SGP - TR - 30

PROCEEDINGS
FOURTH WORKSHOP
GEOTHERMAL RESERVOIR ENGINEERING

Paul Kruger and Henry J. Ramey, Jr.
Editors

December 13-15, 1978

Stanford Geothermal Program
INTERDISCIPLINARY RESEARCH
IN ENGINEERING AND EARTH SCIENCES
Stanford University, Stanford, California

DISCLAIMER

PROCEEDINGS OF THE FOURTH WORKSHOP ON GEOTHERMAL RESERVOIR ENGINEERING

PAUL KRUGER AND HENRY J. RAMEY, JR.
STANFORD GEOTHERMAL PROGRAM
STANFORD UNIVERSITY
STANFORD, CALIFORNIA

DECEMBER 13-15, 1978

CONDUCTED UNDER SUBCONTRACT No. 167-3500
WITH LAWRENCE BERKELEY LABORATORY
UNIVERSITY OF CALIFORNIA
SPONSORED BY THE GEOTHERMAL DIVISION OF THE DEPARTMENT OF ENERGY

TABLE OF CONTENTS

Page

Modelling

INTRODUCTION TO THE PROCEEDINGS OF THE FOURTH GEOTHERMAL RESERVOIR ENGINEERING WORKSHOP, STANFORD GEOTHERMAL PROGRAM

Henry J. Ramey, Jr.
Co-Principal Investigator, Stanford Geothermal Program
Department of Petroleum Engineering
Stanford University
Stanford, CA. 94305

The First Stanford Geothermal Reservoir Engineering Workshop was held in mid-December, 1975. The RANN research programs, funded by the National Science Foundation, were just getting underway, and the international geothermal industry was quite small. The program committee for the first workshop in 1975 used as guidelines the selection of papers from industry, educational research, and various state and federal institutions involved in the newborn geothermal industry. Much of the information presented at this workshop was a recounting of research plans for the future. The meeting was fully attended, and a good cross-section of national and international interests in geothermal energy was represented at the first workshop. A complete spectrum of attendees from national and international geothermal organizations indicated the growing importance of reservoir engineering to the rapid development of geothermal energy.

The Second Geothermal Reservoir Engineering Workshop was held in mid-December, 1976. This meeting was truly exceptional in that many of the attendees were now reporting accomplished research and results from actual field operations. This was contrasted to the previous meeting, which focused mainly on research intentions. Dr. Carel Otte, president of Union Oil Company's Geothermal Division, presented the keynote address at the second geothermal workshop and focused his attention on the impending importance of federal, state, and local regulation of the new geothermal industry. This workshop, like the first one, was sold out, and it was necessary to limit papers presented at the workshop. However, a policy was set by the program committee for the second workshop to publish papers offered for the meeting in the Proceedings. The Proceedings of the first two geothermal workshops became important references during the third year.

The Third Geothermal Workshop was held in mid-December, 1977. Dean Richard H. Jahns presented the keynote address for the Third Workshop, welcoming an international group of geothermal reservoir engineers. The Third Geothermal Reservoir Engineering Workshop was truly remarkable in that candid, open presentations of results of field experimentation with geothermal energy were presented by many of the speakers. The nature of the presentations underlined the importance of free exchange of information to augment the development of geothermal energy to meet national needs. Again, a large international contingent of attendees was present at the meeting. Important and unique field information was presented, and the Proceedings of this workshop now appear to join those of the first two workshops as unique references in this field of geothermal reservoir engineering.

The program committee for the Fourth Geothermal Workshop, presented in mid-December, 1978, decided that the format of the last two geothermal workshops should be continued; that is, the objective should be documented talks on field phenomena and reports on important results of research directly applicable to geothermal energy development. An arranged panel discussion of problems of common importance was also built into the program. Finally, it was decided to publish all submitted papers in the proceedings, but to select papers for presentation at the workshop program. The keynote speaker for the Fourth Geothermal Workshop program was Dr. Robert Rex, president of Republic Geothermal Corporation, who spoke on "Credibility of Geothermal Reservoir Engineering Calculations." The main thrust of this talk was focused on the reception of reservoir engineering work by financial institutions involved in funding geothermal energy developments.

The Department of Energy was the funding agency for both the third and fourth workshops. The Introduction to the fourth workshop pointed out that geothermal reservoir engineering had finally come of age. The hallmarks of the geothermal reservoir engineering workshops had clearly become (1) an open exchange of information, and (2) the presentation of results, as opposed to plans or intentions. The main focus of the Stanford geothermal reservoir engineering program has become augmentation of ongoing field operations. The papers presented at the fourth workshop indicated that other participants were dedicated to the same objective.

Attendees at the Fourth Geothermal Reservoir Engineering Workshop in December, 1978, were enthusiastic about the scheduling of a fifth workshop in December, 1979. Plans have already been set for this meeting. We offer the Proceedings of the Fourth Geothermal Reservoir Engineering Workshop to the geothermal reservoir engineering community in anticipation of important presentations to come during the fifth workshop in December, 1979.

RECENT DEVELOPMENTS IN THE DGE PROGRAM

Marshall Reed, Program Manager
Division of Geothermal Energy
Department of Energy
20 Massachusetts Av. N.W.
Washington, D.C. 20545

This Fourth Workshop on Geothermal Reservoir Engineering demonstrates the success of this workshop series at Stanford. The Division of Geothermal Energy of the U. S. Department of Energy funds this and other geothermal workshops to accomplish a transfer of technology and exchange of information between the research community and the geothermal industry. The active participation of industry representatives in this workshop is an indication of its worth.

On December 8, 1978, the Division of Geothermal Energy was reorganized into technical disciplines. Rudy Black, the past Director of the division, has become the Resource Manager for Geothermal Energy under the Assistant Secretary for Resource Applications. He and eight other persons from the Division are now responsible for the commercialization of geothermal energy. Bennie DiBona, the Acting Director of the Division of Geothermal Energy, and the 24 remaining staff members are organized as shown on the accompanying chart.

The Reservoir Engineering Program is now under the purview of the Reservoir Assessment Section in the Hydrothermal Support Branch. The Reservoir Assessment Section also handles programs in Exploration Technology, Industry-Coupled Drilling, and State Cooperative Low-Temperature Assessment. It is planned that this new organization will be more responsive to the needs of the geothermal industry and will be better able to coordinate related activities within the Division of Geothermal Energy.

I want to thank you all for the contribution you have made to this workshop and to the field of geothermal reservoir engineering. I look forward to the continued success of this program and to the fruitful exchange of ideas at future workshops.

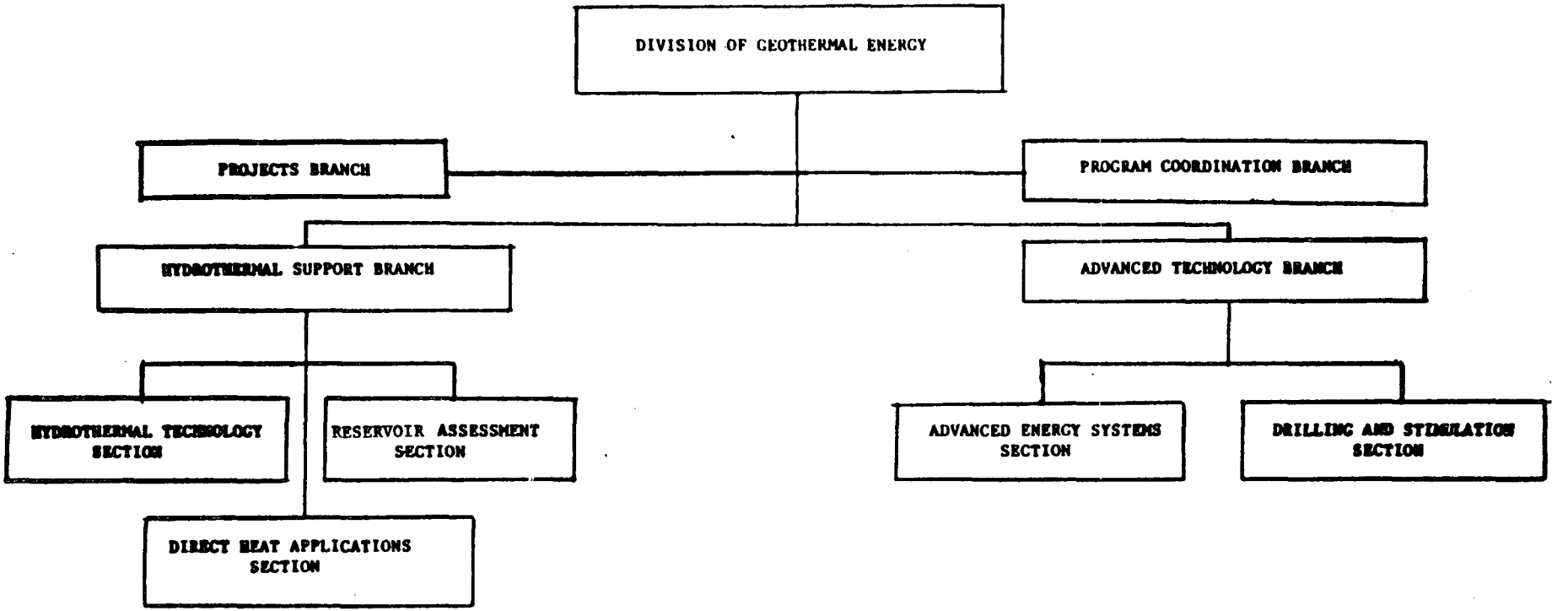
DIVISION OF GEOTHERMAL ENERGY
PROJECTS BRANCH
PROGRAM COORDINATION BRANCH
HYDROTHERMAL SUPPORT BRANCH
ADVANCED TECHNOLOGY BRANCH
HYDROTHERMAL TECHNOLOGY SECTION
RESERVOIR ASSESSMENT SECTION
DIRECT HEAT APPLICATIONS SECTION
ADVANCED ENERGY SYSTEMS SECTION
DRILLING AND STIMULATION SECTION

RECENT ACTIVITIES AT THE CERRO PRIETO FIELD

Alonso E., H.[1], Domínguez A., B.[1], Lippmann, M.J.[2],
Manon M., A.[1], Schroeder, R.C.[2], and Witherspoon, P.A.[2]

[1]Comisión Federal de Electricidad
Coordinadora Ejecutiva de Cerro Prieto
Mexicali, Baja California, México

[2]Lawrence Berkeley Laboratory
Earth Sciences Division
Berkeley, California 94720

INTRODUCTION

The purpose of this paper is to describe some of the latest activities of interest to reservoir engineers at the Cerro Prieto geothermal field. Special emphasis is given to the wells drilled in 1978 for exploration purposes and to provide steam to the existing and future power plants. The present power output is 75MW. Two additional 37.5MW units are scheduled to go on line in March and May 1979, while the total generating capacity at Cerro Prieto will reach about 400MW in 1985. Additional information is available in a number of papers in References 1 and 2.

NEW WELLS (Figure 1)

At the present time (December 1978), there are six drilling rigs active, four for new wells and two to repair old ones. Because of generally different reservoir conditions and depths, the Cerro Prieto field can be divided into three blocks: Block I, presently the main producing area, centered around M-5; Block II, south of a line which approximately passes through wells M-35 and M-46; and Block III, NE of the railroad track which roughly coincides with the trace of the Cerro Prieto fault.

In 1978 twelve wells have been completed and three are presently being drilled.

Production Wells: M-43, M-102, M-103, M-104, M-114, M-130, M-181, T-366
Exploration Wells: M-93, M-94, M-96, S-262
Wells Being Drilled: M-107, M-123, M-150

Depth: The average depth of these wells is 2000m; the deepest are T-366 (2980m) and M-96 (2728m). The new production wells have reached the hot water reservoir(s) between: 1500 and 1700m (Block I, Wells M-43, M-114, M-130), 1453 and 1610m (Block II, Well M-181), and 1800 and 2000m (Block III, Wells M-102, M-103, M-104).

Lithologic and Temperature Characteristics: In Block I the downhole temperatures measured were: 294°C (M-130), 271°C (M-114), 265°C (M-43), which are only moderate for this block, while in Block II, 287°C was measured at the bottom of M-181.

In Block III, the downhole temperatures in M-102 and M-104 are about 345°C, similar to M-53. To the NW, in M-94, it only reached 208°C. The lithologic column and structural conditions found in M-53, drilled in 1974, are generally repeated in wells M-102, M-103 and M-104. Nevertheless, towards the SE the

permeable hot zone deepens quite appreciably. It was found between 2400 and 2560m in M-93, and between 2427 and 2922m in T-366. In these two wells the characteristic of the productive intervals is quite different. In M-93 high permeability zones were indicated by large lost circulations. On the other hand, in T-366 these losses were minimal, and visual inspection of the recovered cores indicate low permeabilities. (A relatively long perforated interval was installed in this well.) The temperatures measured in the drilling muds at rest in the well were 221°C (M-93) and 230°C (T-366). These values suggest that after cleaning the wells and a heating up period, the temperatures will reach at least 340°C. This seems to indicate that Block III may have production potential, independent of an apparent decrease in permeability and increase of depth towards the SE. This area, which already has seven completed wells, will supply steam to the Cerro Prieto II plant (additional 110MW by 1983 and 220MW by 1985).

Exploration well M-96, NW of the main production area, reached basement at about 2713m. The maximum temperature (108°C) was reached at 1977m; 97°C was measured at 300m indicating a shallow hot aquifer. South of the field another exploratory well, S-262, penetrated basement at 1470m. There, the highest temperature was measured at the bottom of the hole (100°C).

Casings (Figures 2 and 3): In most of the wells built in 1978 a 7-5/8" Ø, K-55, 45.3 lb/ft. casing with Hydrill Super EU thread was used. When required, as in M-102 and M-94, a 5" Ø, K-55, 23 lb/ft. liner with Super EU thread was installed. Recently it was decided to change the diameter of the production casing to 9-5/8" Ø to increase steam production and because it is easier to obtain commercially. In M-103 and T-366 a 9-5/8" Ø, N-80, 47 lb/ft. production casing with Buttress thread and 7" Ø, N-80, 29 lb/ft. hanging and cemented liner with Hydrill Super EU thread were installed. With the new grade of casing larger mechanical capacity has been sought to better withstand the tension and compression stresses which have created many problems at Cerro Prieto. Nevertheless, one will have to wait to find out the corrosive effect of the geothermal fluids on this type of casing.

DRILLING PROBLEMS

Three main problems during the drilling of these wells have been encountered: a) lost circulation during drilling and cementing operations, b) fishing problems, and c) cave-ins and stuck tools.

Lost Circulation: During drilling and cementing, this is the most important problem. In some cases, circulation losses could be controlled. In other cases, like in M-93, almost 100m were drilled with complete loss of circulation in order to clearly penetrate into the producing layer and get good production. This may result in stuck pipes and in cementing problems. With this procedure, the probability of losing cement slurry into the formation is increased. This is a severe problem because the production casing could fail when the well is heated up. In some cases, like in M-93, M-123 and M-150, in addition to losses near the production zones, lost circulation has occurred in the upper 1000m, while cementing the 11-3/4" Ø or 13-3/8" Ø surface casing. This situation is very serious because the safety of the anchor and seals which prevent upward flows depend heavily on a good cement job. This problem was only encountered in Block III, and is related to the high permeability of its sandy layers.

Fishing Problems: These problems are closely related to circulation losses since they create conditions which may end with tools getting stuck in the borehole. Then, if the tools fail mechanically a fishing problem results. Some fishing operations were successful, but in M-94 and M-103 they failed.

In M-94 it was decided to hang a 5" Ø production casing in the upper part of the producing zone which remained open. Pipes which could not be fished out were left in the hole from 2328 to 2601m. This lower part of the well showed high temperatures but low permeability. Another interval of high temperature, presently covered by the casing, was detected at 1600m. It showed a maximum of 214°C.

In M-103 because of the good thermal characteristics of the well, it was decided to slant-drill above the fish. The drilling was successful but there exists uncertainty about the behavior of the 9-5/8" Ø production casing when the well heats up. The thermal expansion in the area of deviation may produce collapse or fracture of the casing. This is being watched as the well begins to heat up.

Cave-Ins and Stuck Tools: Another problem is the caving of shales near the high temperature zones. This occurs when the drilling operation takes too long, because of lost circulation or other causes. This is well known in the oil industry when the drilling lasts more than 60 days. In Cerro Prieto it is complicated by the presence of fractures or possibly faults which increase the probability of cavings. This results in stuck or caught tools.

When this situation develops, special mud conditions are used in the hole. But if this does not stop the caving, temporary plugs of cement bridging the zones affected are used to stablize the formations. This will allow the installation and cementing of casing which will definitely solve the problem.

In Blocks I and II these types of problems have not occurred or have been easily solved following the procedure described, but in Block III they have been more severe.

DEVELOPMENT OF NEW WELLS

A number of wells drilled before 1978 were developed this year. The chemical characteristics of the separated brine produced are given in Table 1.

From the 1978 wells M-102, M-114 and M-130 have been developed. Figure 4 shows the evolution of the characteristics of M-102 during the later part of its development. With time and orifice-diameter changes there is a marked variation in the wellhead pressures. However, chemical indices and the "Na-K-Ca" geothermometer remain essentially constant. At Cerro Prieto when orifices (or purges) are changed, these parameters are used to detect any possible variation in the downhole source of the produced steam-brine mixture.

Total production of M-102 was 120 tonnes/hr. of steam and 180 tonnes/hr. of brine at 13.8 bars (200 psig). This is a good well, and even better characteristics are expected to be found in the rest of the wells in Block III, especially in T-366 and M-93 which are only beginning to heat up.

TABLE 1

CHARACTERISTICS OF CERRO PRIETO WELLS DEVELOPED DURING 1978

WELL	DATE	PERFORATED INTERVAL (depth m)	FLOW CONDITIONS	WELLHEAD PRESSURE bars (g)	Na mg/l	K mg/l	Ca mg/l	Cl mg/l	TEMP. (°C)	ENTHALPY kJ/kg
M-50	11/24/78	1144-1249	6" Ø cone	14.0	7009	1859	337	12958	306	1379
M-51	2/8/78	1245-1567	6" Ø orif.	23.1	10600	3342	551	20534	335	1561
M-53	6/20/78	1845-1996	5-1/2"Ø orif.	12.1	10396	3454	429	19692	345	1632
M-84	8/4/78	1536-1691	5" Ø cone	22.1	10341	3118	486	19694	325	1494
M-90	2/20/78	1221-1379	5" Ø orif.	15.1	6221	1773	242	12242	320	1460
M-91	2/2/78	2133-2294	6" Ø orif.	17.9	9281	2476	405	16757	318	1448
M-101	5/19/78	1193-1394	6" Ø orif.	6.4	2703	423	3	4310	241	1042
M-102	10/20/78	1793-1990	6" Ø orif.	19.3	11266	3342	481	21019	329	1519
M-105	10/18/78	1480-1673	6" Ø cone	15.7	9793	2851	529	18794	320	1462

WELL TESTING

Measurements of temperatures, pressures, flow-rates, and enthalpies have been made for several years at Cerro Prieto. During 1978 several well tests have been performed, and data from long-term measurements in M-6 and M-10 have been collected. Preliminary analyses of data have been made for the measurements listed in Table 2. The water-level data from M-6 is quite satisfactory, but are not considered to be reliable due to the different depths of penetration, and large differences in temperature at M-6 and within the producing field. When reservoir simulation is used this data will be very valuable. The well test involving M-101 has been analyzed, but the values for kh/μ and ϕch cannot be considered to be satisfactory, since recent reservoir models suggest that two or more separate aquifers are penetrated at different depths by the five wells involved in the test. The measurements made when M-53 was brought on-line would have made a contribution to our knowledge of that portion of the field, but anomalous increases in water level (downhole pressure) completely obscured the M-53 production effect for several weeks. The anomalous behavior has been ascribed to a medium-scale earthquake (5.3 Richter) whose epicenter was about 20km south of the production field. The water levels rose before the earthquake (in spite of the drawdown), and began to decrease slowly soon after the major shock.

Several productivity tests have been made using two or more rate changes as a means of determining near-well parameters. The data for three such tests carried out during the long interference test with M-101 has been studied, but the multiple aquifer effects have made the parameter values difficult to determine.

Presently, there are additional analyses, simulation of well tests, and new measurements in the planning stage for 1979. Efforts will be made to determine the hydrological characteristics of the stratigraphic discontinuity between Blocks II and III.

TABLE 2

SUMMARY OF WELL TEST RESULTS

OBSERVATION WELL	PRODUCING WELLS	kh/μ md-ft/cp	φch ft/psi
M-6	Entire Wellfield	4.7×10^{6}	
M-101	M-50,51,90, 91	1.5×10^{6}	2.3×10^{-2}
M-104 M-10	M-53 Entire Wellfield	Earthquake	
Two-rate Tests	M-51 M-90 M-91	Inhomogenieties	

FINAL REMARKS

The drilling activity at Cerro Prieto will continue at least at the present pace: six rigs will be operating in the field, about 20 new wells are scheduled to be completed in 1979.

As new wells become available two-rate flow tests and long-term interference tests have been planned to establish the characteristics of different blocks of the Cerro Prieto reservoir(s).

REFERENCES

1. "Proceedings Second United Nations Symposium on the Development and Use of Geothermal Resources," San Francisco, Calif., May 20-29, 1975, U.S. Gov. Printing Office, 3 Vols., 2466 p., 1976.

2. "Proceedings First Symposium on the Cerro Prieto Geothermal Field, Baja California, Mexico," San Diego, Calif., September 20-22, 1978, Lawrence Berkeley Laboratory, Rept. LBL-7098 (in preparation).

ACKNOWLEDGMENTS

Work partially performed under the auspices of the U.S. Department of Energy.

GLOSSARY OF TERMS USED IN FIGURES 2 AND 3

C.C.R.B. (Cople corto, rosca Buttress): Short connector, Buttress thread
C.C.R.R. (Cople corto, rosca redonda): Short connector, round thread
Cementada: Cemented
Colg. (Colgador): Hanger
Cond. (Conductor): Conductor casing
Cople Especial: Special connector
Cople Flotador: Floating collar
Cople Retén: Baffle connector
Cuñas Sencillas: Simple wedges
Lastrabarrenas: Drill collars
Pérdida de Ciculación: Lost Circulation
Perf. (Perforación): Wellbore
Pescado: Fish
Plano: Flat
Pozo: Well
Ranurada: Slotted
R.B. (Rosca Buttress): Buttress thread
R.H.S.E.U. (Rosca Hydrill Super EU): Super EU Hydrill thread
S.L.: Slotted liner
Tapón Cemento: Cement plug
Tapón de Fondo: Downhole plug
T.R. (Tubería): Casing
Tubo: Pipe

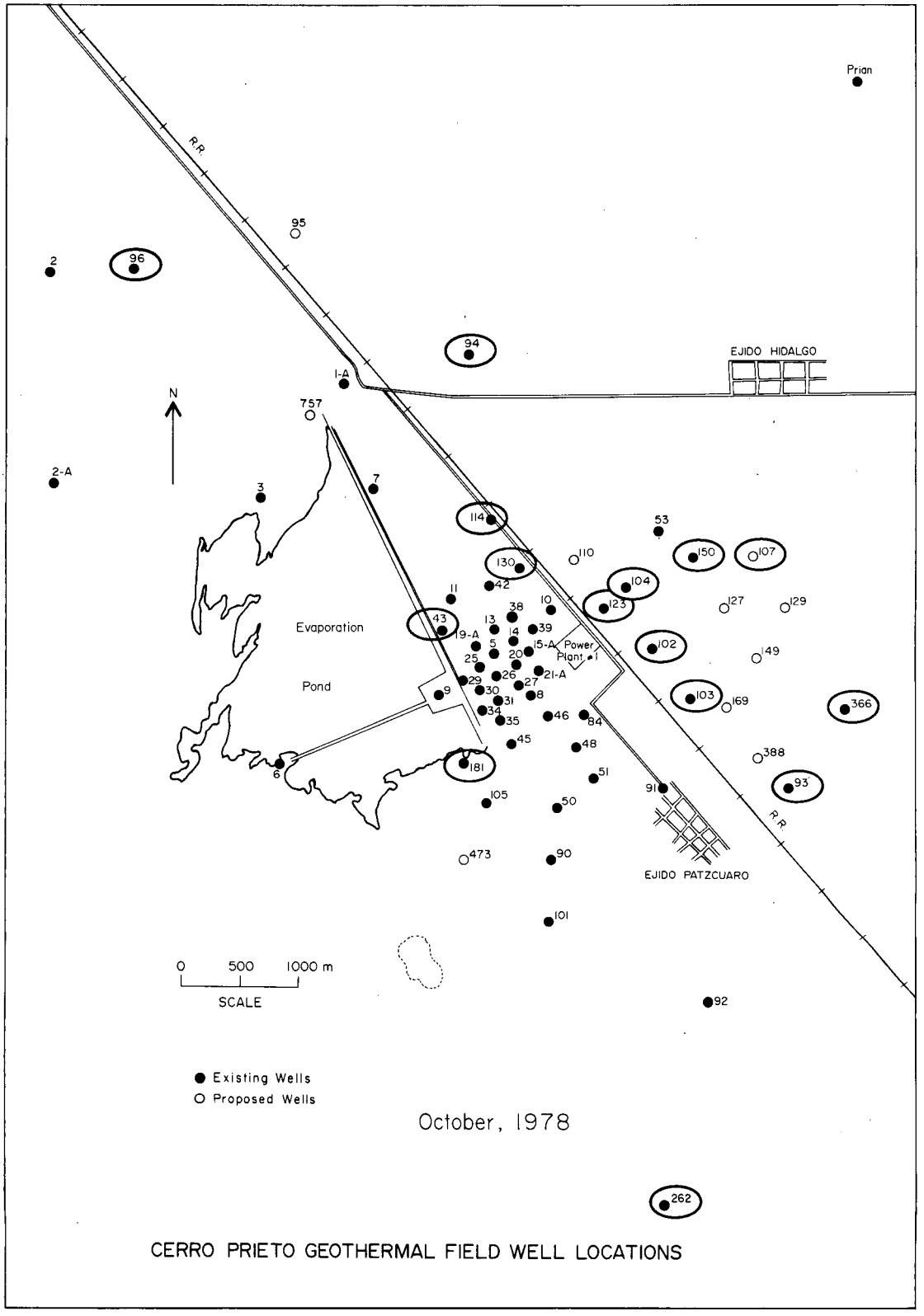

Figure 1: Location of 1978 Wells (Well numbers are circled).

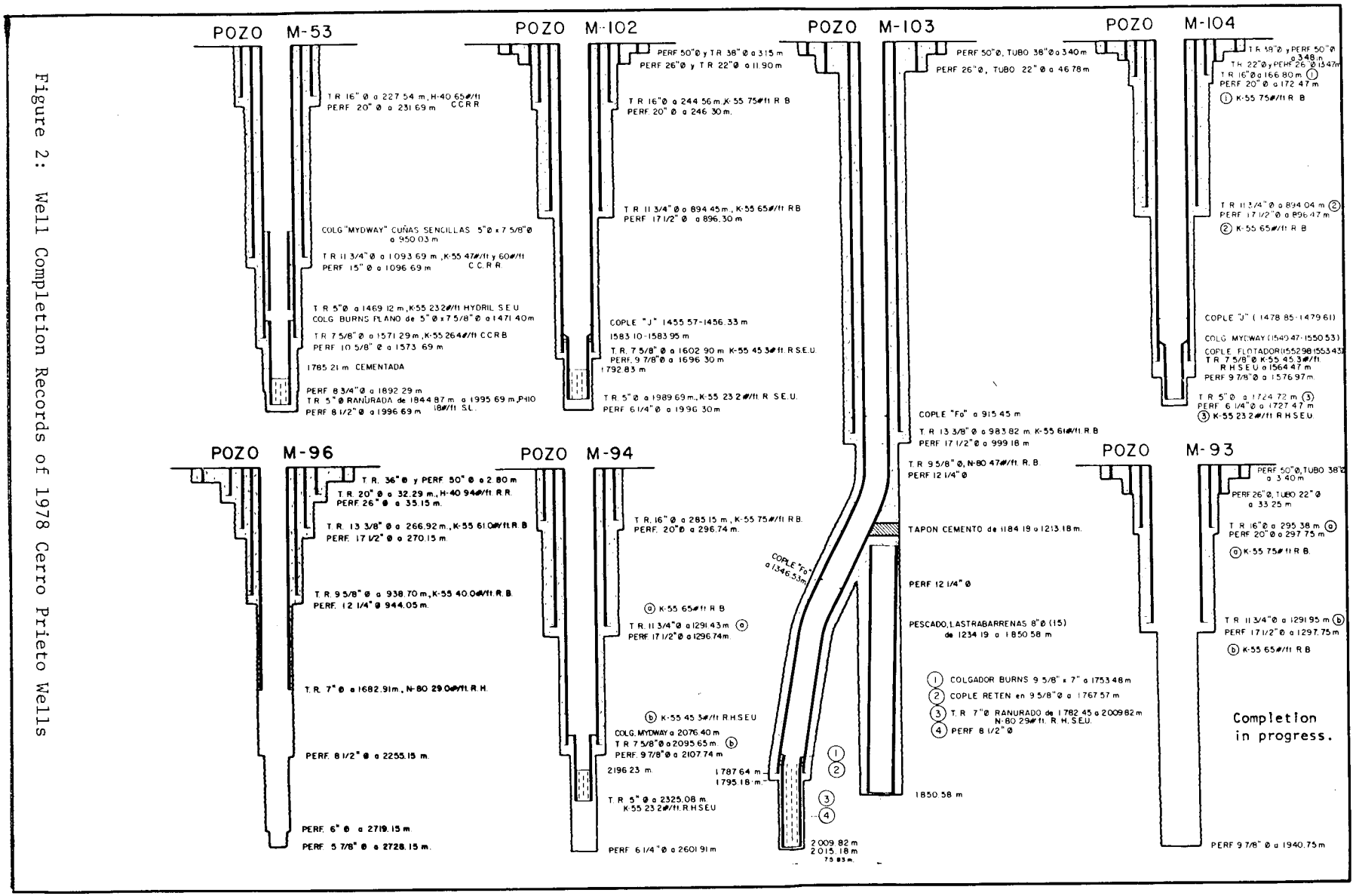

Figure 2: Well Completion Records of 1978 Cerro Prieto Wells

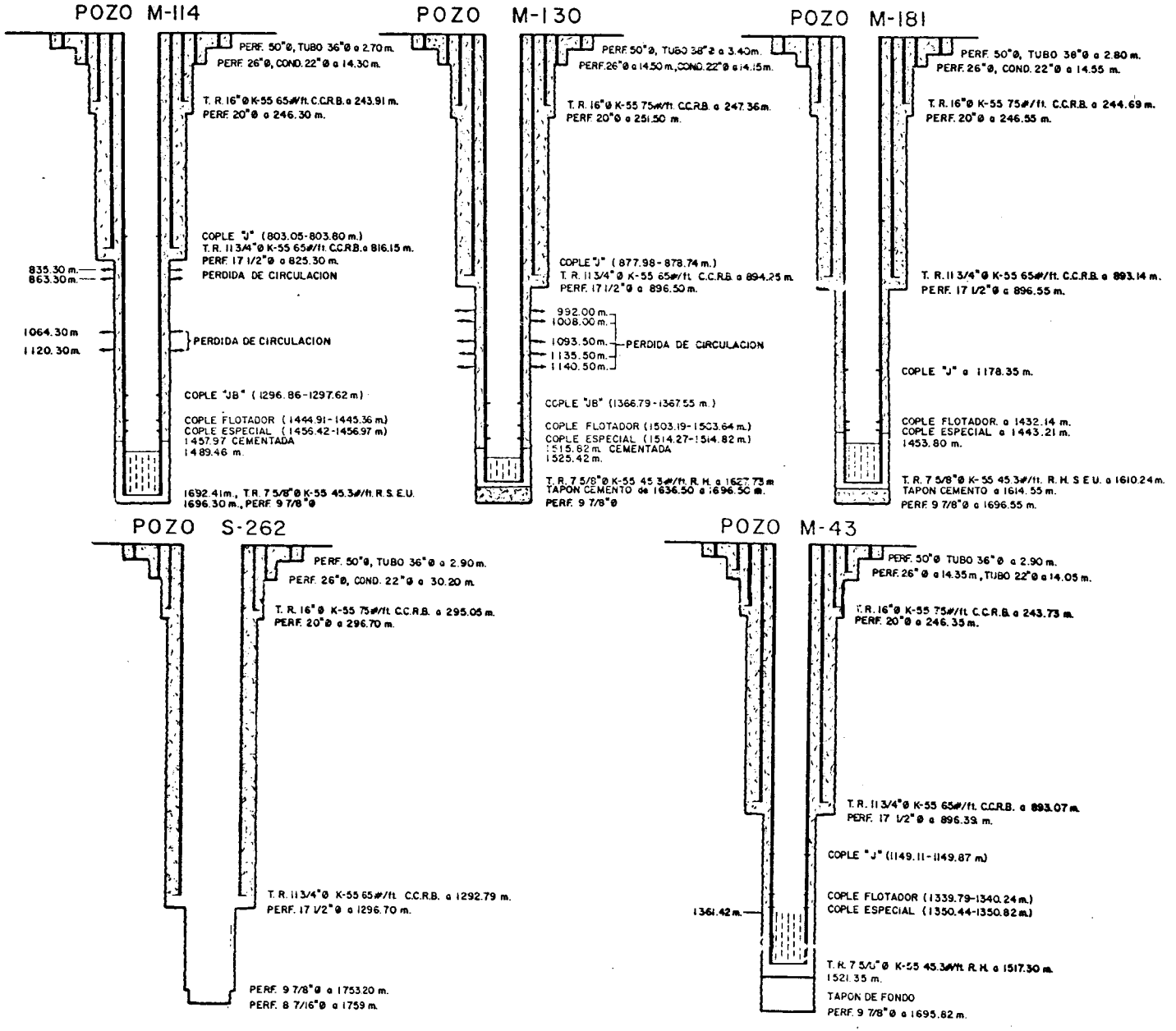

Figure 3: Well Completion Records of 1978 Cerro Prieto Wells

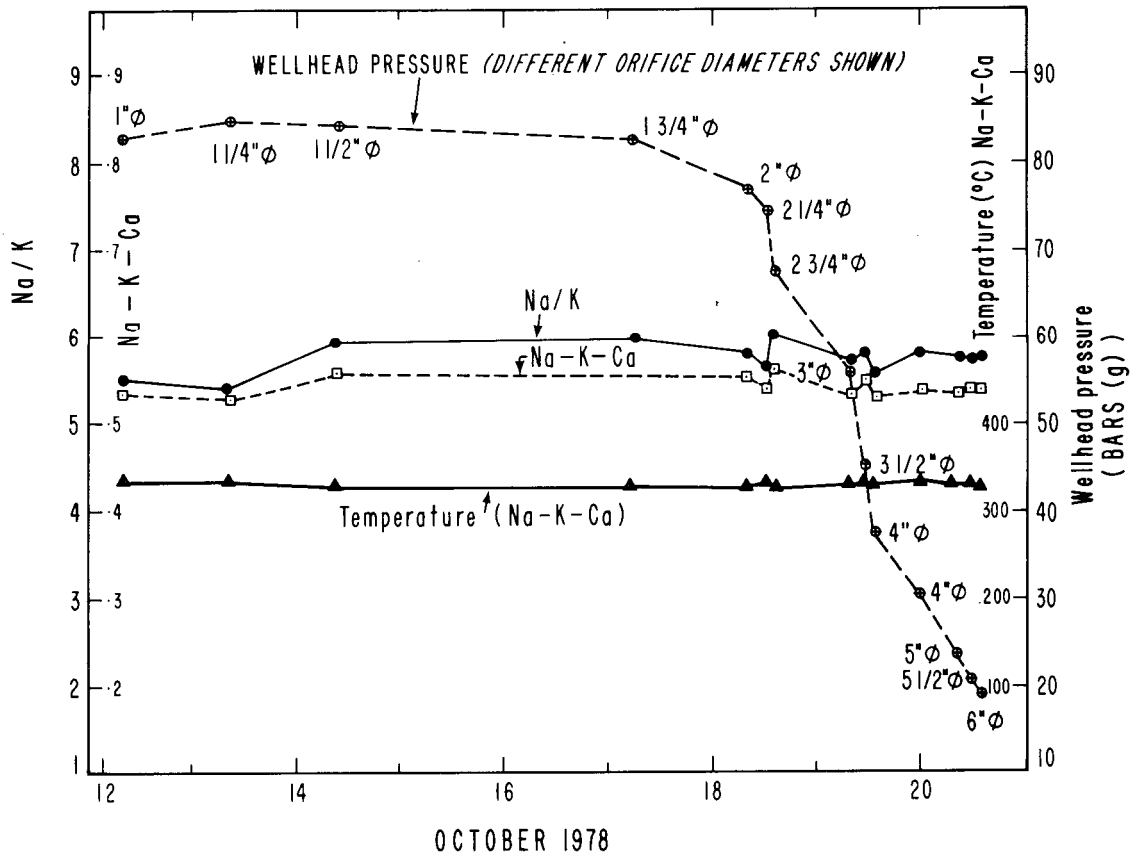

Figure 4: Change in Well M-102 Characteristics During its Development

PROGRESS REPORT ON THE DOE/DGE/LBL RESERVOIR ENGINEERING AND SUBSIDENCE PROGRAMS

J.H. Howard, J.E. Noble, W.J. Schwarz, and A.N. Graf
Earth Sciences Division
Lawrence Berkeley Laboratory
University of California
Berkeley, California 94720

THE GEOTHERMAL RESERVOIR ENGINEERING MANAGEMENT PROGRAM
(Including projects continued from the former NSF-RANN Geothermal Program)

Fiscal year 1978 was the second year of LBL's responsibility for the Geothermal Reservoir Engineering Management Program ("GREMP") on behalf of the Division of Geothermal Energy of the Department of Energy.

The history of this program through FY 1977 is explained in LBL's Earth Sciences Division Annual Report for 1978. Administrative highlights of the program in FY 1978 are as follows:

1. All projects started under the NSF-RANN program were continued. These include work done at Stanford University; Princeton University; Systems, Science and Software; University of California at Riverside; and the University of Colorado. All of these programs were further extended into FY 1979 with the exception of the University of Colorado who chose to conclude their program.

2. Seven new projects were started. These projects are indicated in Table 1.

3. The Division of Geothermal Energy re-emphasized its concern that all projects under the GREMP program clearly and directly relate to DGE's "power-on-line" mission. The Review Task Force originally constituted to overview the GREMP program was dissolved, and plans were made to assemble a new task force. LBL was urged to solicit industry to assure that there is Federal support of research to all reservoir engineering-related technical "hangups" to "power-on-line." LBL was requested to revise and update the original GREMP planning document (LBL-7000).

4. With the exceptions noted below, all project areas of the original GREMP plan have been addressed as have all known serious technical reservoir-related impediments to geothermal resource development,

---

This work is sponsored by the Division of Geothermal Energy of the U.S. Department of Energy under Contract W-7405-ENG-48

e.g., formation damage during drilling. Important projects that have not yet received this full measure of support are work on mass flow measurement techniques, on use of tracers, and on decline curve analysis, particularly enthalpy decline curve analysis. Also, in keeping with the recommendation of the Review Task Force, essentially nothing has been done on economics and on exploitation strategies.

5. A so-called GREMP publication series was started. Henceforth all reports prepared under GREMP contracts will be published or reprinted as part of this series. S^3's summary of the Wairakei field and Terra Tek's bibliographic review will be the first two publications of this series.

6. The program began issuing a "Newsletter." The first was issued Aug. 1, 1978; the second, Nov. 3. The purpose of the newsletter is to summarize the highlights of progress in research and to direct readers to new, complete reports on the research. The newsletter is available by requesting addition of one's name to the GREMP Newsletter mailing list.

7. A plan for support of new work in the GREMP program through FY 1980 has been developed. The plan is shown in Figure 1.

Technical and scientific progress accomplished during the year can be related to five work areas. These work areas and the contracts within them are shown in Table 1. Brief sketches of these contracts and their achievements are shown in Table 2.

Technical progress on the program has been very satisfactory. Worthy of special note are the following accomplishments:

1. Completion of a comprehensive bibliographic review of the literature pertaining to geothermal reservoir exploitation (Terra Tek).

2. Development of a quantitative model of a prototype geothermal resource, namely one dominated by a vertical fault (University of Colorado).

3. Compilation of the entire production history of an important liquid dominated geothermal reservoir, namely Wairakei (Systems, Science and Software).

4. Increasing awareness of the importance of lithology logging as a practical tool during drilling of geothermal wells (University of California at Riverside).

5. Meeting for the third time at the annual Stanford Geothermal Workshop. This Workshop has become the outstanding public forum for exchange of ideas and information in geothermal reservoir engineering.

Table 1. GREMP MAJOR PROGRAM AREAS AND CONTRACTS

PROGRAM AREAS	CONTRACTS
1. Status of Geothermal Reservoir Engineering	A. Terra Tek* - review of the literature in geothermal reservoir exploitation engineering.
2. Measurements of Interest to Exploitation Engineers	A. Measurement Analysis Corporation* - review of the status of instrumentation to make measurements of interest to reservoir engineers, e.g., temperature, mass flow rate, etc.
	B. UC/Riverside - use of mineral species as an indicator of reservoir temperatures; use of stable isotopes to determine temperatures and total fluid flux throughout the reservoir.
	C. Battelle Memorial Institute/Pacific Northwest Laboratory* - measurement of well head enthalpies on a real-time basis.
	D. Terra Tek* - measurement of non-condensable gases, particularly carbon dioxide, in the flow stream on a real-time basis.
	E. Stanford University - techniques for measuring saturation and relative permeability and for use of natural tracers (radon) in reservoir studies; rock to fluid heat transfer; thermal stress cracking.
3. Analytical Tools	A. Terra Tek* - analysis of near-bore formation damage as a consequence of mud-type, and drilling and completion practices.
	B. Republic Geothermal Incorporated* - analysis of calcium carbonate precipitation in the near bore area due to inappropriate pressure drawdowns there.
	C. Stanford University - development of parallelpiped models for use in well testing to obtain lumped reservoir properties; decline curve analysis; incorporation of high non-condensable gas content into analytical mathematical models.

* New contract in FY 1978.

Table 1 (continued)

PROGRAM AREAS	CONTRACTS
3. Analytical Tools (cont'd)	D. Intercomp* - development of analytical techniques for interpretation of wellhead temperature, pressure, and mass flow rate data when the reservoir is in part in two-phase flow.
4. Forecasting Reservoir Performance	A. Princeton University - codes for the simulation of mass and energy transport in fractured reservoirs.
	B. University of Colorado - analytical model for mass and energy transport in a half space characterized by a vertical conduit (i.e. fault).
5. Synthesis of Data and Applications of Forecasting and Analytical Tools	A. Systems, Science and Software - synthesis of data for the Wairakei geothermal field.
	B. Stanford University - synthesis and analysis of data from the Travale-Radicondoli field and the Bagnore field.
	C. Systems, Science and Software - analysis of production history of the Wairakei field.
	D. University of Colorado - application of analytical model to the East Mesa field.
	E. University of California at Riverside - synthesis of subsurface geology based on lithology logging at the Cerro Prieto field.

* New contract in FY 1978.

TABLE 2. GREMP CONTRACTS - STATUS AND RESULTS

SUBJECT AREA	CONTRACT AND STATUS AND RESULTS
1. Status of Geothermal Reservoir Engineering	A. Terra Tek - • The objectives of this contract have been to develop an annotated bibliography, narrative review and thesaurus of geothermal reservoir engineering in a broad sense. Literature in English, Russian Italian and Japanese has been searched using computer search services, abstracts, and index services. Topics include: analytical modeling, numerical modeling, physical modeling, formation evaluation (including well testing and case studies, but not well logging), exploitation strategies (including production-disposal strategies, stimulation, well spacing), and interpretation of production trends (including isotope analysis, heat and mass flux histories, and tracer injection techniques). • There has been a need to gather together and synthesize the literature pertaining to reservoir engineering in order to understand more clearly where this technology and science now stands and accordingly to plan more effectively for support of research in the future. • The contract has essentially been completed as of December 1, 1978 and a report (the second in the GREMP series) which includes thesaurus, annotated bibliographic entries, and short narrative review has been prepared.
2. Measurements of Interest to Exploitation Engineers	A. Measurement Analysis Corporation - • The objective of this project is to evaluate measurement needs and existent measurement methods for geothermal reservoir related parameters, including permeability, flow rate, particulate count, conductivity, density, void fraction, quality, pH and others. • There is a need to determine what measurements are sought and desired in the geothermal resource exploitation community and to evaluate the current capability to make those measurements reliably.

Table 2 (continued)

SUBJECT AREA	CONTRACT AND STATUS AND RESULTS
2. Measurements of Interest to Exploitation Engineers (cont'd)	• To date the contract has reported high interest in detection and measurement of fractures and in a non-fouling temperature probe. Mass flow measurement and enthalpy measurement at the wellhead appear to be of lesser interest. B. UC/Riverside - • An objective of the program at UC/Riverside is to map mineral assemblages and other indices of temperatures in order to determine the maximum temperatures to which the strata in a geothermal reservoir have been subjected. • Although supported originally as a topic of basic research, this task of the UC/R program has turned out to have appreciable practical value as a guide to decisions regarding progress of drilling toward zones sufficiently hot to be interesting economically. • UC/R has reported its results in many publications among the most recent being publication of UCR/IGPP 78/8, 78/9 and 78/10 in the proceedings of the Hilo Geothermal Resources Council meeting in July 1978. C. Battelle Memorial Institute/Pacific Northwest Laboratories - • The objective of this study is to evaluate calorimetry systems that will permit economical, reliable and accurate measurement of enthalpy values at the geothermal wellhead. • The saleable product from a geothermal well is the energy contained in the wellhead fluid. The energy content per mass unit passing from the well should therefore be known. Furthermore for power plant design purposes it is important that enthalpy of the wellhead product be known as a function of time. • The project began November 1, 1978, and Phase 1 is to conclude on March 30, 1979.

Table 2 (continued)

SUBJECT AREA	CONTRACT AND STATUS AND RESULTS
2. Measurements of Interest to Exploitation Engineers (cont'd)	D. Terra Tek - • The objective of this project is to develop a simple and convenient instrument to measure non-condensable gases on a real-time basis in geothermal discharges. • Information on the non-condensable content in the flow stream is needed in order to estimate the power potential of a well and reservoir and also to design power stations. • A draft final report on the instrument design has been written. Construction of the instrument should begin following design approval. Laboratory and field testing are scheduled for completion by September 1979. E. Stanford University - • Among the many objectives of this program is a project to better understand the petrophysics of rock/high salinity fluid systems including: - techniques for measuring liquid content in brine/steam systems using a capacitance probe. - effect of salinity on surface tension and related phenomena. - effect of temperature on permeability and relative permeability. • Also, a project to evaluate the utility of radon in understanding geothermal reservoir behavior and response during production. • Also a project to evaluate heat flux from collections of rock fragments of various shapes and sizes to geothermal fluids. • Also a project to evaluate thermal stress cracking in rocks of known geometry. • All these projects are necessary in order to understand the fundamental behavior of mass and energy distribution and transport in geothermal reservoirs.

Table 2 (continued)

SUBJECT AREA	CONTRACT AND STATUS AND RESULTS
2. Measurements of Interest to Exploitation Engineers (cont'd)	E. Stanford University (cont'd) - • Stanford has issued annual reports and topical reports on their findings.
3. Analytical Tools	A. Terra Tek - • The objective of the project is to evaluate the consequences of mud-type and drilling and completion practices on the development of a "baked" skin around the well bore. • It has been proposed that several geothermal wells have been essentially non-producing because of formation damage in the near-bore area as a consequence of standard drilling and completion practice applied to very high temperature environments. • To date Terra Tek has acquired some core material, has begun evaluation of operating practices and choices for mud, and has begun conceptualization of a laboratory program to simulate formation damage in order to understand the factors controlling it.
	B. Republic Geothermal Incorporated - • The objective of this program is to empirically evaluate the consequence of pressure drop in the near bore area on the precipitation of carbonate minerals from calcium carbonate carbon dioxide rich geothermal fluids. Such fluids are to be flushed through core by a pressure differential. • Carbonate precipitation is well known as a fouling agent in geothermal wells and is suspected to be a cause of impaired permeability around well bores. • The contract is about to begin.

Table 2 (continued)

SUBJECT AREA	CONTRACT AND STATUS AND RESULTS
3. Analytical Tools (cont'd)	C. Stanford University - • Among the many activities underway at Stanford is a project to develop analytical mathematical models for well response of wells drilled into a parallelpiped, the shapes of which can be suitably and quickly changed in order to approximate the geometry of all or part of a reservoir. • There is an advantage to reservoir analysts to have available to them a suite of rapidly solvable analytical mathematical solutions. Review of pressure signatures for well tests with respect to various choices of these models can lead quickly to perspective on the intrinsic parameters and the possible geometries a reservoir may have. • Stanford has used these models to analyze data from certain Italian fields. • Decline curve analysis and treatment of non-condensables in analytical mathematical models have also been addressed in the program. D. Intercomp - • The objectives of this project are to develop an understanding of well testing under situations where there is two-phase flow in the reservoir and to explain, if such is possible, how analysis based on single phase reservoir analysis need be modified to account for the presence of two phases in the reservoir. • The consequence of two-phases present in the reservoir need to be understood in order that they can be properly taken into account when estimating reservoir parameters. • The contract started at the beginning of the fiscal year.

Table 2 (continued)

SUBJECT AREA	CONTRACT AND STATUS AND RESULTS
4. Forecasting Reservoir Performance	A. Princeton University - • There are multiple objectives to this project, the general objective of which is to improve the methodology for geothermal reservoir simulation. Particular objectives include: - development of non-isothermal three-dimensional, two-phase code for heat transport in fractured geothermal reservoirs. - investigate (using finite element techniques) the solution of transient partial differential equations of special importance to such a code. • There has been a great deal of interest in a capability to simulate and forecast geothermal reservoir performance, particularly for fractured reservoirs. • Princeton has made significant progress in the formulation of the theoretical basis for the code and has developed certain important codes and subroutines particularly those useful in solving non-linear coupled PDE's. B. University of Colorado - • The objective of this project has been to develop a semi-analytical model for naturally occurring mass and energy transport in a half space in which the system is charged at some depth within an imbedded vertical conduit (i.e., fault). The model has been applied to the East Mesa field, California. • There has been and continues to be interest in understanding prototype models of geothermal reservoirs. The project has developed one such model. • The project has ended with publication of a final report.

Table 2 (continued)

SUBJECT AREA	CONTRACT AND STATUS AND RESULTS
5. Synthesis of Data and Applications of Forecasting and Analytical Tools	A. Systems, Science and Software ("S^3") – • The objective of this project was to compile all possible reservoir related data on the Wairakei field, New Zealand. • Interest in case histories for purposes of sharing experience and as opportunities for use in history matching with simulators, etc. has always been evident in the development of geothermal resources. • This project has been completed, and both a comprehensive report and executive summary report have been issued. B. Stanford University – • Among the objectives of the Stanford program are activities to synthesize certain data from the Larderello area, Italy. Stanford investigators have, for example, constructed for different times in the development of the field in the Larderello vicinity, pressure maps of the fields and graphs of reservoir static pressures vs masses produced. • Many people interested in vapor dominated reservoirs have also expressed interest in learning from the experiences in the Italian fields. • The project has issued quarterly reports as well as specific reports at the Italian/Larderello-1977 and Stanford-1976 and 1977 workshops. C. Systems, Science and Software ("S^3") – • The objective of this project of S^3, which is a continuation of their earlier work on data compilation at Wairakei, is to construct a geologic model of the field and to match production and subsidence history in the field from 1953 to 1976. S^3 will also forecast future production from the field under different assumptions for the imposed production rates.

Table 2 (continued)

SUBJECT AREA	CONTRACT AND STATUS AND RESULTS
5. Synthesis of Data and Applications of Forecasting and Analytical Tools (cont'd)	C. Systems, Science and Software ("S^3") (cont'd) - • Because of its exceptional data base, Wairakei offers an unusual opportunity for reservoir simulation. • This project was initiated in September 1978 and is to conclude in May 1979. D. University of Colorado - • The University of Colorado has applied an analytical model (described above) to the East Mesa reservoir in order to gain insight into the natural phenomena that may have lead to the occurrence of the geothermal resource there. • This project has been completed. E. University of California at Riverside - • An objective of the UC/R program is to develop an advanced model of the subsurface geology in the Cerro Prieto field, noting in particular the distribution of temperature, porosity and temperature related mineral assemblages. • This project is a significant part of the cooperative Mexican-U.S. project to elucidate the Cerro Prieto geothermal resource. • UC/R continues to issue reports on a regular basis.

Figure 1

PLANNED GREMP PROJECTS AND RFP SCHEDULE FY '79/80

GREMP CATEGORY	SUBJECT	RFP/CONTRACTOR	TYPE OF CONTRACT	FY 1979 1	FY 1979 2	FY 1979 3	FY 1979 4	FY 1980 1	FY 1980 2	FY 1980 3	FY 1980 4
New Contracts											
I. Well Testing	Decline curve analysis	FY 1979 RFP	Competitive (FP)	+ — •	——	——	——	——	——	Δ	
	Two-phase mass flow	FY 1979 RFP	Competitive (FP)				•	——	——	Δ	
II. Geochemical-technical	Tracers to follow flow	FY 1979 RFP	Competitive (FP)	+ — •	——	——	——	——	——	Δ	
	Trace element studies	FY 1978 RFP	Competitive (FP)	•	——	——	——	——	——	——	Δ
III. Properties of Materials	Permeability/porosity from cuttings	FY 1979 RFP	Competitive (FP)				•	——	——	——	Δ
IV. Numerical Modeling		FY 1979 RFP	Competitive (FP)			+ —	•	——	——	——	Δ
V. Site-Specific Studies		FY 1979 RFP	Competitive (FP)			+ —	•	——	——	——	Δ
VI. Fundamental Studies		FY 1979 RFP	Competitive (FP)			+ —	•	——	——	——	Δ
VII. Analytical Modeling		FY 1979 RFP	Competitive (FP)				+	——	——	——	——
VIII. Surface Geophysics		FY 1979 RFP	Competitive (FP)								
IX. Physical Modeling		FY 1979 RFP	Competitive (FP)				+	——	——	——	——
X. Economics		FY 1979 RFP	Competitive (FP)			+	——	•	——	——	Δ
XI. Exploitation Strategy		FY 1979 RFP	Competitive (FP)			+	——	•	——	——	Δ

Legend

- • Proposed start of project/task.
- + CBD announcement or existing qualified contractors list.
- Δ Anticipated report, project milestone, or termination.

THE SUBSIDENCE R&D MANAGEMENT PROGRAMS

A major consequence of development of a geothermal reservoir may be subsidence occurring due to withdrawal of voluminous amounts of fluids. Unexpected and uncontrolled subsidence can have detrimental social, environmental, and economic impact. In order to better understand subsidence, its causes and effects, Lawrence Berkeley Laboratory initiated the Geothermal Subsidence Research Program (GSRP).

The goals of the GSRP are to develop methods for assessing naturally occurring subsidence, for inferring a geothermal reservoir's compaction potential, and for minimizing potential subsidence effects during exploitation of a geothermal reservoir. Attainment of these goals is expected to provide the tools needed for geothermal developers to measure subsidence and to predict subsidence potential of a reservoir. For regulatory agencies, the program is expected to lead to guidance with which to recommend appropriate action to minimize impact of subsidence.

The GSRP is organized into four independent elements:

1. Subsidence Characterization - Subsidence characterization is concerned with studying examples of subsidence and subsidence effects. Research has been conducted to document cases of known subsidence in geographic areas having geological and physical environments representative of geothermal areas. Where data were available, i.e., Wairakei, New Zealand, and The Geysers, California, case histories have been written. Associated studies have also been conducted on the economic and environmental impact of subsidence. These studies indicated that there is an inadequacy of the latter data.

2. Subsidence Mensuration - Research has developed guidelines for surface monitoring surveys to establish background deformation rates and monitor possible deformation induced by geothermal development. Research to date has also assessed the state-of-the-art of well bore extensometers to directly measure vertical distances between points in the wellbore. Several suggestions for improved instrumentation that have resulted from this research will make substantial contributions toward creating direct measurement instrumentation for use in geothermal wells.

Indirect measurement methods, i.e., gravity, resistivity and microseismic, have promise as inexpensive, areal survey techniques. Research will be conducted to evaluate the ability of these methods to detect changes in the physical properties of a geothermal reservoir, and to relate these changes to reservoir compaction and subsidence.

3. Subsidence Prediction - Ultimately, the ability to predict subsidence is dependent upon an understanding of the response of geologic materials and systems to natural and man-made stress fields. To gain this understanding, the Geothermal Subsidence Research Program has initiated research to study the response of reservoir material to various stress field changes.

   Other research will assess various subsidence models, review their relative analytical merits, and, if necessary, make recommendations for new models. A related project will develop methods for physical modeling using a centrifuge. Predictions of subsidence made by numerical modeling can thus be evaluated by comparison with a centrifuge model.

   Out of these efforts may evolve better understanding of how geologic materials and systems respond to stress field changes, and enable earth scientists to more accurately predict subsidence over a given reservoir. A step toward greater predictive capability is the assessment of existing theory and its applicability to geothermal reservoirs. Most subsidence theories were developed to describe the compaction of oil and gas reservoirs or of relatively shallow unconsolidated aquifers. The applicability of these theories to deep, thermodynamically complex geothermal systems needs to be examined.

4. Reservoir Operating Policy - The final element in the GSRP is the development policies that minimize effects of subsidence. These policies are derived from the research results of the previous three elements and should provide regulators with:

   (a) the ability to distinguish naturally occurring subsidence from that possibly caused by geothermal operations, and

   (b) the basis to operate or control a geothermal field such that adverse subsidence effects are minimized or avoided.

ACCOMPLISHMENTS

Case Histories

Most documented subsidence has been due to extraction of hydrocarbons or ground water. Useful analogies may be drawn for the production of geothermal fluids. In some cases, deep extraction of fluids has produced little or no subsidence. A case history of the geologic and physical environments, the stress history, and the response or lack of response at land surface, has proved useful in making comparisons to similar potential geothermal systems.

Four case histories were completed by Systems Control, Inc. in the following areas: Wairakei, New Zealand; Chocolate Bayou, Texas; Geysers, California; and Raft River, Idaho. The four subsidence sites were selected on the basis of: (1) physical relevance of subsidence areas to high priority U.S. geothermal sites in terms of withdrawn geofluid type, reservoir depth, reservoir geology and rock characteristics, and overburden characteristics, and (2) data completeness, quality, and availability.

A review of potential geothermal sites was made in order to determine the physical relevance (i.e., analogies) of areas with past subsidence to the potential geothermal sites. These case histories may serve as models for developers and/or regulators in assessing comparable areas.

Surface Monitoring - Guidelines Manual

The fundamental objective of a monitoring program is to quantify the magnitude and direction of surface movements that may occur in a geothermal reservoir area immediately prior to, during, and immediately following the removal of geothermal fluids.

A geothermal development program must include monitoring of horizontal and vertical displacements at the surface and at depth before and during production. It should be possible to differentiate between subsidence caused by geothermal operations and that caused by other man-induced activities, or those occurring naturally.

Thus, guidelines need to be developed to obtain data directly related only to geothermal fluid production. These guidelines should consider the geologic structure, stratigraphy, and seismicity of the area, as well as the existing and proposed ground water, gas, and oil developments. The guidelines should also consider, if available, any known ground deformation characteristics of the region and any man-induced deformations of nearby fluid producing fields.

Woodward Clyde Consultants have produced a manual that reviews various surface monitoring methods and compares their installation, utilization, and accuracy. Utilization of these methods should enable planners and regulators to determine the natural rate of subsidence. In addition, such a manual can be used to ascertain induced subsidence during development and production of a geothermal field.

Direct Measurements of Changes in Vertical Distances in a Wellbore

Woodward Clyde Consultants have recommended hostile environment component testing for the following four tools: 1) induction coil with slip collar well casings, 2) reed switches with magnets emplaced in slip collars, 3) electromagnetic oscillators with magnets emplaced in slip collars, and 4) radioactive logging with tracers emplaced in either slip collars or directly into the formation.

The study reviewed instruments available for monitoring subsurface displacements, both vertical and horizontal. Techniques and materials for improving existing or developing new instruments were evaluated. Elements of sensor and signal technology with potential for high temperature monitoring of subsidence were identified.

Environmental and Economic Effects

A contract with EDAW/Earth Science Associates resulted in assessment of data available from areas that have experienced geothermal and non-geothermal subsidence. A detailed appraisal was made of areas with the most comprehensive data base. Areas studied included desert basins in central and southern Arizona; Baldwin Hills and Inglewood, California; Galveston, Texas; Las Vegas Valley, Nevada; Mexico City, Mexico; San Joaquin Valley, California; Santa Clara Valley, California; Wairakei, New Zealand; and Wilmington-Long Beach, California.

Final reports from all these contracts will be available as part of an LBL subsidence report series.

In FY 1978 and early in FY 1979 seven contracts were let. Four of these are near completion while three others are continuing into FY 1979. These contracts are summarized in Figure 2.

Programs scheduled for FY 1979 are summarized in Figure 3.

During the Subsidence Workshop held at Asilomar, October, 1978, recommendations for the revision of the Subsidence Management Plan were made. Figure 4 illustrates a suggested revision for the plan.

The Geothermal Subsidence Research Program is directly responsive to the DOE/DGE goal of "power-on-line." The subsidence risk of geothermal development can be reduced by utilization of techniques and tools developed through the GSRP. Operational methodology developed by the program can provide guidance to regulators and developers to prevent or minimize subsidence.

The first Subsidence Newsletter is scheduled to be issued on February 1, 1979. It will be sent to all who request it and to those who currently receive the GREMP Newsletter.

Figure 2

STATUS OF CURRENT SUBSIDENCE CONTRACTS

TITLE	CONTRACTOR	TYPE	MODE OF PROCUREMENT	STARTING DATE (ESTIMATED OR ACTUAL)	TERMINATION DATE (ESTIMATED OR ACTUAL)
Case Histories (Category 1)	Systems Control	FP	Competitive	10/7/77	10/31/78
Guidelines Manual (Category 2)	Woodward-Clyde	FP	Competitive	11/18/77	10/31/78
State-of-the-Art Assessment (Category 3)	Woodward-Clyde	FP	Competitive	8/29/77	10/31/78
Environmental and Economic Effects (Category 4)	EDAW - Earth Sciences	FP	Competitive	9/20/77	10/31/78
Subsidence Models (Category 8)	Golder Associates	CPFF	Competitive	6/19/78	9/30/79
Physical Processes (Category 5)	Colorado School of Mines	CPNF	Competitive	9/15/78	9/30/79
Physical Processes (Category 5)	Terra Tek, Inc.	CPFF	Competitive	11/5/78	12/31/79

FP - Fixed Price
CPFF - Cost Plus Fixed Fee
CPNF - Cost Plus No Fee

Figure 3

PLANNED SUBSIDENCE PROJECTS FOR FY 1979

GROUP	SUBJECT	RFP DUE	TYPE OF CONTRACT ANTICIPATED
1	Case Histories	--	FFP
1	Risk Analysis	Jan.	FFP
2	A. Hostile Environment	Dec/Jan	FFP
2	B. Radioactive Bullets	Dec/Jan	CPFF
2	Indirect Methods	Dec/Feb	FFP/CPFF
3	Physical Methods	Feb.	FFP
3	Creep Phenomena	April	CPFF

FFP - Firm Fixed Price
CPFF - Cost Plus Fixed Fee

Figure 4

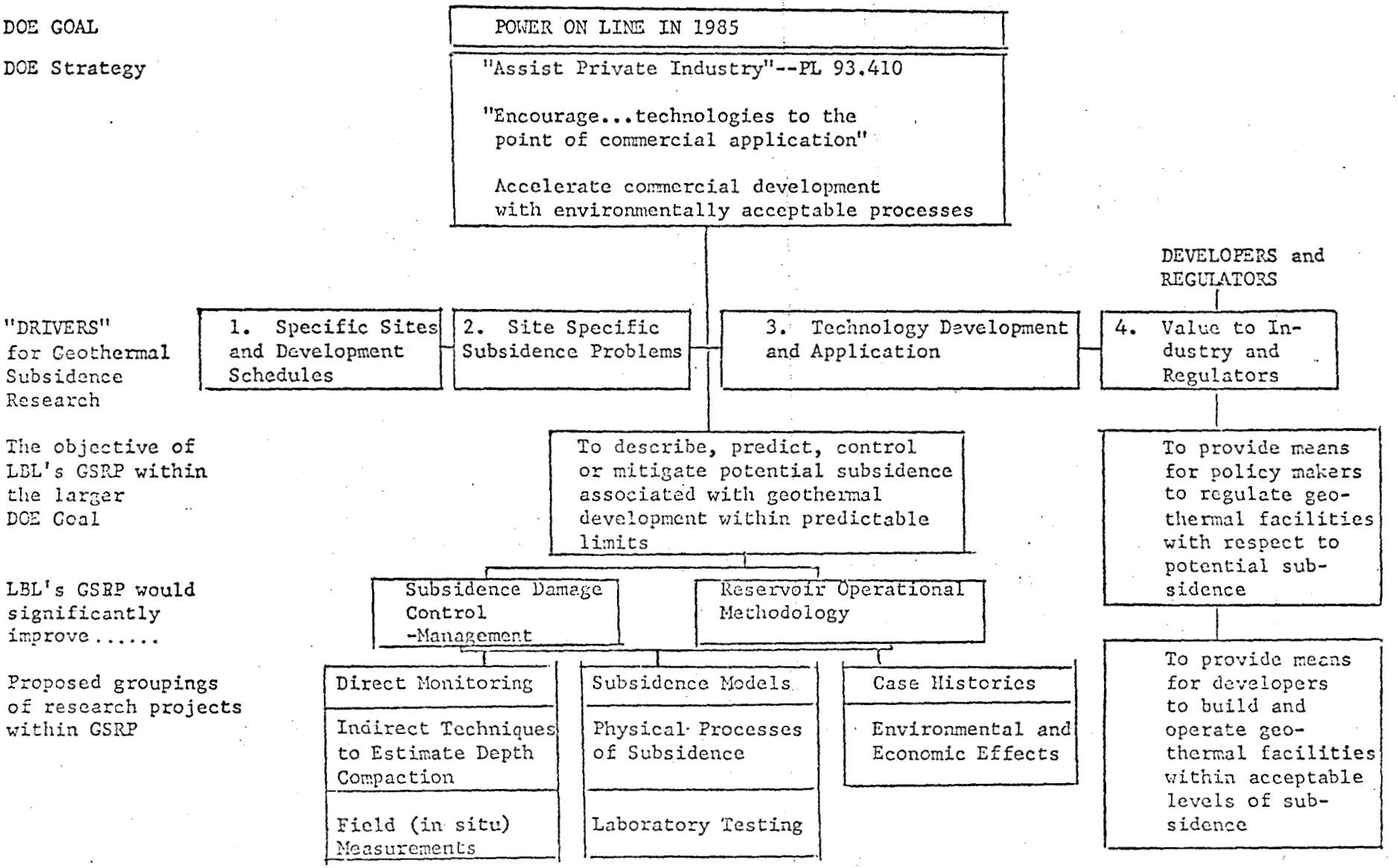
DOE GOAL
POWER ON LINE IN 1985
DOE Strategy
"Assist Private Industry"--PL 93.410
"Encourage...technologies to the point of commercial application"
Accelerate commercial development with environmentally acceptable processes
DEVELOPERS and REGULATORS
"DRIVERS" for Geothermal Subsidence Research
1. Specific Sites and Development Schedules
2. Site Specific Subsidence Problems
3. Technology Development and Application
4. Value to Industry and Regulators
The objective of LBL's GSRP within the larger DOE Goal
To describe, predict, control or mitigate potential subsidence associated with geothermal development within predictable limits
To provide means for policy makers to regulate geothermal facilities with respect to potential subsidence
LBL's GSRP would significantly improve.....
Subsidence Damage Control -Management
Reservoir Operational Methodology
Proposed groupings of research projects within GSRP
Direct Monitoring
Indirect Techniques to Estimate Depth Compaction
Field (in situ) Measurements
Subsidence Models
Physical Processes of Subsidence
Laboratory Testing
Case Histories
Environmental and Economic Effects
To provide means for developers to build and operate geothermal facilities within acceptable levels of subsidence

GEOTHERMAL RESERVOIR ENGINEERING RESEARCH IN NEW ZEALAND.

A SIMPLISTIC MODEL AND THE WAIRAKEI GEOTHERMAL RESERVOIR

Ian G. Donaldson
Physics and Engineering Laboratory
Department of Scientific and Industrial Research
Lower Hutt, New Zealand

Although nowadays much of the New Zealand geothermal reservoir research effort is still being concentrated on the older fields of Wairakei and Broadlands there has been a definite advance over recent years in our approach to the studies. On the practical side, long term reinjection trials are now in progress at Broadlands, and drilling, for field evaluation, is well underway at Ngawha, a field characterised by a steam discharge coupled with a hydrostatic pressure gradient.

On the theoretical side, well pressure transient analysis and reservoir behaviour modeling are probably the primary interests. For the former both multi-element computer modeling programs and two-phase pressure diffusion analysis (Grant, 1978, Grant and Sorey, 1979) are being used by M.A.Grant, E.Bradford and F.Sutton (AMD*) and M.L.Sorey (PEL). Geometry and boundary influences are dominant and estimated steam flows are higher than are consistent with the Corey (1954) expressions for relative permeability. Both of these effects are probably due to the fracture permeability of the reservoirs. A.McNabb (AMD) is currently taking this into account by determining the response to discharge in a fracture-block medium. He is working with 100 metre blocks, consistent with data from lumped parameter models and from well records, with a block permeability of 10^{-15} m^2.

Reservoir behaviour modeling is probably the research area of greatest current interest with most research groups here involved to some extent. The models range over a wide spectrum, from extreme simplification to sophisticated detail. At the simpler extreme is the model of J.Elder (AU). This consists of two resistors and a condenser in electrical analog form but is coupled with models of the well system and the above surface plant to enable overall system effects and interactions to be assessed.

L.Ju.Fradkin (PEL) is also working with one of the simpler models. This is one representing the gross field pressure behaviour with the equation

$$\frac{dp}{dt} = A(p-p_o) + Bq + C$$

---

*The initials indicate the research groups, listed later, with whom these researchers are associated.

where p is a representative field pressure (for Wairakei at 580m) at time t, p_o is the initial value of this pressure, q is the mass discharge from the wells, and A, B and C are coefficients characterising the system. She is using field data and system identification methods to estimate these coefficients, as functions, and hence as variables with time, for Wairakei.

Among the more complicated models are those of R.A. Wooding (AMD) for the Tauhara field, adjacent to and affected by Wairakei, and the detailed model of the two-phase zone of Broadlands being set up on the computer by M.J.O'Sullivan and G.Zyvoloski (AU). They are first trying a horizontal section. Sorey (PEL) is using both their technique and that of Mercer and Faust (1978) on local sections of geothermal reservoirs to check ideas and assumptions being put forward by other workers in this field.

It is to an intermediate model, however, that I wish to address the remainder of this paper. This is what is now generally here called the "drainage" model. I will concentrate on one recent variant of this model and will use the Wairakei reservoir as my example.

The "drainage" model

The variant of this model discussed here is illustrated in Figure 1. In this the geothermal reservoir is pictured as a column of rock matrix saturated at depth with hot water but overlain in turn by columnar layers saturated with water and steam and with cold water. This reservoir is assumed to be surrounded by, and directly connected with, the cooler outside water. There are thus no structural boundaries as such although some permeability variation is anticipated. The circular cylinder of the Figure is also purely illustrative. The shape of the actual column will be defined by the reservoir and it may vary significantly from level to level. For the majority of the exercise only the integrated flows up the column are of interest, but horizontal flows and the pattern of vertical flow across the reservoir have been taken into account.

The history of this model is now somewhat shady as most New Zealand geothermal researchers can probably see some of their own previous work in its development. As a full drainage model, however, its appearance is only recent with its application to Wairakei by McNabb in 1975. In that application the cold upper layer was not present and the two-phase layer was not treated in detail. Nonetheless a good match with the pressure drawdown in the Wairakei field was obtained.

With its application to other geothermal reservoirs several variants on this basic model have evolved but for Wairakei the cooler upper layer has been added to permit the accounting for the quenching recently of the shallow well WK 107. It is hoped that it may also assist in explaining, quantitatively, the slow reduction in temperature of the main water zone of the reservoir. This is dropping in temperature by 1-2^{o}C per year.

The model reservoir in the undisturbed state

In the undisturbed state hot water at enthalpy H_b is assumed to enter the bottom of the hot water section of the reservoir at the rate M_b (mass flux). This is the integrated flux at this level and for Wairakei it would be 430 kg s^{-1}. This flow then moves up through the various layers to the surface. Under the assumed steady conditions the flow up through the lower water layer is isenthalpic, and hence, due to the small variation in enthalpy with pressure, virtually isothermal.

This means that the temperature, and hence the pressure, at the two-phase/lower single-phase interface is defined and we may thus work back down from the surface to determine this level if so required.

As cool water hydrostatic conditions apply both the steam and the water at saturation conditions move up through the two-phase layer, again under isenthalpic conditions until the influence of the cooler near surface water is encountered. Some cooling, and thus drop in enthalpy, will then take place and the boundary zone here will be somewhat diffuse. Beneath the zones of greatest cold water movement the cooling zone would be quite marked. Beneath zones of low movement, it is the heating of the water that would take precedence. In some areas, as evidenced by the surface manifestations of the system, the hot water and steam will continue right through to the ground surface. In the steady system, assuming no crossflow of the colder water, the fluid mass escape at the surface must match that entering at depth.

The model reservoir under exploitation

With the discharging of wells tapping the lower single-phase section of the reservoir, a local drop in pressure must occur. This pressure drop will, however, propagate quickly throughout this zone due to the low compressibility of the liquid water. Some pressure decay will thus soon occur at the side boundaries of the system and the gradient established here will result in the gradual incursion of cold outside water into the reservoir. This cold water will extract heat from the rock and a slowly thickening temperature front will thus begin to move in towards the wells. In a homogeneous system this frontal movement would be maximal at the well level and reduce as we move both above and below this level. With structure certain other levels may dominate. If the withdrawal is below the natural hot water influx, M_b, this frontal movement will slowly decay and a new stable situation will develop. For higher discharges, however, the front must continue its inward movement.

As this aspect of the process has already been documented by McNabb (1975), I will concentrate here on the conditions above the main well production zone. As the temperature of this lower water system is set, the drop in pressure due to the discharge must result in a drop in level of the boiling interface. In fact, it is the level of this interface that, in effect, controls the pressures throughout the water zone.

These pressures have dropped by about 26 bars since production commenced in 1953.

Above this interface in the two-phase zone the pressure gradient must decrease and although the upward vapour flow will be reduced relatively little, the upward water flow will quickly decrease. Surface manifestations are thus expected to become drier, although the total heat, controlled mainly by the steam flow, may not drop much. This is in fact what happened at Wairakei. With a higher discharge, however, the upward water flow in the two-phase zone will cease altogether and downward drainage of this water will commence. This drainage will have several effects. It will supply water to the lower water zone and thus decrease the rate of pressure decay. It will extract some heat from the rock in the two-phase zone (even without the cool overlying water the water temperature decreases as we approach the surface). And it will either create some drier zones near the top of the layer or permit the cooler water from above to flow into the system. In Wairakei evidence suggests that both of these mechanisms are in progress in various local regions. Some shallower wells, for example, became significantly drier over the years of exploitation, while well WK 107 has been quenched. If this cooler water from above establishes preferred paths to the lower hot water system, and such preferred paths may only be the reverse of those previously established by the natural flow, the potential further exists for the cooling of this well water and the adjacent rock.

The Wairakei application

On account of the apparent high degree of horizontal connection in the Wairakei geothermal reservoir, it is thought to be an ideal field for application of this model. In this case the three elements of the model, the upper and lower water zones and the intermediate two-phase one, are defined by their moving interfacial boundaries and hence can be treated independently, although interactively.

In the lower water element the wells are assumed to act as a local three-dimensional sink and thus draw in fluid from all around. The base flow, M_b, at some depth, is only minimally affected and the side flow is reduced in vertical extent by an assumption of an enhanced horizontal permeability. In the initial exercise this enhancement is by a factor of 10. The interface between this layer and the two-phase one above is, however, assumed horizontal.

In the other two layers only vertical flow is taken into account. Well withdrawals are thus distributed horizontally and the other water/two-phase interface is also horizontal. It should be noted that at that interface the water temperature must be in excess of 100°C as the pressure must be above 1 bar. The upper layer thus transports some heat.

This study is currently still in progress with analytic solutions being developed for the three zones. If the results are satisfactory, extension to the Broadlands system, in which

vertical connection has already shown up in shallow reinjection tests, will probably have priority.

References

Corey, A.T., 1954. The interrelation between gas and oil relative permeabilities. Producers Monthly, 19, 38-41.

Grant, M.A., 1978. Two-phase geothermal pressure transients = a comparison with single-phase transients. N.Z. Journal of Science, (in press).

Grant, M.A. and Sorey, M.L., 1979. The compressibility and hydraulic diffusivity of a water-steam mixture. Water Resources Research, (submitted).

Mercer, J.W. and Faust, C,R., 1978. Geothermal reservoir simulation. A U.S.Geological Survey report in three parts (unpublished).

McNabb,.A., 1975. A model of the Wairakei geothermal field. An Applied Mathematics Division, D.S.I.R., N.Z. report (unpublished).

Research Groups

AMD Applied Mathematics Division, Department of Scientific and Industrial Research, P.O. Box 1335, Wellington, N.Z.

AU Auckland University, Private Bag, Auckland, N.Z.

PEL Physics and Engineering Laboratory, Private Bag, Lower Hutt, N.Z.

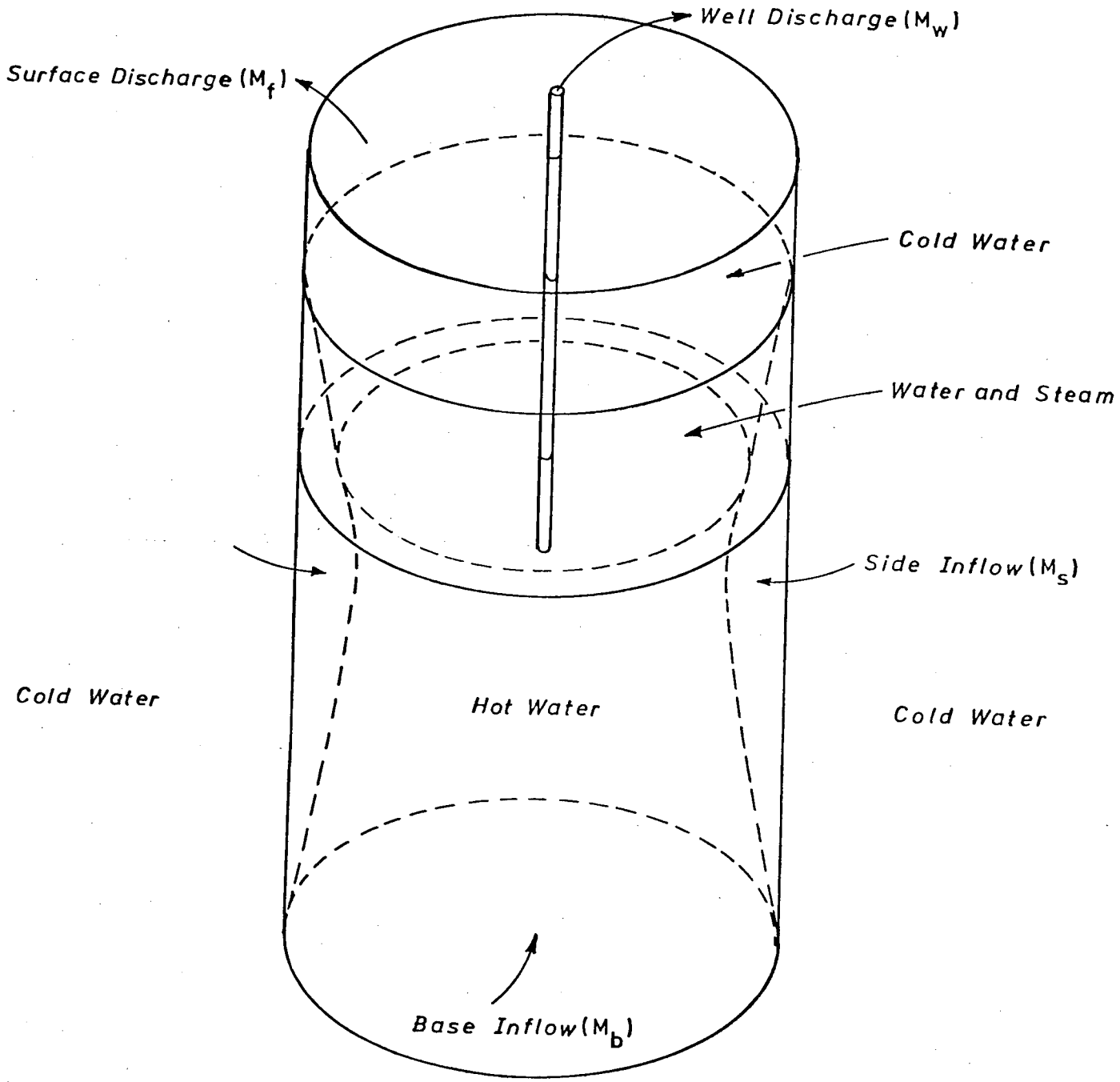

FIGURE 1. The Drainage Model.

THE REPLACEMENT OF GEOTHERMAL RESERVOIR BRINE AS A MEANS OF REDUCING SOLIDS PRECIPITATION AND SCALE FORMATION

by
John C. Martin
Chevron Oil Field Research Company
P. O. Box 466, La Habra, CA 90631

INTRODUCTION

A number of technical difficulties are encountered in producing geothermal energy from reservoirs containing brines with high concentrations of dissolved solids. The reduction in temperature and pressure associated with brine production results in the precipitation of solids which can form heavy scale in producing and injection wells and in surface equipment. Evidently under many conditions precipitates form in the reservoir surrounding producing wells, thereby reducing their productivity. In some cases the precipitation of solids is so severe that it can prevent economic production.

This paper presents results of an investigation of the possibility of injecting a different water in a geothermal reservoir as a means of reducing problems caused by solids precipitation and scale formation. Corrosion problems may also be reduced depending upon the water-rock-metal behavior. The results are confined chiefly to reservoir mechanics, a logical first step in evaluating the process for a given reservoir. Water-rock chemistry, water treating, water supply, brine disposal and overall economics are discussed only briefly or are beyond the scope of this paper.

In general the composition of water injected into geothermal reservoirs does not remain the same. In addition to mixing with the original water the injected water tends to equilibrate with the reservoir rock. If fresh water is injected it may pick up such minerals as silica, carbonate, iron, sulphur, etc. These minerals may precipitate and cause problems in producing the reservoir. Nevertheless, under suitable conditions, a change in the reservoir water may be an attractive alternative to cycling the original reservoir brine.

DISCUSSION

Figures 1 and 2 illustrate one method of replacing the original reservoir brine with injected water. Figure 1 illustrates a single well injecting water. Region 1 contains injection water that has cooled the reservoir rock. Region 2 contains injection water that has been heated by the rock and adjacent formations. Region 3 contains the original brine at high temperatures. Figure 2 illustrates cycling operations. The original injection well continues as an injection well and two producing wells produce hot injection water from Region 2.

An alternate method to that illustrated is to produce the reservoir heat by continuous water cycling. The original reservoir brine is produced but a different water is injected. This method may be particularly

attractive for very low porosity reservoirs in which many pore volumes of water are required to produce the heat by water cycling.

The ratio of the volume of Region 1 to the volume of Regions 1 and 2 of Figures 1 and 2 is the ratio of the cold water volume to the injection water volume. This ratio is determined by the ratio of the velocity of the cold bank separating Regions 1 and 2 and the velocity of the injection water bank separating Regions 2 and 3.

The velocity of the injection water bank, u_f, is:

$$u_f = \frac{u_{w2}}{\phi} \tag{1}$$

Where ϕ is the porosity and u_{w2} is the volumetric flow rate of the hot injection water per unit cross section area. The relation for the velocity of the cold bank, u_c, can be obtained by applying mass and heat balances across the cold bank

$$\frac{u_c}{u_{w2}} = \frac{1}{\phi\left[1+\left(\frac{1-\phi}{\phi}\right)\frac{\rho_r}{\rho_{w2}}\frac{(h_{r1}-h_{r2})}{(h_{w1}-h_{w2})}\right]} \tag{2}$$

Where the subscripts 1 and 2 refer to Regions 1 and 2 respectively, and

h_r is the enthalpy of the solid portion of the rock
h_w is the enthalpy of the water
ρ_r is the density of the solid portion of the rock
ρ_w is the density of the water

The desired ratio, u_c/u_f is (from equations 1 and 2)

$$\frac{u_c}{u_f} = \frac{1}{1+\left(\frac{1-\phi}{\phi}\right)N} \tag{3}$$

where

$$N \equiv \frac{\rho_r(h_{r1}-h_{r2})}{\rho_{w2}(h_{w1}-h_{w2})} \tag{4}$$

In most potential applications N lies between .5 and 1.0. Using the porosities found in oil and gas reservoirs as a guide, one would expect the porosities of geothermal reservoirs to vary from about .01 for some fractured reservoirs with no matrix porosity to about .35 for highly porous sandstone reservoirs. These ranges of N and ϕ result in a range of u_c/u_f from about .01 to about .50. Thus, the volume of injection water may vary from about twice that of the cold water to perhaps as much as 100 times larger.

The proposed method of water injection appears favorable for low values of u_c/u_f. These low values correspond to low porosity reservoirs where flushing the brine from the reservoir and replacing it with injection water might remove only a small fraction of the useful heat initially contained in the reservoir. The prospects are much less favorable for highly porous reservoirs as illustrated by the example discussed in the following paragraphs.

Performance predictions were made for an idealized, uniform, two-dimensional, radially symmetric reservoir with the initial temperature distribution given in Figure 3-a. The calculations were made using a stream tube model in which the fluid mobility varies along the stream tubes as required by the temperature-viscosity relation. A constant pressure difference of 1000 psi was maintained between injection and production wells, and a constant pressure outer boundary was assumed at a radial distance of 20,000 feet. No heat recharge was assumed, the change in water density was neglected, and heat conduction effects were ignored. Other parameters were: porosity .25, permeability 500 md, u_c/u_f fixed at .257, and well bore radii of .46 feet.

Figure 3 presents the temperature distribution, the stream lines, the well patterns, and the injection water and the cold banks at various times. Continuous over-injection was maintained over most of the life of the reservoir in order to maintain a sufficiently wide region of hot injection water in which to locate the production wells. In general, at cold water breakthrough producing wells were either converted to injection wells or shut in until a more appropriate time to convert them to injectors. The production wells were located and operated so that none of the original brine was produced.

The cumulative water injected and produced and the temperature of the produced water versus time are presented in Figure 4. The two sharp drops in temperature of the produced water during the first five years and the sharp drop during the twenty-fourth year are the result of cold water breakthrough into the production wells. The other three sharp temperature drops result from locating production wells in areas with lower temperatures. The gradual rises following these three drops are caused by higher temperatures being propagated outward from the center of the reservoir.

The average injection rate per well per foot of interval during the first twenty-three years of production was 676 B/D/ft, and the average production rate was 633 B/D/ft. During this time there was an average of 16 active injection wells, 8 active production wells, 3 wells shut in and 39 wells abandoned. On the average only about 57% of the wells were utilized at any time. Since well cost can be the dominant cost of geothermal reservoir development, the production of injection water heated by the geothermal reservoir as illustrated in this idealized example can add significantly to the production costs in a high porosity reservoir.

The idealized two-dimensional model illustrates some of the problems associated with high porosity reservoirs. As pointed out previously, the processes whereby injection water is heated within the reservoir and then produced should become more economical to apply for reservoirs with smaller porosities. Smaller porosities are associated with smaller values of u_c/u_f. This indicates larger regions containing hot injected water relative to the cold water regions. Results presented in Figure 3 indicate that larger regions containing hot water allow more efficient use of wells.

CONCLUSIONS

1. Problems with solids precipitation and scale formation may be reduced in some geothermal reservoirs by replacing the original reservoir brine with fresh water or a water with a different dissolved solids content.

2. Injection of a water different from the original reservoir brine is particularly attractive for very low porosity reservoirs where many pore volumes of water are needed to produce the reservoir heat by water cycling.

ACKNOWLEDGMENT

The two-dimensional reservoir performance calculations were made by R. E. Wegner assisted by F. J. Kelsey. Appreciation is extended to M. G. Reed for his valuable suggestions.

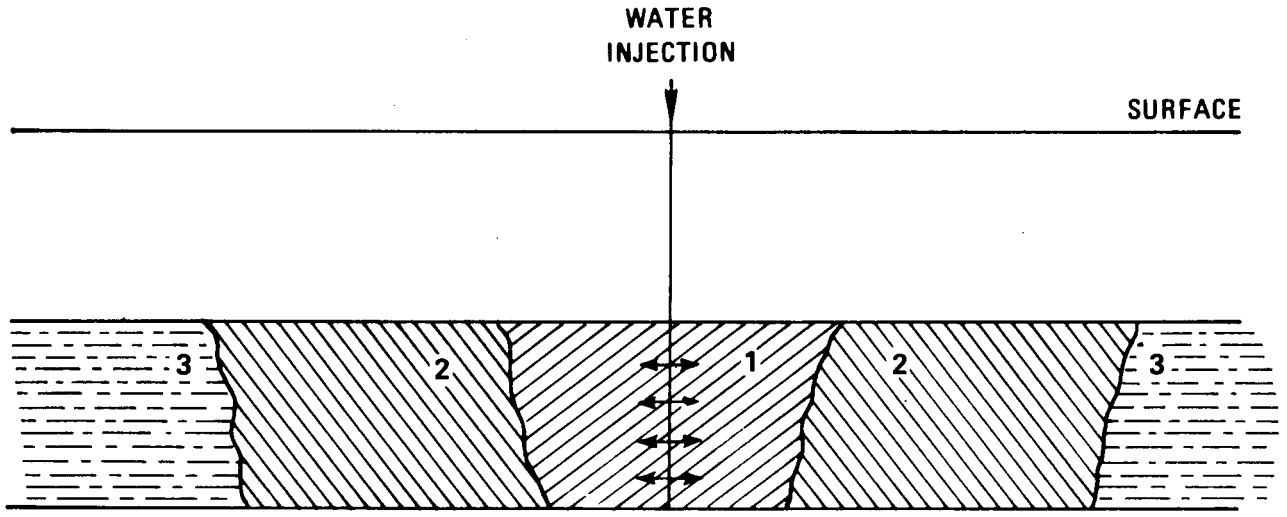

FIGURE 1

AN ILLUSTRATION OF WATER INJECTION INTO A GEOTHERMAL RESERVOIR. REGION 1 CONTAINS COOL INJECTION WATER, REGION 2 CONTAINS HOT INJECTION WATER, AND REGION 3 CONTAINS HOT BRINE.

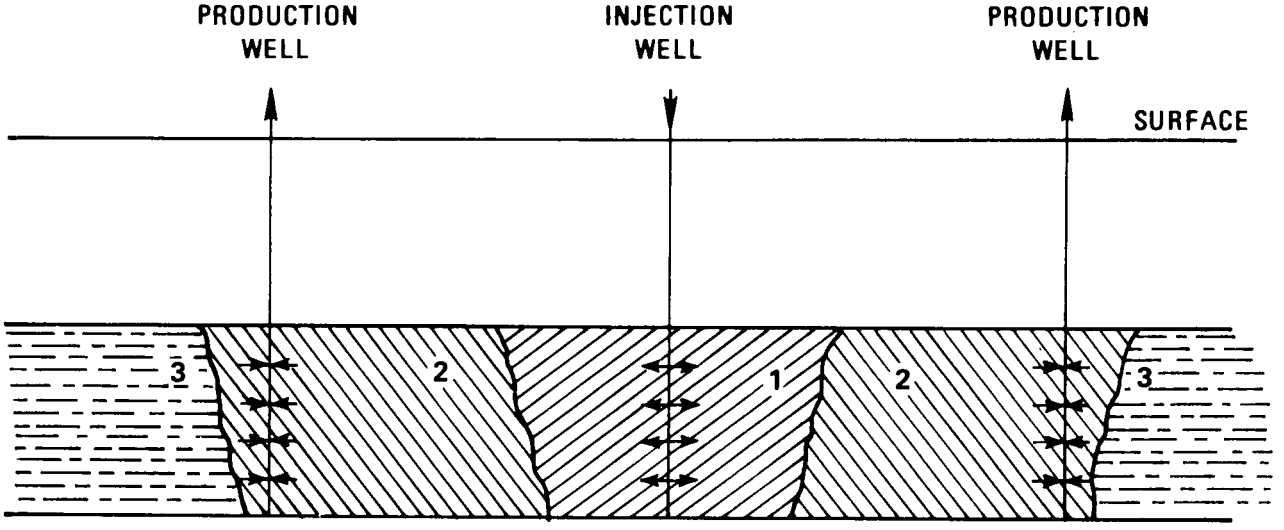

FIGURE 2

AN ILLUSTRATION OF A INJECTION WATER CYCLING OPERATION.

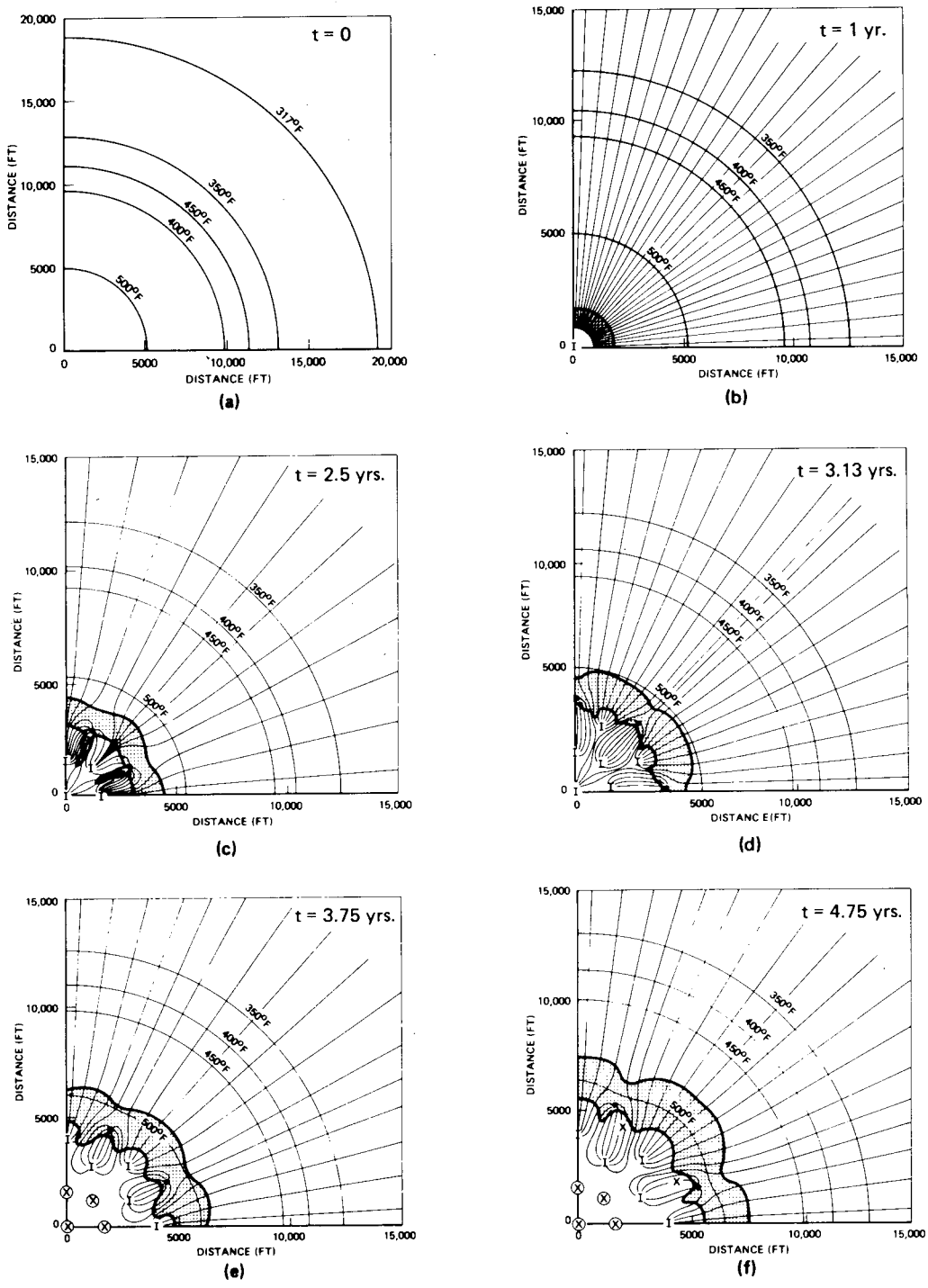

FIGURE 3

POSITIONS OF COLD AND INJECTED WATER BANKS, TEMPERATURE DISTRIBUTIONS, STREAM LINES, AND WELL PATTERNS AT VARIOUS TIMES DURING RESERVOIR PRODUCTION FOR ONE QUARTER OF THE IDEALIZED TWO DIMENSIONAL RESERVOIR.

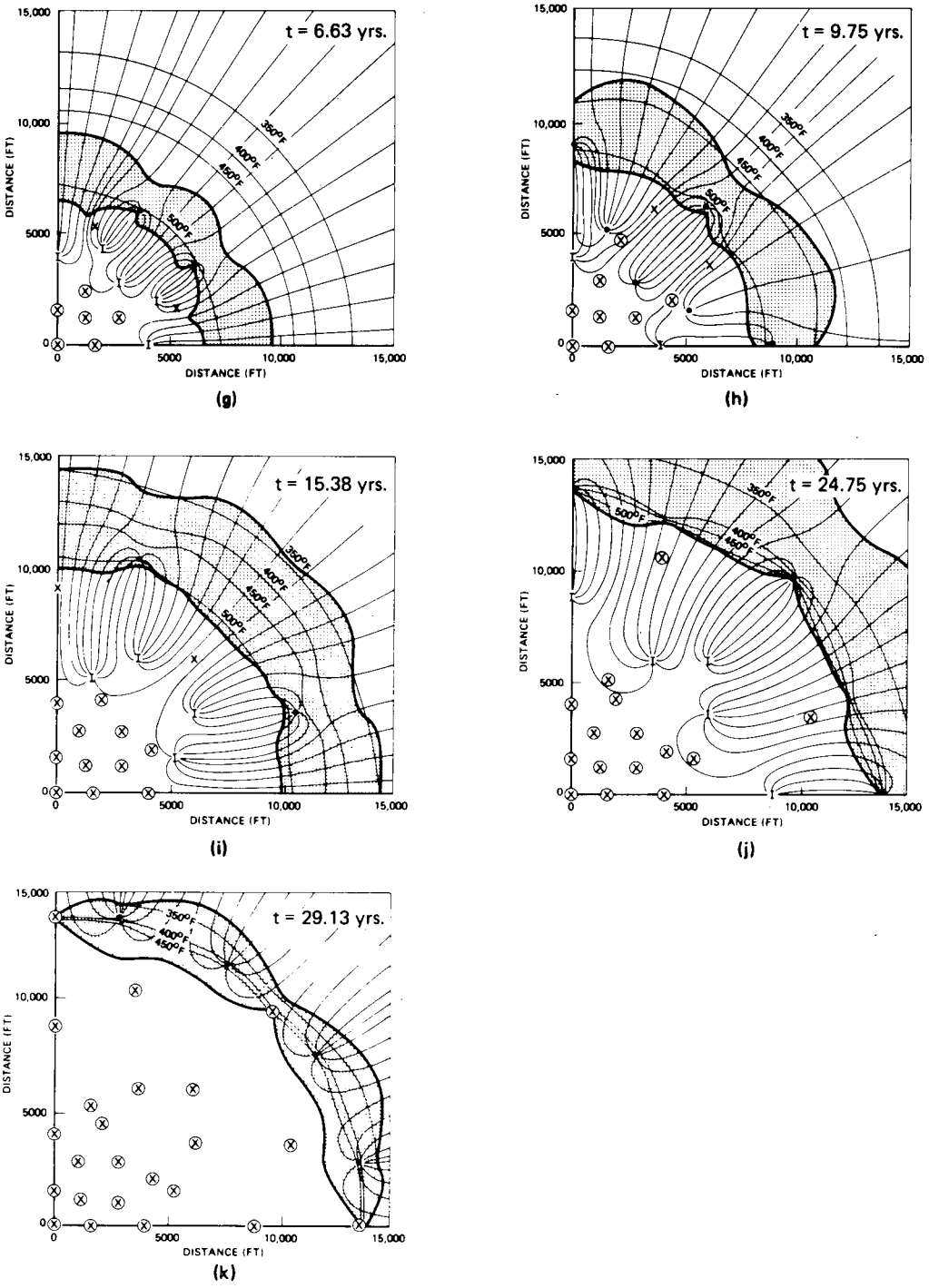

FIGURE 3

CONCLUDED

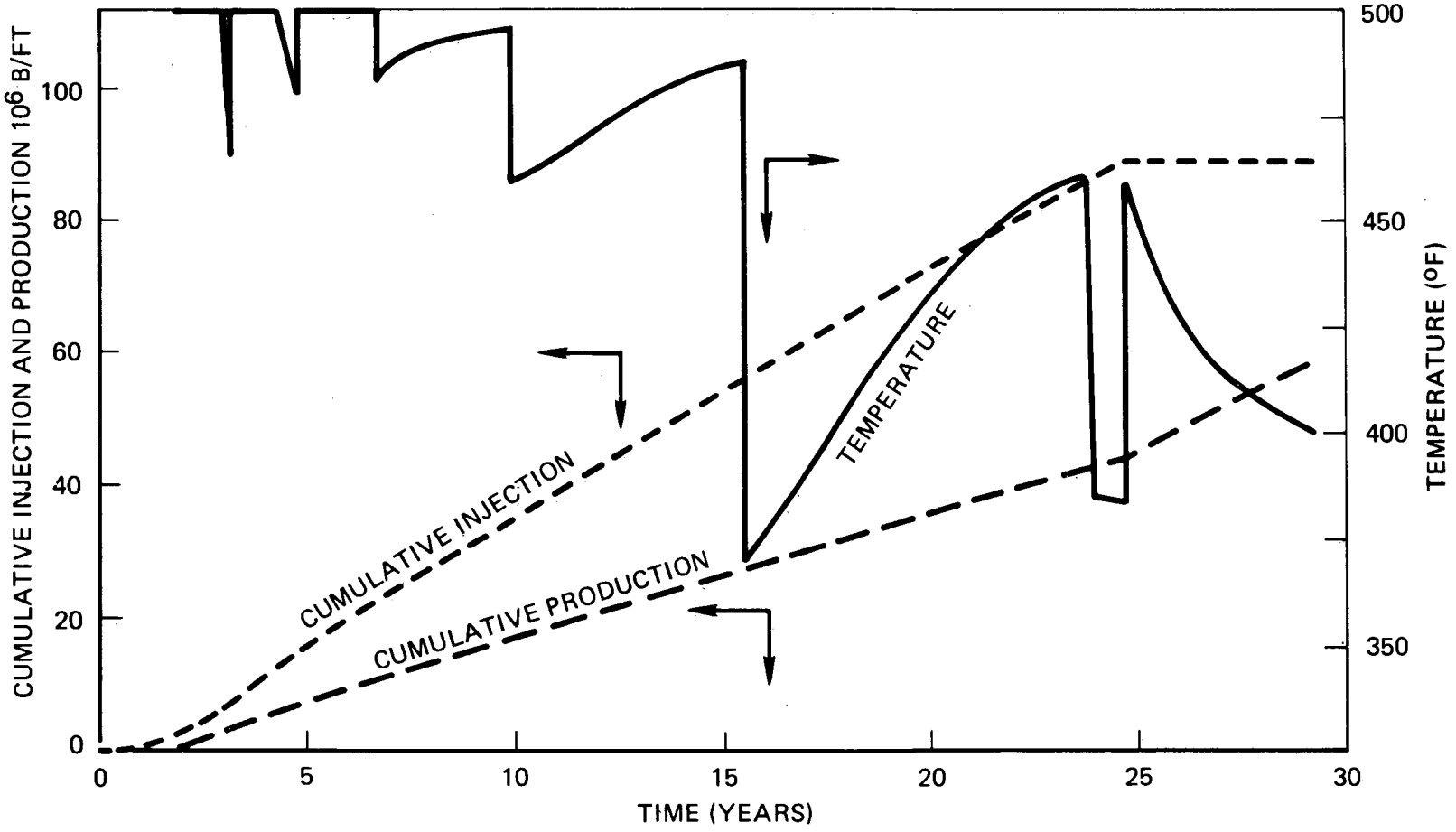

FIGURE 4

TEMPERATURE OF PRODUCED WATER AND CUMULATIVE WATER INJECTION AND PRODUCTION FOR IDEALIZED TWO DIMENSIONAL GEOTHERMAL RESERVOIR

CHANGES IN PERMEABILITY DURING FLOW OF WATER THROUGH GRANITE SUBJECTED TO A TEMPERATURE GRADIENT

D. Lockner, D. Bartz, and J. Byerlee

U. S. Geological Survey

345 Middlefield Road

Menlo Park, CA 94025

The useful lifetime of a geothermal reservoir as an energy source can depend strongly on the technique used to extract heat. In both naturally occurring geothermal fields and artificial geothermal reservoirs, such as the Los Alamos hot dry rock experiment, continuous extraction of heat requires maintenance of a channel of permeable material to and away from the heat source. Since such a system must be recharged to maintain production over a useful period of time, water must be heated and thus transported through rock in the presence of large temperature gradients.

We have designed experiments to study permeability changes in rock due to fluid flow along a temperature gradient to further understanding of how heat production in geothermal reservoirs may depend on these effects. Cylindrical samples of Westerly Granite, 8.9 cm long, 7.6 cm in diameter, and containing a 0.66 cm diameter borehole, were used. A resistance heater was placed in the borehole as a heat source, giving a radially symmetric temperature gradient. Confining pressure and pore pressure were applied to the sample; a pore

pressure gradient was applied to induce radial flow either toward or away from the borehole. Although permeability may not have remained homogeneous during the experiments, an apparent permeability, averaged over the whole sample, was calculated from Darcy's Law by measuring the pore fluid flow rate.

Figure 1 shows the results of two experiments with samples of Westerly Granite; experimental conditions are given in Table I.

Table I

	Experiment I	Experiment II
Confining Pressure (bars)	300	600
Pore Pressure-borehole (bars)	105	200
-jacket (bars)	100	205
Temperature -borehole (^{o}C)	310	358
-jacket (^{o}C)	115	145

In both experiments the permeability decreased. In experiment I, pore fluid flowed away from the hot borehole; the decrease in permeability may have been caused by deposition of dissolved minerals because of a decrease in solubility with lowered temperature. In experiment II, pore fluid flowed toward the borehole. In this experiment, the decrease in permeability may likewise have been due to deposition of dissolved minerals. At pressures below 300 bars the solubility of silica as a function of temperature goes through a maximum between 320^{o} and 340^{o}C. If the pore fluid is saturated at this temperature, it must deposit silica on heating as it moves toward the borehole, thus

decreasing the permeability. Permeability may also have been decreased in both experiments I and II by alteration of minerals in place, resulting in clogging of pores. Further experiments are being conducted to determine the relative importance of these two effects.

These results suggest that under the proper conditions, fluid flowing through rock along a temperature gradient can result in decreased permeability. Although this effect is undesirable in geothermal applications, it may be of use in the disposal of nuclear waste materials. In this case, transportation of nucleides away from the hot disposal site by ground water may be inhibited by decreases in the permeability. The experiments reported here were designed to show that permeability can be decreased by fluid flow. We are currently conducting experiments to study the conditions under which permeability can be increased by fluid flow. When this problem is thoroughly understood, it should be possible to design geothermal heat extraction systems so as to take advantage of these effects and thereby improve energy production.

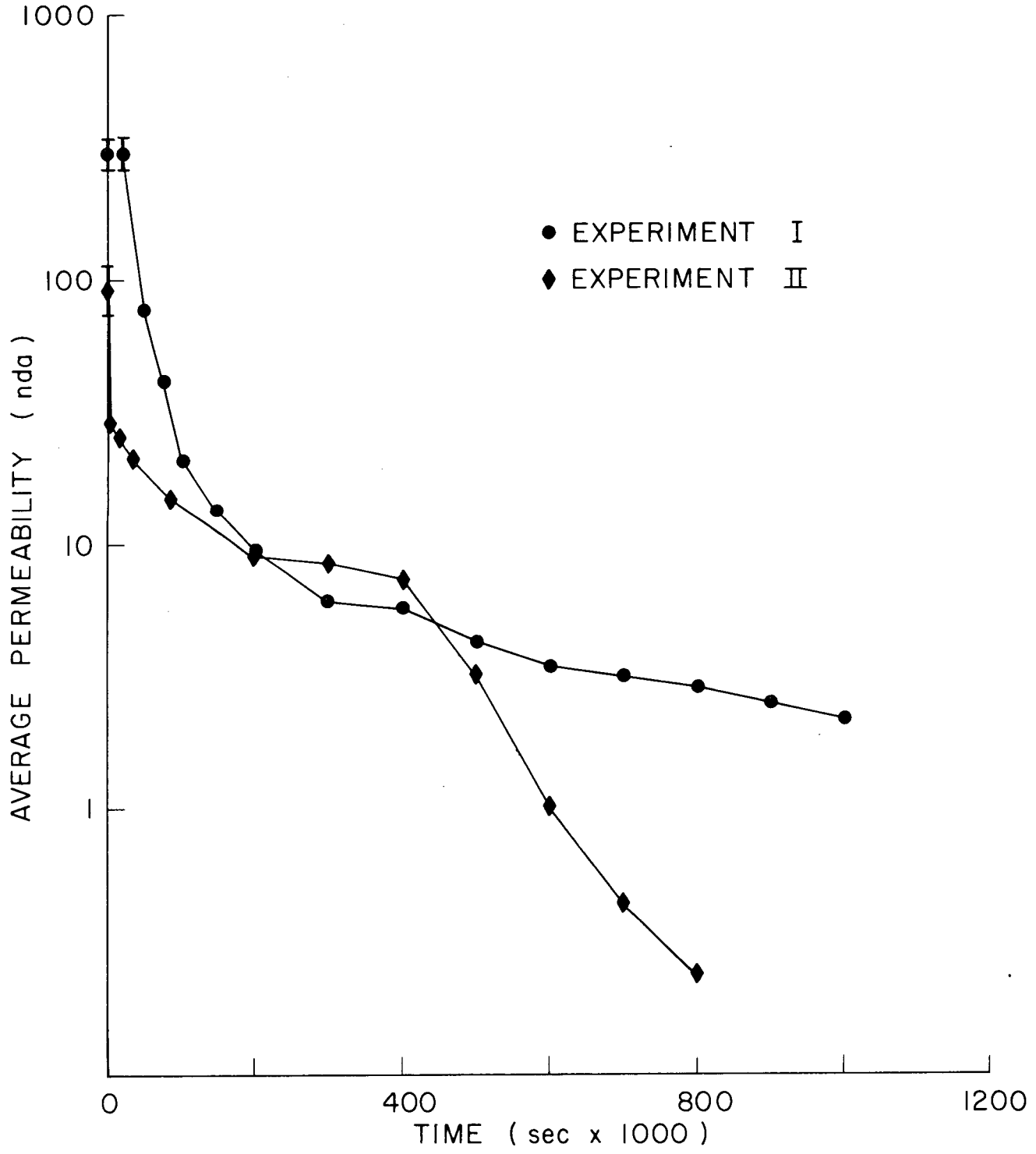

FIG. 1. Plot of average permeability vs time for two samples of Westerly Granite. In Experiment I, water cooled as it flowed away from the borehole. In Experiment II, water flowed toward the borehole, increasing in temperature. In both experiments, permeability decreased with time.

LABORATORY INVESTIGATIONS OF STEAM PRESSURE-TRANSIENT BEHAVIOR IN POROUS MATERIALS

by

W. N. Herkelrath and A. F. Moench
U. S. Geological Survey
Menlo Park, Calif. 94025

Introduction

Transient flow of noncondensable gas in porous materials has been thoroughly investigated, and good agreement between the gas-flow equation and experiments has been reported in the petroleum-engineering literature (Wallick and Aronofsky, 1954). This theory has been widely used in computer simulations of pressure-transient behavior in vapor-dominated geothermal steam reservoirs (e.g., Moench and Herkelrath, 1978).

However, few laboratory experiments involving steam flow in porous materials have been reported. In order to test the applicability of the gas-flow theory to steam flow, we developed a laboratory system to investigate the transient flow of steam through unconsolidated porous materials. Pressure-transient experiments were carried out by imposing a step change in gas pressure at one end of a cylinder of porous material, and measuring the pressure as a function of time at the other end.

Apparatus

A schematic diagram of the experimental apparatus is shown in figure 1. The steam-flow system was enclosed in an oven which had a temperature uniformity of $\pm 0.5^{o}C$. All components, including valves and pressure transducers, operated at high temperatures inside the oven to avoid temperature gradients and steam condensation in the system.

The sample holder consisted of stainless steel pipe in which unconsolidated porous materials were densely packed. The results reported here were obtained with a pack of the 0.053 mm to 0.125 mm sieved fraction of a natural desert sand. The bulk density and porosity of the sample were 1.7 g/cm^3 and 0.32, respectively.

Steam was obtained by boiling pure water or $CaCl_2$ brine stored in a large reservoir inside the oven. At any given temperature the steam pressure above the liquid in the reservoir was approximately equal to the vapor pressure of the solution.

Pressure-transient tests were also run with air or nitrogen gas which was supplied from a pressure regulating system outside the oven.

In the experiments reported here, the sample was brought to a low initial pressure, and then a constant higher gas or steam pressure was applied at the top of the sample by opening the appropriate pneumatic valve. The pressure at both ends of the sample was measured continuously with pressure transducers during the resulting pressure buildup.

Results

Typical pressure buildup curves obtained in the experiment are shown in figure 2. Results of tests with air agreed well with the one-dimensional gas-flow equation (Aronofsky, 1954):

$$\frac{K}{2\mu}\frac{\partial 2p^2}{\partial Z^2} = \phi\frac{\partial P}{\partial t} \qquad (1)$$

In equation 1, P is the gas pressure, Z is the distance from the top of the sample, μ is the fluid viscosity, ϕ is the sample porosity, K is the intrinsic permeability, and t is the time. A good fit to the air pressure buildup data was obtained by assuming a permeability of 3.0 Darcys in the theoretical calculations.

However, when the same pressure boundary conditions were imposed using steam as the fluid, large time delays in the pressure response were observed. The time required for pressure buildup was increased by as much as a factor of thirty. This is illustrated by comparing the curves for air buildup and steam buildup at 100°C in figure 2. A fit to the standard theory could only be obtained by assuming an unreasonably low permeability of 0.1 Darcy.

Discussion

The delayed pressure response was probably caused by condensation. Despite the fact that the steam pressure was less than the saturation vapor pressure throughout the experiment, condensation occurred in the sample. A liquid saturation as high as three percent by volume was measured by weighing the sample at the end of pressure-transient runs.

Condensation of the steam probably occurred because the vapor pressure of liquid water in a porous medium is reduced. This "vapor-pressure-lowering" effect, commonly observed in soil systems, is caused by adsorption and gas-liquid interface curvature in the small pores of the medium. The dependence of the liquid saturation in the sample upon vapor pressure was determined at high temperature by allowing the sample to equilibrate with salt solutions of known vapor pressure in the reservoir. The results of these tests are shown in figure 3. Also shown for comparison are room temperature data published by Westcot and Wierenga (1974).

When condensation occurs, a sink term for steam should be added to equation 1 to preserve the mass balance. Moench and Atkinson (1979) showed that the rate of steam condensation, q_s, can be expressed as

$$q_s = \frac{H_c}{L}\frac{\partial T}{\partial t} \qquad (2)$$

in which H_c is the heat capacity of the porous medium, L is the latent heat of vaporization, and T is the temperature.

Vapor-pressure lowering can be incorporated into this theory by assuming that T is a function of both steam pressure and liquid saturation, S. The steam-flow equation for small changes in temperature and liquid saturation can be expressed as

$$\frac{\partial}{\partial Z}\left(\frac{\rho K}{\mu}\frac{\partial P}{\partial Z}\right) = \phi\,[1-S]\,\rho C_t\,\frac{\partial P}{\partial t} + \frac{H_c}{L}\left(\frac{\partial T}{\partial P}\frac{\partial P}{\partial t} + \frac{\partial T}{\partial S}\frac{\partial S}{\partial t}\right) \qquad (3)$$

in which ρ and C_t are the density and compressibility of steam, respectively. Estimates of the sink term indicate that it is one to two orders of magnitude larger than the compressibility term. Accounting for condensation in this way results in an increase in the predicted response time which is of the same order of magnitude as found in the experiments. However, possibly because of errors in the determination of system parameters, good quantitative agreement between the modified theory and the experimental results has not yet been achieved.

References

Aronofsky, J. S., 1954, Effect of gas slip on unsteady flow of gas through porous media: Journal of Applied Physics, v. 25, p. 48-53.

Moench, A. F., and Atkinson, P. G., 1979, Transient-pressure analysis in geothermal steam reservoirs with an immobile vaporizing liquid phase: Geothermics (in press).

Moench, A. F., and Herkelrath, W. N., 1978, The effect of vapor-pressure lowering upon pressure drawdown and buildup in geothermal steam wells: Transactions, Geothermal Resources Council Annual Meeting, Hilo, Hawaii, July 25-27, p. 465-468.

Wallick, G. C., and Aronofsky, J. S., 1954, Effect of gas slip on unsteady flow of gas through porous media - experimental verification, Transactions of AIME, Petroleum Branch, v. 201, p. 322-324.

Westcot, D. W., and Wierenga, P. J., 1974, Transfer of heat by conduction and vapor movement in a closed soil system: Soil Sci. Soc. Amer. Proc., v. 38, p. 9-14.

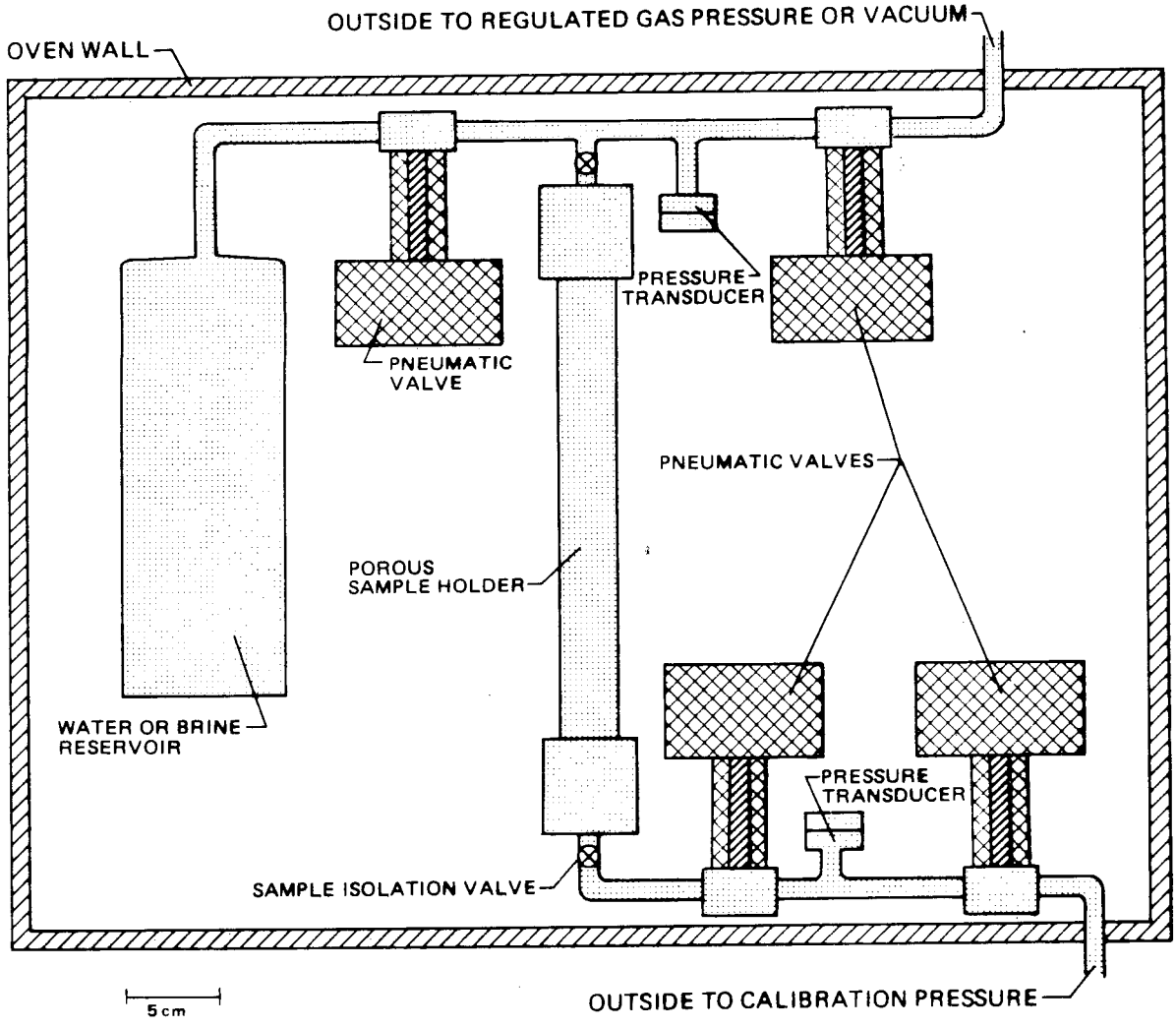

FIGURE 1 – Schematic diagram of stream-pressure-transient apparatus

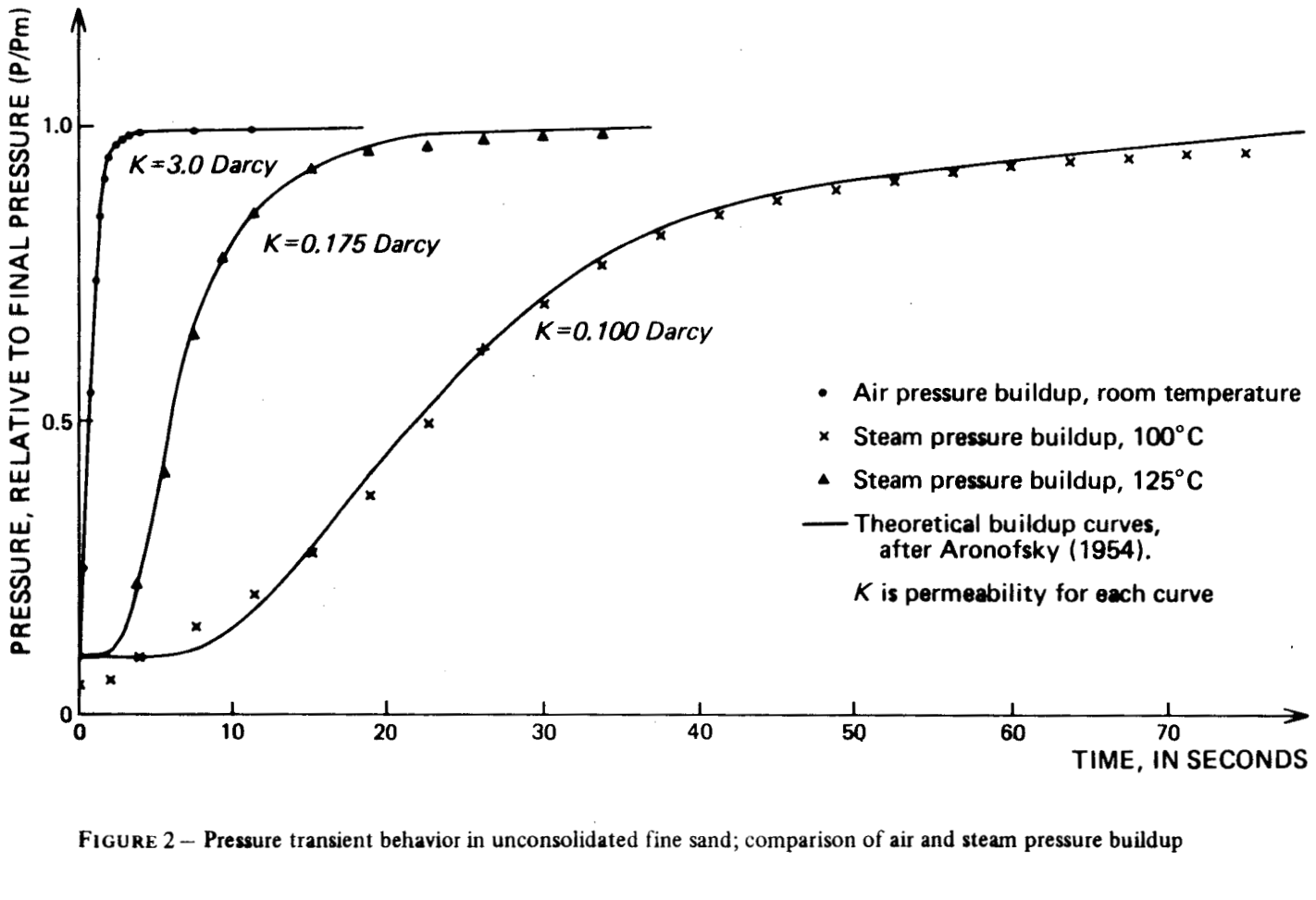

FIGURE 2 – Pressure transient behavior in unconsolidated fine sand; comparison of air and steam pressure buildup

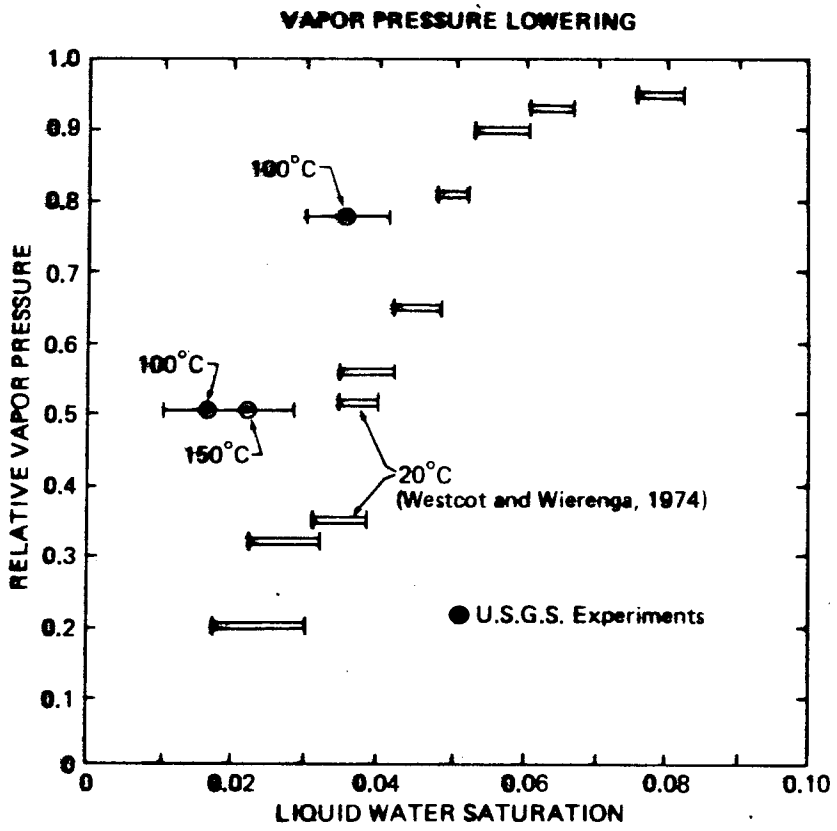

FIGURE 3. -Dependence of relative vapor pressure upon liquid saturation in a fine sand. All of the measurements with doubled error bars were made at 20°C by Westcot and Wierenga (1974).

BENCH-SCALE EXPERIMENTS IN THE STANFORD GEOTHERMAL PROJECT

J.R. Counsil, C.H. Hsieh, C. Ehlig-Economides, A. Danesh and H.J. Ramey, Jr.
Department of Petroleum Engineering, Stanford University,
Stanford, California 94305

The Stanford Geothermal Project bench-scale experiments are designed to improve the understanding of geothermal reservoir physics. Three sets of experiments are discussed in the following sections: (1) vapor pressure lowering in porous media due to capillarity and adsorption, (2) the effect of temperature on absolute permeability, and (3) the determination of steam-water relative permeability for drainage processes.

Vapor Pressure Lowering

Vapor pressure lowering in porous media may be important to both reserve evaluation and geothermal reservoir performance prediction. Vapor pressure lowering is a lowering of the vapor pressure curve. As shown schematically in Fig. 1, it occurs at low water saturations. The lowering may be caused by (1) capillarity, i.e., curved liquid-vapor interfaces in porous media and/or by (2) surface adsorption of fluid molecules at the solid-fluid interface. It is believed that capillary effects occur at low water saturations, but that vapor pressure lowering is minor until saturations are so low that adsorption phenomena dominate (Hsieh et al., 1978).

The importance of vapor pressure lowering is further demonstrated by the following hypothetical situation. If the temperature and pressure of a geothermal reservoir are determined to be that of point A in Fig. 1, a reservoir engineer may use the flat surface vapor pressure curve and assume the reservoir is 100% dry steam and contains no liquid water. In actual practice, further lowering of reservoir pressure may allow capillary or adsorbed water to vaporize. Thus, both the reserves and the rate of production are increased beyond that predicted with the assumption of no vapor pressure lowering (and no liquid water saturation).

The following calculation demonstrates the possible importance of surface adsorption. A reservoir rock of 1 m^2/gm surface area, 25% porosity, and 10.6 $Å^2$ surface area per H_2O molecule will have 7.95 m^2 surface area per cc pore volume and 2.24×10^{-3} gm H_2O per cc pore volume.

At the arbitrary condition of 200°C and 15 bars, saturated steam density (should use superheated) is .00786 gm H_2O/cc. Using the above unconfirmed assumptions, one layer of adsorbed H_2O will increase reservoir water content by 29%. Ten layers of adsorbed H_2O will further increase

reservoir water content. One unanswered question remains: "How much of the adsorbed H_2O can be produced?"

The experimental apparatus required for this study is now assembled. Vapor pressure lowering will be determined as a function of pressure, temperature, and amount of H_2O, using the apparatus shown in Fig. 2. However, it is expected that at each temperature level studied, results will demonstrate multilayer adsorption "plateaus" as shown in Fig. 3. To better understand the adsorption phenomena and to try to estimate the number of adsorption layers, the BET cell shown in Fig. 4 has already been used to determine nitrogen surface areas of consolidated sandstones (Berea) and unconsolidated sand packs. These studies may be extended to include natural gas adsorption phenomena as they occur in natural gas reservoirs.

Effect of Temperature on Absolute Permeability

Experimental results of Weinbrandt (1972), Cassé (1974), Aruna (1976), and others suggest the absolute permeability of sandstones and unconsolidated sands to water is reduced up to 65% at elevated temperatures and confining pressures. Permeability reductions with increased temperature were not observed for nitrogen, oil, or octonol. In addition, permeability reduction was not observed for water flowing through limestone. Recently, Dr. A. Danesh, visiting professor from Abadan Institute of Technology, Iran, performed additional experiments flowing water and oil through unconsolidated sand and unconsolidated stainless steel. His results were similar to those of Cassé and Aruna, but similar reductions in permeability also occurred for unconsolidated stainless steel (Danesh et al., 1978).

Subsequent experiments were recently completed using water and either unconsolidated sand or limestone ground and sieved to a similar mesh size. These experiments did not reproduce the temperature level effects. The reason the results were different may be due to a different experimental procedure. In particular, water was pumped through the core during the entire experiment. In the earlier experiments, water may not have flowed through the core during heating and cooling between measurements at different temperatures. The solid-liquid boundary layer, intermolecular force mechanism, as suggested by Danesh to explain the permeability reductions, may indicate that such procedural differences are important. Future experiments will attempt to verify Danesh's conclusions.

Steam-Water Relative Permeability

Steam and liquid relative permeabilities, expressed as a function of liquid saturation, are required in the numerical models used to calculate mass and energy recovery from two-phase geothermal reservoirs. Currently, modified Corey-type equations are used because adequate techniques for determining proper steam-water relative permeabilities are still under development. Relative permeabilities are often expressed as equations for convenience.

Sufficient data can be obtained from steady, two-phase, non-isothermal flow experiments to allow the construction of steam-water relative permeability curves for a drainage process. Water saturation can be measured with a capacitance probe (Chen et al., 1978). A preliminary relative permeability curve is shown in Fig. 5. The data has not been corrected for temperature or Klinkenberg slip effects, and the core has not yet been analyzed for nonhomogeneity caused by possible hydrothermal alteration.

In addition, isothermal nitrogen-displacing-water experiments were performed to provide gas-water drainage relative permeabilities at a variety of temperatures. These gas-water relative permeabilities provide an interesting comparison to the steam-water relative permeabilities. One example is shown in Fig. 6. Data analysis is not yet complete, and differences between the two curves have not yet been explained. Stewart et al. (1953) has stated that gas-expansion and gas drive drainage relative permeabilities are identical for hydrocarbons in homogeneous sandstone cores. For this reason, the steam-water and the nitrogen-water experiments are expected to yield similar, and possibly identical, results. Future effort will focus on refining the quality of data obtained from these two types of experiments.

References

Aruna, M.: "The Effects of Temperature and Pressure on Absolute Permeability of Limestone," Ph.D. Dissertation, Stanford University, 1976.

Cassé, F.J.: "The Effect of Temperature and Confining Pressure on Fluid Flow Properties of Consolidated Rocks," Ph.D. Dissertation, Stanford University, 1974.

Chen, H.K., Counsil, J.R., and Ramey, H.J., Jr.: "Experimental Steam-Water Relative Permeability Curves," Geothermal Resources Council Transactions (1978), 2, 103-104.

Danesh, A., Ehlig-Economides, C., and Ramey, H.J., Jr.: "The Effect of Temperature Level on Absolute Permeability of Unconsolidated Silica and Stainless Steel," Geothermal Resources Council Transactions (1978), 2, 137-139.

Hsieh, C.H., and Ramey, H.J., Jr.: "An Inspection of Experimental Data on Vapor Pressure Lowering in Porous Media," Geothermal Resources Council Transactions (1978), 2, 295-296.

Stewart, C.R., Craig, F.F., Jr., and Morse, R.A.: "Determination of Limestone Performance Characteristics by Model Flow Tests," Trans. AIME (1953), 198, 93-102.

Weinbrandt, R.M., Cassé, F.J., and Ramey, H.J., Jr.: "The Effect of Temperature on Relative and Absolute Permeability of Sandstones," Soc. Pet. Eng. J. (Oct. 1975), 376.

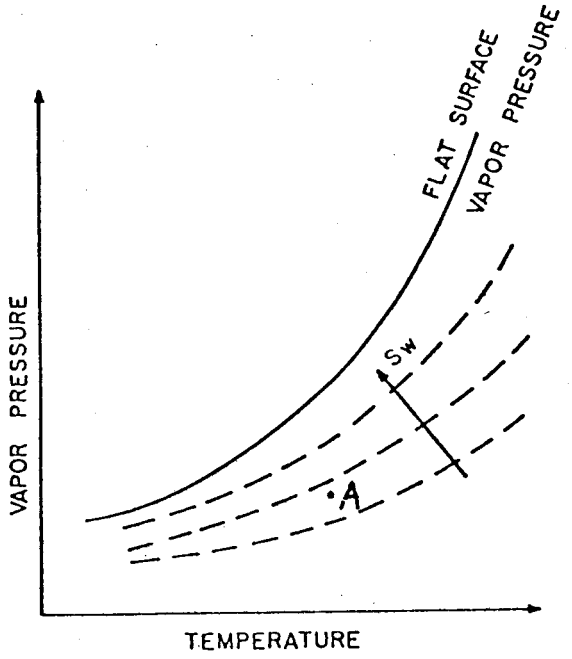

FIGURE 1. HYPOTHETICAL VAPOR PRESSURE CURVE DEPENDENCE ON WATER SATURATION (S_W)

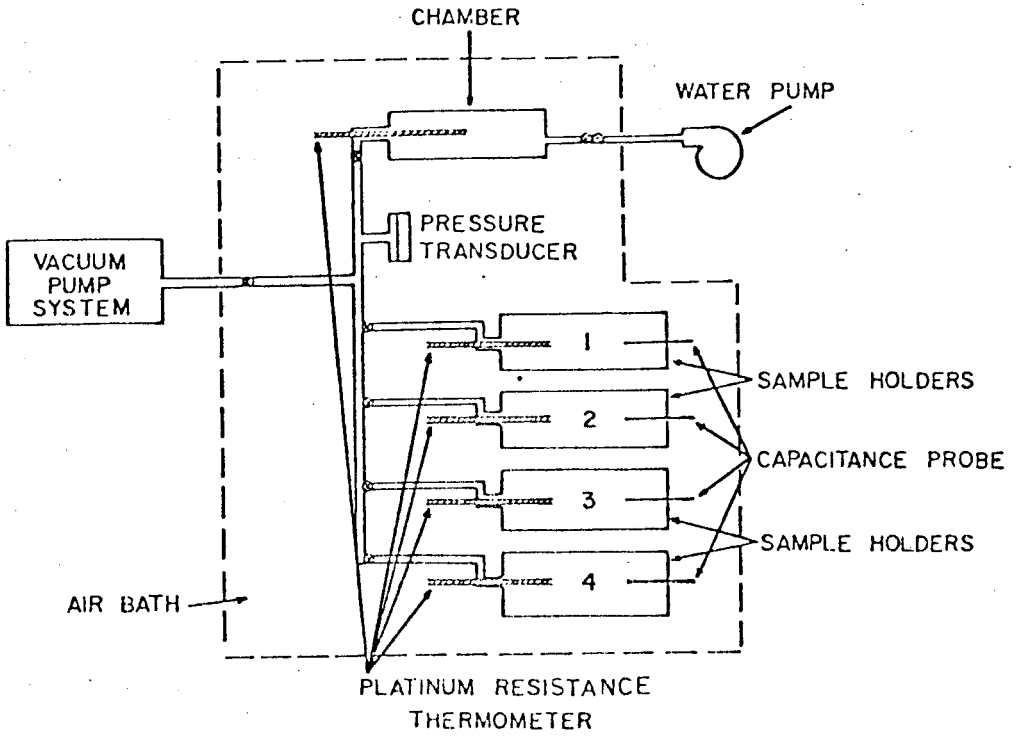

FIGURE 2. APPARATUS USED TO DETERMINE WATER ADSORPTION AND VAPOR PRESSURE LOWERING

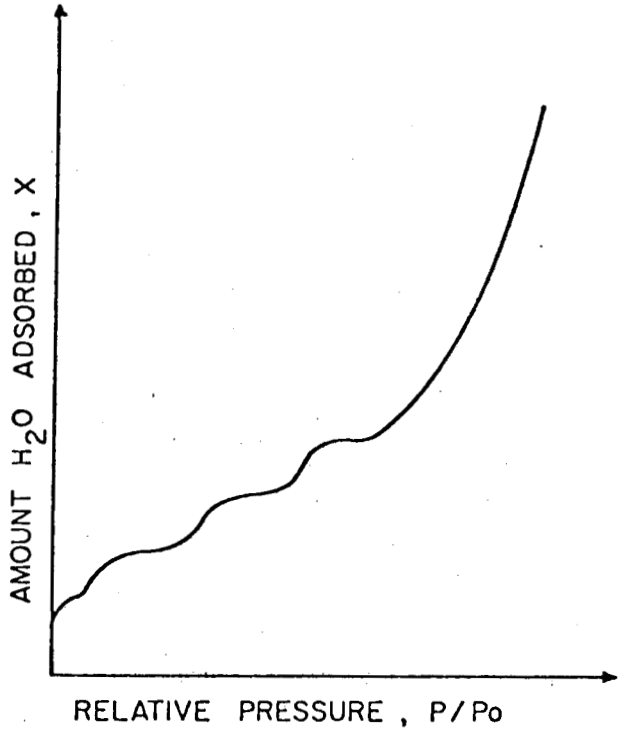

FIGURE 3. SCHEMATIC FIGURE SHOWING AN ADSORPTION ISOTHERM FOR H_2O - S_iO_2

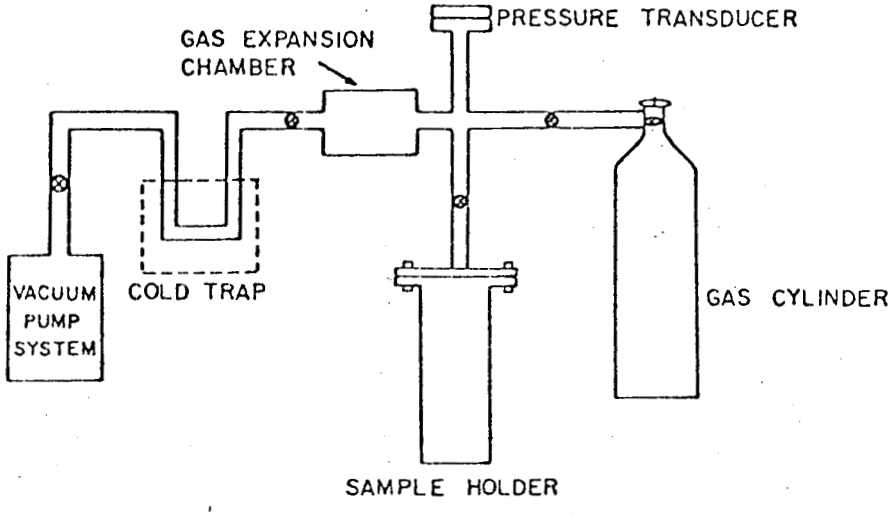

FIGURE 4. BET CELL USED TO DETERMINE ROCK SURFACE AREA

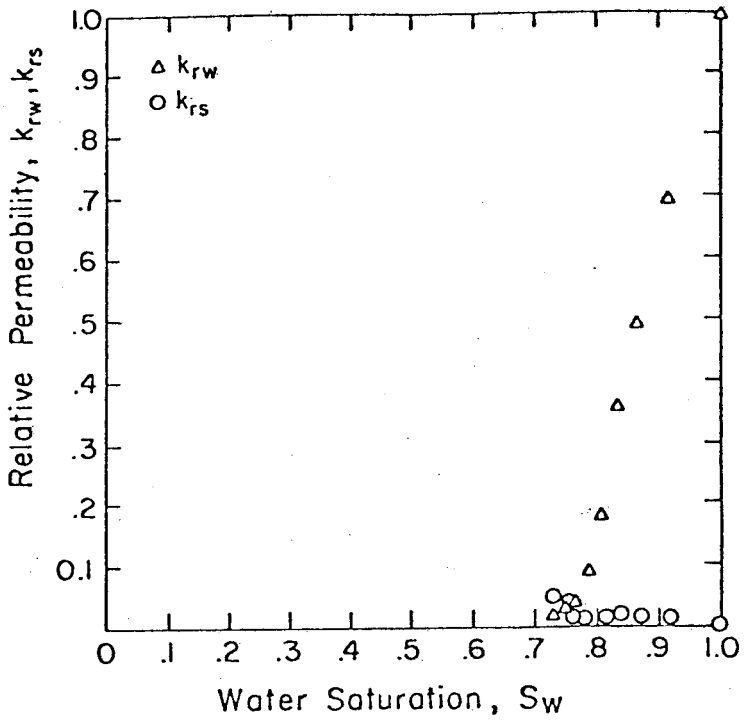

FIGURE 5. STEAM-WATER RELATIVE PERMEABILITY DETERMINED FROM NONISOTHERMAL, BOILING FLOW EXPERIMENT (330-280°F)

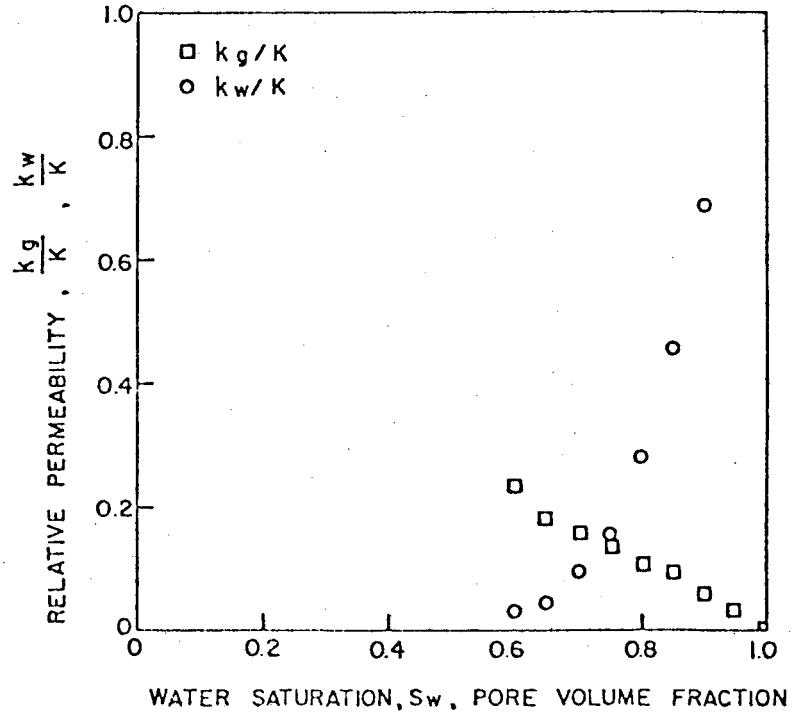

FIGURE 6. NITROGEN-WATER RELATIVE PERMEABILITY DETERMINED FROM ISOTHERMAL GAS-DRIVE EXPERIMENT (300°F)

AN EXPERIMENTAL STUDY OF THE PHASE CHANGE BY IN-SITU VAPORIZATION IN POROUS MEDIUM

L. Castanier* and S. Bories
GE-1FP-1MF, Enseeiht 2 rue Carmichel
31071 Toulouse-Cedex, France

Introduction

A natural geothermal reservoir is an aquifer generally in liquid phase confined between two impermeable layers of rock. Drilling of such reservoirs causes a decompression which allows the in-situ vaporization of some water and the development of a dual-phase flow.

Dual-phase flow is directed by the fractures of the reservoir; energy extinction is mainly determined by heat and mass transfers between the rock and the fluids. A large part of the energy stored in the reservoir is the heat of the rock, so the knowledge of these two interconnected mechanisms is very important to appreciate the behavior of geothermal reservoirs.

Mathematical Model (inspired by Luikov's model)

ASSUMPTIONS

a. The porous medium is homogeneous and deformable.
b. Fluids and porous medium are supposed to be a fictitious equivalent continuous medium.
c. Viscous works are neglected.
d. Capillarity effects are neglected.

LOCAL EQUATIONS

With these hypotheses the following equations are available:

Continuity: $$\Phi \frac{\partial}{\partial t} (\rho_i S_i) = - \nabla \cdot (\rho_i \vec{V}_i) + I_i$$

Flow: $$\rho_i \vec{V}_i = - \frac{K K_{ri}}{V_i} \nabla P$$

Enthalpy: $$\frac{\partial}{\partial t} (1-\Phi) \rho_r h_r + \sum_i \rho_i S_i \Phi \left(\frac{\partial h_i}{\partial t} \right) = \nabla \cdot (h^* \nabla T) - \sum_i (\rho_i \vec{V}_i) \cdot \nabla h_i - \sum_i h_i I_i + \frac{dP}{dt}$$

Equations of State: $\rho_i = f(p_i,T)$; $V_i = g(p_i T)$; $K_{ri} = k(S_i,p,T)$

*Visiting Scholar at Stanford University

A definite fluid heat and mass transfers will depend on:

- porosity,
- nature and granulometry of the porous medium,
- initial thermodynamic conditions,
- liquid saturation,
- exploitation conditions.

Experimental Apparatus (Fig. 1)

The simulation of auto vaporization phenomena was made on a simple geometrical shape of the porous medium in which heat and mass transfers are mono-directional.

The experimental installation was set up with the following:

1. A cylindrical cell

It allows the average thermodynamic conditions of T = 180°C and P = 10.5 bars. The problem of the conciliation of good performances in pressure and low thermic perturbations caused by the envelope in contact with the porous medium was solved by using two concentric tubes, the internal in epoxy resin and the external in duraluminum. The external tube can be heated by electric resistances controlled by an electronic regulation chain which can work at two levels:

- in relation with a fixed temperature to obtain a regular heating of the porous medium, or
- to minimize the gap of temperature between the axis of the porous medium and the exterior. The heat losses in this position can be assumed to be equal to zero.

2. Fluid alimentation

It is made by a nitrogen-pressurized reservoir containing a deformable envelope. Water goes to the ends of the cylindrical cell through porous plaques. Ends of the cell are kept at constant temperature by oil circulation.

3. Fluid production

This is initiated by opening a micrometric valve at the end of the condensor. This condensor allows the access to the enthalpy of the produced fluid. The flow rate is determined by weighting the condensed fluids.

4. Measurements

There are 24 thermocouples and 12 pressure gauges distributed along the cell; liquid saturation is measured by γ-ray absorption. The source is 1 C_i of AM241. The accuracy of the method is around 5%.

5. Porous media

At the beginning of experiments glass balls were used. After many problems with the silicate dissolution, a quartz sand was utilized and gave complete satisfaction.

Experimental Results

A. Influence of some parameters

1. Porosity

The fraction produced in vapor phase is more important at low porosity (Fig. 2). However, with the horizontal configuration the total massic-produced fraction is not affected by porosity. The fact that the enthalpy of produced fluids is better at low porosity shows clearly the importance of the solid matrix heat in the vaporization process.

2. Speed of decompression (Figs. 3 and 4)

If the decompression is too fast, a great quantity of water in liquid phase is expulsed. Then a large fraction of the energy stored in the solid matrix cannot be used for vaporization.

3. Initial liquid saturation

When the initial liquid saturation is low, the produced fraction is low, but the enthalpy and vapor quality of the produced fluids are better. The results agree with the numerical studies of Toronyi and Martin (Figs. 5 and 6).

4. Heat influx or heat losses

Heat influx or heat losses have a strong effect on the behavior of the model; some critical studies were made to estimate the envelope contribution to the phenomena. Such effects must be carefully checked to insure accuracy of the measurements.

B. Energy extraction efficiency

Energy extraction efficiency is defined by $\eta = E_p/E_i$, where E_p is the produced energy and E_i the initial energy of the reservoir; both of them are calculated from a temperature level of 100°C. We can see in Fig. 7 that:

- All the runs have the same shape of the graphs of $\eta(P/P_o)$
- η is maximum for the runs with Sol = 1 and in-situ vaporization (H5, H6). The run H1 (high-speed run) shows an initial expulsion of liquid water producing a large depletion without any energy extraction by in-situ vaporization. Then the behavior of this run is similar to the behavior of low initial liquid saturation runs.
- A large part of the energy remains in the reservoir for the low saturation runs. This result shows clearly the interest of reinjection for vapor-dominated or very low-porosity reservoirs.

C. "Black box" model based on mass and energy balances

A comparison of numerical and experimental data shows excellent results (Fig. 8). A model similar to those of Whiting and Ramey and of Brigham and Morrow describes an experimental simulation very well.

Conclusions

This study shows some qualitative results on the problem of in-situ vaporization in porous media; however, these results cannot be applied directly for reservoir exploitation. Among the problems remaining we can show the improvement of some numerical models based on local equations, the determination of the relative permeabilities curves, and the behavior of geothermal reservoirs at very low initial liquid saturation with the influence of capillarity effects.

References

BORIES, S., and GHALLEB, K. Transferts de chaleur et de masse dans les milieux poreux non saturés. 1972, G.E. I.F.P.-I.M.F., ENSEEIHT, Toulouse.

BORIES, S., CASTANIER, L., KLOCKENBRING, F., and MONFERRAN, L. Transferts de chaleur avec changement de phase en milieu poreux -- Application à la géothermique. Contrat D.G.R.S.T., G.D. I.F.P.-I.M.F. 1977, ENSEEIHT, Toulouse.

BRIGHAM, E., and MORROW, B. P/Z behavior for geothermal steam reservoirs. 1974, Congrès de l'AIME, SPE Paper No. 4899.

LUIKOV, A.V. Heat and mass transfer in capillary porous bodies. Pergamon Press, 1966.

LUIKOV, A. V., and MIKHAYLOW. Theory of energy and mass transfer. Prentice Hall, Inc., Englewood, 1961.

MARX, J. W., and LANGENKEIM, R. H. Reservoir heating by fluid injection (1959). AIME 216, AIME 312.

PELLERIN, MAUBOURGUET MM. Contribution à l'étude par voie numérique des transferts de chaleur conjugués. Thèse de Spécialité, Université de Toulouse, Novembre, 1977.

MARTIN, J. C. Analysis of internal steam drive in geothermal reservoirs. 45th Annual California Regional Meeting of the SPE of AIME, Apr. 2, 1975, Ventura, SPE Paper No. 5382.

MERCER, J. W., and FAUST, C. R. Simulation of water and vapor dominated hydrothermal reservoirs. 5th Annual Fall Meeting of the SPE of AIME, Dallas, Sept. 28, 1977, SPR Paper No. 5520.

TORONYI, R. M., and FAROUK ALI, S. M. Two-phase, two-dimensional simulation of a geothermal reservoir and the welbore system. 50th Annual Fall Meeting of the SPE of AIME, Dallas, Sept. 28, 1977, SPE Paper No. 5521.

Geothermal Energy
Review of research and development, UNESCO, Paris, 1973.

WHITING, R. L., and RAMEY, H. J., Jr. Application of Material energy balances to geothermal steam production, Journal of Petroleum Technology, 893-900, 1959.

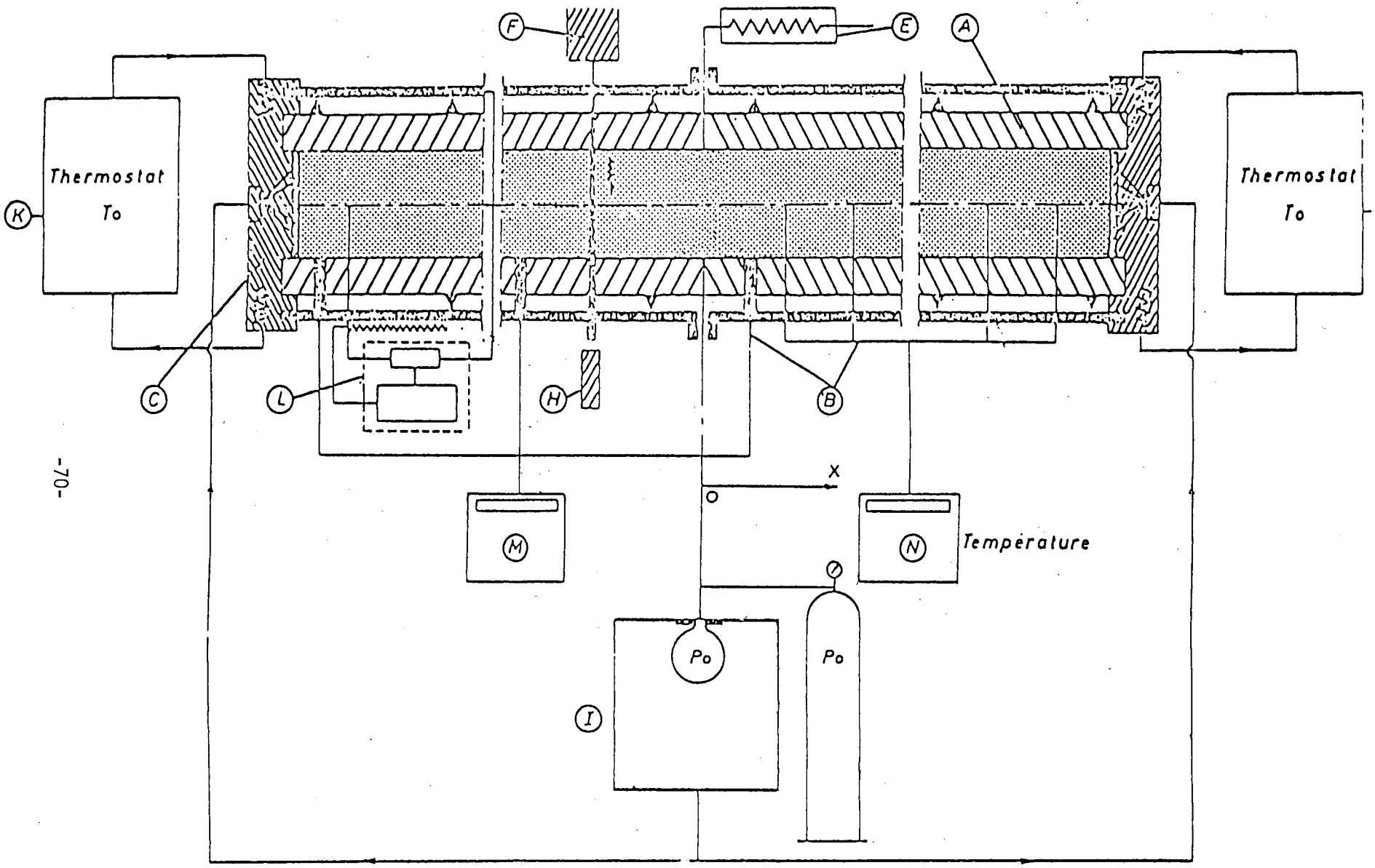

EXPERIMENTAL APPARATUS

FIGURE 1

A - Epoxy tube
B - Thermocouples
C - Oil circulation
E - Condenser
F - γ Ray source
H - γ Ray absorbtion
I - Water injection
K - Thermostats
L - Electric heating regulation
M - Pressure recorder
N - Temperature recorder

FIGURE 2 -

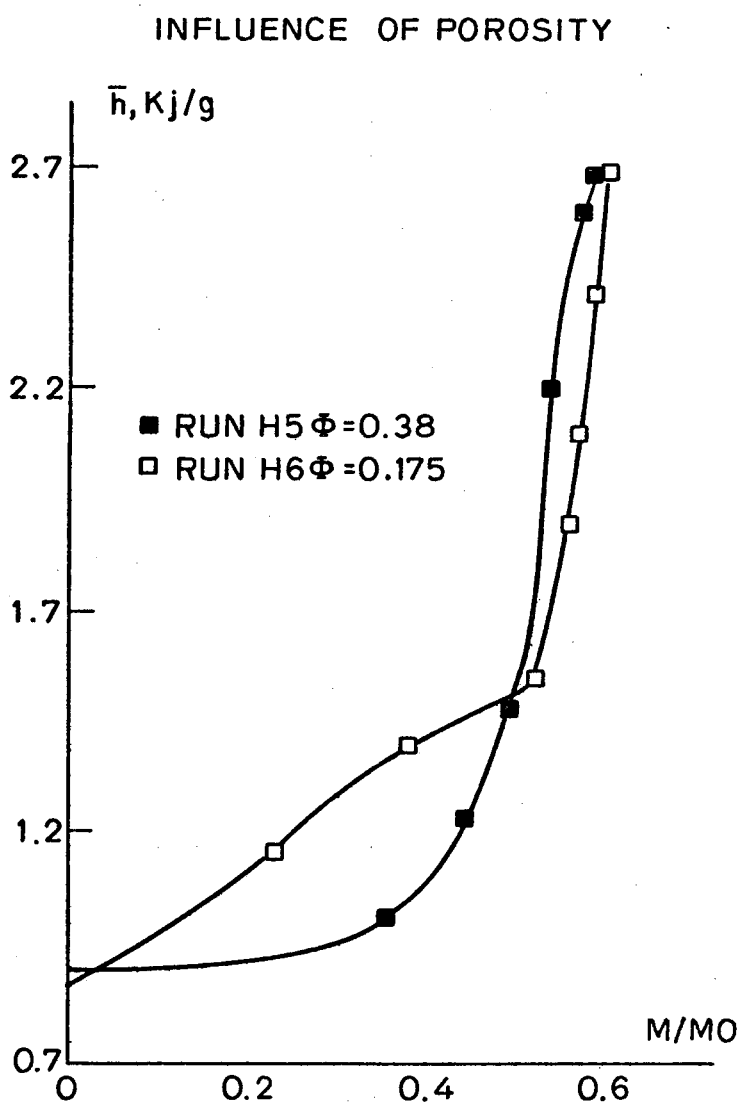
INFLUENCE OF POROSITY
$\bar{h}$, Kj/g
2.7
2.2
1.7
1.2
0.7
RUN H5 Φ=0.38
RUN H6 Φ=0.175
M/MO
0
0.2
0.4
0.6

FIGURE 3 -

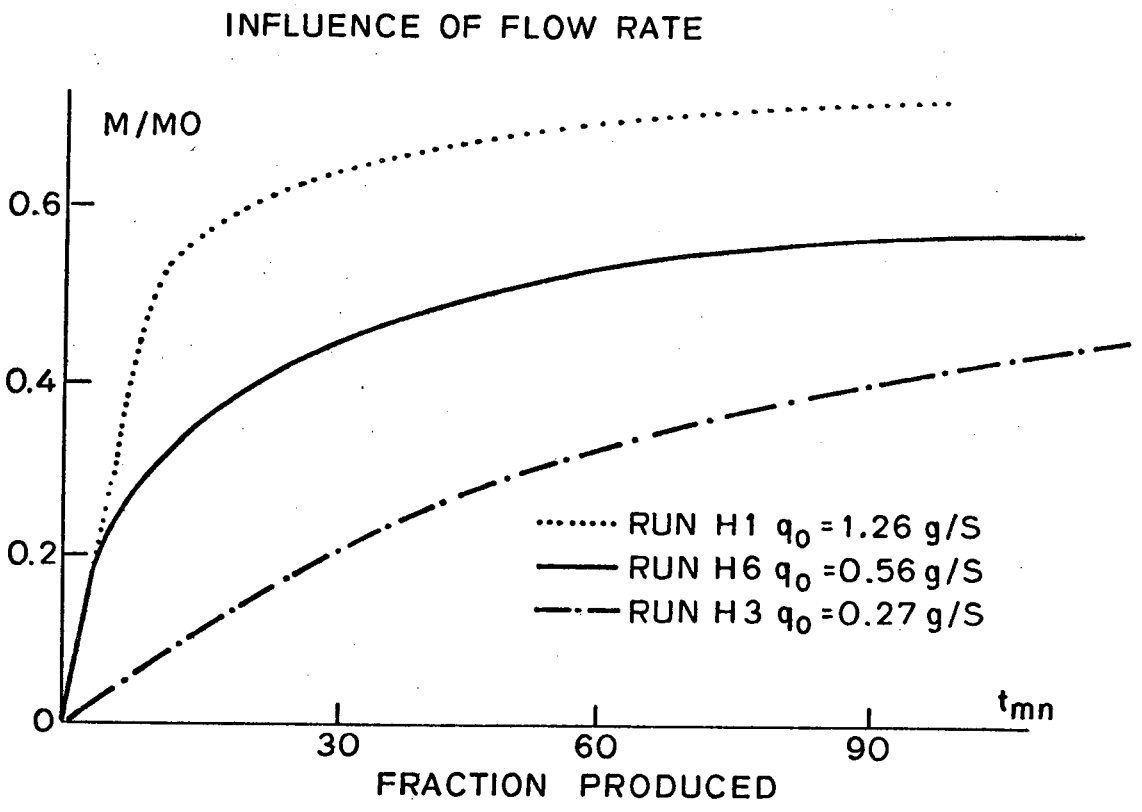
INFLUENCE OF FLOW RATE
M/MO
0.6
0.4
0.2
0
30
60
90
t_{mn}
RUN H1 q_0 = 1.26 g/S
RUN H6 q_0 = 0.56 g/S
RUN H3 q_0 = 0.27 g/S
FRACTION PRODUCED

FIGURE 4 -

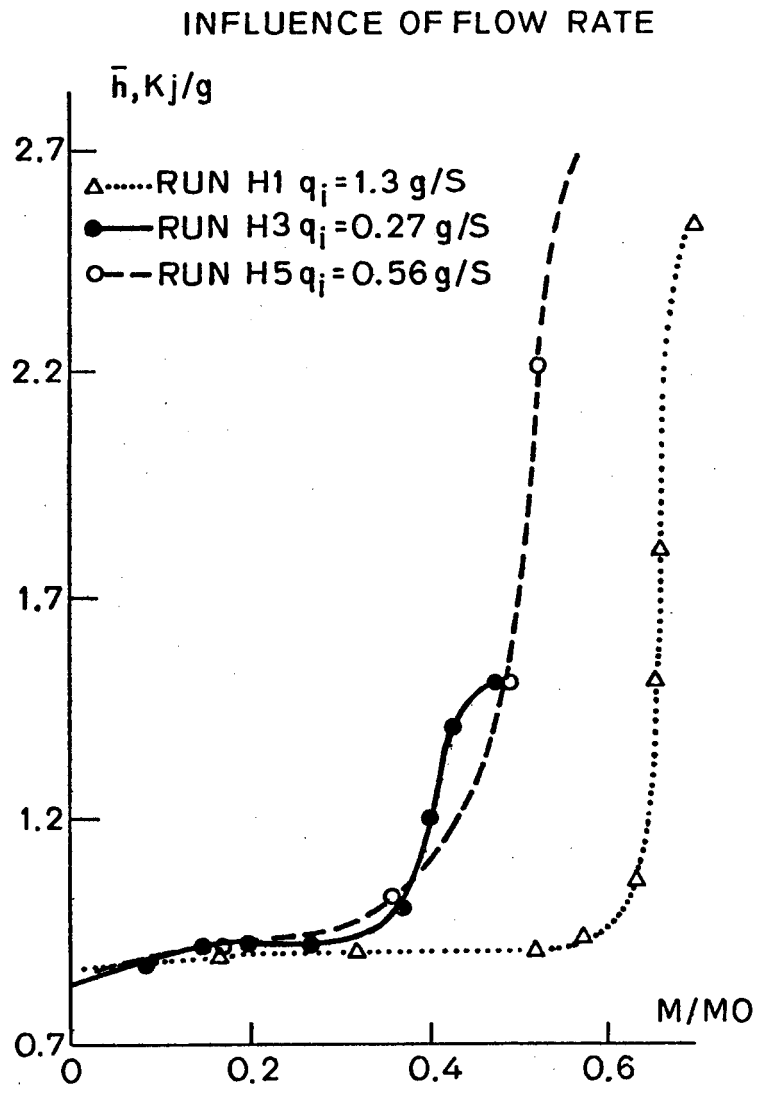
INFLUENCE OF FLOW RATE
$\bar{h}$, Kj/g
2.7
2.2
1.7
1.2
0.7
RUN H1 q_i = 1.3 g/S
RUN H3 q_i = 0.27 g/S
RUN H5 q_i = 0.56 g/S
0
0.2
0.4
0.6
M/MO

FIGURE 5 -

INFUENCE OF INITIAL LIQUID SATURATION

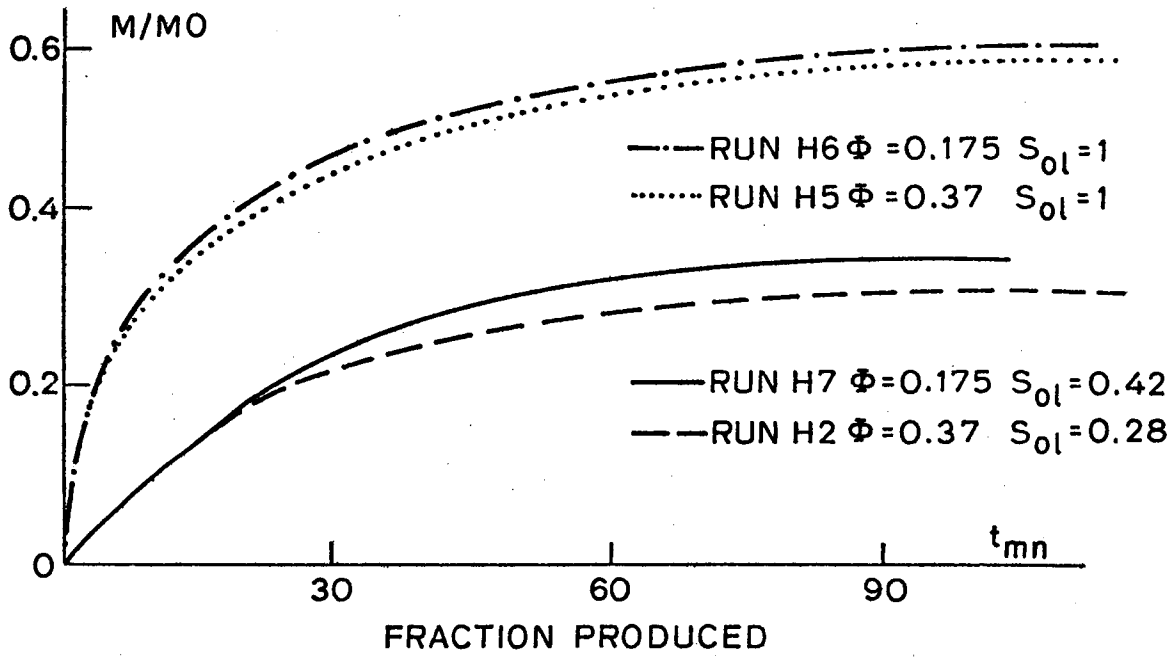

FIGURE 6 -

INFLUENCE OF SATURATION

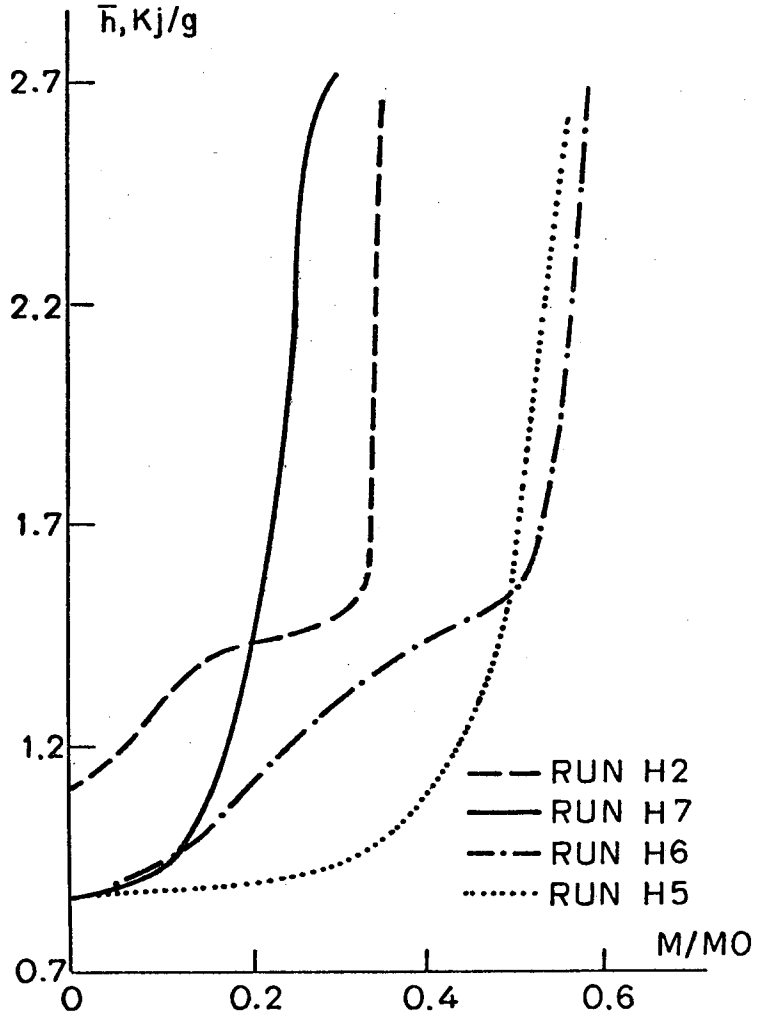

FIGURE 7 -

ENERGY EFFICIENCY

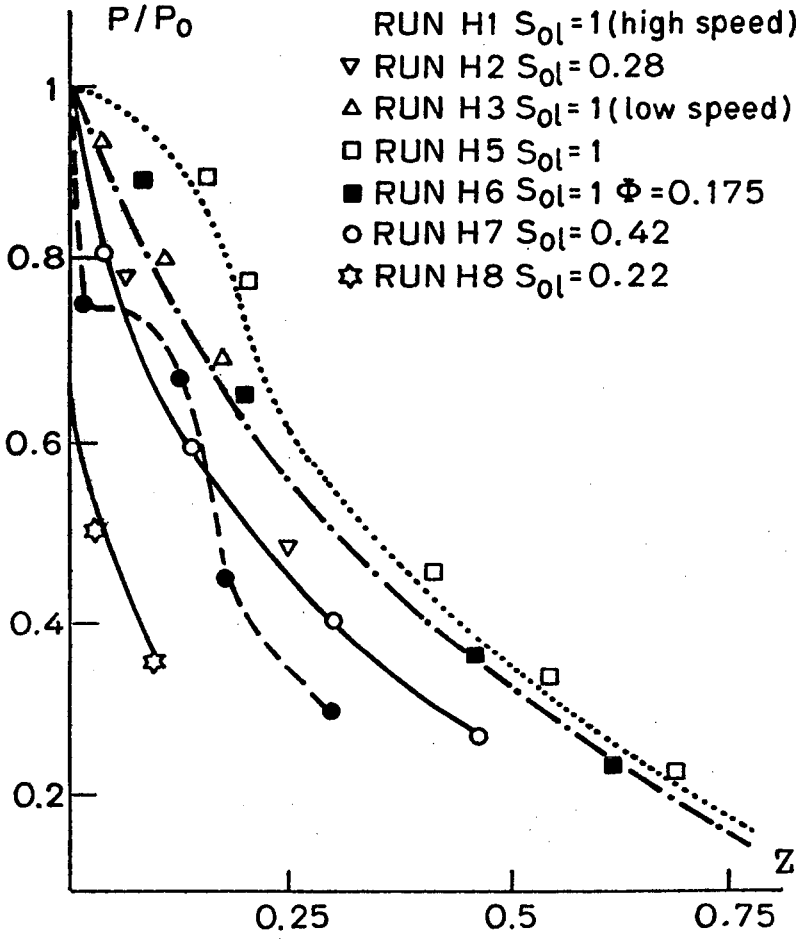

FIGURE 8.

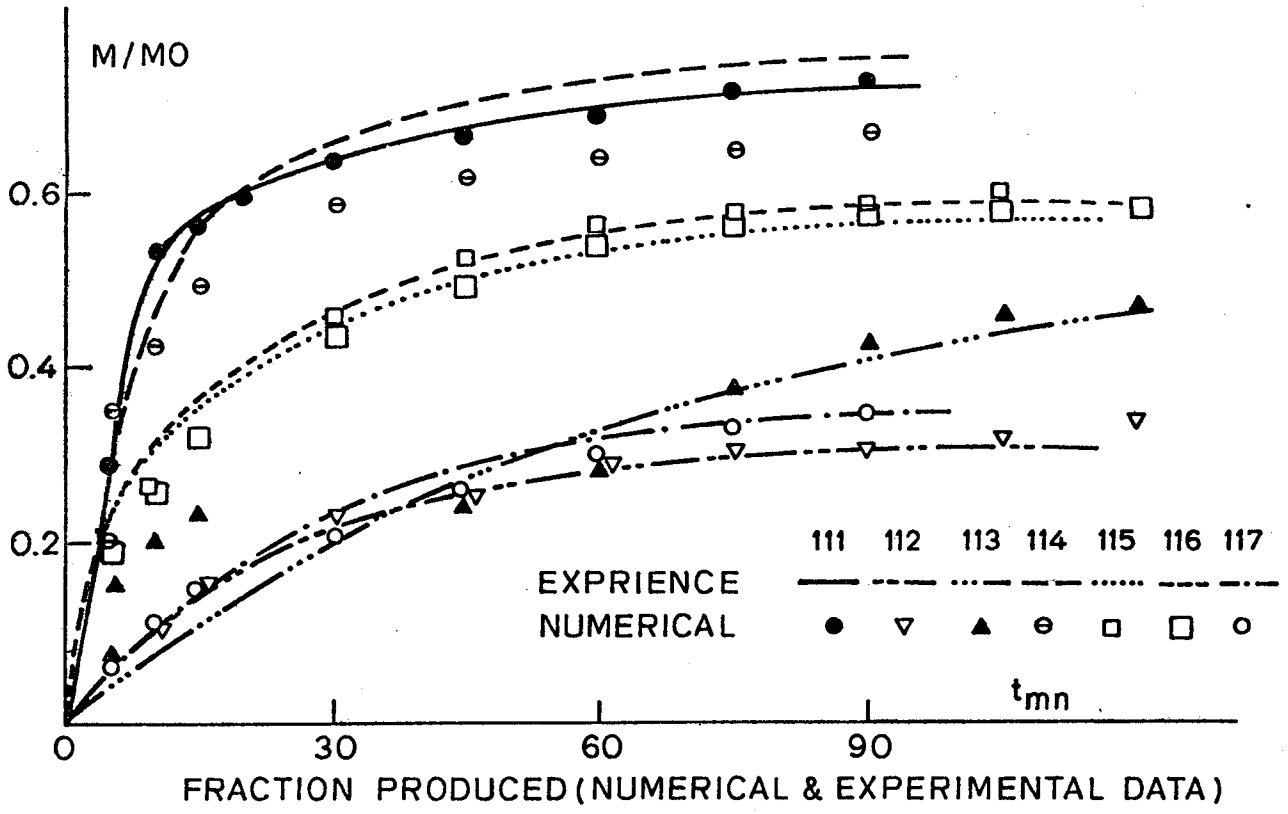
M/MO
0.6
0.4
0.2
0
30
60
90
t_{mn}
111 112 113 114 115 116 117
EXPRIENCE
NUMERICAL
FRACTION PRODUCED (NUMERICAL & EXPERIMENTAL DATA)

THE PSEUDOPRESSURE OF SATURATED STEAM

Malcolm A. Grant
D.S.I.R., P. O. Box 1335, Wellington, New Zealand

1. Definition and use of the pseudopressure

In a porous medium containing steam and immobile water, the equation for the flow of (saturated) steam is (Grant 1978):

$$(H_s - H_w)\frac{dp_s}{dT} k \nabla\cdot\left[\frac{\rho}{\mu}\nabla p\right] + \rho_m C_m \frac{\partial p}{\partial t} = 0 \qquad (1)$$

and $p = p(T)$.

This is a nonlinear diffusion equation, nonlinear because of the $\frac{\rho}{\mu}$ multiplying $\nabla\rho$, and because the coefficient of $\frac{\partial p}{\partial t}$ is also a function of T and hence P. It can be linearised in P, to obtain

$$\nabla^2 p = \frac{1}{\kappa_o}\frac{\partial p}{\partial t} \qquad (2)$$

where $$\kappa_o = \frac{k}{\rho_m C_m}\left[\frac{\rho_s}{\mu_s}\frac{dp_s}{dT}(H_s - H_w)\right]_o$$

is evaluated at the assumed initial uniform state.

We can also write

$$m^* = \int\frac{\rho}{\mu}\,dp = \int\frac{dp}{\nu} \qquad (3)$$

so that

$$\nabla^2 m^* = \frac{1}{\kappa}\frac{\partial m^*}{\partial t} \qquad (4)$$

This can again be linearised by setting κ equal to its initial value κ_o:

$$\nabla^2 m^* = \frac{1}{\kappa_o}\frac{\partial m^*}{\partial t} \qquad (5)$$

The nonlinearity caused by the coefficient of ∇p has been

removed, but the variation in κ has not been accounted for. However, it is nearly always better practice, with nonlinear diffusion equations, to represent the divergence terms exactly (here $\nabla^2 m$). The errors incurred by ignoring the variations in κ seem less important. A rough reason can be advanced. Both (5) and (2) are valid if the pressure changes are small. But (5) is also valid for steady pressure changes of any magnitude. If a bore is running for a long time, there is a quasi-steady region near the bore. The approximation (5) may better represent this, for large drawdowns, than (2).

It should be noted that the pseudopressure defined here does not have the dimensions of pressure, but $\rho p/\mu$ (= $kg/m^3 s$). Conventional gas pseudopressures are differently defined. Such a pseudopressure for superheated steam is given by Atkinson and Mannon (1977).

The boundary conditions are also scaled. If we have two-dimensional flow to a bore producing at a rate q (m^3/sec) = W^* (kg/sec), the condition is

$$2\pi r \left(\frac{\kappa}{\mu} \frac{\partial p}{\partial r}\right)_{r=a} = q \qquad (7)$$

this is $$2\pi r \left(k \frac{\partial m^*}{\partial r}\right)_{r=a} = W^* \qquad (8)$$

Thus, where the expression $q\mu$ occurs, it is replaced by W^*. For example, in the standard 2-d solution

$$\Delta p = p - p_o = \frac{qu}{4\pi kh} E_1\left(\frac{a^2}{4\kappa t}\right) \qquad (9)$$

we have, using the pseudopressure,

$$\Delta m^* = m^* - m_o^* = \frac{W^*}{4\pi kh} E_1\left(\frac{a^2}{4\kappa t}\right) . \qquad (10)$$

Since it is usually mass flow rates that are specified, use of the pseudopressure usually makes some small saving of effort in looking up densities and viscosities.

2. Formulae for $m^*(p)$

Use of the pseudopressure is convenient only if there is a simple expression for it as a function of pressure. Fortunately this is so. In any approximate formula for pseudo-pressure, we need its derivative dm^*/dp represented to some order of accuracy, for we always use differences $m^*(p_1) - m^*(p_2)$. Thus we approximate ρ/μ to some order of accuracy, and integrate to get m^*.

The following expression is accurate to 1% (130-240°C) 2% (100-260°C).

$$\frac{1}{\nu} = \frac{\rho}{\mu} = 4.793 \times 10^4 \, p^{6/7} \qquad (11)$$

where p is in bars. Keeping p in bars from now on:

$$\frac{dm^*}{dp} = 10^5 \frac{\rho}{\mu} = 4.793 \times 10^4 \, p^{6/7}$$

$$m^* = 2.58 \times 10^9 \, p^{13/7} \qquad (12)$$

For convenience, define

$$\boxed{m(p) = p^{13/7}} \qquad (13)$$

$$= m^*/(2.58 \times 10^9) \qquad (14)$$

3. Equations in field units

3.1. Units bar, tonne/hr, darcy-metre

It is simplest to work with these units, and the function

$$\boxed{m(p) = p^{13/7}} \quad .$$

The standard drawdown formula (10) now becomes:

$$m^* = 2.58 \times 10^9 \, p^{13/7} = 2.58 \times 10^9 \, m$$

$$W^* = W/3.6$$

$$kh \rightarrow 10^{-12} \, kh$$

$$2.58 \times 10^9 \, \Delta m = \frac{W}{3.6} \frac{1}{4\pi \, 10^{-12} \, kh} E_1 \left(\frac{a^2}{4\kappa t}\right)$$

or $$\boxed{\Delta m = 8.57 \frac{W}{kh} E_1 \left(\frac{a^2}{4\kappa t}\right)} \quad . \qquad (15)$$

If a bore is running for time t, and then switched off for time Δt,

$$\Delta m = -8.57 \frac{W}{kh} \left\{E_1\left(\frac{a^2}{4\kappa \Delta t}\right) - E_1 \left(\frac{a^2}{4\kappa}(t+\Delta t)\right)\right\}$$

$$\simeq 8.57 \frac{W}{kh} \ln \left(\frac{t + \Delta t}{\Delta t}\right)$$

$$\simeq 19.7 \frac{W}{kh} \log_{10} \left(\frac{t + \Delta t}{\Delta t}\right) \qquad (16)$$

Then, if M is the slope of a plot of $p^{13/7}$ vs t, or $\frac{t+\Delta t}{\Delta t}$, on semilog paper (slope of M per cycle),

$$M = 19.7 \, W/kh$$

or $$\boxed{kh = 19.7 \, W/M} \quad . \qquad (17)$$

Summary

$$m(p) = p^{13/7}$$

$$\Delta m = m - m_o = 8.57 \frac{W}{kh} E_1 \left(\frac{a^2}{4\kappa t}\right)$$

$$kh = 19.7 \, W/M \qquad (M = \text{slope of } m \text{ per cycle.})$$

3.2. Units kg/cm^2, tonne/hr, darcy-metre

It is simplest to redefine

$$\boxed{m(p) = p^{13/7}} \qquad (18)$$

Since 1 kg/cm^2 = 0.981 bar, a factor of $(0.981)^{13/7}$ multiplies the formula for m^*

$$m^* = 2.49 \times 10^9 \, p^{13/7} = 2.49 \times 10^9 \, m \, .$$

Then the drawdown formula is

$$\boxed{\Delta m = 8.88 \, \frac{W}{kh} \, E_1 \left(\frac{a^2}{4\kappa t} \right)} \qquad (19)$$

and $$\boxed{kh = 20.4 \, W/M} \, . \qquad (20)$$

M = slope of a plot of $p^{13/7}$ vs t

or $(t + \Delta t)/\Delta t$ on semilog paper

(slope of M per cycle).

References

1. U.K. Steam Tables in S.I. Units, 1970.

2. Abramowitz & Stegun, "Handbook of Mathematical Functions", Dover, 1965.

3. Grant, "Two-phase Linear Geothermal Pressure Transients - A Comparison with Single-Phase Transients", N.Z. Jl. Sci., Sept. 1978.

4. Mannon & Atkinson, "The Real Gas Pseudo-Pressure for Geothermal Steam", Third Workshop on Geothermal Reservoir Engineering, Stanford, 1977.

NOTATION

SI units are used unless otherwise specified.

t	time
μ	dynamic viscosity
ν	kinematic viscosity
ρ	density
T	temperature
p	pressure (also bar and ksc)
p_s	saturation pressure of steam
H	specific enthalpy
C	specific heat
ϕ	porosity
k	permeability (also darcy)
h	aquifer thickness
m^*	pseudopressure
m	$= p^{13/7}$ = scaled pseudopressure
W^*	mass flow
W	mass flow, tonne/hr
κ	diffusivity
M	slope of m vs $\log_{10} t$

$$E_1(x) = \int_x^\infty \frac{1}{u} e^{-u}\, du$$ (Abramowitz & Stegun 1965)

a	bore radius
r	radial distance

Suffices:

o	initial state
m	medium
s	steam

COMPRESSIONAL AND SHEAR WAVE VELOCITIES IN WATER FILLED ROCKS DURING WATER-STEAM TRANSITION

Hisao Ito,* John DeVilbiss and Amos Nur
Rock Physics Project
Department of Geophysics
Stanford University
Stanford, California 94305

ABSTRACT

Both compressional and shear wave velocities were measured in water-filled Berea sandstone as a function of pore pressure under a constant confining pressure of 200 bar. At 145.5°C, compressional velocity increased from steam-saturated (low pore pressure) to water-saturated (high pore pressure) rock, whereas shear wave velocity decreased. Furthermore, a velocity minimum, attenuation and dispersions occur at water-steam transition for compressional wave. Results at 198°C show that both compressional and shear velocities decrease from steam-saturated to water-saturated rock, and a small velocity minimum is observed for compressional waves, but no attenuation nor dispersion occur. At both temperatures, the V_p/V_s ratio and Poisson's ratio increased from steam-saturated to water-saturated rock.

The results are reasonably compatible with the mechanical effects of mixing steam and water in the pore space near the phase transition, and may be applicable to in situ geothermal field evaluation.

INTRODUCTION

One of the methods of exploration for geothermal resources is seismic surveying, including microearthquake studies, V_p/V_s ratios, and seismic wave attenuation.

However, few laboratory measurements of velocity of rocks at high temperature with hot water or steam have been made (e.g., Spencer and Nur, 1976). It is important therefore to extend our knowledge of velocities in water-filled rocks at high temperature with an emphasis of difference between the liquid (water) and gas (vapor) phase of pore fluid, which we have done in this study. Specifically, we have measured both compressional V_p and shear V_s velocities and wave amplitudes in porous rock at geothermal temperatures, as the water in the pores is converted to steam and steam to water, with particular attention to the effects of the phase transition itself. From the velocities, we also computed Poisson's ratio.

Experimental Procedure

The basic method used is the measurement of pulse travel time through rock samples with pore water. At fixed temperature, we vary the pore pressure P_p back and forth across the transition from steam (low P_p) to water (high P_p). The transition pressures for the temperatures used, 145.5°C and 189°C, were taken from Keenan et al., 1969.

Ultrasonic compressional and shear wave velocities and amplitudes were measured by the conventional pulse transmission method, with a mercury delay line as a reference. 1 MHz PZT ceramic transducers were used for generating compressional and shear waves.

Results

We measured both compressional and shear wave velocities at a constant confining pressure (300 bar) and temperature (19.5°C, 145.5°C, and 189°C) as a function of pore pressure. The pore pressure was changed from high pore pressure to low pore pressure (decreasing pore pressure cycle) and then increased again (increasing pore pressure cycle). Varying the pore pressure over the range of 7.0 bars in a saturated sample at 19.5°C produced almost no changes in either V_p or V_s.

In contrast, marked changes of velocities, Poisson's ratios, and wave amplitudes with changing pore pressure were observed at the higher temperatures of 145.5°C and 198°C. The results show:

(1) There is a minimum for compressional velocity at pore pressure of 4 bar (Fig. 2) which is very close to the water-vapor transition pressure of 4.212 bar at 145.5°C (Keenan et al., 1969). Below this pore pressure, water is in vapor phase (steam) and above the transition pressure it is in liquid phase. No minimum is observed for shear wave velocity (Fig. 3).

(2) Compressional wave velocity of steam-filled rock is lower than that of water-filled rock. Shear wave velocity in steam-filled rock is higher than that of water-filled rock.

(3) Poisson's ratio and V_p/V_s ratio calculated from compressional and shear wave velocities increase from steam-saturated to water-saturated rock, as shown in Fig. 4.

(4) We observe changes of wave amplitude vs pore pressure (Fig. 5 and Fig. 6). We notice a sharp drop in the compressional wave amplitude at the water-vapor transition, which is reproducible with pore pressure cycling. However, no minimum of shear wave amplitude is observed. In Fig. 5, the time intervals from first arrival to the first, second, and third peaks are plotted vs pore pressure with a large time interval corresponding to lower frequency of the wave. Again the water-steam transition, a peak time interval, was observed for compressional wave but not for shear wave. This suggests that high frequency components of the compressional wave are significantly more attenuated at the water-vapor transition.

Because attenuation depends so sensitively on many factors, and because the sample length is short, we cannot yet calculate exact Q values for these data. Nevertheless, it is obvious that attenuation and dispersion occur at the water-steam transition in our rock sample for compressional waves, but not for shear waves.

CONCLUSION

We have studied experimentally the nature of wave propagation in steam-, water-, and mixture-saturated sandstone. The results show that the P wave velocity is abnormally low in the phase transition region at 145°C and 198°C, whereas the shear velocity has no minimum there. Poisson's ratio undergoes a marked increase upon the transition from the steam-saturated to water-saturated state. The amplitude of the P wave at 145°C also has a strong minimum at the transition region, whereas the S amplitude does not.

All these results can be explained by the effects of a mixture of steam, vapor, and water in the pores at the transition conditions: for a few percent steam, the density of the mixture is relatively high, similar to water, whereas the bulk modulus, $\bar{K}$, is low, similar to steam. The shear velocity, which is insensitive to the bulk modulus of the fluid inclusion, is therefore barely influenced, whereas the compressional velocity is sensitive to $\bar{K}$, and thus undergoes a measurable change. Furthermore, the large relative P attenuation at the transition is probably due to local flow in the partially saturated state.

The results of this study suggest that in situ interfaces between steam and hot water, if they exist, may be recognizable using the seismic method. Furthermore, regions with both steam and hot water should exhibit anomalous low velocity and high attenuation of P waves, but not of S waves. Furthermore, Poisson's ratio is, as expected, a good discriminator between steam and hot water in the pore space and may be a useful tool, as suggested in previous work (e.g., Combs and Rotstein, 1976) on the basis of room temperature measurements. The data presented here demonstrate that the conclusion is valid also at temperatures anticipated in a geothermal area.

ACKNOWLEDGEMENTS

We thank John Weeks, who helped in the design and initiation of this project. We are grateful to P. Gordon for the design, construction, and maintenance of the special equipment used in the experiments. We are also indebted to J. Walls for the shear transducer design and extensive discussions. This study was supported by grant EY-76-S-03-0326 PA#45, from the Office of Basic Research, the Department of Energy.

References

Anderson, D.L., and J.H. Whitcomb, Time-dependent seismology, J. Geophys. Res. 80, 1497-1503, 1975.

Combs, T., and Y. Rotstein, Microearthquake studies of the Coso geothermal area, China Lake, California, Proc. 2nd U.N. Symp., Develop. use of Geothermal Res., v. 2, 909-916, 1976.

Domenico, S.N., Elastic properties of unconsolidated porous sand reservoirs, Geophysics 42, 1339-1368, 1977.

Elliot, S.E., and B.F. Wiley, Compressional velocities of partially saturated, unconsolidated sand, Geophysics 40, 949-954, 1975.

Hayakawa, M., The study of underground structure and geophysical state in geothermal areas by seismic exploration, Geothermics, Spec. Issue 2, v. 2, pt. 1, 347-357, 1970.

Keenan, J.H., F.G. Keyes, P.G. Hill and J.G. Moore, Steam Tables, John Wiley & Sons, New York, 1969.

Mavko, G.M. and Amos Nur, Wave attenuation in partially saturated rocks, Geophysics, in press, 1978.

Nur, A. and G. Simmons, The effect of saturation on velocity in low porosity rocks, Earth Planet. Science Lett., 7, 183, 1969.

O'Connell, R.J. and B. Budiansky, Seismic velocities in dry and saturated cracked solids, J. Geophys. Res., 79, 35, 5412, 1974.

Richter, D., and G. Simmons, Thermal expansion behavior of igneous rocks., Inter. J. Rock Mech. Min Sci., 11, 403-411, 1974.

Spencer, J. and A.M. Nur, The effects of pressure, temperature, and pore water on velocities in Westerly granite, J. Geophys. Res. 81, 899-904, 1976.

Takeuchi, S., and G. Simmons, Elasticity of water-satured rocks as a function of temperature and pressure, J. Geophys. Res. 78, 3310-3320, 1973.

Todd, T. and G. Simmons, Effect of pore pressure on the velocity of compressional waves in low porosity rocks, J. Geophys. Res., 77, 3731-3743, 1972.

Toksoz, M.N., C.H. Cheng and A. Timur, Velocities of seismic waves in porous rocks, Geophysics 41, 621-645, 1976.

Walsh, J.B., New analysis of attenuation in partially melted rock, J. Geophys. Res., 74, 4333, 1969.

Walsh, J.B., Wave velocity and attenuation in rocks undergoing polymorphic transformations, J. Geophys. Res., 78, 1253-1261, 1973.

White, J.E., Computed seismic speeds and attenuation in rocks with partial gas saturation, Geophysics 40, 224-232, 1975.

Winkler, K., and Amos Nur, Attenuation and dispersion in partially saturated rocks, (abstract) SEG meeting, San Francisco, 1978.

Zoback, M.D., High pressure deformation and fluid flow in sandstone, granite and granular materials: Ph.D. thesis, Stanford Univ., 1975.

TABLE 1

Physical Properties of Berea Sandstone

grain density	2.66	*
total porosity	18.9%	*
	18.75%	**
crack porosity	0.25%	**
pore porosity	18.50%	**
water permeability	160 md	**

* present measurement

** Zoback

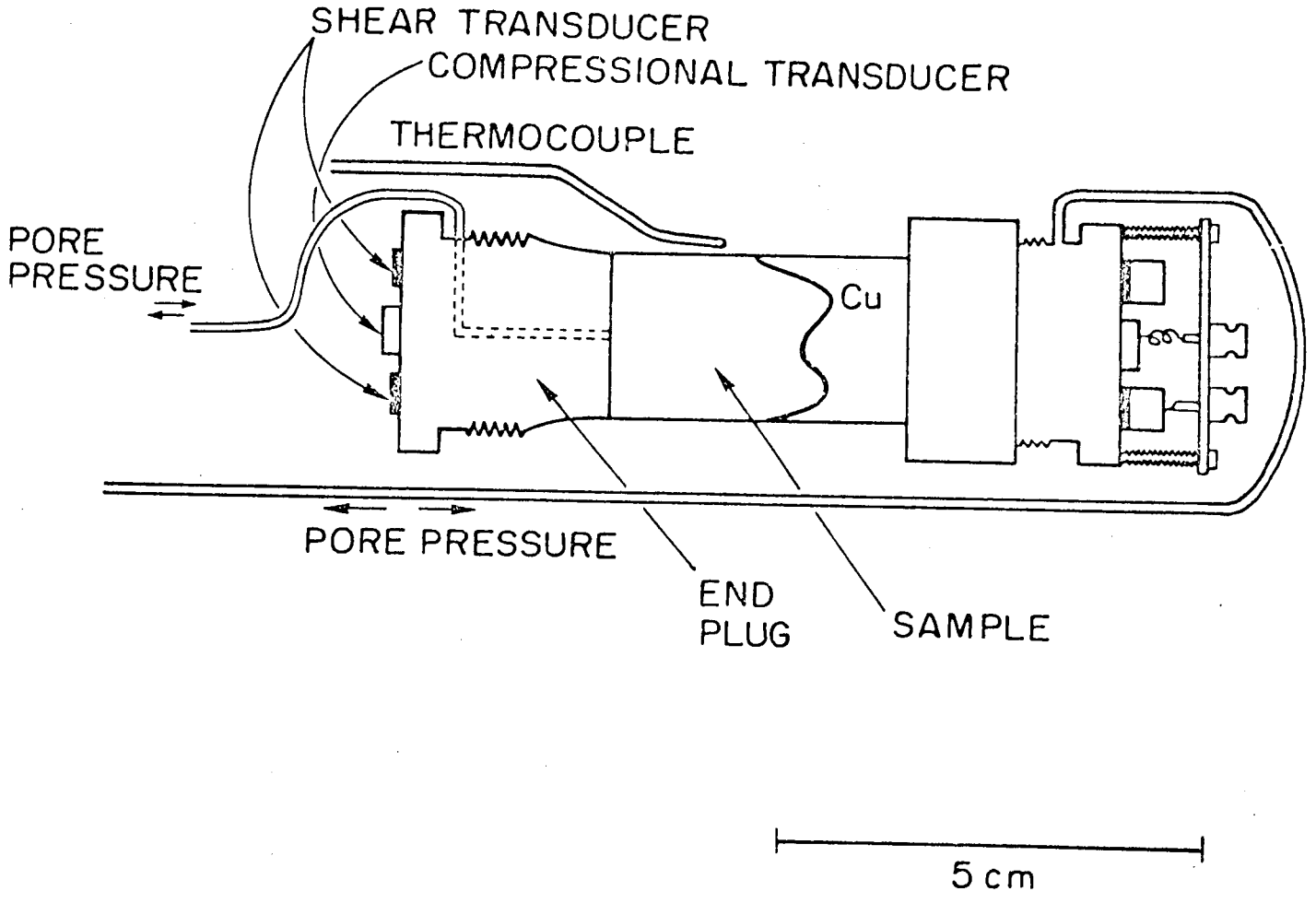

FIGURE 1. SCHEMATIC DIAGRAM AT SAMPLE ASSEMBLY

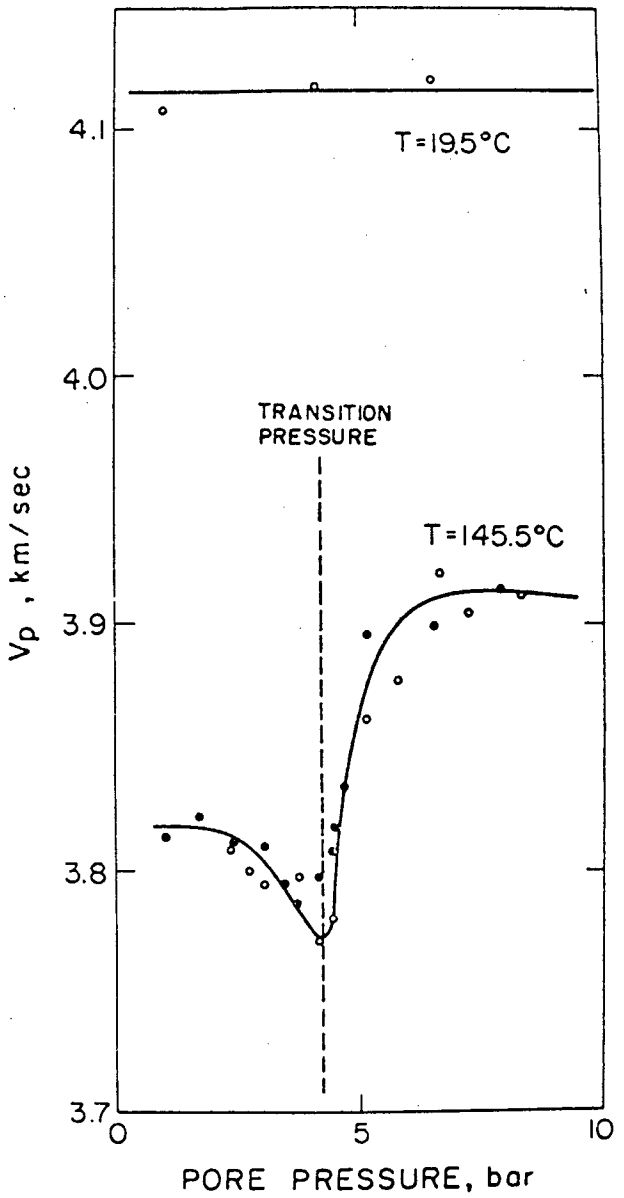

FIG. 2. Compressional wave velocity V_p vs pore pressure at 19.5°C and 145.5°C. Open circles show the data during decreasing pore pressure cycle, closed circles show the velocities during increasing pore pressure cycle. Saturation pressure at 145.5°C is also shown.

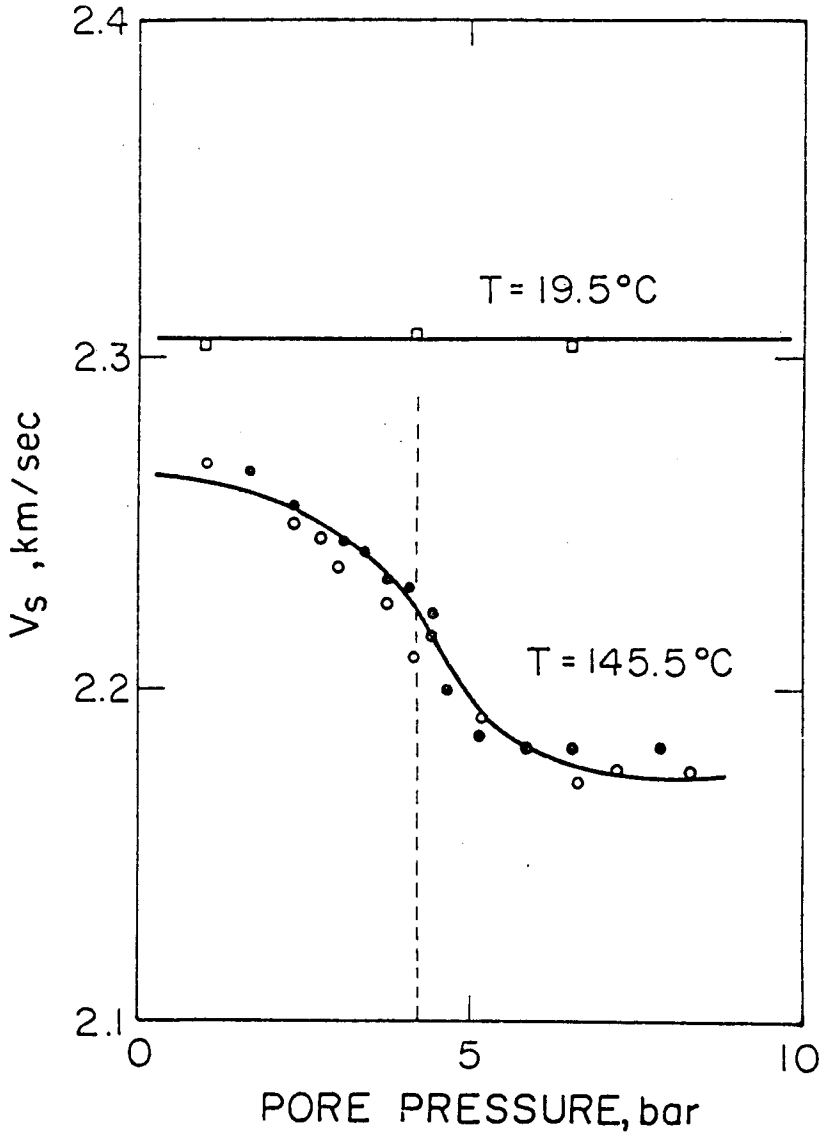

FIGURE 3. Shear wave velocity V_s vs pore pressure at 19.5°C and 145.5°C.

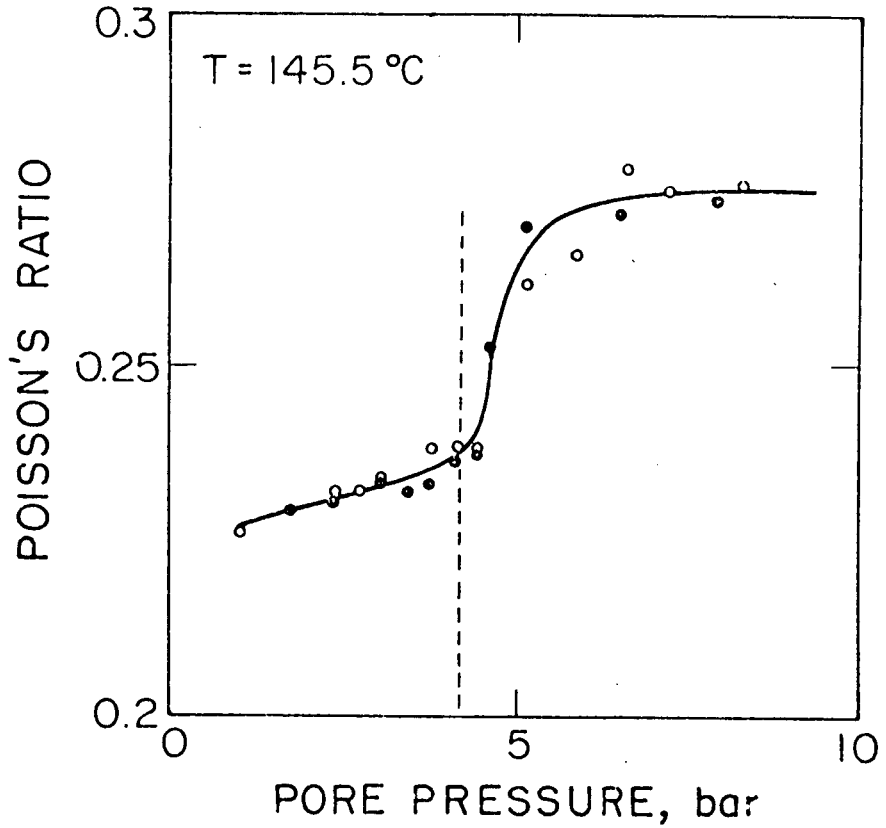

FIGURE 4. Poisson's ratio vs pore pressure calculated from compressional and shear wave velocities at 145.5°C.

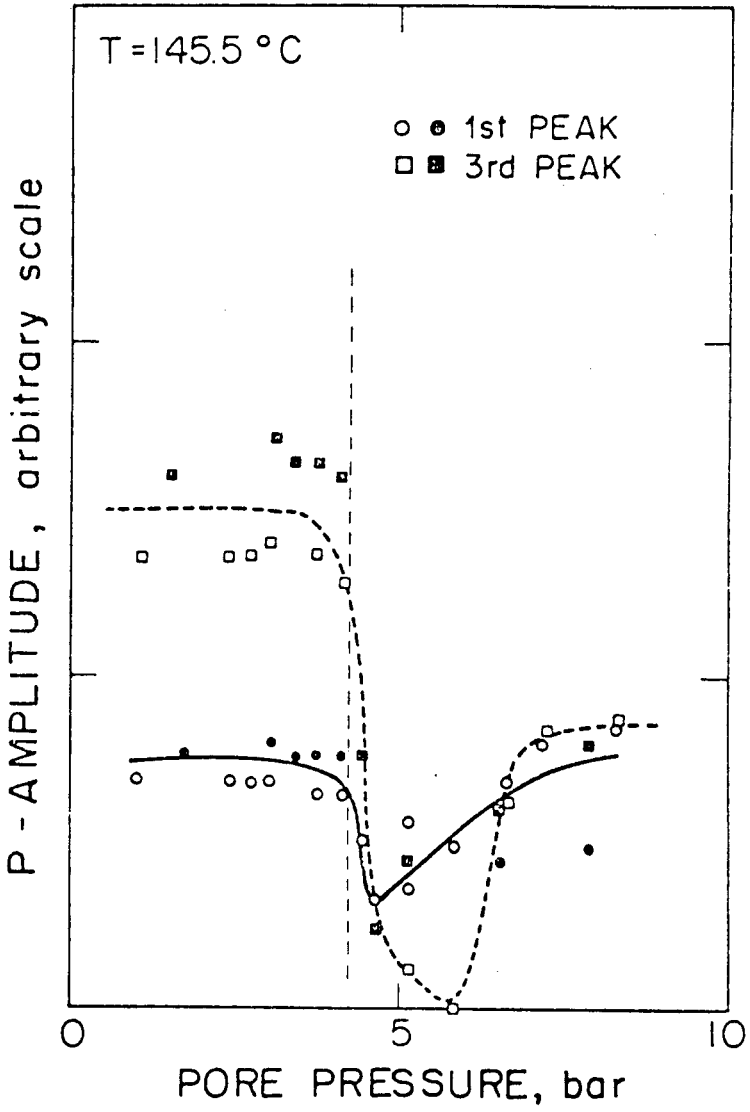

FIGURE 5. V_p/V_s ratio vs pore pressure at 145.5°C.

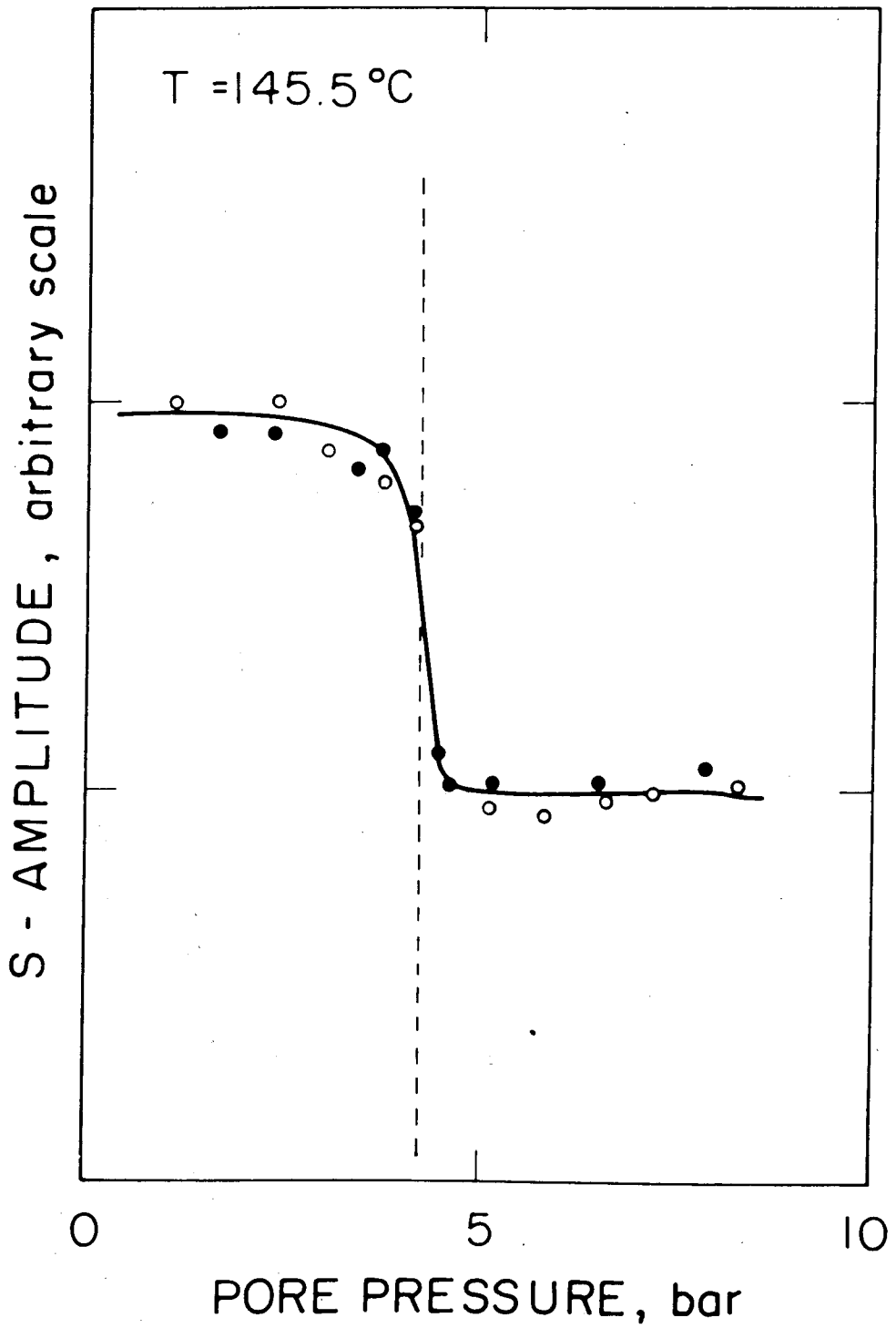

FIGURE 6. Peak amplitude (first and third) of compressional wave vs pore pressure at 145.5°C.

DOWNHOLE MEASUREMENTS AND FLUID CHEMISTRY OF A CASTLE ROCK STEAM WELL, THE GEYSERS, LAKE COUNTY, CALIFORNIA

Alfred H. Truesdell, U.S. Geological Survey, Menlo Park, Calif.
George A. Frye, Aminoil U.S.A., Santa Rosa, Calif.
Manuel Nathenson, U.S. Geological Survey, Menlo Park, Calif.

Introduction

Certain wells within The Geysers steam field have standing water columns either when first drilled or when produced at low flow rates. These water columns have been attributed by Lipman et al. (1978) to accumulation of water condensing in the well bore. Alternative explanations are that perched water bodies exist within the reservoir or that a deep water body underlying the steam reservoir has been tapped. A well in the Castle Rock field of The Geysers drilled by Signal Oil and Gas Company (now Aminoil, U.S.A.) with such a water column was sampled in 1976 for water, gas, and isotope chemistry in hopes of distinguishing between these possible origins; the results along with the well history and downhole pressure and temperature measurements are reported here.

The well is located in Lake County, California, in the central part of the Castle Rock field, 4.8 km west-northwest of the town of Anderson Springs. Drilling was started in mid 1970 on a ridge at an elevation of 700 m above sea level. Steam entries were encountered at depths (below land surface) of 1,899, 1,902, 2,176, 2,248 2,288, and 2,295 m; the total depth drilled was 2,498 m. Large volume water entries above 685 m were cased off to 762 m.

Downhole Measurements

Static downhole pressure and temperature surveys were made each year from 1973 to 1977. During that period the well was held at a small bleed flow through a 2.5-cm orifice, except during short (usually less than 8 hour) performance tests. The results of the downhole surveys are shown in figures 1 and 2. In each of these surveys standing water was found in the well below a vapor zone. Temperatures and pressures above the water level generally decreased with time, and the level of water in the well rose. The pressure in the water zone was remarkably constant at each depth and the pressure and temperature near the bottom of the well at 2,484 m remained at 53.6 ±0.3 bars and 247.7 ±1.6°C from 1973 to 1976. (Measurements in 1977 were not made below 2,164 m.) The variations of pressure and temperature at this depth are well within the expected instrumental reproducibility of ±2% of full range or ±0.8 bars and ±2.2°C.

Above the level of standing water the measurements indicate the presence of vapor (steam + gas). Below 610 m in this vapor zone the temperatures were those expected for steam-water saturation at the measured pressures within less than ±0.7°C in 1973, 1974, and 1977, with larger differences (to 2.7°C) in 1975 and 1976 possibly due to instrumental error. Above 610 m the temperature differences increased probably due to accumulation of gas. The pressure gradients (near 0.17 bars/100 m) were also close to those calculated for columns of

saturated steam except in 1976 and 1977 when the observed gradients were almost twice those calculated. These high gradients could be produced by accumulation of nearly 100% CO_2 in the well but this was not observed in the chemical samples. Pressure gradients near the surface were slightly higher due to gas accumulation.

Below the water level, pressure gradients were equal to those calculated for pure water; and temperatures, although greater than in the vapor zone, were much lower than those expected for saturation at the observed pressures indicating absence of steam.

Pressures and temperatures in the water zone were remarkably constant despite large changes in the vapor zone above. This suggests that the physical conditions within the well were controlled by the reservoir away from the well. The temperature at the well bottom is close to that at similar depths in Castle Rock wells without standing water and similar to the temperature at the bottom of the vapor zone in 1973 (at 2,270 m). Pressures at 2,286 m have remained at 38 ± 0.3 bars, close to field pressures for this depth as observed or extrapolated from other wells without standing water.

These observations suggest that steam enters the well from the deepest observed steam entries (at 2,290 ± m) and the pressure in the water column is controlled at this depth by the pressure of steam outside the well. Temperatures at this point have been below the field average for this depth after 1973 but pressure communication could be maintained even if the formation cooled off locally.

The standing water may be local to the well or could represent the top of a more extensive water body. Nearby wells did not enounter water but were not drilled to as great a depth. Redrilling of this well to 2,714 m in early 1977 did not encounter any deeper steam zones nor did it greatly affect the water level when measured in May 1977. This suggests that the rocks drilled were impermeable or that the water, if perched, extends at least to 2,714 m.

The cooling off of the well and the accumulation of gas in the upper 600 meters both suggest that a large proportion of the steam flowing up the well is condensing in the well bore and flowing down the well. This is the probable origin of the water in the well, although this water may have mixed with water of a larger water zone. The continuing decrease in temperature and pressure in the well suggest that steam entry to the well at its normally low flow rate was not sufficient to maintain reservoir pressure and temperature conditions in the well and that condensed water continued to flow away from the well. During a full flow test the accumulated water clogging the steam entries (probably near 2,290 m) was expelled and steam access was sufficient to temporarily heat the well bore. A shorter period of rest after testing may explain the inconsistently high downhole pressures and temperatures measured in 1976.

Collection and testing on March 9, 1976.

Samples of condensed steam, gas, and expelled water were collected during a flow test on March 9, 1976. The samples were taken on bleed (2.5-cm orifice) and at various intervals after the well was opened (at 12:45 p.m.) to flow through a 10-cm orifice. Liquid water was ejected from the well immediately after increasing its flow. This

ejected water was sampled at the lip of the horizontal silencer before it stopped flowing at about 1:15 p.m. A second slug of water was ejected from the well at 3:30 p.m. and sampled at 4:00 p.m. Again the flow lasted only a short time. Throughout the test the steam which had been initially wet and opaque at the mouth of the silencer became gradually drier and more transparent. During ejection of the second slug of water the steam was again opaque. Samples of steam condensate and gas were taken 15 minutes before the flow was increased and 2-1/4 and 4-1/4 hours afterwards. Chemical and isotopic analyses of steam condensate and ejected water (along with earlier condensate analyses from Aminoil Laboratories) are shown in table 1 and gas analyses in table 2.

Water Analyses

The condensate analyses show that compared to bleed steam, full flow steam contained higher concentrations of chemical constituents more soluble in liquid (Cl, B, NH_4) and lower concentrations of constituents more soluble in vapor (CO_2 as HCO_3, H_2S). These observations are consistent with partial condensation during bleed and removal of liquid-soluble constituents to the water draining down the well bore and concentration of gas-soluble constituents in the bleed steam. The ejected water was much higher than either condensate in most salts because salts are only slightly soluble in steam at these pressures. The salts contained in the ejected water could all have been leached from reservoir rock and their concentrations are quite consistent with this water originating as steam condensate rather than from the deep brine body which has been hypothesized to underlie the field.

The second slug of ejected water was more concentrated in most constituents than the first slug suggesting a longer period of rock leaching. It is possible that this slug represented relatively stagnant water below the main steam entry to the well. This water may have been ejected when a deeper steam passage was cleared and steam entered the well at a lower point.

Gas Analyses

The gas/steam molal ratio of the bleed steam (1/1,720) was much lower than that of full flow steam ($\sim$1/4,500, table 2). This is consistent with partial condensation of steam in the well bore when the well is on bleed flow. If it is assumed that negligible condensation occurs on full flow and that the amount of gas dissolved in the liquid water is negligible it is possible to calculate the relative amounts of steam condensing and flowing out of the well near the bottom and of steam (and entrained water) flowing out at the wellhead when the well is on bleed. Calculations from the gas/H_2O ratios suggest that 40% of the total steam is leaving at the top of the well with 60% condensing and flowing down and out at the bottom.

Hydrogen and oxygen isotopes.

Oxygen-18 and deuterium were measured in the condensates from bleed and full flow steam and in the ejected water (table 1 and figure 3). The isotopic composition of the ejected water appears to bear little relation to the calculated composition of water condensed in the well bore and the second sample appears to have been in isotopic equilibrium with full flow steam at 95°C. It is suggested that the

isotopic composition of the ejected water was rapidly altered in the silencer at temperatures near surface boiling (97°C at this altitude) by exchange with steam blowing over it. This alteration was partial when the first sample was collected and complete when the second sample was collected.

The ratio of change in oxygen-18 to the change in deuterium for bleed versus full flow steam indicates partial isothermal separation of steam and water at about 250°C (figure 3). This suggests that the temperature of separation between steam entering the well and liquid water leaving it is close to the reservoir temperature, and is consistent with the pressure control mechanism suggested earlier of a steam entry at 2,290 m from the main reservoir initially at 247°C. The precision of the deuterium measurement ($\pm 1°/_{oo}$) is not however sufficient to indicate the temperature of separation to better than ±25°C so this slope is consistent with separation at the temperatures observed in the well.

The isotopic changes can also be used to calculate the fraction of steam leaving the wellhead and the fraction condensing and draining down the well. Assuming that the bleed steam may actually have some entrained water, the initial flow of saturated steam divides into three streams. Part of the steam remains vapor and flows out of the well; part of the steam condenses to liquid water and is entrained in the bleed steam and leaves the well with it; and finally, part of the steam condenses to liquid water and flows down the well and out into the formation. Applying conservation of energy to this process including the effects of wellbore heat loss (Ramey, 1962), the enthalpy of the bleed steam may be determined as a function of $m/m_s(0)$ where m is the mass flow rate of bleed steam and entrained condensate out of the well and $m_s(0)$ is the mass flow rate of saturated steam into the well at the bottom. If the enthalpy of the bleeding mixture were known, this ratio could be determined directly. The enthalpy was not measured, but this energy balance provides upper and lower bounds on the ratio $m/m_s(0)$. The enthalpy of the bleeding discharge must be between that for saturated liquid and saturated vapor at 230 to 240°C, and these bounds constrain $m/m_s(0)$ to be between 0.42 and 0.74 for the bleed steam and between 1.0 and 0.90 for the full flow steam.

Isotopic fractionation of oxygen-18 and deuterium between the steam flow and the condensing water flows may also be modeled by writing conservation of mass (steam up, water up and down), conservation of isotopes in those flows, and the equilibrium fractionation factors between water and steam (Truesdell, et al., 1977). These equations may be used to derive the isotopic composition of feed steam from the measured compositions of surface bleed steam and water as a function of the ratio of mass of bleed flow to initial mass flow of steam $m/m_s(0)$. For each isotopic ratio ($^{18}O/^{16}O$, D/H) two curves are shown on figure 4 for the compositions of feed steam derived from the measured isotopic composition of bleed steam and water, one for assumed fractionation at 230°C and one for 240°C. The curves are only plotted in the range of $m/m_s(0)$ of 0.42 to 0.74 as determined by the enthalpy calculation. Also shown are two short curves marked "full flow." Each full flow curve is for the average of the two measured contents of deuterium and of oxygen-18

isotopes given in table 1. For $m/m_s(0)$ of one, all the flow exits the well. Since the enthalpy was not measured, there is some possibility of condensation and flow down the well, so the curves have been calculated down to $m/m_s(0)$ of 0.9. For the oxygen-18 contents of the source steam to have been the same from full flow and bleed measurements, the bleeding well would have to produce about 55% of the inlet steam with 45% draining down the well at either 230 or 240°C. For deuterium, the two sets of measurements are only consistent for an assumed 240°C fractionation temperature. Deuterium measurements have, however, standard deviations of ±1‰. This large error compared to oxygen-18 measurements, means that the failure of consistency for deuterium values at 230°C is hardly significant. The ratio of 55% of the inlet mass of steam being produced by the bleeding well is in reasonable agreement with a value of 40% based on the gas analyses and with the 42% to 74% indicated by heat transfer calculations.

Summary

Standing water in a Geysers steam well has been shown from physical measurements and chemical and isotopic analyses of bleed and full flow steam to result from condensation in the well bore. Pressures and temperatures in the standing water suggest pressure communication with the steam reservoir at a point below the standing water level. Limited inflow of steam and outflow of condensed water has allowed the well bore and surrounding rock to decrease markedly in temperature and pressure over the period 1973-1977. Chemical analyses of condensate and ejected liquid water show significant differences, although ejected water also appears to originate as steam condensate.

Gas and isotopic analyses of bleed and full flow steam agree with heat transfer calculations that indicate that about half of the steam entering the well during bleed flow is condensed in the well bore. We conclude that the chemical and isotopic composition of steam collected from this well and probably also from other wells on bleed is dominated by condensation and phase separation in the well and only full flow steam can be clearly related to field conditions.

References

Lipman, S. C., Strobel, C. J. and Gulati, M. S., 1978, Reservoir performance of The Geysers field: Proceedings, Larderello Workshop on Geothermal Resource Assessment and Reservoir Engineering, September 1977. Geothermics (in press).

Ramey, H. J., Jr., 1962, Wellbore heat transmission: Transactions AIME, v. 225, p. 427-435.

Truesdell, A. H., Nathenson, Manuel, and Rye, R. O., 1977, The effects of subsurface boiling and dilution on the isotopic compositions of Yellowstone thermal waters: Journal of Geophysical Research, v. 82, p. 3694-3704.

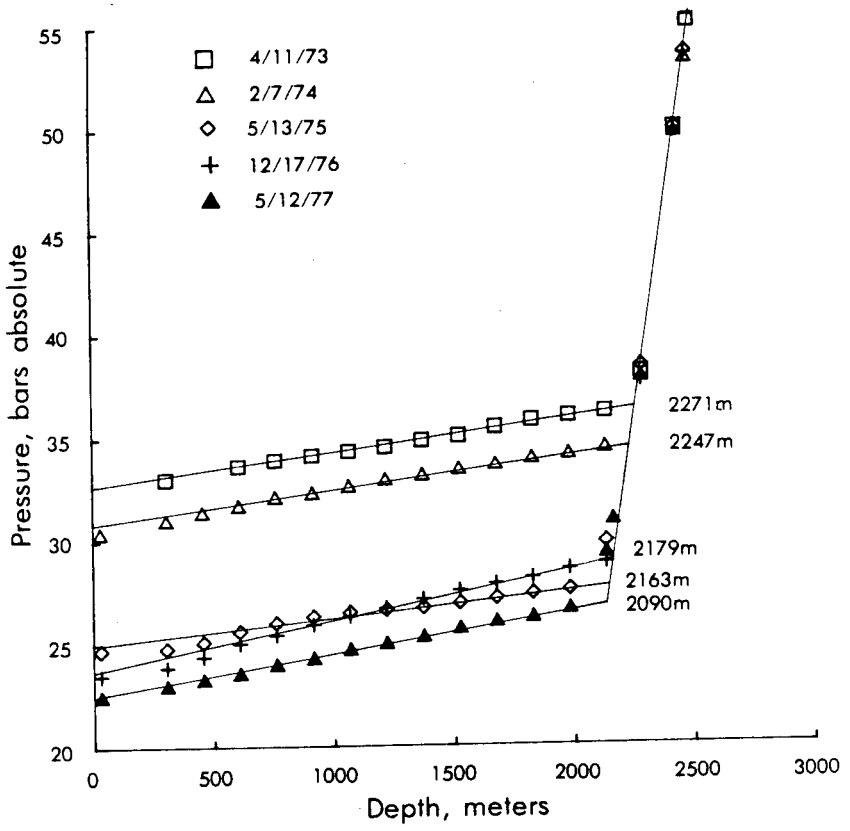

FIGURE 1 Downhole pressures measured from 1973 to 1977 in the Castle Rock steam well with position of water-steam interface indicated.

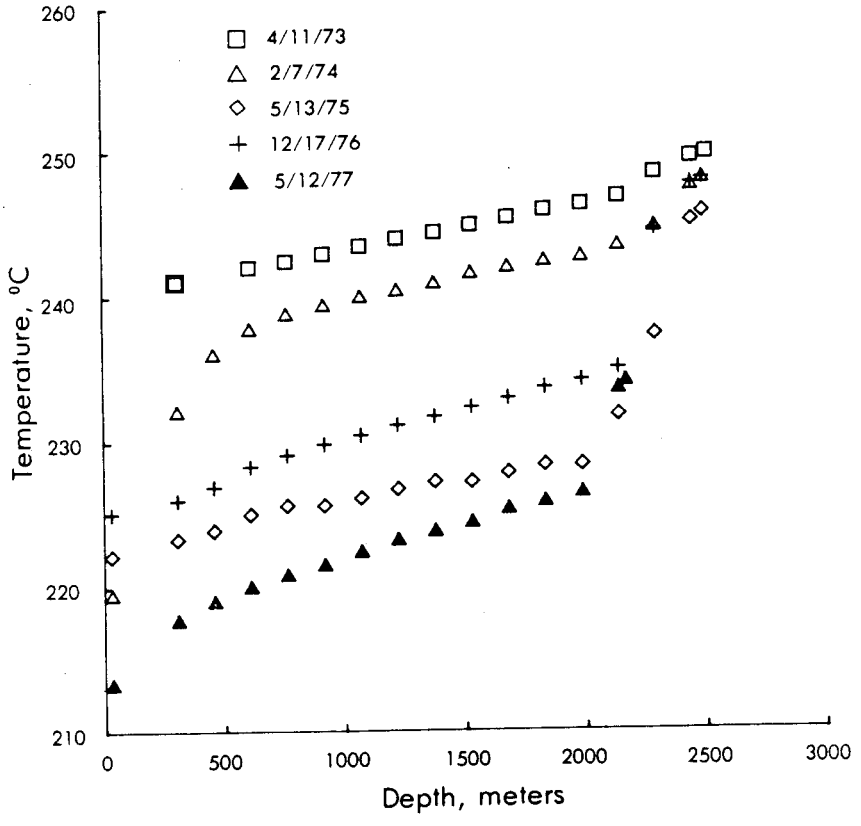

FIGURE 2 Down hole temperatures measured from 1973 to 1977 in the Castle Rock steam well.

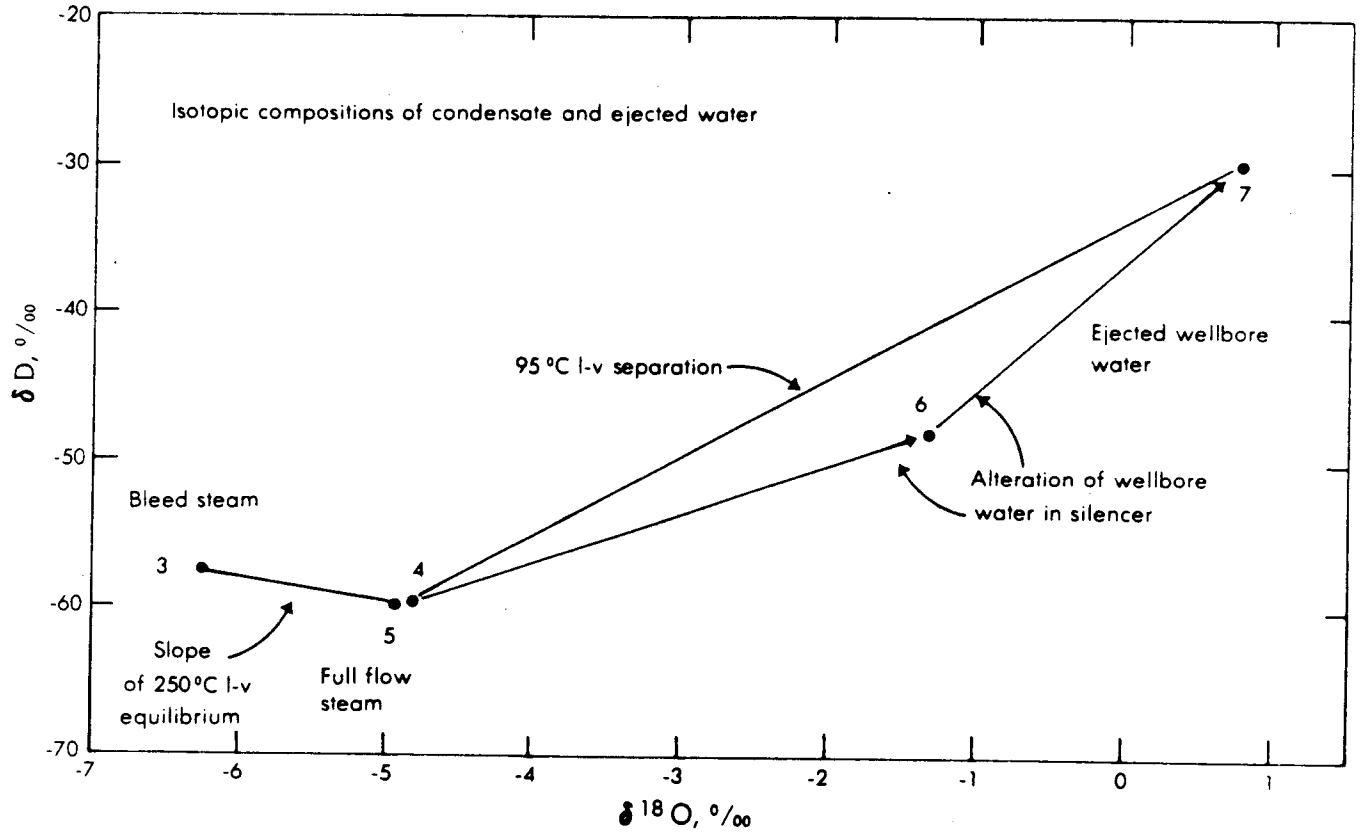

Figure 3 Oxygen-18 and deuterium compositions of bleed and full flow steam condensates and of ejected liquid water collected March 9, 1976 from the Castle Rock steam well with equilibrium slopes indicated for water-steam separation at reservoir and silencer temperatures.

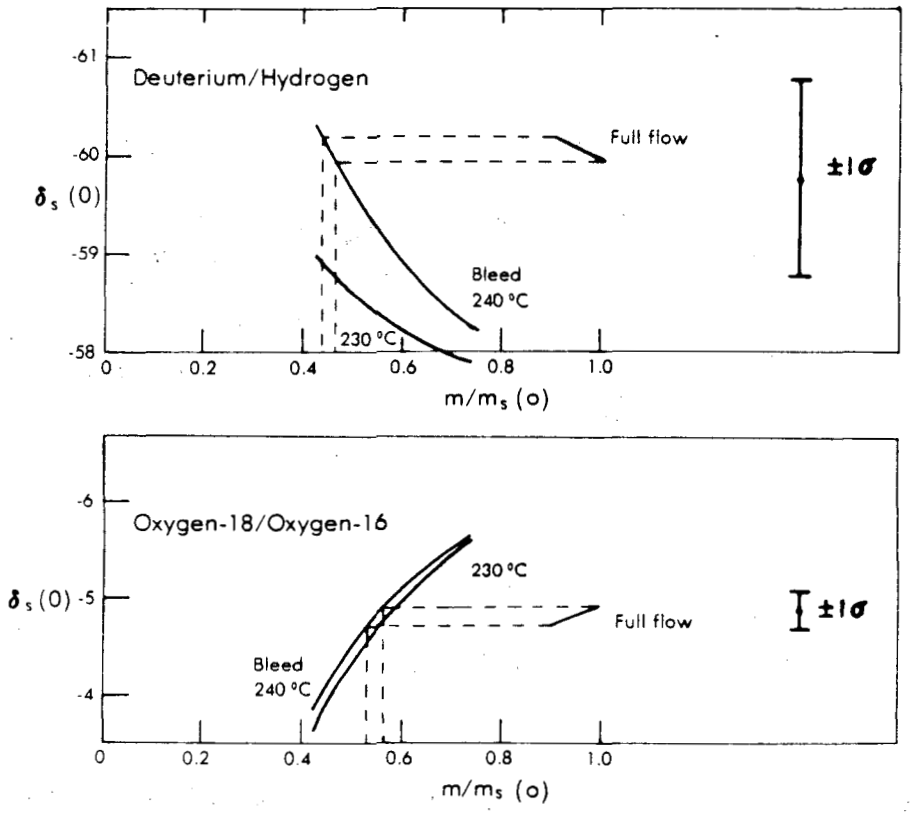

Figure 4 Isotopic compositions of source steam derived from measurements under full flow and bleeding conditions as a function of ratio of mass flow measured at the surface to input mass flow of saturated steam. Curves for bleeding flow calculated for two assumed temperatures of isotopic equilibration. Assuming the isotopic composition of feeding steam to be the same under full flow and bleed, a horizontal projection from the full flow values implies that the bleeding flow was only about 55% of the input steam flow. Standard deviations for deuterium and oxygen-18 measurements are shown on the figure.

Table 1. Chemical and isotopic analyses of steam condensate and ejected water from the Castle Rock Springs well (in mg/ℓ unless otherwise noted)

	Steam condensate			--	--	Ejected water	
Analysis	1	2	3	4	5	6	7
Data and time of collection	7/7/75	2 PM 3/9/76	3/9/76 12:30 PM	3 PM	5 PM	1 PM	4 PM
Well condition	flowing	10 cm orifice	2.4 cm orifice	10 cm orifice			
WHP bars gauge	--	--	25.6	5.2	5.2	5.2	5.2
pH	5.7	5.4	6.1	5.7	5.7	8.9	7.8
Ca	0.6	<0.1	0.1	<0.1	<0.1	1.8	2.9
Mg	0.2	<0.1	0.04	0.04	0.03	1.0	0.7
NH_4	10.6	<0.2	5	9	n.d.	n.d.	n.d.
Na	<0.5	<0.05	<0.5	<0.5	<0.5	18	71
K	<0.005	<0.05	<0.5	<0.5	<0.5	7.8	12
Li	n.d	n.d.	<0.01	<0.01	<0.01	0.12	0.6
Cl	24	52	7.1	10	10	7.1	18
F	0.01	<0.1	<0.1	<0.1	<0.1	0.5	3.7
HCO_3	28	22	95	46	38	64	162
SO_4	8.4	5	13(4)*	7.3	10(3)*	9	40
NO_3	0.4	1.7	n.d.	n.d.	n.d.	n.d.	n.d.
B	0.4	2.3	0.1	1.2	2.2	42	n.d
SiO_2	<0.3	0.4	4.3	4.3	4.3	46	80
H_2S	33	122	40	35	35	n.d.	n.d.
Hg (µg/ℓ)	n.d.	0.6	n.d.	n.d.	n.d.	n.d.	n.d.
$\delta^{18}O(H_2O)$	n.d.	n.d.	-6.26	-4.83	-4.95	-1.34	+0.75
$\delta D(H_2O)$	n.d.	n.d.	-57.5	-59.8	-60.1	-48.2	-29.8

Analysts: 1, 2 J. Muggee and D. Sarkaria, Aminoil USA, Huntington Beach, Calif.
3-7 Water chemistry; J. M. Thompson
^{18}O, D; N. L. Nehring and L.D. White } U.S. Geol. Surv., Menlo Park, Calif.

*sulfate in parentheses determined on samples with H_2S fixed in the field as CdS to prevent oxidation. H_2S analyses are also on these samples.

Table 2. Gas analyses of steam collected 3/9/76
Condensate includes dissolved gases.

Analysis #	1				2				3			
Time of coll.	12:30				3:00				5:00			
Orifice	2.5 cm				10 cm				10 cm			
gas phase/ condensate molal	1/2250				1/8580				1/8630			
gas/H_2O molal	1/1720				1/4300				1/4600			
	mole % in gas	moles/1000 moles in gas		H_2O total	mole % in gas	moles/1000 moles in gas	in cond	H_2O total	mole % in gas	moles/1000 moles in gas	in cond.	H_2O total
CO_2	93.4	0.42	0.11	0.53	92.2	0.11	0.093	0.20	94.4	0.11	0.078	0.19
H_2S	0.53	0.0024	0.022	0.024	0.22	2.6×10^{-4}	0.020	0.020	0.10	1.2×10^{-4}	0.020	0.020
H_2	4.5				4.4				3.5			
Ar	0.001				0.003				0			
O_2	0				0				0			
N_2	0.33				0.57				0.32			
CH_4	1.9				2.8				1.9			

Analyst: N. L. Nehring, U.S. Geol. Surv., Menlo Park, Calif.

FORMATION PLUGGING WHILE TESTING A STEAM WELL AT THE GEYSERS

Calvin J. Strobel
Union Oil Company of California
Santa Rosa, California

SUMMARY

During testing of a steam well at The Geysers steam field in Sonoma County, California, rate suddenly dropped by 17,500 lb/hr and wellhead pressure simultaneously increased by 30 psi. There was no evidence of plugging in any of the surface facilities downstream of the wellhead. Pressure buildup tests before and after the incident show that there was a 15% reduction in permeability-thickness. Analysis of pressure losses in the wellbore due to friction showed that all of the rise in wellhead pressure could be explained by the reduction in mass flow that occurred as a result of the 15% reduction in kh. The change in wellhead enthalpy from 1200 Btu/lb and 4°-5°F superheat prior to the incident to 1197 Btu/lb and 0-1.4°F superheat after the incident indicates the well became slightly wet. One possible explanation for this reduction in kh is that movement of free water caused a plugging action or a reduction of mobility to steam in one or more steam entries.

STATEMENT OF THE PROBLEM

On the first day of testing, the well was produced for 8.5 hours with a final rate of 195,640 lb/hr at 168 psig wellhead pressure. The following day this well was re-tested (see Table 1). After 5 hours, with the well producing 194,466 lb/hr at 174 psig, wellhead pressure suddenly jumped up 30 psi and rate dropped to 177,000 lb/hr. This was observed by personnel on site at the time. Inspection of test tube, orifice, throttling valve and muffler did not reveal any evidence of plugging. On the third day of testing, this well was re-tested at 172 psig wellhead pressure for 8.3 hours and final production rate was 171,000 lb/hr, indicating that there had been a permanent loss of about 13% in productivity. This test data is on Table 2.

Analysis of pressure buildup tests prior to and after the incident described above shows that there was a 15% loss in permeability-thickness, which is sufficient to account for all of the loss in productivity. The first buildup test, Figure 1, was done after flowing the well for 8.5 hours at 195,640 lb/hr on the first day of testing. The kh product calculated from this test was 75,000 md-ft. The loss in productivity occurred while flowing on the second day of testing, Table 1. A second buildup, Figure 2, was recorded after flowing for 8.3 hours at 171,000 lb/hr on the third day of testing, Table 2. The kh product calculated from this test was only 63,400 md-ft, 15% lower than what it was prior to the loss in productivity.

REASON FOR RISE IN FLOWING PRESSURE

Normally when wellhead pressure rises suddenly as rate drops off, plugging action downstream of the wellhead is commonly thought to be the cause. This case study shows that the same thing can happen in a steam well if there is a sudden plugging action in the the formation. Wellhead pressure rises because there is less friction drop at the lower rate. This was verified by friction drop calculations using the Cullender and Smith[1] equation. Results of this calculation, summarized below, show that friction loss dropped from 199 psi at the higher rate to 155 psi at the lower rate, and that static head (i.e. the gradient due to vapor density changes) increased from 34 psi to 38 psi for a net decrease of 40 psi in the vertical pressure gradient. The change in formation permeability caused bottomhole flowing pressure to be 10 psi lower at the lower rate. The 40 psi decrease in flowing pressure gradient was therefore reflected at the surface as a 30 psi rise in flowing wellhead pressure.

Rate lb/hr	Wellhead Pressure psig	Bottom Hole Pressure psig	Static Head psi	Friction Loss psi
194,466	174	407	34	199
177,027	204	397	38	155

POSSIBLE PLUGGING MECHANISM

Comparison of Tables 1 and 2 shows that prior to the loss in productivity the steam was superheated about 4°F with an enthalpy

1 Theory and Practice of the Testing of Gas Wells, (Oil and Gas Conservation Board, Calgary, Alberta, 1965) p. 146.

of 1200 Btu/lb, but after the loss in productivity the steam was only slightly superheated or just at saturation with an enthalpy of 1200 Btu/lb, slightly lower than before. The sudden change in enthalpy along with the reduction in reservoir permeability strongly suggests that water influx may have caused a reduction in mobility to steam at one or more steam entries.

TABLE 1

SECOND FLOW TEST

Time min	Wellhead Pressure psig	Enthalpy Btu/lb	Superheat °F	Rate lb/hr
70	182	1201	4	185,571
85	188	1201	3.4	174,265
115	172	1199	3.3	196,026
145	172	1199	3.3	196,026
175	172	1199	3.3	196,522
220	172	1200	4.3	195,624
280	174	1200	3.4	194 446
310	204	1203	5.0	177,027

TABLE 2

THIRD FLOW TEST

Time min	Wellhead Pressure psig	Enthalpy Btu/lb	Superheat °F	Rate lb/hr
75	173	1197	0	174,460
150	172	1197	1.4	173,429
240	172	1197	1.4	172,543
360	172	1197	0.4	170,903
480	174	1197	-0.5	171,137

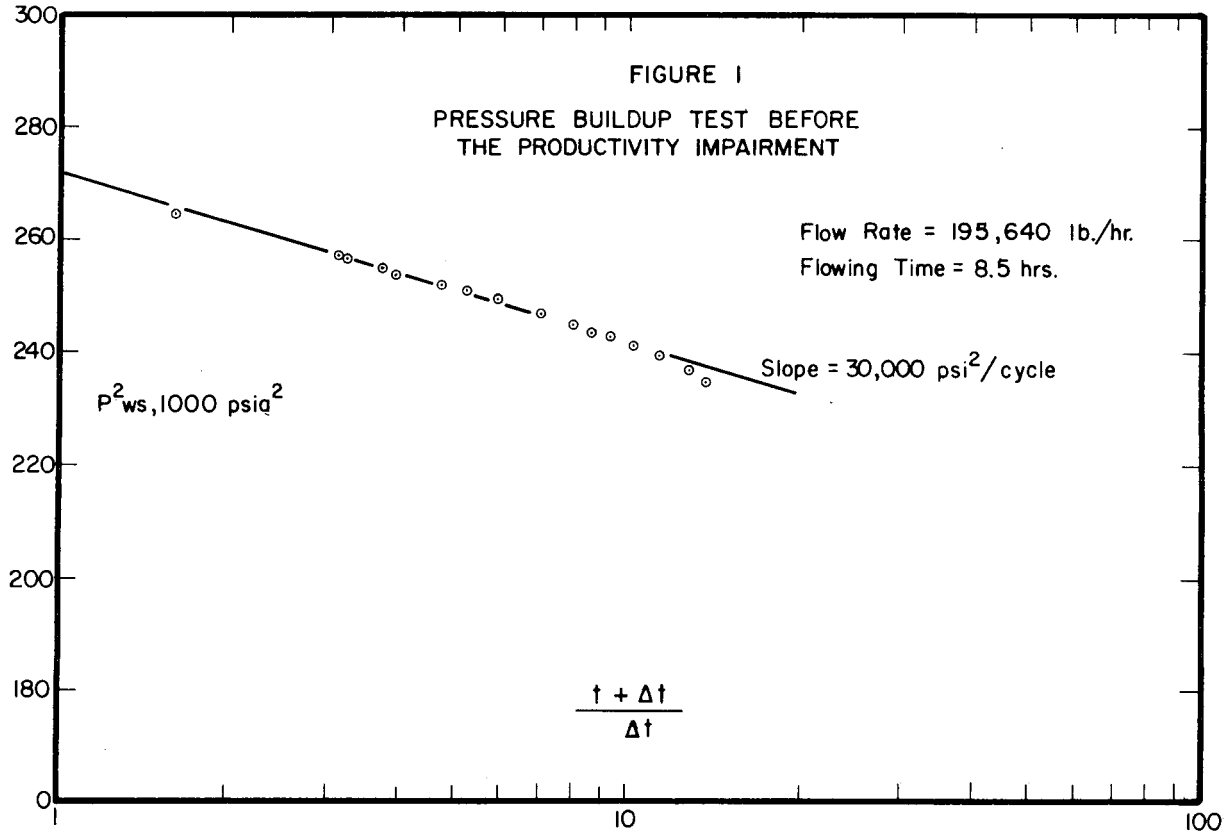

FIGURE 1

PRESSURE BUILDUP TEST BEFORE THE PRODUCTIVITY IMPAIRMENT

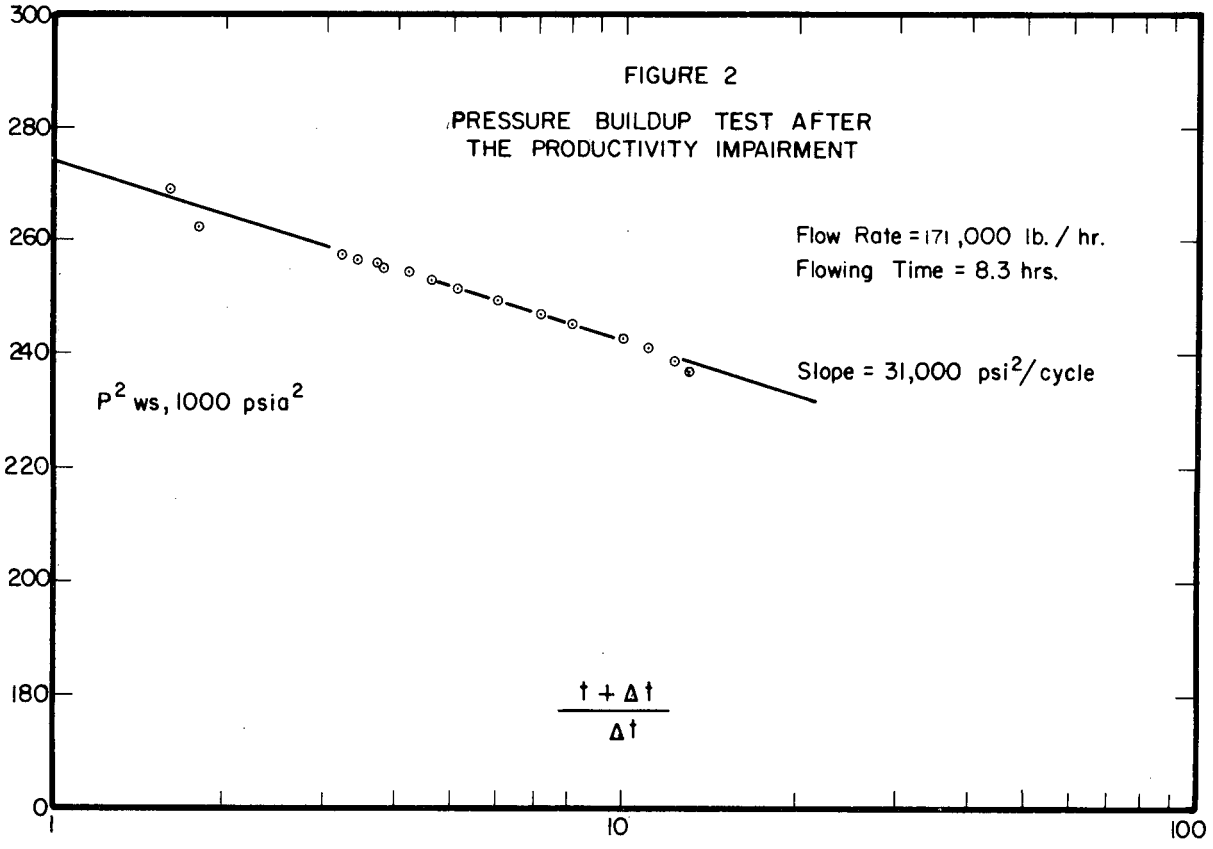

FIGURE 2

PRESSURE BUILDUP TEST AFTER THE PRODUCTIVITY IMPAIRMENT

THE EFFECT OF THERMAL CONDUCTION UPON PRESSURE DRAWDOWN AND BUILDUP IN FISSURED, VAPOR-DOMINATED GEOTHERMAL RESERVOIRS

A. F. Moench
U.S. Geological Survey
Water Resources Division
345 Middlefield Road
Menlo Park, CA 94025

Introduction

An analysis of steam-pressure behavior in a vapor-dominated geothermal reservoir with an immobile vaporizing liquid phase was presented by Moench and Atkinson (1977) at the Third Stanford Workshop on Geothermal Reservoir Engineering, and later expanded by Moench and Atkinson (1978). In that study a finite-difference model was used to demonstrate the effects of phase change in the reservoir upon pressure drawdown and buildup. In this paper that model is modified to incorporate heat transfer from blocks of impermeable rock to thin, highly-permeable, porous fissures. The purpose of this study is to demonstrate the added effect of heat transfer of this type upon the transient pressure response of a vapor-dominated geothermal reservoir.

Hypothetical Model

In the present study the vapor-dominated reservoir is assumed to be composed of a random assortment of highly permeable, porous fissures separated by blocks of impermeable rock, as illustrated in figure 1a. The fissures and blocks are initially at the same constant temperature throughout. With the onset of well discharge, pressure reductions induce vaporization of liquid water within the fissures. The resulting temperature decline induces transfer of heat by conduction from the adjacent blocks.

In order to make the problem mathematically tractable, the conceptual model is idealized as shown in figure 1b. Alternating layers of fissures and blocks of constant thickness are assumed to extend in the radial direction to infinity. The thickness of the impermeable block is assumed to represent the average thickness of the blocks in the actual reservoir. The fissures are assumed to be filled initially with a uniform distribution of liquid water and steam at a fixed saturated-vapor pressure. The initial water content of the fissure is sufficiently low that changes in saturation do not appreciably change the permeability to steam. Well discharge and fissure permeability, porosity, and thermal properties are assumed constant to simplify interpretation of the results.

It is also assumed, as in the model of Moench and Atkinson (1978), that steam and liquid water in the fissure are in local thermal equilibrium with the solid material in the fissure and that effects of vapor-pressure lowering are negligible. Effects of the latter type were considered by Moench and Herkelrath (1978).

Approach

Theoretical equations for the flow of steam through porous reservoirs in the presence of immobile vaporizing or condensing liquid water are given by Moench and Atkinson (1978). In that study it was assumed that the only temperature changes to occur in the reservoir are those due to vaporization or condensation. In this analysis temperature changes are also assumed to occur in response to heat conduction from impermeable rocks bounding permeable fissures. Moreover, in the approach that follows it is assumed that the temperature distribution across the fissure is constant and that smoothly varying temperature changes can be approximated by step changes.

The finite-difference model of Moench and Atkinson (1978) computes temperature changes at each node. These time-varying temperature changes are used to compute the flux of conductive heat normal to the fissure, at the boundary between fissure and block. A convolution equation for this calculation was derived using an analytical expression for temperature response in a slab of finite thickness, insulated at one end, and subject to an instantaneous change in temperature at the other (Carslaw and Jaeger, 1959, p. 97).

Calculated heat conduction to or from the fissure is averaged over the width of the fissure and put into the energy equation as a source term for calculation of the necessary temperature changes. Values of the thermal conductivity and diffusivity used in the analysis are given in table 2. Computation of the distributions of pressure, temperature, and saturation is carried out in the manner described by Moench and Atkinson (1978).

Results

Figure 2 shows computed dimensionless pressure drawdown (P_D vs. log t_D) in the producing well with and without effects of thermal conduction. As shown previously by Moench and Atkinson (1977), pressure drawdown is delayed in time over that expected for a noncondensable gas. This delay depends upon the initial liquid-water saturation and upon the heat capacity of the reservoir rock. In figure 2 the exponential integral solution for noncondensable gas is shown for comparison to illustrate the delay. Parameters used are listed in table 1. Heat conduction is computed for a block of infinite thickness. The addition of heat to the producing fissures can be seen to cause only a slight decrease in the rate of pressure decline at large times.

Figure 3 shows computed dimensionless pressure buildup in the production well as influenced by heat conduction from a block of infinite thickness. As explained by Moench and Atkinson (1977), pressure buildup exhibits an anomalous plateau caused by condensation in the reservoir near the well. In the examples shown by Moench and Atkinson (1977), obtained without the influence of heat conduction, the shape of the recovery curve is independent of production time for a radially ininfinite system. An example is shown in figure 3 for comparison. Figure 3 shows that the greater the production time the higher the computed pressure plateau when heat conduction is included.

Figures 4 and 5 illustrate the effect of heat conduction from blocks of finite thickness upon computed pressure buildup. Figure 4 shows that increased production time causes no further shift in the computed pressure buildup. Figure 5 shows the effect of various block thicknesses upon pressure buildup after a large production time. Thicker blocks are able to supply more heat and hence able to shift the pressure plateau to a higher level than thinner blocks.

Liquid-water saturation in the fissure near the wellbore increases to the value it had prior to production if pressure buildup is allowed to continue indefinitely. Figure 6 shows the effect of thermal conducting layers of different thickness upon the rate of saturation recovery. The rate of recovery in the case of no conduction is shown for comparison. The thicker the impermeable block, the longer it takes for the liquid saturation to recover fully.

The liquid-saturation distribution at different times during production is shown in figure 7 under conditions with and without conduction. At early times the effect of conduction is negligible but with the passage of time the shape of the saturation distribution curve changes as thermal conduction becomes significant. Conduction of heat into the fissure tends to steepen the saturation distribution.

Conclusions

It has been shown that the conduction of heat into highly permeable fissures from blocks of impermeable rocks might have a significant effect upon the pressure transient behavior of wells in vapor-dominated geothermal reservoirs. The effect upon drawdown is to bring about a slight decrease in the rate of pressure decline. The effect upon pressure recovery is more profound as the heat input brings about a significant shift in the location of the condensation plateau. Conduction of heat also steepens the saturation profile in the flashing zone and decreases the rate of condensation in the vicinity of the wellbore.

References

Carslaw, H. S., and Jaeger, J. C., 1959, Conduction of Heat in Solids: Oxford at the Clarendon Press, London.

Moench, A. F., and Atkinson, P. G., 1977, Transient-pressure analysis in geothermal steam reservoirs with an immobile vaporizing liquid phase-summary report: Proceedings of the Third Workshop on Geothermal Reservoir Engineering, Stanford University, Stanford, Calif., Dec. 14-16.

Moench, A. F., and Atkinson, P. G., 1978, Transient-pressure analysis in geothermal steam reservoirs with an immobile vaporizing liquid phase: Geothermics (in press).

Moench, A. F., and Herkelrath, W. N., 1978, The effect of vapor-pressure lowering upon pressure drawdown and buildup in geothermal steam wells: Transactions, Geothermal Resources Council Annual Meeting, Hilo, Hawaii, July 25-27, p. 465-468.

Table 1. Notation

P_D (dimensionless pressure) $= \frac{\pi k h M_w}{q \mu Z_i \bar{R} T} (P^2_i - P^2)$

t_D (dimensionless time) $= \frac{k P_i t}{\phi \mu r_w^2}$

r_D (dimensionless distance) $= r/r_w$

r radial distance

r_w well radius

q production rate

P pressure

P_i initial pressure

k permeability

h fissure thickness

t time

R gas constant

T temperature

μ steam viscosity

K thermal conductivity of impermeable block

α thermal diffusivity of impermeable block

ℓ thickness of impermeable block

S liquid-water saturation (percent of void space)

S_i initial liquid-water saturation

t_0 production time

Δt time since shut in

Z_i initial compressibility factor

M_w molecular weight of water

ϕ porosity

Table 2. Values of Parameters Used

P_i	30×10^6 dynes/cm^2	ϕ	0.10
k	10×10^{-8} cm^2	T	507 K
K	1.67×10^5 dyne/(°C s)	S_i	0.10
α	8.4×10^{-3} cm^2/s	ρ_s	2.3 g/cm^3
h	100 cm	$c_{\rho s}$	9.6×10^6 dyne-cm/(g°C)
q	6.94×10^3 g/s	r_w	100 cm

NOTE: Remaining parameters are known properties of water at prevailing temperature and pressure

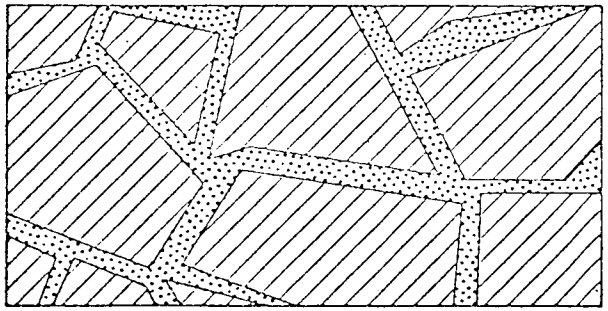

A.

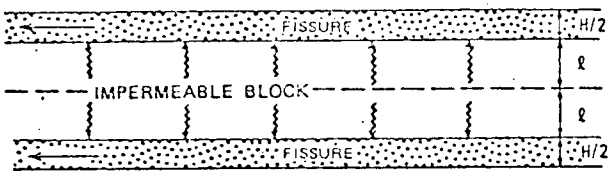

B.

Figure 1. Vapor-dominated geothermal reservoirs

A. Hypothetical fractured reservoir composed of porous fissures and impermeable blocks

B. Idealized block and fissure reservoir used in the model

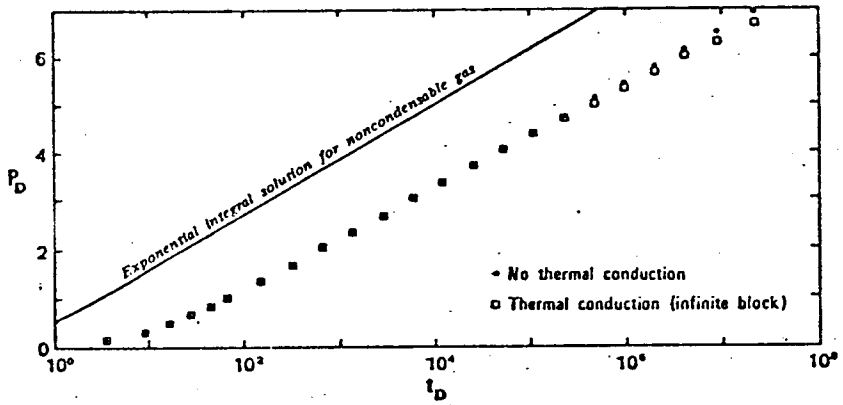

Figure 2. Pressure drawdown in producing well with and without thermal conduction

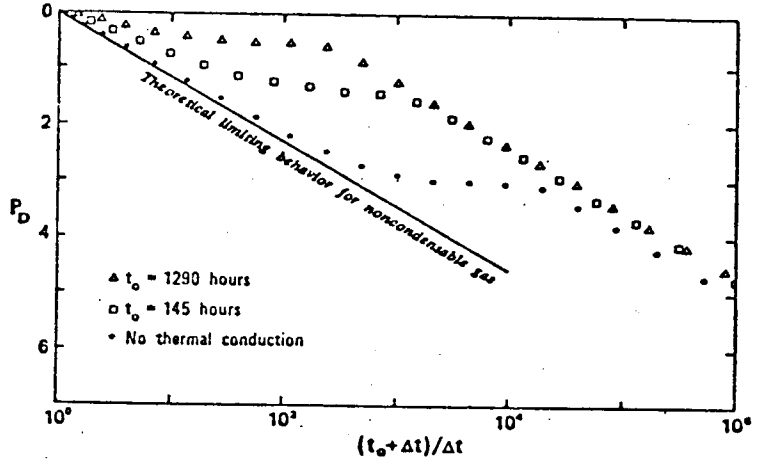

Figure 3. Pressure buildup after different production times — fissure bounded by conducting layers of infinite thickness

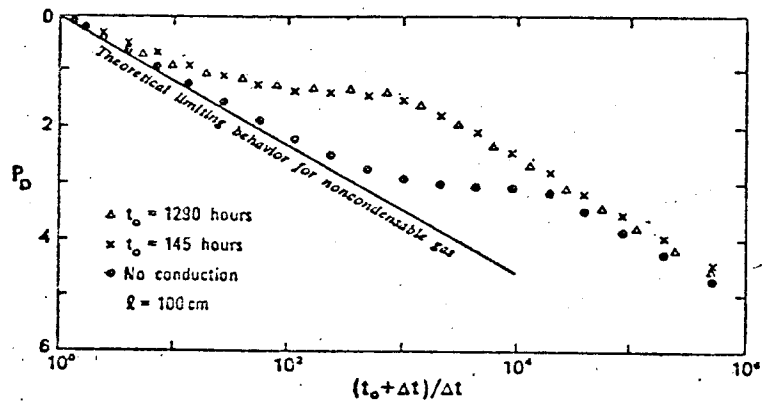

Figure 4. Pressure buildup after different production times — fissure bounded by conducting layers of finite thickness

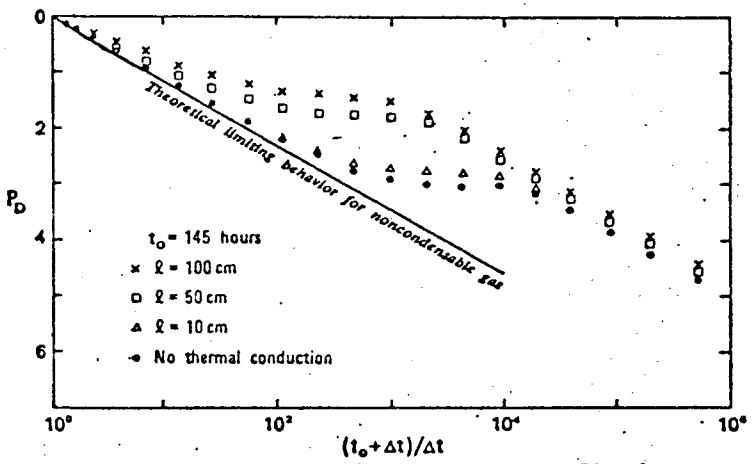

Figure 5. Pressure buildup after a fixed production time — fissure bounded by conducting layers of different thicknesses

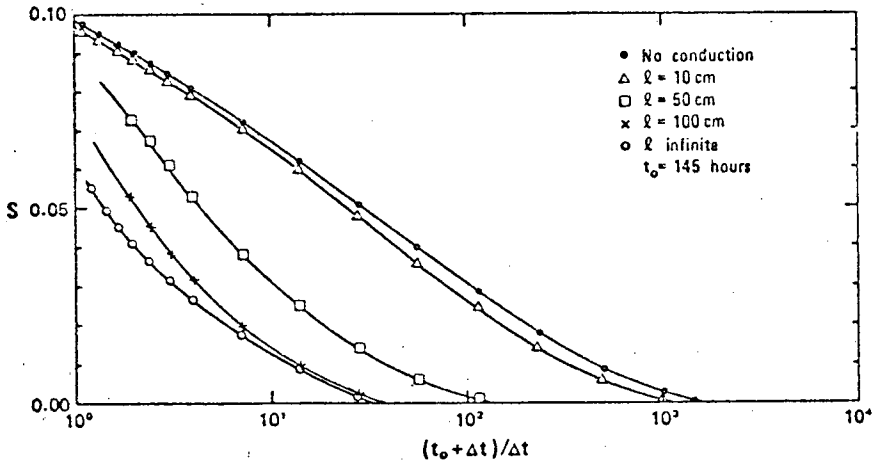

Figure 6. Saturation buildup near well bottom — fissure bounded by conducting layers of different thicknesses

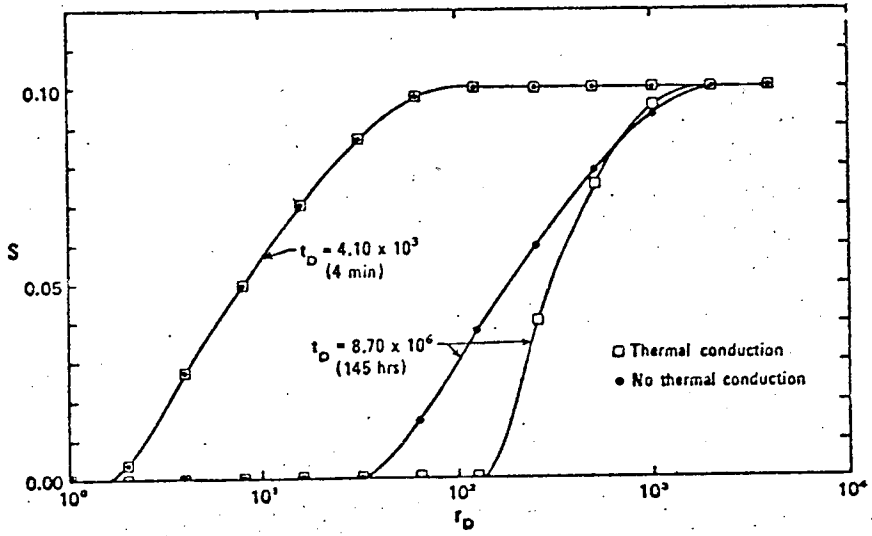

Figure 7. Radial saturation distribution at different times with and without thermal conduction

Dup

EVALUATION OF COSO GEOTHERMAL EXPLORATORY HOLE NO. 1 (CGEH-1) COSO HOT SPRINGS KGRA, CHINA LAKE, CA

C. Goranson, R. Schroeder, and J. Haney
University of California
Lawrence Berkeley Laboratory
Berkeley, California 94720

The well CGEH-1 (Coso Geothermal Exploratory Hole No. 1) was drilled at the China Lake Naval Weapon Center under the supervision of DOE/NVO and CER Corporation by Big O Drilling Company. They started drilling on 2 September 1977 and completed the well on 1 December 1977 to 4845 feet. The well is an exploratory hole to determine geological and hydrothermal characteristics of the Coso Hot Springs KGRA. During drilling, numerous geophysical and temperature surveys were performed to evaluate the geological characteristics of CGEH-1. LBL performed eight temperature surveys after completion of the well to estimate equilibrium reservoir temperatures. Downhole fluid samples were obtained by USGS and LBL, and a static pressure profile was obtained.

Two flow tests were attempted in 1978. The first test began September 5, 1978 used nitrogen stimulation to initiate flow, but resulted in small flow and subsequent filling of the bottom hole with drill cuttings. The second test, on November 2, 1978, utilized a nitrogen-foam-water mixture to clean residual particles from bottom hole and nitrogen was then used to stimulate the well. The well again was dry after stimulation. Water influx was calculated at 4-5 gal/min as the well filled after unloading of the wellbore.

Figure 1 shows the location of Coso Hot Springs. Figure 2 illustrates the location of CGEH-1 relative to heat flow contours obtained by ARPA (Advanced Research Projects Agency) and DOE heat flow holes. Numerous geological and geophysical studies were performed (1-18) prior to the drilling of CGEH-1. However, the geological characteristics of the Coso area are rather complex. This is illustrated in the aforementioned references. The area consists essentially of a ring fracture zone located in the basin and range province east of the Sierra Nevada range (19). Figure 3 illustrates generalized alteration, geophysical characteristics, and active thermal areas in the Coso Hot Springs area.

WELL COMPLETION--CGEH-1

The drill site is on rhyolite pyroclastic debris covering a granite complex. Rhyolite dikes intrude and are probably contemporaneous with the extruded rhyolite domes in the vicinity. Faults and fracture zones had a strong influence in hole direction and penetration rates. Figure 4 shows the surface projected horizontal deviation of the well. Maximum horizontal displacement was calculated to be 375 feet at S70° 20'W. As shown in the figure, three large meanders in the wellbore occurred during drilling. Final bottom hole vertical depth is approximately 4815 feet (total drilled depth, 4845).

Figure 5 is a synopsis of the completion record. Three large mud losses occurred along the cased portion of the well (CGEH-1 is cased to 3488 feet). An influx of water at a rate of 90 BPH was observed at about 1900 feet. Above this zone, at about 1660 feet, running clay and gravel entered the wellbore. The gravel was subangular and the clay is actually powdered granite with clay-sized particles. Numerous mud losses occurred below 3500 feet. However, it is not known whether this mud went into the fractured zone near 3500 feet or if other fractures intersect the well below this point.

THERMAL EQUILIBRIUM PERIOD, December 1977--September 1978

LBL performed eight temperature surveys (21) before the first flow test. The final recorded maximum temperature was 382°F at 1900 feet. The water level varied, but was found at approximately 890 feet. Figure 6 shows five of eight temperature surveys. The figure illustrates that zones above 3500 feet (1900, 2700, 3500 feet) where large mud losses occurred during drilling show atypical temperature distribution indicating that the formation was cooled from mud entry. However, zones below 3500 feet where numerous mud losses are observed do not illustrate this abnormal behavior. This seems to indicate that the mud losses below 3500 feet probably entered the large fracture zone above 3500 feet and not into fractures below the portion of the well that was subsequently cased. However, there was a large mud loss at T.D.

Downhole chemical samples (21) of wellbore fluid were also obtained during this initial equilibrium period. Dissolved silica concentrations from bottom hole sampels indicate a temperature of 338°F (201/mb/1). Silica temperatures at 2740 feet were calculated to be 194°F (40 mb/1).

The cause of these discrepancies is unknown. However, the drill pipe was stuck at 3488 for a short period. Pipe release and diesel fuel were added to free the drill bit. The presence of residual organics in the wellbore might explain low silica concentrations observed at the 2700 foot depth. (23)

FLOW TEST 1

The first extended flow test was carried out September 5 to 8, 1978. During the well stimulation and subsequent flow the wellhead temperature was 262.5°F (128°C) and the discharge tube temperature was 250°F (123°C). This occurred during the nitrogen lift at 300 CFM of heated N_2 with the tube at 2060 feet. The nitrogen flow rates were varied as the tube was lowered to the final depth, 4590 feet. When the nitrogen was shut off, the flow decreased to nearly atmospheric pressure at the discharge tube within one-half hour. The wellhead temperature dropped at 95°C at this point. Within five minutes of shutting off the nitrogen, the flow had decreased appreciably. The well was then pressured with 2000 psi pressure at the nitrogren truck for one-half hour. At this time, the tubing was terminated at 4590 feet downhole. The wellhead pressure at this time was 370 psi and nitrogen was pumpted at 200 cfm. The well was open and unloaded an unknown quantity of water, then died. An attempt was made to find a liquid level with the N_2, but the attempt was unsuccessful. The N_2 tubing was then lowered to 4700 feet but no nitrogen returns were observed and the nitrogen pressure reached 3000 psi. When the tubing was removed, the lower 250 feet of tubing was plugged with sand and clay. At this point the flow testing was terminated.

FLOW TEST 2

The second flow test utilized a nitrogen-foam-water mixture to clean the bottom portion of the well below 4700 feet. The well cleanup and stimulation began on November 5,1978 by injecting foam at 1000 feet and slowly lowering the injection tube while continuing to pump foam. Good returns were obtained during the descent. A wellhead sample of the foam was taken for analysis. The sample showed large amount of grey clay-like material entrained in the foam. Subsequent analysis by R. Clark (DOE/NVO) indicated that the material was fine

powdered granite, not clay. At this point over 100 feet of material was being circulated out of the well, but further progress was not possible due to an obstruction at 4695 feet. An attempt was made to withdraw the tubing, but it could only move a maximum of about 60 feet upward. The tubing moved freely downward, but could not be withdrawn more than about 60 feet upward. The tubing was worked up and down a few times and finally came free. However, when it came to the surface there was about 145 feet that had been left in the well.

During the cleanout procedure, fluid samples were taken from a tube at the wellhead using a high-pressure needle valve for metering. This valve was subsequently plugged with sand grains brought up with the foam. The sand was retained as a sample of the material removed from the well. Before removing the nitrogen injection tube, the well was cleaned to 4695 feet by circulating a water-foam mixture for four hours. After four hours, the well was cleaned by pumping clean water for one hour followed by nitrogen until the well reached its maximum flowing temperature and pressure at the critical discharge tube. The nitrogen was shut in and the well flowed for less than five minutes, after which the temperature and flow decreased rapidly. The wellhead temperature was 95^{o}C and flow was essentially pure steam. After the nitrogen tube was brought to the surface a different end was made up to try to pass the blockage at 4695 feet. The well was again foamed (this time at 3500 feet) and the tubing was lowered after returns were obtained. The tubing encountered a block at 4490 feet. The well was again cleaned and stimulated with nitrogen. The well again died in less than five minutes after stimulation. The nitrogen was then pumped at 3000 psi with the wellhead shut in for about 15 minutes. The 2" and 4" discharge tubes were then opened. No show of water was seen, only nitrogen. No subsequent show of water was found with the well open for 12 hours. A water-level tool was then used to monitor the position of the water level in the well. The water level was first found at 3645 feet. This was about 23 hours after the final pressurization and flow of the well, and 12 hours after shutting in the well. This is an average increase in water level of about 1.3 ft/min $\simeq$ 4 gal/min. The water level was subsequently monitored closely and it was seen that the time required for the water level to rise 1 foot was <u>decreasing</u> slightly as the height of the water column increased. This continued

up to 3460 feet, at which time the rate of filling began to decrease. Since the latter depth is approximately the depth to which the well is cased, we are forced to conclude that the well was not filling from the bottom, but instead the water was coming from the well annulus at the bottom of the casing. Following the well fill-up measurements, the testing was terminated.

CONCLUSIONS

The well was drilled in very hard rock. It was extremely difficult to prevent drill bit wandering, and the final bottomhole location is ∿ 374 feet (horizontal) from the wellhead location with three serious meanders (see Figure 1). During the monitoring of the thermal equilibration, at least 15 downhole surveys were run over a period of about 10 months. Our final surveys, before the workover began, indicated considerable friction below the casing. During the cleanout the nitrogen tubing was broken with a piece apparently lodged between 4490 and 4635 feet. This suggests that the well is currently unuseable at the present time below about 4000 feet due to either cable and wireline cuts in the uncased curved well, fractures which have been opened during the downhole activity, or opening of a fracture during drilling. (The drill bit was stuck temporarily at 4771 feet.) [20] Since the well had about 200 feet of fill, and since the flow seems to come down the wellbore, the tension could also have been due to a sticky layer of clay (powdered granite) in the well. It is not likely that there are serious cable grooves below 4500 feet, and the origin of the fill is unknown, hence it is likely that the tubing was stuck in a fracture.

During drilling there were several circulation losses while using mud. The deepest circulation loss occurred at bottomhole, where more than ∿ 1400 bbls (∿ 59,000 gals) of mud was lost, as shown in Figure 5. This large quantity of mud, plus the material added to the mud to prevent further losses to the fracture, make production from this zone questionable. The apparent lack of significant influx from the lower zone (recall that the maximum influx during well fill-up after cleanout was about 5 gals/min) leads us to conclude that the lower zone is not of significant interest for production of geothermal fluids at this time. When the temperature log is examined, the bottomhole can be seen to be about 40°F cooler than the zones which are about half as deep.

The well was cased to about 3500 feet. The largest mud losses during drilling occurred in the zone adjacent to the casing shoe, i.e., in the zone from 3260 to 3500 feet, as shown in Figure 2.[20] In this zone, up to 4000 bbls (168,000 gals) of drilling mud and lost circulation material was lost (note that this follows only if the mud losses while drilling from 3600 to ∿ 4500 feet are all assumed lost in this interval). This zone shows up as a broad temperature depression in the temperature logs taken during thermal equilibration of the well as shown in Figures 5 and 6. It is likely that this zone is contributing the 3-6 gpm of influx that fills the well when the latter is emptied during the flow tests. The mud lost in this zone has a volume equal to about 20,000 ft^3. Assuming an effective porosity of 10 percent we have a damage radius which is at least 17 feet. If this zone contributes all of the flow to the well, the head is 3260-900 = 2360 ft. = 1015 psi. At ∿ 385°F this is well above the saturation curve for pure water, and implied that the fluid source is liquid, not steam. The chloride content of the well was the same as that at Coso Hot Springs.[14] The pieziometric head at both Coso Hot Springs and CGEH-1 is approximately 3500 feet about sea level.

While the mud losses are not quite so enormous in the two zones about 3200 feet they are still appreciable. One fracture was encountered at ∿ 2750 feet where more than 2100 bbls (∿ 88,000 gals) of mud and various materials were lost during drilling. The shallowest and hottest zone was at 2060 feet, where more than 900 bbls (37,800 gals) were lost. It is also noteworthy that at 1900 feet a water influx of at least 60 gpm occurred while drilling under pressure with air. A switch to mud was made at that point, hence there is no indication of how much the formation could flow from that zone.

Several water samples have been taken during the course of the well equilibration and during the well tests. These water samples probably came from the zone near the bottom of the casing. It is also likely that there has been contamination of the fluid samples by drilling mud and other foreign material. It is unlikely that we have sampled the uncontaminated reservoir fluid. On the other hand, it is

equally unlikely that the source of fluid near CGEH-1 is at an appreciably higher temperature than observed in this well (< 390°F). All of the sand, clay, and fluid samples that were taken during the recent work are being held at LBL.

Although numerous problems were encountered during the drilling of CGEH-1, it has proved valuable in the initial hydrogeological evaluation of the Coso Hot Springs area. Further drilling in the area is necessary to provide a more complete evaluation, and the Coso Hot Springs KGRA shows promise for development of power production or direct heat utilization.

ACKNOWLEDGEMENTS

We wish to thank many people for their assistance during these studies. In particular, R. Clark (DOE/NVO) has provided valuable suggestions, corrections, and encouragement. The work could not have been completed without the assistance of the NWC geothermal group or Captain R. Wilson (USN).

REFERENCES

1 Austin, C.F., Austin, W.H., Jr., and Leonard, G.W., 1971, Geothermal science and technology--a national program: Naval Weapons Center Tech. Ser. 45-029-72, 95 pp.

2 Austin, C.F., and Pringle, J.K., 1970, Geologic investigations at the Coso thermal area: Naval Weapons Center Tech. Pub. 4878, 40 pp.

3 Chapman, R.H., Healey, D.L., and Troxel, B.W., 1973, Bouguer Gravity Map of California, Death Valley Sheet: California Division Mines and Geology, Scale 1:250,000.

4 Combs, J., 1975, Heat flow and microearthquake studies, Coso Geothermal Area, China Lake, California: Final Report to Advanced Research Projects Agency, ARPA Order No. 2800, Contract No. N00123-74-C-2099, 65 pp.

5 Combs, J., and Rotstein, Y., 1976, Microearthquake studies at the Coso Geothermal Area: in Proceedings of Second United Nations Symposium on the Development and Use of Geothermal Resources, in press.

6 Duffield, W.A., 1975, Late Cenozoic ring faulting and volcanism in the Coso Range area of California: Geology, v.3, p. 335-338.

7 Frazer, H.J., Wilson, H.B.D., and Hendry, N.W., 1943, Hot springs deposits of the Coso Mountains: California Jour. Mines and Geol., v. 38, p. 223-242.

8 Furgerson, R.B., 1973, Progress report on electrical resistivity studies, Coso geothermal area, Inyo County, California: Naval Weapons Center Tech. Pub. 5497, 38 pp.

9 Godwin, L.H., Haigler, L.B., Rioux, R.L., White, D.E., Muffler, L.J.P., and Wayland, R.G., 1971, Classification of public lands valuable for geothermal steam and associated geothermal resources: U.S. Geol. Survey Circ. 647, 18 pp.

10 Koenig, J.B., Gawarecki, S.J., and Austin, C.F., 1972, Remote sensing survey of the Coso geothermal area, Inyo County, California: Naval WEapons Center Tech. Pub. 5233, 32 pp.

11 Lanphere, M.A., Dalrymple, G.B., and Smith, R.L., 1975, K-Ar ages of Pleistocene rhyolitic volcanism in the Coso Mountains, California: Geology, v. 3, p. 339-341.

12 Teledyne Geotech, 1972, Geothermal noise survey of the Coso Hot Springs area, Naval Weapons Center, China Lake, CA: unpublished Technical Report No. 72-6 produced under contract for the Naval Weapons Center, 18 pp.

13 Hulen, J.B., 1978, Geology and alteration of Coso Geothermal area, Inyo County, California, UURI-ESL Report DOE Contract EG-78-C-07-1701.

14 R.M. Gailbraith, Geological and Geophysical Analysis of Coso Geothermal Exploratory Hole No. 1 (CGEH-1), Coso Hot Springs KGRA, California, May 1978. UURI-ESL Report.

15 Fox, R.C., 1978a, Dipole-dipole resistivity survey of the Coso Hot Springs KGRA, Inyo County, California, UURI-ESL Report.

16 Fox, R.C., 1978b, Low-altitude aeromagnetic survey of the Coso Hot Springs KGRA, Inyo County, California, UURI-ESL Reprot.

17 Le Shack, L.A., 1977, Preliminary 2-meter temperature map 22-23 September, Coso, California: Development and Resources Transportation ERDA Contract No. EG-77-C-01-4021.

18 Roquemore, G. R., 1978a, Active faults and related seismicity of the Coso Mountains, Inyo County, California: Seism. Soc. America Earthquake Notes, v.49, no.1, p.24.

19 Roquemore, G.R., 1978b, Evidence for basin and range/Sierra Nevada transitional zone structures in the Coso Mountains, California: Geol. Soc. America Abstracts w/programs, v. 10, no.3, p. 144.

20 Coso Geothermal Exploratory Hole No. 1, CGEH No. 1, Completion Report, March 1978. NVO 0655-04.

21 State Downhole characteristics of Well CGEH-1 at Coso Hot Springs, California, June 1978. LBL-7059, C. Goranson, R. Schroeder.

22 Combs, J. February 1978, Geothermal exploration techniques: A case study. University of Texas at Dallas, EPRI, ER-680 project 375. Final Report pps. 27-65.

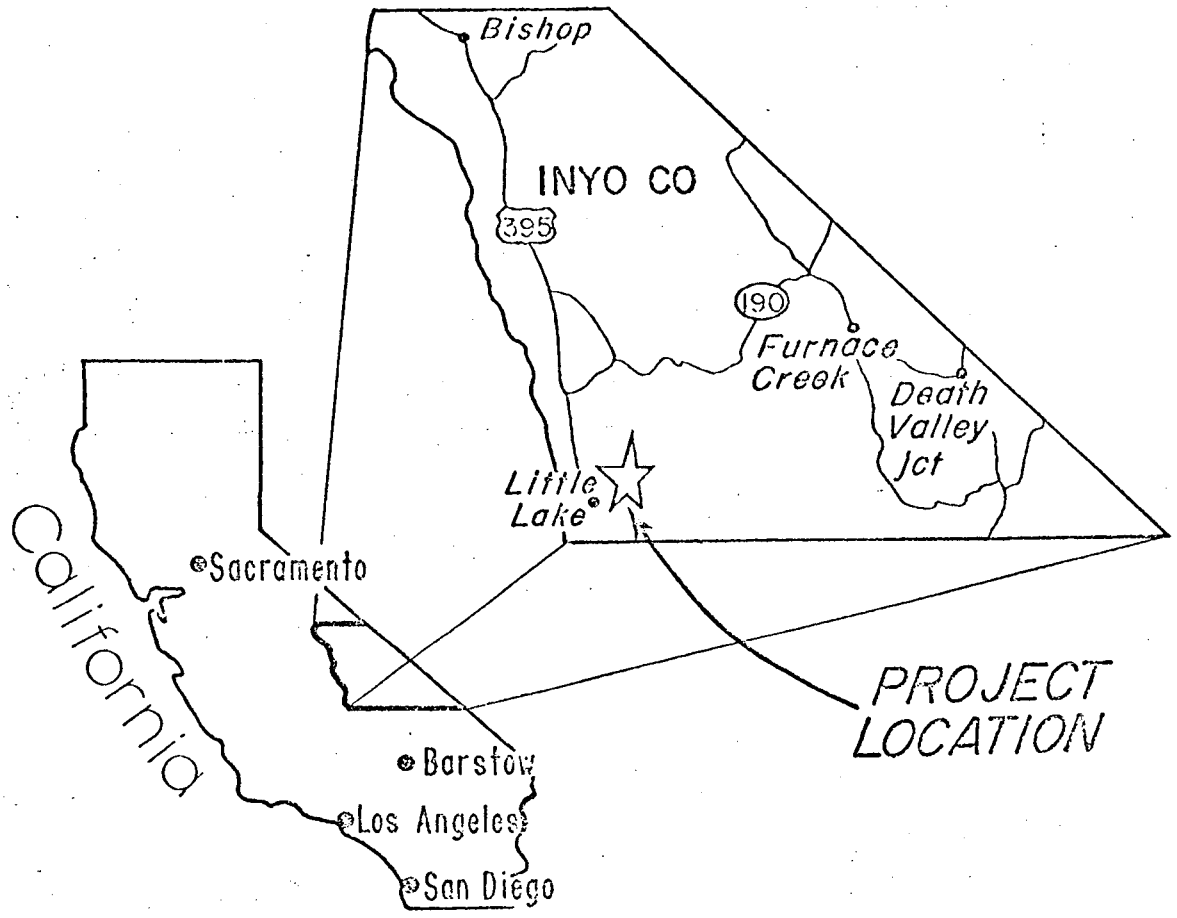

Figure 1. The location of the China Lake Naval Weapons Center.

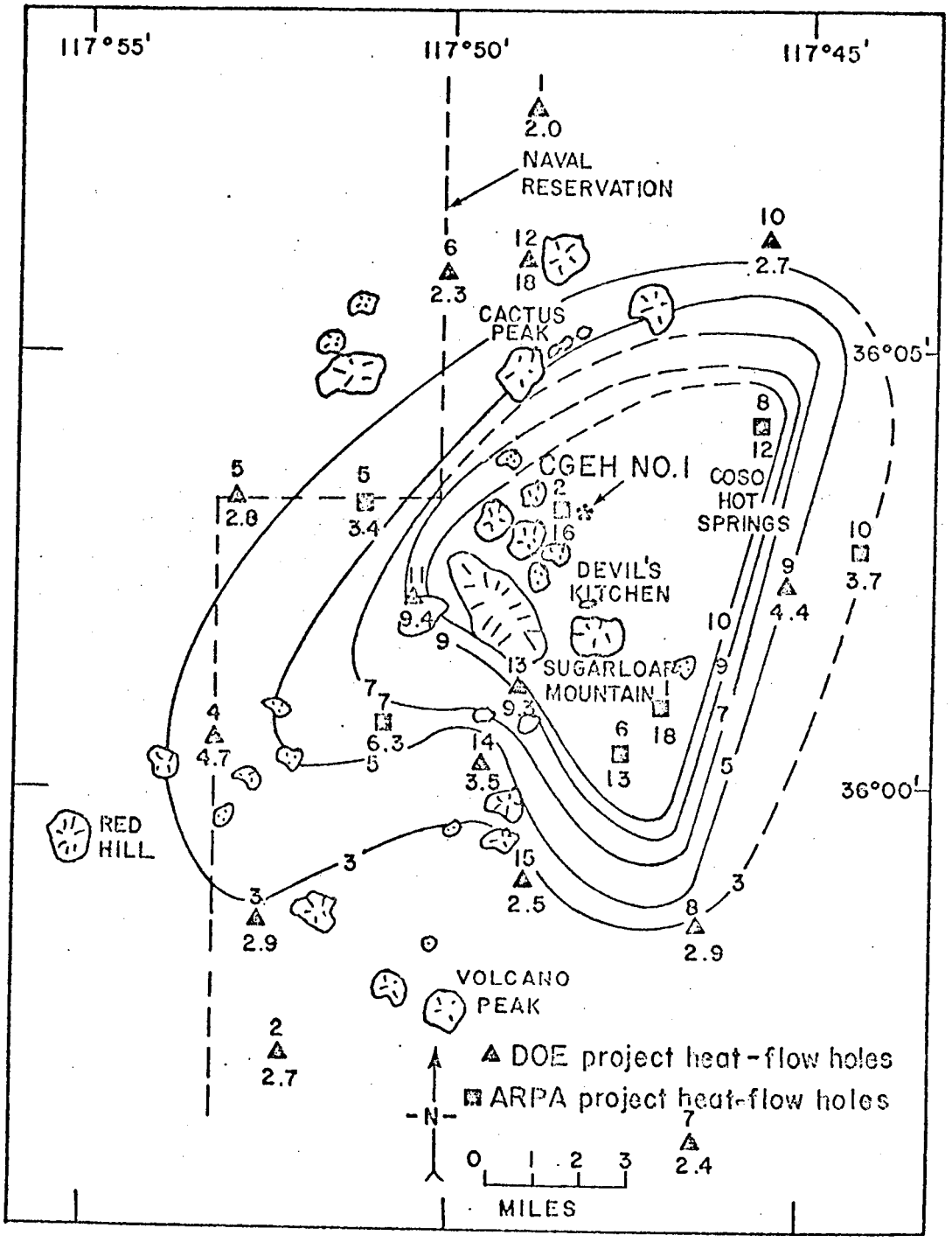

Figure 2. Generalized map of thermal anomalous region and CGEH No. 1 well location. The numbers in the figure identify the hole and (below) give the heat flow in HFU.

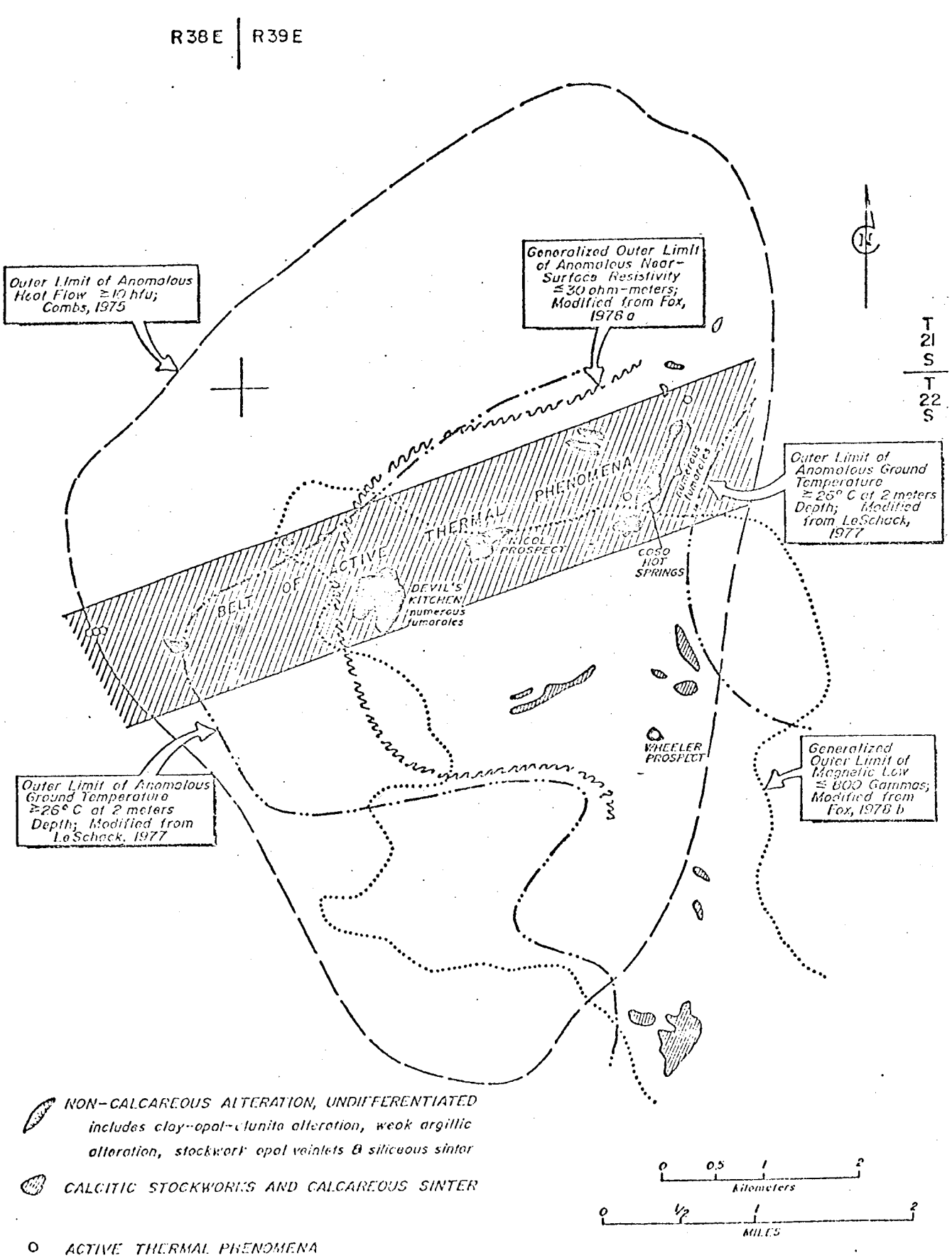

FIGURE 3
GENERALIZED ALTERATION AND GEOPHYSICAL MAP

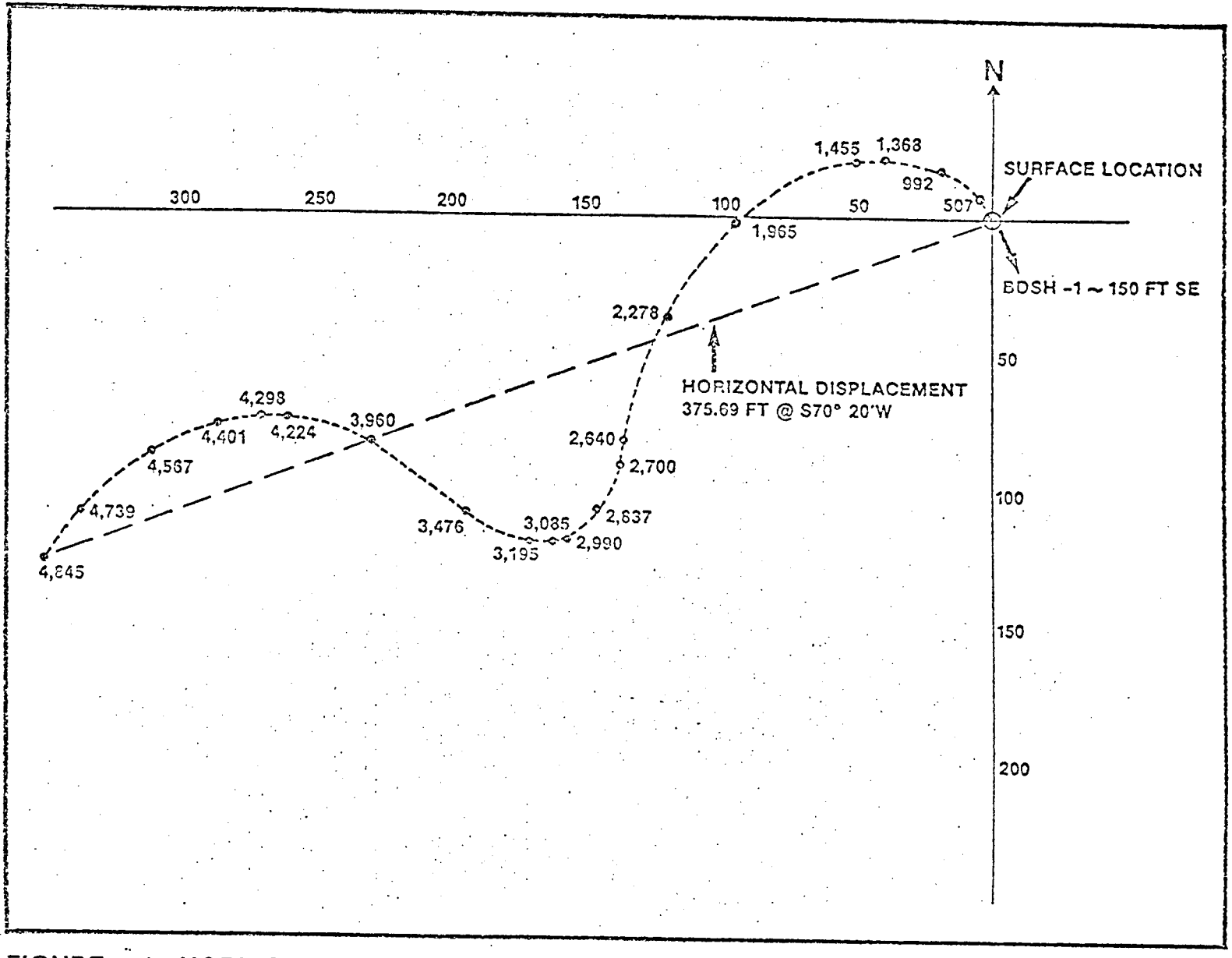

FIGURE 4 : HORIZONTAL PROJECTION OF DISPLACEMENT IN FEET PLOTTED AS A FUNCTION OF MEASURED DEPTH

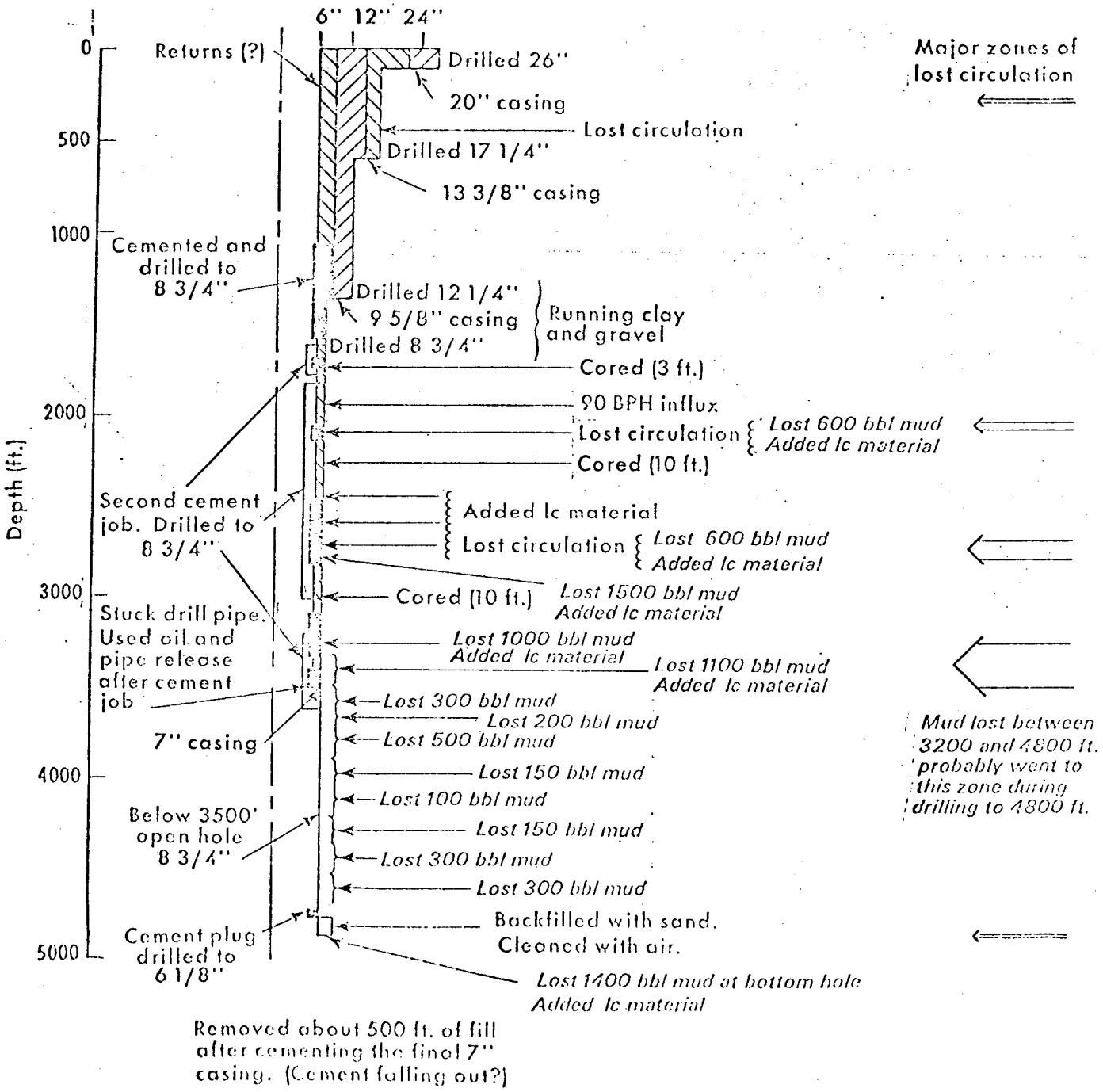
6" 12" 24"
0
500
1000
2000
3000
4000
5000
Depth (ft.)
Returns (?)
Drilled 26"
20" casing
Lost circulation
Drilled 17 1/4"
13 3/8" casing
Cemented and drilled to 8 3/4"
Drilled 12 1/4"
9 5/8" casing
Drilled 8 3/4"
Running clay and gravel
Cored (3 ft.)
90 BPH influx
Lost circulation
Lost 600 bbl mud
Added lc material
Cored (10 ft.)
Second cement job. Drilled to 8 3/4"
Added lc material
Lost circulation
Lost 600 bbl mud
Added lc material
Lost 1500 bbl mud
Added lc material
Cored (10 ft.)
Stuck drill pipe. Used oil and pipe release after cement job
Lost 1000 bbl mud
Added lc material
Lost 1100 bbl mud
Added lc material
Lost 300 bbl mud
Lost 200 bbl mud
Lost 500 bbl mud
7" casing
Lost 150 bbl mud
Lost 100 bbl mud
Below 3500' open hole 8 3/4"
Lost 150 bbl mud
Lost 300 bbl mud
Lost 300 bbl mud
Backfilled with sand. Cleaned with air.
Cement plug drilled to 6 1/8"
Lost 1400 bbl mud at bottom hole
Added lc material
Removed about 500 ft. of fill after cementing the final 7" casing. (Cement falling out?)
Major zones of lost circulation
Mud lost between 3200 and 4800 ft. probably went to this zone during drilling to 4800 ft.

FIGURE 5

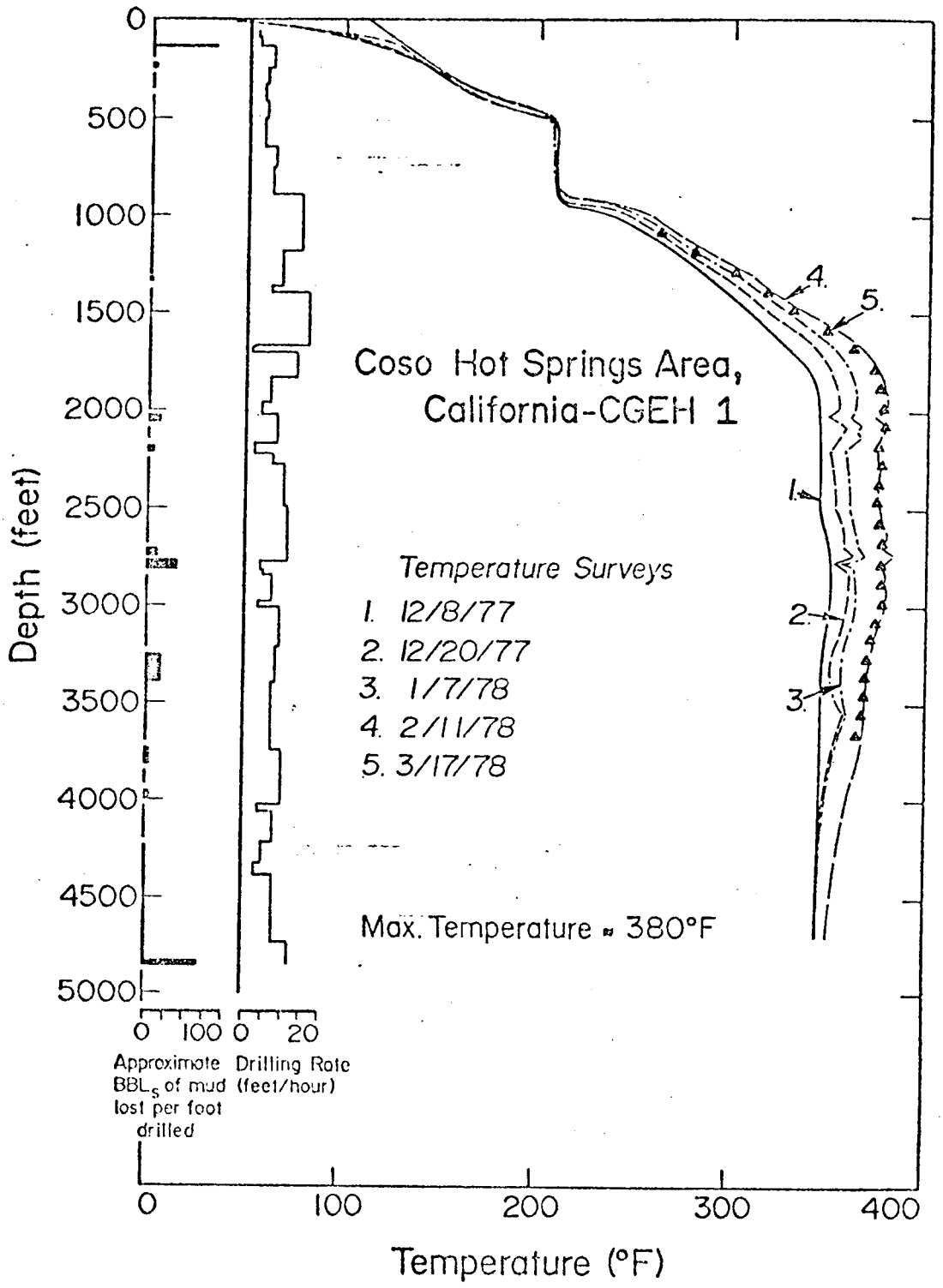

Figure 6. Temperature Surveys in the Static Steam and Water Column at Coso Hot Springs.

LOCATING THE PRODUCING LAYERS IN HGP-A

D. Kihara, B. Chen, A. Seki, and P. Yuen
University of Hawaii
Honolulu, Hawaii 96822

The characteristics of the Hawaii Geothermal Project well HGP-A were presented last year in terms of flow rates under throttled conditions, downhole pressure and temperature profiles, and pressure drawdown and buildup tests. In particular, the more recent pressure buildup analyses have indicated the possibility of multiple production zones. In an attempt to locate these production zones, two tests have been conducted during the past six months.

A direct means of determining the locations of the permeable layers is to measure the flow rates at the suspected depths. However, two difficulties immediately arise. Since the flow in HGP-A is a mixture of saturated liquid and vapor, the mass flow rate cannot be measured using a conventional spinner (which is a volumetric flow meter). Furthermore, the temperature encountered in the wellbore exceed the temperature limits of that instrument. To circumvent both of these difficulties, the well was allowed to produce only under severely throttled conditions. This had the effect of keeping the well fluid in a liquid state at temperatures well within the capability of the flow meter. The flow meter setup used for the production and pumpdown tests is shown in Figure 1.

The presence of a slotted liner in the bottom 4200 feet of the wellbore does not allow unequivocal interpretation of the data; however, a comparison of the maximum flow rate measured within the slotted liner and that measured at the weir on the surface shows that only a small fraction of the flow passes through the annular region outside the slotted liner.

The results for a flow meter run are shown in Figure 2. The well was producing at a flow rate of 44 gallons/minute of liquid only (22,000 lb/hr) as compared to 100,000 lb/hr of 65% quality steam at wide open conditions. This indicates that for these slow, all-liquid flow conditions, roughly 75% of the production is occurring between the depths of 4550 to 6250 feet.

The second series of tests consisted of cold water being pumped downhole at 115 gallons/minute while temperature and flow rate were monitored at selected depths. In all of the attempts,

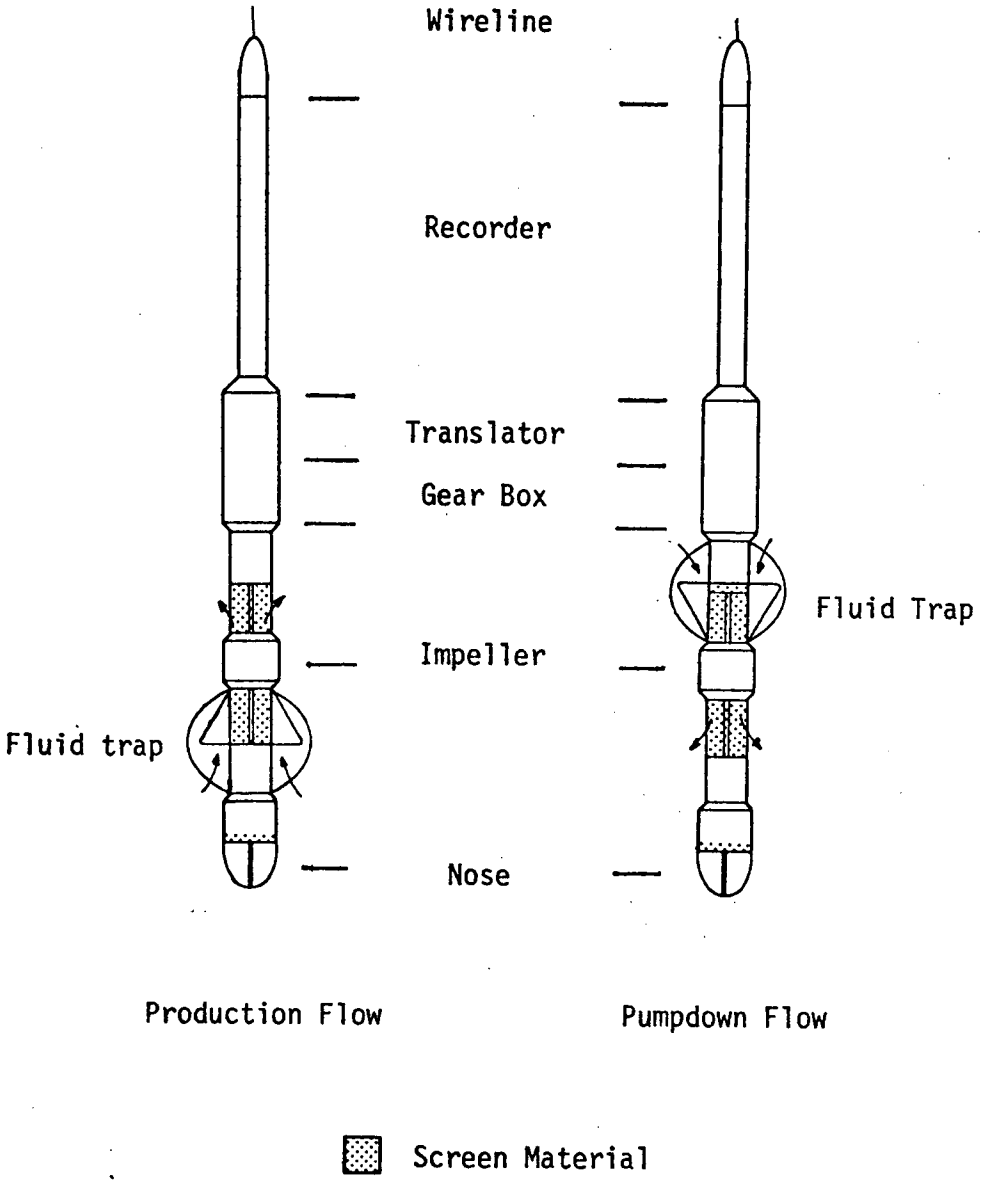

Figure 1. Flowmeter Setup

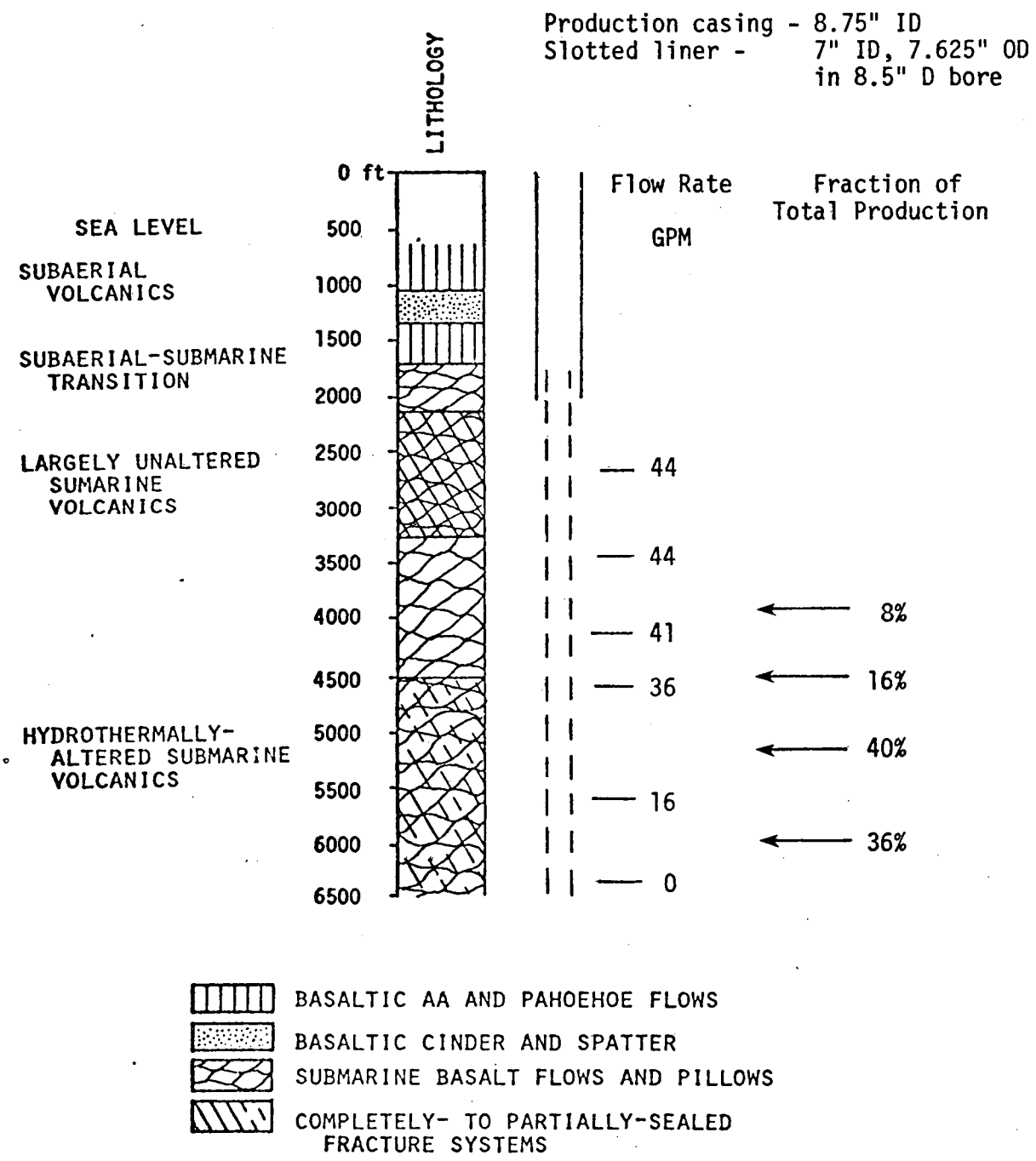

Figure 2. Summary of Flow Meter Test

a substantial amount of debris, analyzed later to be silica crystals, got past the filter screens, clogging the impeller which prevented the proper functioning of the flow meter.

The temperature profiles obtained during these tests are plotted in Figures 3 and 4. In both of these figures the temperatures measured prior to pumping (static condition A) are shown as circles while triangles and squares indicated temperatures measured while cold water was being pumped down (conditions B and C). The curve labelled (A on B) is the static temperature profile (A) moved parallel to itself so that a reasonable fit with profile (B) is obtained.

The matching of the displaced temperature profiles would lend weight to the assertion that the cold water being pumped down is pushing wellbore fluid down the wellbore and forcing the fluid back into the reservoir near bottomhole.

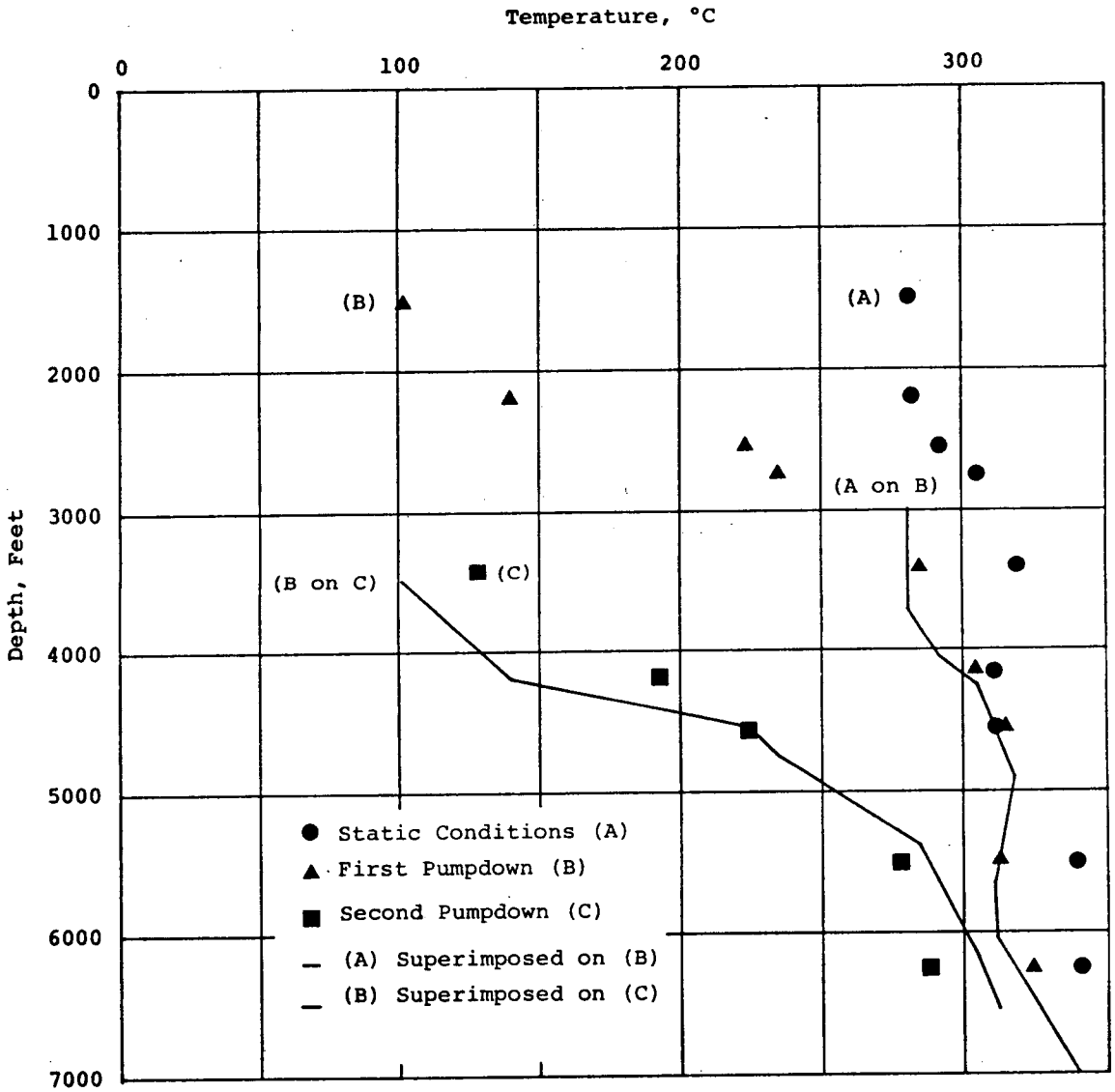

Figure 3. Results of First Pumpdown Test

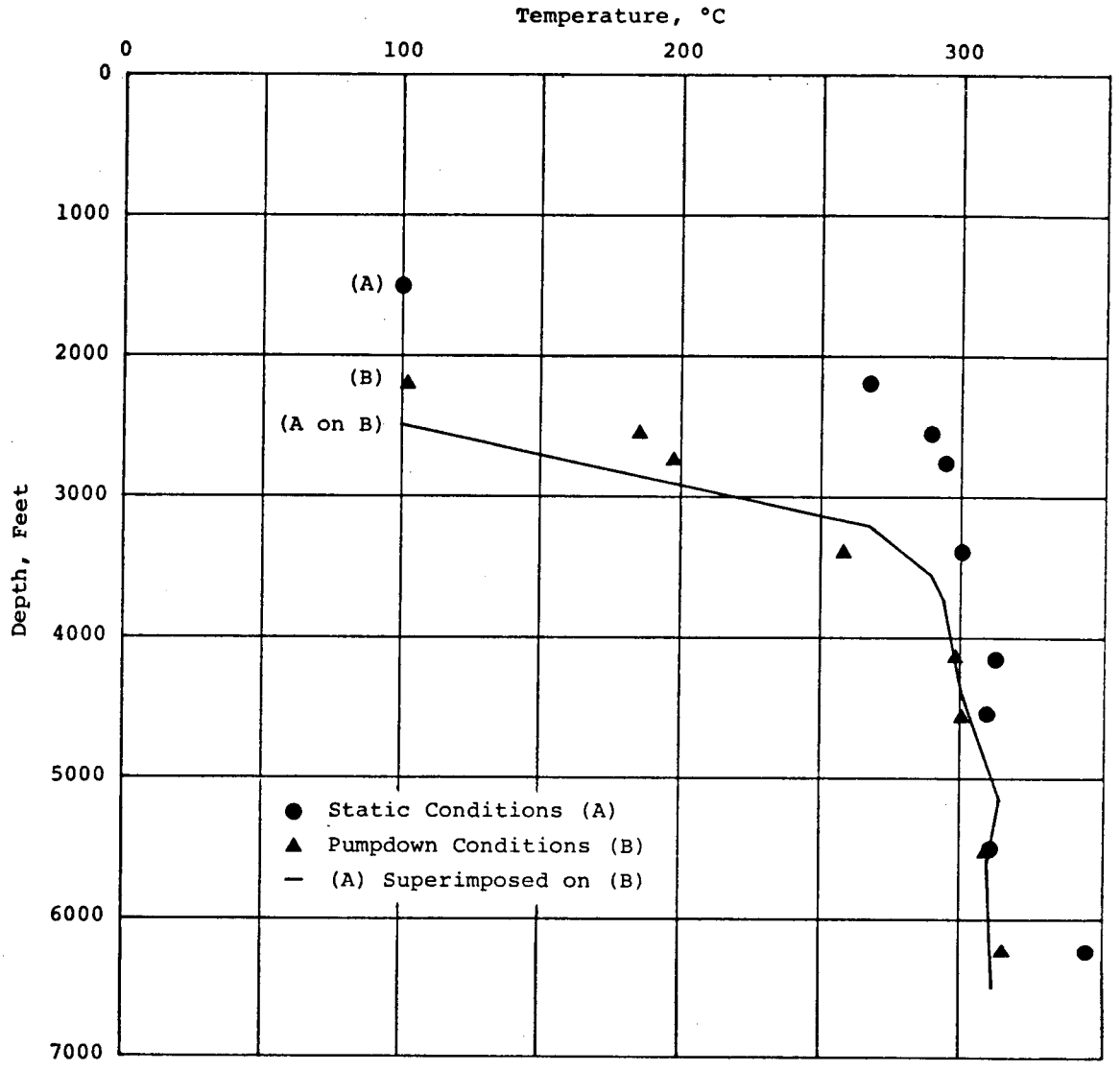

Figure 4. Results of Second Pumpdown Test

RESULTS OF WELL-TESTING IN THE BROADLANDS GEOTHERMAL FIELD, NEW ZEALAND

Roland N. Horne*, Malcolm A. Grant†, Robert O. Gale*
*University of Auckland †D.S.I.R. Wellington

Summary

Although not the first hot-water geothermal field under development, the Broadlands geothermal field has shown itself to be quite different in behaviour to other hot-water fields. The field was discharged some five years between 1966 and 1971, and has provided a large source of data in its as yet undeveloped state. This paper presents some of the results inferred from well-testing and highlights (1) the complexity of the system, (2) the importance of wellbore storage effects and (3) the effects of reinjection.

Introduction

The Broadlands geothermal field has had long delays in coming into production (for non-technical reasons), which has permitted a quite lengthy investigation of its properties. The field is largely hot-water dominated, however is different from the hot-water dominated Wairakei field in several ways. Firstly the Broadlands field has a much less homogeneous permeability and demonstrates preferred flow paths and barriers. Secondly the water in the system has already reached two-phase conditions at production depth (2000-3500 ft), whereas at Wairakei most of the production depth is still liquid. A much more significant difference however is not the early appearance of the steam phase, but the continued presence of dissolved gas i.e. carbon dioxide (Grant 1977). The contribution of the partial pressure of the CO_2 results in a lower effective pressure of the H_2O component with resulting boiling at apparently high (total) pressure. As a consequence of the two-phase conditions the diffusion time of a pressure change is very long (~1 year) compared to Wairakei (~ several hours), and the wells tend to act independently of one another to a large extent. As a result single well pressure transients tend to reflect conditions close to the well rather than properties of the reservoir at large, so it is particularly difficult to interpret well test results. This difficulty is compounded by the fact that several of the wells produce from more than one interval, thus the response depends firstly on the position of the recording instrument and secondly on whether or not the alternative feed points are producing or accepting fluid - sometimes in fact they do both, and the pressure response shows an oscillatory behaviour. In this paper some of the initial results are summarised, and the effects of the various complicating factors are discussed.

Initial Analysis

During 1977 and 1978, Grant (unpublished reports) has analysed a

number of pressure transient tests using more or less standard Horner buildups line source or spherical flow models. The results of some of these analyses are summarised in table 1. Although there is wide variability in the results due to local variations and also to the various complicating factors mentioned before, there is an interesting trend in the results in that the single well tests show permeability depth products (kh) of order 1-10 darcy-meters while the interference tests show values more of order 100. There are several possible explanations for this. Firstly the single well tests may be indicative of conditions only in the vicinity of the well (this is highly likely to be so since the pressure response is very slow moving in a two-phase system, and the well tests are of short duration), while the interference tests more clearly indicate reservoir permeabilities further away from the well. A second explanation is that the flow is essentially through fractures rather than through a porous medium (this is most certainly the case) and that each well intersects only a single or very few fractures while the pressure response further away is through many intersecting fractures. A third explanation is that the single well tests experience a comparatively low permeability due to relative permeability effects caused by flashing close to the well - this explanation does not hold up in the case of a pump test however.

It is apparent then that single well tests are dominated by effects close to the well, an observation which suggests greater emphasis be placed on well conditions at the time of the tests. These early analyses have not specifically investigated the effects of well-bore damage and well-bore storage, and it was with this in mind that the results of the well tests were examined a second time.

Storage and Skin Effects

Pressure transients from the Broadlands geothermal field are notoriously problematical in that they frequently show unpredictable fluctuations. However amongst the anomalous responses there are many that show a more normal behaviour. Taking as an example a buildup test on BR9 shown in table 2, the Horner plot shows a fairly straightforward straight line - see figure 1 - with a slope of about 6 bars/cycle. This slope implies a permeability depth of about 1800 md-ft or 0.6 d-m. However examination of the log-log plot (figure 2) reveals that the flow is dominated by storage effects during almost the entire test period, and thus no confidence can be placed on this permeability estimate. A longer buildup test on the same well illustrated in figure 3 indicates a semilog straight line of slope 9 bar/cycle (~ 1200 md-ft or 0.4 d-m). After some two weeks of production the pressure recovery declines, suggesting the intersection of some boundary. BR18 shows a similar buildup behaviour (figure 4), with an implied kh of less than 300 md-ft (0.1 d-m), and a levelling off at about 60 days.

The quantity and quality of data available does not permit quantitative statements, however it is clear that storage effects are not the cause of the difference between single well tests and interference tests. This is not to say that storage effects do not exist, and in fact it was an early conclusion of this investigation that essentially all of the

pressure transient tests performed using Amerada-type gauges are completly masked by wellbore storage. Since these effects may last for a time of the order of weeks in some wells it is definitely inappropriate to perform permeability tests in this manner. The longer type of test provides much useful permeability estimates. It was not possible to reach any reliable estimates of the order of magnitude of any skin effects due to the lack of a long enough semi-log straight line. Values of skin factor obtained for BR18 were in the vicinity of +1, however this figure is not a reliable one.

Complications

The Broadlands geothermal wells are particularly difficult to interpret in that they often behave unpredictably. For example BR7 (figure 5), which shows oscillations in its pressure recovery - in this case probably due to production from more than one level (Grant, D.S.I.R. report Jan. 1978). As another example BR11 shows order of magnitude changes in permeability due to scaling up of its slotted liner. However in considering the various misbehaving responses of the many wells it must be remembered that the wells interfere to a very mcuh greater extent than would be expected from their own single well behaviour.

The reason for the difference between single well and interference test permeabilities is still not clear, however the following explanation is suggested. If the permeability exists in fractures, then each well will have only limited accessibility to the fracture system, since it may only intersect one or two fractures which may not necessarily be very conductive. However after some time and distance the original fracture will intersect other fractures, some of which may be very much more conductive, thereby providing more permeable paths through the reservoir. Thus the pressure response of a distant well will be "seen" through the more permeable system. This explanation fits both the observed single well and interference test results. The single well tests show a flattening of the Horner plot after a period of 2 weeks to 2 months, which is indicative of an increase in permeability or alternatively of the intersection of a constant pressure boundary such as a fault.

Reinjection

There have been a number of reinjection tests at Broadlands, two into the reservoir proper (BR7 and BR33) and one on the outside (BR34). Some interesting results have been obtained, in that no confirmed recirculation of cold water has been found, despite the demonstrated interference between wells. About 200 t/h was injected into BR33 for 6 months. A rapid return of isotope tracer occurred to the production wells BR8,11, which have good connection to BR33 (see Table 1). But no observable cooling happened. The reasons for this are twofold. Firstly the injected fluid experiences a negative buoyancy of 0.06 psi/ft due to its higher density, while the driving force between wells (assuming a permeability depth of 200 d-m) would be 0.005 psi/ft (Grant internal report 1977). Note that the removal of cold water by negative buoyancy can only be effective in such highly-permeable rock as this. Secondly the relative

permeability effects would result in a greater permeability to the two-phase production fluid than to the injected water (Grant 1977, Horne and Ramey 1978) - permitting a greater access to new production than to reproduction of the injected water.

BR7 is an isolated well, and fluid has been injected into it for two years. Immediately on shutting, hot water begins to flow in the well, as indicated by the pressure rise (Fig.5). Further measurements show a complicated structure of permeability, with some levels discharging hot water during injection, and others accepting the mixture of hot and cold water in the well.

BR34 lies outside the production field (temperature 80°C). It has excellent connection to BRM2. With three weeks' injection at BR34, no thermal effects have been confirmed at BRM2, although chemical changes occurred in less than a day.

Acknowledgement

We thank Ministry of Works and Development for the data used here, and in particular P.F. Bixley for helpful comment.

References

Grant, M.A., "Broadlands - A Gas-Dominated Geothermal Field", Geothermics 6 (1977), 9-29.

Horne, R.N. and Ramey, H.J. Jr., "Steam/Water Relative Permeabilities from Production Data", Geothermal Resources Council, Transactions 2 (1978), 291.

Table 1

Broadlands Well-tested Results

Well	23/19	34/M2	M2	11	7	26	33/11	33/8
Kh(d-m)	150-190	1200	0.8	3,6,8,40	1	0.14	250-350	225
Test type	interf.	interf.	buildup	buildup/ drawdown	injection	injection	interf.	interf.

Table 2

BR9 Buildup Data

Production time 1 year, Production rate 61t/hr, Depth 3600', Enthalpy 1.09-1.69 MJ/kg.

Δt (mh)	Δp (bar)
1.43	0.67
2.86	1.30
4.30	1.97
5.73	2.56
7.16	3.18
8.59	3.64
10.03	3.98
11.46	4.36
12.89	4.69
14.32	4.99
15.76	5.28
17.19	5.53
18.62	5.78
20.05	6.03
22.00	6.33

Figure 1 - Horner buildup graph for BR9.

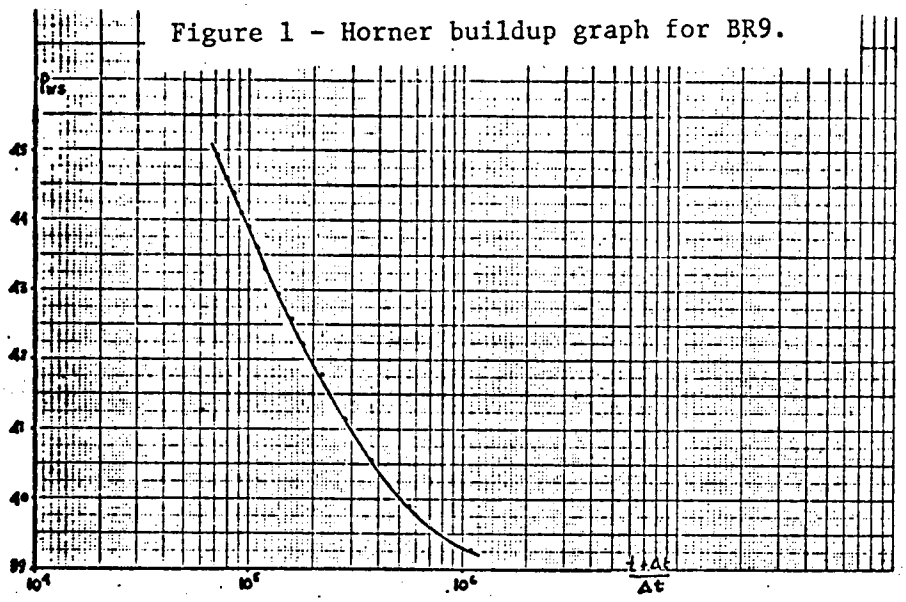

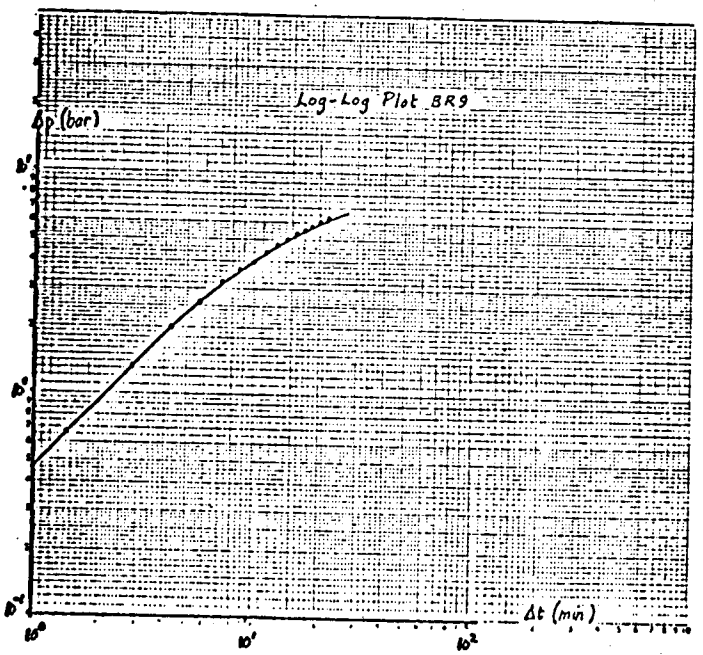

Figure 2 - Log-log pressure buildup for BR9.

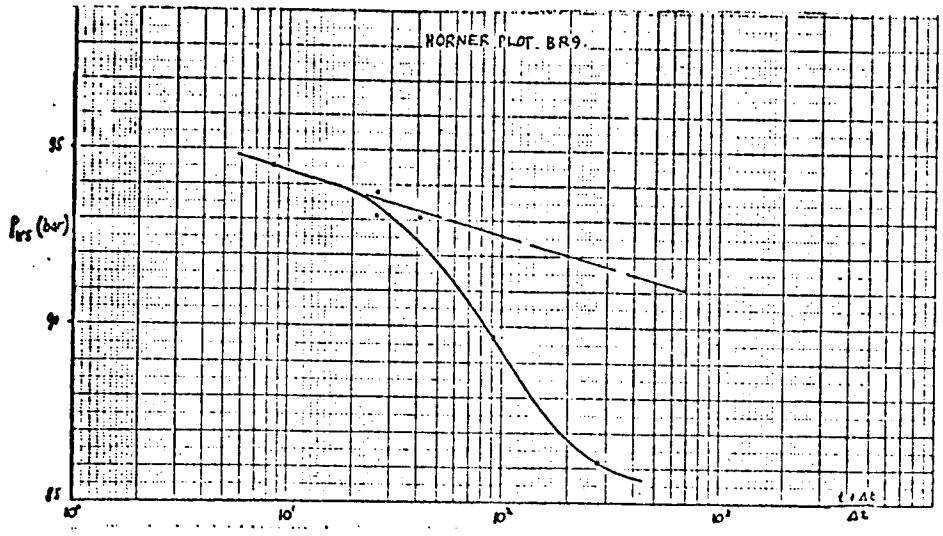

Figure 3 - Longer buildup test on BR9.

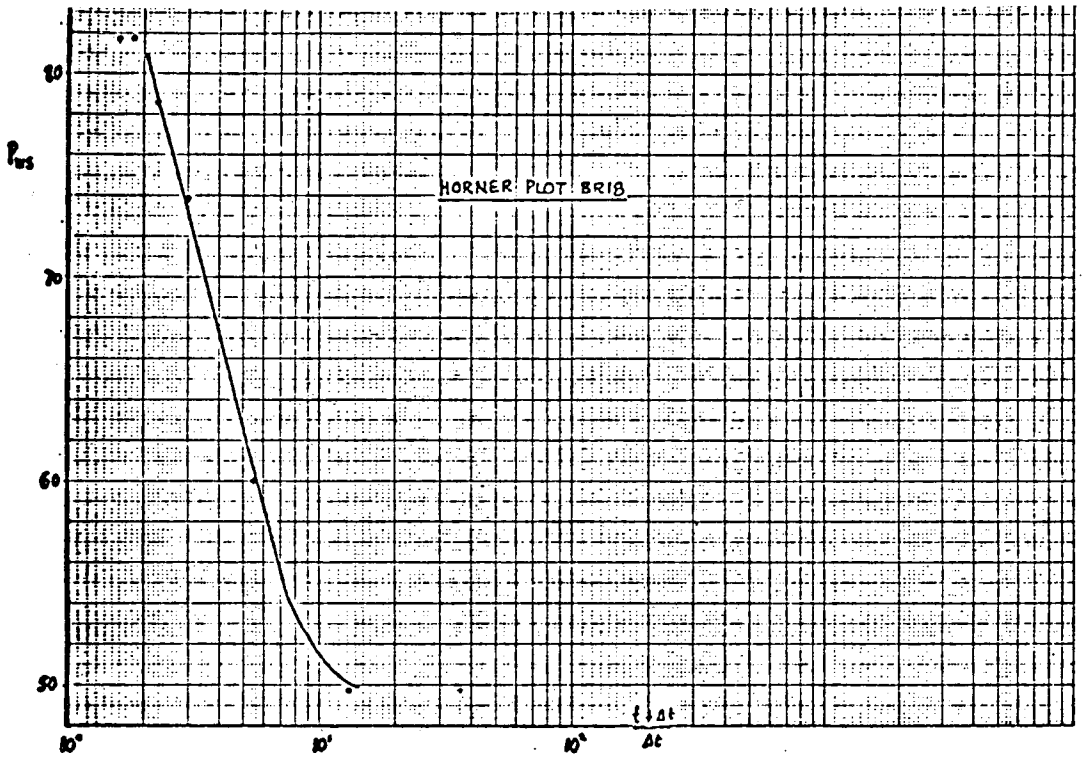

Figure 4 - Buildup test on BR18.

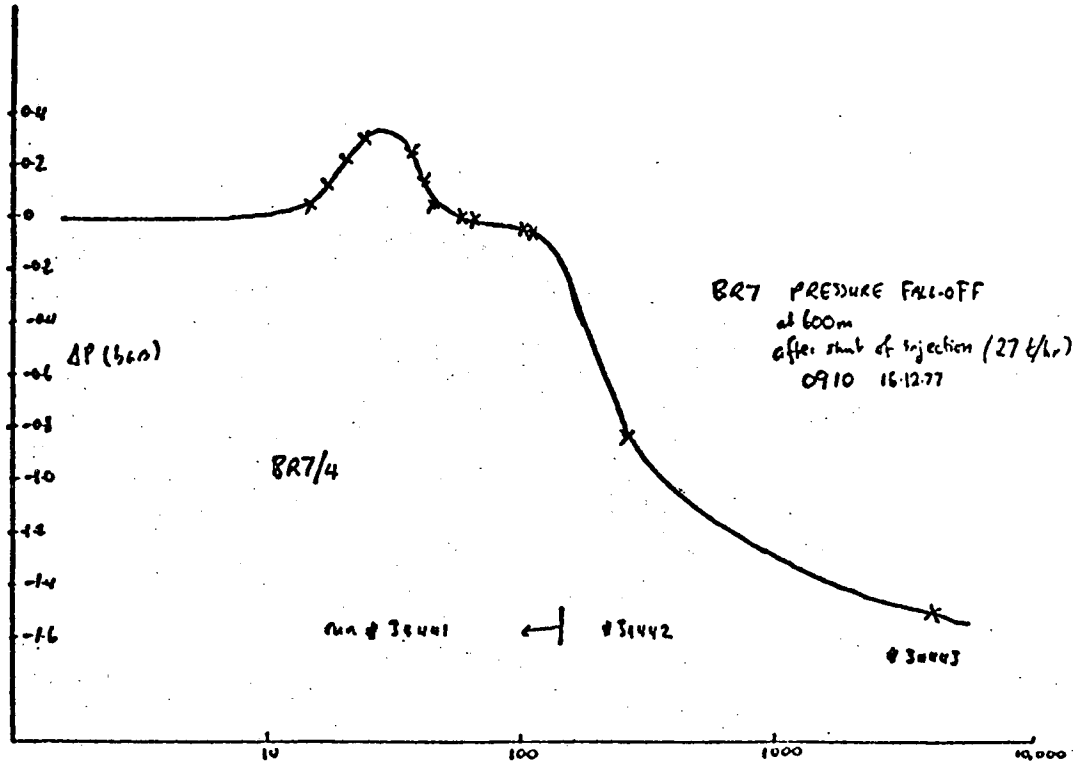

Figure 5 - BR7 injection test.

MECHANISM OF RESERVOIR TESTING

Gunnar Bodvarsson
School of Oceanography
Oregon State University
Corvallis, Oregon 97331

(1) Introduction

In evaluating geothermal resources we are primarily interested in data on the distribution of temperature and fluid conductivity within the reservoir, the total volume of the productive formations, recharge characteristics and chemical quality of the thermal fluids. While geophysical exploration by surface methods may furnish some data on the temperature field and give indications as to the reservoir volume, they furnish practically no information on the fluid conductivity and production characteristics. Such information will generally have to be obtained by tests performed within the reservoir, primarily by production tests on sufficiently deep wells. Reservoir testing is therefore one of the most important tasks in a general exploration program.

In principle, reservoir testing has much in common with conventional geophysical exploration. Although the physical fields applied are to some extent different, we face the same type of selection between controlled and natural drives, forward and inverse problem setting, etc. The basic philosophy (Bodvarsson, 1966) is quite similar.

In the present paper, we will discuss some fundamentals of the theory of reservoir testing where the fluid conductivity field is the primary target. The emphasis is on local and global aspects of the forward approach to the case of liquid saturated (dominated) Darcy type formations. Both controlled and natural driving pressure or strain fields are to be considered and particular emphasis will be placed on the situation resulting from the effects of a free liquid surface at the top of the reservoir.

(2) Relations governing the pressure field in Darcy type formations

Let $p(t,P)$ be the pressure field at time t and at the point P in a Darcy type domain B with the boundary surface Σ. Consider a general setting where the permeability k is a linear matrix operator and the kinematic viscosity of the fluid ν is also taken to be variable. It is convenient to introduce the fluid conductivity operator $c = k/\nu$ and express Darcy's law

$$\vec{q} = -c\nabla p \tag{1}$$

where $\vec{q}$ is the mass flow density. Moreover, let ρ be the fluid density, s the capacitivity or storage coefficient of the formation and f be a source density. Combining (1) with the equation for the conservation of mass, we obtain the diffusion equation for the pressure field

$$\rho s \partial_t p + \Pi(c)p = f \tag{2}$$

where $\Pi(c) = -\nabla(c\nabla)$ is a generalized Laplacian operator. Appropriate boundary

conditions that may be of the Dirichlet, Neumann, mixed or more complex convolution type, have to be adjoined to equation (2). The case of a homogeneous/isotropic/isothermal formation results in the simplication $\Pi(c) = c\Pi = -c\nabla^2$ where c is a constant. Moreover, stationary pressure fields satisfy the potential equation

$$\Pi(c)p = f. \tag{3}$$

The eigenfunctions $u_n(P)$ of $\Pi(c)$ in B satisfy the equations

$$\Pi(c)u_n = \lambda_n u_n, \quad n = 1,2, \ldots \tag{4}$$

where the constants λ_n are the eigenvalues and the boundary conditions on Σ are homogeneous of the same type as those satisfied by p(t,P) in (2) and (3).

(3) Types of solutions

It is of interest to consider some general expressions for the solutions of equations (2) above. The key to the equation is the causal impluse response or Green's function G(t,P,Q) which represents the pressure response of the causal system to an instantaneous injection of a unit mass of fluid at t = 0+ at the source point Q. This function satisfies the same boundary conditions as the eigenfuctions $u_n(P)$. Solutions to (2) in the case of a general source density f(t,P), non-causal initial values and general boundary conditions can then be expressed in terms of integrals over the Green's function (Duff and Naylor, 1966).

Two fundamental types of expressions for the Green's function are available. First, in the case of simple layered domains B with a boundary Σ composed of a few plane faces, G(t,P,Q) can be expressed as a sum (or integral) over the fundamental source function

$$p = (8\rho s)^{-1}(\pi at)^{-3/2}\exp(-r_{PQ}^2/4at)U_+(t) \tag{5}$$

and its images. The symbol $U_+(t)$ is the causal unit step function and r_{PQ} is the distance from Q to P. Whenever applicable, sums of this type represent the most elementary local and/or global expressions for G(t,P,Q).

Second, the Green's function can be expanded in a series (in integral) over the eigenfunctions of $\Pi(c)$. If ρ and s are constant, then

$$G(t,P,Q,) = (1/\rho s)\sum_n u_n(P)u_n(Q)\exp(-\lambda_n t/\rho s). \tag{6}$$

The series expansion (6) is of a more general applicability than solutions of the type based on the fundamental source function (5). However, because of quite poor convergence properties, (6) is largely of a more global long-term relevance. It is less suited for the computation of local values. The formal link between the two types of solution (5) and (6) is provided by the Poisson summation formula (Zemanian, 1965).

A different type of solution of (2) that is of interest in the present context can be obtained by operational methods. Limiting ourselves to the pure initial value problem with $p(0,P) = p_0(P)$ in the case of an infinite domain, we can, since ρ, s and $\Pi(c)$ are independent of t, formally express the solution of the homogeneous form of (2) as

$$p = \exp[-t\Pi(c)/\rho s]p_0 \tag{7}$$

where the exponential operator is to be interpreted as a Taylor series in the operator $\Pi(c)$

$$\exp[-t\Pi(c)/\rho s] = 1 - [t\Pi(c)/\rho s] + (1/2)[t\Pi(c)/\rho s]^2 - \ldots \tag{8}$$

The series represents an iteration process where the convergence is limited to (properly defined) small values of t. The practical applicability is therefore fundamentally different from (6). Moreover, it is of considerable interest that rather general situations with regard to $\Pi(c)$ can be admitted in (7) and (8).

Three simple but fundamental physical parameters are associated with processes governed by the diffusion equation (2). First, the local diffusivity $a = c/\rho s$. Second, the skin depth $d = (2c/\rho s\omega)^{\frac{1}{2}}$ which is a measure of the penetration of a wave of angular frequency ω (Bodvarsson, 1970). Finally, the relaxation time $t_0 = 1/ak^2$ which is a measure of the attenuation in time of a one-dimensional wave like pressure field of wave number k. The time t_0 is the time during which the wave amplitude decreases from unity to 1/e. This parameter is obtained by inserting a solution of the form $\exp[(-t/t_0)+ikx)]$ into the one-dimensional form of (2).

(4) Effects of a free liquid surface

The presence of a free liquid surface in a reservoir requires the introduction of a rather complex surface boundary condition. Let Σ now represent the free liquid surface at equilibrium and Ω be the free surface in a perturbed state. The boundary Ω is a surface of constant pressure which without loss of generality can be taken to vanish. The free surface condition (Lamb, 1932) is then expressed

$$Dp/Dt|_{p=o}=0 \tag{9}$$

where D/Dt is the material derivative. This is an essentially non-linear condition which leads to a much more complex problem setting. Losing the principle of superposition the construction of solutions to the forward problem becomes a difficult task.

Bodvarsson (1977a) has shown that when Ω deviates only little from Σ, (9) can be simplified and linearized. For this purpose we place a rectangular coordinate system with the z-axis vertically down such that the (x,y) plane coincides with Σ. Moreover, let the amplitude of Ω relative to Σ be u and the scale of the undulation of Ω be L. Then provided $|u/L|<<1$, the condition (9) can be replaced by the approximation

$$(1/w)\partial_t p - \partial_z p = 0, \tag{10}$$

where $w = cg/\phi$ is a new parameter, namely, the free sinking velocity of the pore liquid under gravity (g = acceleration of gravity). Under these circumstances, the solution of the forward problem is obtained by constructing a solution to (2) which satisfies (10) at the free surface and appropriate conditions at other sections of the reservoir boundary.

The presence of a first order derivative with respect to time in the free-surface condition (10) obviously leads to an additional relaxation process analog to the purely diffusive phenomena associated with the first order time derivative in the basic equation (2). As we shall conclude below, the individual time scales of the two phenomena are, however, quite different.

For the sake of brevity, we shall limit the present discussion to the simplest but practically quite relevant case of the semi-infinite liquid saturated homogeneous, isotropic and isothermal half-space. To consider the pure free-surface related phenomena, we eliminate pressure field diffusion by neglecting the compressibility of the liquid/rock system. In this setting we can combine the potential equation (3) and the surface condition (10) in one single equation confined to the Σ plane (Bodvarsson, 1978a), which expressed in terms of the fluid surface amplitude $u(t,x,y) = p/\rho g$ takes the form

$$(1/w)\partial_t u + \Pi_2^{\frac{1}{2}} u = f/\rho g c \qquad (11)$$

where $\Pi_2^{\frac{1}{2}} = (-\partial_{xx}-\partial_{yy})^{\frac{1}{2}}$ is the square root of the two-dimensional Laplacian and f is an appropriately defined source density. To obtain the pressure field in the space $z>0$, the boundary values derived from (11) have to be continued into the lower half-space on the basis of standard potential theoretical methods. The fractional order of the Laplacian in (11) is quite unusual, but the operator is well defined and poses no mathematical problems. For a further discussion of such operators in a slightly different setting, we refer to a paper by Bodvarsson (1977b).

Consider the attenuation of a wave formed pressure field of the form $\exp[-(t/t_0)+ikx]$ where t_0 is the relaxation time and k is the wave number. Inserting into equation (11), we find that $t_0=1/wk$. Comparing this result with the case of the purely diffusive pressure field we find that the ratio of the free surface/diffusion relaxation times is $ak^2/wk=k\phi/g\rho s$. The assumptions of waves of lengths 10 to 10^3 meters and porosities of 10^{-2} to 10^{-1}, results in ratios ranging from about 10^2 to 10^5. The relaxation times of diffusion phenomena are therefore orders of magnitude shorter than for free-surface phenomena of a comparable spatial scale. As a result, we can conclude that in most cases of practical relevance, the two phenomena can be separated and treated individually.

Some solutions of equations (11) of practical interest have been obtained by Bodvarsson (1977a). Confining ourselves again to the simple semi-infinite half-space, the most important result is given by the causal impluse-response function G(t,S,Q,) which represents the response of the surface amplitude at the point S = (x,y) in Σ and time $t\geq 0+$ to an instantaneous injection of a unit mass fluid at a point Q in the half-space at time t=0+. The system is assumed to be in equilibrium for $t\leq 0$. Let Q = (0,0,d), the resulting expression for the surface amplitude is

$$G(t,S,Q) = (1/2\pi\phi\rho)(wt+d)[x^2+y^2+(wt+d)^2]^{-3/2}U_+(t) \qquad (12)$$

where $U_+(t)$ is the causal unit-step function. The impluse response is essentially the key to the solution of (11) for more general conditions. The pressure field in the half-space is obtained from (12) by a simple continuation technique where the singularity at Q has to be taken into consideration. The long term response of the surface amplitude to a periodic source function at Q is of particular interest in the present context. Let the mass flow injected at Q=(0,0,d) take the form $\exp(-i\omega t)$. The amplitude of the frequency response is then obtained by

$$F(S,Q,\omega) = \int_0^\infty G(S,Q,\tau)\exp(i\tau\omega)d\tau \qquad (13)$$

The present results on the dynamics of the free surface amplitude provide the basis for a technique of reservoir probing and testing which yields results on c and ϕ that are supplementary to the conventional well test techniques (see Bodvarsson and Zais, 1978, this volume).

(5) Testing with controlled signals

Local. Reservoir tests with controlled drive yielding mostly local parameter values include primarily the driving point tests which are usually referred to as pressure buildup and/or drawdown tests on single wells. Pioneering work on the development of this technique has been carried out at Stanford, and there exists considerable literature (see e.g. Ramey, 1976). Interpretation is based on appropriate solutions of equation (2).

Interference. The spatial scale of well-to-well interference tests depends on the distances involved. Short distances tend to yield only local parameter values whereas long distances may lead to results of a more global nature. In the case of simple systems of sufficient extend, the interpretation is to be based on the following concentrated source unit-step responses obtained on the basis of equation (2) (Carslaw and Jaeger, 1959).

axi-symmetric two-dimension	point-symmetric three-diemsion
$-(m/4\pi c)Ei(-F^{-1})$,	$(m/4\pi Cr)\mathrm{erfc}(F^{-\frac{1}{2}})$ (14)

where $F = 4at/r^2$ is the Fourier number and m is the appropriately defined (constant) mass flow applied. Again, there is very considerable literature on the subject (Matthews and Russell, 1967; Earlougher, 1977) mostly emphasizing the two-dimensional axi-symmetric situation.

It is important to note that in the above expressions, the complementary error function (erfc) and the exponential integral (Ei) will in the interval $0<F<0.5$ yield very similar values when taken as functions of time at a fixed field point. The short-term well interference test is therefore largely "blind" with regard to the space dimensions involved. Although the value of the amplitude factor is observable, its structure depends critically on the space dimension and this data does therefore not convey any information unless strong assumptions are made with regard to the underlying model. Considerable caution is therefore called for in the interpretation of well interference data, and it would appear that too much confidence has been placed in the applicability of the axi-symmetric two-dimensional Theis-type solution.

Global. Tests of this nature can be carried out only when there is sufficient data on the global characteristics of the pressure/flow field. An important case consists in the use of global free liquid surface data. A brief review of the theory involved has already been given in section (5) above. Forward solutions based on the type of Green's function expression given by (6) above are of particular relevance in global work.

(6) Testing with natural signals

Types of drive. Available natural driving strain or force fields are of the following LF (low-frequency) to ULF (ultra-low-frequency) types (period range in parenthesis): seismic strain (1 to 10^3s), hydroelastic oscillations and noise (two-phase flow, etc.)(10 to 10^5s), tidal strain (10^4 to 10^6s), atmospheric pressure variations (10^4 to 10^6s), precipitation load (10^4 to 10^6s) and seasonal water-level variations (10^6 to 10^8s).

Local. The most obvious applications of natural drive are to the local type of testing. For the sake of brevity, we will limit our attention to VLF and ULF test signals where the mass forces on liquid columns in boreholes can be ignored. Moreover, in the single borehole case the essential results are obtained by deriving the pressure amplitude in an open hole (free liquid surface) to a homogeneous harmonic formation dilatation drive of amplitude b and angular frequency ω. Responses to other types of signals can then be easily derived with the help of a Fourier transform analysis. Under some further plausible simplifying assumptions, the following essential results for the pressure amplitude p in a single borehole of cross section f were presented at the 1977 Stanford Symposium (Bodvarsson, 1977c and 1978a), namely,

$$p = p_0 T/(1+T), \quad \text{where } p_0 = \varepsilon b/s, \text{ and } T = -4i\pi g r_0 c/\omega f = -iAS/\omega. \qquad (15)$$

Here, p_0 is the static pressure amplitude, ε the formation matrix coefficient characterizing the relation between the imposed strain and the porosity, r_0 the radius of the (spherical) well cavity, $A = 4\pi r_0 c$ the admittance of the cavity and $S = dp/dm = g/f$ is the mass stiffness of the well. The first two relations in (15) are general, but the third one is obtained on the basis of the assumption that $d/r_0 >> 1$ where d is the skin depth of the formation at tidal frequencies.

The case of pressure oscillations of tidal nature in closed well-reservoir systems has been discussed recently by Arditty, Ramey and Nur (1978). By a proper definition of the well mass stiffness S, the relations (15) would also be applicable to systems of this type.

The application of seismic signals in reservoir testing offers interesting possibilities. Mainly because of vertical displacement oscillations, the forward theory for this case is more complex than the results given above and can therefore not be discussed in this brief note. The subject has been investigated by Bodvarsson (1970). Forward solutions based on the iteractive type of series given by (8) are of particular interest in the interpretation of local tests based on natural drive.

Interference and global. More global type interference tests can, in principle, be carried on the basis of natural pressure or strain signals. Because of the well/well pressure field scattering processes involved, the theory cannot be discussed within the framework of this short note.

(7) Fractured reservoirs

The discussion above has been devoted entirely to formations which are of the Darcy type or can be approximated by such media. Largely fractured reservoirs have not received any attention. The theory of such cases differs from the material presented above and will not be discussed here. It is of interest to note that the mechanism of pressure field propagation in fractures with elastic walls has been discussed by Bodvarsson (1978b).

References

Arditty, P.C., Ramey, H.J., Jr., and A.M. Nur, 1978. Response of a closed well-reservoir system to stress induced by earth tides. SPE paper 7484 Houston, Texas.

Bodvarsson, G., 1966. Direct interpretation methods in applied geophysics. Geoexploration 4:113-138.

Bodvarsson, G., 1970. Confined fluids as strain meters. J. Geophys. Res. 75 (14):2711-2718.

Bodvarsson, G., 1977a. Unconfined aquifer flow with a linearized free surface condition. Jokull, 27:1977.

Bodvarsson, G., 1977b. An equation for gravity waves on deep water. Jokull, 27:1977.

Bodvarsson, G., 1977c. Interpretation of borehole tides and other elasto-mechanical oscillatory phenomena in geothermal systems. Workshop on Geothermal Reservoir Engineering, December, 1977, Stanford University, Stanford, California.

Bodvarsson, G., 1978a. Convection and thermoelastic effects in narrow vertical fracture spaces with emphasis on analytical technique. Final Report for U.S.G.S. pp. 1-111.

Bodvarsson, G., 1978b. Pressure field propagation and density currents. 2nd Invitational Well Testing Symposium, Lawrence Berkeley Laboratory, Berkeley California.

Bodvarsson, G., and E. Zais, 1978. A field example of free surface testing. 4th Stanford Workshop on Geothermal Reservoir Engineering.

Carslaw, H.S. and J.C. Jaeger, 1959. Conduction of Heat in Solids. 2nd ed., 496 pp., Oxford.

Duff, G.F.D. and D. Naylor, 1966. Differential Equations of Applied Mathematics. John Wiley and Sons, New York, 423 p.

Earlougher, R.C. Jr., 1977. Advances in Well Test Analysis. Society of Petroleum Engineers of AIME, New York, N.Y., and Dallas, Texas.

Lamb, H., 1932. Hydrodynamics. 6th ed., 738 pp., Dover Publications, New York, N.Y.

Matthews, C.S. and D.G. Russell, 1967. Pressure buildup and flow tests in wells. Society of Petroleum Engineers of AIME. New York, N.Y. and Dallas, Texas.

Ramey, H.J., Jr., 1976. Pressure transient analysis for geothermal wells. 2nd U.N. Symposium on the Development & Use of Geothermal Resources, San Francisco.

Zemanian, A.H., 1965. Distribution Theory and Transform Analysis. McGraw-Hill Book Company, New York, N.Y.

A FIELD EXAMPLE OF FREE SURFACE TESTING

Gunnar Bodvarsson
School of Oceanography
Oregon State University
Corvallis, Oregon 97331

and

Elliot Zais
Elliot Zais & Associates
Corvallis, Oregon 97330

Introduction

Theoretical results on free liquid surface dynamics presented by Bodvarsson (1978, this volume), provide the basis for a technique of reservoir probing and testing which can yield results that are supplementary to conventional well testing data. The Laugarnes geothermal area in Iceland which is one of the sources of the Reykjavik District Heating System is a case where both methods are applicable and appear, interestingly, to yield quite different results. A brief account of the free surface results will be presented below.

The Laugarnes geothermal source area

The Laugarnes geothermal area (see Fig. 1) has been described in some detail by Thorsteinsson and Eliasson (1970). The active reservoir underlies an area of 5 km^2 within the city of Reykjavik and has a base temperature about 145°C. The reservoir is embedded in a flood basalt series of more than 3 km thickness. Fluid conductivity is mainly along the contacts of lava beds and up through dikes and fracture zones. Evidently, the permeability is quite heterogeneous and anisotropic.

Several dozen production wells have been drilled in the area during the past decades. The maximum depth is now of the order of 3 km. The productivity of individual wells obtained with the help of submerged pumps placed at depths up to 100 meters varies from 1 to 50 kg/s with well-head temperatures mostly in the range of 125°C to 135°C. The main production is obtained from an aquifer extending between the depths of 730 and 1250 meters. The pumping load is governed by the demand on the heating system during the course of the annual cycle and varies from about 100 to 300 kg/s. As a consequence of the varying production rate, the elevation of the piezometric surface fluctuates in a quasi-periodic way with the year as a basic period. Thorsteinsson and Eliasson (1970) have during the period 1965 to the end of 1969, collected a considerable amount of water level data from 60 observation wells in the area. Fig. 2 gives an example of their water level data on a day in November of 1967. Moreover, Fig. 3 illustrates the relation between the integrated production rate and the water levels as observed in two centrally located wells. These data furnish a quite interesting picture of the hydrological characteristics of the reservoir.

Very few quantitative data are available on the permeability and porosity characteristics of the Laugarnes reservoir. Using conventional well interference test techniques in field experiments of 10 to 20 hours duration, Thorsteinsson and Eliasson (1970) have estimated the permeability of the reservoir to be of the order of 10 darcys.

Bodvarsson (1975) arrived on the basis of water level recovery data from one well at a permeability value of a few darcy. No results were obtained on the porosity but field observations on outcrops indicate very low values, perhaps a few parts per thousand.

Relevant theoretical results presented by Bodvarsson (1977a & b, 1978) permit an analysis and interpretation of the available observational data in terms of estimates of the more global permeability and porosity characteristics of the reservoir. Two different procedures are available for carrying out this analysis, namely, 1) the production data can be taken to represent a periodic process with an approximately sinusoidal input/output, or 2) short sections of the graphs can be analyzed individually as independent processes.

On the first approach, input-output amplitude and phase relations for the annual cycle can be estimated with the help of the production rate and water level data in Fig. 3. Unfortunately, the present observational material is deficient in that the peak-to-peak input-output phase lags are small and quite poorly defined. Nevertheless, on the available data, estimates of roughly 1.5 months equivalent to a phase angle of 45 degrees are indicated.

Carrying out a numerical evaluation of the complex integral for the frequency response as given by equation (13) in the paper by Bodvarsson (1978 , this volume) for the case of various values of the sinking velocity parameter w, and comparing the results with the observational data, we obtain on the basis of the phase difference a best fit for a value of $w = 4 \times 10^{-4}$ m/s. With the help of the amplitude ratio, permeability estimates of roughly 10 millidarcy and porosity estimates of 10^{-3} are obtained.

An alternative approach to the periodic input/output data based on a simple lumped system model is discussed in the Appendix. The resulting estimates of the permeability and porosity are of the same order of magnitude as the data given above.

On the individual event analysis of the water level responses to the changes in the production rates, we obtain quite similar results. The theory is based on the following results by Bodvarsson (1977b) for the response of the free water surface to sinks at depth in homogeneous and isotropic Darcy type solids. First, let the initial free surface be at equilibrium and a point-sink of volume rate V be placed at the depth d and start production at t = 0. The initial rate of drawdown of the free surface vertically above the sink is then

$$u = V/2\pi\phi d^2 \qquad (1)$$

where ϕ is the porosity. Moreover, let k be the permeability of the solid, ν the kinematic viscosity of the fluid and therefore $c = k/\nu$ the fluid conductivity. The long term stationary value of the free surface drawdown vertically above the sink is then found to be

$$h_s = V/2\pi gcd \qquad (2)$$

where g is the acceleration of gravity.

We apply these results to the production event from September 1968 to March 1969 and assume that the point source model can give reasonable estimates of the parameters of interest. During the event in question, the flow rate was increased quite abruptly from 2.5 to $7 \times 10^5 m^3$/month, that is, by about 0.17 m^3/s. To correct for local precipitation we assume that the increased input flow to the local reservoir is 0.15 m^3/s. From the initial slope of the water level graph given in Fig. 3, we derive an initial rate of drawdown in response to the increased production of $u = 1.1 \times 10^{-5} m/s$. Assuming that the production depth is about 10^3 m we find on the basis of equation (1) an estimate of the porosity of about $\phi = 2 \times 10^{-3}$.

Since equilibrium was not approached during the present event, we are unable to apply equation (2) to obtain a numerical estimate of the fluid conductivity c. However, since the graph in Fig. 3 furnishes us with a lower bound h_m for the stationary drawdown h_s, we can convert equation (2) to an inequality

$$c \leq V/2\pi g h_m d \qquad (3)$$

and obtain an upper bound for c. Taking on the basis of the graph $h_m = 60$ m, we obtain the upper bound of $4 \times 10^{-8} s$. Assuming the kinematic viscosity to be $3 \times 10^{-7} m^2/s$ (100°C) we obtain that the permeability $k \leq 1.2 \times 10^{-14} m^2$ = 12 millidarcy.

The above estimates of the global permeability turn out to be two to three orders of magnitude lower than the values quoted above as the results of the short-term well interference tests. There appears to be an inverse relation between the time scale of the test signal and the magnitude of the estimate. The longer the time scale, the lower the estimate.

Although a much more elaborate analysis of the Laugarnes data is indicated, the above discrepancies may be quite real and reflect the very considerable heterogeneity and fracturing of the reservoir. Due to local interconnection by fractures, the short-term interference tests performed on adjacent wells give much higher permeability estimates than the more intergrated global values obtained with the help of the total production rate and well data. The result indicates that considerable caution is called for in the interpretation of relatively short-term well interference tests on complex reservoirs.

Appendix

In processing the periodic data, we can also base our estimates on a lumped model as shown in Fig. 4. The model is characterized by a single input conductance K and a single capacitance S. In the physical sense, the capacitance simply represents the effective pore area of the container shown in Fig. 4. Let f be the volume rate produced from the container, h be the average liquid level in the container counted positive down and assuming that the ambient water level is zero, we arrive at the following equation governing the lumped system

$$S(dh/dt) + Kh = f \tag{4}$$

In the case of periodic flow $f = Fexp(i\omega t)$ where F is the amplitude and ω the angular frequency. Let the response of the liquid level be $h = Hexp(i(\omega t-\alpha))$, and inserting in equation (4) the resulting output-input amplitude ratio is found to be

$$H/F = (K^2+S^2\omega^2)^{-\frac{1}{2}} \tag{5}$$

and the phase angle

$$\alpha = \tan^{-1}(S\omega/K) \tag{6}$$

From the graphs in Fig. 3, we find that we can on the average take $F = 0.07$ m^3/s, $H = 19m$ and $\alpha = 0.78$ radians. Solving equations (2) and (3) for the system parameters we obtain

$$K = 2.7x10^{-3}m^2/s = 2.5x10^{-4}Kg/sPa, \quad S = 1.4x10^{4}m^2 \tag{7}$$

To translate these results into estimates of the average permeability k and average porosity ϕ we observe that the ground water level depression in Fig. 2 has the shape of a slightly elongated flat disk with an area of approximately $A = 4\ km^2$. For the present purpose we replace this disk by a circular one with a radius $R = 1.13$ km. On the basis of simple potential theoretical relations (Sunde, 1968), we find that the contact conductance of a flat circular disk of radius R immersed in a porous medium of fluid conductivity c is simply 8cR. In the present case, where the disk is placed on the surface of the half-space the contact conductance is consequently 4cR. Since the value of K given in (4) above is to be taken as an observed value of the actual contact conductance, we obtain the estimate for c as

$$c = K/4R = 2.5x10^{-4}/4x1.13x10^{3} = 5.5x10^{-8}s \tag{8}$$

Since $c = k/\nu$ where k is the permeability and ν the kinematic viscosity, and moreover, the porosity $\phi = S/A$, we obtain by assuming $\nu = 3x10^{-7}m^2/s$ (100°C) the following estimates

$$k = 1.7x10^{-14}m^2 = 17 \text{ millidarcy and } \phi = 3.5x10^{-3} \tag{9}$$

which is of the same order of magnitude as the results given above.

References

Bodvarsson, G., 1977a. Interpretation of borehole tides and other elasto-mechanical oscillatory phenomena in geothermal systems. Third Workshop on Geothermal Reservoir Engineering, December, 1977, Stanford University, Stanford, California.

Bodvarsson, G., 1977b. Unconfined aquifer flow with a linearized free surface condition. Jokull, 27:1977.

Bodvarsson, G., 1978. Mechanism of reservoir testing. Fourth Workshop on Geothermal Reservoir Engineering, December, 1978, Stanford University, Stanford, California (this volume).

Sunde, E.D., 1968. Earth Conduction Effects in Transmission Systems. Dover Publications, Inc., New York.

Thorsteinsson, T., 1976. Redevelopment of the Reykir Hydrothermal System in Southwestern Iceland. Second U.N. Symposium on the Development & Use of Geothermal Resources, San Francisco, 1975.

Thorsteinsson, T., and J. Eliasson, 1970. Geohydrology of the Laugarnes hydrothermal system in Reykjavik, Iceland. U.N. Symposium on the Development and Utilization of Geothermal Resources, Pisa.

Tomasson, J., and T. Thorsteinsson, 1976. Use of injection packer for hydrothermal drillhole stimulation in Iceland. Second U.N. Symposium on the Development and Use of Geothermal Resources, San Francisco, 1975.

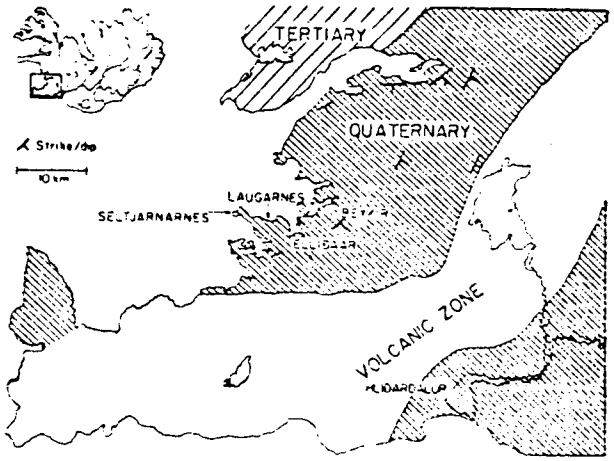

Figure 1. Geological map of southwest Iceland with index map.

From: Tomasson and Thorsteinsson (1976).

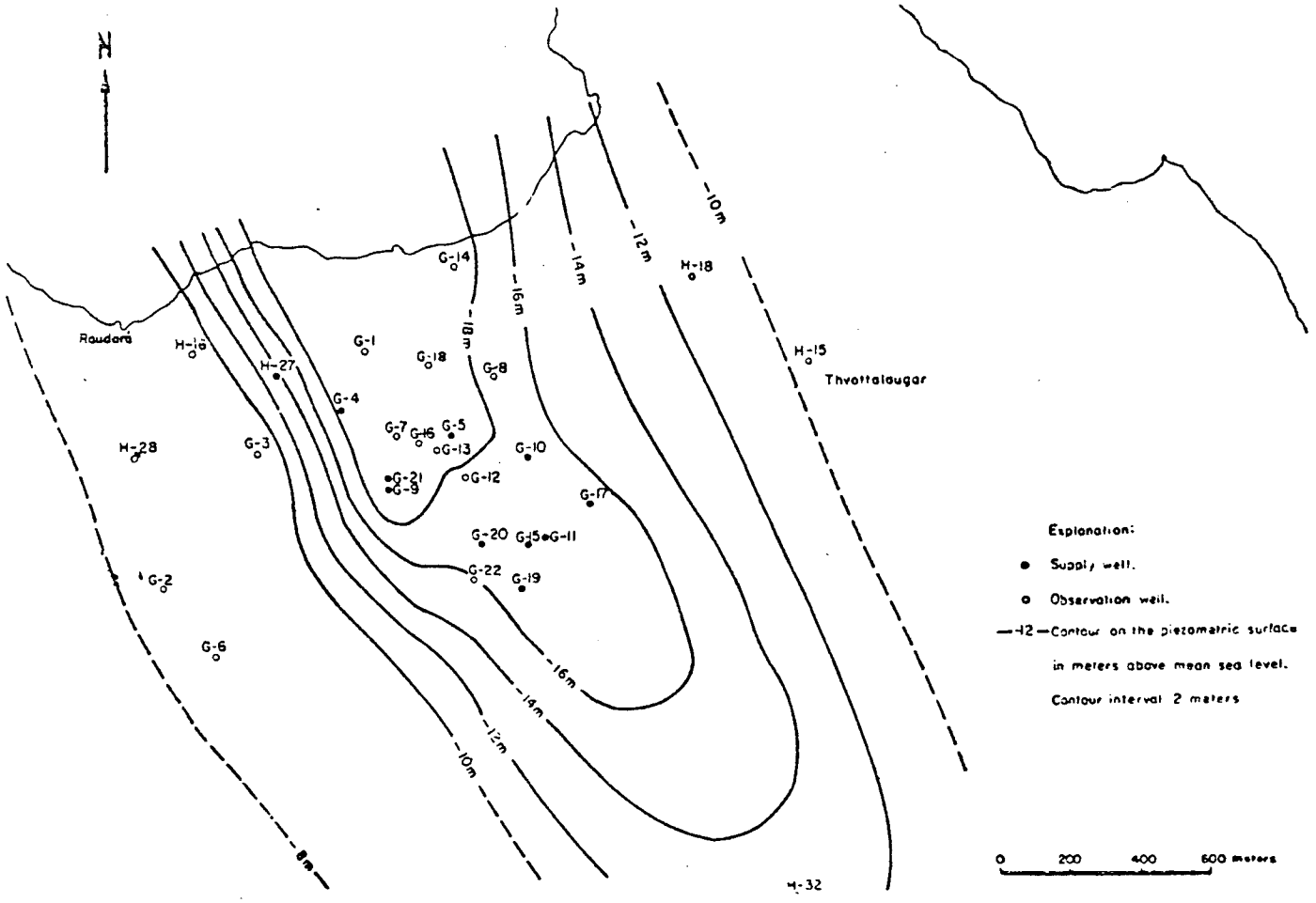

Figure 2. Elevation of the piezometric surface in the Laugarnes hydrothermal system on November 15, 1967.

From: Thorsteinsson and Eliasson (1970).

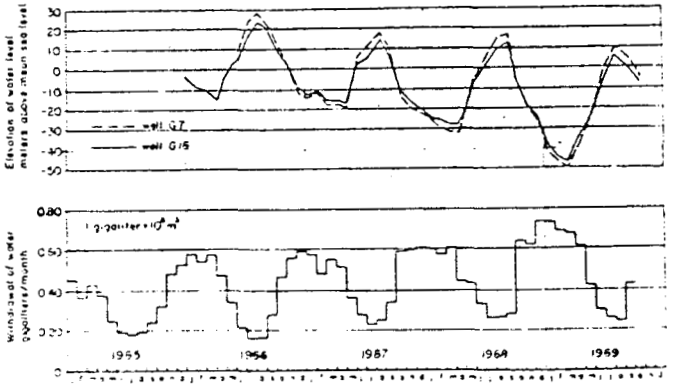

Fig. 3. Hydrographs of wells G7 and G16 and monthly withdrawals of water from 1965 to 1969.

From: Thorsteinsson and Eliasson (1970).

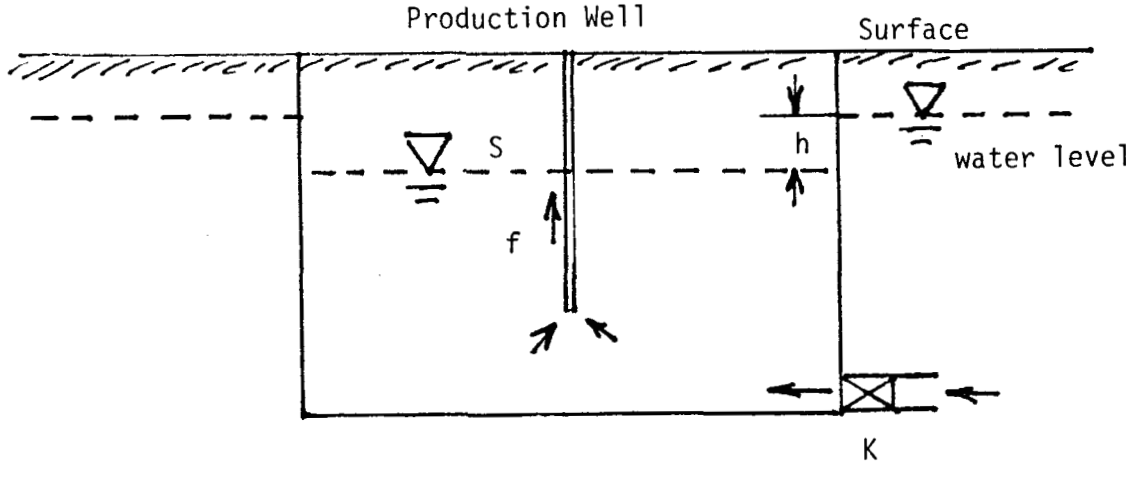

Fig. 4. Lumped model of input conductance K and capacitance S.

GEOTHERMAL RESERVOIR TESTING BASED ON SIGNALS OF TIDAL ORIGIN

Gunnar Bodvarsson
School of Oceanography
Oregon State University
Corvallis, Oregon 97331

and Jonathan Hanson
Lawrence Livermore Laboratory
University of California
Livermore, California 94550

Introduction

The theory of pressure and water level oscillations of tidal origin in Darcy type aquifers and petroleum reservoirs has been discussed in a number of recent publications (see for example, Bredehoeft, 1967; Bodvarsson, 1970, 1977, 1978a, 1978b; and Arditty et al., 1978). There is a general agreement that observational data on the tidal pressure phenomena may be applied to obtain useful estimates of important reservoir parameters such as the permeability.

A Simple Basic Model

In the simplest setting involving a single open well connected by a small spherical cavity to a large homogeneous and isotropic reservoir, the mechanism of the tidal well test is easily comprehended on the basis of the model illustrated in Fig. 1 below. Let the permeability of the porous medium be k, the density of the fluid by ρ, its kinematic viscosity be ν and hence the fluid conductivity of the medium be $c=k/\nu$. Moreover, let s be the hydraulic capacitivity or storage coefficient of the medium and the diffusivity therefore $a=c/\rho s=k/\mu s$ where μ is the absolute viscosity of the fluid. The skin depth of the medium at an angular frequency ω is then $d=(a/2\omega)^{\frac{1}{2}}$ (Bodvarsson, 1970). For the present purpose, concentrating first on cases where boundary effects can be ignored, we assume that the skin depth of the reservoir material at tidal frequencies is smaller than the extent of the reservoir including the depth of the well. In other words, the reservoir can be assumed to be infinite as viewed from the well-cavity. Introducing a spherical coordinate system with the radial coordinate r and with the origin placed at the center of the cavity, the fluid pressure field p(r,t) in the porous medium is governed by the diffusion equation (Bodvarsson, 1970).

$$\partial_t p - a[\partial_{rr} + (2/r)\partial_r]p = -(\varepsilon/s)\partial_t b \qquad (1)$$

where t is time, b(t) the tidal dilatation of the medium and ε is the formation matrix coefficient. Let r_o be the radius of the cavity, f the cross section of the well and g the acceleration of gravity. The boundary condition at $r = r_o$ is then

$$(f/g)\partial_t p - Fc\partial_r p = 0, \qquad (2)$$

where $F = 4\pi r_o^2$ is the surface area of the cavity.

The expression for the oscillations of the water level in the well in response to the dilatation is obtained by solving equation (1) with the

boundary condition (2) and deriving the pressure at the cavity which is equal to the pressure at the well bottom. To simplify our results without any appreciable loss of generality, we can in most cases assume that the skin depth of the medium is much larger than the dimensions of the cavity, that is, $d >> r_o$. Assuming therefore an infinite medium and that b and $p \propto \exp(i\omega t)$, the solution of (1) in terms of amplitudes is (Bodvarsson, 1970)

$$p = (B/r)\exp[-(1+i)r/d] - (\varepsilon b/s), \tag{3}$$

where B is a constant to be determined by the boundary condition (2). Inserting (3) into (2), we finally obtain for the amplitude of the water level in the well

$$h = -(\varepsilon b/\rho g s)T/(1+T), \tag{4}$$

where b is the dilatation amplitude and T is the tidal factor,

$$T = -4i\pi g s c r_o/f\omega, \tag{5}$$

An elementary potential theoretical argument shows that the admittance or conductance of the cavity is

$$A = 4\pi c r_o, \tag{6}$$

and we can define the mass stiffness of the well

$$S = dp/dm = g/f, \tag{7}$$

This quantity measuresthe increase in well bottom pressure when a unit mass of liquid is added to the well. Using these expressions, the tidal factor can be expressed

$$T = -iAS/\omega \tag{8}$$

which along with (4) is our final result for the above simple model illustrated in Fig. 1.

It is to be noted that the above expression (8) will also hold for a closed well situation. We have then only to redefine the mass stiffness

$$S = dp/dm = 1/\beta M \tag{9}$$

where M is the liquid mass in the well and β is the compressibility of the liquid. In the case of a gas cap, (9) will have to be adjusted accordingly. In the case of a closed well equation (4) will have to be expressed in terms of the well-head pressure rather than a water level.

Interpretation of Well Data

In the relatively simple situation described above, the interpretation of well data is based on equations (4) and (8). Invariably, ρ and f can be

taken to be known. Since in most practical cases, the effective dilatation εb and formation capacitivity s are of less interest than the formation fluid conductivity c, the latter quantity is generally the primary target of any interpretation of observational tidal well data. Equations (4), (8) and (6) show that c has to be derived from the tidal factor T and that this factor can be separated if we are able to observe the water level amplitude at two different tidal frequencies. Since the tidal force field includes a number of frequencies this will generally be possible. Being, in principle, able to obtain T and thus on the basis of (8) the admittance A, the fluid conductivity will have to be derived with the help of (6). In the rather idealistic situation with a spherical well-cavity of known radius r_o, we are therefore, in principle, able to reach our goal of obtaining a numerical estimate of c.

From the practical point of view, the procedure will, however, break down if $T >> 1$. The factor $T/(1+T)$ is then approximately equal to unity and the water level amplitude h will be independent of the fluid conductivity. In practice, we can expect this difficulty to become serious when about $T > 3$. Since in most cases the factor $4\pi g/f\omega$ will be of the order of 10^7 (MKS), we see that the above inequality implies $r_o c > 3\times10^{-7}$(MKS). For water at 100°C with $\nu = 3.10^{-7} m^2/s$ we obtain then in terms of permeability $r_o k > 3\times10^{-7}\times3\times10^{-7} \approx 0.1$ darcy-meters. Therefore, taking, for example, $r_o = 0.5$ m, we find that the above difficulty becomes serious for permeabilities in excess of 200 millidarcy. In other words, the tidal test based on open well situations is sensitive only to small to medium permeabilities. Due to increased stiffness S, the applicability in the case of closed wells is more restricted.

Deviations from the basic model

Non-spherical well-reservoir connection. The assumption of a spherical cavity is perhaps to most obvious idealization in the above basic model. Unfortunately, the symmetry of the pressure field will be broken in the case of a non-spherical cavity, and the above simple relations may, in principle, not apply. However, provided the dimensions of a non-spherical cavity are much smaller than the skin depth d of the medium, and this will mostly be the case, the difficulties arising are not too important from the more global point of view. The global pressure field at some proper distance from the cavity will be approximately spherically symmetric and the above analysis will largely be valid. The most serious casualty is that the cavity admittance is not given by the simple relation (6) and other analog relations have to be relied on. In practical cases, there may be difficulties in establishing the form of the cavity. Most frequently, however, the well-reservoir connection consists of an open section of the well. Let the radius of the well be r_1 and the length of the open section be L. An elementary potential theoretical exercise shows that when $L >> r_1$ the admittance can then be (Sunde, 1968) approximated by

$$A = 2\pi cL/\ln(L/r_1) \qquad (9)$$

It is of interest to point out that an open section of L = 10m and r_1 = 0.1m has approximately the same admittance as a spherical cavity of r_o = 1.1 m.

Multi-well setting. Another important deviation from the basic model involves cases where there is more than one well opening into the reservoir. This situation may lead to a well-well interaction and pressure field scattering. The practical criterion for interaction is obtained by comparing the well-well distance to the skin depth d of the medium. In general, two wells will interact noticeably if the distance between the well-reservoir cavities is approximately equal or less than the skin depth at tidal frequencies.

The analysis of multi-well situations is more complex than the results given above. In the case of spherical cavities, the solution for the pressure amplitude field will then have to be constructed as a sum over solutions of the type (3), that is

$$p = \sum_j (B_j/r_j)\exp[-(1+i)r_j/d] - (\varepsilon b/s), \qquad (10)$$

where the j^{th} summand is centered at the j^{th} well-cavity, r_j is the distance from the field point to the center of the j^{th} cavity and the B_js are integration constants. A boundary condition of the type (2) applies at each well-cavity and the constants B_j are obtained by solving a set of linear algebraic equations. An estimate for the fluid conductivity can then be obtained along similar lines as indicated above. We will, however, refrain from a further discussion. Obviously, neglecting well-well interaction M multi-well situations leads to an underestimate of the formation fluid conductivity c.

References

Arditty, P.C., Ramey, H.J., Jr., and A.M. Nur, 1978. Response of a closed well-reservoir system to stress induced by earth tides. SPE paper 7484 Houston, Texas.

Bodvarsson, G., 1970. Confined fluids as strain meters. J. Geophys. Res. 75(14):2711-2718.

Bodvarsson, G., 1977. Interpretation of borehole tides and other elastomechanical oscillatory phenomena in geothermal systems. 3rd Workshop on Geothermal Reservoir Engineering, December, 1977, Stanford University, Stanford, California.

Bodvarsson, G., 1978a. Convection and thermoelastic effects in narrow vertical fracture spaces with emphasis on analytical techniques. Final Report for U.S.G.S. pp. 1-111.

Bodvarsson, G., 1978b. Mechanism of reservoir testing. 4th Workshop on Geothermal Reservoir Engineering, December 1978, Stanford University, Stanford, California (this volume).

Bredehoeft, J.D., 1967. Response of well-acquifer systems to earth tides. J. Geophys. Res., 72(12), 3075-3087.

Sunde, E.D., 1968. Earth Conduction Effects in Transmission Systems. Dover Pulications, Inc., New York. pp 370

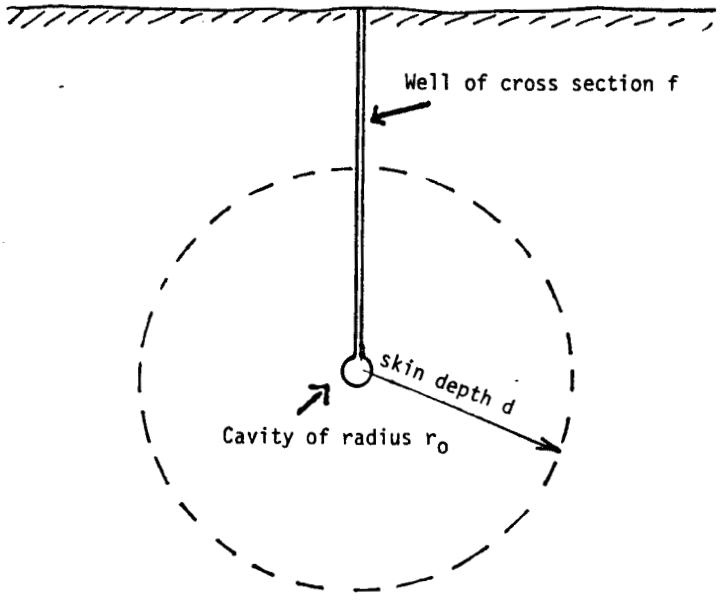

Figure 1. Single well model.

PRESSURE DRAWDOWN ANALYSIS FOR THE TRAVALE 22 WELL

A. Barelli, W.E. Brigham, H. Cinco, M. Economides, F.G. Miller,
H.J. Ramey, Jr., and A. Schultz
Department of Petroleum Engineering
Stanford University
Stanford, California 94305

Introduction

This work presents preliminary results on the analysis of drawdown data for Travale 22. Both wellhead pressure and flow rate data were recorded in this well for over a period of almost two years.

In the past, Barelli et al. (1975) and Atkinson et al. (1977) presented the analysis of five pressure buildup tests. Figure 1 shows the Horner plot for these cases. They found that to have a good match in all cases, it was necessary to assume that the Travale 22 well is intersected by a partially penetrating vertical fracture in a parallelepiped whose bottom side is maintained at constant pressure (boiling front), as shown in Fig. 2.

Atkinson et al. also presented an analysis for a pressure interface test run in the Travale-Radicondoli area. In this case, the Travale 22 well was flowing and the pressure recorded at wells R1, R3, R5, R6, R9, and Ch1 (see Fig. 3). Analysis of these data showed that pressure interference in this reservoir can be matched by considering pure linear flow (Figs. 4 and 5). This indicated the possible presence of a vertical fracture intersecting the Travale 22 well. It was determined that fracture is oriented along the N73°W direction. In addition, the pressure interference data showed that no boundary exists within 2 kilometers from the fracture plane. It was mentioned that linear flow should take place in both horizontal and vertical directions.

Analysis of Drawdown Data

As mentioned previously, both wellhead pressure and flow rate were measured when this well was continuously flowing during almost two years. First the bottomhole pressure was calculated and plotted on a semilog paper (Fig. 6). Data on this graph show a curve of increasing slope similar to a fractured well case. The pressure seems to stabilize at 400 days, indicating a possible constant pressure boundary.

A log-log graph of the pressure data is shown in Fig. 7. It can be seen that the first data points follow a one-half slope straight line, suggesting linear flow.

Since previous buildup analysis and interference analysis suggested that the well is intersected by a fracture and the reservoir has a constant pressure boundary, two models are used to analyze the pressure drawdown data:

1) a well intersected by a fully penetrating vertical fracture in a finite system (Gringarten, Ramey, and Raghavan), and,

2) a well intersected by a partially penetrating vertical fracture in a parallelepiped whose bottom side is a constant pressure boundary.

Figure 8 presents the application of the type-curve matching technique by using the first model. Agreement between most of the pressure data and the dimensionless pressure curve is good; however, at very long time (about 400 days), the system seems to reach steady-state flow, indicating the existence of a constant pressure boundary.

Figure 9 presents the match of data with the second flow model (parallelepiped model). The data appears to match the curve for dimensionless formation thickness ≈ 2.5.

Results from this analysis and from previous work are summarized in Table I. It can be seen that although both the results from buildup and drawdown analysis suggest the same type of geometry for the system, they do not agree regarding the dimensions of the reservoir.

Further effort is needed in the analysis of additional drawdown data not presented in this work. At this point, the results from the buildup data are more reliable because the analysis was based on several tests.

Conclusions

A preliminary analysis of the drawdown data for the Travale 22 well seems to indicate the following:

1) the well is intersected by a highly conductive fracture, as found from the buildup and interference data, and

2) a constant pressure boundary seems to exist, causing the system to reach pseudosteady flow at about 400 days.

References

Atkinson, P., Barelli, A., Brigham, W.E., Celati, R., Manetti, G., Miller, F., Nery, G., and Ramey, H.J., Jr.: "Well-Testing in Travale-Radicondoli Field," Proc., Lardarello Workshop on Geothermal Resource Assessment and Reservoir Engineering, Pisa, Italy, Sept. 12-16, 1977.

Barelli, A., Celati, R., Manetti, G., and Neri, G.: "Horner's Method Applied to Buildup Tests on Travale 22 Well," Summaries of the Second Workshop on Geothermal Reservoir Engineering, Stanford University, Stanford, California, Dec. 15-17, 1975.

Nomenclature

c_t = compressibility $(Kg/cm^2)^{-1}$

h = reservoir thickness (m)

k = permeability (m)

p = pressure (Kg/cm^2)

q = flow rate (tons/hour)

t = time (days)

x_f = half fracture length (m)

ϕ = porosity

μ = viscosity (cp)

TABLE I: RESULTS FROM PRESSURE TESTS

	kx_fh_f (Darcy m^2)	$\phi h_f x_f$ (m^2)
Interference	$5x10^4$	$1.5x10^4$
Buildup	$2.5x10^5 k$	$2.5x10^4$ (ϕ=.1)
Drawdown (Parallelepiped)	$1.4x10^3$ (ϕ=.1)	$1.2x10^4$ (ϕ=.1)
Drawdown (Vertical Fracture)	$6.552\ x_f$	$3.66x10^6/x_f$

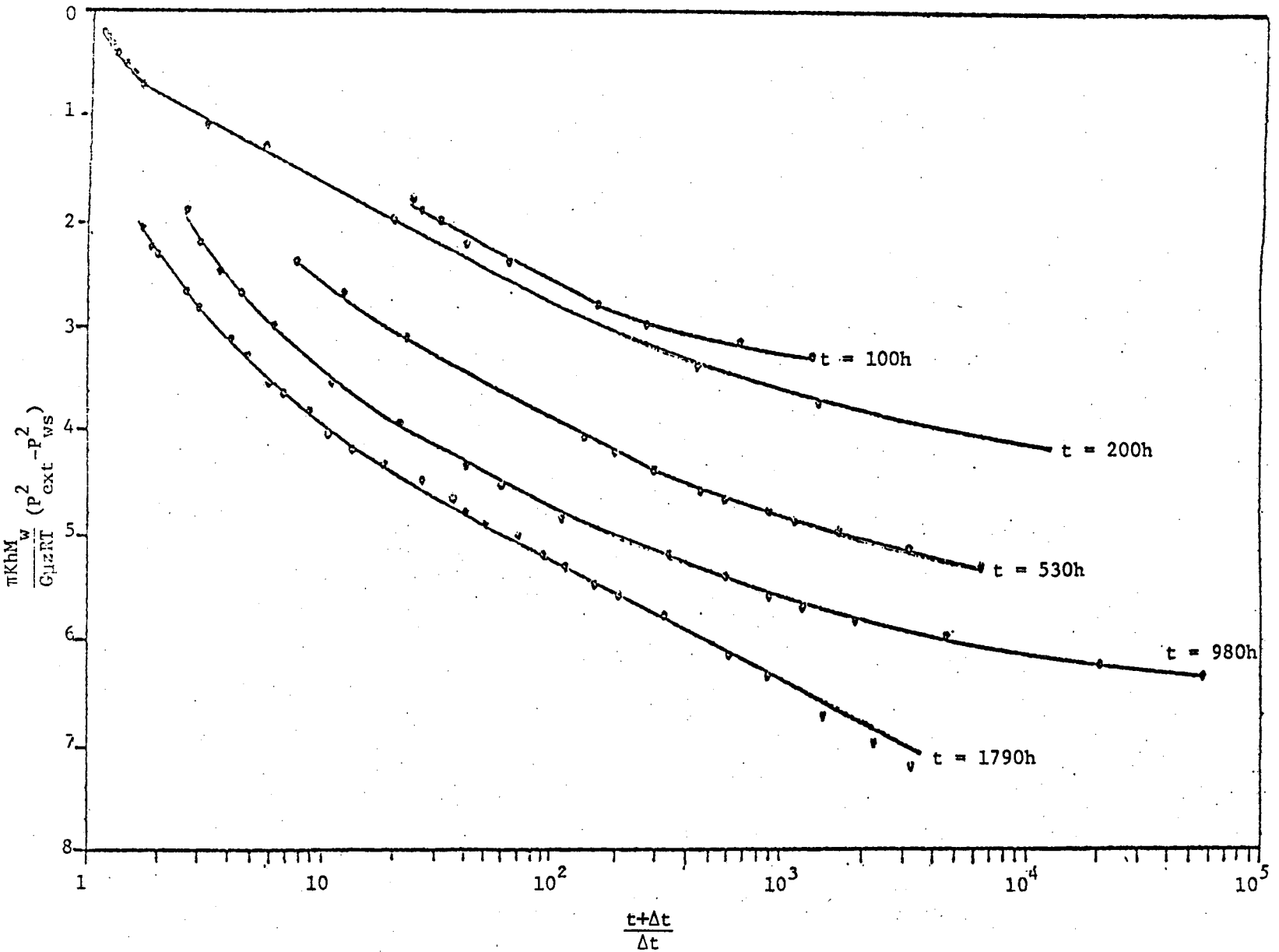

FIG. 1: RECONSTRUCTED HORNER BUILDUP GRAPH FOR T-22 WELL, 1972-1973 (Barelli et al., 1975)

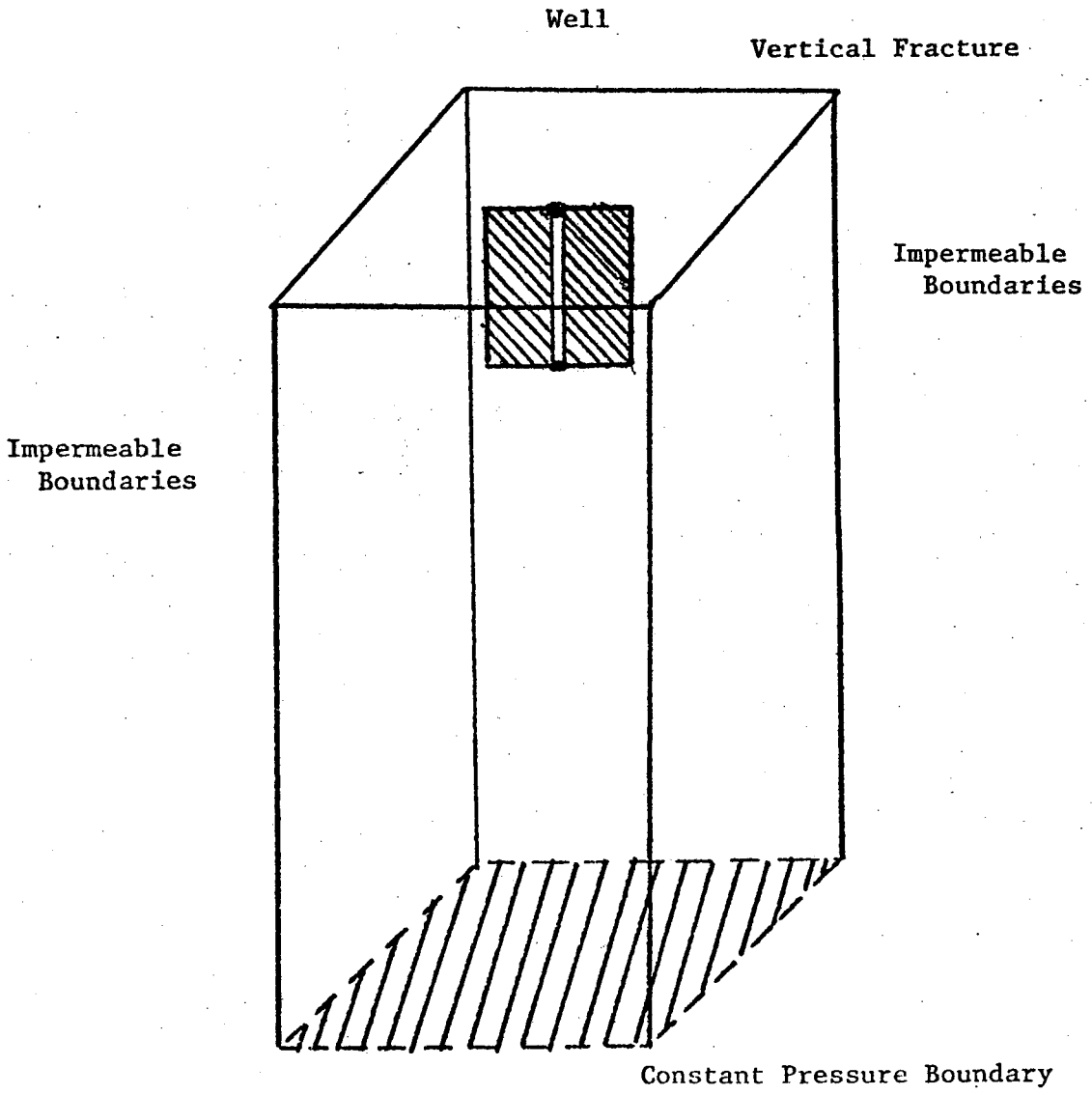

FIG. 2: PARALLELEPIPED MODEL FOR A WELL INTERSECTED BY A PARTIALLY PENETRATING VERTICAL FRACTURE

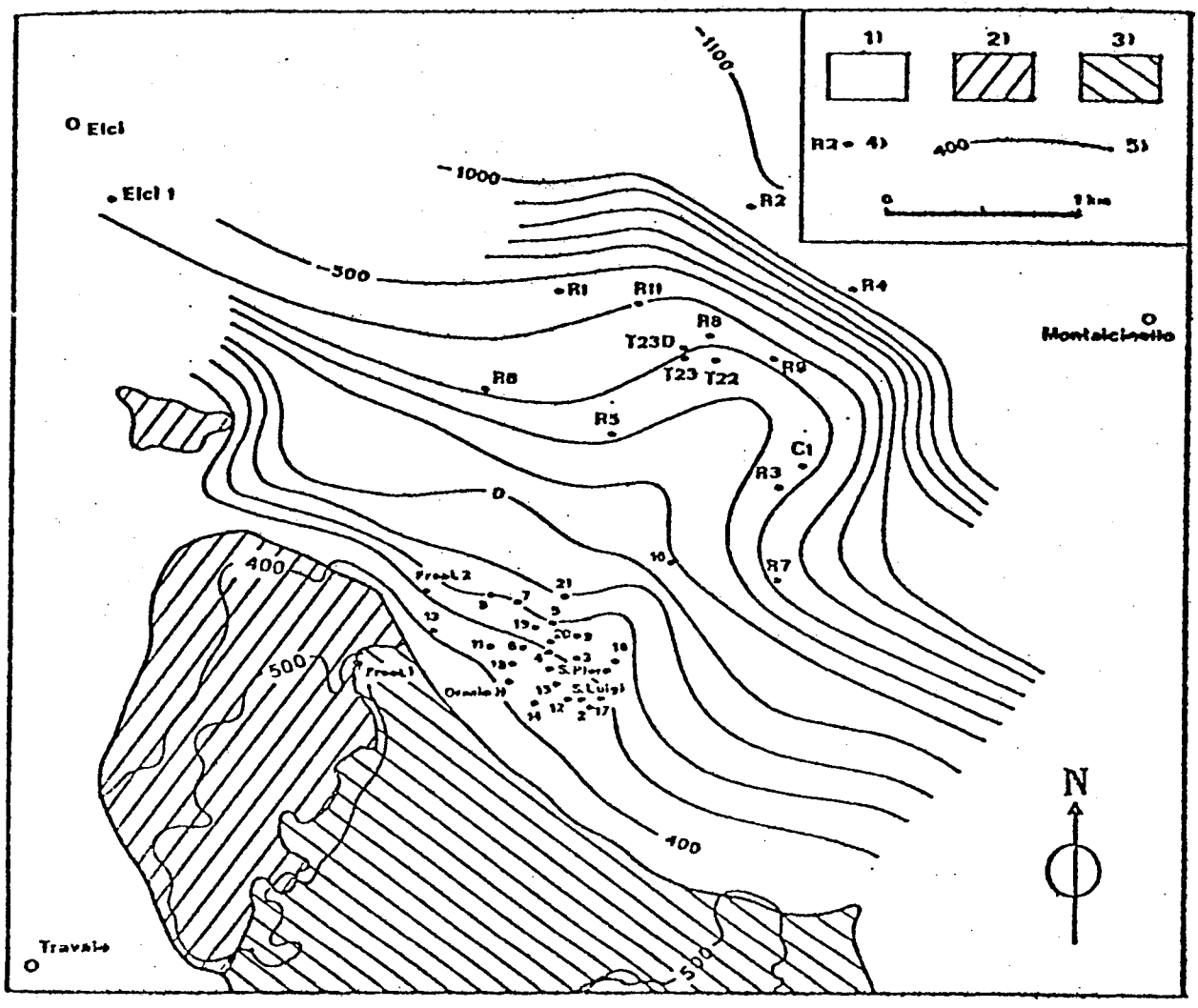

FIG. 3: TRAVALE GEOTHERMAL FIELD. STRUCTURAL MAP OF THE RESERVOIR TOP.
1: COVER COMPLEX: 2: RADIOLARITES AND LIMESTONES (PREDOMINATING);
3: CAVERNOUS LIMESTONES; 4: WELLS; 5: ISOBATHS (ELEVATION m a.s.l.)

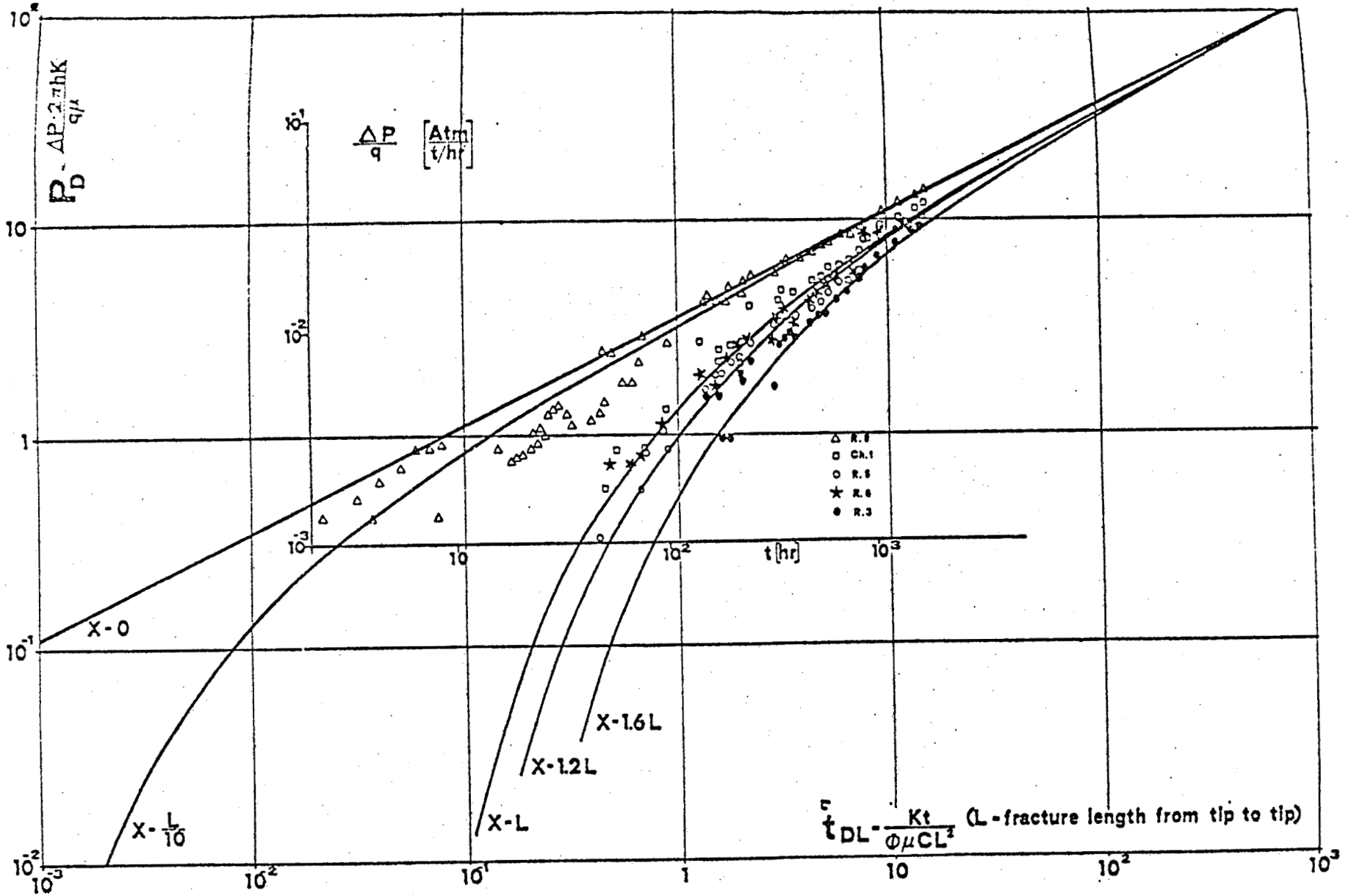

FIG. 4: INTERFERENCE DATA MATCHED WITH TYPE CURVES (Atkinson et al.)

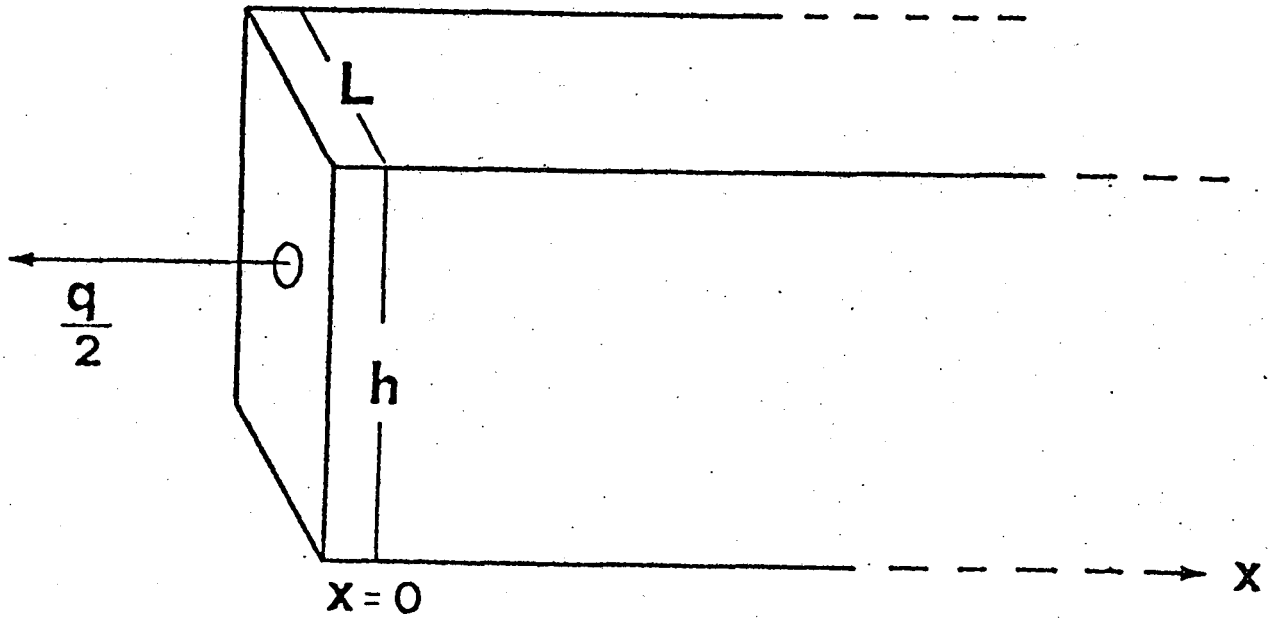

FIG. 5: LINEAR FLOW GEOMETRY (Atkinson et al.)

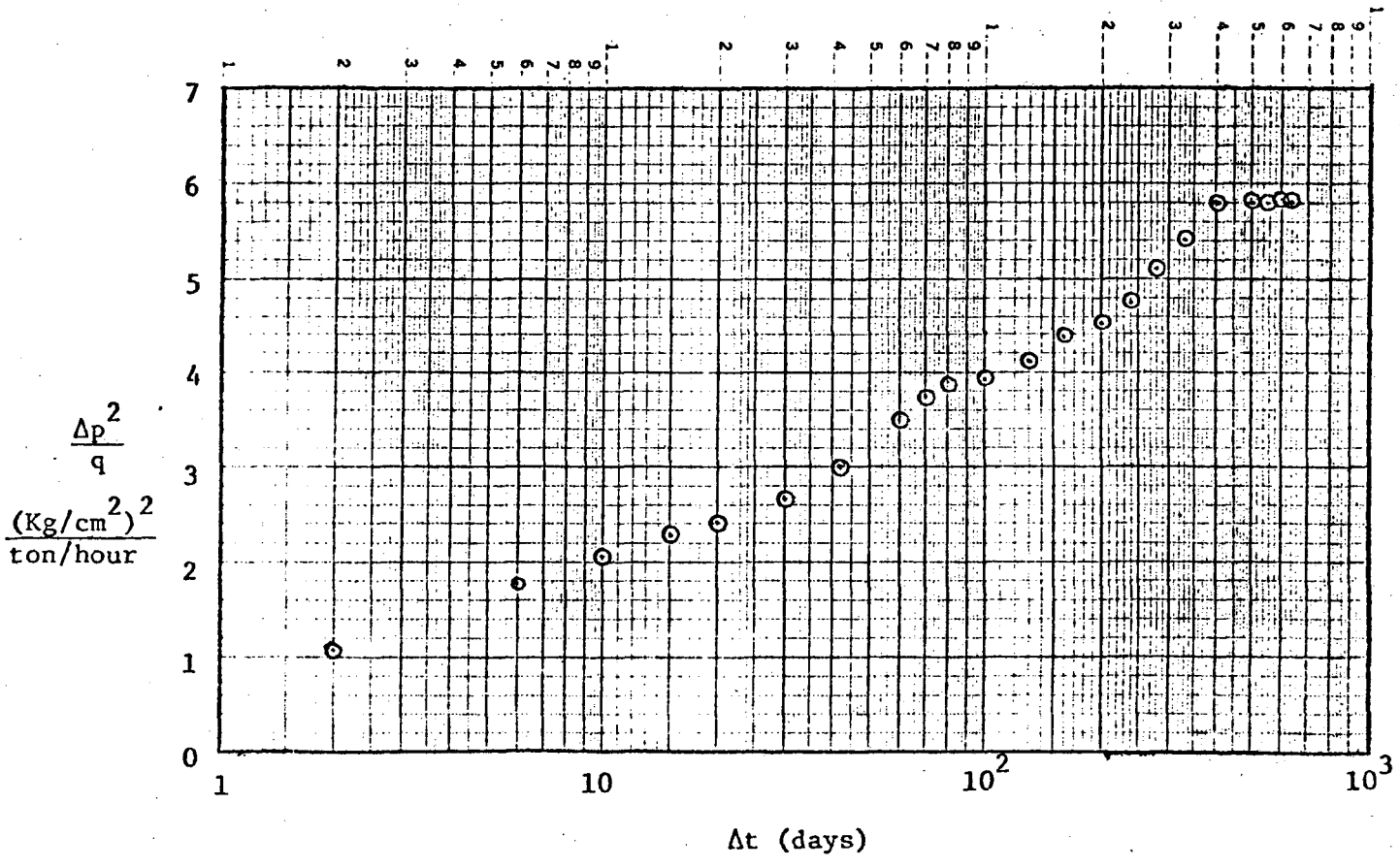

FIG. 6: SEMILOGARITHMIC PLOT FOR THE TRAVALE 22 WELL DRAWDOWN DATA

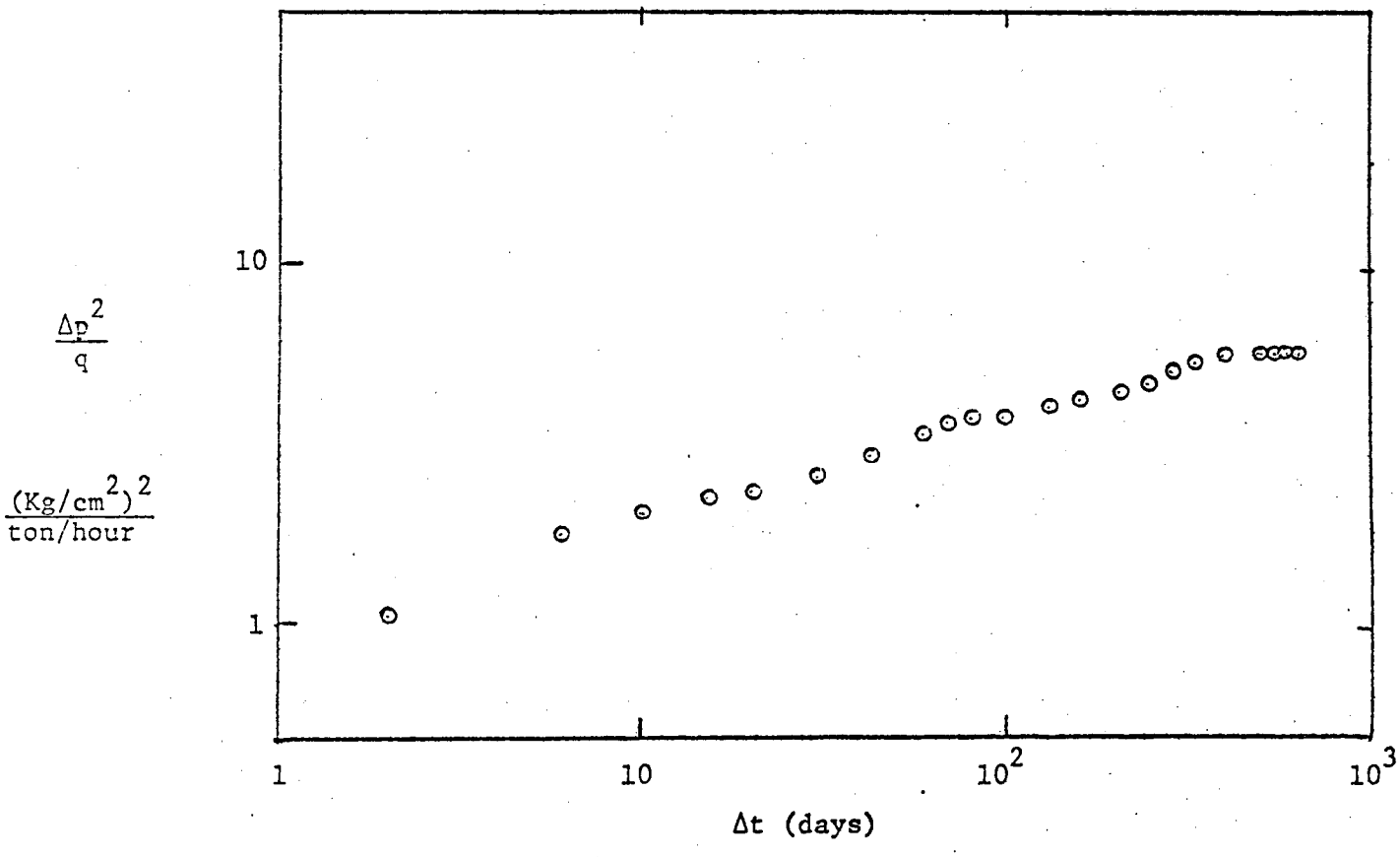

FIG. 7: LOG-LOG GRAPH OF DRAWDOWN DATA

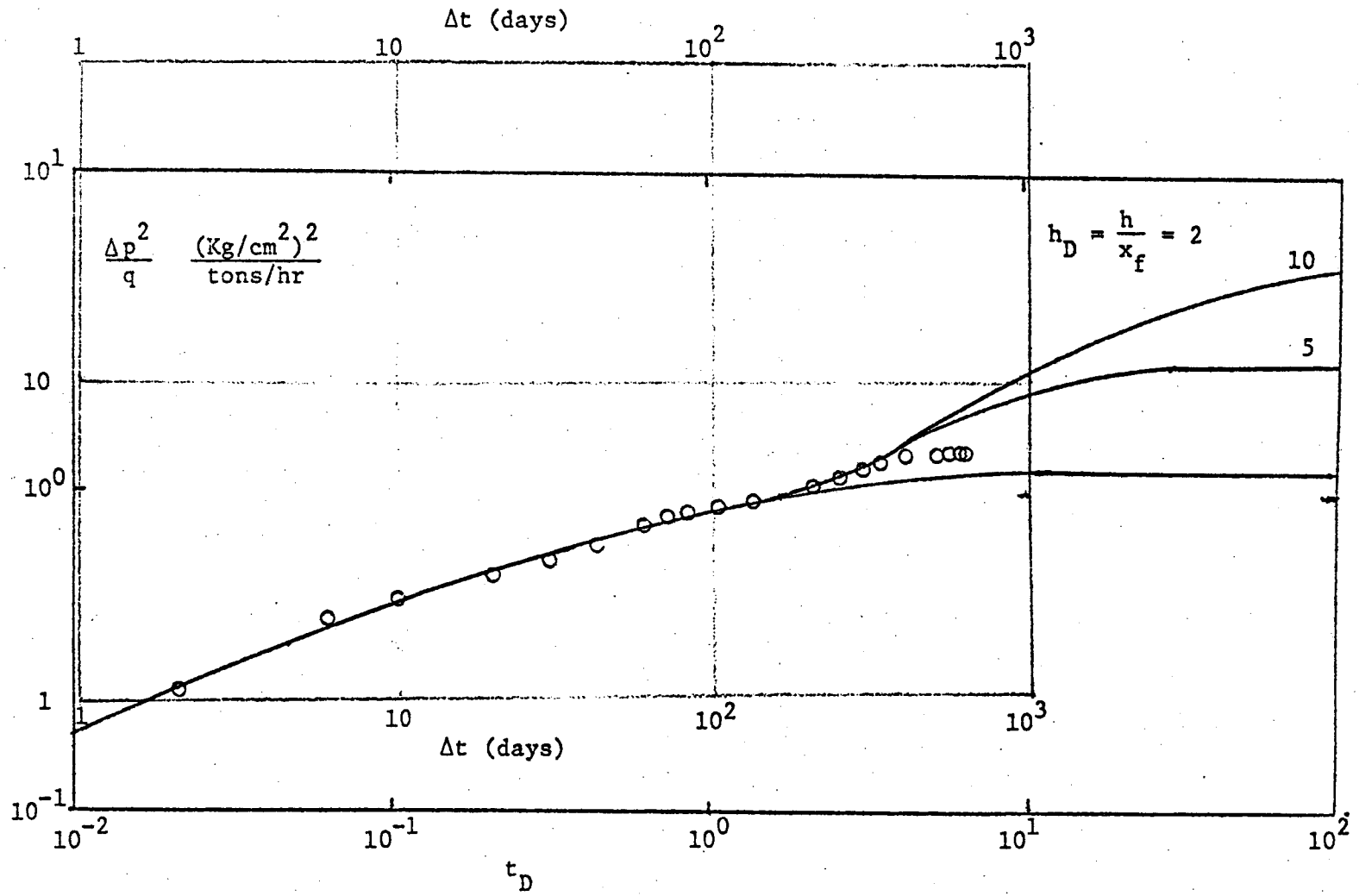

FIG. 8: TYPE-CURVE MATCHING WITH PARALLELEPIPED MODEL

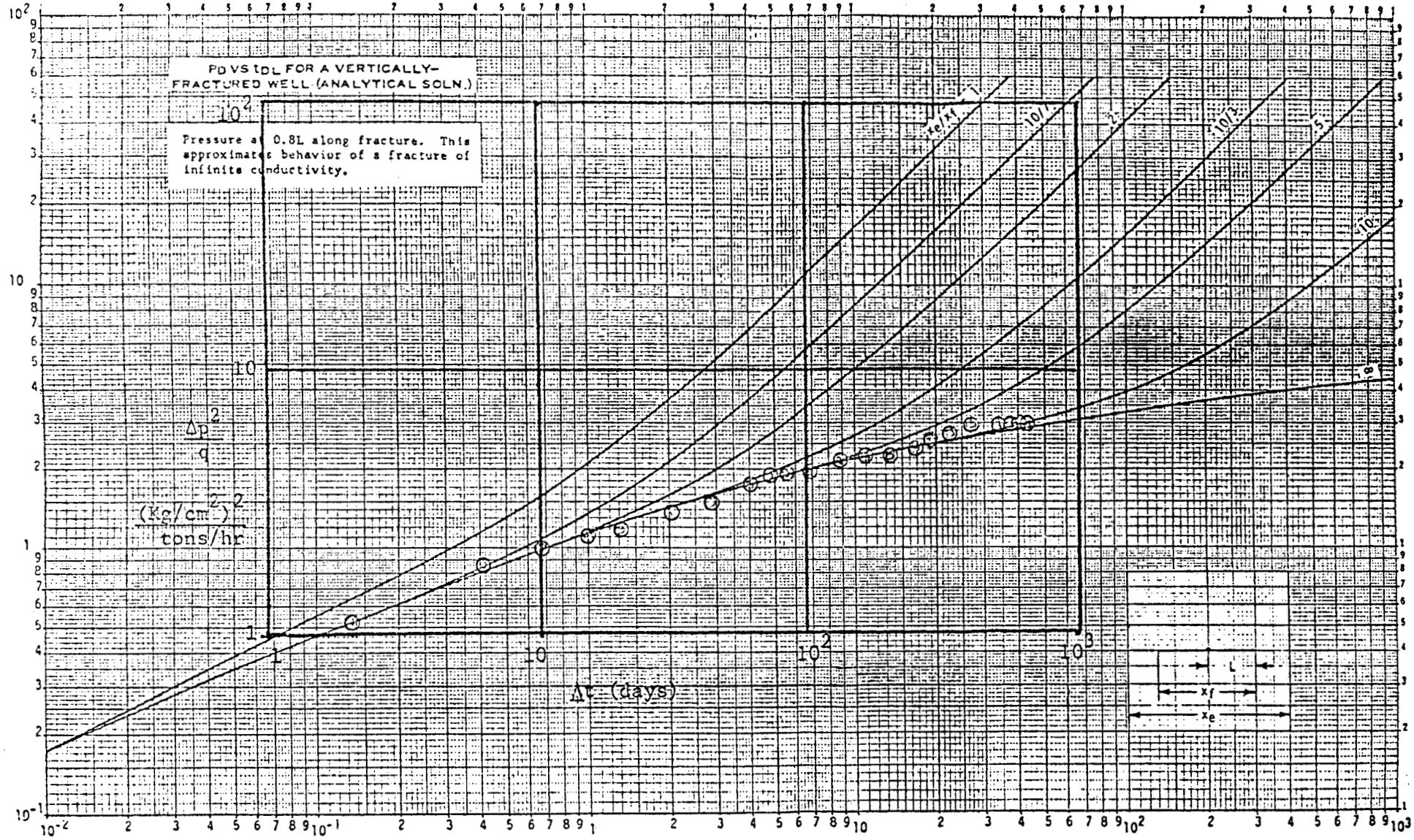

FIG. 9: TYPE-CURVE MATCH FOR THE DRAWDOWN DATA BY USING THE INFINITE CONDUCTIVITY VERTICAL FRACTURE SOLUTION

INJECTION TESTING IN GEOTHERMAL WELLS.

MEHMET SALTUKLAROGLU.
ELC-ELECTROCONSULT.
MELCHOR OCAMPO No. 463 3°piso
MEXICO 5, D.F.
(8 VIA CHIABRERA, 20151)
MILANO ITALY).

JESUS RIVERA RODRIGUEZ.
COMISION FEDERAL DE ELECTRICIDAD.
MELCHOR OCAMPO No. 463 3° piso.
MEXICO 5, D.F.

ABSTRACT.

Transient pressure analysis methods were applied to analyze the results of injection tests carried out in a recently completed geothermal well in Los Azufres Geothermal field in Mexico. Potential use of those methods (employing injection, two rate injection and fall off tests) is ilustrated in obtaining important well and reservoir parameters at the well completion stage and in predicting future well perfor mance. Also, based on the experience obtained with this well and other similar wells, suggestions are made on the type of analysis which is most applicable.

INTRODUCTION.

Injection tests are carried out as a part of completion procedures of geothermal wells in the Los Azufres Geothermal Field, Michoacan,Mexico. The main purpose of these tests is to obtain early information about the well and reservoir parameters in order to predict future well performance. Injection tests are considered especially useful to achieve this objective, as the problems associated with two phase flow conditions observed during draw-down and build-up tests are avoided, making the eventual analysis simpler.

Moreover, injection tests are easier to carry out than the drawdown and build-up tests.

In this paper the application of different pressure analysis methods to the results of several injection tests carried out in a geothermal well in Los Azufres is illustrated; and the potential of these methods in reaching the above objective, even with incomplete data, is demonstrated.

GENERAL BACKGROUND.

Los Azufres Geothermal Field is located in the State of Michoacan in Central Mexico. It is on the E-W oriented neo-volcanic axis and is covered by neo-quaternary volcanic deposits overlying a basement of lutites and sands. Microgranular andesites form the lower part of the volcanic formations and are overlaid at places by riolites and pyroclastics.

Alteration zones and thermal manifestations are clearly related to tectonic activity and are located near faults and fracture zones. The wells so far drilled in this area are sited near the known major faults in order to encounter secondary permeability associated with them.

The main production is thought to come through fractures.

The completion of the well is shown in Fig. 1 which also includes the data on circulation fluid losses and percentage core recovery.

It was drilled almost completeley in fractured andesitas. The fractures were usually filed with silica, chlorite and epidote. The portion of the well below 2200 m was highly fractured and fragmented as was observed from the last two cores taken and as confirmed by very poor core recoveries.

The well was drilled using bentonitic mud from surface up to 1500 m and with water from 1500 m downwards.

The circulation was totally lost at 2224 m for one hour, then partially recovered and was lost again completeley at about 2332 m. The last part of the well was drilled with total loss of circulation.

The first series of tests were carried out when the well was at 2404 m, after a core had been taken at this level. Here when the first attempt was made to core, it was found that there was an accumulation of cuttings 50 m thick at the bottom, and after several trials these cuttings were cleaned with a batch of mud.

The second series of tests were run after deepening the well to 2450 m and putting a liner as shown in Fig. 1. The well was stopped at this depth for reasons of well safety, problems with water supply and materials.

TEST PROCEDURE.

Before the injection tests were run two temperature surveys had been carried out (5 and 7 hours after circulation stopped) to determine the distribution of the permeable

Type Curve Matching Using the Curves of Earlougher and Kersch.(3).

The results of the analysis with this method are also presented in tables II and III.

Although two or three different matches could be made for earch test, an average of the parameters obtained with different matches give a reasonable indication of the order of values sought. One can also observe that the average values obtained by this method compare reasonably well with the average values obtained by the log-log method.

With Semi-Log Method.

In order the confirm the conclusions obtained by the log-log analysis semi-log standard plots of data were also made.

It was found that wellbore storage effects were dominating almost all or a very large portion of the data; and either the semi-log straight line data were lost completely (because of not having sufficient clock time) or only the beginning of the required data were recorded. Therefore, it was impossible to analyse the data by this method.

However, the semi-log plot of the results of the first test (the longest recorded test) are presented in Fig. 13 as an example. It can be seen that towards the end of the data semi-log straight line conditions are being reached, and the slope of the drawn lines may give an idea about the lower limit of the transmissivity value. One can also observe a high skin effect.

Other methods of analysis were also tried. In Figure 14 one can see the results of the conventional two rate analysis (2) of the second test. It will be noted that the proper straight line portion of the data had not been reached.

The method suggested by Gladfelter et al. (4) for the data dominated by wellbore storage effects, was also applied to the results of some of the tests.

Although it was possible to obtain reason ably good semi-log straight lines in every case, the transmissivity obtained was very low (in the order of 1.60 d.m./cp) compared to the values shown in tables II and III. However, in plotting the graphs, a figure of 0.0351 m^3/m (0.0672 bbl/ft) was used (as calculated using the actual hole, casing and pipe dimensions during the tests) for casing capacity. This figure gives a C value of 0.1551 bbl/psi. On the other hand the tests results indicate a C value of about 0,250 bbl/psi.

When a correction was made to the casing capacity using this latter value, it was found that the slope of the semi-log straight line diminished giving transmissivity values slightly smaller than those obtained by type curve matching methods. Also it has been observed with the method that unless one uses very small time intervals (one or two minutes) one gets a large dispersion of points.

It was also found that with this type of wells one can not use methods of analysis employing logarithmic pressure change versus time. This is probably because the late time transients are short and the early time transient data are masked by wellbore storage effects. Therefore, it is very difficult to select the plot which gives the right straight line for the evaluation of the parameters sought.

In the case of the five tests considered usually there were not any late time transient data, and when they were recorded either they were not sufficient or they could not be used for analysis for the above reasons.

DISCUSSION.

Although the results obtained by the type curve matching methods vary from match to match and from one method to other, they are all of the same order and give a good indication in what range the actual values lie. In fact the average values obtained by both type curves agree very well and give a very good idea about the parameters sought.

It seems the log-log method gives results with less dispersion and for the data used appears to be superior to the other as it also enables us to calculate the storitivity.($\emptyset hc_t$).

It will be noted that the second series of tests indicate a transmissivity 10% higher than the value obtained by the first series of tests. This is quite logical as the additional drilling of 40 m after the first series of tests, through an obviously fractured formation, must have increased the transmissivity by increasing the h.

The skin damage appears to be high, but understandable when it is remembered that almost 220 m were drilled with no return of the circulation fluid and the cuttings were obviously pushed into the fractures, causing a skin damage. It clearly lies between 5 and 10.

The storage coefficient indicated by both series of tests is about 0.250 bbl/psi which is about twice as high as the value calculated taking into account the profile of the well (0.1578 bbl/psi). The discrepency may be due to the fractured nature of the tested formation, with the fractures acting as a part of the well storage.

This may be supported by the increase in storitivity after the deepening of the well by40 m. It will be noted that the storitivity is nearly doubled after this

zones along the well depth. The results of these tests are plotted in Figure 2. It can be noted that although the formations below 2200 m were generally permeable, several well defined zones had higher permeability and might be associated with fractures and/or fractured zones. The best permeable feature appears to be the zone where the first total loss of circulation was observed (at about 2224 m).

Also a pressure-depth survey was made to determine the standing water level in the well. It was found to be at about 672 m.

The tests were carried out using a Kuster pressure gauge to monitor the pressure changes. Three-hour clocks were used as clocks of larger capacities were not available.

The first series of testing consisted of three tests as follows:

I.- With the pressure gauge at 1472 m, injection at the rate of 500 litres/min., for 370 minutes, then recovery for 236 minutes.

II.- With the pressure gauge at 1472 m, injection at a rate of 1000 litres/min for 75 minutes and then raising the injection rate to 1500 litres/min and injection at this rate for 45 minutes. At the end of this period water was injected at a rate of 2050 litres/min and there was a partial return of water after about 4 minutes.

III.-With the pressure gauge at 1500 m, injection at the rate of 800 litres/min for 136 minutes.

The second series of tests were carried out as follows:

I.- With the pressure gauge at 2000 m, injection at 800 litres/min for 258 minutes, and then recovery for 140 minutes.

II.-With the pressure gauge at the same level, injection at 1000 litres/min. (Data monitored for 124 minutes). During this test, the injection could not be kept constant.

The results of these tests are plotted in Figures 3 through 7.

ANALYSIS OF THE RESULTS.

With Log-Log Method.

Although, almost always the tendency is to analyze the results by means of the semi-Log method, it has been found with similar tests that in almost all cases the well-bore storage effects dominate and mask a large part of the data, and it is difficult to define the proper semi-log straight line.

Therefore, the results were first plotted in a log-log form, and analysed by means of the"Type Curve Matching" technique using the type curves of Ramey et al (1), enlarged versions of the curves presented as Fig. C.6 in monogram Vol.5 of the SPE (2).

The matching procedure for four tests using the log-log plots is illustrated in Figures 8 through 12. The well and reservoir parameters were calculated using the formulae for dimensionless pressure, dimensionless time and dimensionless storage coefficient, as shown in apendix A. The results of the analysis are presented in tables II and III.

The results of the last test were not analyzed for the reason that the injection rate during this test was not constant.

With the results of some tests one could obtain more than one good match. In these cases the best match was selected by comparing the value of the storage coefficient obtained by the formula 3 in Apendix A with the value obtained by using the - data on the unit slope parts of the log-log graphs and the formula 4 in Apendix A. In some cases, however, it was difficult to select the best match amongst two matches and the parameters obtained by both matches were presented in tables II and III.

In the case of the analysis of the recovery part of the first test the differences between the C values indicated that the beginning of the recovery was perhaps 3.7 minutes later than assumed. The data were adjusted taking this time difference into account and a new match was obtained. The results of the new match are not significantly different from the previous match.

The results calculated by this method indicated that with the data used, semi-log straight line should start about 3 hours after the beginning of the test. It was clear that in some tests the useful part of the data for semi-log analysis was lost during the period when the Kuster gauge was raised and relowered, after re-winding or changing the clock; and in others only the beginning of the semi-log data was recorded within the first 3 hours of clock time.

It is well known that the "Type Curve Matching Techniques" are especially useful when the wellbore storage effects last a long time and early time transient data exist, as it was the case with the tests carried out. However under these circumstances the methods give only aproximate values.

Therefore, the results were analyzed by means of another"Type Curve Matching" technique, using the type curves of Earlougher and Kersch (3). (Larger scale versions of the curves presented as Fig. C.7 in Monograph Vol. 5 of the SPE (3).

additional drilling, indicating that the additional 40 m were highly fractured forming a psuedo-porous medium.

The storitivity value obtained from the first series of tests is quite acceptable, because if one assumes $\phi = 0.1$ and $c_t = 5.7 \times 10^{-5}$ $(Kg/cm^2)^{-1}$ one gets $h = 298$ m which is very close to the permeable interval observed (2410 - 2200 = 210 m).

The tests during which late data were registered do not show the typical fractured reservoir behaviour, indicating that the formations are behaving like porous. However, typical semi-log curves of fractured formations were observed with the data of another well in the same field.

Finally, if the flow efficiency is calulated using the results of first and fourth test, a value between 0.51 and 0.52 is obtained. When one takes into account that when the well was eventually induced, it produced 63 t/h, it indicates that if the skin damage can be removed the well will produce about 123 t/h.

CONCLUSIONS.

I.- Injection tests can be successfully used to determine well and reservoir parameters at the completion stage of a well and the results can be analysed with the established methods.

II.- They are easy to perform and Kuster pressure gauges are sufficient to record the pressure changes. However clocks of at least 6 hours period are required to register all the necessary data.

III.- Injection data are usually dominated by well bore storage effects and the parts which can be analysed by semi-log methods are short. For this reason it is absolutely necessary to make log-log plots to define the data which can be analyzed by the semi-log methods.

IV.- In cases where a large part of the semi-log straight line data is missing, or too short to be identified, the type curve matching techniques using the type curves of Ramey et al and Earlougher and Kersch can be successfully used to analyse the early time transient data. Although the results obtained are approximate when several tests are carried out reasonably reliable average values can be determined.

The log-log analysis with the type curves of Ramey et al are likely to give more consistent results.

V.- Experience with this and other wells indicate that the methods of analysis using log pressure-time plots are not recommendable for these wells.

ACKNOWLEDGEMENTS.

The authors express their gratitude to - C.F.E.(Comision Federal de Electricidad) of Mexico for permitting the publication of the data.

The authors also state that the opinions expressed are their own and not necessarily of their respective organizations.

REFERENCES.

1.- Agarval, R.G.; Al Hussainy, R.; Ramey H.J. Jr. (1970) "An Investigation of Wellbore Storage and Skin Effect in Unsteady Liquid Flow, I, Analytical Treatment" Soc. Pet. Eng. J. Sept. 1970.

2.- Earlougher, R.C., Jr. (1977) "Advances in Well Test Analysis" Monograph Volume 5, Society of Petroleum Engineers of AIME.

3.- Earlougher, R.C. Jr.; Kersch K.M. - (1974) "Analysis of Short Time Transient Test Data by Type Curve Matching J. of Pet Tech. July 1974.

4.- Gladfelter,R.E.; Tracy, G.W. and Wilsey, L.E. (1955) "Selecting Wells which Will Respond to Production Stimulation Treatment" , Drill and Prod. Prac. API (1955) 117.

TABLE I

NOMENCLATURE

Symbol	Meaning	Units: Conventional	Units: Metric
K	Effective average permeability	millidarcy	darcy
h	Net formation pay thickness	ft.	m
p	Pressure	psi	kg/cm^2
q	Injection Rate	SBD	
W			t/h
μ	Viscosity	centipoise	centipoise
t	time	hour	hour
B	Formation volume factor (reservair volume/standard volume = $\frac{Vr}{Vsc}$)		
ϕ	porosity	fraction of bulk volume	
c_t	Total system effective isothermal compressibility	$(psi)^{-1}$	$(Kg/cm^2)^{-1}$
r_w	welbore redius	ft	m
c	Wellbore sturage coefficient	bbl/psi (1 bbl/psi = 2.2615 $m^3/Kg/cm^2$)	$m^3/Kg/cm^2$
P_D	Dimensionless pressure		
t_D	Dimensionless time		
C_D	Dimensionless storage coefficient		
ΔP	Pressure change	psi	Kg/cm^2
Δt	Time change	hour	hour
m	Slope of Semi-log Straight line	psi/log cycle	Kg/cm^2/log cycle
Vsc	Specific Volume at standard conditions		m^3/t
Vr	Specific volume at reservoir conditions near the injection (assumed to be 1.0435 m^3/t in all calculations)		m^3/t
s	Skin effect (dimensionless)		
Δps	See equation 7.		
$\bar{p}$	Volumetric average plessure within drainage volume	psi	Kg/cm^2

TABLE II

RESULTS OF THE ANALYSIS OF THE TESTS

WITH THE WELL AT 2,404 M .

Type of Test	Analysis Method	$\frac{Kh}{\mu}$ d.m/cp	mdft/cp	ϕhc_t m/Kg/cm^2	ft/psi	C bbl/psi	S
Injection 500 litres/min	Semi-log	There are not enough data.					
	Log-Log (Ramey)	14.34 ?	49018 ?	7.46×10^{-3} ?	1.72×10^{-3} ?	0.251$^+$ 0.241	20 ?
		8.72	28620	7.37×10^{-3}	1.70×10^{-3}	0.238	10
	E-K	7.65	25088			0.290	12.39
		7.02	23027			0.290	3.18
		7.33	24057			0.290	7.79
Recovery after injection with 500 litres/min	Semi-log	5.49 ?	18013 ?				
		4.12 ?	13518 ?			0.350$^+$	
	Log-Log (Ramey)	8.01	26281	8.32×10^{-3}	1.92×10^{-3}	0.269	10
		8.01	26281	7.00×10^{-3}	1.61×10^{-3}	0.280$^+$	10
						0.235	
	E - K	No good match					
Injection with 1,000 litres/min	Semi-log	There are enough data.				0.246$^+$	
	Log-Log (Ramey)	8.58	28151	6.10×10^{-3}	1.41×10^{-3}	0.198	10
	E - K	4.63	15193			0.190	3.39
		11.23	36860			0.199	14.88
		7.93	26026			0.195	3.14
Injection with 800 litres/min	Semi-Log	There are not enough data.				0.298$^+$	
	Log-Log (Ramey)	6.31	20703	8.4×10^{-3}	1.94×10^{-3}	0.272	5
		9.38	30776	8.0×10^{-3}	1.84×10^{-3}	0.261	10
	E - K	9.81	32193			0.254	10.15
		5.34	17510			0.248	4.41
		7.57	24852			0.251	7.28
Average Representative Values		8.00	26248	7.36×10^{-3}	1.70×10^{-3}	0.250	8.82

+ Calculated using the data on the unit slope part of the log-log plots.

NOTES : 1 E-K stand for analysis using Earlougher + Kersch curves (2). Skin values were obtained by assuming $\phi = 0.1$ and $c_t = 5.7 \times 10^{-3}$ $(Kg/cm^2)^{-1}$. h = 910 m.

2 Figures underlined are the average values obtained using Earlougher + Kersch curves.

TABLE III

RESULTS OF THE ANALYSIS OF THE TESTS

WITH THE WELL AT 2430 M.

Test	Analysis Method	Kh/μ d.m./cp	Kh/μ md.ft/cp	ϕhc_t m/kg/cm2	ϕhc_t ft/psi	C bbl/psi	S
Injection with 800 litres/min	Semi-log	There are not enough data					
	Log-log (Ramey)	9.38	30776	13.66×10^{-3}	3.15×10^{-3}	0.262 0.256	10
	E - K	6.20	20351			0.210	3.55
		15.25	50151			0.230	18.45
		8.53	27577			0.220	6.96
		10.00	32826			0.220	8.87
Recovery after injection with 800 litres/min	Semi-log	There are not enough data					
	Log-log (Ramey)	6.75	22147	15.52×10^{-3}	3.58×10^{-3}	0.269* 0.267	5
	E - K	9.14	30000			0.255	5.73
		8.99	29500			0.236	5.77
		9.07	29750			0.246	5.75
Injection with 1000 litres/min	E -K	9.32 ?	30590 ?			0.345 ? 0.370 ?	4.78?
Average Representative Values		8.80	28856	14.59×10^{-3}	3.37×10^{-3}	0.248	7.31

* Calculated using the data on the unit slope part of the log-log plots.

NOTES: 1. E-K stand for analysis using Earlougher + Kersh curves (2). Skin values were obtained by assuming $\phi = 0.1$ and $c_t = 5.7 \times 10^{-5}$ $(Kg/cm2)^{-1}$, $h = 250$ m.

2. Figures underlined are the average values obtained using Earlougher + Kersch curves.

FIGURE 1

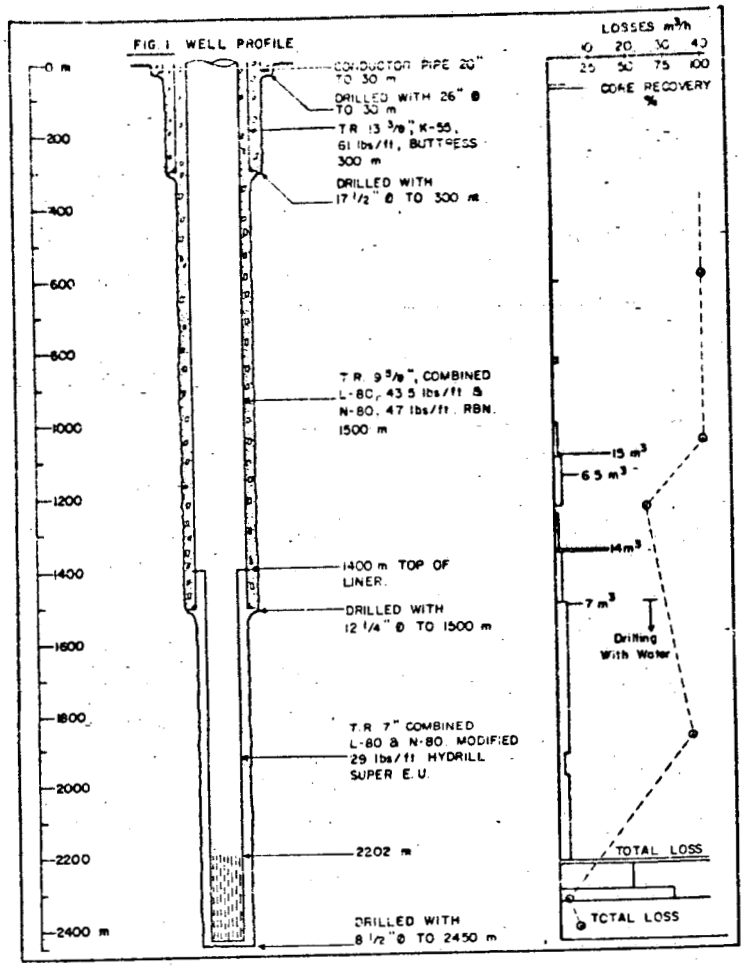

FIGURE 2

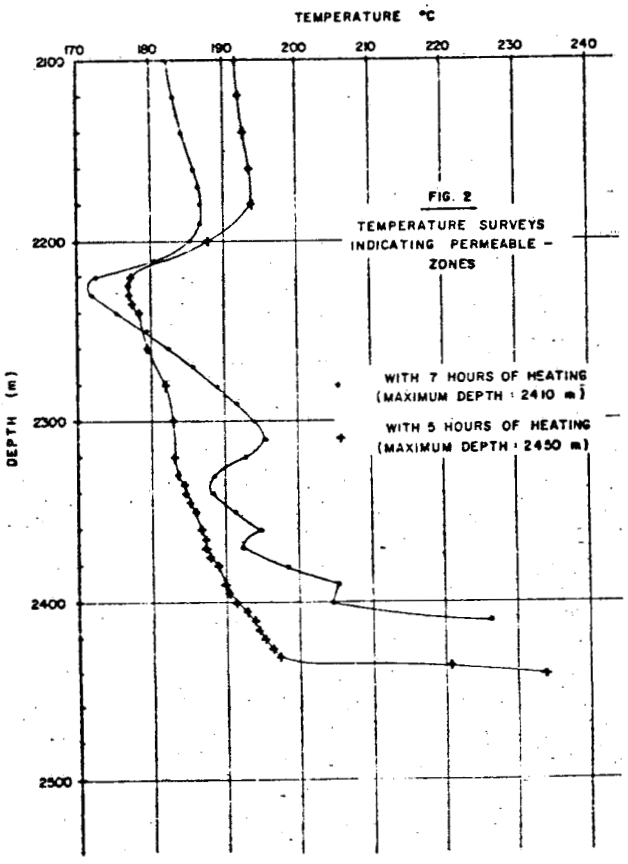

FIGURE 3

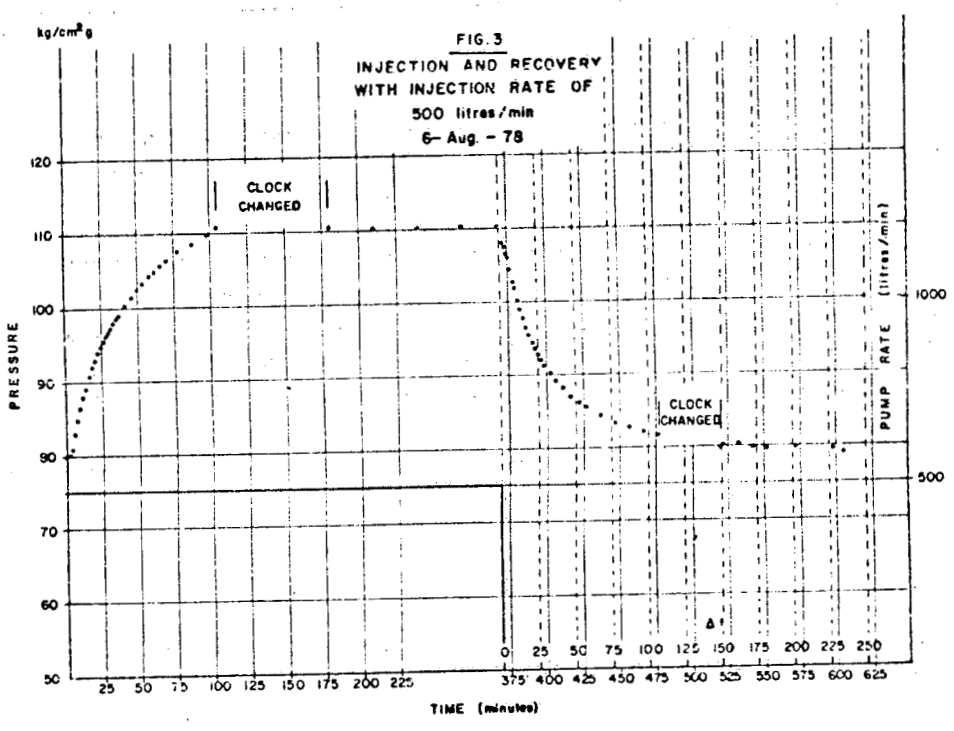

FIG. 4
TWO RATE INJECTION TEST
6 - Aug. - 78

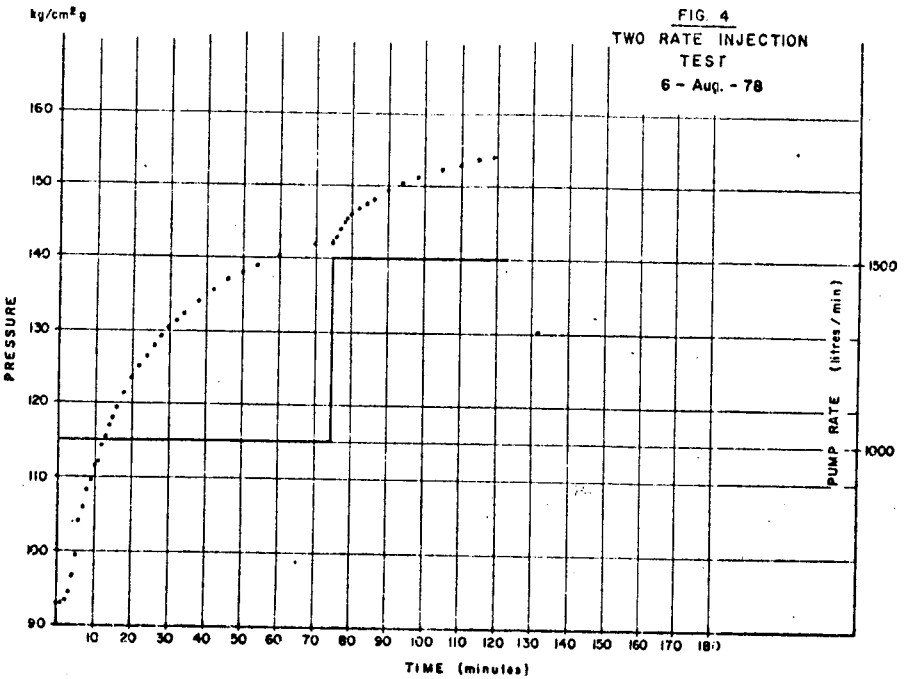

FIG.5
INJECTION WITH 800 l/min
7 - Aug. - 78

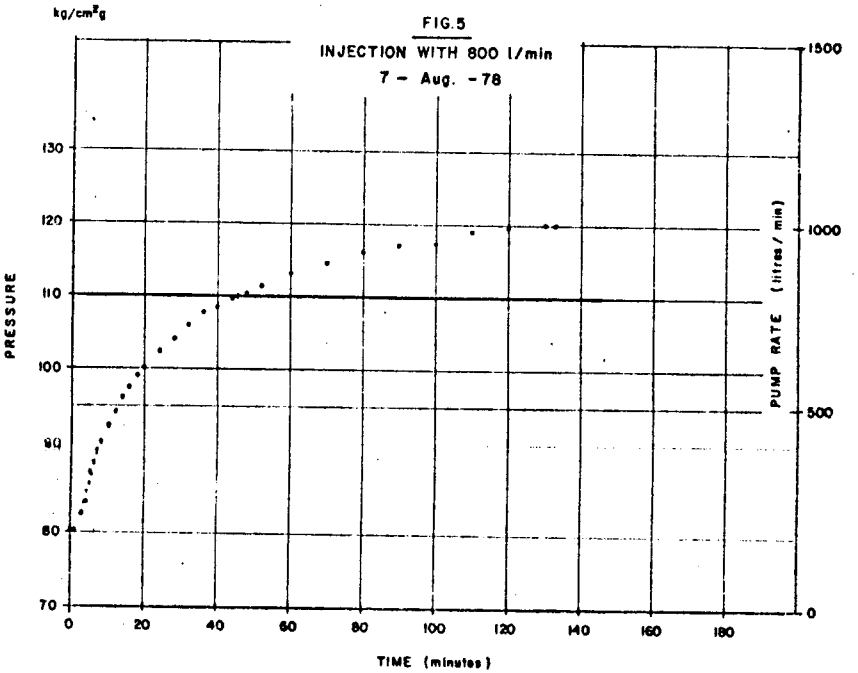

FIG. 6
INJECTION AND RECOVERY
WITH 800 litres / min
12 - Aug. - 78

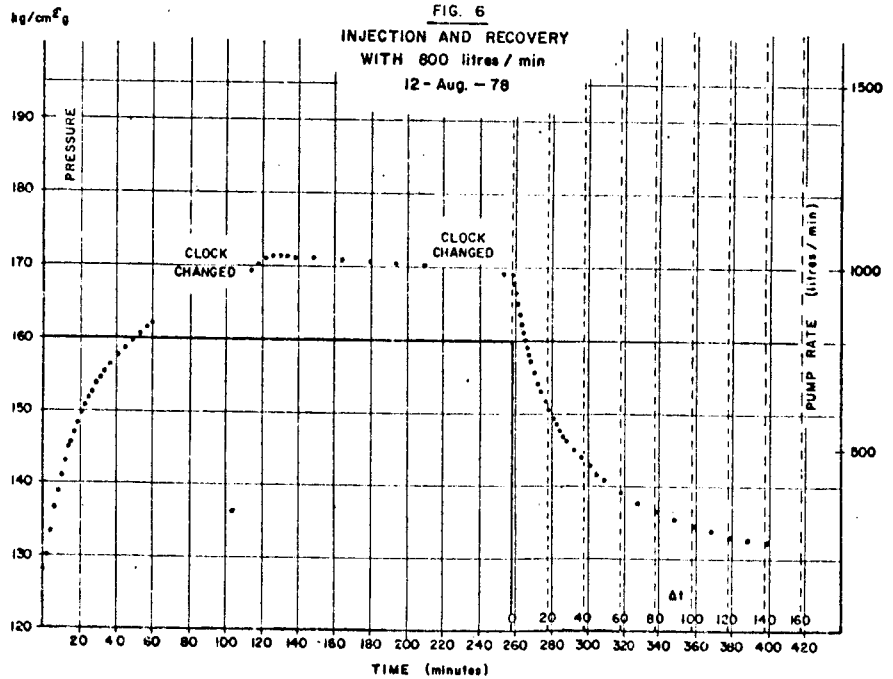

FIG. 7
INJECTION WITH
1000 litres / min
12 - Aug. - 78

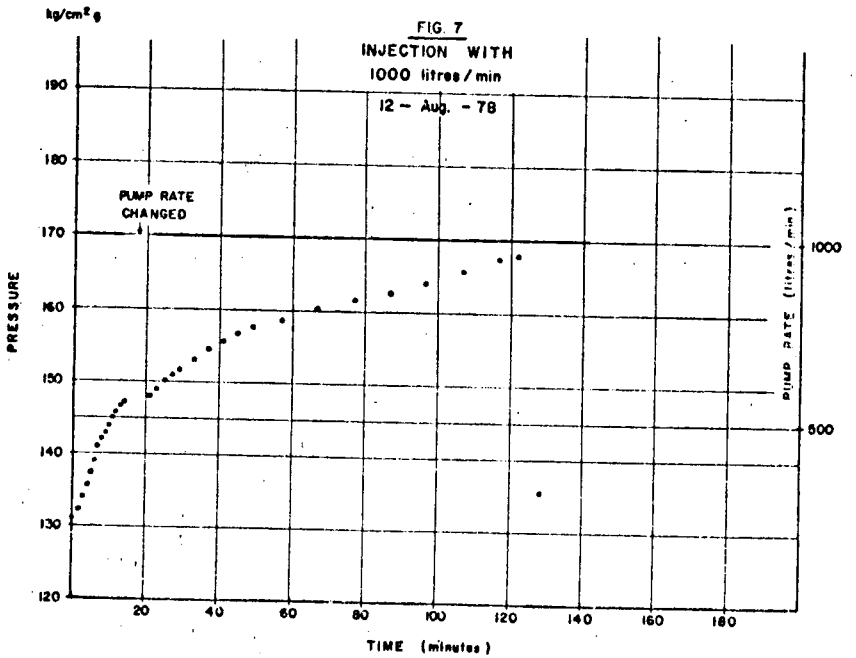

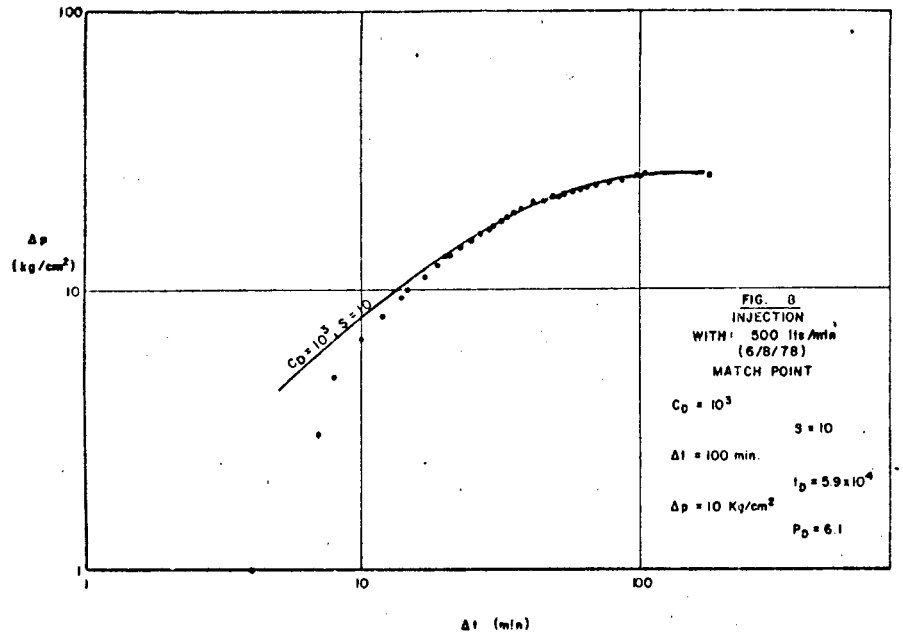

FIG. 8
INJECTION
WITH : 500 lts/min
(6/8/78)
MATCH POINT

$C_D = 10^3$ S = 10

Δt = 100 min. $t_D = 5.9 \times 10^4$

Δp = 10 Kg/cm² $P_D = 6.1$

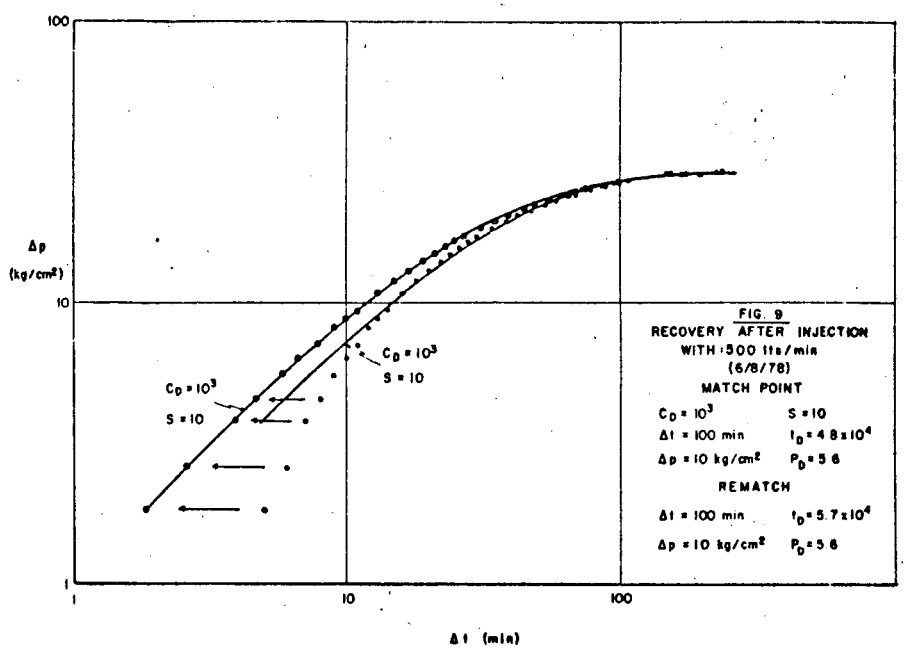

FIG. 9
RECOVERY AFTER INJECTION
WITH : 500 lts/min
(6/8/78)
MATCH POINT

$C_D = 10^3$ S = 10

Δt = 100 min $t_D = 4.8 \times 10^4$

Δp = 10 kg/cm² $P_D = 5.6$

REMATCH

Δt = 100 min $t_D = 5.7 \times 10^4$

Δp = 10 kg/cm² $P_D = 5.6$

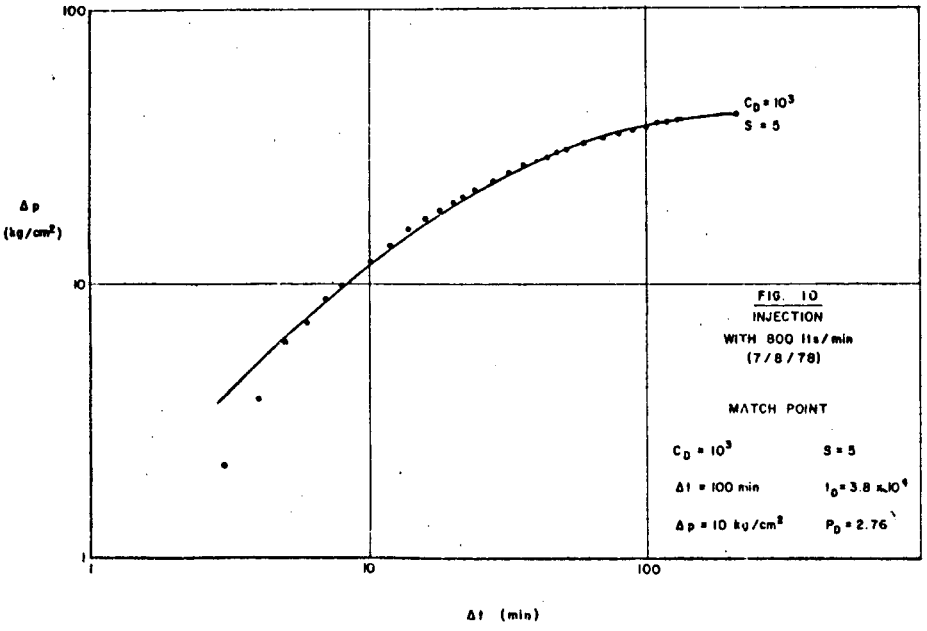

FIG. 10
INJECTION
WITH 800 lts/min
(7/8/78)

MATCH POINT

$C_D = 10^3$ S = 5

Δt = 100 min $t_D = 3.8 \times 10^4$

Δp = 10 kg/cm² $P_D = 2.76$

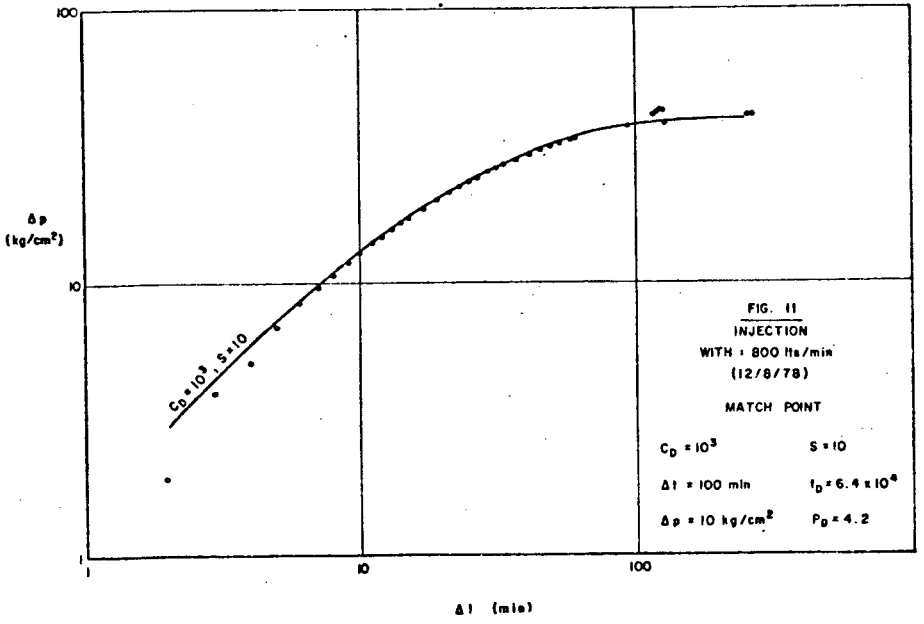

FIG. 11
INJECTION
WITH : 800 lts/min
(12/8/78)

MATCH POINT

$C_D = 10^3$ S = 10

Δt = 100 min $t_D = 6.4 \times 10^4$

Δp = 10 kg/cm² $P_D = 4.2$

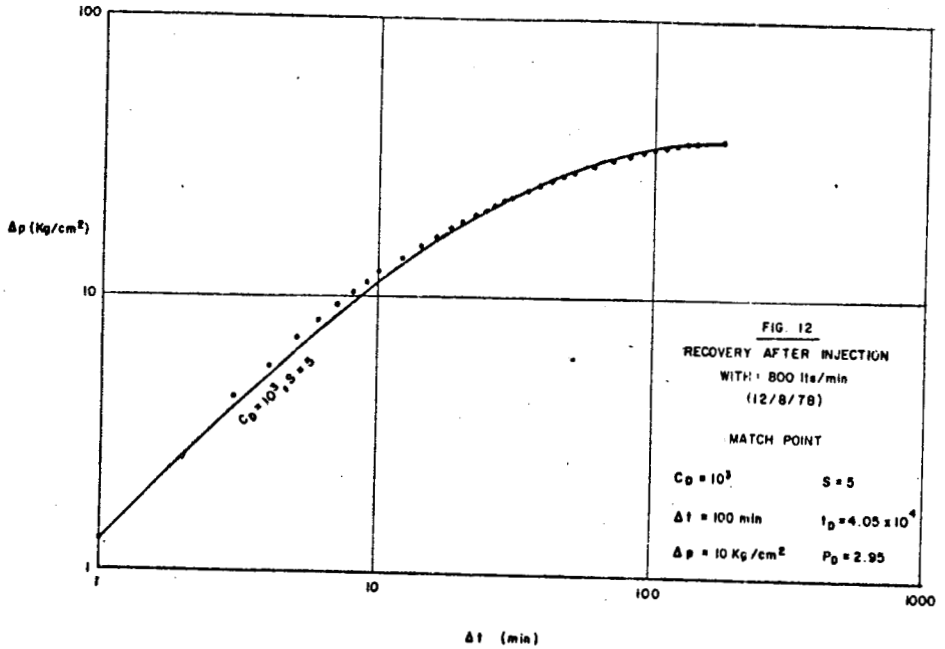

FIG. 12
RECOVERY AFTER INJECTION
WITH 800 lts/min
(12/8/78)

MATCH POINT

$C_D = 10^3$ S = 5

Δt = 100 min $t_D = 4.05 \times 10^{-4}$

Δp = 10 Kg/cm² $P_D = 2.95$

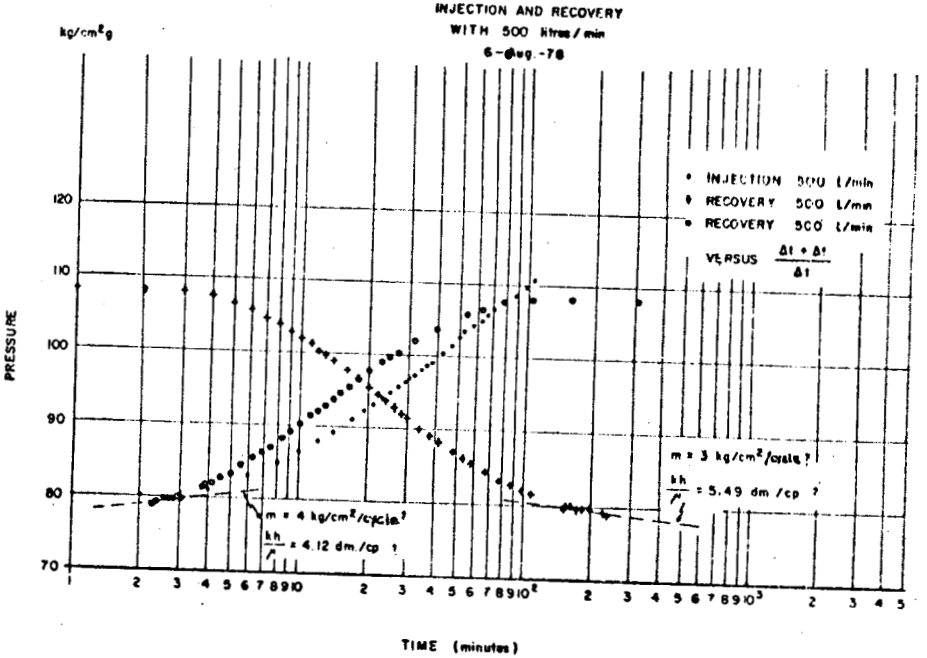

FIG. 13
INJECTION AND RECOVERY
WITH 500 litres / min
6-Aug.-78

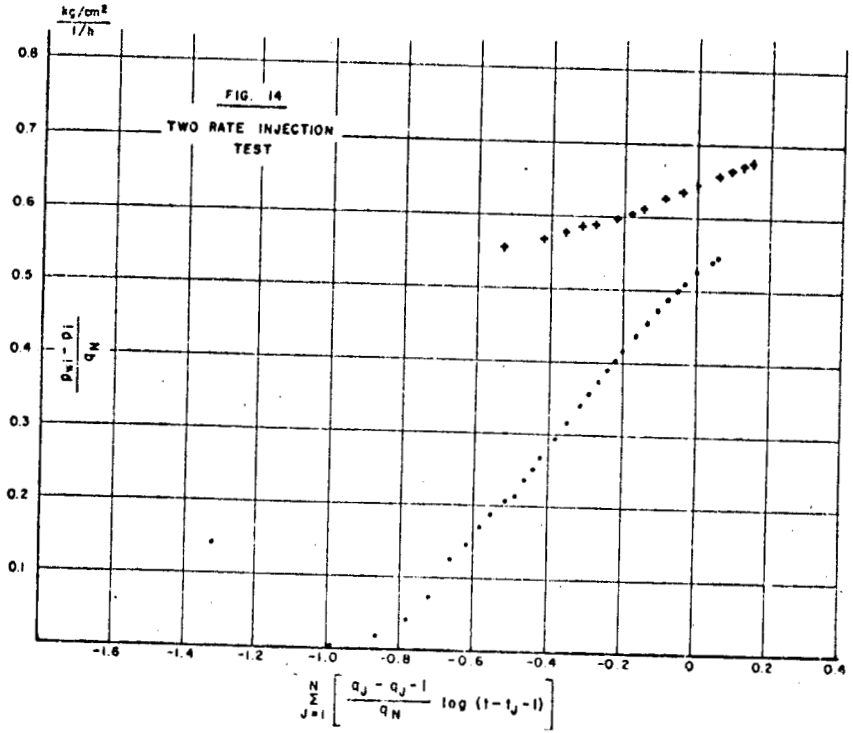

FIG. 14
TWO RATE INJECTION
TEST

Appendix A:

Formulae Used :

Conventional Reservoir Engineering Units		Metric Units
$P_D = \frac{\Delta pkh}{141.2\ q\ B\mu}$	(1)	$P_D = \frac{2.1891\ \Delta pkh}{sc\ W\ B\mu}$
$t_D = \frac{0,0002637\ kt}{\phi \mu c_t\ h\ r^2_w}$	(2)	$t_D = \frac{0,3485\ kt}{\phi \mu c_t r^2_w}$
$C_D = \frac{5.6146\ C}{2\ \phi\ C_t\ h\ r^2_w}$	(3)	$C_D = \frac{C}{2\pi \phi\ c_t h\ r^2_w}$
$C = \frac{qB\ \Delta t}{24\ Ap}$	(4)	$C = \frac{W\ Vsc\ B\ \Delta t}{\Delta p}$
$m = \frac{162.6\ q\ \mu\ B}{Kh}$	(5)	$m = \frac{0.5258\ Vsc\ q\ B\mu}{Kh}$
$t = \frac{(200000 + 12000\ s)}{(kh/\mu)}$	(6)	$t = \frac{(200000 + 12000\ s)}{3281\ (kh/\mu)}$

$$\text{Flow efficiency} = \frac{\bar{p} - pwf - \Delta ps}{\bar{p} - pwf} = 1 - \frac{\Delta ps}{\bar{p} - pwf}$$

$\Delta p_s = 0.87$ m.s. (7)

RECENT DEVELOPMENTS IN WELL TEST ANALYSIS IN THE STANFORD GEOTHERMAL PROGRAM

C. Ehlig-Economides
Department of Petroleum Engineering
Stanford University
Stanford, California 94305

In the past year a number of studies pertaining to geothermal well test analysis were conducted. In this paper a brief overview of progress on the following six subjects is presented: (1) earth tide effects on a closed reservoir, (2) transient pressure analysis of multilayered heterogeneous reservoirs, (3) interference testing with wellbore storage and skin at the producing well, (4) steam/water relative permeabilities, (5) transient rate and pressure buildup resulting from constant pressure production, and (6) transient pressure analysis of a parallelepiped reservoir.

Earth Tide Effects

The gravitational attraction between the sun, moon, and earth induces a radial deformation of the earth which results in the readily observable oceanic tides. The same mechanism also generates a state of stress on the surface of the earth which has been referred to as earth tides. Due to the low compressibility of the earth compared to that of water, the pressure transients caused by earth tides are of small amplitude. However, the pressure changes are of sufficient magnitude to cause water level variations in open wells and pits, and several investigators have indicated that a relationship exists between the amplitude of the response of an open well system and the characteristics of the formation and the fluid contained therein.

P. Arditty[1,2] modified the equations solved by Bodvarsson[3] for an open well in a finite closed reservoir to apply to a shut-in well with the borehole completely filled with formation fluid. Only one phase is flowing in the reservoir, and the reservoir is confined and infinite in radial extent. The expression for pressure induced by an applied tectonic pressure, p_c, is given by:

$$p = p_{SD}\left(1 - \frac{ae^{n(a-r)}}{r\left[1+\frac{B}{i\omega}\left(\frac{1}{a}+n\right)\right]}\right) \qquad (1)$$

with:

$$p_a = p_{SD}\left(1 - \frac{1}{1+\frac{B}{i\omega a}(na+1)}\right) \qquad (2)$$

where $B = 4k/c_f\mu\ell$, $n^2 = i\omega/d$, ω = oscillation frequency, d = diffusivity $k/\phi\mu c$, a = wellbore radius, and r = radial distance from well. The static pressure $p_{SD} = p_c(4G_m c_f - c_m)/(3+4G_m c_f)$, where p_c is an applied tectonic pressure, G_m is the rock matrix shear modulus, c_f is fluid compressibility, and c_m is matrix compressibility. The amplitude of the relative response p_a/p_{SD} is:

$$R_e(p_a/p_{SD}) \cong R_e\left(\frac{4k/i\omega\mu a\ell c_f}{1 + \frac{4k}{i\omega\mu a\ell c_f}}\right) \qquad (3)$$

The critical frequency, ω_c, for which the response amplitude exhibits an abrupt decrease is defined by:

$$\omega_c = \frac{4k}{\mu a\ell c_f} \qquad (4)$$

Tides are classified according to length of period, T: long period tides (T = 16 days); diurnal tides (T = 1 day), semidiurnal tides (T = 1/2 day); and terdiurnal tides (T = 1/3 day). If $\omega_c/2\pi \gg 2$, then the critical frequency exceeds both the diurnal and semidiurnal frequencies, and $A_D/A_{SD} \simeq 1$, where A_D and A_{SD} are the diurnal and semidiurnal amplitudes of the earth tide effect. If $1 < \omega_c/2\pi < 2$, then $1.25 < A_D/A_{SD} < 2$. If $\omega_c/2\pi \ll 1$, both amplitudes will be small, and undetectable. Thus, the ratio of the two amplitudes determines limits on the value of ω_c, which in turn gives an approximation for $k/\mu c_f$ since a and ℓ are known. If ω_c is computed from $k/\mu c_f$, an explanation for existence or nonexistence of tidal effects is provided.

A graph of amplitude versus period for a typical sandstone reservoir containing gas is shown in Fig. 1. From these results we would expect the diurnal tide amplitude to exceed the semidiurnal tide amplitude and both should be detectable.

Figure 3 shows raw data from a fluid test. Figure 4 shows the data in Fig. 3 modified to show relative pressure variations. Spectral analysis using Fast Fourier Transforms provides the results shown in Fig. 5. The two small peaks in amplitude are due to diurnal and semidiurnal tide effects. The reader is referred to Ref. 1 and Ref. 2 for more detail.

Multilayered Systems

A mathematical model was derived by S. Tariq[4,5] to satisfy the following conditions for a multilayered reservoir: each layer is horizontal and circular, homogeneous and isotropic, and bounded by impermeable formations at the top, bottom, and at the external drainage radius. Each layer has constant porosity and permeability, and

uniform thickness, but the drainage radius may be different for different layers. The fluid in each layer has small and constant compressibility. Initial reservoir pressure is the same for each layer; and instantaneous sandface pressure is identical for all layers. Pressure gradients are small and gravity effects negligible. The total production rate, q, is constant, but the production rate for each layer may vary in time. The model for n layers is specified by the following equations:

$$\frac{\partial^2 p_j}{\partial r^2} + \frac{1}{r}\frac{\partial p_j}{\partial r} = \frac{\phi_j \mu_j c_j}{k_j}\frac{\partial p_j}{\partial t}\ ;\ p_j(r,t) = p_i - p_j(r,t),\ r\varepsilon[r_{wj}, r_{ej}] \quad (5)$$

$$p_j(r,0) = 0 \quad (6)$$

$$\frac{\partial p_j}{\partial r}(r_{ej},t) = 0 \quad (7)$$

$$p_{wf}(t) = p_j(r_w,t) - S_j\left(r\frac{\partial p_i}{\partial r}\right)_{r_w} \quad (8)$$

$$q = C\frac{\partial p_{wf}}{\partial t} + \sum_{j=1}^{n} q_j(t)$$

$$= C\frac{dp_{wf}}{dt} - 2\pi \sum_{j=1}^{n}\left(\frac{kh}{\mu}\right)_j\left(r\frac{\partial p_j}{\partial r}\right)_{r_{wj}} \quad (9)$$

where $j = 1, 2, \ldots, n$; s_j = skin factor for each layer; and C = wellbore storage constant, cc/atm.

The system of equations is transformed into and solved in Laplace space. The resulting solution is then numerically inverted using the algorithm by Stehfest.[6]

A thorough analysis of drawdown data generated for different types of layered systems was conducted. The cases investigated included layers having different permeabilities, thicknesses, radii, and skin effects. Log-log type curves for analysis of multilayered systems were developed, and techniques for analyzing two-layered systems using semilog graphs of pressure vs time were described. The reader is referred to Ref. 4 and Ref. 5 for more detail.

Interference Testing

As more sensitive pressure gauges have become available, interference testing, that is, observation of the pressure changes at a shut-in well resulting from a nearby producing well, has become feasible. Interference testing has the advantage of investigating more reservoir volume than a single-well test. For a producing well with considerable wellbore storage and skin effects, the combined effects of the storage and skin is to prolong the time it takes for the sandface flow rate to become equal to the surface flow rate. Since the sandface flow rate is not constant during this time period, conventional interference testing, which assumes a constant rate, is not valid.

The mathematical model used in this study by H. Sandal[7,8] assumes the flow is radial, the medium is infinite, homogeneous, and isotropic with constant porosity and permeability, the single-phase fluid is slightly compressible with constant viscosity, pressure gradients are small, and wellbore storage and skin are constant. The equations which represent this system are the following:

$$\frac{\partial^2 p_D}{\partial r_D^2} + \frac{1}{r_D}\frac{\partial p_D}{\partial r_D} = \frac{\partial p_D}{\partial t_D} \; ; \; p_D = p_D(r_D, t_D), \; r_D > 1, \; t_D > 0 \qquad (10)$$

$$p_D(r_D, 0) = 0 \; ; \; r_D > 1 \qquad (11)$$

$$C_D \frac{\partial p_{wD}}{\partial t_D} - \left.\frac{\partial p_D}{\partial r_D}\right|_{r_D=1} = 1 \; ; \; t_D > 0 \qquad (12)$$

$$p_{wD} = p_D - S \left.\frac{\partial p_D}{\partial r_D}\right|_{r_D=1} \; ; \; t_D > 0 \qquad (13)$$

$$\lim_{r_D \to \infty} p_D(r_D, t_D) = 0 \; ; \; t_D > 0 \qquad (14)$$

where p_D, r_D, t_D, and C_D are dimensionless pressure drop, radius, time, and storage, respectively, p_{wD} is the pressure drop inside the wellbore, and S is the wellbore skin factor.

The equations are transformed into and solved in Laplace space. The resulting Laplace space solution is numerically inverted using the Stehfest[6] algorithm.

Results were compared with the study by Garcia-Rivera and Raghavan[9] which was based on the superposition of a series of line source solutions combined with sandface flow rates obtained for a finite radius well (Ramey and Agarwal,[10] and Ramey, Agarwal, and Martin[11]). The comparison indicated that for low values of the effective wellbore radius, $C_D e^{2s}$, the Garcia-Rivera and Raghavan study may be in error. Figure 5 shows the close agreement between the two solutions for large values of $C_D e^{2s}$. Figure 6 shows an example of discrepancies between the two solutions. The reader is referred to Ref. 7 and Ref. 8 for more detail.

Steam/Water Relative Permeabilities

Using production data from the Wairakei field, R. Horne[12] and K. Shinohara[13] demonstrated that steam/water relative permeability curves can be generated from field data. The method of analysis was suggested by Grant,[14] but improvements were made on the production data. Specifically, assuming negligible wellbore heat loss, steam and water discharges at the wellbase were back calculated from the surface values. The wellbore heat loss was less than 1% in the wells tested because they have been flowing for a long period of time. Total discharge values were divided by the wellhead pressure in order to filter out changes in discharge due only to pressure depletion in the reservoir. Thus, changes in discharge due to relative permeability effects were isolated. The actual downhole temperature was used to determine fluid densities, viscosities, and enthalpies. Finally, flowing water saturation was determined from the back-calculated wellbase steam and water discharges. They did not take into account the immobile fluid in the reservoir.

Relative permeabilities were computed from equations for Darcy's law and the flowing enthalpy given below:

$$q_w = -\rho_w \frac{k}{\mu_w} F_w(S_w)\ A\ p' \tag{15}$$

$$q_s = -\rho_s \frac{k}{\mu_s} F_s(S_w)\ A\ p' \tag{16}$$

$$h = \frac{\rho_w h_w F_w(S_w)/\mu_w + \rho_s h_s F_s(S_w)/\mu_s}{\rho_w F_w(S_w)/\mu_w + \rho_s F_s(S_w)/\mu_s} \tag{17}$$

where q is the discharge rate, ρ is one-phase fluid density, μ is viscosity, A is flow area, p is the pressure gradient, F is the fractional flow, S_w is the flowing water saturation, and subscripts

s and w refer to the steam and water phases. Figure 7 shows the resulting permeability curves.

Future improvements on this method will include incorporation of wellbore heat loss in the back calculation of fractional flow, and use of irreducible water saturations estimated from results of experimental studies in the Stanford Geothermal Program.

Constant Pressure Production

Conventional well test analysis has been developed primarily for constant rate production. Since there are a number of common reservoir production conditions which result in constant pressure production, there is a need for a more thorough treatment of transient rate analysis and pressure buildup after constant pressure production.

In this work by C. Ehlig-Economides, the following assumptions are needed: flow is strictly radial, and the porous medium is homogeneous and isotropic, with constant thickness h, porosity ϕ, and permeability k. The fluid viscosity is constant, and the total compressibility of the fluid and the porous medium is small in magnitude and constant. The equations to be solved are the following:

$$\frac{\partial^2 p_D}{\partial r_D^2} + \frac{1}{r_D}\frac{\partial p_D}{\partial r_D} = \frac{\partial p_D}{\partial t_D} \; ; \quad p_D = p_D(r_D,t_D), \; r_D \varepsilon [1,R], \; t_D > 0 \qquad (18)$$

$$p_D(r_D,0) = 0 \; ; \; r_D \varepsilon [1,R] \qquad (19)$$

$$p_D(1,t) = 1 + S \lim_{r_D \to 1^+} \frac{\partial p_D}{\partial r_D} \; ; \; (t_D > 0) \qquad (20)$$

$$\lim_{r_D \to \infty} p_D(r_D,t_D) = 0 \; ; \; (t_D > 0) \text{ for unbounded reservoir} \qquad (21)$$

$$\frac{\partial p_D}{\partial r_D}(R,t_D) = 0 \; ; \; (t_D > 0) \text{ for closed bounded reservoirs, } R = \frac{r_e}{r_w} \qquad (22)$$

$$p_D(R,t_D) = 0 \; ; \; (t_D > 0) \text{ for constant pressure bounded reservoir} \qquad (23)$$

$$q_D(t_D) = - \lim_{r_D \to 1^+} \frac{\partial p_D}{\partial r_D} \qquad (24)$$

where:

$$r_D = r/r_w,\ t_D = \frac{kt}{\phi\mu c r_w^2},\ p_D(r_D,t_D) = \frac{p_i - p(r_D,t_D)}{p_i - p_w},$$

$$q_D = \frac{q\mu}{2\pi kh(p_i - p_w)},\ \text{and S is wellbore skin factor.}$$

Transient rate solutions have been tabulated in the literature. In this work, the numerical Laplace inverter by Stehfest[6] is used to generate solutions for the transient wellbore rate, the radial pressure distribution, and cumulative production including boundary and skin effects.

Pressure buildup after constant pressure production has not been properly handled in the literature. It can be shown that the following equation exactly represents pressure buildup after constant production under the conditions mentioned at the beginning of this section.

$$p_{DS}(\Delta t_D) = 1 + \int_{t_{Df}}^{t_{Df}+\Delta t_D} q_D(\tau)\,\frac{dp_{Dw}}{d\tau}\,(t_{Df}+\Delta t_D-\tau)\,d\tau \qquad (25)$$

where p_{DS} is the dimensionless shut-in pressure at the wellbore, t_{Df} is the flowing time before shut-in, Δt_D is the elapsed time after shut-in, q_D is dimensionless rate, defined above, and p_{Dw} is the dimensionless wellbore pressure drop for constant rate production, defined by:

$$p_{Dw}(t_D) = \frac{2\pi kh}{q\mu}\,(p_i - p[1,t_D]).$$

This work is nearing completion. The author may be consulted for more information.

Parallelepiped Model

The parallelepiped model has been proposed as a reasonable approximation for both The Geysers and the Italian geothermal reservoirs. Through use of source functions, Green's functions, and the Neumann product method described by Gringarten,[15] solutions are readily available for a number of related problems. The model assumes three-dimensional flow in a reservoir bounded by impermeable and/or constant pressure boundaries with a well located at any point which may be

fully or partially penetrated and which may intersect a horizontal or a vertical fracture. Solutions are in the form of infinite sums and integrals which must be integrated by computer. Type-curves are being developed which will shed new light on the behavior of geothermal reservoirs. In particular, detection of a boiling front may be possible in a dry steam reservoir bounded at its base by boiling water. This constitutes a constant pressure boundary if the reservoir is isothermal.

References

1. Arditty, P.C., and Ramey, H.J., Jr.: "Response of a Closed Well-Reservoir System to Stress Induced by Earth Tides," Paper SPE 7484, presented at the 53rd Annual Fall Meeting of the SPE of AIME, Oct. 1978, Houston, Texas.

2. Arditty, P.C.: "The Earth Tide Effects on Petroleum Reservoirs, Preliminary Study," Engineer's Degree Thesis, Stanford University Petroleum Engineering Department, 1978.

3. Bodvarsson, G.: "Confined Fluid as Strain Meters," J. Geoph. Res. (1970), 75, No. 14, p. 2711.

4. Tariq, S.M., and Ramey, H.J., Jr.: "Drawdown Behavior of a Well with Storage and Skin Effect Communicating with Layers of Different Radii and Other Characteristics," Paper SPE 7453, presented at the 53rd Annual Fall Meeting of the SPE of AIME, Oct. 1978, Houston, Texas.

5. Tariq, S.M.: "A Study of the Behavior of Layered Reservoirs with Wellbore Storage and Skin Effect," Ph.D. Dissertation, Stanford University Petroleum Engineering Department, 1977.

6. Stehfest, H.: "Numerical Inversion of Laplace Transforms," Communications of the ACM (Jan. 1970), 13, No. 1, Algorithm 368.

7. Sandal, H.J., Horne, R.N., Ramey, H.J., Jr., and Williamson, J.W.: "Interference Testing with Wellbore Storage and Skin Effect at the Produced Well," Paper SPE 7454, presented at the 53rd Annual Fall Meeting of the SPE of AIME, Oct. 1978, Houston, Texas.

8. Sandal, H.J.: "Interference Testing with Skin and Storage," Engineer's Degree Thesis, Stanford University Petroleum Engineering Department, 1978.

9. Garcia-Rivera, J., and Raghavan, R.: "Analysis of Short-Time Pressure Transient Data Dominated by Wellbore Storage and Skin at Unfractured Active and Observation Wells," Paper SPE 6546, presented at the 47th Annual California Regional Meeting of the SPE of AIME, Apr. 1977, Bakersfield, CA.

10. Ramey, H.J., Jr., and Agarwal, R.G.: "Annulus Unloading Rates and Wellbore Storage," Soc. Pet. Eng. J. (Oct. 1972), 453-462.

11. Ramey, H.J., Jr., Agarwal, R.G., and Martin, I.: "Analysis of 'Slug Test' or DST Flow Period Data," J. Can. Pet. Tech. (July-Sept. 1975), 34-47.

12. Horne, R.N., and Ramey, H.J., Jr.: "Steam/Water Relative Permeabilities from Production Data," Geothermal Resources Council, Trans. (July 1978), 2.

13. Shinohara, K.: "Calculation and Use of Steam/Water Relative Permeabilities in Geothermal Reservoirs," M.S. Report, Stanford University Petroleum Engineering Department, 1978.

14. Grant, M.A.: "Permeability Reduction Factors at Wairakei," presented at the AIChE-ASME Heat Transfer Conference, Salt Lake City, Utah, Aug. 15-17, 1977.

15. Gringarten, A.C., and Ramey, H.J., Jr.: "The Use of Source and Green's Functions in the Solution of Unsteady Flow Problems in Reservoirs," Soc. Pet. Eng. J. (Oct. 1973), 285-296; Trans. AIME, 255.

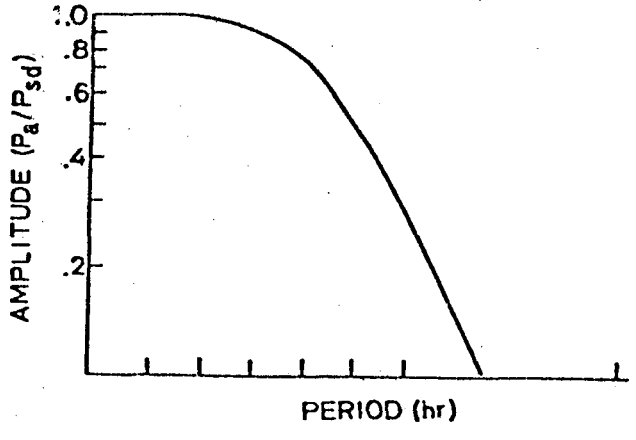

FIG. 1: RESPONSE (p_a/p_{SD}) OF A CLOSED-WELL RESERVOIR SYSTEM FOR A SANDSTONE CONTAINING GAS

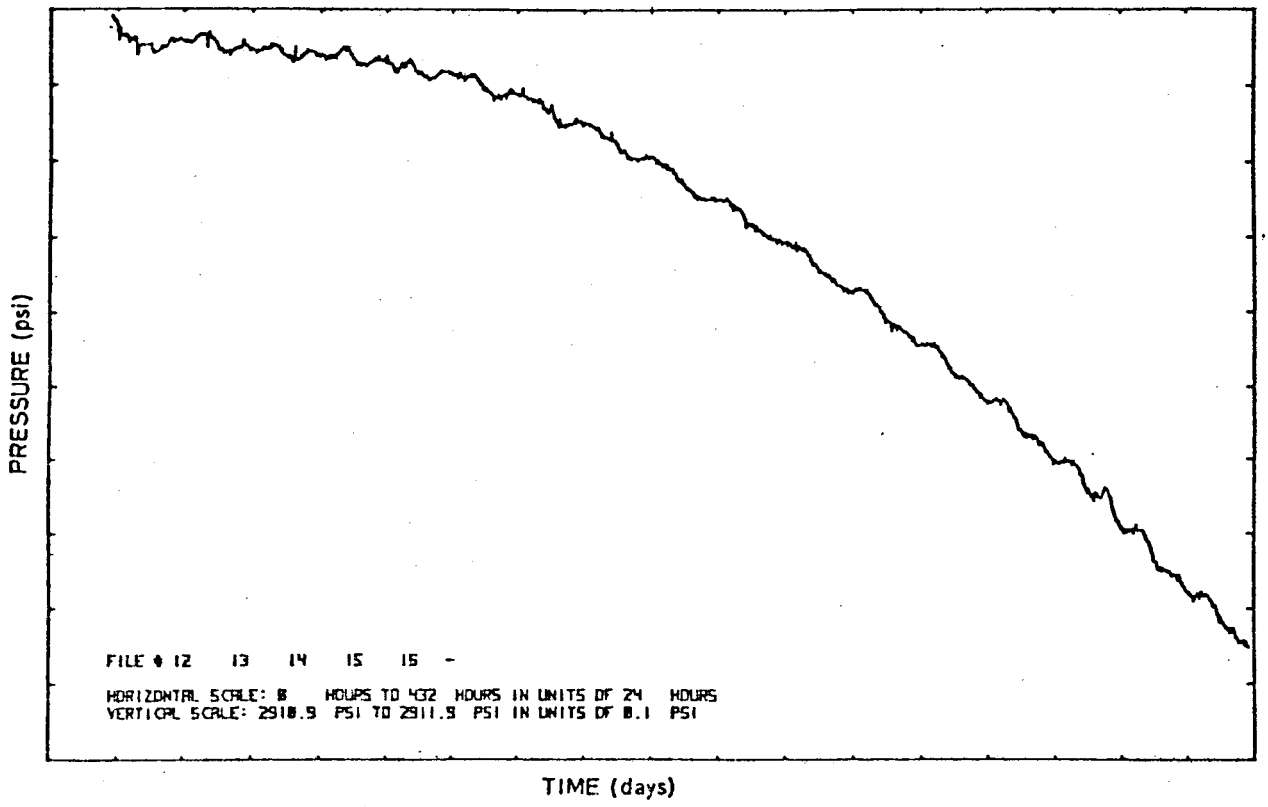

FIG. 2: INITIAL DATA FOR THE "A" FIELD

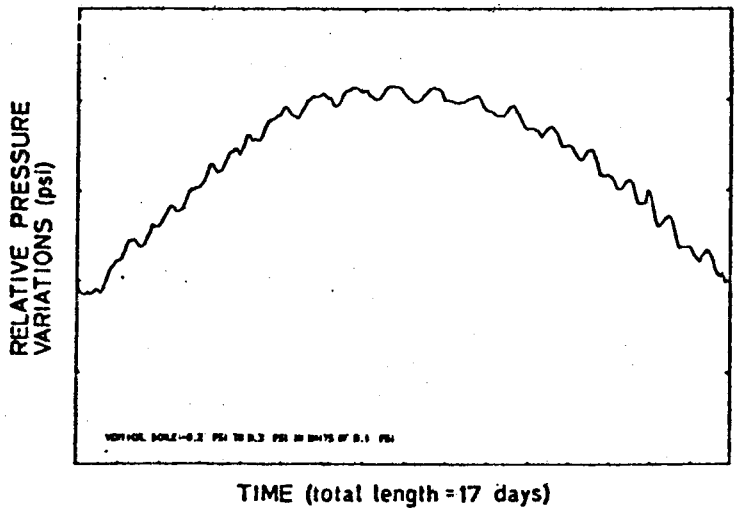

FIG. 3: MODIFIED DATA FOR THE "A" FIELD

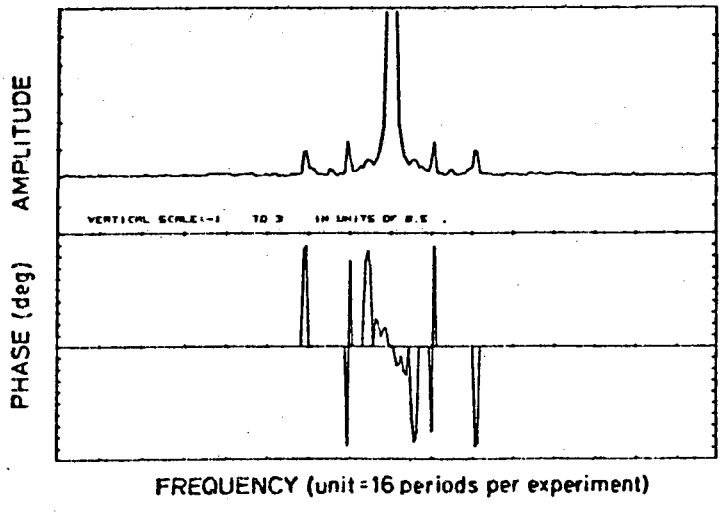

FIG. 4: SPECTRUM ANALYSIS BY FFT FOR "A" FIELD

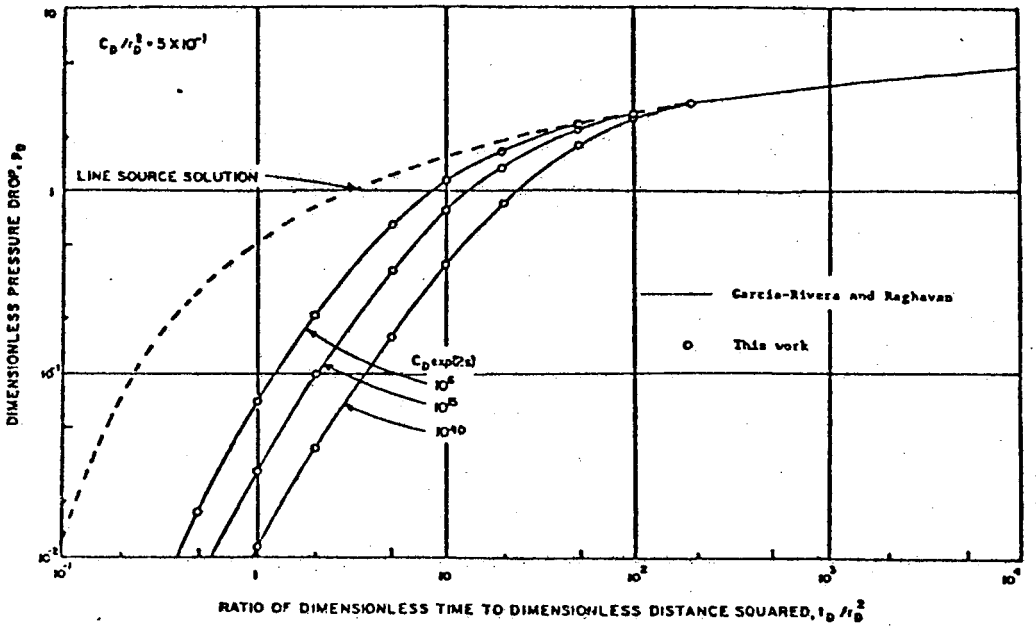

FIG. 5: COMPARISON OF RESULTS OF THIS STUDY WITH THE GARCIA-RIVERA AND RAGHAVAN STUDY

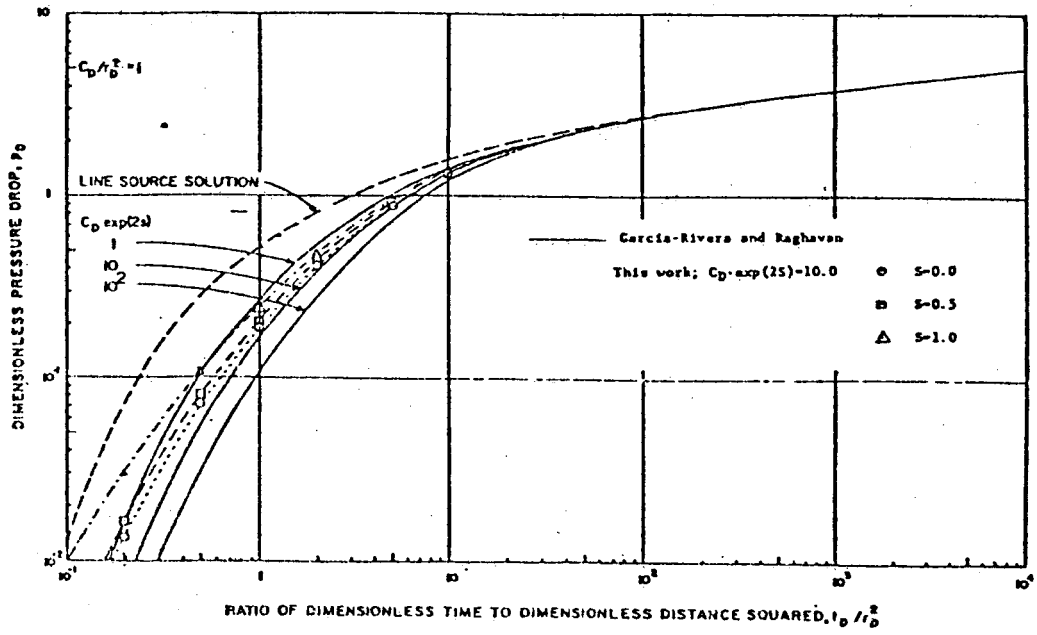

FIG. 6: COMPARISON OF RESULTS OF THIS STUDY WITH THE GARCIA-RIVERA AND RAGHAVAN STUDY

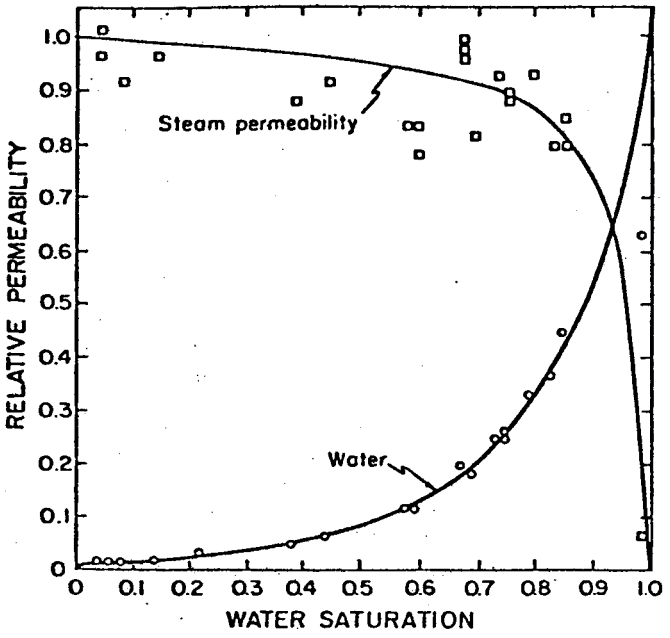

FIG. 7: STEAM-WATER RELATIVE PERMEABILITIES FROM WAIRAKEI WELL DATA

RECENT RADON TRANSIENT EXPERIMENTS

P. Kruger, L. Semprini, G. Cederberg, and L. Macias
Stanford Geothermal Program
Stanford University
Stanford, CA 94305

Radon transient analysis is being developed as a method complementary to pressure transient analysis for evaluation of geothermal reservoirs. The method is based on the observations of Stoker and Kruger (1975) that radon concentration in produced geothermal fluids is related to geothermal reservoir type, production flow rates, and time. Stoker and Kruger showed that radon concentrations were markedly different in vapor-dominated and liquid-dominated systems, and varied not only among wells of different flow rate in an individual reservoir, but also varied timewise in individual wells. The potential uses of radon as an internal tracer for geothermal reservoir engineering were reviewed by Kruger, Stoker, and Umaña (1977). Also included were results of the first transient test performed with rapid flow rate change in a vapor-dominated field. The results of the next four radon-flow rate transient experiments were summarized by Kruger (1978) in which effects of well interference and startup production in a new well were demonstrated. Four of these first five radon transient experiments have been carried out in vapor-dominated reservoirs at The Geysers in California and Serrazzano in Italy. The systematics of the transients of radon concentration following abrupt changes in flow rate is being evaluated by Warren and Kruger (1978). The fifth test was at the HGP-A well in Hawaii, the first transient test in a liquid-dominated reservoir.

Three additional radon transient tests have been carried out, each in a different type of geothermal resource. The first test was in a petrothermal resource, the reservoir created by hydraulic fracturing by LASL in the hot, dry rock experiment in New Mexico. The results of this first 75-day production test of continuous forced circulation, during January-April, 1978, are given by Tester, et al (1978). The results of the radon concentration measurements made during this test are summarized by Kruger, Cederberg, and Semprini (1978). The second test was a second transient test at the HGP-A well in the liquid-dominated reservoir at Pohoiki, Hawaii, and the third test was a second transient test at the Grottitana well in the Serrazzano field at Larderello, Italy. The general observations of these tests are listed in Table 1. A summary of each of these three tests follows.

During the LASL hot dry rock flow test, five samples of recirculating production fluid were obtained by wellhead sampling. Two samples were obtained during the following shutin and venting periods of the test, and one sample of makeup water was analyzed during the test. The radon concentration data are given in Figure 1. The data show a quasi-exponential growth in radon concentration

TABLE 1

RECENT RADON TRANSIENT EXPERIMENTS

Site	Date	Test Conditions	Observations
LASL Hot, Dry Rock Fenton Hill, New Mexico	Spring, 1978	Recirculated water as forced circulation through hydraulic cracks	Logistics Growth of [Rn]
Univ. Hawaii HGP-A Pohoiki, Hawaii	(1) July, 1977 (2) July, 1978	Short period ($\sim$4 hr) flow tests through two orifice sizes	(1) [Rn] constant with flow rate (2) [Rn]/Q growth with production?
ENEL Grottitana Serrazzano Italy	(1) Nov-Dec, 1976 (2) Aug-Sep, 1978	Long period (3 week) flow tests with two rapid changes in flow rate, Q	(1) [Rn]/Q constant (2) [Rn]/Q = $F(Q_{th})$?

during the 75-day test period. The first sample, collected 6 hours after initiation of the flow test period, was water resident in the large fracture volume during the prior 3-month shutin period and should represent geofluid radon in equilibrium with radon emanation from the fractured rock. The second sample indicated a dilution of this concentration with the large amount of makeup water required during the first 20 days of flow. The rise in concentration during the remainder of the test can be described by exponential growth of the form

$$[Rn] = [Rn]_o \; e^{+kt}$$

where k is a growth constant with the value 0.035±0.005 for the first four samples. The fifth sample showed a value of $k = 0.071$ indicating a trend toward a logistics growth of the form shown in Figure 2 by

$$[Rn] = \frac{[Rn]^{\infty}}{1 + ae^{-bt}}$$

where $[Rn]^{\infty}$ is the infinite-time steady-state radon concentration for finite radium concentration and constant emanation and thermodynamic conditions; and a and b are empirical constants estimated by least-square fit as given in Figure 2. The value of $[Rn]^{\infty} = 11.2$ nCi/l is based on the LASL measurement of [Ra] = 1.7 pCi/g in core rock and assumed values of emanating power, rock porosity and density, and the volumetric estimates of the fracture volume and total circulation volume. Four mechanisms for the observed quasi-exponential growth in radon concentration have been evaluated.

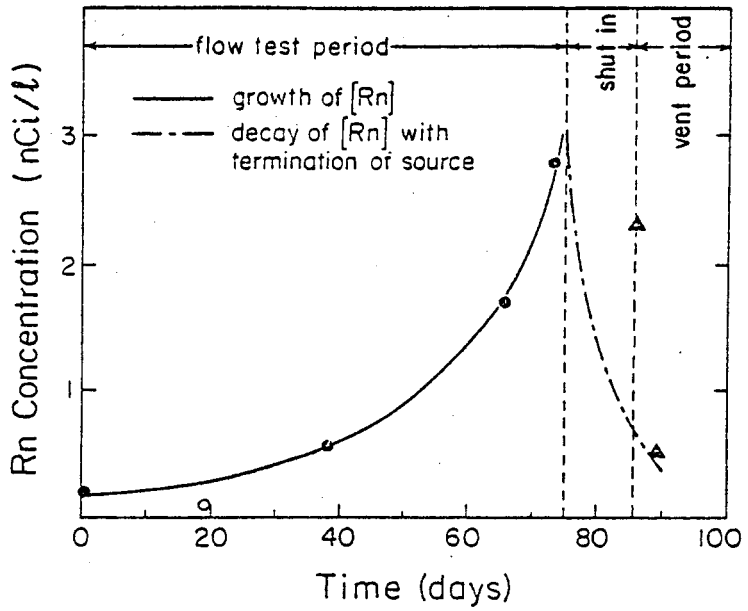

Figure 1. Radon data from the LASL Phase I test

Two of these, (1) the possibility of continuous radium dissolution and (2) the increase of radon solubility with decreasing reservoir temperature, have been discarded. The two remaining mechanisms, (3) an increase in emanating power of radon by recoil or diffusion from the rock to the recirculating fluid, or (4) an increase in the area of fractured rock surface (at constant emanating power) through increased fracturing of the formation by the recirculating fluid pressure and temperature differential cannot be distinguished. Current investigations by Macias (private communication) to determine the dependence on radon emanation on the pressure, temperature, and pore fluid density in fractured rock should assist in examining these two mechanisms.

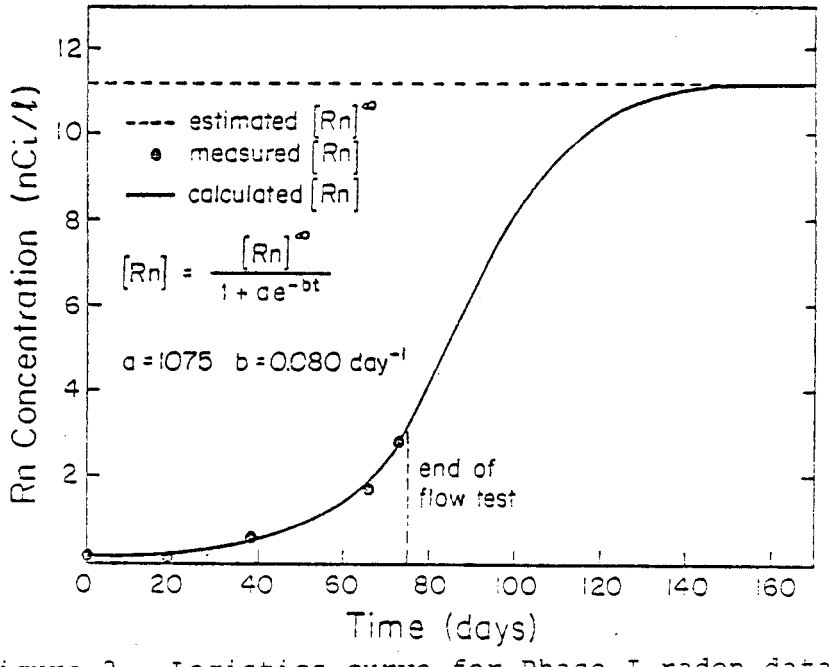

Figure 2. Logistics curve for Phase I radon data

The second test at the HGP-A well in Hawaii was run in July, 1978 in a manner similar to the first test of July, 1977 described by Kruger (1978). Both tests, with flow duration limited by environmental constraints, were run with changes in orifice plates to provide maximum flow through an 8" hole and minimum flow through a 1-3/4 - 2" hole. Flow rates were measured by the Russell James lip-flow pressure method (1962). The radon concentration and flow rate data are shown in Figure 3. Both short-period tests show essentially a constant radon concentration, independent of flow rate, in accordance with the horizontal flow model proposed by Stoker and Kruger (1975). However, the short flow periods preclude observation of any longer period transient. Several interesting trends are noted in the mean value data given in Table 2, primarily the increase in radon concentration per unit flow rate resulting from both an increase in mean radon concentration and a decrease in flow rate between the two tests. This observation may be consistent with the growth in radon concentration noted by Warren and Kruger (1978) for a newly producing well in a non-producing section of The Geysers geothermal field. If the model of "boil out" of condensed fluid near the wellbore is valid, observation of increased radon concentration per unit flow rate with further production in the HGP-A well can be predicted.

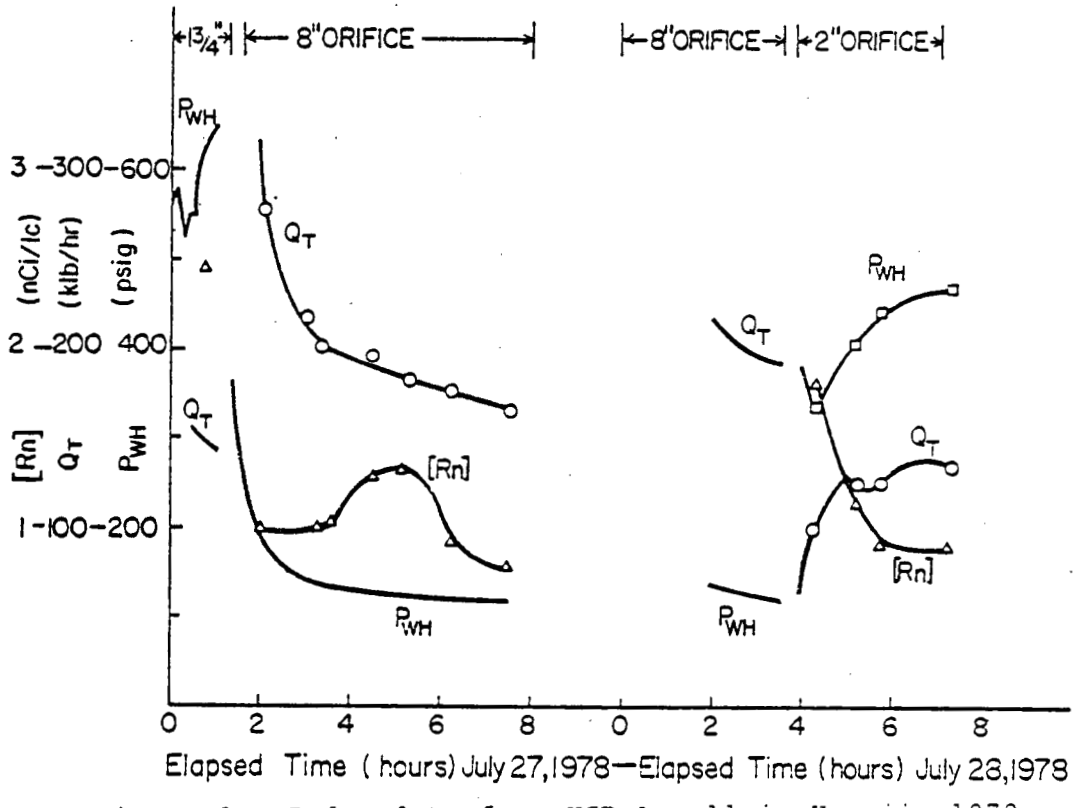

Figure 3. Radon data from HGP-A well in Hawaii, 1978

The second test at the Grottitana well at Serrazzano, Italy was run in August 1978 in cooperation with the ENEL staff in Castelnuovo. The preliminary results of this test, shown in Figure 4, agree well with the results of the November 1976 test, again showing a strong dependence of radon concentration on flow rate. However, Table 3 shows an interesting difference in this dependence related to the range of flow rates obtained. In the initial test, the flow rate was decreased from the full normal of about 11.8 t/hr to a value of about 7.5 t/hr. The observed transient was rapid (less than 1 day) and the radon concentration per unit flow rate was constant at a value of 7.33±0.76 over the entire flow rate range. In the current test, the flow rate was reduced in two stages, from 11.3 t/hr to 8.1 t/hr and then to about 5 t/hr. The two samples obtained for the first reduced flow rate showed a [Rn]/Q value in agreement with the previous value for the same flow rate change, but differed markedly for the lowest flow rate. Three possible physical reasons could account for this non-linear dependence on the lowest flow rate: (1) the increased reservoir pressures associated with the lowest flow rate sufficient to result in increased emanation from the reservoir rock (as indicated in the LASL hot dry rock experiment); (2) the possibility of a non-linear contribution from radon emanated from the boiling front to the well, as suggested for steam systems by Warren and Kruger (1978); and (3) the possibility of partial condensation of the steam under subcooled conditions during transit to the well. Here again the experimental data of Macias on emanation under known reservoir conditions will be of value in distinguishing between these possibilities.

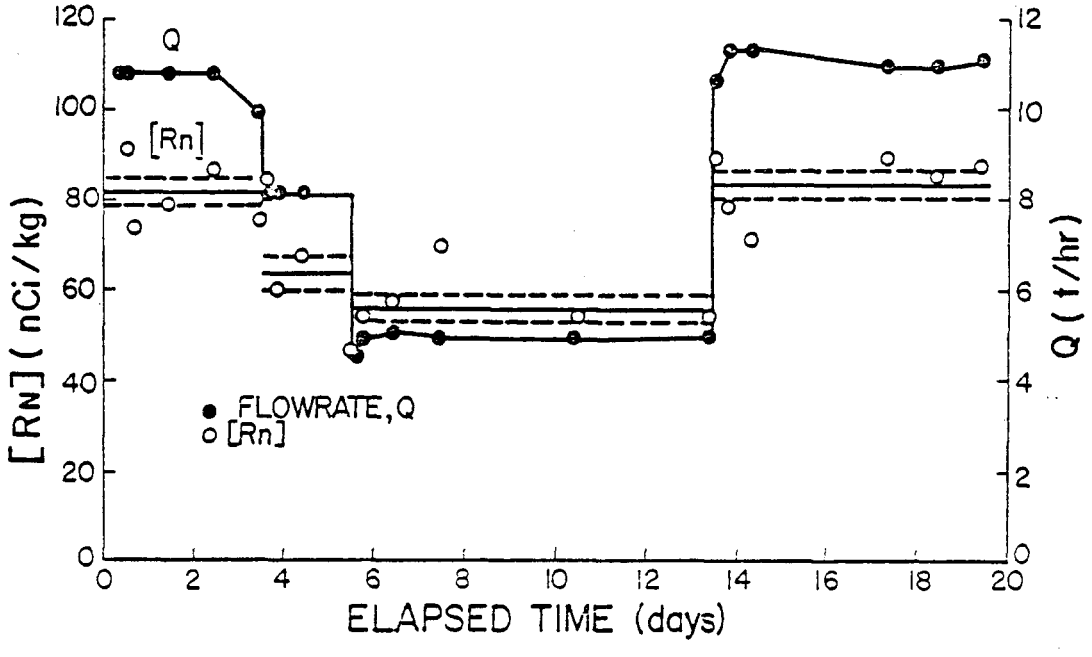

Figure 4. Radon data from Grottitana Well, Italy

TABLE 2

RADON TRANSIENT TESTS - POHOIKI, HAWAII

Date	Orifice (inches)	$\bar{Q}$ (klb/hr)	$[\bar{Rn}]$ (nCi/kg)	$\frac{[\bar{Rn}]/Q}{(\frac{pCi/kg}{mt/hr})}$
July, 1977	8	286	0.89	1.41
	1-3/4	137	0.85	2.82
July, 1978	8	201	1.22	2.76
	2	121	1.20	4.50

TABLE 3

RADON TRANSIENT TESTS - GROTTITANA, ITALY

Test Dates	[Rn]/Q Ratio	Q Range (t/hr)
Nov - Dec 1976	7.33 ± 0.76	7.5 - 11.8
Aug - Sep 1978	7.8 ± 0.3	8.1 - 11.3
	11.5 ± 0.6	4.6 - 5.0

REFERENCES

James, R. (1962), Steam-Water Critical Flow through Pipes, Inst. Mech. Engrs. Proc. 176, No. 26, 741.

Kruger, P. (1978), Radon in Geothermal Reservoir Engineering, Trans. Geothermal Resources Council 2, 383-385.

Kruger, P., G. Cederberg, and L. Semprini (1978), Radon Data - Phase I Test LASL Hot Dry Rock Project, Tech. Report SGP-TR-27.

Kruger, P., A. Stoker, and A. Umaña (1977), Radon in Geothermal Reservoir Engineering, Geothermics 5, 13-19.

Stoker, A. and P. Kruger (1975), Radon in Geothermal Reservoirs, Proceedings Second U. N. Symposium on the Development and Use of Geothermal Resources, San Francisco, CA.

Tester, J., et al (1978), Report on Phase I Test Results, LASL Hot Dry Rock Project, in preparation.

Warren, G. and P. Kruger (1978), Radon in Vapor Dominated Geothermal Reservoirs, Tech. Report SGP-TR-22, in preparation.

AN EVALUATION OF JAMES' EMPIRICAL FORMULAE FOR THE DETERMINATION OF TWO-PHASE FLOW CHARACTERISTICS IN GEOTHERMAL WELLS

P. Cheng and M. Karmarkar
University of Hawaii
Honolulu, Hawaii 96822

Introduction

One of the most economical and simple methods of determination of two-phase flow parameters in geothermal well testing is the so-called James' method [1,2]. The method consists of the measurements of lip pressure (p), and the flow rate of water (w) by a conventional weir. The stagnation enthalpy (h_o) is then determined from a plot showing h_o versus $w/p^{0.96}$ which is empirically determined by James [1,2]. The mass flow rate is then determined from the following empirical formula

$$G = 11{,}400 \frac{p^{0.96}}{h_0^{1.102}} \tag{1}$$

where G is the total mass flow rate in $lb_m/sec\text{-}ft^2$, p is the lip pressure in psia, and h_0 is the specific enthalpy in BTU/lb_m. The above relation is empirically determined for discharge pressure up to 64 psia and pipe diamters up to 8". For pipe diamters smaller than 0.2", it has been suggested that the value of 11,400 be replaced by 12,800. In view of the widespread use of the James' method, it is important to assess its accuracy and range of applicability.

Two-Phase Critical Flow Theory

In this paper we shall compare the wellbore discharge characteristics obtained from James' empirical formulae to those predicted by Fauske's two-phase critical flow theory [3]. Fauske suggested that in two-phase flow the maximum discharge rate may not necessarily be accomplished by a shock front. He proposed that at the critical flow condition the absolute value of the pressure gradient at a given location is maximum but finite for a given flow rate or quality, i.e.,

$$(dp/dz)_{G,x} = \text{maximum and finite}, \tag{2}$$

where z is the coordinate along the streamwise direction, and x the quality of the saturated mixture.

Under the assumptions of (i) annular flow pattern, (ii) two-phases

in thermal equilibrium, (iii) negligible frictional loss, and (iv) one-dimensional steady flow, Fauske [3] obtained the following analytical expression for the critical flow rate of a saturated mixture:

$$G_{critical} = \left[g_c k/Q\right]^{1/2} \tag{3}$$

where $Q = -[(1-x+kx)\, x\, (dv_g/dp) + (v_g(1+2kx-2x) + v_f(2xk-2k- - 2xk^2+k^2))\, dx/dp]$,

$g_c = 32.2 \dfrac{lb_m\text{-}ft}{lb_f\text{-}sec^2}$, and $k = (v_g/v_f)^{1/2}$ with v_g and v_f denoting the specific volume of the saturated vapor and liquid respectively. Thus, the critical flow rate can be calculated from Eq.(3) if the steam quality and the lip pressure are known.

The corresponding stagnation enthalpy can be determined from

$$h_0 = h_f(1-x) + h_g x + (G^2/2g_c)((x^3 v_g^2/Rg^2) + (1-x)^3 v_f^2/(1-Rg)^2)/J \ , \tag{4}$$

where R_g is the gas void fraction which is related to steam quality [4]. In comparison with experimental data, Levy [4] found, however, that using Eq.(4) for the computation of h_0 would lead to under-prediction of the mass flow rate. For this reason we shall compute the stagnation enthalpy on the basis of a homogeneous model, i.e.,

$$h_0 = h_f(1-x) + h_g x + G^2 v_h^2/2g_c J \ , \tag{5}$$

where $v_h = v_f(1-x) + v_g x$ and $J = 778$ ft-lb$_m$/BTU .

The weir flow rate is then determined from

$$w = G(1 - x) \ . \tag{6}$$

Results and Discussion

For a given set of values of lip pressure and steam quality and with the data of saturated steam-water properties [5], Eq.(3) can be used for the computation of total mass flow rate G . The stagnation

enthalpy and the weir flow rate are then determined from Eqs.(5) and (6). The results of the computations for the lip pressure from 14.7 psia to 200 psia for geothermal well testing applications are plotted in Figs. 1 and 2. When the lip pressure and the weir flow rate are measured in a geothermal well test, the stagnation enthalpy of the reservoir, the steam quality at the well head, and the total mass flow rate can easily be determined from these plots.

To assess the accuracy of the James' method, calculations were carried out for five different sets of lip pressure and weir flow rate using James' empirical formulae and Fauske's theoretical prediction (i.e., Figs. 1 and 2). The results for total mass flow rate, the stagnation enthalpy, and the steam quality are tabulated in Table 1 for comparison. It is shown that the results based on the two methods differ within 8%.

References

1. James, R., "Measurement of Steam Water Mixtures Discharging at the Speed of Sound to the Atmosphere, New Zealand Engineering, pp. 437-441 (1966).

2. James, R., "Steam-Water Critical Flow Through Pipes," Proc. Inst. Mech. Engrs., v. 176, pp. 741-748 (1962).

3. Fauske, H., "Contribution to the Theory of Two-Phase, One Component Critical Flow," Argonne National Laboratory, Rept. No. ANL-6633 (1962).

4. Levy, S., "Prediction of Two-Phase Critical Flow Rate," A.S.M.E. Paper 64-HT-8.

5. Keenan, J. and Kays, Keys, F. G., Steam Tables, John Wiley and Sons, Inc., New York, N.Y. (1969).

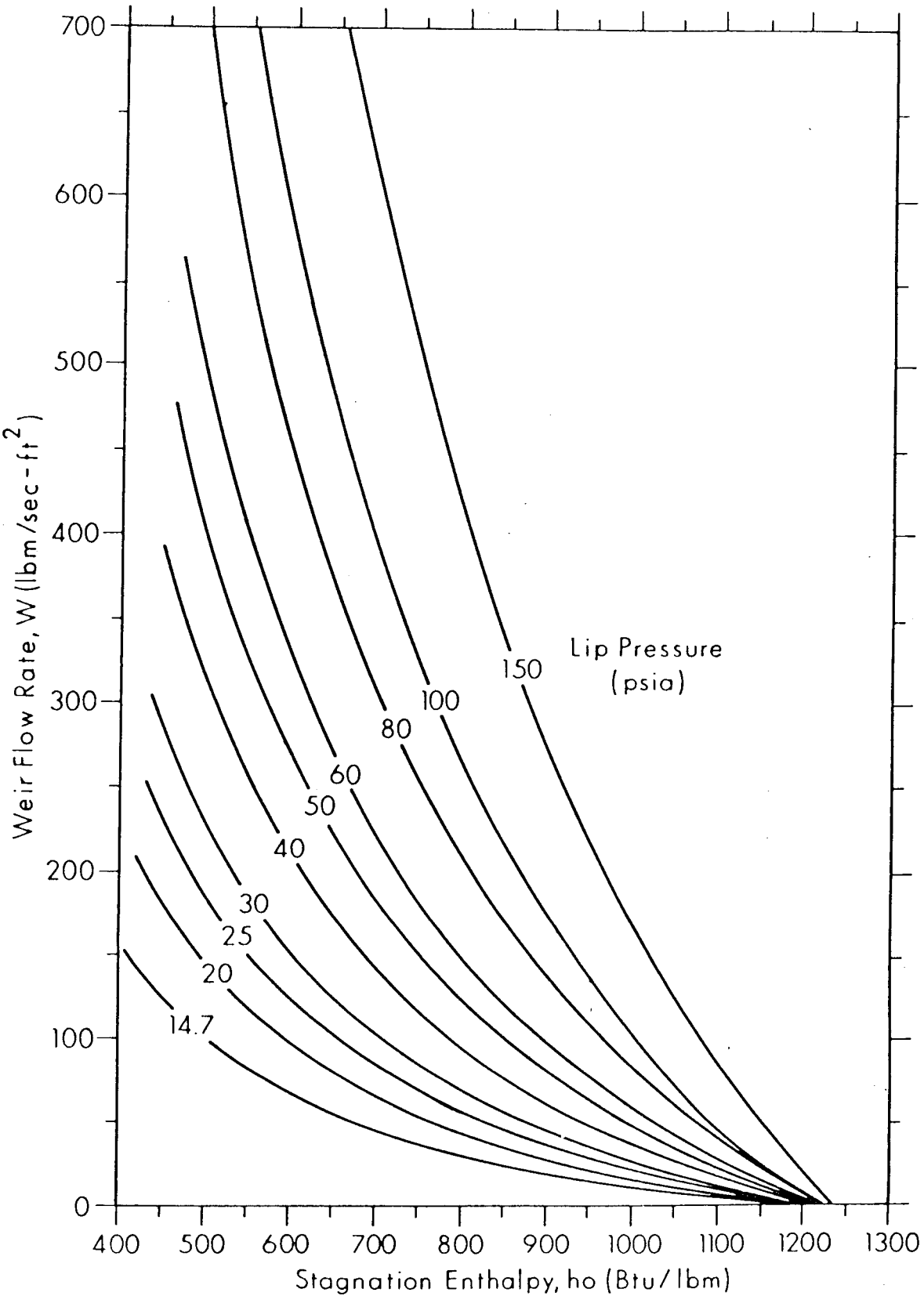

Fig. 1. Weir Flow Rate vs. Stagnation Enthalpy at Selected Values of Lip Pressure According to Fauske's Theory

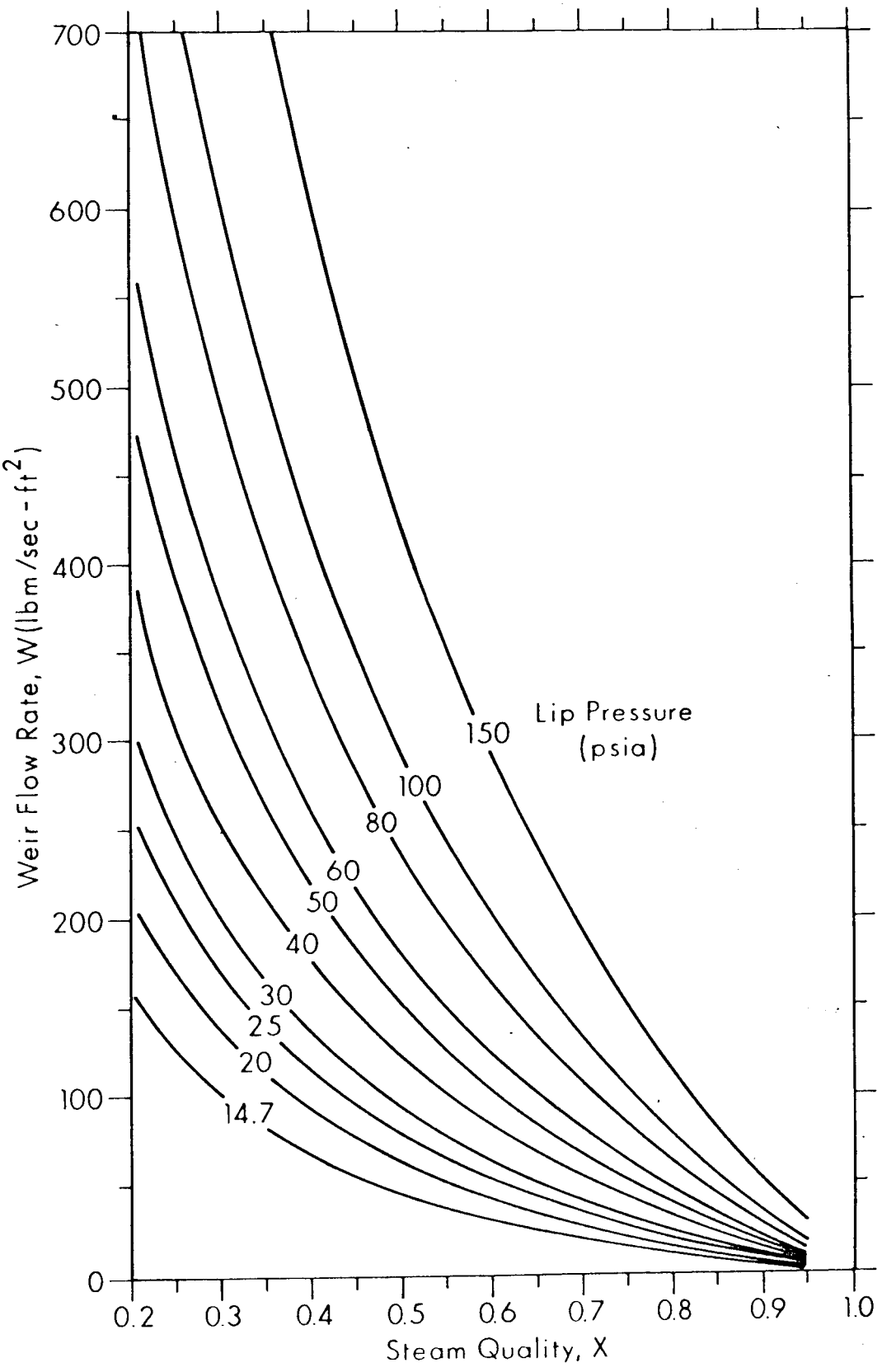

Fig. 2. Weir Flow Rate vs. Steam Quality at Selected Values of Lip Pressure According to Fauske's Theory.

Table 1. COMPARISON OF RESULTS BASED ON THE JAMES' METHOD AND FAUSKE'S ANALYTICAL MODEL

Case	p (psia)	w ($lb_m/sec\text{-}ft^2$)	h_o BTU/lb_m	G $lb_m/sec\text{-}ft^2$	x	Method
1	14.7	40	736.90	88.44	.54	Fauske (F)
			800.00	95.13	.58	James (J)
2	25.0	85.5	698.78	164.59	.48	F
			750.00	170.06	.50	J
3	60.0	226.0	697.79	403.39	.44	F
			715.00	415.42	.46	J
4	100.0	105.0	1004.52	419.84	.75	F
			985.00	476.60	.78	J
5	150.0	53.0	1148.87	523.41	.90	F
			1130.00	590.00	.90	J

Evaluation of a Geothermal Well Logging, DST and Pit Test

Erdal O. Tansev
Chevron Resources Company
P.O. Box 3722, San Francisco, CA 94119

Introduction

This paper briefly discusses logging and testing operations and certain related physical aspects in geothermal well evaluations.

A good understanding of thermal and hydrological characteristics of geothermal reservoirs are essential in geothermal well evaluations. Within geothermal reservoirs, in evaluating the wells, the two most important parameters that first could be estimated, then measured or calculated, are temperature and productivity. Well logs and wireline surveys are means of measuring formation temperatures. Drill Stem Tests (DST's) or Pit Tests are means of determining formation productivity.

Geochemistry and Petrology are currently accepted as two evaluation yardsticks in geothermal well evaluations. Investigations of cuttings and cores during drilling operations, along with studies on formation waters could be used in a predictive nature for temperature and productivity and could yield useful information on the resource.

Logging in Geothermal Wells

Logs in general are extremely useful devices in single or multiwell reservoir evaluations. Formation Density, Neutron, Induction, Sonic, SP, Gamma-Ray, Caliper and Dipmeter logs are widely accepted by the geothermal industry. Depending on the types of formations penetrated by the well, some logs are preferred or rather have a higher priority than others. For example, in volcanic rocks density and sonic logs could be preferred to dipmeter and to neutron logs.

The above formation logs could also be used in estimation of static formation temperatures at various depths. The temperatures, obtained from maximum reading thermometers attached to these logs in individual logging runs, are used in a buildup analysis to estimate final temperatures.

A current problem with the use of some logs is their temperature limitations. This limitation sometimes proves troublesome and costly in geothermal well evaluations. However, careful plans relating to a) type of logs, b) the number of logs to be run, c) their schedule, could result in significant time savings and cost reduction.

A critical review of available literature and field evaluations revealed the current temperature limitations for some of the existing logs:

Type of Log		Temperature Rating (^{o}F)
Resistivity	Standard: Dual Induction (DIL)	350
	Hot Hole: Single Induction (IL)	500
Porosity	Borehole Compensated Sonic (BHC)	350
	Hot Hole BHC, No Sp, No GR	500
	No SP, with GR	400
	Long Spaced Sonic	350
Density	Formation Density Compensated (FDC)	400
	Compensated Neutron Log (CNL)	400
Dipmeter	Four Arm High Resolution	350

For example, in evaluating a +500^{o}F well, at a depth of 6,000 to 10,000 feet, it becomes difficult, even with a cooling run, to obtain a DIL, or a Long Spaced Sonic or a Dipmeter for the entire well depth.

Given the above limitations, in hot water geothermal wells with static temperatures around 500^{o}F, it is recommended that SP be run with the Hot Hole Single Induction Log. The Hot Hole BHC Sonic could be run alone. FDC-CNL-Gamma Ray-Caliper could be run in combination on one trip, preferably after a second cooling run. If Dipmeter Log is desired it should be scheduled immediately after a cooling run.

If lost circulation is expected, further planning is necessary in an attempt to obtain some of the logs. If total lost circulation occurs and if one is unable to continue circulation to cool the well, the chances of obtaining logs are drastically reduced.

To increase the chances of obtaining all desired logs, and to save considerable time by eliminating the prerequisite temperature surveys along with multiple cooling runs, logging industry is pursuing research and development on tools for high temperature environments. DOE sponsored programs in advanced high temperature electronics for geothermal well logging applications are also continuing.

A Drill Stem Test (DST) vs. a Pit Test

A DS or a Pit test is usually conducted as a first step in the productivity evaluation of a geothermal well. The objective is to gather flowing bottom hole and wellhead data. Analysis of successful tests can yield information on a productivity index for the well, and a permeability-thickness product, preferably from a pressure buildup. Usually a DST is run in an open hole while rigged up, a pit test is run in a cased hole, after the rig release and installation of a X-mas tree. The costs of these tests, though relatively comparable, are beyond the scope of this discussion. If a DST is elected in evaluation of

the well, the results of this test could be used in a decision to run a liner, to abandon the well without running a liner, or possibly to continue drilling.

There is a greater chance of getting (good) bottom hole data through a DST. In a pit test one relies on either a) wireline pressure and temperature bombs at mid-perf's, or b) bottom hole pressure (only) estimation through nitrogen tubing pressure, which is surface recorded, and the nitrogen volume data.

A disadvantage in both DST and Pit tests with bottom hole recordings is that the data is not available until the tests are over. Surprises and disappointments are not uncommon when tools or charts are brought to surface.

A severe limitation for both tests is the limited water volumes that can be produced during a relatively short time. Often these tests only serve in a partial cleanup of lost circulation, or they merely enable production of few wellbore volumes before running out of storage capacity. Disposal of the produced formation brine and mud proves costly and time consuming. Higher production rates and slightly longer test times, however, are possible through a pit test.

DST was designed by the oil industry to test the hydrocarbon potential of limited intervals, usually $\ll$200 feet. In geothermal wells the intervals of interest are usually greater. Therefore, DST's are not suitable, neither for the large intervals to be tested nor the high flow rates desired.

One practice is to attach both outside and inside pressure recorders and the temperature bomb to the end of the drill pipe, and set the packers, as deep as possible, between the drill pipe and the intermediate casing. A 15-25 feet perforated tail pipe preferably above the pressure and temperature bombs, permits the entire hole below to be open to flow. See Figure 1A.

An alternate, in an open hole test, is to run the drill pipe to the desired depth and inject nitrogen, producing the well through the annulus. Pressure and temperature bombs could be attached to the bottom of the drill pipe. This method eliminates the cost of a drill stem test and avoids the possible - high temperature related - problems with the packers. See Figure 1B.

Flow rates in both tests are usually estimated by volumetric measurements. An estimation of wellhead steam quality is also necessary to determine the total mass rate from the well. Numerical wellbore models could be used to estimate wellbore heat losses and pressure drops, hence wellhead qualities. In the absence of bottom hole data wellbore models could also be used, starting with wellhead data, to predict flowing bottom hole pressures and temperatures.

Given these limitations of Drill Stem and Pit tests, long term production tests, where a nearby injection well is available, becomes necessary in further or final evaluation of a well. Long term tests are especially important for wells with fracture production.

More research is required to find new ways and means of short time testing hot water geothermal wells.

FIG. 1

TWO CURRENT PRACTICES IN GEOTHERMAL WELL TESTING

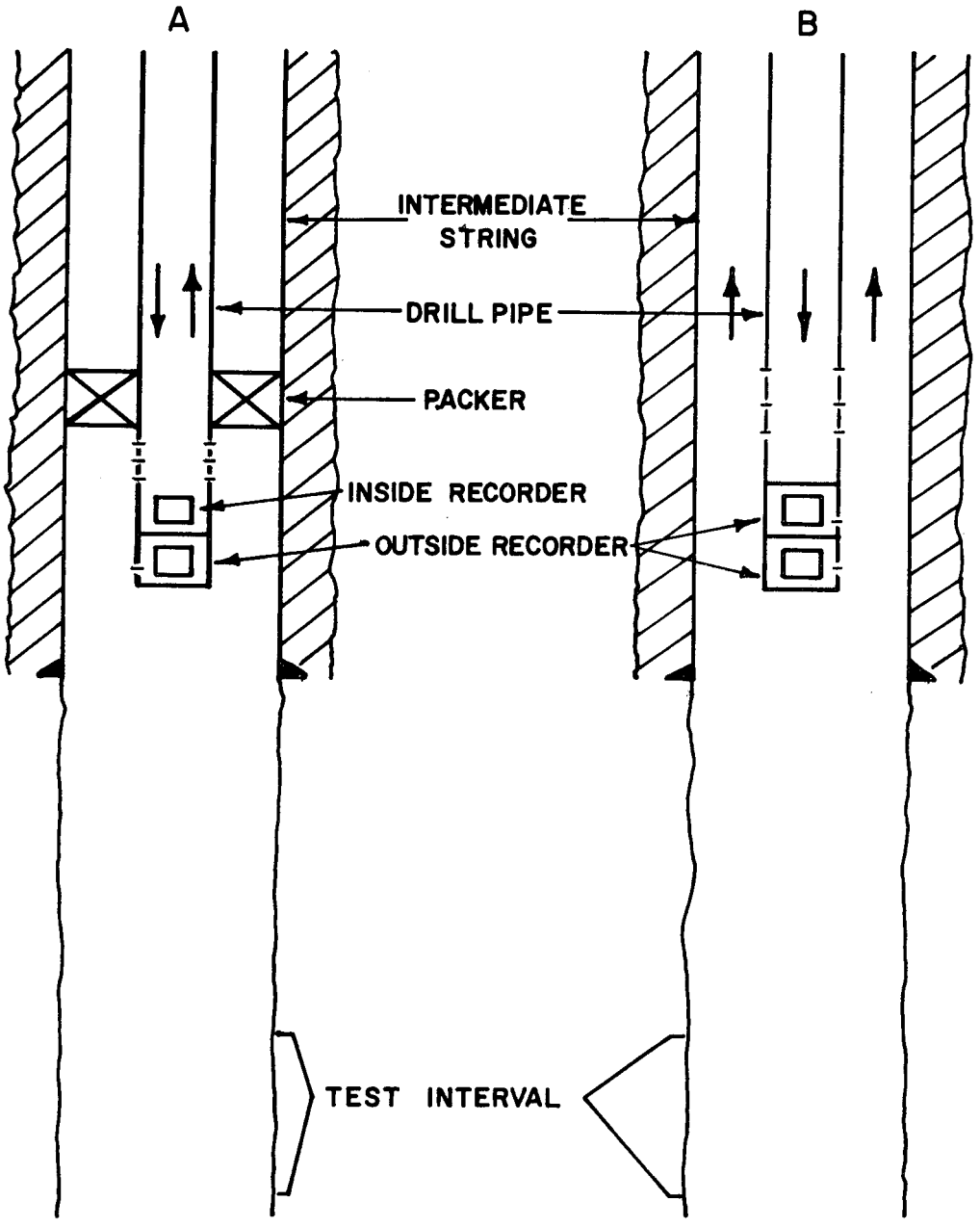

WAIRAKEI GEOTHERMAL FIELD RESERVOIR ENGINEERING DATA*

J. W. Pritchett, L. F. Rice and S. K. Garg
Systems, Science and Software
La Jolla, California 92038

Systems, Science and Software (S^3) has prepared an extensive collection of fundamental field information concerning the history of the Wairakei geothermal field in New Zealand. The purpose of the effort was to accumulate any and all pertinent data so that various theoretical reservoir simulation studies may be carried out in the future in a meaningful way. Categories of data considered include electrical resistivity measurements, magnetic force surveys, surface heat flow data and a catalog of surface manifestations of geothermal activity, geological and stratigraphic information, residual gravity anomaly surveys, laboratory measurements of formation properties, seismic velocity data, measurements of fluid chemical composition, monthly well-by-well mass and heat production histories for 1953 through 1976, reservoir pressure and temperature data, and measurements of subsidence and horizontal ground deformation. The information is presented in three forms. A review of all the data is contained in the final project report.[1] An abbreviated version of the final project report has also been prepared by S^3 for wide distribution by the Lawrence Berkeley Laboratory (LBL).[2] In addition, a magnetic tape suitable for use on a computer has been prepared. The magnetic tape contains a bank of information for each well in the field, on a well-by-well basis. For each well, the tape contains the completion date, the surface altitude, the bottomhole depth, the geographic location, the slotted and perforated interval locations, the bottomhole diameter, locations of known casing breaks, the geologic drilling log, fault intersections, shut-in pressure measurements, and month-by-month production totals of both mass and heat for each month from January 1953 through December 1976. The magnetic tape, as well as the complete and summary reports are available through the Lawrence Berkeley Laboratory.

REFERENCES

1. Pritchett, J. W., L. F. Rice and S. K. Garg, "Reservoir Engineering Data: Wairakei Geothermal Field, New Zealand," Systems, Science and Software Report, SSS-R-78-3591, March, 1978.

2. Pritchett, J. W., L. F. Rice and S. K. Garg, "Summary of Reservoir Engineering Data: Wairakei Geothermal Field, New Zealand," Lawrence Berkeley Laboratory Contractor Report, 1978.

* Work performed for the U. S. Department of Energy under Lawrence Berkeley Laboratory Purchase Order No. 3024102.

RECENT RESERVOIR ENGINEERING DEVELOPMENTS AT BRADY HOT SPRINGS, NEVADA

J. M. Rudisill
Thermal Power Company
601 California St.
San Francisco, California 94108

Brady's Hot Springs is a hydrothermal area located approximately 28Km northeast of Fernley, Nevada. Surface manifestations of geothermal activity occur along a north - northeast trend fault zone (herein referred to as the Brady Thermal Fault) at the eastern margin of Hot Springs Flat, a small basin. Since September, 1959, Magma Power Company, its subsidiaries, and Union Oil Company (as Earth Energy Company) have drilled numerous wells in the area. In 1977 Magma's 160 acre lease in Section 12 was assigned to Geothermal Food Processors (GFP) for the purpose of providing heat from the wells on this acreage for the dehydration of food. GFP made application to the Geothermal Loan Guarantee Program (GLGP) for assistance in financing the effort, and consequently the GLGP office turned to the USGS for a resource evaluation. The USGS in turn recommended that a pumped flow test was necessary to truly determine the ability of the acreage's wells to provide the requisite water flow rate, temperature, and composition for the plant's operating lifetime of at least 15 years. Consequently, Thermal Power Company was contacted and procured to design, arrange, conduct, and evaluate a pumped flow program to satisfy these questions.

Brady's Geology

Brady's is easily accessed from Reno, Nevada by driving 88Km eastward on U.S. Interstate 80, taking the Nightingale-Hot Springs exit, and heading eastward toward the Hot Springs Mountains, on whose northwest flank lies the area. Small steam vents, areas of warm ground, and spring sinter deposits are present for 4Km (2.5m) along the zone of the N 19°E trending Brady Thermal Fault. The fault itself extends some 9.6Km (6m) through the area. It is a normal fault of small displacement (100') dipping 70 -80 NW with the downthrown side to the west. The fault is typical of the basin and range type faults in the western U.S.[2] Fluid emergence has been occurring for a minimum of 10,000 years as evidenced by the sinter deposits[3] sandwiched between Pleistocene Lake Lahontan sidements.

Four main rock types are exposed in the Brady Hot Springs area[3]:

1. Volcanic rocks of Tertiary/Quaternary age, chiefly basalt in the mountains east of the springs;

2. Sedimentary rocks of Tertiary age consisting of sandstone, shale, tuff, diatomite, and minor limestone;

3. Lake deposits, of late Pleistocene Lake Lahontan;

4. Coarse alluvial fan and pediment deposits.

"Regional gravity and magnetic surveys do not suggest the presence of an upper crustal heat source."[2] Thus, a cooling magma or other intrusive body does not appear to be supplying heat to the Brady system. The geology suggests that the system is the result of deep circulating water, typical of basin and range hydrothermal systems.[2]

Production Test

A pumped flow test was designed to evaluate whether this complex reservoir could support GFP's dehydration plant with 700 gpm of 270°F (132°C) water for the plant's 15 year life. A shaft-driven turbine pump capable of pumping 600 gpm of water was purchased by GFP and installed in the designated producer, well Brady 8. The pump's bowls were set at 500 ft. to provide sufficient net positive suction head to prevent the entering water from flashing before entering the pump. The nearby artesian well Earth Energy 1 (EE-1) was instrumented with a Sperry-Sun Pressure Transmission System (PTS) with a ¼ of 1% accurate Bourdon tube gauge to measure interference effects. Three more distant wells (see Figure 1), Bradys 1, 3, and 4, were monitored for interference effects by measuring their changing water levels, with a Powers Portable Well Sounder. Some baseline data was gathered and the pump, driven by a portable diesel engine, was activated. A back pressure was maintained at the surface on the pump sufficient to both regulate the flow rate at 650 gpm and to allow the measurement of the water in a single liquid phase by means of an orifice.

The test began shakily as a lack of constant supply of bearing flush water prevented continuous operation. Finally this logistical problem was overcome and a test of >300 hours of virtually continuous, 650 gpm pumping was accomplished. Unfortunately, drawdown levels in the producer, Brady 8, couldn't be measured because the proper instrumentation was not installed with the pump. However, build-up after shut-in of the producer was measured and plotted semi-logarithmicly in Figure 2. The response of wells Brady 1 and 4 was accurately measured during both drawdown and building and are presented in Figures 3 and 4. EE-s displayed no measurable response.

The conclusion of the test wells were 1) that Brady 8, although cased to 1048', appeared to be drawing production from a zone from 610 ft. to 800 ft. which is open to the shallow wells Brady 1 (1567 ft.) and Brady 4 (723 ft.). (See Figure 5). (2) EE-1 appeared to be isolated from this region by casing to 894'. (3) From the drawdown curves of Brady 4 and Brady 1, it appeared that the shallow reservoir being drawn upon is being fed by a deep, vast reservoir (probably

deep circulating up the Brady Thermal Fault) which would cause the pressure decline of the field to slow greatly over time. The build-up behavior of the wells confirmed the recharging ability of the system as wells B1, 4, and 8 logarithmicly approached their original water level. Finally, (4), water composition and temperature remained constant throughout the test, indicating a reliable, continuous reservoir composition. Thus, it was concluded that the Brady reservoir has a reasonable chance of providing the required flow rate for the 15 year plant life.

Injection Test

A short term injection test was then designed to answer the following questions:

1. Determine the injectivity of EE-1, the most prospective injection candidate due to its apparent isolation from Brady 8's production zone.
2. Determine the zones in the well which accept water during injection.
3. Determine as quantitatively as possible the relative ability of each of these zones to accept water.
4. Use the data gained above to ascertain the suitability of EE-1 for GFP on a production basis.

To accomplish these objectives in an expeditious manner it was decided to store fresh water on site, inject water in the well at initially varying rates, log the well while injecting at a constant rate, and then re-test the injection of injectivity of the well to determine whether any changes of the well's injectivity had occurred over time. Neighboring well's water levels were to be measured throughout the testing of EE-1.

Performance of the Injection Test

The performance of the injection test consisted of the following actions:

(a) Static temperature surveys.
(b) Wellhead selection and installation.
(c) Pre-injection surveys.
(d) Injectivity tests.
(e) Injection surveys.
(f) Survey at varied flow rates.
(g) Interference effects.

EE-1's Suitability as an Injector

From the field work, it was apparent that EE-1 in its present condition did not accept the design injection rate of 700 gpm without pressure interference at B-8, the producer. Water injected down EE-1 leaves the wellbore through 3 exit points:

1. the 9 5/8 in. - 7 in. lap at 371 ft.

2. the perforations at 1880 ft. - 1940 ft.

3. the perforations at 3200 ft. - 3300 ft.

It appears that the upper regions are causing interference with B-8. Accordingly, the injecting of water in zones above 2000 ft. must be avoided if EE-1 is to be used as an injector. Referring to the schematic of EE-1 in Figure 6, this could be accomplished by running smaller pipe into the 4½-in. liner below 2000 ft. and cementing back to surface. The tremendous pumping penalty imposed prevents this course of action from being a viable option. Alternatively, one could consider pulling the 4½-in. liner, reaming out a larger hole below the 7-in., and running a somewhat larger casing through the 7-in. down to the preferred depth. This operation poses a high drilling risk as well as a rather severe pumping penalty, and was thus also deemed a less-than-preferable action.

Two other alternatives appeared available to GFP. A temporary surface disposal system could be cleared with the applicable Nevada State agencies. This system could be employed until GFP determined the ultimate course of action to take - whether to drill a new injection well, or attempt to rework EE-1 in the latter manner detailed above. It was recommended to GFP to pursue all alternatives with the ultimate objective of disposing the water underground.

The GFP plant has operated using surface disposal one month as of December 3, 1978 without problems from the geothermal reservoir. Unfortunately, preoccupation with operational problems concerning the food dehydration equipment has precluded the gathering of even rudimentary reservoir data. Hopefully, as the everyday plant operations smooth out more attention can be turned towards the reservoir.

References

1. Olmstead, et al., 1975 Preliminary hydrogeologic appraisal of selected hydrothermal systems in northern and central Nevada: USGS Survey Open-File Report 75-76, 267 p.

2. Evaluation - GFP, Inc. Loan Guarantee Application, USGS, July 15, 1977.

3. de Leon, Thermal Power Company Geotechnical Summary of Brady Hot Springs - unpublished report.

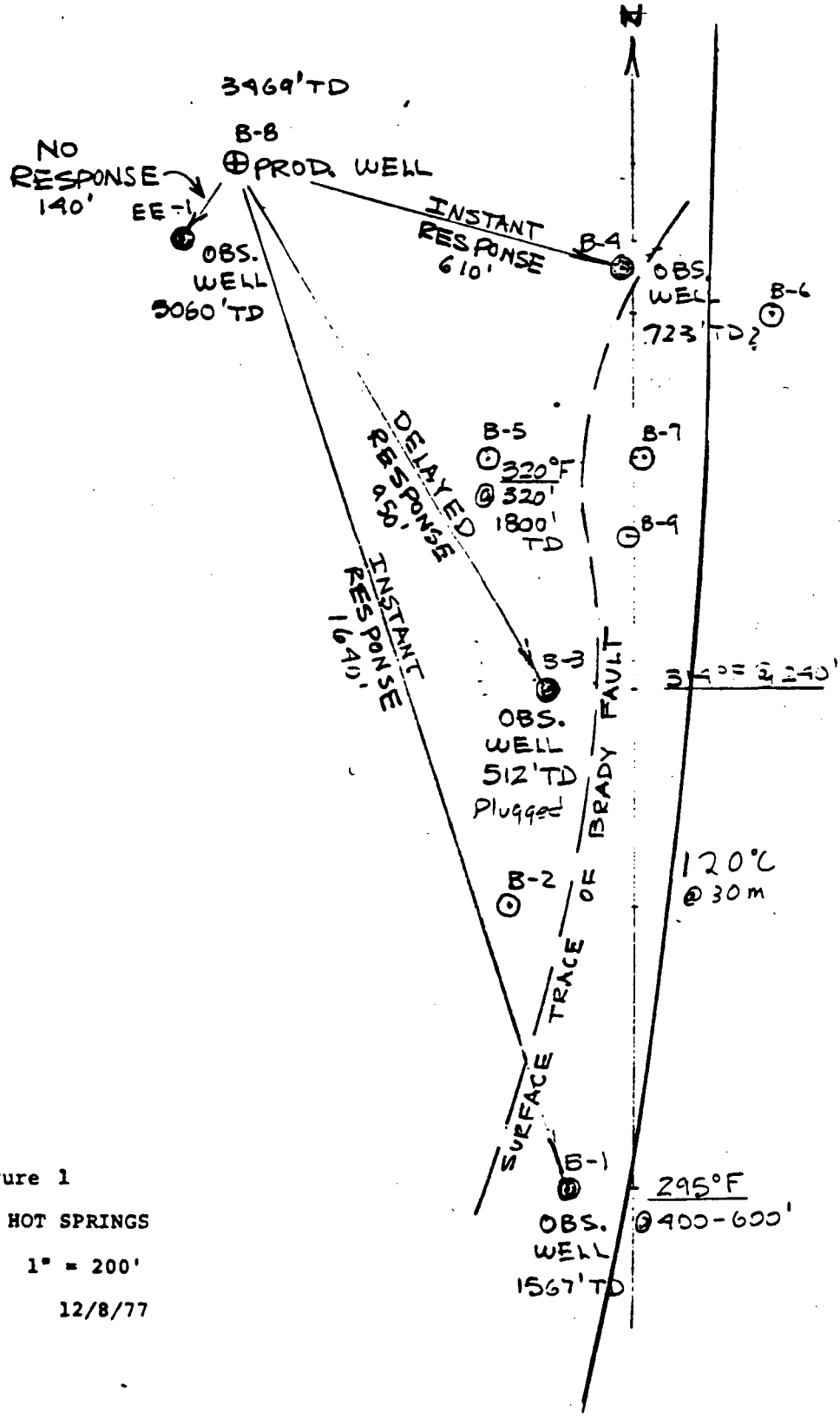

Figure 1

BRADY HOT SPRINGS

Scale 1" = 200'

HD 12/8/77

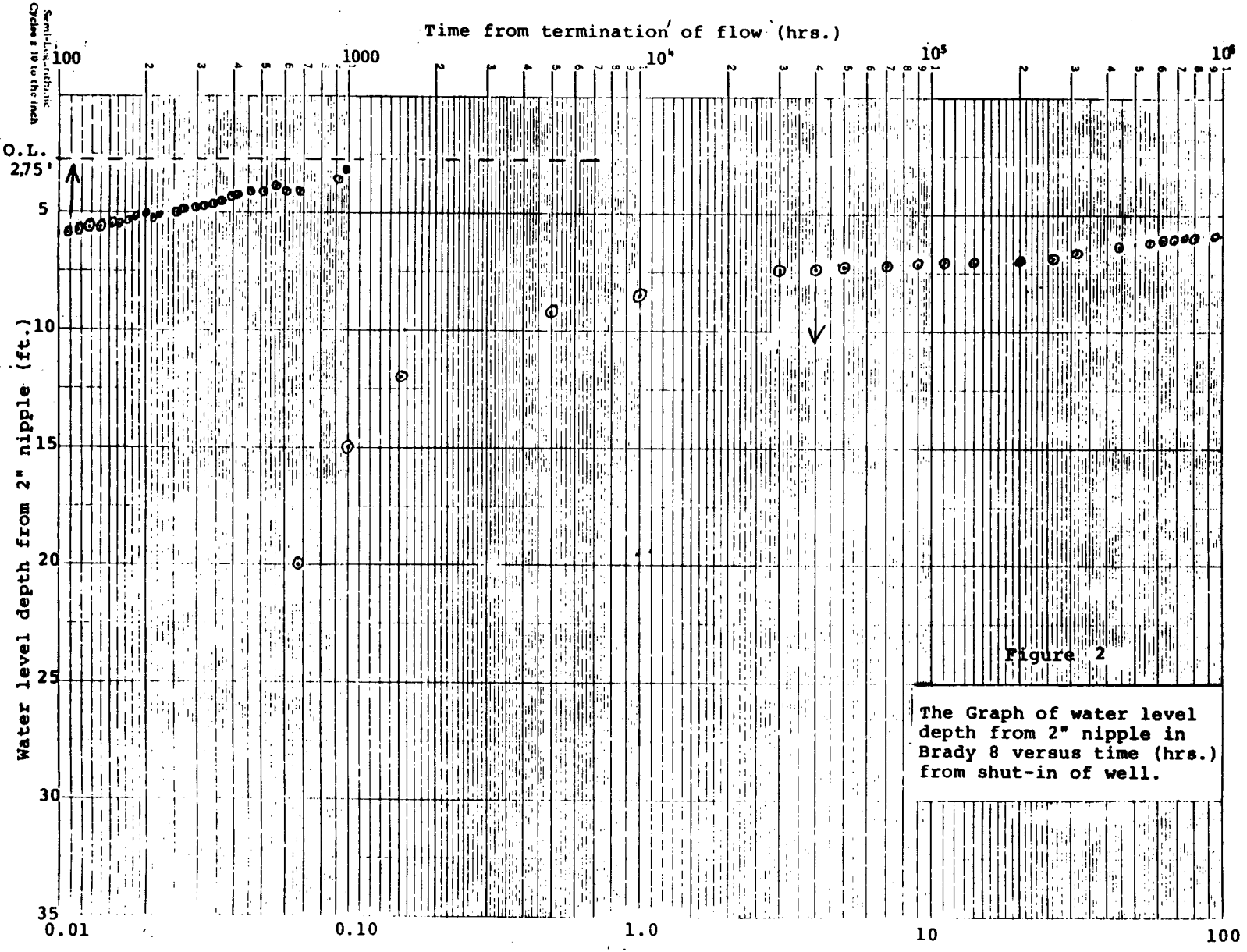

Figure 2

The Graph of water level depth from 2" nipple in Brady 8 versus time (hrs.) from shut-in of well.

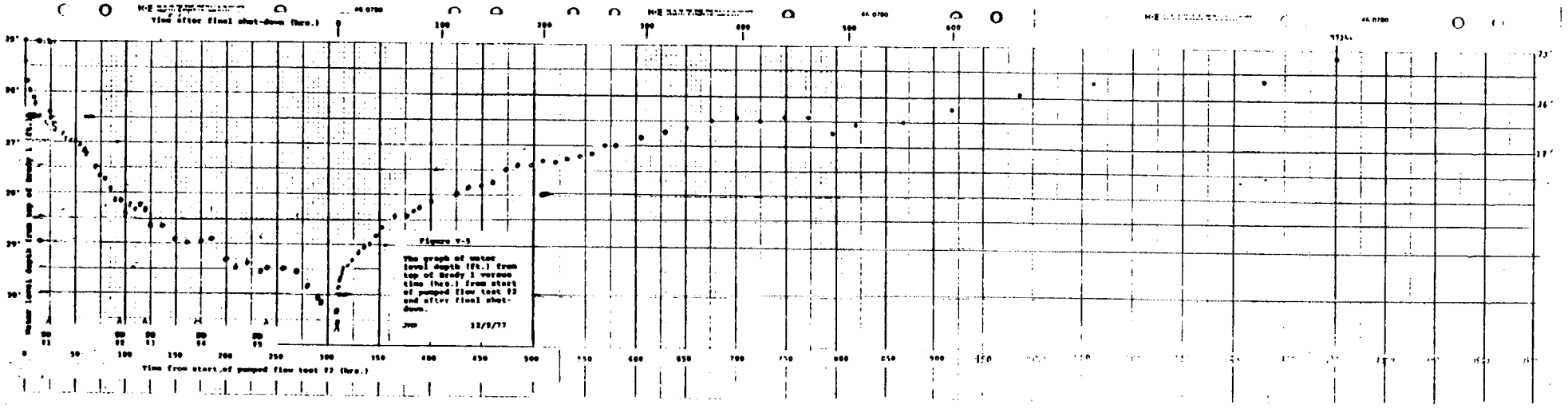
Time after final shut-down (hrs.)
Time from start of pumped flow test 02 (hrs.)
Figure V-5
The graph of water level depth (ft.) from top of Brady 1 versus time (hrs.) from start of pumped flow test 02 and after final shut-down.
JMH 12/9/77

Figure 3

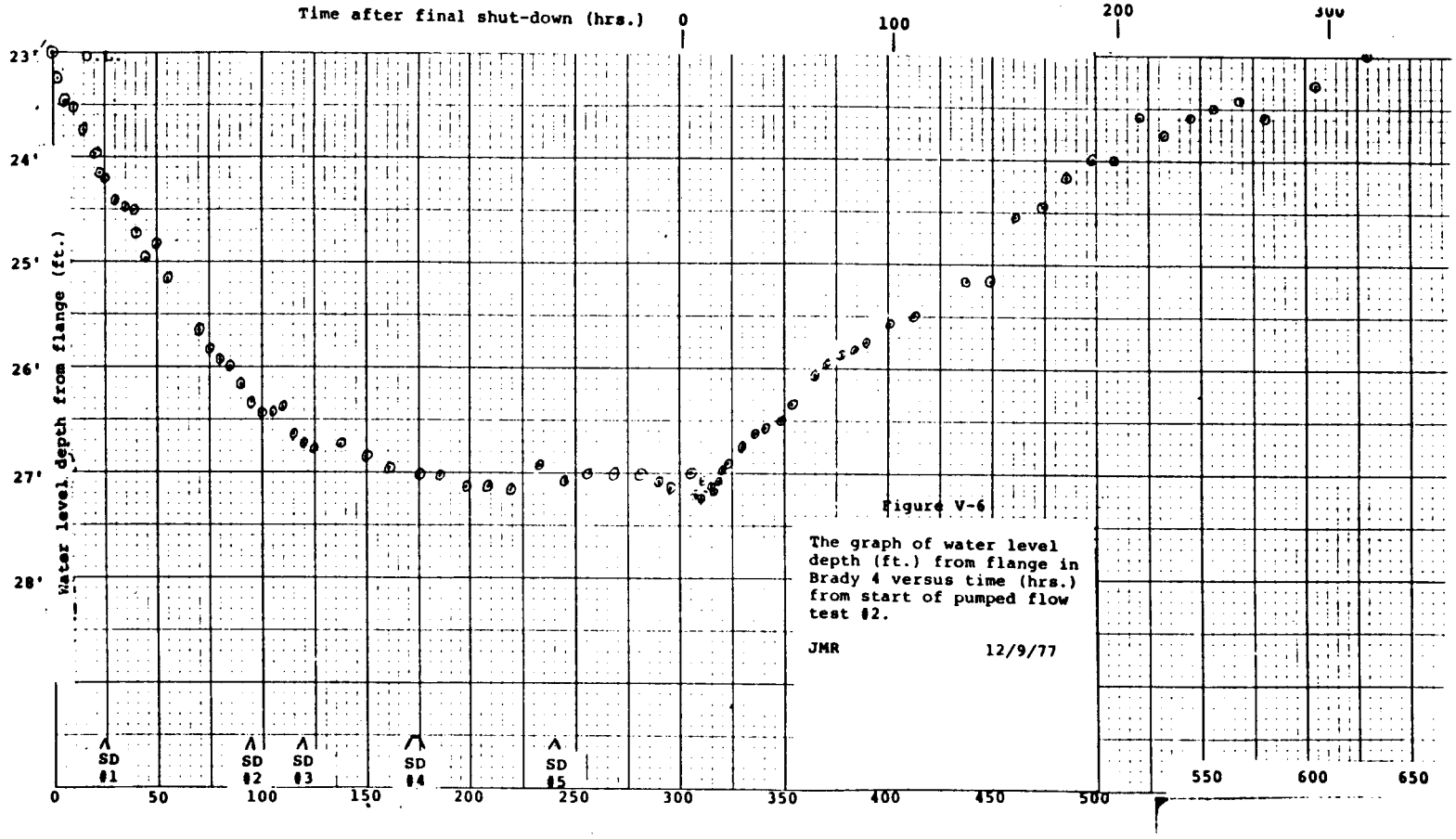
Time after final shut-down (hrs.)
0
100
200
300
D.L.
23'
24'
25'
26'
27'
28'
Water level depth from flange (ft.)
SD #1
SD #2
SD #3
SD #4
SD #5
0
50
100
150
200
250
300
350
400
450
500
550
600
650
Figure V-6
The graph of water level depth (ft.) from flange in Brady 4 versus time (hrs.) from start of pumped flow test #2.
JMR
12/9/77

Figure 4

FIGURE 5.

A CARTOON DEPICTING
THE DYNAMICS OF THE
BRADY HOT SPRINGS RESERVOIR

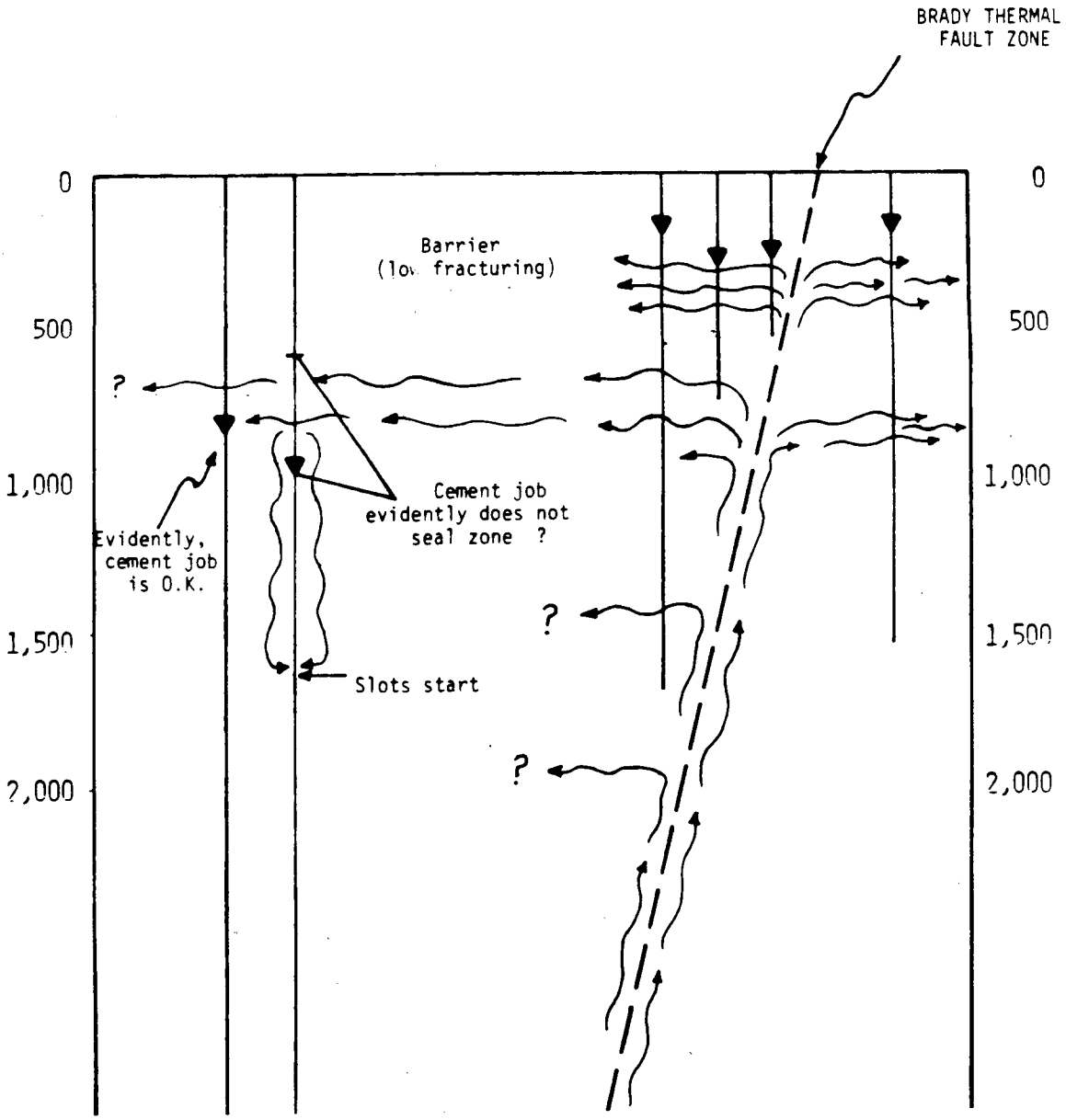

FIGURE 6

EE-1 Schematic
as of 2/78

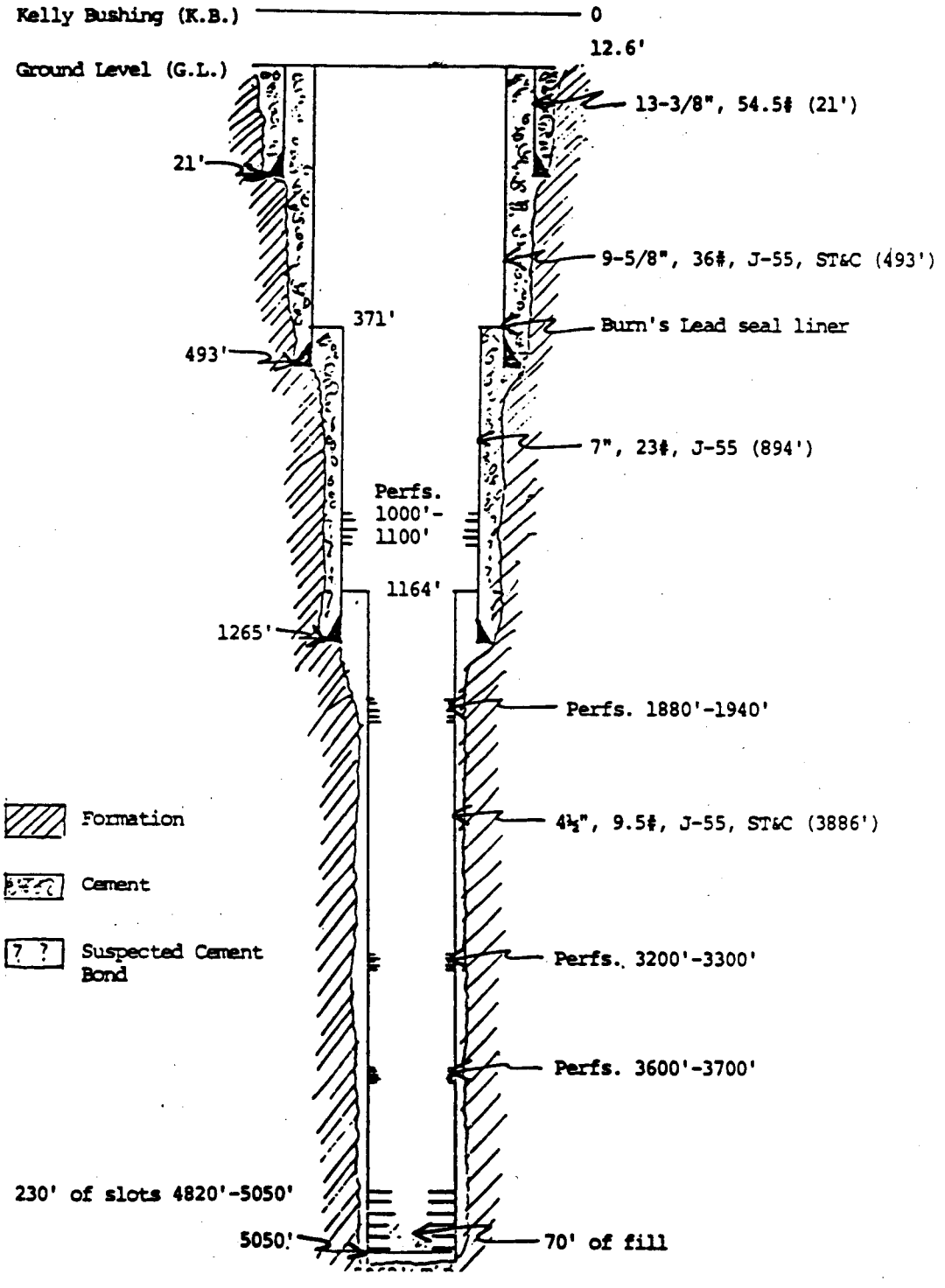

THE BULALO GEOTHERMAL RESERVOIR MAKILING-BANAHAO AREA, PHILIPPINES

Philip H. Messer and Val F. de las Alas
Philippine Geothermal, Inc.
P.O. Box 7336, Airport, Metro Manila, Philippines

The Bulalo field, located within the Makiling-Banahao geothermal prospect, is being explored and developed by Philippine Geothermal Incorporated (PGI), a branch of the Union Oil Company of California. During the past four years, twenty-eight wells have been drilled and completed in the Bulalo heat anomaly. These wells have defined a large geothermal reservoir characterized by a high-temperature effluent which can be spontaneously produced to generate commercial power.

An extensive flow testing program has resulted in the production of over thirteen billion pounds of reservoir effluent. After flashing the steam to atmospheric conditions, nearly seven billion pounds of produced reservoir fluid have been reinjected into the Bulalo reservoir. In spite of the large quantity of reservoir effluent that has been produced and reinjected, insufficient testing has been conducted to determine the total commercial power generating capacity of this large liquid-dominated reservoir.

The preliminary estimate of generating capacity has led to the current installation of 220 MW. Field development for the installation of four 55 MW units is in progress. The initial 55 MW unit is scheduled for operation in July, 1979, with Unit 2 to operate in the fourth quarter of 1979. Continued drilling and production testing up to the initiation of commercial operation will afford periodic reserve updating and confirmation for additional power generating units. After commercial power generation commences, data will be available to establish a more reliable estimate of the Bulalo field potential.

INTRODUCTION

As a result of the increasing worldwide energy crisis, the economic harnessing of alternate energy sources has become more attractive. Of particular interest in the Philippines is the development of geothermal energy which has been encouraged because of its relatively large potential. Several geothermal areas have been appraised and recognized by the Philippine government as having potential for power generation. One such area, the Makiling-Banahao region, has been contracted to PGI for further exploration and subsequent development.

The Bulalo geothermal anomaly is one field within the Makiling-Banahao area that has been discovered and is being developed by PGI. During the past four years, twenty-eight wells have been drilled and completed in the Bulalo heat anomaly. These wells have defined a large, liquid-dominated geothermal reservoir characterized by a high-temperature effluent which can be produced to generate commercial power.

PGI has developed an active drilling and exploration program which has investigated approximately 7.3 square kilometers (1800 acres) of the Bulalo field prospect. Continual expansion of this exploration acreage is augmented by the drilling and completion of an additional well nearly every month. A comprehensive well testing program has been developed to understand and define the geothermal reservoir characteristics. However, the ultimate productive capacity and extent of the Bulalo anomaly will only be determined by future drilling and long-term production. This report describes what is currently known about the Bulalo field within the Makiling-Banahao area.

GEOLOGY

The Makiling-Banahao contract area, as shown in Figure 1, is located in the Laguna province southeast of Manila, below the Laguna de Bay. The area is characterized by surface hot springs most prevalent near the town of Los Baños at the northern base of the Makiling volcano. Spas and thermal baths are popular in this area. Other hot springs and geothermal surface manifestations are widely spread between the Makiling and Banahao volcanoes in an area of several hundred square kilometers.

The Bulalo field is located to the south of the Makiling volcano. The prospect is currently the southernmost geothermal anomaly that is being actively developed by PGI within the Makiling-Banahao contract area. The Bulalo field is located approximately sixty kilometers southeast of Manila as shown in Figure 1. The area lies between the Banahao and Makiling volcanoes and is, in general, characterized by tuffs, lahars and lava flows of the basaltic-andesite type. The Makiling volcanics are older and are overlain in areas by the Banahao volvanics leading to difficulty in accurately defining the stratigraphy.

The drilling and production testing programs have defined the subsurface Bulalo structure as a large heat anomaly principally composed of a fractured andesite formation in the north and central portions, and a fractured tuff to the southeast. The fracture system within the reservoir is believed to be controlled by major faulting, oriented according to the main north-south regional trend, with transverse faulting trending in the east-northeast direction.

SUMMARY OF DRILLING OPERATIONS

Twenty-eight wells have been completed in the Bulalo field by PGI since January, 1975. These completions comprise the total Bulalo field exposure to date. The wells have been drilled on a 0.26 square kilometer (65 acre) pattern, in general, with approximately 7.3 square kilometers (1800 acres) of total reservoir exposed to date. The degree of infill drilling over the economic project life will be dependent upon a more accurate assessment of the reservoir. Each completion is composed of a seven-inch perforated liner suspended in a 9-5/8-inch cemented casing. Total depths range from nearly 3,000 feet for completions located in the central portion of the field, to over 9,000 feet in the flank completions. Wellbore exposures reflect the commercial temperature gradients and productive intervals encountered in each completion.

Cooling of the geothermal formation results from the circulation of the mud fluids during drilling. Normally, several months of a static wellbore condition must follow the drilling and completion phases of a well to adequately define the static bottomhole temperature profile. Maximum static bottomhole temperatures range from 520°F to 655°F. Individual well production is a result of the fluids associated with the most permeable zones exposed to the wellbore, which may not be of maximum exposed temperature.

SUMMARY OF WELL TESTS

Production testing has been regarded as an important phase in the assessment of the Bulalo reservoir. Surface production equipment has been constructed to afford a variety of flow testing conditions to characterize each completion. During each test the well is generally produced at commercial operating conditions for sufficient flow periods to define the stable flow characteristics of each well.

Most of the Bulalo completions have been subjected to several flow tests; however, three flank completions were initially assessed as having marginal productive capacity and were converted to injectors. The produced fluid in the Bulalo field has always been reinjected into the reservoir. This produced effluent has been flashed to atmospheric conditions and subsequently reinjected.

RESERVOIR ASSESSMENT

The twenty-eight completions in the Bulalo field have defined two types of geothermal formations. The northern and central completions have defined a highly productive andesite formation, with an apparently well-defined fracture network of

good permeability and commercial temperature. The southeastern completions have exposed a fractured tuff formation of high temperature and lower flow capacity. Both formations are believed to have similar fluid-in-place characteristics and the reserve potential is comparable for both types of formation.

Productivity Characteristics The production testing program has defined the stable total mass flow rates at a commercial operating pressure of 140 psia. Production at this pressure is a mixture of steam and water, the relative proportions depending primarily upon the reservoir fluid enthalpy. Commercial total mass flow rates for the Bulalo field vary from 130,000 lbs/hr to 833,000 lbs/hr. Commercial steam rates for individual completions range from 50,000 lbs/hr to over 275,000 lbs/hr.

Individual steam rates have been found to vary moderately within a controlled range of economic pressure conditions. The first 110 MW plant, composed of Units 1 & 2, will require 2.1 million lbs/hr of steam. Nineteen producers have been allocated to supply the required steam for Units 1 & 2 operation.

Injectivity Characteristics. The produced water from all the flow testing has been reinjected into the reservoir. No measurable injectivity loss or static reservoir pressure alteration has been detected. Although the temperature of the reinjection fluid to date has been 135°F, commercial operation will involve the disposal of produced fluid at 325°F. The reinjection of fluid at the elevated temperature will have the benefit of reducing any long-term damage phenomena; and less fluid heat-up will be required prior to any subsequent production of the reinjected fluid, if such occurs.

The steam production requirements for Units 1 & 2 will lead to a reinjected demand of 6.0 million lbs/hr of produced fluid. Five injection wells are currently planned to dispose of the 3.0 million lbs/hr of produced fluids associated with Unit 1. Additional injection capacity will be required for commercial operation of subsequent units.

Long-Term Production Test. A long-term production test involving the production of four wells and reinjection into one well has just been completed. The production for over six months demonstrated the very stable flowing conditions of the Bulalo completions. Sensitive reservoir pressure recording instruments were located in three idle wells surrounding the producers. Pressure data monitored in each observation well indicated a pressure response resulting from the production test. Analyses of this pressure interference test are ongoing.

Reservoir Definition. Along with the extensive production testing, a comprehensive reservoir engineering program has been developed to define the productive formation characteristics. Pressure response data following the majority flow tests have been monitored and the analyses of the results have indicated a definite trend. The central completions, which are generally the shallower wells, behave as a radial flow system with high flow capacity.

The deeper flank completions are generally dominated by vertical fracture behavior with less flow capacity. These results have led to the current feeling that the central reservoir portion is composed of a fractured matrix with well-defined horizontal and vertical fracture exposure. The deeper flank completions are believed to expose primarily a vertically fracture-dominated system. Pressure buildup analysis has indicated that these flank completions expose vertical fractures ranging from 25 to 175 feet in fracture half-length.

Chemical analyses of the produced fluids have defined a reservoir brine characterized by 2330 ppm chlorides, 16 ppm calcium, 385 ppm potassium, and 615 ppm silica with pH of 6.6.

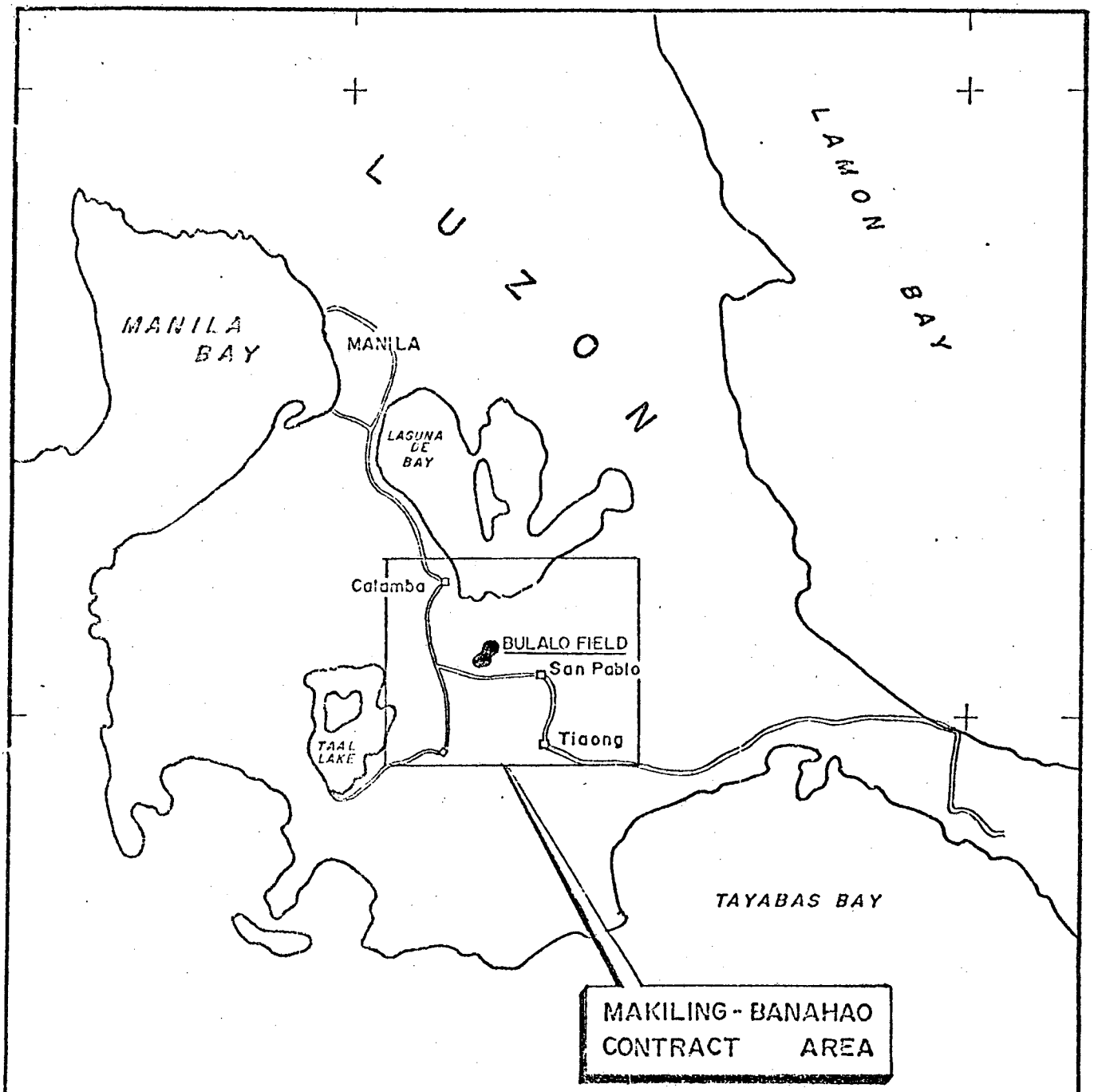

FIGURE 1

PHILIPPINE GEOTHERMAL, INC.

INDEX MAP

MAKILING - BANAHAO

CONTRACT AREA

0 10 20 30 40 50 KMS.

SCALE 1:1,000,000

SYSTEM APPROACH TO GEOTHERMAL FIELD DEVELOPMENT

Seiichi Hirakawa
The University of Tokyo
Department of Mineral Development Engineering
Faculty of Engineering
7-3-1 Hongo, Bunkyo-ku, Tokyo 113, Japan

INTRODUCTION

Geothermal energy will play an important role. Thanks to the great endeavors of those engaged in the geothermal field development in Japan, it has become possible to generate 50MW/hr of electricity per unit field. Up to this day, as is often the case with its stage in the cradle, the main purpose has been to produce electricity from geothermal steam. The target of exploitation has mainly been the area by surface geological survey and the reservoirs are located not deeper than 1500 meters.

The technology for geothermal resource development necessitate full application of every essential technique in order to cope with the various types of objective geothermal resources, and, since it has direct influence on the profitability of investment, it needs to be evaluated from an overall viewpoint. The evaluation, at the same time, must be carried out efficiently, invoking various effective methods.

Therefore, it is expected to develop a simulation model which gives rational data for a judgement in working out strategies, such as the scale of the exploration, installation of utilities and schedules of investment and development. With a view to it, the model should be able to simulate both physical and economical phenomina through the life of the geothermal field, that is, from the beginning of exploration to development and utilization. It also should at once determine the optimum conditions the static and dynamic characteristics of the reservoir, the depth and the number of production and injection wells, the fittest layout and specifications of the site including surface facilities, the behavior of pressure, enthalpy and other behaviors of the geothermal fluids flowing from the bottom to the head of the well and the costs associated with exploration, production and operation.

The purpose of this study is to develop simulation models for optimizing the scheme from exploration to utilization and to compose simulation programs for a digital computer.

CONCEPTS

Generally system approach seems to be advantageous when applied to a large scale project such as the geothermal field development. The process of the study on geothermal resource development system starts with planning, selection, analysis and composition of the system. Design of a system, reliability analysis and evolvement of the composition accompany the process, employing various techniques of simulation, optimization and computation. Thus the development pattern for economical operation is drawn - how should geothermal energy be extracted from a specific reservoir and utilized at the lowest cost or with the best recovery rate with economy assumed to be of second importance?

Hitherto the main concern of geothermal resource development in Japan has been geothermal steam production for generation of electricity. Each essential technology for exploration, drilling, development, production, transportation and generation of electricity is open to the charges of being rather separate and desultory. Utilization of geothermal energy other than for electricity generation has been mostly for recreation and therapy in baths and spas at low temperature levels, but recently there has been a trend toward multipurpose usage of hot water. And the target of exploitation is not necessarily the area of shallow zones; every type of geothermal reservoir is now explored.

It is important to categorize the results of research work on each elemental technique, to make up a formula for geothermal exploitation and development and for effective utilization of various types of promising resources macroscopically, to develop the knowhow for establishing the most appropriate conditions for exploitation and development, to rearrange different priorities for future development, and to point out hardware items which should be investigated and tried out.

A model for exploration of large scale deep geothermal resources should be able to simulate the layout, depth, number of production and injection wells, well head pressure, and steam composition and enthalpy of hot fluids, to estimate drilling and operating costs, discharge of hot fluid and the option and layout of surface facilities and to print out the optimum condition of the system. This is of great significance in determining the most efficient system for geothermal resource development.

OUTLINES OF SUBSYSTEMS

The outlines of each subsystem which is the component of the total system for geothermal field development are explained below.

(1) Subsystem for exploration investigation

Preliminary surface and subsurface surveys are the first step taken. Surface survey is classified roughly into two categories, one of geological structure and the other of anomalies caused by the existance of geothermal fluid. The former consists of geologic surveys and gravity, magnetic and seismic prospecting. The latter includes

surveys of hydrothermally altered rock, electrical conductivity surveys, geochemical surveys, geothermal gradient surveys, heat-flow determinations and microearthquake measurements. Meanwhile subsurface survey comprizes structural boring, drilling of exploratory and reinjection testing wells, geological and geochemical logging, core analysis and other types of logging. The objective of these exploration surveys is to locate geothermal reservoirs.

As there are many types of geothermal resources, it is necessary to establish the exploration system which suits one of each type. In a broad way, geothermal heat itself and/or geologic structure are the keys to the exploration. A structural boring is done into the geothermal reservoir recognized by compiling every result of the surveys and all the cores are preserved for the analysis of reservoir characteristics. After the rough surveys, detailed surveys follow drilling at least three exploratory wells (six wells in a practical manner in Japan.) The reservoir size, reserves, fracture distributions and production ability are evaluated to provide data for the next development subsystem.

(2) Development and production subsystem

A reservoir model is composed as a function of outer valuables such as the reservoir delimitations assumed by the above submodel, the location, number and depth of exploratory wells, information obtained from them, and geological, topographical and environmental factors. Then the optimum project scheme is set up and carried out. In the development stage, the data from drilling of the production wells and various well tests performed at the same time are put together for the necessary calibration of the model.

It proceeds to the production stage and providing data for the next production and transportation subsystem. In the production stage in accordance with the various accumulated data, the optimum condition of the project is obtained by defining the uncertain factors involved with the heat source and the discharge mechanics. Therefore the production system from the reservoir to the well head is independently designed to be made optimum at each time step. The principles of the model of the development and production system are as follows.

1) Objective process

When the project is concluded to be feasible and the development starts, the subsystem deals with software which covers to the start of operation, field works such as drilling of wells and the progress to the well head of a production well in the operation stage. The system is devided into following steps.

1 decision whether the site be developed or not
2 reservoir investigation
3 development scheme
4 from the reservoir to the bottom hole of development and production wells
5 from the bottom hole to the well head
6 from the well head to the bottom of an injection well
7 from the bottom hole of injection well to the reinjected reservoir

2) The function of the system

1 As a part of the total system, it can simulate various characteristics of above process (costs, efficiency etc.)

2 It can simulate the process independently when provided with data from other subsystems. Bases for the evaluation of the optimization are;

A) Before and during the stage of development

i) minimization of drilling, operation and construction costs

ii) maximization of efficiency (recoverability, lifespan) from a macroscopic view point (volmetric method, material balance method)

iii) fracturing according to circumstances

iv) steam quality etc.

B) In the stage of production

i) minimization of production or discharge decline (operation cost)

ii) maximization of efficiency from a microscopic view point (simulation of the reservoir) for example; minimization of pressure loss at given production rate and enthalpy

iii) others

(3) Transportation and multipurpose utilization subsystem

The produced geothermal fluid from the production well is sent to a separator where it is separated into vapor, liquid and solid. The vapor is transported to a power plant, while the portion of the hot water is delivered through pipes to be utilized multipurposely, the rest being reinjected through injection wells. The subsystem involves the fluid transportation from the site to the power plant and to other utilizing facilities, various problems of fluid treatment and the systematization of the large scale, multipurpose utilization of the hot water at discrete temperature.

(4) Power plant subsystem

Though there are different kinds and types of geothermal reservoirs which may well vary widely, the minimization of unit cost of electricity or sometimes even the maximization of output assuming economy of second importance, is required without exception. The power plant subsystem is needed to draw the optimum project of power generation which satisfies the given conditions. There are broadly two types of power generating method, one uses natural geothermal steam, the other runs the steam separated from hot water.

i) produced steam is sent directly to a turbine.

ii) the steam separated from hot water through a separator is sent to a turbine.

iii) flashed steam under the reduced pressure is used to run a turbine.

Binary cycle plant and total flow plant are now under development in Japan.

(5) Environmental preservation subsystem

The subsystem provides various countermeasures against the environmental impact which has been predicted in advance and which occurs during the period of development of the geothermal field. It should be used in accordance with every other subsystem. Climate, atmosphere, waters, noises, vibrations, ground animals and plants

and landscape scenery are to be carefully monitored.

ACKNOWLEDGMENT

This paper is much indebted to the achievements of the committee (chairman Prof. Seiichi Hirakawa) of "Research for the effective development of geothermal energy", which is a link in the chain of the 1977 Sunshine Project. So, acknowledgment is due to the "Sunshine Project Group" of the Industrial Technology Agency, The Geological Survey of Japan, Nippon Steel Corporation, Geothermal Energy Research and Development Co., Japan Metals and Chemicals Co., Japan Oil Engineering Co., LTD. and Toshiba Electric Co.

THE USE OF FLUID GEOCHEMISTRY TO INDICATE RESERVOIR PROCESSES AT CERRO PRIETO, MEXICO

Alfred H. Truesdell,
U.S. Geological Survey, Menlo Park, Calif.

Regular chemical sampling and analysis of fluids produced from the hot-water geothermal system of Cerro Prieto, Mexico has provided early warning of reservoir processes (Manon et al., 1977). The changes in chloride concentration, sodium to potassium ratio and measured fluid enthalpy are shown in the figures for wells M-5, M-26, M-21A, and M-11 of the Cerro Prieto field. The concentration of chloride, a "conservative" constituent, is characteristic of different water masses and is affected by a change of water source, by mixing of waters and by boiling and steam loss but not by reaction with rock minerals. The ratio of sodium to potassium is a temperature-sensitive geothermal index resulting from rock-water reaction and is not affected by boiling and steam loss or by mixing of water masses provided these processes occur at constant temperature. The enthalpy is related to the fluid temperature and to boiling in the aquifer with "excess" steam entering the well. These indices provide a reasonably complete picture of major reservoir processes occurring in hot water systems. Silica analyses have not been reliable from Cerro Prieto but should be used in addition to Na/K as a temperature indicator. Analysis of fluids from a producing geothermal field must of course include other constituents for study of environmental effects, scaling, corrosion, etc.

Well M-5 at Cerro Prieto shows uncomplicated behavior in which a single liquid phase with little "excess" aquifer steam was tapped and production has shown little change over the life of the well (fig. 1). Before April 1973, initial production was through a small diameter pipe and was cooled conductively so little evaporative concentration of chloride from steam loss occurred and the chloride concentrations of produced fluids approximated that in the aquifer. After April 1973, water was collected from the production separator and flashed to atmospheric pressure during sampling. Steam separation in the separator and during sampling resulted in a 35% loss of water as steam and a 1.6x concentration of chloride in the remaining liquid. From 1973 to the present the chloride concentrations after flashing have decreased slightly as the fluid temperature and the amount of steam separated have decreased. The decrease in temperature is indicated by the increase in the Na/K ratios and the decrease in enthalpy. The temperature drop indicated by Na/K was from about 313 $\pm 3^{\circ}C$ to 302 $\pm 2^{\circ}C$ (the variation depending on the geothermometer scale used) and that indicated by enthalpy was from 312 to $281^{\circ}C$. The larger drop and lower absolute temperature indicated by enthalpy may result from initial excess aquifer steam or from inaccuracies in this rather difficult measurement. The downhole

temperature of 299°C measured in 1977 (F. J. Bermejo, unpublished data, 1977) agrees more nearly with the Na/K temperatures and aquifer chloride concentrations based on Na/K temperatures are more constant (at 8,960 ±20 mg/kg by one scale) than are those based on enthalpy which show an apparent increase from 8,700 to 9,700 mg/kg.

The other wells show less regular behavior. The chloride concentration after flashing of water from M-26 declined suddenly in mid-1975 indicating drawdown of lower chloride fluids into this part of the production aquifer. Temperatures calculated from Na/K ratios and enthalpies also declined but showed no discontinuity in 1975. This suggests that the fluid temperature was maintained by heat transfer from rock minerals.

Fluids from well-21A had initial enthalpies of 420 to 480 cal/gm equivalent to a temperature of 360 to 370°C if the aquifer fluid were entirely liquid water. The initial chloride concentrations were also unusually high. By 1977 both the enthalpy and the chloride had declined rapidly to values similar to those of M-5 fluids. The Na/K ratio was initially only slightly lower than that of most well fluids but showed a normal increase with time and the Na/K indicated temperature was 315 ±5°C throughout the period shown. The probable explanation for the unusual behavior of M-21A is that initial fluids contained large amounts of excess steam from boiling in the aquifer and these were replaced with more normal fluids as production continued. The high chloride concentrations resulted from boiling in the aquifer with heat re-supplied to the fluids from rock minerals.

Well M-11 suffered a casing break in 1975 and higher level fluids with lower enthalpy and chloride and much higher Na/K ratio entered the well. When the break was repaired and an upper production interval near 900 m cased off, the well performance was greatly improved, with production of high Cl, high enthalpy, low Na/K fluids similar to early production fluids.

Regular collection and analysis of water (and gas) samples from a hot-water geothermal well is an essential part of a well-testing or monitoring program. The chemical data obtained complements physical measurements and may give the earliest warning of breakthrough of natural or reinjected cold waters. Analyses should be as complete as possible but constituents indicating reservoir processes (Cl, Na, K, Ca, SiO_2) and mineral deposition (pH, HCO_3, CO_2) should be analyzed with special care.

References

Manon, A., Mazor, E., Jimenez, M., Sanchez, A., Fausto, J., and Zenzio, C., 1977, Extensive geochemical studies in the geothermal field of Cerro Prieto: Lawrence Berkeley Lab. Report LBL 7019, 113 p.

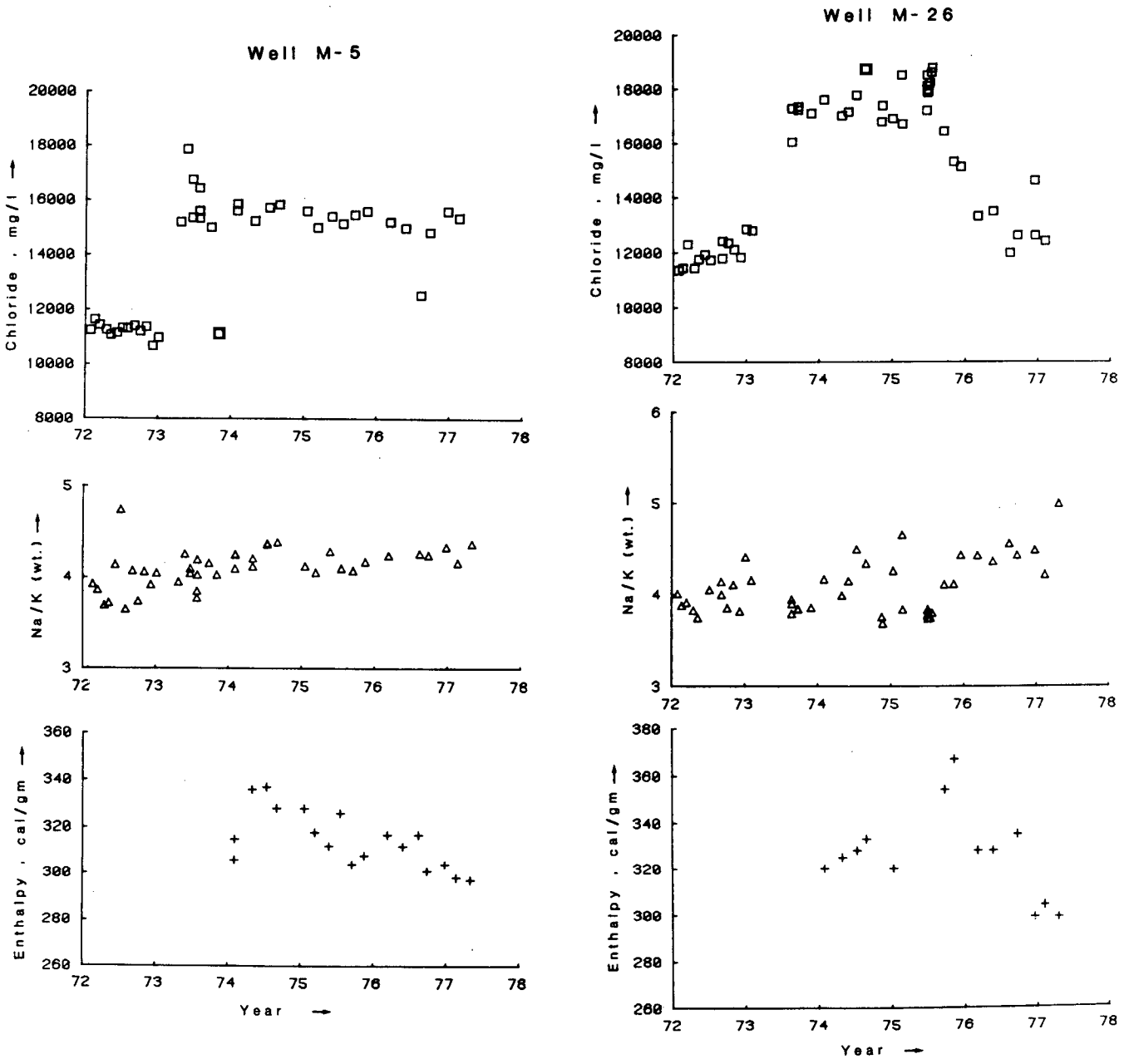

Figure 1. Chloride concentrations after flashing, Na/K ratios of brine and enthalpies of the total discharge of wells M-5 and M-26 from 1972 to mid 1977. Data from Manon et al. (1977). Units are mg/kg, weight ratio and Kcal/kg.

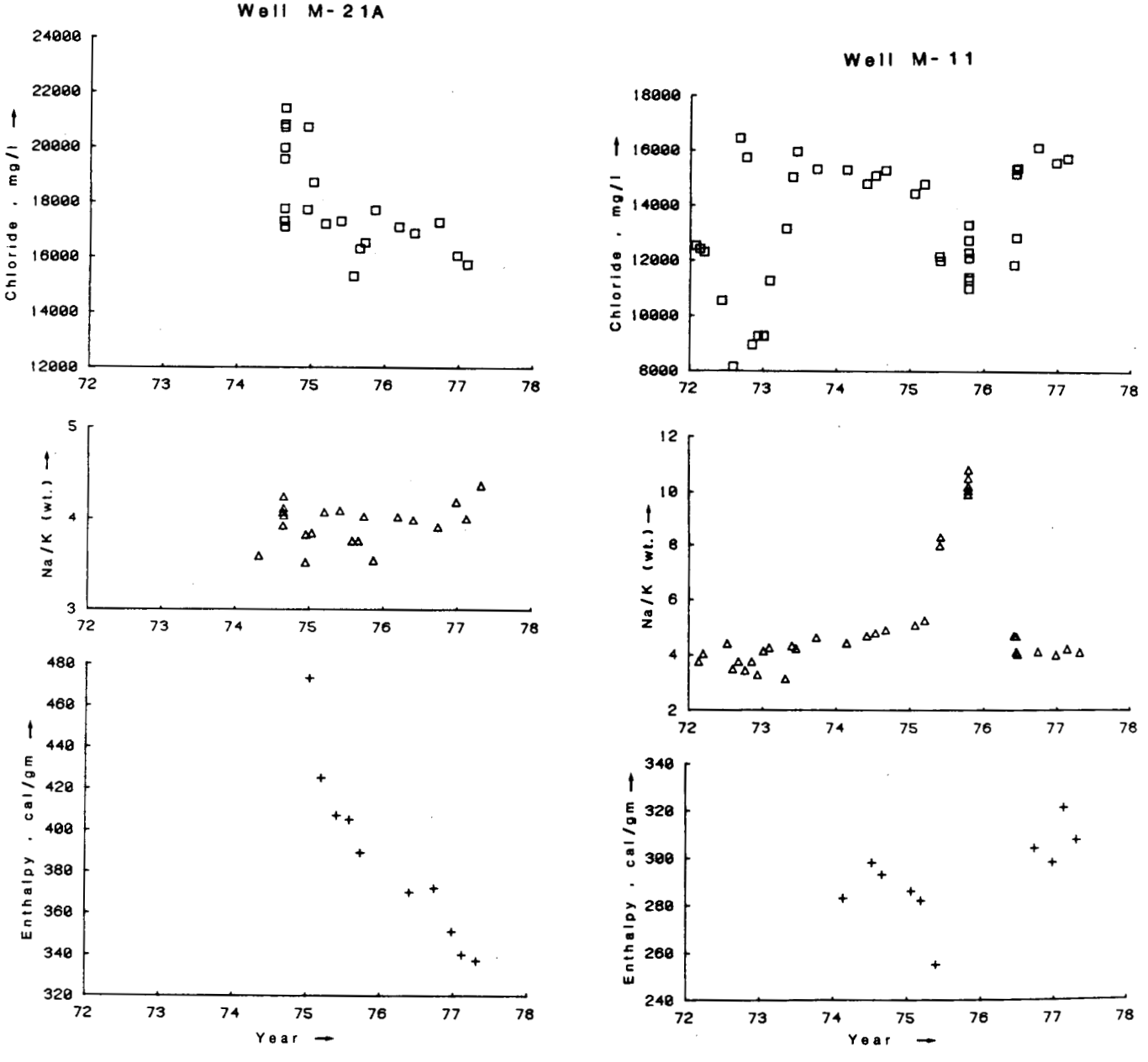

Figure 2. Chloride contents after flashing and the sodium to potassium ratio of brine and enthalpy of the total discharge of well M-21A from 1975 to mid-1977 and well M-11 from 1972 to mid-1977.. Data from Manon et al. (1977). Units are mg/kg, weight ratio and Kcal/kg.

Dup

EVALUATION OF THE FENTON HILL HOT DRY ROCK GEOTHERMAL RESERVOIR

PART I - HEAT EXTRACTION PERFORMANCE AND MODELING (H. D. Murphy)

PART II - FLOW CHARACTERISTICS AND GEOCHEMISTRY (C. O. Grigsby and J. W. Tester)

PART III - RESERVOIR CHARACTERIZATION USING ACOUSTIC TECHNIQUES (J. N. Albright)

Geothermal Technology Group
Los Alamos Scientific Laboratory
Los Alamos, New Mexico 87545

ABSTRACT

On May 28, 1977, as the production well GT-2 at Fenton Hill was being redrilled along a planned trajectory, it intersected a low-impedance hydraulic fracture in direct communication with the injection well, EE-1. Thus, a necessary prerequisite for a full-scale test of the LASL Hot Dry Rock Concept, that of establishing a high flow rate between wells at low wellhead differential pressures, was satisfied. Previously, communication with EE-1 had been through and between high-impedance fractures, and flow was insufficient to evaluate the heat-extraction concept.

In September a preliminary test of the entire system-surface plant and downhole flow paths was conducted. During 96 h of closed-loop circulation, fluid total dissolved solids remained low (<400 ppm), water losses continually decreased, and no induced seismic activity occurred. The operating power level was 3.2 MW (thermal) and fluid temperature reached 130°C at the surface. This test demonstrated for the first time that heat could be extracted at a usefully high rate from hot dry rock at depth and transported to the surface by a man-made system.

Full-scale operation of the loop occurred for 75 days from January 27 to April 12, 1978. This test is referred to as Phase 1, Segment 2 and was designed to examine the thermal drawdown, flow characteristics, water losses, and fluid geochemistry of the system in detail. Results of these studies are the major topic of this paper which is divided into three separate parts covering first the heat extraction performance, second the flow characteristics and geochemistry and third the use of acoustic techniques to describe the geometry of the fracture system. In the third section, dual-well acoustic measurements used to detect fractures are described. These measurements were made using modified Dresser Atlas logging tools. Signals intersecting hydraulic fractures in the reservoir under both hydrostatic and pressurized conditions were simultaneously detected in both wells. Signal attenuation and characteristic waveforms can be used to describe the extent of fractured rock in the reservoir. A detailed account of the field test can be found in ref. [1].

EVALUATION OF THE FENTON HILL HOT DRY ROCK GEOTHERMAL RESERVOIR

PART I. HEAT EXTRACTION PERFORMANCE AND MODELING

H. D. Murphy

During the 75-day long heat extraction test, a LASL-developed temperature surveying tool with 0.05°C resolution employing a thermistor was positioned downhole in the GT-2B production well. A total of 58 logs or surveys were taken during the 75-day run. Between surveys the tool was stationed at 2.6 km (8500 ft), just above all the known producing zones in GT-2B. In this fashion the mean temperature due to the mixed fluid flows converging upon GT-2B was continuously monitored. A typical set of temperature surveys is presented in Fig. I-1. Only the downhole region where the produced fluid enters the well is shown. The uppermost survey was obtained on Feb. 4, 1978, seven days after the start of power production, while the middle and lower surveys were obtained after 12 and 16 days, respectively. Even a cursory look at these surveys indicates a complex reservoir-to-producing well connectivity. The major temperature changes at the depths indicated with arrows are associated with flow connections identified in earlier testing.[1] The middle survey, and even more pronouncedly the lower survey, show the development of new flow connections between the previously established major connections 1 and 2, and in fact, the magnitude of the temperature change at 2.68 km (8790 ft) suggest that a major connection has developed there. This information was later corroborated with flowing spinner surveys and radioactive tracer logs to characterize the production and injection zones.

Figure I-2 presents the variation of temperature at 2.6 km (8500 ft) with time. As stated earlier the measurement is made downstream of all the flow connections so that the temperature represents the mean temperature of the mixed fluid in the production wellbore, and thus provides an indication of the overall thermal drawdown of the reservoir. The "scallop" in the data and the theoretical curve that appears at day 24 is the result of a doubling of the injection rate, from 8×10^{-3} to 1.6×10^{-2} m^3/sec (125 to 240 gpm). This flow increase became possible because of the large flow

impedance reductions that occurred during heat extraction. (These are discussed in Part II). Figure I-3 presents the net thermal power produced using a constant 25°C reinjection temperature in the calculation. Despite the declining production temperatures, the increasing flow rate allowed the power to be kept roughly constant for the last 40 days. Peak power was 5 MW(t).

Thermal Drawdown Analysis. To interpret the drawdown results of Fig. I-2 in terms of effective heat transfer area it was assumed that the fracture system could be described as a single circular fracture. This is indeed an approximation -- the actual fracture need not be circular, and furthermore the temperature surveys and other evidence accumulated to date suggests that instead of a single fracture, heat was extracted from one main hydraulic fracture which was connected to the producing well by a multitude of natural joints of limited heat transfer area. Rather than modeling this more complicated geometry however, initial attention was restricted to a model of a single circular fracture in order to provide an approximate estimate of the effective heat transfer area. This model has been described in reference 1 and employs numerical techniques to solve the two-dimensional fluid motion and energy equations as well as the one-dimensional, but transient, rock energy equation. Property variations with temperature, fracture aperture changes due to thermal contraction, and natural convection effects are included. Because the hydraulic fracture itself is much more permeable than the surrounding rock, it was assumed that fluid was confined to the fracture and that heat was transported from the rock to the fluid in the fracture solely by means of thermal conduction in the rock. The possible enhancement of heat transfer area because of thermal stress cracking was not considered in the model. In actuality, a small amount of fluid did penetrate the surrounding rock, particularly at very early times as indicated by the formation water losses shown in Fig. I-4. To correct for this effect the fluid loss was assumed to occur uniformly over the fracture area so that on the average, heat was removed from the reservoir by all of the produced water flow and half the difference between the injected and produced water flows.

In the calculations, the observed time variations of production and injection flow rates as well as the reservoir injection temperature were

used. Initial equilibrium rock temperatures and their variation with depth was determined from previous borehole equilibrium temperature surveys. The downhole temperature variation due to heating of the injected fluid within the well was calculated with a one-dimensional convection and radial conduction code. To start with, a constant value of 0.1 mm was taken for the fracture aperture. This value resulted in an initial overall flow impedance of 15 bars per liter per second, in accordance with the early observations.

The radius of the modeled fracture was then varied until the predicted thermal drawdown matched the measurements. The results for a 60-meter (200 ft) radius fracture agreed quite well with the measurements, as previously shown in Fig. I-2. Because of hydrodynamic flow inefficiencies only about 75% of the circular area actively transferred heat, so the effective heat transfer area was only 8000 m^2 (one side of the fracture).

We emphasize that this is not a measure of the total fracture area accessible to water. The effective heat transfer area is strongly influenced by the vertical separation of the fracture water inlet and outlet locations. Unless buoyant forces significantly affect flow (corresponding to fracture impedances lower than those measured) the water only partially fans out from the inlet and then flows fairly directly to the outlet, and thus the effective heat transfer area swept by this flow is a direct function of the inlet and outlet spacing. In the present case the spacing between the inlet, located at 2.76 km (9050 ft) in the injection well, and the production well connection with the highest flow capacity is approximately 100 meters. Roughly speaking, then, the effective area would be that of a circle 50 m in radius, namely 7900 m^2, very close to that derived with the simulation model.

The possibilities of reducing flow impedances and enhancing heat transfer area by means of thermal cracking as the reservoir cools and contracts have been discussed by Murphy.[4] Subject to the large uncertainties in our knowledge of the maximum horizontal earth stress, it was estimated that the effects of thermal cooling might be apparent after a cooling of about 75°C or more. A close scrutiny of the temperatures of Fig. I-2 shows that starting at 48 days there is a period of eight days in which the temperature was constant. Additional constant temperature intervals are noted starting at day 58, and then again on day 68. Each of these plateaus were terminated

by stepwise decreases in temperature. While this behavior may have resulted from thermal stress cracking, the evidence is far from conclusive; we hope to resolve the issue in future experiments with higher capacity pumps which will permit faster and larger thermal drawdowns.

Formation Water Loss Rates. Figure I-4 presents the accumulated water volume lost by means of permeation to the formation. The rate of loss, i.e. the slope of Fig. I-4, declined from an initial value of 3×10^{-3} m^3/sec (50 gpm) to only 1×10^{-4} m^3/sec (2 gpm). The theoretical fit represents the solution to the nonlinear, pore-pressure-diffusion equation for a diffusion parameter (consisting of the product of the fracture area and the square root of the rock permeability and compressibility) of $2.3 \times 10^{-7} m^3 bar^{-1/2}$. In this model the rock permeability and compressibility are very pressure dependent and this dependency has been derived from previous flow and pressurization experiments. More details can be found in references 1 and 4.

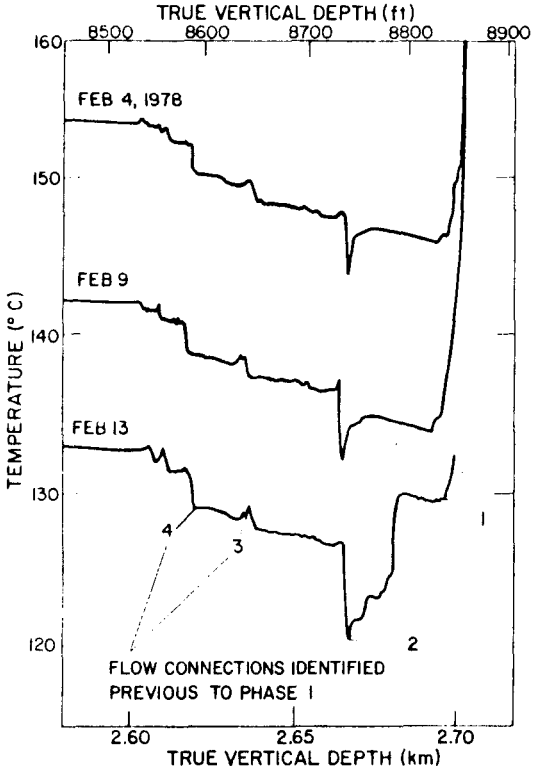

Figure I-1. Three temperature surveys taken in the bottom section of GT-2B during Phase 1.

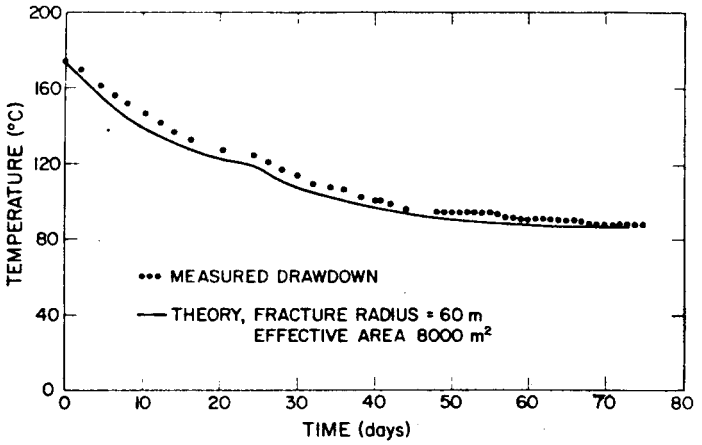

Figure I-2. Thermal drawdown of produced fluid measured at a 2.6 km (8500 ft) depth in GT-2B.

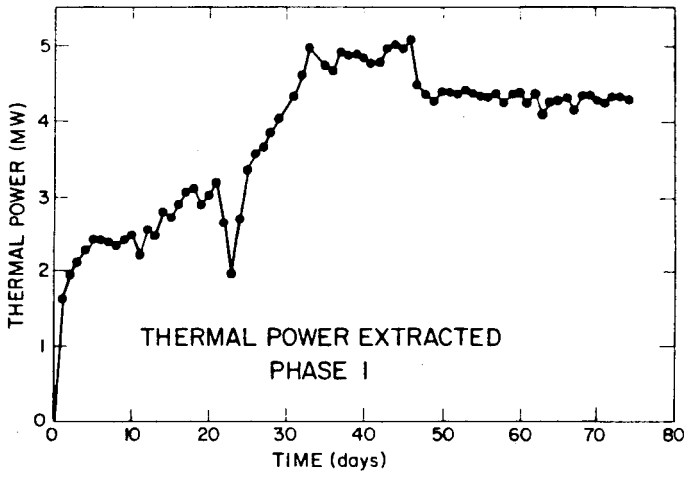

Figure I-3. Net thermal power extracted.

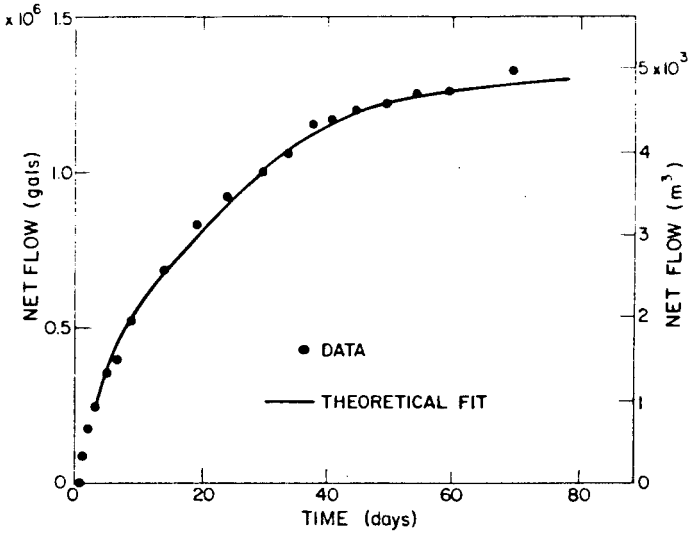

Figure I-4. Total accumulated water loss or storage by permeation into the formation.

EVALUATION OF THE FENTON HILL HOT DRY ROCK GEOTHERMAL RESERVOIR

PART II. FLOW CHARACTERISTICS AND GEOCHEMISTRY

Charles O. Grigsby
Jefferson W. Tester

Flow Impedance

For the circulation system, the flow impedance is defined as the pressure drop through the fracture system connecting the production and injection wellbores divided by the production flow rate. Figure II-1 shows the measured impedance corrected for buoyancy effects between the cold and hot wellbores. The large decrease in impedance is attributed to changes in the fracture system and its connections to the wellbores caused by localized cooling (thermal stress) and/or pore pressure induced "stress relief" effects. Changes in impedance have been attributed to shear-like, discrete events occurring within the reservoir. These changes are apparently irreversible and indicate that the rock may have undergone considerable dislocation during the flow test.

Fracture Volume and Degree of Mixing

Dye tracer techniques developed previously were used to characterize the fracture system volume under flow conditions and the fluid residence-time distribution (RTD) within the reservoir.[1] In the four experiments run during the 75-day test, a 200 ppm, 100 gal (400 liter) pulse of sodium-fluorescein dye was injected into the EE-1 wellhead, pumped down EE-1 and through the fractured region, and up the GT-2B wellbore. Dye concentration in the produced fluid was monitored spectrophotometrically at the surface as a function of time and volume throughput. The results of the four experiments are described by plotting normalized tracer concentration as a function of effective fracture system or throughput volume as shown in Fig. II-2.

Flow in the fracture system can be described as well-mixed with no major short circuits. The degree of mixing cannot be adequately accounted for by dispersion of flow in a single hydraulic fracture. Because of this fact and of the known existence of multiple flow paths between EE-1 and GT-2B, the observed shape of the RTD is caused by dispersion within individual flow paths as well as superposition from mixing of various production flows in the wellbore. Consequently, several statistical quantities are needed to

describe flow in the system. The median volume reasonably represents the flow through the major production paths in GT-2B while the increase in the spread of the distribution is indicative of longer residence time paths possibly through more circuitous routes in the rock.

Several general comments can be made: (1) the fracture flow system has grown considerably in size during the 75-day test, the integrated mean fracture system volume was 14,900 gal on 4/7/78, up from 9090 on 2/9/78 and the median volume is larger, 12,800 gal versus 6750 gal, (2) there is evidence for the development of additional secondary flow paths, that is the tendency toward earlier and later arrival of dye with smaller and larger residence times (or volumes) causing an increase in the spread of the distribution, (3) the apparent degree of mixing or dispersion is virtually unchanged between the 3/1/78 and 4/7/78 experiments as shown by the similar shapes of the phase 1-2, 1-3, and 1-4 curves when plotted on normalized volume coordinates.

Fluid Geochemistry

Samples of the circulating fluid were collected periodically at the injection wellhead, the production wellhead, and from the makeup system. A mass balance of dissolved material in the fluid circulating through the surface system indicates that no deposition or scaling occurred in the surface equipment. The change in concentration with time of various dissolved species in the recirculating fluid should be consistent with the models which have been derived from geophysical mapping techniques, flow and temperature surveys and radioactive tracer experiments.

The graphs of SiO_2, Cl^- and HCO_3^- concentrations and solution conductivity vs time shown in Fig. II-3 illustrate the general behavior of the reservoir during the 75-day test. Samples taken early in the test have high concentrations of dissolved species (TDS$\sim$3300 ppm) and represent undiluted fluid contained in the reservoir several months prior to this experiment. Relatively fresh makeup water ($\sim$400 ppm TDS) is injected into the reservoir where it mixes with and dilutes the fluid contained in the fracture system. Initially, when the makeup water rate is high, the dilution effect dominates and concentrations are low. As recirculation continues and the water loss rate to permeation decreases, the concentration of dissolved material rises and eventually approaches an asymptote. The sharp peak on day 23 corresponds

to a sudden change in flow impedance, a short shutdown and a resulting partial flow back of fluid (see Fig. II-1). Water which had been forced into the rock pores returned to the circulating system because of a transitory pressure decline, providing a source of high concentration fluid. As the system returned to its initial injection pressure, the fluid which returned from the pores was replaced and high makeup flows were required. The dilution effect of this high makeup rate is seen for 10 to 15 days in the SiO_2 concentration vs time graph (Fig. II-3).

Assuming quartz-controlled saturation of SiO_2 in solution, the asymptotic value of SiO_2 concentration shown in Fig. II-3 suggests a reservoir temperature of 188°C.[2] The temperature of the water leaving the fracture system and entering the wellbore was measured downhole. Within three days of circulation this downhole temperature was below 160°C corresponding to a quartz-controlled saturation concentration of less than 147 ppm. Clearly the declining mean reservoir temperature could not account for the increasing SiO_2 content in the fluid. A secondary flow path at the initial reservoir temperature is required. According to a simple kinetic model, the change in silica concentration with time for that fraction of the flow corresponds to a first order rate depending on the difference between the silica saturation value of the highest reservoir temperature in contact with flowing fluid and the average silica concentration at any particular time:

$$\frac{d(\overline{SiO_2})}{dt} = ka^* \left({SiO_2}^{sat}_{T=T_{max}} - \overline{SiO_2} \right) \qquad \text{(II-1)}$$

where ka^* is a constant which includes relevant mass transfer rates, dissolution kinetics rates, and a rock surface area to fluid volume parameter. Assuming no dissolution or reprecipitation occurs in the cooler main flow path, a differential material balance shows that the rate of accumulation of SiO_2 is due to three principle effects: the relative volumes of each flow path, the fluid loss rate due to permeation, and the production of SiO_2 due to active dissolution and/or displacement in the hot region. If the circulation time is large compared to the overall mean residence time τ, the material balance is written as:

$$V \frac{d\bar{C}}{dt} = \dot{q}_T (C_{in} - \bar{C}) + \dot{q}_2 (1-e^{-ka^*\tau_2 f}) (C^\infty - C_{in}) \qquad \text{(II-2)}$$

where

$$C_{in} = \frac{\dot{q}_T - \dot{q}_{loss}}{\dot{q}_T} \bar{C} + \frac{\dot{q}_{loss}}{\dot{q}_T} C^M$$

V = total volume of primary and secondary flow paths = V_1+V_2

C^M = (SiO_2) makeup = concentration of SiO_2 in the makeup water

C^∞ = $(SiO_2^{sat})_{T=T_{max}}$ = quartz controlled saturation concentration of SiO_2 at T_{max}

$\bar{C}$ = $(\overline{SiO_2})$ = average concentration of SiO_2 at time t

k = dissolution mass transfer coefficient, cm/sec

a^* = rock surface area to fluid volume ratio, cm^{-1}

$\dot{q}_2$ = fluid circulation rate through hot region at time t

$\dot{q}_T$ = total fluid circulation rate at time t

$\dot{q}_{loss}$ = $\dot{q}_{makeup}$ = fluid loss rate to permeation at time t

τ_2 = mean residence time in hot region (secondary flow path)

f = fraction of plug flow conversion = function of dispersion in hot region ($f < 1$)

In the case of low water loss and rapid reaction in the hot region ($ka^*\tau_2 f \gg 1$), eq (II-2) reduces to

$$\bar{C} = C^\infty - (C^\infty - C_o)e^{-\dot{q}_2 t/V} = C^\infty - (C^\infty - C_o)e^{-\zeta t} \qquad \text{(II-3)}$$

The solution to this equation with $\zeta = .04\ sec^{-1}$, $C^\infty = SiO_{2_{T=180°C}}^{sat}$ = 220 ppm SiO_2 and $C_o = SiO_{2_{initial}}$ (t=0) = 80 ppm (the SiO_2 concentration of the initial EE-1 injected water, is shown as the dotted line on the SiO_2 plot of Fig. II-3. Rate equations of the same form were applied to the fluoride, sulfate and the $^{87/86}Sr$ data with the same success. Remarkably, the value of ζ is in each case 0.04. Since in all probability more than one mineral is dissolving to contribute SiO_2, $SO_4^=$, F^- and Sr to the solution, it would

be quite fortutious that all dissolution rates were equal. Thus it appears that mass transfer rates, specifically mixing rates between various flow fractions, control the concentration history of these particular species in solution.

The possibility remains that saturated pore fluid is merely being displaced from the hot region at a rate $\dot{q}_2$. Further investigation is underway to consider the difference between active dissolution and pore fluid displacement by examining the time dependence of ratios of various ions including Na^+/K^+ /Li^+/Cs^+ and $Cl^-/Br^-/I^-$.

As seen in Fig. II-3 chloride concentrations also show a marked increase in time possibly indicating displacement and/or mixing with saturated pore fluid because no solid mineral source of chloride should exist at the reservoir conditions. In addition, the rate of increase of Cl^- agrees with the empirical model proposed to explain SiO_2 buildup if a constant concentration source of Cl^- is being supplied to the flow path through the hot region.

In the case of the calcium and bicarbonate concentrations vs time, different conditions prevail (see Fig. II-3). Calcite ($CaCO_3$) -- the principal contributor of $CO_3^=$ in solution -- has a retrograde solubility with temperature at a constant CO_2 partial pressure. Therefore, the lowest temperature of the reservoir may control the bicarbonate dissolution, and this lowest temperature is encountered in the main flow path as shown by temperatures measured at the EE-1-to-fracture system connection. In the first 35 days of the run the calcite solubility appears to be controlled by the temperature of the mixed production flow in GT-2B. During the last 40 days, however, the bicarbonate concentration approaches a saturation value corresponding to the calculated EE-1 injection temperature. At least one strong possibility for the apparent shift in control of the calcite solubility to the EE-1 injection temperature is the major change in downhole impedance and a doubling of the EE-1 flow rate that was observed during this period.

Calcium concentrations in equilibrium with calcite and (HCO_3^-) were calculated from the thermodynamic data (equilibrium constants from Garrels and Christ)[3] assuming unit activity coefficients. Graphs of Ca^{++} in ppm corresponding to values of HCO_3^- at the GT-2 production temperature are also plotted in Fig. II-3. Notice that the calculated Ca^{++} based on observed

HCO_3^- approaches the Ca^{++} observed at day 45. Until that time, however, the Ca^{calc} is much higher than the Ca^{obs}. Assuming that all the HCO_3^- originally came from calcite, the observed Ca^{++} is an order of magnitude too low during the first 25 days of operation. This could be the result of precipitation of a noncarbonate Ca rich mineral such as phillipsite $(K_2Na_2Ca)(Al_2Si_4)O_{12} \cdot 4\text{-}5\ H_2O$. (See ref. 1 for details.)

The discussion above serves to illustrate the complex relationships that exist between the geometric, thermal, and chemical properties of the fracture system. We have been motivated toward selecting simple models and testing their consistency rather than adding unwarranted complexity to improve their fit to the data.

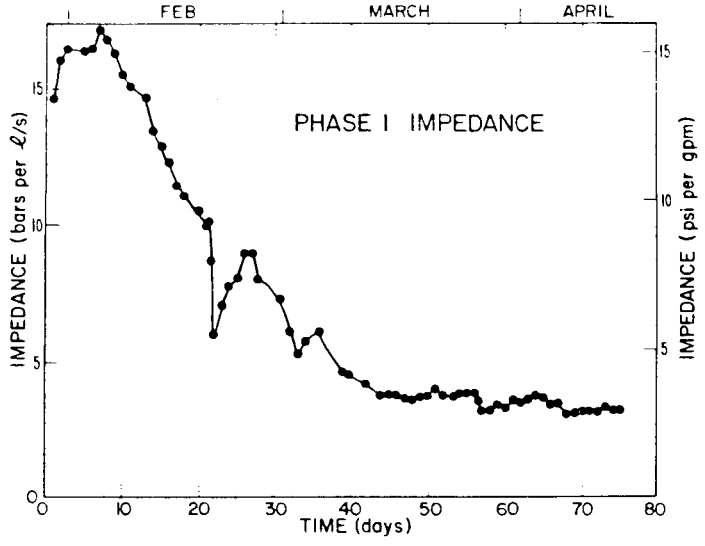

Figure II-1. Net flow impedance between the GT-2B production and EE-1 injection wellbores with buoyancy corrections included.

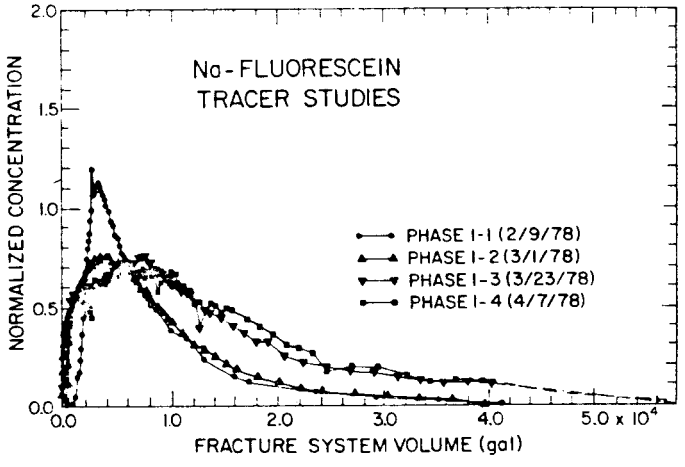

Figure II-2. Normalized tracer concentration as a function of fracture system volume.

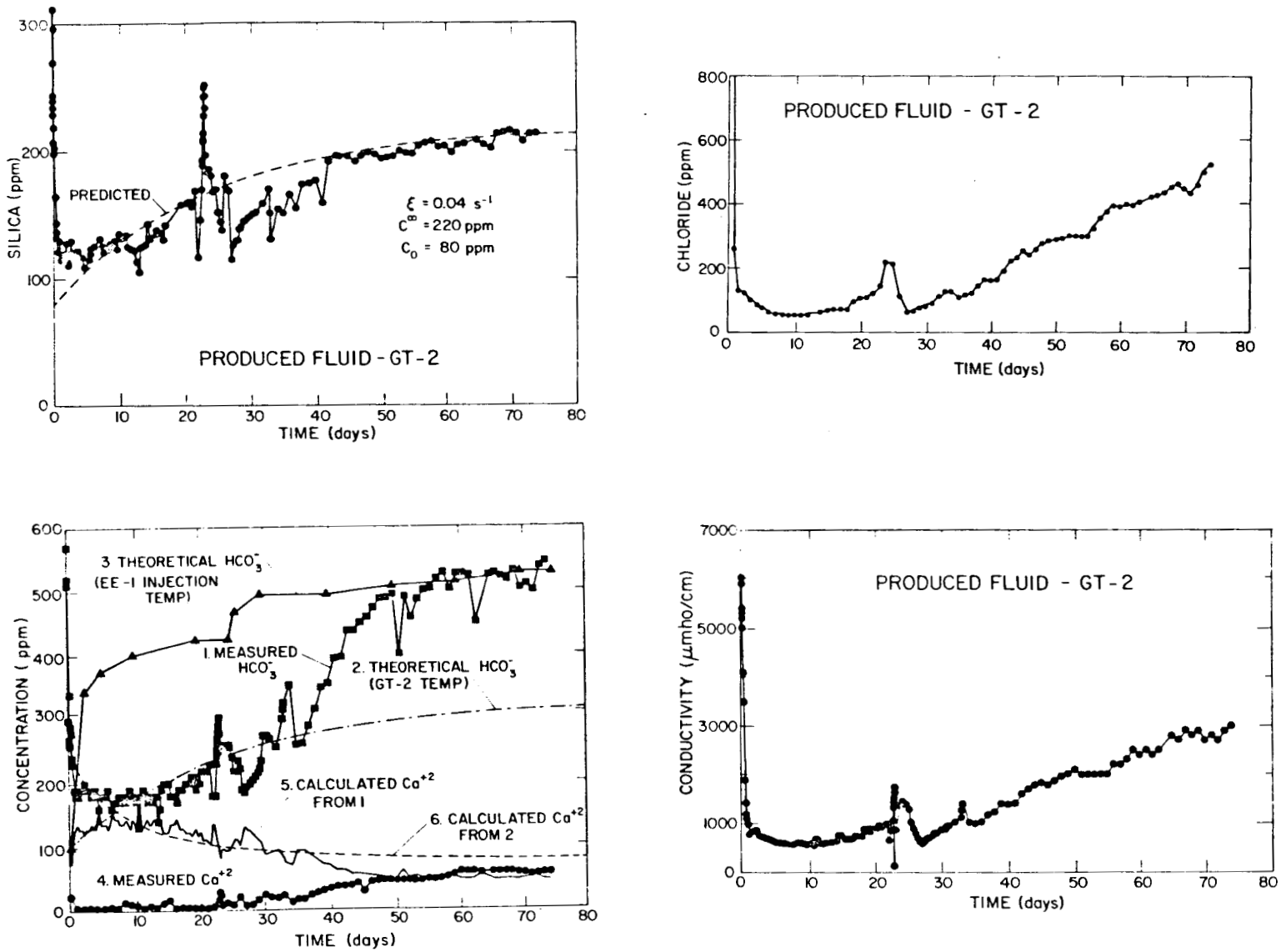

Figure II-3. Concentration histories of dissolved silica (SiO_2), chloride (Cl^-), calcium (Ca^{+2}), and bicarbonate (HCO_3^-) and electrical conductivity of the fluid produced at the GT-2B wellhead during the 75-day Phase 1 test.

EVALUATION OF THE FENTON HILL HOT DRY ROCK GEOTHERMAL RESERVOIR

PART III. RESERVOIR CHARACTERIZATION USING ACOUSTIC TECHNIQUES

J. N. Albright

Introduction

The success in establishing flow between wells at Fenton Hill is due in part to the development of crude acoustic measurement techniques which enabled targeting of a hydraulically fractured rock volume for the final directional drilling of the production well.[4,5,6] Our purpose here is to review subsequent efforts to detect pressurized hydraulic fractures in the Fenton Hill reservoir that are based on the acquisition of data using commercially available acoustic logging tools and signal processing techniques developed at LASL. Only the dual-well measurements made with these tools will be discussed. In the application of these methods at Fenton Hill, results of the earlier work have been substantiated and more detailed information regarding fractures in the reservoir has been obtained.

The Fenton Hill Reservoir

The downhole arrangement at Fenton Hill is shown in Fig. III-1. Energy Extraction Well No. 1 (EE-1) and Granite Test Well No. 2 (second redrilled section, GT-2B) are the injection and production wells respectively. GT-2B terminates at 2.7 km (8882 ft) and EE-1 at 3.0 km (10,000 ft) at a greater depth than represented in the figure. Both wells penetrate basement rocks at approximately 0.7 km (2400 ft) and terminate in granodiorite. Four fractures in GT-2B account for 90% of production. In order of decreasing flow, the fractures are located at 2.64 km (8665 ft) (35%, 2.70 km (8857 ft) (24%), 2.67 km (8750 ft) (19%) and 2.69 km (8815 ft) (12%). GT-2B is cased to 2.60 km (8541 ft). The bottom casing in EE-1 is at 2.92 km (9578 ft), but 90% of the flow moves behind casing from 2.92 km to 2.76 km (9053 ft) where it enters the reservoir through a hydraulic fracture. Water then moves vertically 64 m (210 ft) before the lowest entry point in GT-2B is reached. Several other fractures over the depth interval 2.1-2.9 km (7000 to 9600 ft) accept water on pressurization of the injection well, but these account for only a small percentage of the injection into the reservoir. Because of the depth of the reservoir, the major fractures are believed to be always vertical or nearly so.

Logging Tools and Acquisition of Data

Two acoustic logging systems, one for use in each well, were provided under subcontract for this work by Dresser Atlas, Dresser Industries, Inc. One system is that used by Dresser Atlas in providing their Acoustilog logging service. The second system is a modified version of the first with the principal difference being the use of a more powerful transmitter. The bandpass of the detected signals transmitted between wells was 12 kHz $\pm$ 2 kHz. A signal repetition rate of 5 signals/second and a logging rate of 0.1 m/s (20 ft/min) was used when either tool was in operation.

The sequence of transmitter and receiver movements for the dual-well measurements is illustrated in Fig. III-1 and is as follows. With the receiver in fixed position in GT-2, the transmitter in EE-1 was moved from an inclination of 45° above the receiver to 45° below it. Next, the receiver was moved in the same manner. This sequence was followed until the depth interval of interest was logged. A staggered sequence was followed in logging upwards. The entire sequence of operations was conducted twice: first, when the wells and reservoir fracture system were at a hydrostatic or unpressurized condition and subsequently when reservoir pressure was elevated to values approaching that believed necessary to part fracture faces.

Direct ray paths of the signals transmitted between wells traversed slant distances up to 46 m (150 ft) and horizontal distances as short as 15 m (48 ft). Volume elements as small as 16 cm^3 in the region between wells were traversed by at least two signals having direct ray paths of different incidence in both unpressurized and pressurized conditions.

Results

An interesting picture of the Fenton Hill experiment emerges when recent analyses of the waveform of signals transmitted between wells is viewed in terms of the acoustic attenuation in the reservoir. Such a study is greatly facilitated using Power logs and Equi-Power logs (NEP logs) of the kind reviewed in references 7 and 8. The recent work shows that characteristic acoustic waveforms identified using the NEP representation can be used to simply describe the extent and nature of the reservoir. Each waveform finds representation over large vertical dimensions in the reservoir under hydrostatic conditions. The significance of each of the waveforms is not understood in detail: reasonable hypotheses can be advanced which are constrained

by the changes in attenuation that were observed on pressurization of the reservoir.

The signals transmitted between wells have been found to have one of three distinctive waveforms. Figure III-2 shows the waveforms which we have designated as S, P, or D type, depending on the relationship between the peak amplitude of the compressional wave arrival and the peak amplitude of the shear wave arrival. The S-type exhibits a strong S-wave arrival whereas in the P-type for comparable P-wave amplitudes, the amplitude of the shear wave is severely attenuated or not observed within reasonable limits to its appropriate arrival time. The D-type shows an emergent P-wave onset and peak P-wave amplitudes comparable to that observed anywhere in the signal coda.

The Power logs for signals transmitted between wells is given in Fig. III-3. The logs are subdivided in segments according to receiver position. With increasing depth the horizontal distance between wells decreases. The logs are not corrected for geometric spreading. This correction however is independent of pressure conditions in the reservoir.

Shown in the Power log is a general increase in attenuation on reservoir pressurization with depth below 2.67 km (8450 ft). A marked discontinuity in attenuation is noted in the center of both unpressurized and pressurized sections of the 2.63 km (8642 ft) segment. On pressurization, attenuation changes by a factor of 10 greater throughout the sections below the discontinuity than above it. We call the discontinuity the top of the primary attenuator in the reservoir. The discontinuity is well within the bounds of the granodiorite section of the reservoir. A primary attenuator is probably not one but perhaps the several mega-fractures which formed the primary flow paths prior to the 1000-hr heat extraction experiment. The producing fractures all intersect GT-2B below this depth.

Of special interest is the 2.7 km (8850 ft) section. The magnitude of the attenuation increases with depth throughout the shallower sections in both pressurized and unpressurized reservoir conditions even though wellbore distances have closed from 37 to 21 m (120 to 70 ft). In the 2.7 km (8850 ft) section the magnitude of the attenuation is reduced by a factor of nearly 100. The increase in attenuation with pressurization however is large -- a factor of 1000. This section of the reservoir is unique in other respects which cannot be discussed here.

The spatial distribution of the waveforms transmitted through the reservoir is shown in Fig. III-4 as the variously colored areas. Also indicated are the locations of the injection point in EE-1, the production points in GT-2 and the top of the primary attenuator.

Now take the liberty of associating the P- and D-type signals with two different fractured regions even though the nature of these systems has not been thus far established. In the unpressurized system an S-type region caps the reservoir, a P-type region dominates, and small wedges of each type including D, are found in the lower section of the reservoir. On pressurizing the system the S-type cap region transforms to a P-type and the mixed types of the lower part convert to D-type. One can reasonably assume that prior to hydraulic stimulation, the reservoir consisted of entirely S-type regions, the red lithology in Fig. III-4. Clearly the waveform types, their spatial distribution in the reservoir, and the changes in waveform effected by pressurization are of global significance in understanding the reservoir. Changes in signal type occur even above the contact, a region quite removed from the injection and production fractures. A communitivity of waveform modification appears to exist, such that on pressurization of S-type regions are converted to P-type, and P-type in turn are converted to D-type. There can be little disagreement that the S-type rock supports shearing stresses of the magnitude associated with high frequency acoustic signals. Further, in the absence of fractures, shear phases will not vanish with pressurization. Our observations indicate to the contrary that within the reservoir under investigation the only S-type region observed in the reservoir converted to P-type on pressurization. Shearing stresses were not transmitted hence fractures are present in the S-type region. The fractures must however have sufficient contact area in the unpressurized state so that loss of shear waves by scattering or back reflection does not occur.

Because P-type regions do not transmit shear waves, it may imply that these regions contain mega-fractures which have single or multiple single parted surface areas exceeding several acoustic signal wavelengths in one dimension. One anticipates that only regions containing mega-fractures pressurized above the least confining stress should be P-type. Somewhat

unexpected is that this condition is met locally in the reservoir without pressurization. Indeed one is led to the conclusion that the fractures do exist which have mismatched parted surfaces caused by relative displacements or chemical dissolution resulting in a self-propped condition.

The existence of P-type regions and the absence of a clear transition between S and P is an apparent contradiction. Components of shearing stress (shear waves) normal to parted fracture surfaces should propagate through the fracture even though that component parallel to the fracture surfaces is reflected. The arrival of a shear phase through P rock should be observed but in fact is not. A solution to this dilemma has not been found.

Several observations provide information regarding the nature of D-type regions. Most of the reservoir when pressurized is D-type. A wedge of D-type bounded successively by P- and S-type regions, exists in the reservoir at hydrostatic pressure. Compressional waves transmitted through D-type regions are not minimum phase, rather they are emergent. Obvious shear wave arrivals are absent. The section of the reservoir exhibiting conversion to D-type on pressurization shows high relative attenuation. By inference D-type regions may contain, in addition to parallel striking mega-fractures, conjugate mega-fractures, or numerous fractures with sufficiently small parted areas so that transmitted compressional and shear waves are scattered.

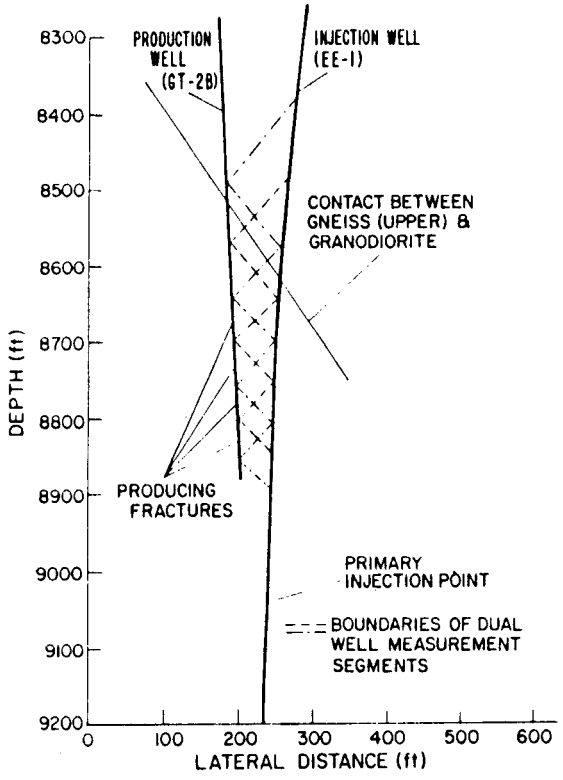

Figure III-1. Logged sections of the Fenton Hill man-made geothermal reservoir.

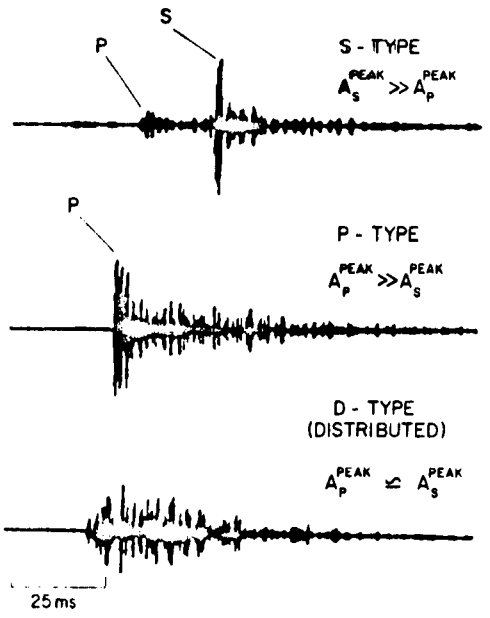

Figure III-2. S-, P-, and D-type waveforms.

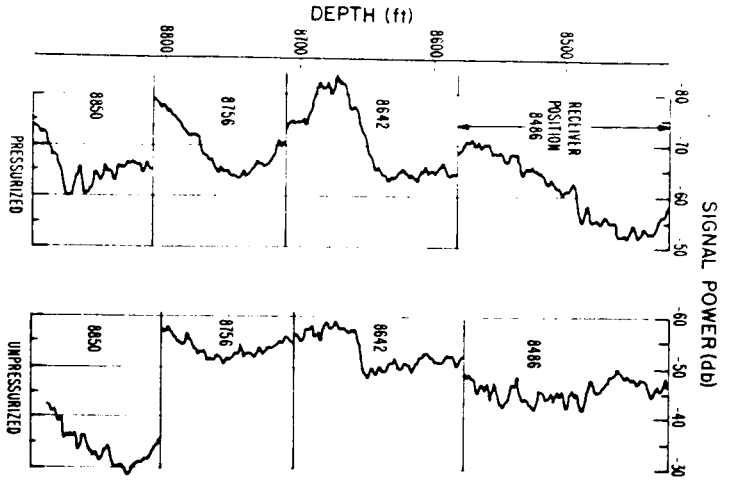

Figure III-3. Power Logs - dual well.

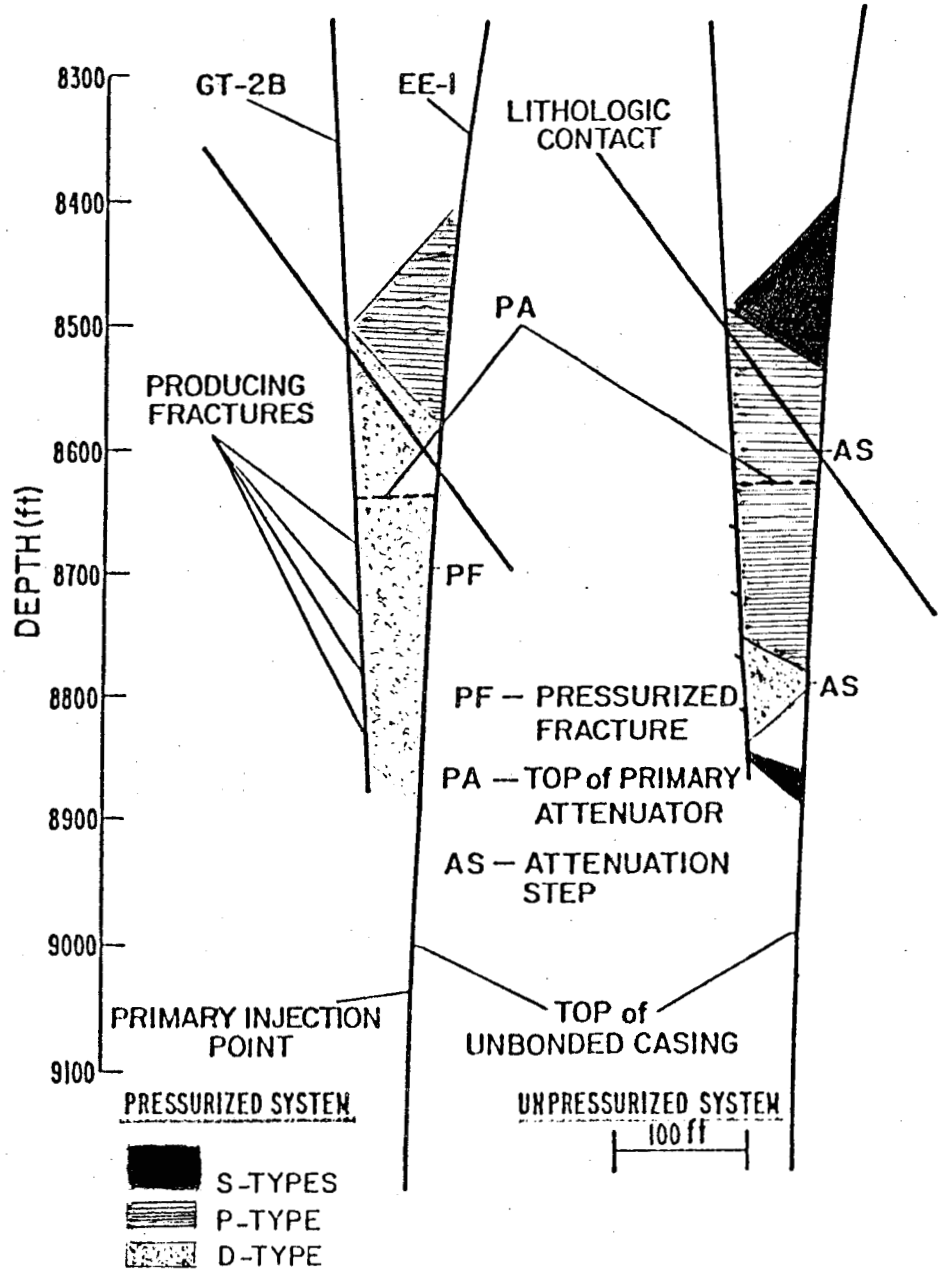

Figure III-4. Spatial relationship between region of high relative attenuation and characteristic waveform.

References

1. Tester, J. W. and J. N. Albright,"Hot Dry Rock Energy Extraction Field Test: First 75 Days of Operation of a Prototype Reservoir at Fenton Hill." Los Alamos Scientific Laboratory Report (to be published, Feb. 1979).

2. Fournier, R. O., "Chemical Geothermometers and Mixing Models for Geothermal Systems," Geothermics 5, 41-50 (1977).

3. Garrels, R. M. and C. L. Christ, Solutions, Minerals and Equilibria, Harper and Row, New York, NY, pp. 408-409 and 418, (1965).

4. LASL Hot Dry Rock Project Staff: "Hot Dry Rock Geothermal Energy Development Project Annual Report, Fiscal Year 1977," Los Alamos Scientific Laboratory Progress Report, LA-7109-PR, Los Alamos, NM, 1978.

5. Albright, J. N., R. L. Aamodt, and R. M. Potter,: "Detection of Fluid-Filled Fractures in Basement Rocks," ERDA Symposium on Enhanced Oil and Gas Recovery Proceedings and Improved Drilling Procedures, Vol. 2 - Gas and Drilling, Tulsa, OK, Aug. 30, 31, Sept. 1, 1977.

6. Albright, J. N. and R. J. Hanold: "Seismic Mapping of Hydraulic Fractures Made in Basement Rocks," ERDA Symposium on Enhanced Oil and Gas Recovery Proceedings, Vol. 2 - Gas, Tulsa, OK, Sept. 9-10, 1976.

7. Albright, J. N., R. L. Aamodt, R. M. Potter, and R. W. Spence: "Acoustic Methods for Detecting Water-Filled Fractures Using Commercial Logging Tools," DOE Symposium on Enhanced Oil and Gas Recovery Proceedings, Vol. 1, F-6, Tulsa, OK, Aug. 29-31, 1978.

8. LASL Hot Dry Rock Project Staff: "Hot Dry Rock Geothermal Energy Development Project Annual Report, Fiscal Year 1978," Los Alamos Scientific Laboratory Progress Report (in preparation).

STRESS AND FLOW IN FRACTURED POROUS MEDIA

Mohammad Sadegh Ayatollahi
Lawrence Berkeley Laboratory, University of California
Berkeley, California 94720

INTRODUCTION

The purpose of the present study is to develop a method for simultaneous solution of stress and flow in a deformable fractured isotropic porous medium saturated with a single phase slightly compressible fluid. The system defined as such can be under the effect of body forces, boundary loads, initial stress, and influenced by some fluid pressure disturbance. The method involves application of the theory of elasticity for plane strain systems, Darcy's law for porous medium, and Biot's constitutive equations for the mixture of fluid and solid skeleton. The resulting initial boundary value problem is then numerically formulated into finite element equations using the calculus of variations.

A computer program has been developed by modifying existing programs to consider interactions between fractures and porous medium when both flow and stress fields are coupled. The program is capable of handling problems in rock masses where fractures extend from one boundary to another, intersect each other, or are isolated in the porous medium. The fractures may have random orientations and the rock matrix can be permeable or impermeable. The region under investigation may be two dimensional or axially symmetric. Solutions can be obtained for either a steady-state flow field under static equilibrium or a non-steady flow field in conjunction with quasi-static equilibrium conditions.

Results obtained for certain typical examples are generally in close agreement with analytical solutions available for rigid systems. In addition, some new features on the response of deformable rock masses under the influence of a flow field have been studied. The present development can be extended to handle coupled stress and heat flow problems in rock masses. Such modification requires new sets of constitutive equations and the application of realistic thermomechanical material properties.

DISCUSSION AND CONCLUSIONS

The method described here has been developed to provide a means to understand in a broader sense, the behavior of a system consisting of a porous deformable rock mass saturated with a single phase liquid which is under the combined influence of fluid pressure, boundary flux, and boundary loads. Darcy's law for flow through porous rock and the parallel plate model for flow in fractures have been used to define flow in the porous rock mass. The theory of elasticity together with a non-linear fracture model is used to define deformations in the porous skeleton as well as in the fracture network. In order to provide an interrelation between fluid flow and structural deformations in the rock mass, two constitutive relations introduced by Biot (1941) have been used. In addition, an interconnection between flow in fractures and in the adjacent porous rocks was developed by writing mass balance relations.

A finite element numerical procedure was adopted in this analysis because obtaining analytical solutions for stress and flow problems in porous rock masses with complicated geometries and boundary conditions is a difficult, if not impossible, task. Through proper use of calculus of variations, the governing equations and boundary conditions are cast

into discrete finite element equations--the solution of which gives fluid pressure and structural displacements at all nodal points specified within the region under investigation.

The application of finite element procedures in this study has been quite advantageous. It has provided flexibility in discretization of the region and has offered freedom to describe the geometry in two dimensions. The use of two-dimensional isoparametric elements for defining the porous medium and one-dimensional isoparametric elements which define fracture segments has further contributed to the efficiency of the numerical procedure. Furthermore, the numerical method developed in this study enables one to obtain stresses and flows within each element very efficiently.

The present numerical development has also proved to be capable of handling a wide range of problems from steady-state flow under static equilibrium conditions to transient flow under quasi-static equilibrium conditions. The rock may be porous and permeable or impervious. The rock mass can be deformable or structurally rigid. The pressure or flux source may be located in the porous medium and its boundaries, in a fracture segment or at the intersection of fractures. In addition, isolated or nonintersecting sets of fractures can be incorporated into the region under study.

In the analysis of rigid fractured systems simulated by the present method, it has been shown that the flow into the well is proportional to the total length of the fractures intersecting the well. This has been shown for either one or two fractures that intersect the well.

The study of the response of a deformable fractured porous medium subject to fluid withdrawal from a well intersected by the fractures has revealed that the fractures close more rapidly at early time, while at later time the rate of closing reduces due to the subsequent pressure drop in the porous medium. Such behavior is not expected to occur in fractures in impermeable systems where the deformations will continue with further changes in fluid pressure.

The nonlinear behavior of joints in fractured systems during fluid flow with changing stress can be studied more quantitatively using the present method. It should be possible to use this approach to obtain the variation of fracture stiffness due to fluid pressure. Fluid injection cannot be expected to reduce the stiffness of fractures in a porous medium when highly compressive initial stresses exist. Only where a rock system is subject to small initial compressive stresses will the fracture network be more susceptible to a reduction in stiffness. The variation of the normal stiffness of the fractures due to fluid injection can be approximated by logarithmic functions.

Although the present method is able to handle a wide range of flow problems in rock masses, certain limitations concerning the use of the method should be kept in mind. The existing computer program developed in this study can be used for cases in which gravitational acceleration is negligible. This assumption is valid in most reservoir engineering problems where the aquifer thickness is very small compared to the height of the overburden material. However, further improvements can be made in the program to account for the influence of gravity. Also it is assumed that changes in both the flow and stress fields take place at constant temperature.

Applicability of the present method depends on the availability of geological information on rock mass structures. The geometry of the system including the length, orientation, and initial fracture aperture openings should be known. The fact that these data are not easily accessible for rock mass structures at depth further restricts the use of the method. Such restrictions have directed the attention of some investigators towards statistical approaches.

It should be emphasized that understanding the behavior of fractured rock masses under the combined effects of flow and stress is a complicated process. The numerical method developed in this work represents a first step toward handling this problem. Further complications can be expected if one is concerned with the flow of heat in such systems. However, the present work may be helpful in suggesting a possible approach to non-isothermal problems associated with fractured rocks.

Extension of the present investigation in future work by others is recommended in such areas as:

(A) Development and application of new fracture models that can help one to simulate the behavior of discontinuities in rock masses more efficiently.

(B) Further generalization of the present computer program to include an option for the solution of coupled stress and heat conduction problems in rock masses. Such modification will require new sets of constitutive equations and the application of realistic thermo-mechanical material properties.

(C) If the present method is to be used as a practical tool rather than remaining as a purely idealized simulation technique, it should be applied to field problems where realistic physical data can be obtained on the behavior of rock masses.

REFERENCES

Barenblatt, G.I., Zheltov, I.P., and Kochina, I.N., "Basic Concept in the theory of seepage of homogeneous liquids in fractured rocks" (Translation) P.M.M. Moscow, v. 24, p. 852, 1960.

Barenblatt, G.I. Zheltov, I.P., and Kochina, I.N., "Flow through fissured rocks," P.M.M. Moscow, Tome XXIV, Part 5, 1960.

Biot, M.A., "General theory of three-dimensional consolidation," J. Applied Physcs, v. 12, pp. 155-164, 1941.

Biot, M.A., "Theory of elasticity and consolidation for a porous anisotropic media," J. Applied Physics, v. 26, pp. 182-185, 1955.

Biot, M.A., "Theory of deformations of a porous viscoelastic anistropic media," J. Applied Physics, v. 27, 1956.

Biot, M.A., "Mechanics of deformation and accoustic propagation in porous media," J. Applied Physics, v. 34-A, pp. 1483-1488, 1961.

Duguid, J.O., "Flow in fractured porous media," Ph.D. Dissertation, Department of Civil and Geological Engineering, Princeton University, Princeton, 1973.

Ghaboussi, J. and Wilson, E.L., "Flow of compressible fluids in porous media," SESM Report No. 71-12, University of Califronia, Berkeley, 1971.

Ghaboussi, J., "Dynamic stress analysis of porous elastic solids saturated with compressible fluids," Ph.D. Dissertation, University of California, Berkeley, 1971.

Gurtin, M., "Variational principles for linear elastodynamics," Arch. Rat. Mech. and Anal., v. 16, pp. 34-50.

Louis, C., "A study of groundwater flow in jointed rock and its influence on the stability of rock masses," Rock Mech. Research Report N. 10, Imperial College, 1971.

Noorishad, J., Witherspoon, P.A., and Brekke, T.L., "A method for coupled stress and flow analysis of fractured rock mass," Publication No. 71-6 Department of Civil Engineering, University of California, Berkeley, 1971.

Taylor, R.L., "Analysis of flow of compressible or incompressible fluids in porous elastic solids," Consulting report to the Naval Civil Eng. Lab, Port Hueneme, CA, 1974.

Wilson, C. and Witherspoon, P.A., "An investigation of laminar flow in fractured porous rocks," Ph.D. Dissertation, University of California, Berkeley, 1970.

Witherspoon, P.A., Norrishad, J., and Maini, Y.N.T., "Investigation of fluid injection in fractured rock and effect on stress distribution," USGS Contract No. 14-08-001-12727, 1972.

Witherspoon, P.A., Taylor, R.L., Gale, J.E., and Ayatollahi, M.S., "Investigation of fluid injection in fractured rock and effect on stress distribution," USGS Contract No. 14-08-001-12727, 1973-1974.

SPACING AND WIDTH OF COOLING CRACKS IN ROCK

By Zdeněk P. Bažant[a]

Summary

One important question in the hot dry rock geothermal energy scheme is the spacing and opening widths of secondary cracks that are induced by cooling in the walls of the main crack and propagate into the hot rock mass. To achieve a significant heat extraction rate after longer periods of operation, it would be necessary to have widely opened secondary cracks, which in turn requires a large spacing of these cracks.

The problem may be treated as a cooled halfspace. When a system of equidistant cooling crack propagates into a halfspace, it reaches at a certain depth a critical state at which the growth of every other crack is arrested. Later these cracks reach a second critical state at which they close. The intermediate cracks, at doubled spacing, open about twice as wide and advance further as cooling penetrates deeper. Determination of the critical states requires calculation of the derivatives of the stress intensity factors with regard to crack lengths, which is accomplished by the finite element method.

It is found that the crack depth-to-spacing ratio at which the critical state is reached is extremely sensitive to the temperature profile. It greatly increases as the cooling front becomes steeper, which is not favorable for maintaining a high heat extraction rate. The effect of transverse isotropy of the material upon the location of critical states is found to be relatively small. Approximate formulas for crack spacing as a function of temperature profile, to be used in conjunction with the analysis of water flow and heat transfer in the cracks, are developed.

---

[a]Professor of Civil Engineering, Northwestern University, Evanston, Illinois, 60201.

REFERENCES

1. Bažant, Z. P., and Ohtsubo, H., "Stability Conditions for Propagation of a System of Cracks in a Brittle Solid," Mechanics Research Communications, Vol. 4, No. 5 (Sept. 1977) 353-366.

2. Bažant, Z. P. , and Ohtsubo, H., "Stability and Spacing of Cooling or Shrinkage Cracks," Advances in Civil Engineering through Engineering Mechanics, Reprints of 2nd Annual Eng. Mech. Div. Specialty Conference held at North Carolina State Univ., Raleigh in May 1977, published by Am. Society of Mechanical Engineers.

3. Bažant, Z. P., and Ohtsubo, H., "Geothermal Heat Extraction by Water Circulation through a Large Crack in Dry Hot Rock Mass," Intern. J. of Numerical Methods in Geomechanics, Vol. 2 (1978), No. 4.

ANNOTATED RESEARCH BIBLIOGRAPHY FOR GEOTHERMAL RESERVOIR ENGINEERING

G. S. Randall and R. F. Harrison
TerraTek
University Research Park, 420 Wakara Way,
Salt Lake City, Utah 84108

Despite efforts of conscientious researchers, the current volume of published materials makes it virtually impossible to review all relevant publications in a given field. As a result it has been estimated that approximately one-tenth of the research and development funds expended in the United States has been applied to areas resulting in a duplication of efforts. This has been attributed to inadequate literature review.

An up-to-date annotated bibliography has been prepared which assisted in avoiding duplication of reservoir engineering research and served as a definitive record of the progress and current status of the subject. The bibliography included English, Italian, Russian and Japanese language publications. Individual documents have been grouped under the following major subject categories:

- Formation Evaluation
- Reservoir Modeling
- Exploitation Strategies
- Evaluation of Production Trends

The specific tasks for completing the bibliography included:

- Literature Research
- Thesaurus Development
- Document Evaluation
- Computerized Bibliography
- Report Preparation

It is imperative that the reservoir engineer quantitatively appreciate the physical processes occurring within the geothermal system in order that an exploitation strategy can be selected with confidence. The first step in this process was to develop an appreciation of the general physical processes associated with geothermal systems and use this background to generate a conceptual model of the particular system under study. Secondly the physical properties of the rock and fluid and the structural features of the reservoir must be assessed. These inputs are required before a representative quantitative simulation can be formulated. A mathematical or experimental model must then be developed using the defined physical properties along with identified initial and boundary conditions which can then be used to assess possible production strategies. The actual reservoir response under production must then be used to continuously update and refine the model. This will allow extrapolations of performance to be made with greater confidence.

In the early 1960's the majority of geothermal reservoir engineering concepts relied primarily on experience gained in the oil and gas industries. It was not long however before workers in geothermal research realized the complexity and different nature of geothermal resources from conventional oil and gas resources. High temperature, steam flashing, chemical deposition and nonporous fractured reservoirs are examples of such differences. The recent surge in geothermal energy exploration and exploitation activities has given an impetus to increased effort and progress in geothermal reservoir engineering.

Literature research resulted in approximately 350-400 documents from retrievable sources in the subject areas listed above.

Thesaurus development has expanded on the GRID indexing system developed by Lawrence Berkeley Laboratory. The expansion of a thesaurus of the GRID data base will permit computerized information retrieval.

The document evaluation phone reviewed and retrieved items for subject relevance and compiled annotations of literature included in the bibliography. Computer tasks have entailed keypunching data for automated retrieval.

Final bibliography has been divided into a narrative review, annotations, reference list, and thesaurus.

SIMULATION OF GEOTHERMAL RESERVOIRS INCLUDING CHANGES IN POROSITY AND PERMEABILITY DUE TO SILICA-WATER REACTIONS

Todd M.C. Li, J.W. Mercer, C.R. Faust, and R.J. Greenfield
U.S. Geological Survey
Reston, Virginia 22092

Introduction

Changes in porosity and permeability due to water-rock reactions may affect a geothermal reservoir in two important ways. One is the possibility of clogging of the pore space in the vicinity of a reinjection well. The second concerns the long term evolution of a geothermal system, for example, the development of a self-sealing cap rock. Two major types of reactions that may affect the porosity and permeability in the reservoir are dissolution-precipitation reactions and alteration reactions. Silica precipitation is the major self-sealing process in hot-water geothermal resevoirs (White, 1973). The purpose of this work is to develop a mathematical model which can simulate the changes in porosity and permeability resulting from water-rock reactions in a geothermal reservoir.

The model being developed describes the flow of hot water in an axially symmetric porous medium. The model is a vertical cross-section in r-z coordinates. For simplicity, only a single dissolved chemical species is being modeled. The fluid is single-phase water and only dissolution and precipitation of quartz are considered. The kinetics for silica are those developed by Rimstidt and Barnes (1979) and Rimstidt (1979).

The Basic Equations

The set of basic partial differential equations that describes a hot water geothermal system are the fluid mass balance (continuity equation), the fluid momentum balance (Darcy's Law), the thermal energy balance, and the dissolved species mass balance equations. Additional conditions needed to fully describe the physics and chemistry are an equation of state (that is, density as a known function of pressure, temperature, and concentration), constitutive relations for fluid and rock, chemical rate equations, and initial and boundary conditions. In addition, the rate of change of porosity and permeability as a function of the reaction must be derived.

The final set of partial differential equations is formulated in terms of fluid pressure, temperature, and concentration. Since exact solutions are too idealized, an approximate method is necessary. The method used is a numerical method in which the spatial derivatives are

approximated using a Galerkin finite-element method and the temporal derivatives are approximated using a finite-difference method.

Changes in Porosity and Permeability

To model changes in porosity and permeability it is necessary that changes in porosity be expressed in terms of bulk pore volume changes in the porous medium due to dissolution or precipitation. Furthermore, it is assumed that the changes in permeability can be directly related to changes in porosity by some empirical or theoretical relationship between permeability and porosity. The relationship used is an empirical one from Pearson (1976),

$$k = 10^{(13.614\ \phi\ -\ 1.8126)} \times 9.87 \times 10^{-12} \qquad (1)$$

where ϕ is porosity (volume fraction), and k is permeability (square centimeters).

To obtain changes in porosity in terms of the reaction kinetics, consider the solute mass balance equation:

$$\frac{\partial}{\partial t}(\phi \rho_w C) + \nabla\cdot(\rho_w C \vec{u}) - \nabla\cdot(\rho_w E \nabla C) - q_s C_s + q_{Re} = 0 \qquad (2)$$

Assuming that the only reactive component is quartz and that the changes in rock mass are due to dissolution and precipitation of quartz, a rock mass balance equation is written

$$\frac{\partial}{\partial t}[(1-\phi)\rho_r C_r] = q_{Re} \qquad (3)$$

In equations (2) and (3), ρ_r and ρ_w are the densities of the rock and water, respectively. C_r and C are concentrations (mass fraction) of silica in the rock and water, respectively. $\vec{u}$ is the Darcy velocity and E is the dispersion coefficient. q_s is the mass flux (grams per second per cubic centimeters) due to a well source and C_s is the concentration of the source fluid. The term q_{Re} is the net rate of precipitation. The term q_{Re} may also be thought of as the time rate of loss of dissolved silica mass per unit volume by precipitation. The subscript Re refers to the part of the subscripted expression which is due to the reaction.

The left hand side of equation (3) can be simplified, assuming that ρ_r and C_r are constant;

$$\frac{\partial}{\partial t}\left[(1-\phi)\rho_r C_r\right] = -\rho_r C_r \left.\frac{\partial \phi}{\partial t}\right|_{Re} \tag{4}$$

Therefore, an expression for $\left.\frac{\partial \phi}{\partial t}\right|_{Re}$ can be obtained, which is

$$\left.\frac{\partial \phi}{\partial t}\right|_{Re} = -\frac{1}{\rho_r C_r} q_{Re} \tag{5}$$

The term q_{Re} is evaluated by incorporating the kinetic rate equation for quartz which describes the time rate of change of silica concentration in the fluid as a function of concentration and temperature. This equation is (Rimstidt and Barnes, 1979; Rimstidt, 1979)

$$\frac{\partial m}{\partial t} = \frac{A}{M}\left[k_+ - k_- m\right] \tag{6}$$

where m is molality of dissolved silica, A/M is the ratio of interfacial area to mass of water, and k_+ and k_- are the rate constants for dissolution and precipitation, respectively. The rate constants are exponential functions of temperature.

Numerical Method

The numerical method used to solve for pressure, temperature, and concentration is based on the finite-element method. The essential features of this method are:

1) The spatial derivatives are approximated using a modified Galerkin finite-element method in which upstream weighting of the convective terms is used.

2) The temporal derivatives are approximated using a backward (implicit) finite difference in time.

3) Concentration, temperature, and pressure are solved for sequentially in a manner similar to that outlined by Coats et al. (1974) for finite difference methods. Solving for concentration, temperature, and pressure in that order allows the coefficient matrix for the spatial derivatives to be symmetric. The method also requires lumping of the time derivative matrices.

4) The convective terms in the temperature and concentration equations are evaluated at the new time level using a linearized semi-implicit method. This allows reasonably large time steps without changing the symmetry of the matrices.

5) The reaction term in the concentration equation is treated semi-implicitly.

Examples

The model has been tested against some analytical solutions. The solution for pressure has been compared to the Theis solution from groundwater hydrology (Theis, 1935). The solution for temperature has been compared to an analytical solution to the problem of hot fluid injection into an aquifer, including the effect of conductive heat loss through the confining beds (Avdonin, 1964). A modification of the Avdonin solution without leakage was used to test the solution of the concentration equation. All three finite element solutions compared favorably to the analytical solutions. The differential rate equation for quartz was integrated analytically over time at constant temperature. This was compared to computed concentrations for conditions of no flow and constant temperature. The accuracy of the concentrations computed by the finite element model under these conditions is dependent on the size of the time step.

The relationship between the temperature and the concentration solutions and how this effects the reaction rate for quartz dissolution-precipitation was studied through a series of one-dimensional problems. In these problems, the fronts are caused by the injection of hot water into a cooler aquifer, with the initial fluids saturated with silica. The results suggest that the temperature solution controls the rate of the quartz precipitation-dissolution reaction in two basic ways.

First, the reaction rate is rapid enough that the curvature of the concentration front basically follows that of the temperature front. This implies that thermal dispersion (conductivity) of the reservoir is relatively more important than silica dispersion in controlling the reaction. Precipitation tends to occur on the upstream side of the fronts where hot water mixes with cold water. This results in decreased porosity and permeability in the vicinity of the well.

The second way in which the temperature solution controls the reaction rate is through the exponential temperature dependence of the rate constants. The result is that the reaction rate is more sensitive to changes in concentration and temperature at higher temperatures.

We are presently in the process of designing two-dimensional problems with the purpose of modeling self-sealing in a reservoir.

Acknowledgements

This work is supported by the U. S. Geological Survey, NSF Grant No. AER 74-08473, and The Pennsylvania State University.

References

Avdonin, N. A., 1964, Some formulas for calculating the temperature field of a stratum suject to thermal injection. Neft'i Gaz, 7 (3), 37-41.

Coats, K. H., George, W. D., Chu, C., and Marcum, B. E., 1974, Three-dimensional simulation of steamflooding. Soc. Pet. Eng. J., 14 (6), 573-592.

Pearson, R. O., 1976, Planning and design of additional East Mesa geothermal test facilities (Phase 1B), Volume 1 - Final Report, SAN/1140-1/1, ERDA.

Rimstidt, J. D., 1979, in preparation. The kinetics of silica-water reactions. Ph.D. Thesis, The Pennsylvania State University.

Rimstidt, J. D. and Barnes, H. L., 1979, Kinetics of silica-water reactions, submitted to Geochim. Cosmochim. Acta.

Theis, Charles V., 1935, The relation between the lowering of the piezometric surface and the rate and duration of discharge of a well using ground-water storage. Eos Trans. Am. Geophys. Union, 16, 519-524.

White, Donald E., 1973, Characteristics of geothermal resources, in Geothermal Energy, edited by Paul Kruger and Carel Otte, pp. 69-94. Stanford University Press, Stanford, California.

PRELIMINARY RESERVOIR AND SUBSIDENCE SIMULATIONS FOR THE AUSTIN BAYOU GEOPRESSURED GEOTHERMAL PROSPECT*

S. K. Garg, T. D. Riney and D. H. Brownell, Jr.
Systems, Science and Software, La Jolla, California

For the last several years, the University of Texas at Austin (UTA) has analyzed the geopressured tertiary sandstones along the Texas Gulf Coast with the objective of locating prospective reservoirs from which geothermal energy could be recovered. Of the "geothermal fairways" (areas with thick sandstone bodies and estimated temperatures in excess of 300°F), the Brazoria fairway appears most promising and the Austin Bayou Prospect has been developed within this fairway.[1] A test well (DOE 1 Martin Ranch) is currently being drilled in this area. Pending the availability of actual well test data, estimated reservoir properties have been employed in numerical simulations to study the effects of variations in reservoir properties on the projected long-term behavior of the Austin Bayou Prospect. The simulations assess the sensitivity of the reservoir behavior to variations in estimated sandstone/shale distribution, shale compressibility, and vertical shale permeablity. Further, hypothetical properties for the stress-deformation behavior of the rock formations were employed in a very preliminary study of the potential ground surface displacements that might accompany fluid production.

AUSTIN BAYOU PROSPECT

It is estimated that the Austin Bayou Prospect has a total sandstone thickness of 800-900 ft, average permeability (from unconfined cores) of 40-60 md, fluid temperature in the range of 300°F (at 14,000 ft depth) to 350°F (at 16,500 ft), and salinities in the range of 40,000-100,000 ppm. It is estimated that the test well will drain several sandstone reservoirs (zones A, B, C, D, E and F in Figure 1) in an area of approximately 16 square miles.[1] The net sandstone thickness, inferred from an interpolated spontaneous potential log, is 840 ft. Average porosity of at least 0.20 is predicted for 250 ft of the sandstone; the remaining sandstone has a porosity of between 0.05-0.20 with an average value of 0.15. The total pore volume, water in pores, and gas in place are estimated to be 60 billion cubic ft, 10 billion bbl, and 426 billion cubic ft, respectively.

RESERVOIR RESPONSE CALCULATIONS

It is likely that the test well will first be used to produce from sand bodies located within a single zone; the simulations consider production to be entirely from Zone E which has the thickest sandstone bodies (50-100 ft). A series of four axisymmetric calculations was run

*Work performed for UTA under DOE Contract EY-76-C-5040-1S.

with the S^3 MUSHRM reservoir computer model to simulate the behavior of layered sandstone/shale sequences used to represent Zone E (Figure 1). MUSHRM includes treatment of all the important fluid/rock response mechanisms and their interactions, that are believed to be operative in Gulf Coast geopressured geothermal reservoirs.[2] The reservoir is assumed to be a cylindrical disc with radius R = 3.63 km (corresponding to a block area of 16 square miles) and height 152.4 m (500 ft, corresponding to the top and bottom of Zone E at depths of 15,300 and 15,800 ft, respectively). The net sand thickness (= net shale thickness) is 76.2 m (250 ft). The reservoir fluid is assumed to be liquid water saturated with methane. The initial pore pressure, temperature and methane mass fraction at a depth of 15,500 ft are 793 bars (11,500 psi), 162.7°C (325°F) and 0.007, respectively. The reservoir fluid is assumed to be initially in hydrostatic equilibrium so that the initial values of pore pressure and methane mass fraction vary slightly over the 500 ft reservoir thickness. The reservoir is produced at a constant mass rate of 36.8 kg/sec (20,000 STB/day); all of the production is from the sandstone layers.

For the sandstone layers we assume horizontal permeability = 20 md; vertical permeability = 2 md; grain density of rock = 2.63 g/cm^3; initial porosity of rock = 0.20; rock thermal conductivity = 5.25 ergs/sec-cm-°C; rock specific heat = 0.963×10^7 ergs/g-°C; rock bulk compressibility = 7.25×10^{-9} cm^2/dynes; irreducible liquid saturation = 0.3 and irreducible gas saturation = 0.0. The latter two parameters define the relative permeabilities, in the case of two-phase flow, using the Corey formulation. For the shale layers we assume identical properties as for the sand layers except for horizontal permeability, vertical permeability and rock bulk compressibility. These properties, as well as the sequencing of the sandstone/shale layers, are varied in the four MUSHRM calculations.

Figure 2 shows the numerical grid, along with the sandstone/shale arrangement, used in simulation #1 (base case). In simulation #2 (thick sands), the arrangement shown in Figure 3 was used. For these two cases the shale layers are assumed to have horizontal permeability = 10^{-4} md; vertical permeability = 10^{-5} md; rock bulk compressibility = 14.5×10^{-10} cm^2/dynes. Simulation #3 (high shale k_v) is the same as #1 except the vertical permeability of the shale layer is increased ten-fold to 10^{-4} md. Simulation #4 (small shale C) is the same as #1 except the bulk rock compressibility of the shale layers is decreased ten-fold to 14.5×10^{-11} cm^2/dynes.

Figure 4 shows the time-dependent pressure decline in the various sandstone well-blocks for all four MUSHRM simulations. For simulation #1 (base case) the pressure drops in well-blocks (i = 1, j = 2, 4, 9) are essentially the same but differ substantially from those in well-blocks (i = 1, j = 6, 7). This clearly illustrates the influence of fluid influx from the adjoining shales. Layers j = 2, 4, 9 are each a 50 ft thick sandstone body sandwiched between shale layers, whereas layers j = 6, 7 are contiguous sandstone bodies with a total thickness of 100 ft. We further note, however, that the pressure drop for all of the sandstone layers is very nearly identical for the first year or two; influx from

adjoining shales should have little or no effect for practical drawdown/buildup times employed in well testing.

Simulation #2 (thick sands) uses the same estimated properties for the sandstone and shale layers as for the base case, but the net sandstone of 250 ft is a single thick body sandwiched between 125 ft thick shale bodies. As shown in Figure 4, the pressure drops in the sandstone layers comprising the 250 ft thick body are essentially identical. The drop is nearly the same as for simulation #1 (base case) for $t < \sim 2$ years; this again indicates that the fluid influx from shale layers will be important only for long production times. For $t > \sim 3$ years, higher pressure drops are obtained for simulation #2 (thick sands); the importance of fluid influx from the shales decreases with increasing sandstone thickness. Comparison of simulation #3 (high shale k_v) with the base case shows that the ten-fold increase in the vertical permeability of the shale layers enhances the fluid influx and thus greatly reduces the long-term pressure drop in the sandstone well-blocks (Figure 4). Nevertheless, the influence of the influx is minimal for $t < \sim 1$ year. Finally, comparison of the results for simulation #4 (small shale C) with the base case shows that a ten-fold decrease in the bulk rock compressibility of the shale layers causes a larger pressure drop in the sandstone well-blocks; this effect, however, becomes evident only for $t > \sim 10$ years.

The MUSHRM simulator computes porosity along with the fluid state in each computational cell at each stage of a calculation. Given current and initial porosities, the radial variation of the vertical compaction of the reservoir may be computed; the compaction at t = 30.3 years is depicted in Figure 5 for each of the four reservoir simulations.

PRELIMINARY SUBSIDENCE STUDIES

Estimation of the vertical (subsidence) and horizontal movements of the ground surface that might accompany reservoir compaction requires knowledge of the stress-deformation behavior of the rock units constituting the reservoir (Zone E) and the overlying and underlying strata. Since such data were not available, hypothetical properties were used in the S^3 AGRESS simulator which couples the reservoir response model (MUSHRM) with a rock stress-deformation response model.[2] Figure 6 shows an axial section of the configuration treated. The test well is expected to enter the geopressured zone at a depth of approximately 10,000 ft. Rocks are likely to be competent in the geopressured zone; above that depth the rocks may be unconsolidated. Accordingly, the formation properties of the rocks surrounding the reservoir are permitted to be different in Region I (depth < 10,000 ft) and Region II (depth > 10,000 ft) for the ground movement studies.

We assume that the Zone E sandstone/shale layer arrangement, formation properties, initial fluid state, and the imposed fluid production are identical to those used for reservoir simulation #1 (base case). In addition to the reservoir formation properties given earlier, we assume

the following stress-deformation properties for the reservoir sandstone (shale) layers: bulk modulus of porous rock = 9.20 kb (0.46 kb); shear modulus of porous rock = 3.45 kb (0.17 kb); bulk modulus of rock grain = 300 kb (100 kb). Since the reservoir pore pressure declines monotonically during fluid production, the values selected are for loading conditions. The overburden/underburden rocks are assumed to be linearly elastic; three parametric AGRESS simulations were made to assess the effects of variations in rock properties. Case A (soft) treats both Region I and Region II as unconsolidated rock with bulk modulus = 25 kb and shear modulus = 9.375 kb. Case B (mixed) treats Region I the same as Case A, but assumes the geopressured zone is four times as stiff (Region II bulk modulus = 100 kb and shear modulus = 37.5 kb). In Case C (stiff), both Region I and Region II are treated as competent rock (i.e., bulk modulus 100 kb and shear modulus = 37.5 kb).

The surface vertical and horizontal movements calculated by the three AGRESS simulations at t = 30.3 years are shown in Figure 7. The horizontal movement is directed toward the test well (r = 0). The combined effect of the movements is to form a subsidence bowl. The main effect of an increase in rock stiffness is to reduce the surface displacements. Comparison of Figures 5 and 7 shows that only a small fraction of the reservoir compaction is calculated to appear as surface subsidence.

CONCLUDING REMARKS

The parametric geopressured reservoir simulations strongly suggest that for sandstone thicknesses greater than 50 ft, the effect of shale fluid influx will not be felt for production times less than one to two years. This implies that the effect can be ignored for drawdown/buildup times practical in well testing, but the influx from shales will likely play an important role in determining long-term pressure drop in the sandstones, and also in the associated reservoir compaction. The parametric ground surface displacement simulations suggest that only a fraction of the reservoir compaction will appear as surface subsidence. It should be emphasized that the estimated values for reservoir properties used in the reservoir response calculations must be confirmed by data from the DOE 1 Martin Ranch test well. The preliminary calculations for the ground surface movements are even more tenuous since they are based upon hypothetical overburden/underburden rock properties.

REFERENCES

1. Bebout, D. G., R. G. Loucks and A. R. Gregory, "Study Looks at Gulf Coast Geothermal Potential," Oil and Gas Journal, September 26, 1977. "Texas Geothermal Prospect Slated to Begin Operations at Martin Ranch," Oil and Gas Journal, October 3, 1977.

2. Garg, S. K., J. W. Pritchett, D. H. Brownell, Jr., and T. D. Riney, "Geopressured Geothermal Reservoir and Wellbore Simulations," Systems, Science and Software, La Jolla, California, Report SSS-R-78-3639, 1978.

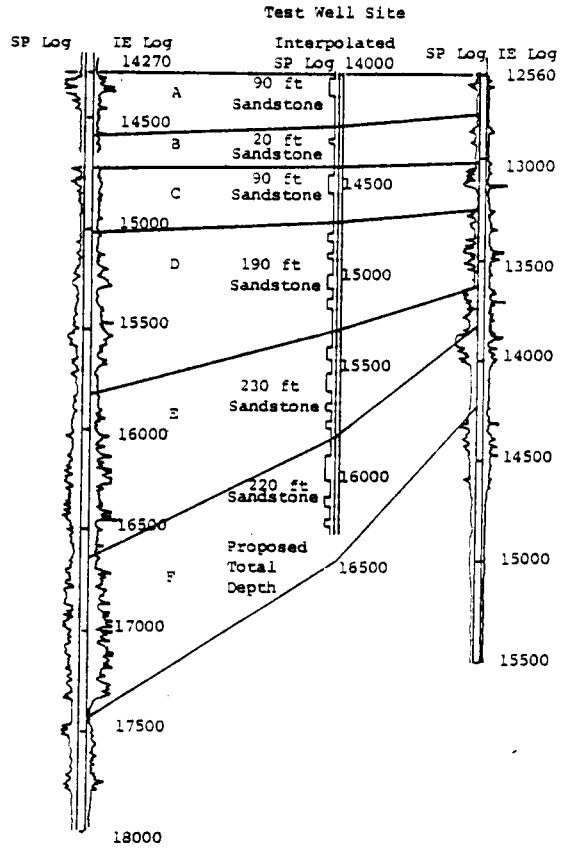

Figure 1. Expected sandstone distribution for the test well site from a synthetic SP log created by interpolation from existing control wells (from Bebout, et al.[1]).

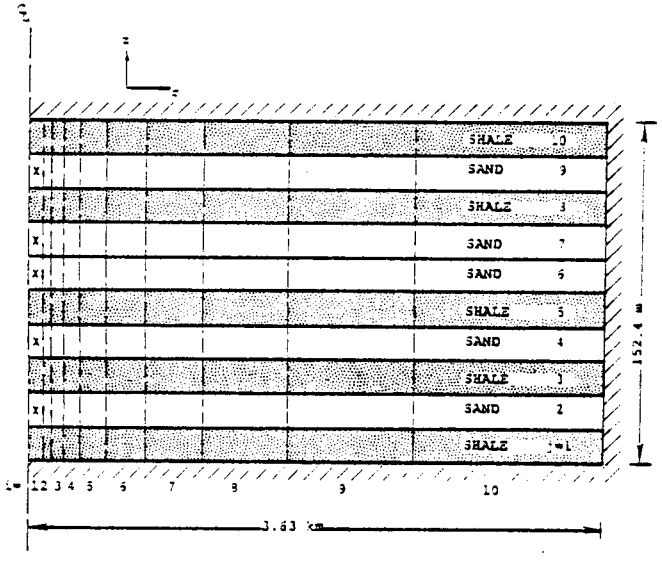

Figure 2. Axial section of the numerical grid and the shale/sandstone arrangement utilized in Cases 1, 3 and 4. The well-blocks from which fluid is produced are indicated by X.

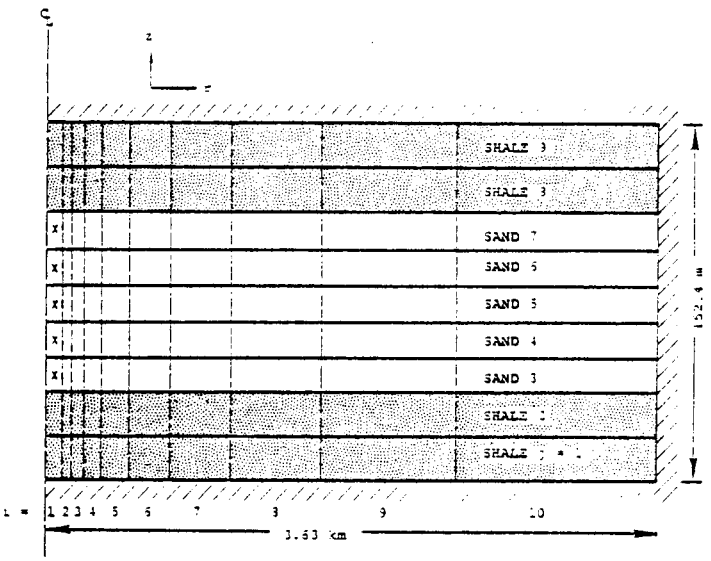

Figure 3. Axial section of the numerical grid and the shale/sandstone arrangement utilized in Case 2. The well-blocks are indicated by X.

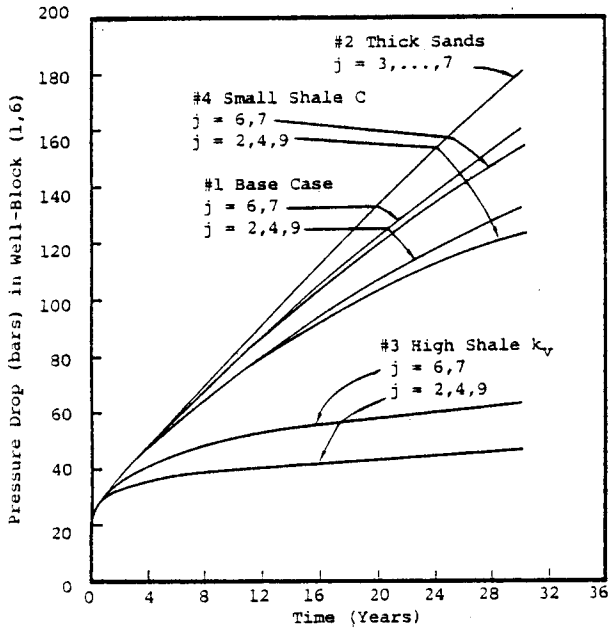

Figure 4. Pressure drop in sandstone well-blocks (i = 1).

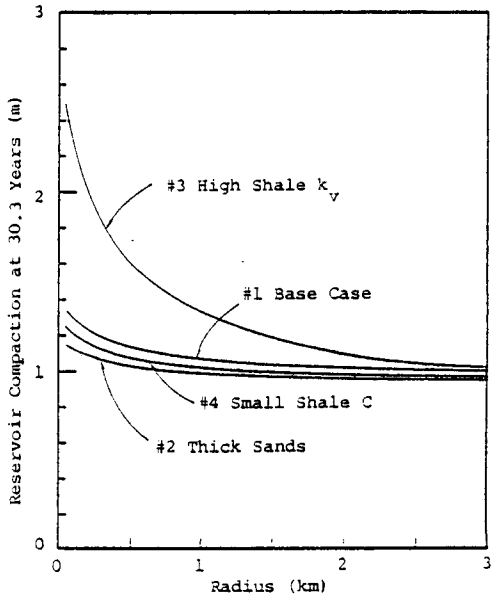

Figure 5. Radial distribution of the vertical compaction of the reservoir.

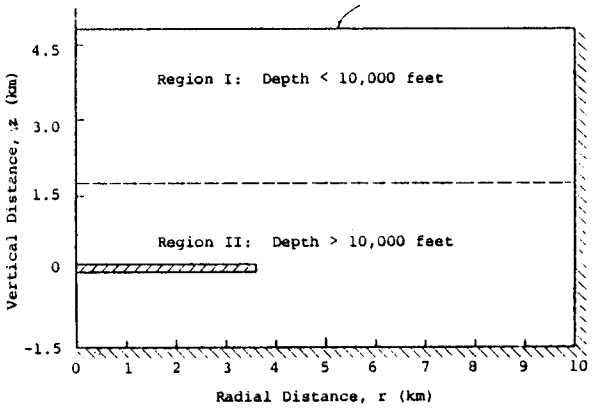

Figure 6. Axial section showing the reservoir (hatched) and the surrounding rocks. Both the bottom and the right vertical (i.e., r=10 km) boundaries are assumed to be fixed.

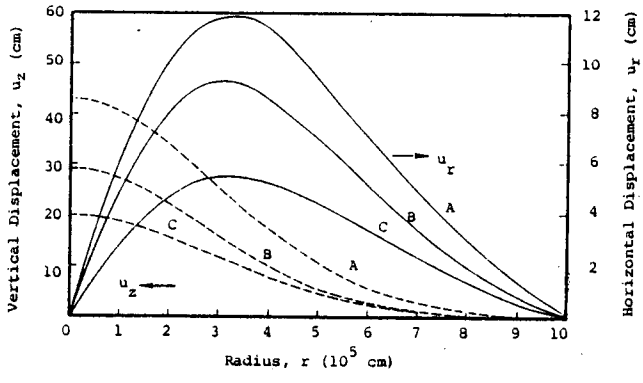

Figure 7. Surface vertical displacement (left) and horizontal displacement (right) at t ∿ 30.3 years for three choices of rock elastic properties.

Clifford I. Voss* and George F. Pinder**

1.0 Introduction

The simulation of geothermal reservoirs involves the solution of the equations describing multiphase, non-isothermal flow in porous media. These equations are highly nonlinear, particularly as the solution encounters the boundary of the two-phase region. There are essentially as many ways of accommodating this nonlinearity as there are numerical models of geothermal reservoirs. However, there is no universally accepted method for establishing the relative accuracy of these techniques. Well-established methodologies such as Fourier analysis and comparison against analytical solutions are simply not applicable to nonlinear systems. A necessary but not sufficient condition for convergence is the conservation of mass energy and momentum. This information is generally provided as an integral part of the numerical solution.

2.0 Governing Equations

One possible form of the equations governing mass and energy transport in geothermal reservoirs is:

$$\left[(1-\theta)\rho_m\left(\frac{\partial h_m}{\partial p_f}\right)_{h_f} - \theta\right]\frac{\partial p_f}{\partial t} + \left[(1-\theta)\rho_m\left(\frac{\partial h_m}{\partial h_f}\right)_{p_f} + \theta\rho_f\right]\frac{\partial h_f}{\partial t} - \left[\left(\frac{\overset{\approx}{k}k_{rs}\rho_s}{\mu_s} + \frac{\overset{\approx}{k}k_{rw}\rho_w}{\mu_w}\right)\right.$$

$$\left.\cdot \nabla_{\sim} p_f - \left(\frac{\overset{\approx}{k}k_{rs}\rho_s^2}{\mu_s} + \frac{\overset{\approx}{k}k_{rw}\rho_w^2}{\mu_w}\right)\cdot \underset{\sim}{g}\right]\cdot \nabla_{\sim} h_f + \nabla_{\sim}\cdot\left\{\left[\left(\frac{1}{\rho_f}\right) S_s S_w \rho_s \rho_w (h_s - h_w)\right.\right. \tag{1}$$

$$\left.\left.\cdot\left(\frac{\overset{\approx}{k}k_{rw}}{S_w\mu_w} - \frac{\overset{\approx}{k}k_{rs}}{S_s\mu_s}\right) - \kappa\left(\frac{\partial T}{\partial p_f}\right)_{h_f}\overset{\approx}{I}\right]\cdot \nabla_{\sim} p_f\right\} - \nabla_{\sim}\cdot\left(\kappa - \frac{\partial T}{\partial h_f}\nabla_{\sim} h_f\right) - \nabla_{\sim}\cdot$$

$$\left\{\left(\frac{1}{\rho}\right) S_s S_w \rho_s \rho_w (h_s - h_w)\left[\left(\frac{\overset{\approx}{k}k_{rw}\rho_w}{S_w\mu_w} - \frac{\overset{\approx}{k}k_{rs}\rho_s}{S_s\mu_s}\right)\cdot \underset{\sim}{g}\right]\right\} - \varepsilon\rho_f(\underset{\sim}{V}_f\cdot\underset{\sim}{g}) = 0 \qquad \text{energy}$$

$$\theta\left(\frac{\partial \rho_f}{\partial p_f}\right)_{h_f}\frac{\partial p_f}{\partial t} + \theta\left(\frac{\partial \rho_f}{\partial h_f}\right)\frac{\partial h_f}{\partial t} - \nabla_{\sim}\cdot\left[\left(\frac{\overset{\approx}{k}k_r\rho_s}{\mu_s} + \frac{\overset{\approx}{k}k_r\rho_w}{\mu_w}\right)\cdot \nabla_{\sim} p_f\right. \tag{2}$$

$$\left. - \nabla_{\sim}\cdot\left[\left(\frac{\overset{\approx}{k}k_{rs}\rho_s^2}{\mu_s} + \frac{\overset{\approx}{k}k_{rw}\rho_w^2}{\mu_w}\right)\cdot \underset{\sim}{g}\right]\right] = 0 \qquad \text{(mass)}$$

*Dept. of Water Resources Eng., The Royal Institute of Technology, S-100 44, Stockholm 70, Sweden.
**Dept. of Civil Engineering, Princeton University, Princeton, N.J.

3.0 Nonlinear Coefficients

These equations are formulated in terms of two dependent variables, h_f and p_f. The remaining thermodynamic properties, e.g., ρ_s, ρ_w, are expressed in terms of h_f and p_f through highly nonlinear relationships. The degree of nonlinearity is apparent in Fig. 1, where a few of the nonlinear coefficients are presented:

$$C_1 \equiv \left(\frac{\underset{\approx}{kk}_{rs} \rho_s}{\mu_s} + \frac{\underset{\approx}{kk}_{rw} \rho_w}{\mu_w} \right)$$

$$C_2 \equiv \theta \left(\frac{\partial \rho_f}{\partial p_f} \right)_{h_f}$$

$$C_3 \equiv \theta \left(\frac{\partial \rho_f}{\partial h_f} \right)_{p_f}$$

$$C_4 \equiv \kappa \left(\frac{\partial T}{\partial p_f} \right)_{h_f} + \frac{1}{\rho_f} \rho_s \rho_w S_s S_w (h_s - h_w) \left(\frac{\underset{\approx}{kk}_{rs}}{S_s \mu_s} - \frac{\underset{\approx}{kk}_{rw}}{S_w \mu_w} \right)$$

Note that at the boundary between the water and two-phase regions the nonlinear coefficients are actually multi-valued, some with a range of several orders of magnitude. Similar relationships are observed for the other nonlinear coefficients on Eqns. (1) and (2). When these coefficients are not handled carefully, instability, oscillations, and non-convergence in the numerical solution result in the neighborhood of the two-phase boundary.

Let us now examine this phenomenon in detail, using the hypothetical step-function coefficient $C(H)$ illustrated in Fig. 2. The behavior of C as a function of the thermodynamic variable H exhibits two undesirable traits: (a) the step does not propagate accurately as a function of H; (b) the value of C is hypersensitive to the value of H. If we assume a simple analytical relationship for H, i.e., $H(x,t) = (ax+b)(ct+d)$, we would observe the propagation of $C(x,t)$ illustrated in Fig. 3(a). However, when this continuous solution is replaced by a finite element approximation, such as illustrated in Fig. 3(b), the nonlinear coefficient is propagated as shown in Fig. 3(c). The numerical scheme clearly introduces a serious error in the propagation of this coefficient.

4.0 The Inverse Iteration Method

This numerical difficulty can be overcome if one employs a weighted-average value of $C(H)$. We will define $C(H)$ at any node i by

$$C(H) = \sigma(C^+ - C^-) + C^- \quad , \quad 0 \leq \sigma \leq 1$$

when the step lies within the region of influence of node i. We will address the problem of computing σ later. A judicious choice of σ generates the step function propagation illustrated in Fig. 4. Notice that now the step travels with a velocity almost exactly equal to the original smooth velocity shown in Fig. 3(a).

To demonstrate the hypersensitivity of $C(H)$, a one-dimensional experiment was conducted. A phase change from water to steam takes place at some point in the domain. Because no constraints were imposed on the system, the solution exhibited instability and oscillations at nodes near the region where the step change in coefficients occurred. It was observed that on some time steps the node nearest the step change in $C(H)$, node k, oscillated exactly between solutions located on either side of the step ($H^* + \varepsilon$ and $H^* - \varepsilon$ of Fig. 2). The associated coefficient oscillation was between C^+ and C^-. When the coefficient was held arbitrarily to C^+, a stable non-oscillatory solution was obtained for node k. The solution, however, was $H^* - \varepsilon$, which is compatible with the coefficient C^-. When $C(H)$ was arbitrarily held at C^-, a solution $H^* = \varepsilon$ was obtained; this is compatible with the coefficient C^+. This perfect oscillation suggests that $H^* + \varepsilon$ and $H^* - \varepsilon$ do not represent the correct solution, and that C^+ anc C^- are not the appropriate coefficients. The correct solution at node k must be exactly at the coefficient step, i.e., H^* and the correct coefficient value must lie between C^+ and C^-. This hypothesis was tested by trying different values of σ, $0 \leq \sigma \leq 1$, to determine whether there was one value which would yield a solution $H|_k = H^*$. Such a value was indeed obtained, and demonstrated that it was possible to have a set of $C(H)$ and H which was self-consistent in the sense that they both were located at the step function change. Thus it is possible to perform an iterative search for a suitable σ using solution consistency as a constraint (see Fig. 5).

5.0 Summary

Whenever one encounters a geothermal reservoir problem wherein the geothermal fluid flashes from water to steam, the governing equations become highly nonlinear. Oscillatory and non-convergent solutions are sometimes encountered for selected nodes and time steps. The correct solution may reside exactly on the two-phase boundary and require coefficient values which are neither those of the single-phase region nor the two-phase region, but rather a weighted average of the two. An inverse iterative scheme based on the requirement of self-consistency in the solution has been developed to identify the value of the optimal weighting coefficient.

6.0 Notation

6.1 Letters

C_α Nonlinear coefficient.

g Gravitational acceleration.

h Enthalpy.

H Thermodynamic property used as independent variable.

k Permeability.

k_r Relative permeability.

p Hydrodynamic pressure.

S Saturation.

T Temperature.

V Velocity.

Δx Spatial increment.

ε^* Small increment.

κ Thermal conductivity.

θ Porosity.

ρ Density.

σ Weighting factor for nonlinear coefficients.

μ Viscosity

6.2 Subscripts

f Reservoir fluid.

i,k Nodal numbers.

m Solid grains.

s Steam phase.

w Water phase.

7.0 References Cited

Voss, C. I., Finite Element Simulation of Multiphase Geothermal Reservoirs. Ph.D. Thesis, Princeton University, 1978.

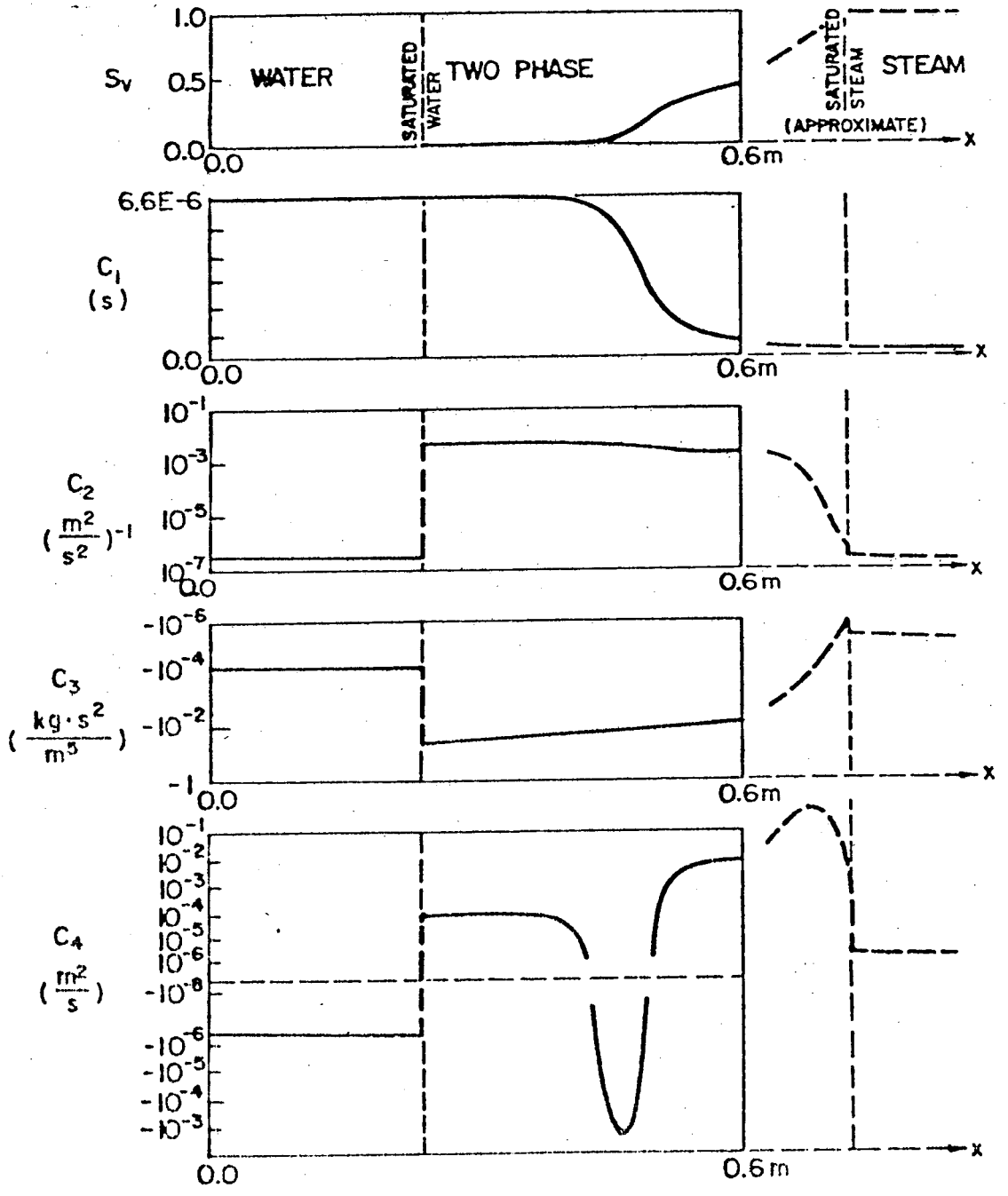

Fig. 1. Nonlinear coefficients for two-phase, non-isothermal problem (after Voss, 1978).

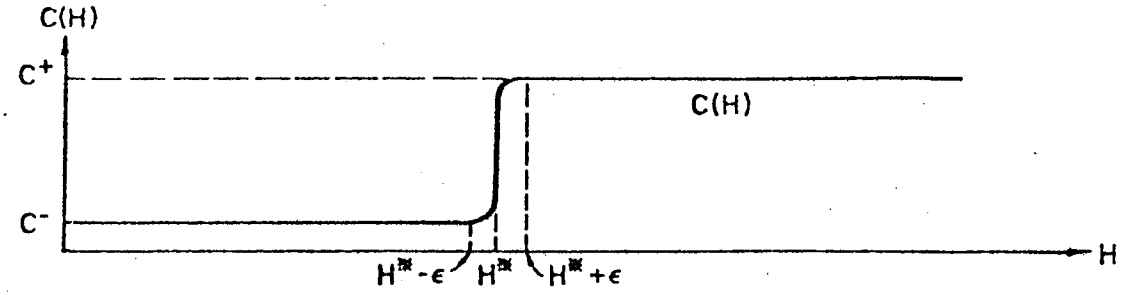

Fig. 2. Hypothetical step-function coefficient C(H) (after Voss, 1978).

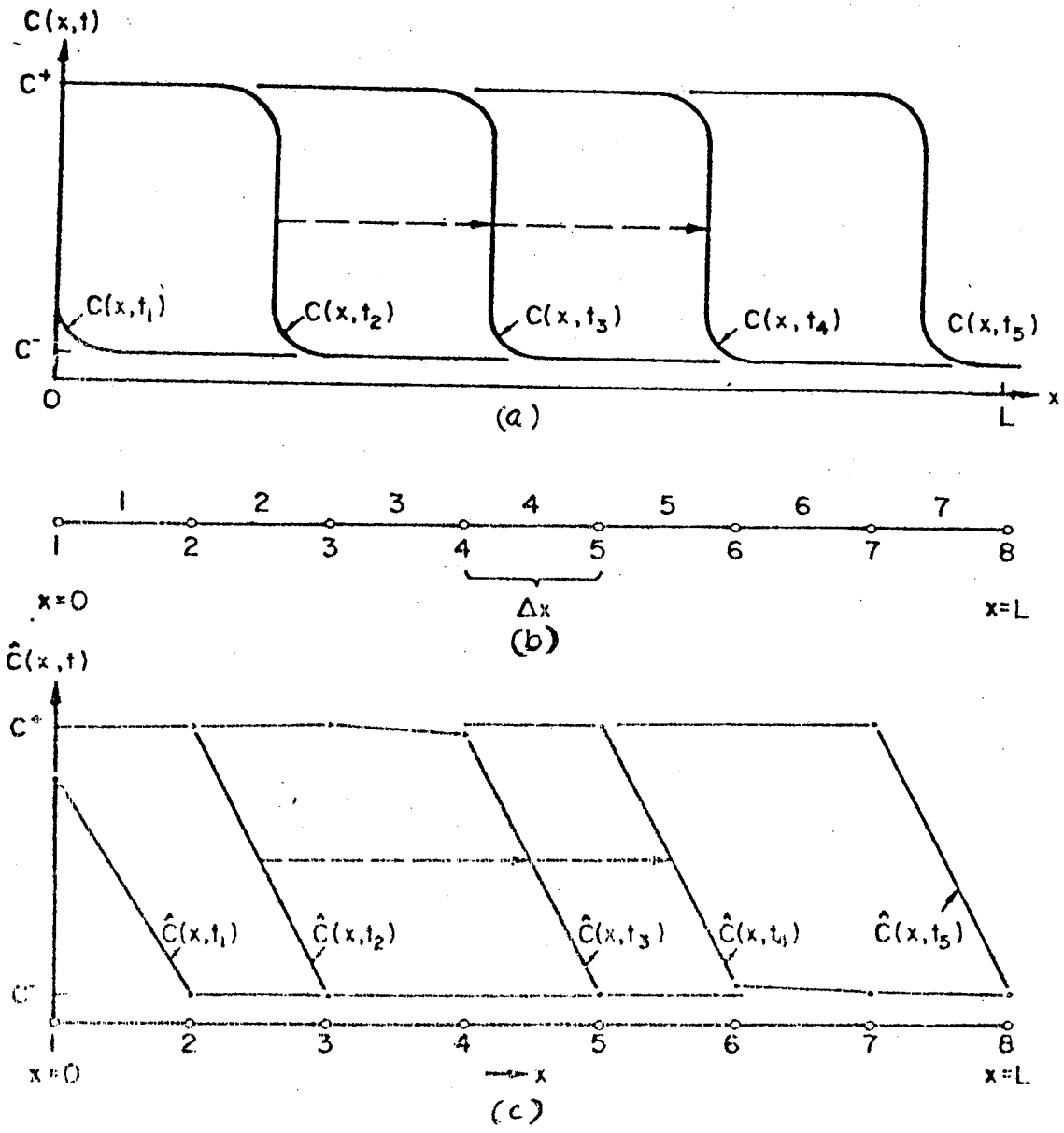

Fig. 3. (a) Smooth progression of nonlinear coefficient, (b) finite element net in one dimension, (c) progression of nonlinear coefficient with discretized operator (after Voss, 1978).

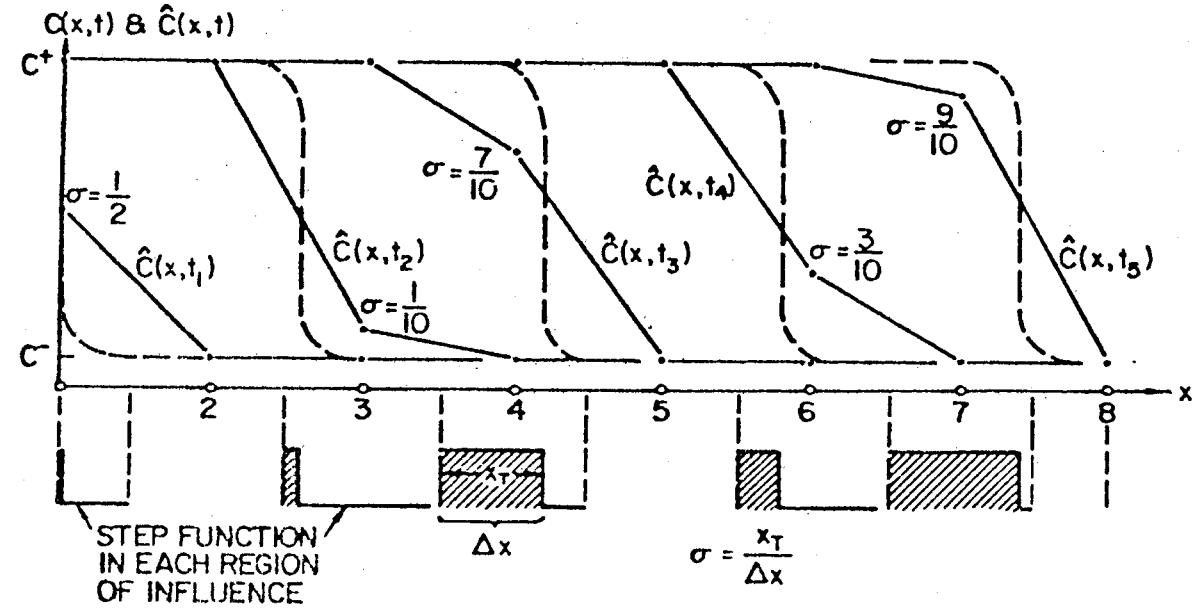

Fig. 4. Propagation of nonlinear coefficient using correction procedure (after Voss, 1978).

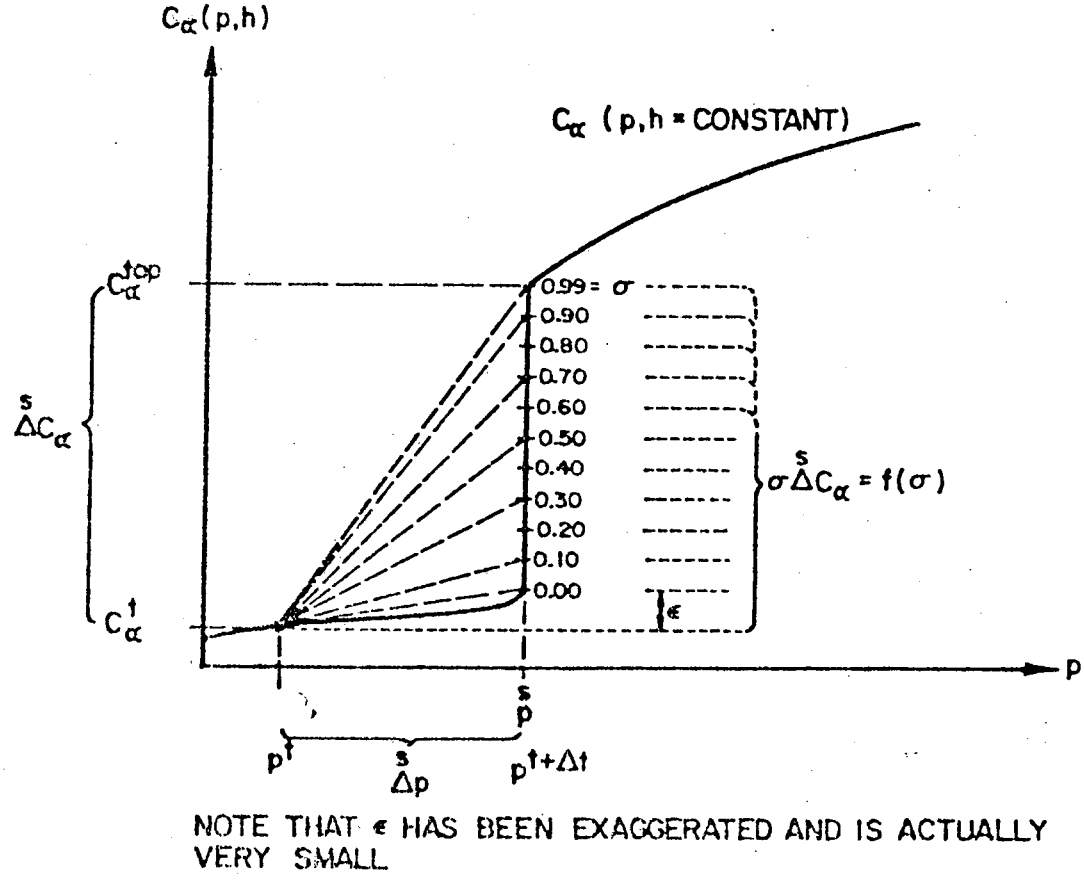

Fig. 5. Inverse iteration algorithm (after Voss, 1978).

PREDICTING THE PRECIPITATION OF AMORPHOUS SILICA FROM GEOTHERMAL BRINES

Oleh Weres, Andrew Yee, and Leon Tsao
Earth Sciences Division
Lawrence Berkeley Laboratory
Berkeley, CA 94720

I. The Homogeneous Nucleation of Colloidal Amorphous Silica

The voluminous gel-like deposits encountered at Cerro Prieto, Wairakei, and Niland consist of flocculated colloidal amorphous silica. The crumbly grey and white scales associated with the gel-like materials are cemented colloidal aggregates. This colloidal silica is produced by homogeneous nucleation in the liquid phase; i.e., nucleation by growth of polymers to critical nucleus size without the participation of some preexisting solid particle.

With most substances heterogeneous nucleation is dominant, and homogeneous nucleation is very slow, rare in nature, and difficult to study in the laboratory. The precipitation of amorphous silica is an apparent exception to this because of the very low surface tension of the silica-water interface - between 35 and 50 ergs cm^{-2} over the range of major practical interest. (By comparison, the surface tension of the water-air interface is about 70-80 ergs cm^{-2}.) This means that enormous numbers of particles can be produced by homogeneous nucleation (on the order 10^{17} to 10^{18} per liter), and this completely swamps the effects of heterogeneous nucleation.

A practical consequence of the dominance of homogeneous nucleation is that the precipitation of amorphous silica is experimentally reproducible and predictable. This is because the rate of homogeneous nucleation is determined by basic thermodynamic and chemical variables (concentration, surface tension, etc.) and not by often unknown trace contaminants as is the case with heterogeneous nucleation.

Figure 1 shows some typical experimental results which depict the decline of dissolved silica with time via the homogeneous nucleation mechanism. These experiments were performed at various pH's in a low salinity buffered medium in which the sodium ion activity was approximately 0.069M, and the time scales were shifted to convert all data to a nominal pH of 7.0. These conditions are approximately equivalent to a .088M (=5200 ppm) NaCl solution at pH 7. Note that the time scale in Figure 1 is logarithmic. With an initial concentration of 1.1g/liter of SiO_2, the reaction runs most of the way to completion in less than 10 minutes.* With an initial concentration of 0.5g/liter, it takes about 5,000 minutes. In

*Here and elsewhere in this paper, concentrations are expressed in terms of grams or moles/liter referred to room temperature. Therefore, we mean that this solution would contain 1.1g/l SiO_2 if cooled to room temperature, but not necessarily at 75°C.

other words, with a large initial saturation ratio, amorphous silica gels may form within the process equipment and associated piping. This is observed at Cerro Prieto and Niland. With small saturation ratios (0.5g/l corresponds to S=1.9 at this temperature), massive precipitation will not occur within the process equipment, but just as certainly will occur somewhere further downstream. Also note that 0.5 and 0.7g/l curves show an induction period during which the concentration does not change noticeably.

We have generated a large quantity of such nucleation data from room temperature to 100°C and have written a computer program which can numerically (and rigorously) model the homogeneous nucleation process; i.e., it can reproduce the curves in Fig. 1. After we have fitted the necessary parameters using our experimental data, we will be able to quantitatively model and predict the process, even under the experimentally inaccessible conditions characteristic of field practice. This program will be documented and made available to interested outside users.

II. Molecular Deposition on Solid Surfaces

By molecular deposition we mean the formation of compact, nonporous amorphous silica by chemical bonding of dissolved silica molecules directly onto solid surfaces.

Below about 100°C, homogeneous nucleation is usually the dominant precipitation mechanism. The major significance of molecular deposition here is that it is the molecular mechanism of the growth of colloidal particles and of the conversion of gel-like deposits to solid scale. However, at higher temperatures molecular deposition from solution may by itself produce scale at a significant rate. Although the deposition rate is very small (about 1 mm/year in the flashed brine pipes close to the steam separators at Cerro Prieto), this scale is almost indestructible once formed.

We studied the molecular deposition process by adding known amounts of colloidal silica of known specific surface area to our solutions. Deposition rates at pH 7, $[Na^+] = 0.069$ and various temperatures and dissolved silica concentrations were calculated (and extrapolated) from our experimental data and are presented in Figure 2. The dashed line represents the approximate concentration limit above which homogeneous nucleation supersedes deposition on added particles as the dominant mechanism. Our data actually covers only the range between 50 and 100°C and below the dashed line. However, we believe the extrapolated values to be good enough for practical application.

At any given concentration, there is a temperature at which the deposition rate has a maximum value. Below this temperature, the rate increases with temperature in the usual way. Above this temperature, the rate of deposition decreases because the increasing solubility of silica causes the rate of the back reaction (i.e., dissolution) to increase even more rapidly. At the saturation temperature for any given concentration, the deposition rate goes to zero. The practical consequence of this is that the molecular deposition rate is a weak function of temperature at temperatures lower than about 15°C below the saturation temperature. However, the rate varies strongly with silica concentration. (Our data is best fitted by an apparent fourth order rate law.)

III. Effects of pH and Salinity

It has long been believed that the rate of amorphous silica deposition is proportional to the surface density of ionized silanol groups on the silica surface. Our experiments on the pH dependence of the rate proved this hypothesis conclusively. We found that the rate as a function of pH calculated from our data matched surface charge vs. pH data in the literature to within experimental error.

The rate as a function of pH for $[Na^+]$ = 0.069 is presented in Figure 3. The function plotted in Figure 3 is the rate at any given pH relative to the rate at pH 7. Increasing the pH at constant salinity increases the rates of molecular deposition and homogeneous nucleation by the same factor. The effect upon the latter is a consequence of the effect upon the former.

We found that the reaction rate ceases to increase in proportion to surface change at about pH 8. This is due to the offsetting effect of the increase of silica solubility with increasing pH. Our data suggest that a constant pH correction factor of about 2.7 is adequate between about pH 8 and 9. The results presented here should not be used above pH 9.

Dissolved salts have two important effects upon these processes:

1) They decrease the solubility of amorphous silica and, thereby, increase the rate of homogeneous nucleation.

2) Increasing the salt concentration at constant pH increases the surface charge density and, thereby, the rate of molecular deposition.

The second effect increases the rates of molecular deposition and homogeneous nucleation by the same factor. The first effect increases only the rate of homogeneous nucleation. It will be discussed in detail elsewhere.

Except at very low salinity, most of the dissociated silanols on the silica surface have cations bound to them - in the case of our experiments, sodium. This means that sodium and hydrogen ion activity do not have independent effects upon the rate; rather, it is the ratio of sodium to hydrogen activity that is important. Therefore, Figure 3 may be used to calculate the effect of salinity upon the molecular deposition rate as well.

To do this, calculate a "nominal pH value" defined by

$$\text{pH nom} = \text{pH} + \log \frac{[Na^+]}{0.069}$$

and then read off the pH correction factor from Figure 3 using the nominal pH value instead of the real one.

For example, to calculate the molecular deposition rate at 100°C, pH 6.5, $[Na^+]$ = 0.69M and 0.7g/l dissolved silica:

First, read the deposition rate at pH7.0 and $[Na^+]$ = 0.069M from Figure 2. This value is 0.22 μm/day. Second, calculate pH nom using the equation above. This is 7.5. Third, read the pH correction factor for pH 7.5 from

Figure 3; this is 1.8. Finally, multiply the two numbers together to obtain the deposition rate which is 0.40 μm/day.

Our data suggest that this procedure is adequate for solutions which contain up to at least 1M NaCl, and it may be adequate at even higher salinities. However, it cannot be recommended for use at salinities much below 5200 ppm. At very low salinities dissociation without ion pairing becomes important, and the basic assumption of the equivalent and opposite effects of hydrogen and sodium activity collapses. We hope to remedy this shortcoming by detailed reanalysis of the low salinity surface charge data in the literature.

The dissolved solids in real geothermal brines are usually predominantly sodium chloride, but other salts are also present. We have found that, in most cases, it is sufficient to use an "effective sodium ion activity" calculated as 0.77 times the (molar) concentration of chloride. If bicarbonate is present as a major ion, use the sum of the chloride and bicarbonate concentrations in place of chloride alone. The rationale for this procedure is that the various other major cations that may be present have essentially the same effects as sodium, and the activity lowering effects of divalent anions approximately compensate for the concentration of the cations that accompany them.

IV. Some Practical Examples; or, How Not to Reinject

Case 1):

Consider a hypothetical geothermal development at which the spent brine contains 5200 ppm NaCl, 0.5g/l dissolved SiO_2, and is delivered to the reinjection well at 75°C and pH 7. The brine delivered to the reinjection well is completely clear and goes right through a membrane filter. The decision is made to reinject. Reinjection commences at 400t/hr into an aquifer of 200°C initial temperature, ϕ=0.1, h=20 m and volumetric solid rock heat capacity = 2460kj/m^3 C. After about 12 days the thermal front is about 60 meters into the formation, and the fluid travel time from wellbore to thermal front is about 50 hour = 3,000 minutes. Referring to Figure 1, we see that there is now ample time for homogeneous nucleation to occur before the fluid reaches the thermal front. The result is that the injectability of that horizon is damaged by silica precipitation. Furthermore, well treatments with caustic or HF are not effective because the damage is 30 to 60 meters away from the wellbore.

Case 2):

Can one reinject straight from the first stage steam separators at Cerro Prieto? Assume the following typical brine conditions at the injection well: 160°C, 0.95 g/l dissolved SiO_2, effective $[Na^+]$ = 0.25, and negligible suspended solids. The brine pH at injection temperature is not known, but is approximately 7.8 at room temperature. This gives a nominal pH of about 8.3 (which is within the range of weak pH dependence) and a pH factor of 2.7 (from Fig. 3). The pH nom = 7.0 deposition rate is read from Fig. 2 as about 1.3μm/day. Correcting for pH, we obtain the actual deposition rate of 3.5μm/day = 1.3 mm/year. This is consistent with the observed rate of vitreous silica deposition near the separators at Cerro Prieto. Because pore permeability is dominant at Cerro Prieto, it is clear that injecting this brine would rapidly plug the injection well.

We hope that such mistakes will be avoided. However, we emphasize that both of these brine streams would be deemed injectible under the criteria presently in vogue: they would be able to pass freely through a micron-sized membrane filter and would not cause visible fouling of metal surfaces during field tests of a few days duration. It is precisely the refinement of such criteria that we hope to have accomplished with the work summarized here.

Acknowledgements

The work reported here was supported by the Division of Geothermal Energy of the U. S. Department of Energy.

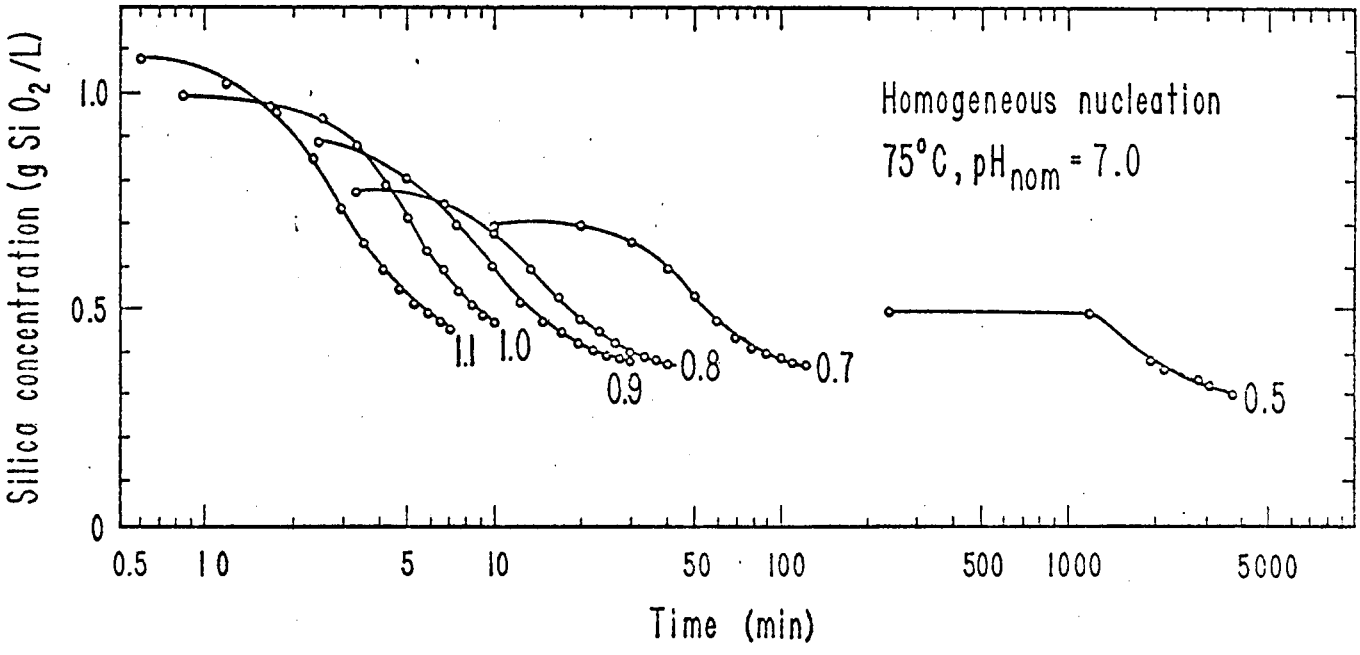

Figure 1. Decrease of dissolved silica concentration with time under conditions of homogeneous nucleation at 75°C, pH 7.0 and sodium activity = 0.069M. Numbers on Figure indicate initial dissolved silica concentrations.

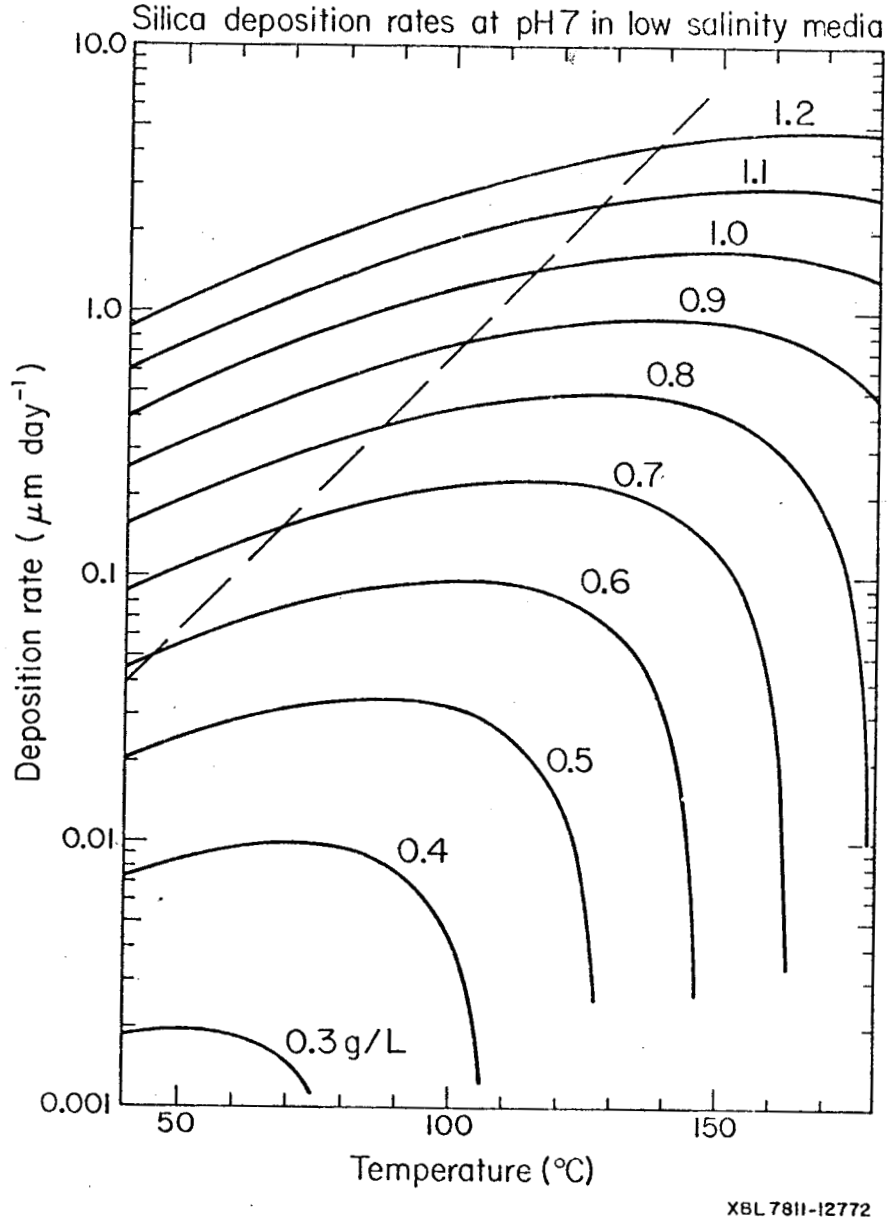

Figure 2. Rates of molecular deposition of silica upon a flat surface at pH 7.0 and sodium activity = 0.069M. Dissolved silica concentrations corresponding to each curve indicated in g/liter referred to room temperature.

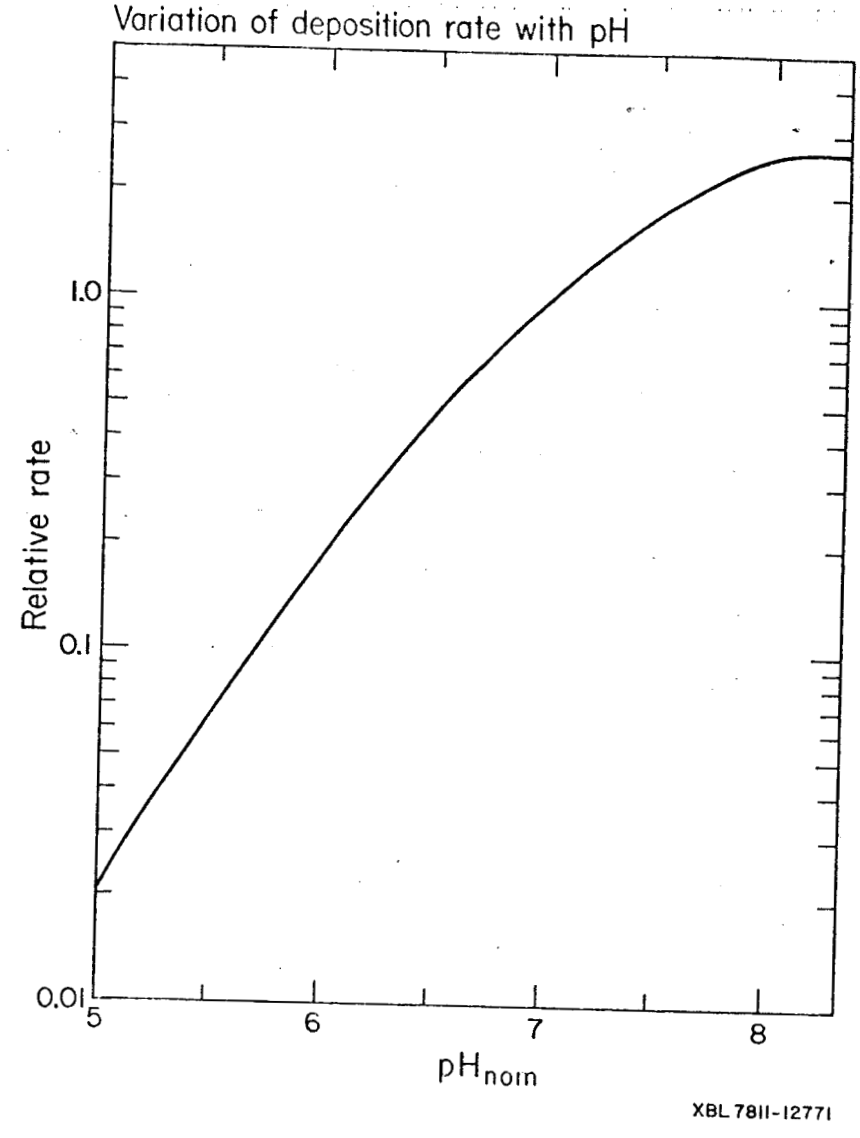

Figure 3. Variation of molecular deposition rate with pH_{nom}. Curve gives the rate as a function of pH_{nom} relative to the rate at pH_{nom} = 7.0. At pH_{nom} greater than 8, use the value 2.7 for the pH correction factor. When sodium activity = 0.069M, pH_{nom} = pH.

Dup

HEAT AND MASS TRANSFER STUDIES OF THE EAST MESA ANOMALY*

K.P. Goyal** and D.R. Kassoy
University of Colorado
Boulder, Colorado 80309

Heat and mass transfer due to convection in a two-dimensional model of the East Mesa geothermal system are presented in this paper. These results are an extension of those presented by Goyal and Kassoy (1977). Geological, geophysical, geochemical, and borehole logging data suggests the existence of four different zones in this anomaly. Basement, the deepest zone, is about 4 km from the surface (Combs and Hadley, 1977) and carries nearly vertical tensile fractures (Bailey, 1977). These fractures would increase the vertical permeability much more than the horizontal permeability. A clay-dominated zone overlies the basement and extends to about 1.9-2.2 km from the surface. The vertical permeability of the sediments in this zone is expected to be good near the fractures. The horizontal permeability is thought to be only moderate because of the presence of clay and dirty sands. Sands dominate the sedimentary zone from about 800-1900 meters depth. Both horizontal and vertical permeabilities in this zone are expected to be better than the underlying zone because of greater sand contents, continuity, and less compaction. The fourth zone, containing large amounts of clay, is represented by the upper 600 meters or so. The vertical permeability is probably very low in these sediments but the numerous shallow wells in them indicate that their horizontal permeability is good. The major source

---

* Research supported by NSF(RANN) and ERDA Geothermal Programs.

** Present address: Earth Science Division, Lawrence Berkeley Laboratory, University of California, Berkeley, California 94720.

of fluid for Southern Imperial Valley brines is the underflow from the Colorado River. This water percolates gradually into sediments and/or fractured basement rock over an area considerably larger than the anomaly itself. Heated at depth by an as yet undefined source, the liquid can rise in the high permeability fractured fault zone, convecting energy toward the surface. When a horizontal aquifer is intersected (relatively large horizontal permeability), reservoir charging will occur.

A two-dimensional mathematical model of this system is shown in Figure 1. The Mesa fault is assumed to act as a conduit for the rising hot water (Combs and Hadley, 1977). Liquid rises in the reservoir section of the fault. The presence of clays in the cap suppresses the vertical transport there. Water pushed out of the fault by the overpressure associated with convection is assumed to flow horizontally in the aquifer. Spatially uniform temperature boundary conditions are imposed on the cold cap surface and at the hot bottom boundary of the reservoir. On the lateral boundary far from the fault (H'>>L'>>ye'), the temperature distribution is assumed to be controlled by vertical conduction. A quasi-analytic theory is developed for high Rayleigh number convection of a liquid in a rigid porous medium. In this approximation liquid rises up the fault and spreads into the near region of the reservoir adiabatically. The cooling effect of the cap in the reservoir is confined to a thin layer adjacent to the interface. The layer grows with distance from the fault. In the far field, full depth of the aquifer is cooled by the surface.

The following simplifying assumptions are made in the analysis:

(i) Flow is steady.

(ii) Physical properties such as coefficient of thermal expansion, specific heat, and medium thermal conductivity are assumed constant.

(iii) Fault medium is isotropic.

(iv) Fault and aquifer are homogeneous in the x-y plane.

(v) Vertical permeability in the aquifer is zero. The presence of shaly layers, associated with the interbedding, makes the vertical transport unimportant in the global sense.

(vi) The ratio (permeability/kinematic viscosity) is a constant. This is a qualitative representation of the decrease of kinematic viscosity with depth (associated with increasing temperature) and the corresponding decrease in permeability due to compaction. In actual situations precise compensation is not achieved.

Figures 2 and 3 show the near fault and far field temperatures in the aquifer and cap at different distances away from the fault. The nondimensional parameters used in these figures are defined as below:

z = actual vertical distance/reservoir depth (L')

y = horizontal distance/reservoir depth (L')

$\hat{y}$ = horizontal distance/reservoir length in y-direction (H')

ℓ = cap thickness/reservoir depth (L')

ye = semi-fault width/reservoir depth (L')

d = an O(1) number

λ = thermal conductivity of the cap/thermal conductivity of the aquifer

M = actual mass flow rate/reference mass flow rate

T = actual temperature/reference temperature

τ = temperature difference across the reservoir/ reference temperature

R = Rayleigh number = reference convection heat transfer/ reference conduction heat transfer

It can be noted that the predicted temperatures in the near field (Figure 2) are quite like that for Mesa well 8-1, 44-7, and 48-7. Far field profiles as in Figure 3 can be related to those in 5-1, 31-1, and the Republic geothermal wells. Surface heat flux ratio (near fault/far field) can be obtained from the Comb's contours (Goyal, 1978) drawn for the East Mesa area. A similar ratio can also be obtained from the Figure 4 which is plotted for the temperature gradient at the surface vs. horizontal distance from the fault. A detailed analysis of this work and the effect of the various parameters is available in Goyal (1978).

References

Bailey, T. (1977). CUMER-77-4-Mechanical Engineering Department, University of Colorado, Boulder.

Combs, J. and Hadley, D. (1977). Geophysics 42, 17.

Goyal, K. P. (1978). PhD thesis, Mechanical Engineering Department, University of Colorado, Boulder.

Goyal, K. P. and D. R. Kassoy (1977). Proceedings of the Third Workshop on Geothermal Reservoir Engineering, Stanford University, pp. 209-213.

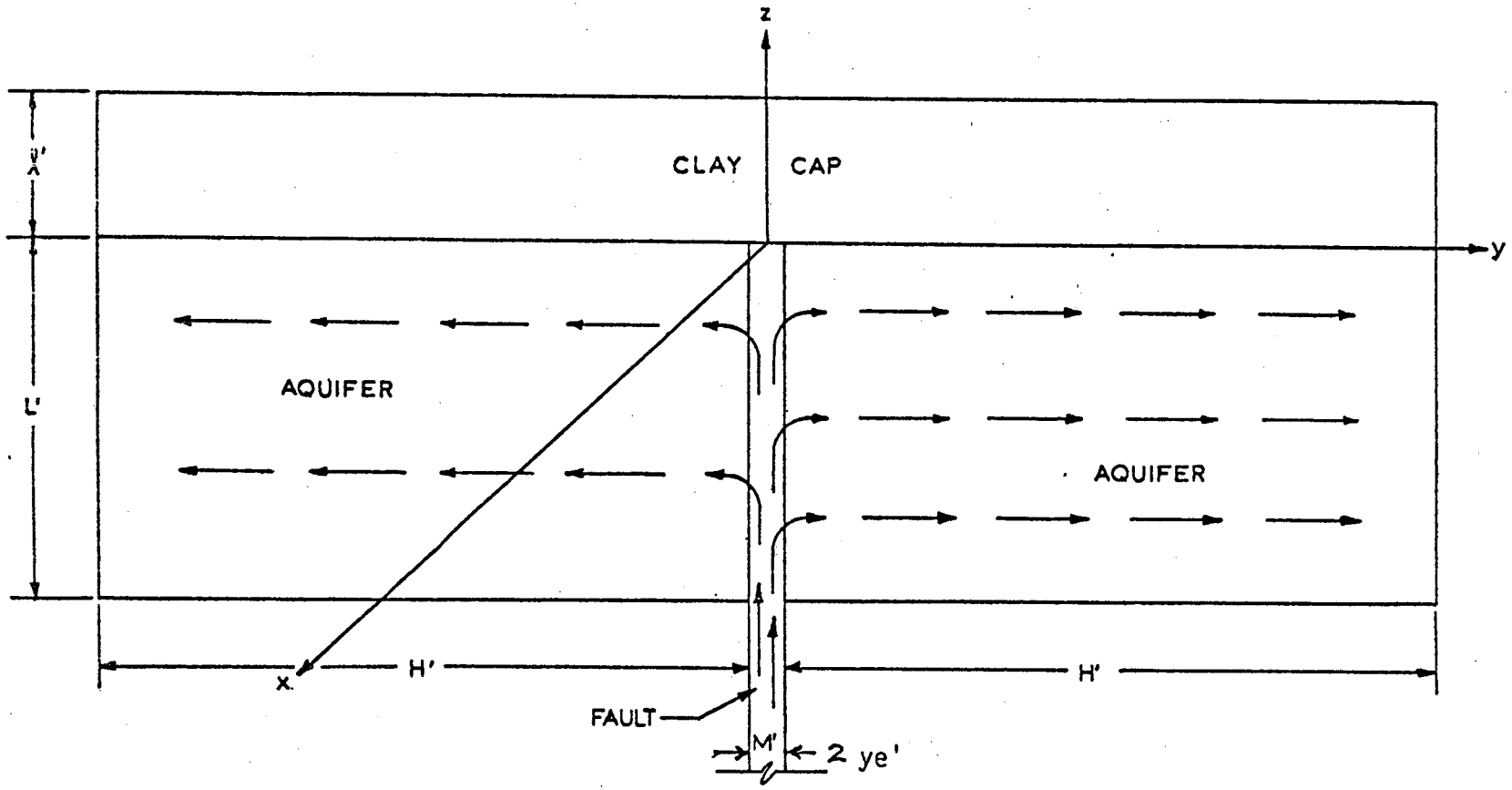

Figure 1: Mathematical Model of the East Mesa Geothermal System.

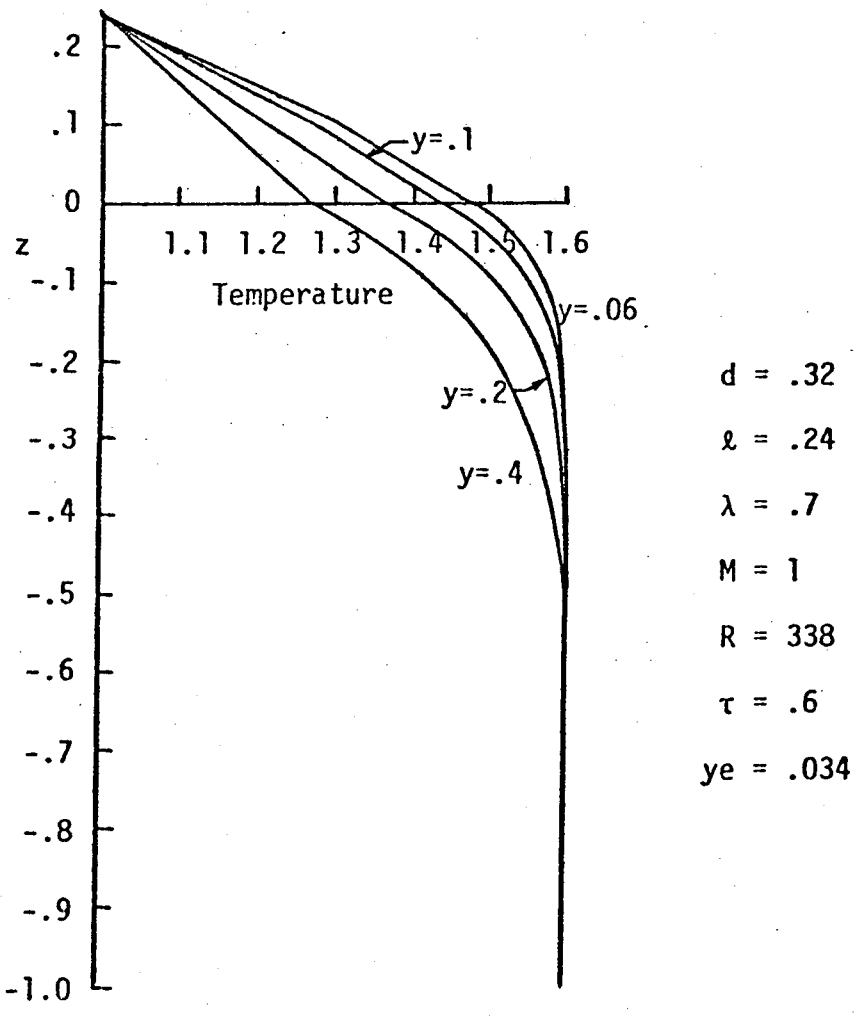

Figure 2: Near Fault Temperatures in the Aquifer and the Cap for Different Values of y

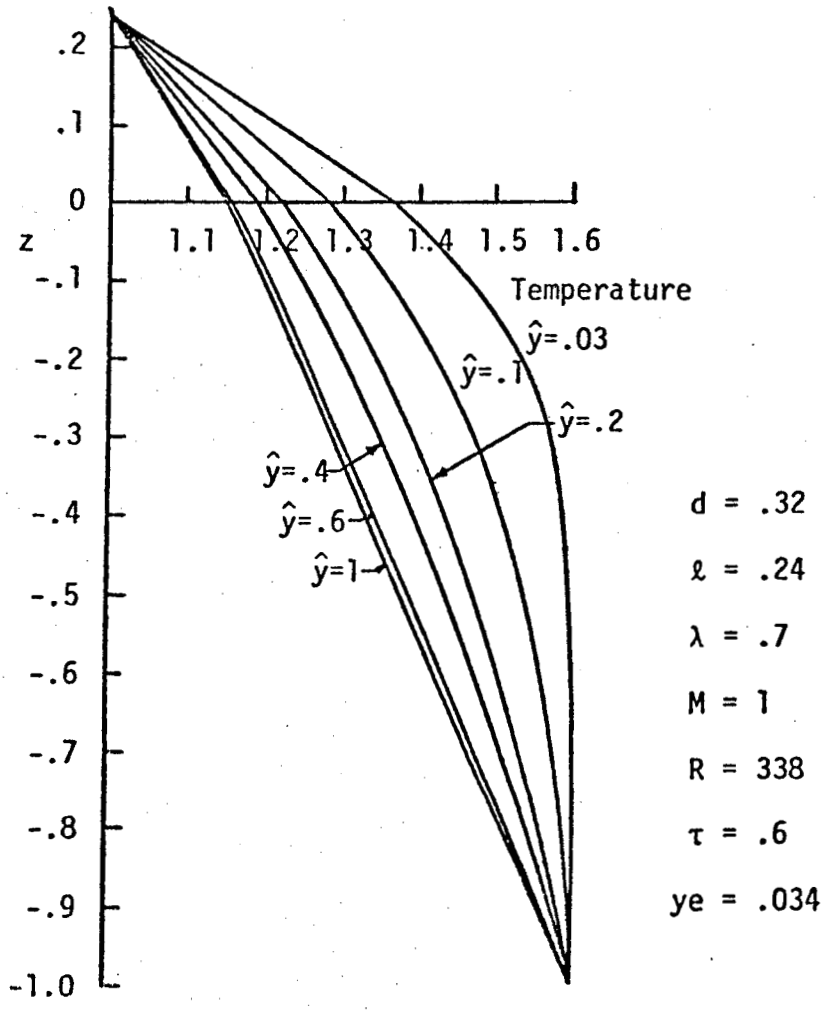

Figure 3: Temperature in the Aquifer and the Clay Cap at Different Locations away from the Fault

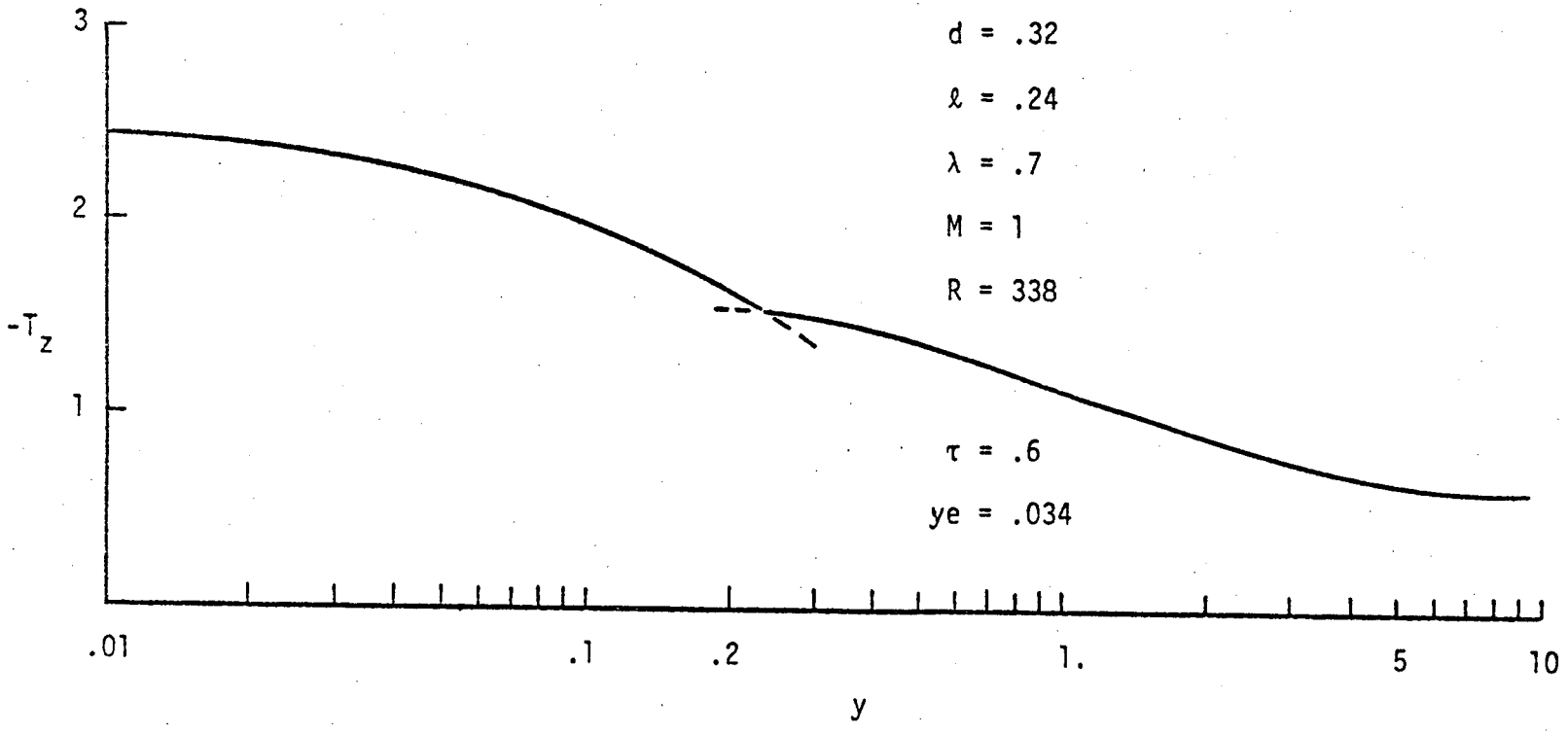

Figure 4: Surface Temperature Gradients vs. Length of the Aquifer

Dup

STUDIES OF FLOW PROBLEMS WITH THE SIMULATOR SHAFT78

K. Pruess, R.C. Schroeder, J. Zerzan
Lawrence Berkeley Laboratory
University of California
Berkeley, California 94720

In recent years, a number of numerical simulators for geothermal reservoirs have been developed. The general purpose of these is to aid reservoir engineers in (i) determining characteristic parameters of reservoirs (most important among those being the reserves of fluid and heat), and (ii) simulating the performance of reservoirs upon production and injection.

The various simulators differ in the approximations made in the underlying physical model (e.g., dependence of rock and fluid properties upon thermodynamic variables), in the geometrical definition of the reservoir (one-, two-, or three-dimensional, regular or irregular shape), in the choice of thermodynamic variables, and in the mathematical techniques used for solving the coupled mass and energy transport equations.

Criteria for desirable performance of numerical simulators depend in part upon the particular problems to be investigated. Different problems will often differ in the required level of detail to be resolved, and in the optimum balance of speed and accuracy of computation. Much can be learned about two-phase flow in porous media from model studies for idealized systems. Such studies can be performed with less-than-three-dimensional models, and algorithms which are based on regular grid spacings will be perfectly acceptable. For modeling natural geothermal reservoirs, on the other hand, it is important that irregular three-dimensional geometries may be handled easily.

In comparison with other two-phase simulators which have been discussed in the literature, the main distinctive feature of SHAFT78 is that it uses an integrated finite difference method (IFD). We solve finite difference equations that are obtained by integrating the basic partial differential equations for mass and energy flow over

discrete surface and volume elements. This method is as easily applicable to irregular geometries of actual reservoirs as it is to idealized, regular geometries; yet the relative simplicity of the finite difference method is retained in the theory and algorithms.

The purpose of this paper is to give a brief review of the basic concepts associated with SHAFT78 and the IFD approach, and to present comparisons of SHAFT78 calculations with some analytical solutions. The comparisons include both single-phase and two-phase water problems and demonstrate the accuracy and calculational stability of the algorithm.

The governing equations for mass and energy transport in porous media when both rock and fluid are in local thermodynamic equilibrium can be written

$$\frac{\partial \phi \rho}{\partial t} = - \vec{\nabla} \cdot \vec{F} + q \qquad \text{(1a)(Mass)}$$

$$\frac{\partial U_{vol}}{\partial t} = - \vec{\nabla} \cdot [\vec{F}_\ell H_\ell + \vec{F}_v H_v - K\nabla T] + \{[\frac{\vec{F}_v}{\rho_v} + \frac{\vec{F}_\ell}{\rho_\ell}] \nabla P + \text{dissipative}\} + Q \qquad \text{(1b)(Energy)}$$

$$\vec{F} = - k [\frac{k_\ell}{\mu_\ell} \rho_\ell (\nabla P - \rho_\ell \vec{g}) + \frac{k_v}{\mu_v} \rho_v (\nabla P - \rho_v \vec{g})] \qquad (2)$$

Under suitable assumptions, we get the integrated form of equations (1)

$$\frac{d}{dt} \int_V \phi \rho dV = \int_A \vec{F} \cdot \vec{n} da + \int_V q dV \quad (\vec{n} \text{ the inward normal}) \qquad (3a)$$

$$\frac{d}{dt} \int_V U dV = \frac{\int_A \{\vec{F}_\ell H_\ell + \vec{F}_v H_v - \vec{F} U_{ave} - K\nabla T\} \cdot \vec{n} da + \int_V (Q - Uq) dV}{\{\phi\rho + (1-\phi) c_{rock} \rho_{rock} [(\frac{\partial T}{\partial U})_\rho + (\frac{\partial T}{\partial \rho}) \frac{(\partial \rho / \partial t)}{U(\partial U / \partial t)}]\}_{ave}} \qquad (3b)$$

The solution to equations (3) is computed on a polyhedral partitioning of the reservoir whose connected components share a common

polygonal interface. Volume and interface averages are computed using standard finite difference techniques.[1,2] The fluid parameters are obtained by bilinear interpolation (triangular interpolation near the saturation line and in the liquid region)[1] using an inverted form of the 1967 ASME Steam Tables.

It is clear on examination that equations (3) are nonlinear and coupled. These are solved by reduction to an appropriate linear approximation at each time step. Accuracy controls are set to allow only small variations in all parameters over a given time step. The energy equation is solved first using density changes predicted by the behavior of the system in the previous time step. Thus, a good estimate for the expected change of fluid energy over the energy time step can be made, which is subsequently corrected during the density time steps. Special interpolation procedures and automatic time-step controls ensure high accuracy of the calculation even when phase transitions occur (elements crossing the saturation line).[2]

An iterative strategy is employed in solving the discretized version of equations (3) after the first-order explicit solution has been generated in each time step. The time-averaged flux terms F (density) or $F_\ell H_\ell + F_v H_v - F\ U_{ave}$ (energy) are written as

$$\overline{F} = \overline{F}(t + \theta\Delta t) = \overline{F} + \theta\Delta t \frac{\partial F}{\partial t} \qquad (4)$$

and an iteration is performed over the whole mesh to minimize the residual term.[1,8]

SAMPLE PROBLEMS

In order to evaluate the SHAFT78 program, calculated results were compared to numerical calculations reported in the literature (e.g., Toronyi[7] and Garg[5]), and to analytic solutions. The remainder of this paper is devoted to a comparison of the computed solutions with the analytic results.

SINGLE-PHASE VAPOR

In 1957 R.E. Kidder presented to the ASME[3] the solution to the problem of isothermal flow of a gas (obeying Darcy's and Boyle's laws) in the semi-infinite homogenous porous solid.

Specifically, the problem solved was

$$\frac{\partial}{\partial x}\left[p\,\frac{\partial p}{\partial x}\right] = \phi\,\frac{\mu}{k}\,\frac{\partial P}{\partial t} \qquad (5)$$

with initial conditions

$$P(x,0) = P_o \quad 0 < x < \infty \qquad (6)$$

and boundary conditions

$$P(0,t) = P_1 < P_o \quad 0 < t < \infty \qquad (7)$$

SHAFT78 was run on a 30-element linear mesh with internode distances of .2m, and large nodes at the boundaries of the grid with the appropriate boundary conditions. Initial conditions were

P_o = 5MPa
T_o = 300 ^oC

with rock properties

$k = 10^{-12}\ m^2$, $K_{rock} = 0$, $c_{rock} = 10^7\ J/kg^oC$, $\rho_{rock} = 2200\ kg/m^3$, $\phi = .2$

Three boundary conditions on the left of the grid

P_1 = 4MPa
P_1 = 2MPa
P_1 = 1MPa

were chosen and the results are compared with the analytic solution for each case in Figure 1.

The computed solution shows a slightly lower pressure drop than the analytic solution. This is probably due to inaccuracies introduced in the boundary approximations.

SINGLE-PHASE LIQUID

To evaluate the performance of SHAFT78 in the liquid region, the "Theis problem"[4] was run on a 15-element mesh with a large element at the outer boundary to simulate the reservoir conditions at infinity.

Reservoir conditions were

Thickness	= 100 m
Initial pressure	= 20.37 MPa
Initial temperature	= 180 ^{o}C
Rock porosity	= .2
Permeability	= 10^{-13} m^2
Rate of fluid withdrawal	= 18 kg/s·m

The results are compared in Figure 2 to the analytic solution of the line source problem (t_D vs P_D on a log-log scale)

$$\nabla^2 P = \frac{\phi\mu c}{k}\frac{\partial P}{\partial r} \tag{8}$$

$$P(r,o) = P_o \quad \text{initial conditions} \tag{9}$$

$$\left.\begin{aligned} \lim_{r\to\infty} P(r,t) &= P_o \\ \lim_{r\to\infty} \frac{2\pi rk}{\mu}\frac{\partial p}{\partial r} &= -q \end{aligned}\right\} \quad \text{boundary conditions (Constant flux with Darcy assumption)} \tag{10}$$

with solution given by the exponential integral

$$P = P_o + \frac{q\mu}{4\pi k}\,\mathrm{Ei}\left\{\frac{-r^2}{4t}\frac{\phi\mu c}{k}\right\} \tag{11}$$

Agreement is close near the sink (to the right of the plot) with deviations increasing to the left. The scatter of computed points around the analytic solution seems to reflect a deviation from the

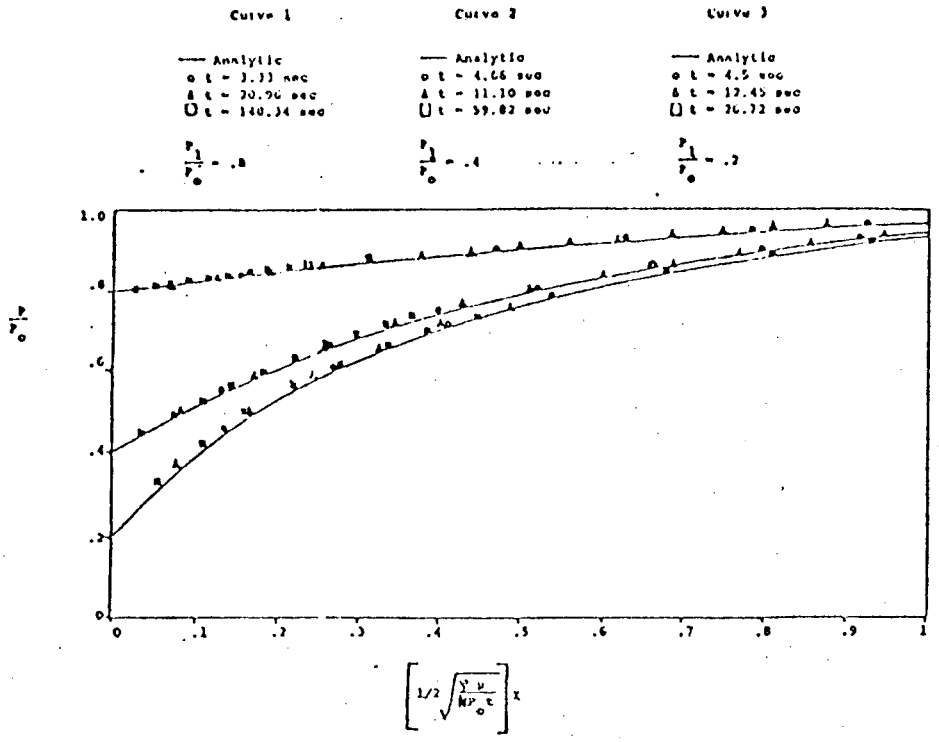

FIGURE 1

KIDDER PROBLEM ANALYTIC VS. COMPUTED SOLUTION

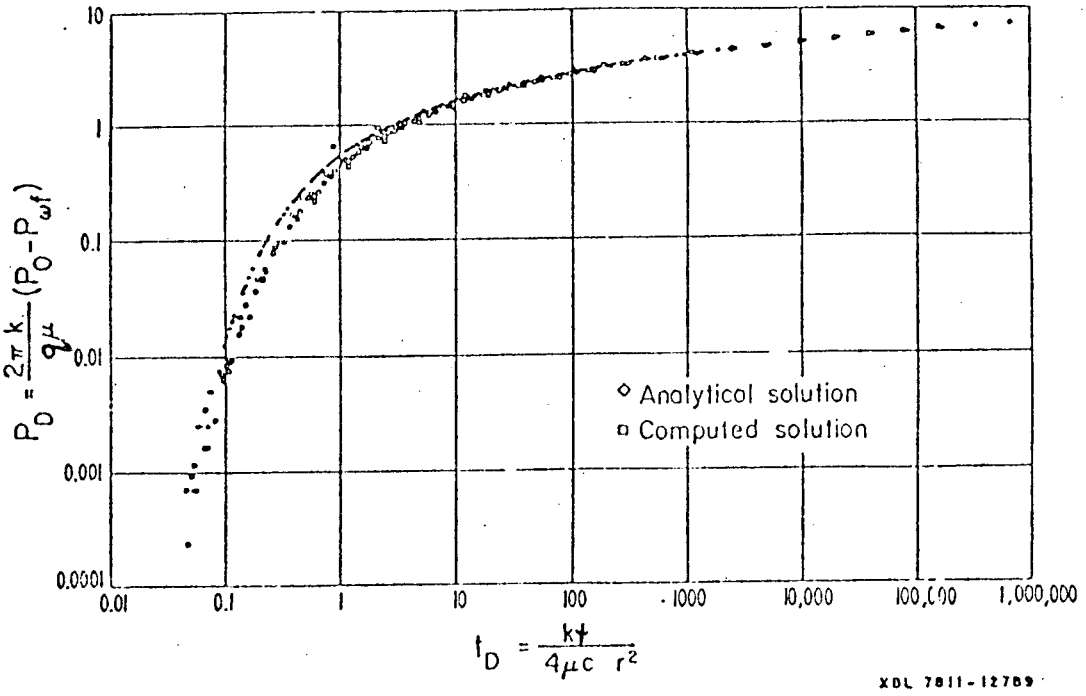

FIGURE 2

THEIS PROBLEM ANALYTIC VS. COMPUTED SOLUTION

solution at late times and large radius when the boundary approximation becomes less accurate.

TWO-PHASE RESERVOIR

Garg derives an approximate diffusivity equation[5] for pressure in a two-phase reservoir initially at equilibrium pressure p_o, which is valid near the wellbore.

$$\frac{\partial P}{\partial t} - \frac{(k/\nu)_T}{\phi \rho C_T} [\nabla^2 P] = 0 \tag{12}$$

Here we have introduced the total kinematic mobility

$$(\frac{k}{\nu})_T = k[\frac{k_\ell}{\mu_\ell} \rho_\ell + \frac{k_v}{\mu_v} \rho_v]. \tag{13}$$

For a line source, we have the boundary conditions at the well

$$r \frac{\partial P}{\partial r}\Big|_{r=r_w} = - \frac{q}{2\pi(k/\nu)_T} \qquad (\nu \equiv \frac{\mu}{\rho}) \tag{14}$$

and at infinity

$$\lim_{r \to \infty} P(r,t) = P_o \tag{15}$$

The solution (after Carslaw and Jaeger) to the above equation is

$$P(r,t) = P_o + \frac{q}{4\pi(k/\nu)_T} \text{ Ei } \{- \frac{r^2}{4t} \frac{\phi \rho C_T}{(k/\nu)_T}\} \tag{16}$$

For sufficiently large t (argument of the exponential integral less than 10^{-2}) we have for the wellbore pressure[5]

$$p_w(t) = P(r_w, t) = P_o - \frac{1.15q}{2\pi(k/\nu)_T} \{\log_{10}(\frac{t(k/\nu)_T}{\phi r_w^2 \rho C_T}) + .351\} \tag{17}$$

This implies that a plot of P_w vs. log t should be a straight line, with slope equal to $1.15q/2\pi(k/\nu)_T$.

SHAFT78 was used to simulate the problem of a mass withdrawal of .14 kg/s·m on a radial grid identical to that reported by Garg[5] with

$$\Delta r_1 = \Delta r_2 = \ldots \Delta r_{11} = 1m$$

$$\Delta r_{12} = 1.2\Delta r_{11}, \ldots, \Delta r_{50} = 1.2\Delta r_{49}$$

using rock properties

$$\rho_{rock} = 2.65 \times 10^3 \text{ kg/m}^3$$

$$\phi = .2$$

$$c_{rock} = 1000 \text{ J/kg}\cdot{}^{\circ}\text{C}$$

$$K_{rock} = 5.25 \text{ W/m}\cdot{}^{\circ}\text{C}$$

Permeability (k) = $1o^{-13}$ m^2 (100 millidarcy)

The relative permeability curves used[6] for the simulation are shown in Figure 6A.

Results of our simulations for three different initial conditions are given in Table 1 and Figures 3-5. P is seen to be a linear function of log t, the slope of which gives a good estimate of the total kinematic mobility $(k/\nu)_T$. We have also plotted P vs $\log(t/r^2)$ for the same simulations, but including all elements, not just the wellblock (Figures 3B, 4B, 5B). Again a straight line results, with slope almost identical to that of the P vs. log t plots. This result, which is outside the scope of Garg's theory, seems to indicate that total kinematic mobilities could also be obtained from observation well data rather than just from flowing wellbore data.

In addition, saturation vs log (t/r^2) was plotted for 3 times for each of the three cases just discussed. As can be seen in Figure 7, saturation appears to be a function of t/r^2 only. At a position proportional to $\sqrt{t}$ there appears a broad saturation front, which becomes more diffuse as vapor saturation increases. Changing the relative permeability curves (Figure 6B) has only a slight effect on the saturation profiles. We are still investigating these results.

Table 1

Results for Total Kinematic Mobilities $(k/\nu)_T$

Initial saturation (S_o) and pressure (P_o)	$(k/\nu)_T$ from P vs log(t) plot	$(k/\nu)_T$ from P vs log (t/r^2) plot	Time (sec)	Actual value of $(k/\nu)_T$
p_o = 8.5 MPa	2.2146×10^{-7}	2.4265×10^{-7}	0.	2.3117×10^{-7}
			1889.	2.2119×10^{-7}
			7490.	2.2154×10^{-7}
S_o = .9			10184.	2.2105×10^{-7}
P_o = 8.6 MPa	1.1610×10^{-7}	1.2266×10^{-7}	0.	1.2633×10^{-7}
			3775.	1.1596×10^{-7}
			7033.	1.1479×10^{-7}
S_o = .5			19268.	1.1404×10^{-7}
			45883.	1.1314×10^{-7}
P_o = 8.6 MPa	3.8239×10^{-7}	4.161×10^{-7}	0.	5.5535×10^{-7}
			2336.	4.0947×10^{-7}
			19327.	3.9253×10^{-7}
S_o = .1			76549.	3.8568×10^{-7}
			142060.	3.7956×10^{-7}
			217406.	3.7866×10^{-7}

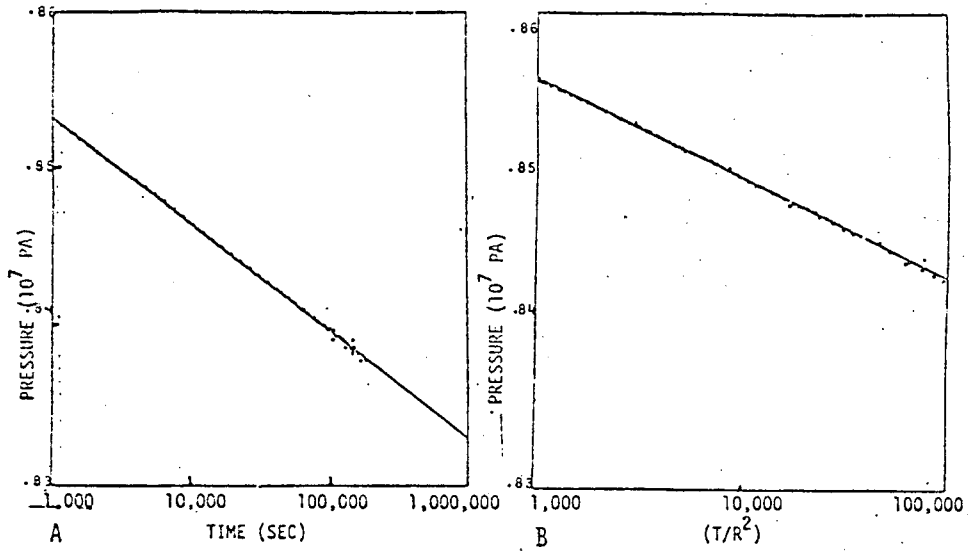

FIGURE 3. GARG PROBLEM - INITIAL RESERVOIR SATURATION = .1

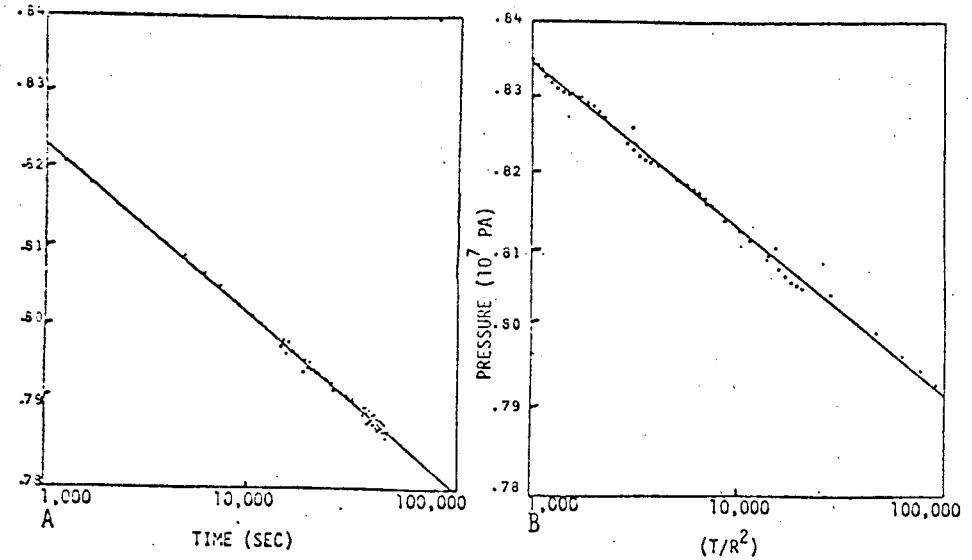

FIGURE 4. GARG PROBLEM - INITIAL RESERVOIR SATURATION = .5

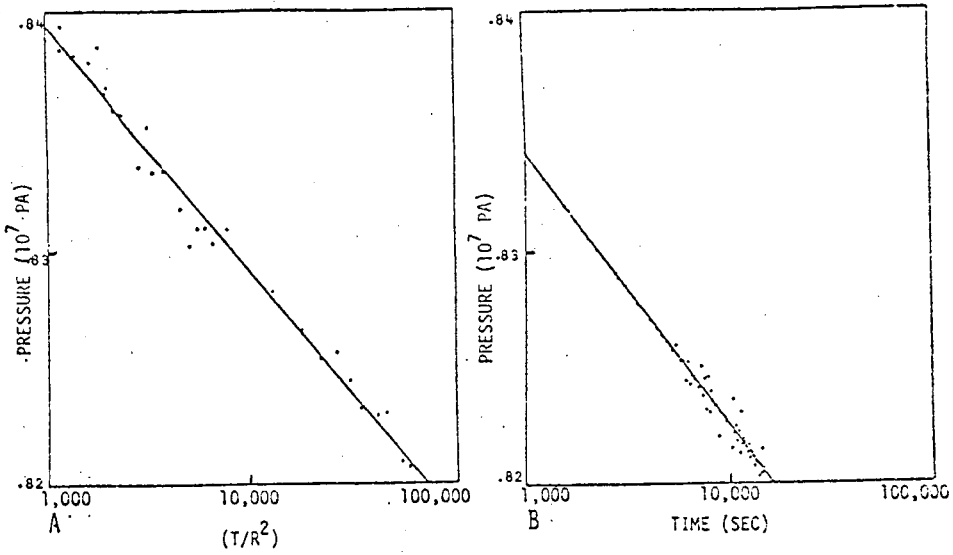

FIGURE 5. GARG PROBLEM - INITIAL RESERVOIR SATURATION = .9

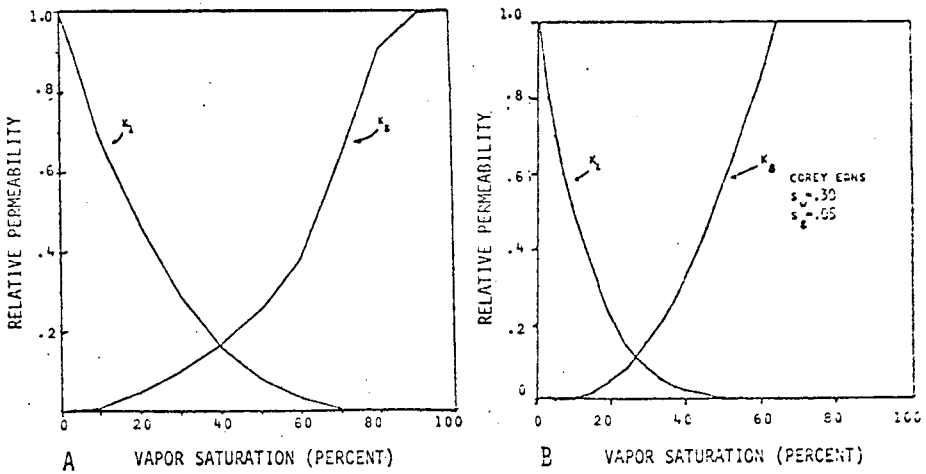

FIGURE 6. RELATIVE PERMEABILITY CURVES

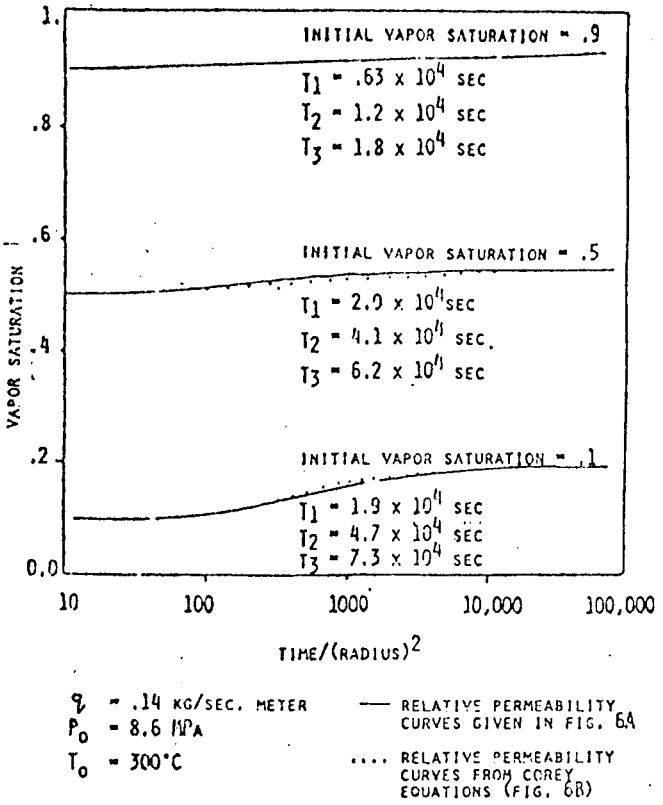

FIGURE 7. PLOT OF VAPOR SATURATION VS. T/R^2 ON A LOG-LINEAR SCALE FOR GARG PROBLEM.

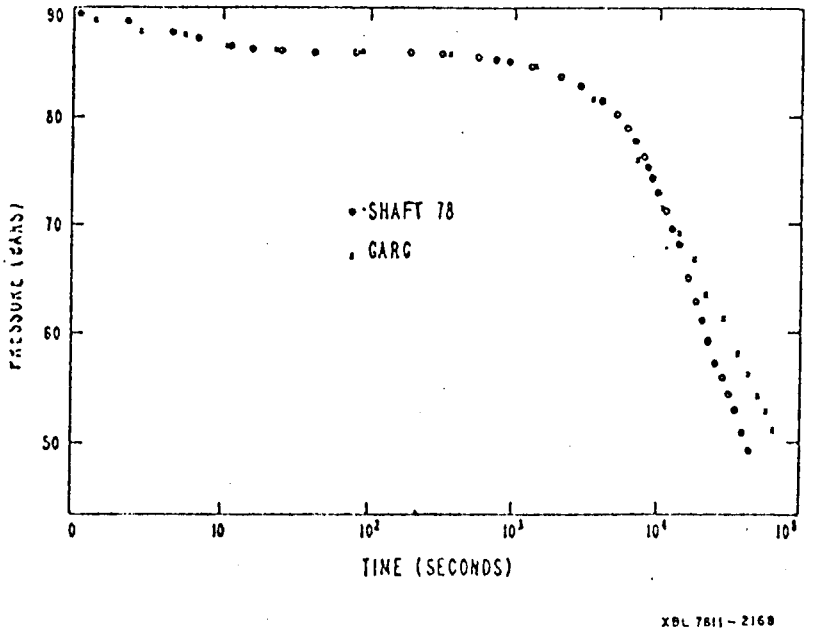

FIGURE 8. DRAWDOWN FROM AN INITIALLY LIQUID RESERVOIR WITH A PROPAGATING TWO-PHASE REGION.

Program SHAFT78 was also run to simulate a drawdown from a liquid reservoir with initial conditions

$$T_o = 300\ ^oC$$

$$P_o = 9.0\ MPa$$

$$k = 10^{-14}\ m^2$$

and the results are compared with Garg's reported results in Figure 8.

For this comparison, the Corey equation was used to generate the relative permeability curves with the parameters

$$S_w = .3$$

$$S_g = .05$$

From the slope of the straight line portion of the curve we compute a $(k/\nu)_T$ value of .86E-8 as compared to numerical values ranging from 1.4E-8 to 1.9E-8. However, $(k/\nu)_T$ values computed from the numerical simulation are decreasing with increasing time, while the straight line portion of the curve appears to be flattening out as time progresses. Thus, it appears that the computed $(k/\nu)_T$ values are converging to the numerically generated values as the flash front passes through the grid blocks.

CONCLUSION

The simulator SHAFT78 has been verified for a number of one- and two-phase flow problems involving subcooled water, water/steam mixtures, and superheated steam. The flow of water and steam in porous media, boiling and condensation, and heat exchange between rock and fluid are all described properly. No difficulties are encountered in crossing the saturation line (phase transitions).

Our simulation results confirm Garg's method of deducing total kinematic mobilities in two-phase reservoirs from production well pressure decline. It is suggested that total kinematic mobilities can also be inferred from observation well data. For uniform initial conditions we observe a simple dependence of vapor saturation upon production time and upon distance from the producing well. This as yet unexplained phenomenon indicates an underlying simplicity of two-phase porous flow.

Apart from idealized model studies, SHAFT78 is also being used for irregular three-dimensional systems. A simulation of production and recharge in the Krafla geothermal field (Iceland) is reported elsewhere.[9] At present, we are developing a history match for production and injection in the highly irregular shaped field of Serrazzano (Italy).[10]

REFERENCES

1. Pruess, K, R. Schroeder, P. Witherspoon, J. Zerzan. "SHAFT78, A Two-Phase Multidimensional Computer Program for Geothermal Reservoir Simulation," (LBL-8264)

2. Pruess, K, R. Schroeder, P. Witherspoon, J. Zerzan. "Description of the 3-D 2-Phase Simulator SHAFT78 for use in Geothermal Reservoir Studies," (SPE-7699), paper to be presented at the 5th SPE-Symposium on Reservoir Simulation, Denver, 31 January—2 February (1979).

3. Kidder, R. 1957, "Unsteady Flow of Gas through a Semi-Infinite Porous Medium," presented at Applied Mechanics Division Summer Conference, Berkeley, California, Paper #57.

4. Matthews, C.S. and D.G. Russell, 1967, "Pressure Build-Up and Flow Tests in Wells," SPE Monographs.

5. Garg, S.K., 1978, "Pressure Transient Analysis for Two-Phase (Liquid Water/Steam) Geothermal Reservoirs," SSS-IR-78-3568(R2).

6. Muskat, M., R.D. Wyckoff, H.G. Botset, and M.W. Meres, 1937, "Flow of Gas-Liquid Mixtures through Sands," Trans. AIME, 123, p. 69.

7. Toronyi, R.M. and S.M. Farouq Ali, "Two-Phase, Two-Dimensional Simulation of a Geothermal Reservoir," Soc. Pet. Eng. J. (June 1977) 171-183.

8. Lasseter, T.J., P.A. Witherspoon, and M.J. Lippmann, "Multiphase Multidimensional Simulation of Geothermal Reservoirs," Proceedings Second United Nations Symposium on the Development and Use of Geothermal Resources, San Francisco, Calif. (1975) vol. 3, 1715-1723.

9. Jonsson, V., "Simulation of the Krafla Geothermal Field," Lawrence Berkeley Laboratory Rept. LBL-7076, Berkeley, Calif. (1978).

10. Weres, O., "A Model of the Serrazano Zone," Proceedings Third Stanford Workshop on Geothermal Reservoir Engineering, Stanford, Calif. (1977) 214-219.

NOMENCLATURE

Latin — Upper Case

C_T = total compressibility
F = mass flux per unit area, kg/m^2s
H = enthalpy per unit mass, J/kg
K = rock heat conductivity, $J/ms\ ^oC$
P = pressure, Pa = N/m^2
P_D = dimensionless pressure
P_w = wellbore pressure, N/m^2
P_o = initial pressure, N/m^2
Q = energy source term, J/m^3s
T = temperature, ^oC
U = energy per unit mass (specific energy), J/kg
U_{vol} = energy per unit volume, J/m^3
S = volumetric vapor saturation

Latin — Lower Case

c = rock specific heat, $J/^oC\ kg$
k = absolute permeability, m^2
$(k/\nu)_T$ = total kinematic mobility, s
q = mass source term, kg/m^3s
r_w = wellbore radius, m
t = time, s

Greek

Θ = time averaging factor (dimensionless)
ρ = density, kg/m^3
ϕ = rock porosity, dimensionless
μ = dynamic viscosity, Ns/m^2
ν = kinematic viscosity, Nsm/kg

Subscripts

ave = average (over volume or surface element)
ℓ = liquid component
rock = referring to rock
v = vapor component
vol = volumetric measurement of the variable (e.g., U_{vol} = Energy/unit volume).

Dup

AN ANALYTIC STUDY OF GEOTHERMAL RESERVOIR PRESSURE RESPONSE TO COLD WATER REINJECTION

Y.W. Tsang and C.F. Tsang
Lawrence Berkeley Laboratory
Berkeley, California 94720

I. Introduction

Various aspects of reinjection of cooled geothermal water into the geothermal reservoir have been studied by many authors. One question of practical relevance is the calculation of reinjection pressures required. These pressures on the one hand determine the pumping requirements which are important inputs to the technical and economical feasibilities of the project. On the other hand, they may also be used as baseline data. As time goes on, if the pressure measured becomes much in excess of the calculated values, some kind of plugging may be occurring and remedial action would have to be taken.

For isothermal cases where the injected water is at the same temperature as the reservoir water, the pressure change is simply given by the Theis solution in terms of an exponential integral. The solution shows that this pressure change is directly proportional to the viscosity. It turns out that the viscosity is a strong function of temperature. Over a range of temperatures from 100°C to 250°C, the viscosity changes by a factor of 3 (whereas the density of water changes by about 20%). This is illustrated in Figure 1.

The injection of cold water into a hot reservoir is a moving boundary problem. On the inside of a boundary enclosing the injection well, the parameters correspond to that of the injected cold water; and on the outside, the parameters correspond to that of the reservoir hot water. The boundary is, of course, not sharp because of heat conduction between the hot and cold water. The width of the boundary depends on the aquifer heat conductivity and capacity, and it increases with time as the boundary (or cold temperature front) moves outward from the injection well.

There exist numerical models to solve such a problem. In an earlier work, we made a simple study using numerical model "CCC" developed at the Lawrence Berkeley Laboratory. A sample of calculated results is shown in Figure 1. The present work is an analytic calculation of such a problem when several approximations are applied. Solutions are obtained in terms of well-known functions or in terms of one integral. These calculations are checked against numerical model results.

Figure 1 also indicates that the temperature boundary effects show up in the pressure change as a function of time. Thus, the pressure data may be analyzed to obtain reservoir transmissivity, storativity, and other reservoir parameters. For such purposes, the numerical modeling approach is limited in its utility because of the complexity of calculations. The present analytical approach will prove more advantageous for such a well-test analysis.

Derivation of the governing equation, including temperature effects, will be given in the following section where the permeability-viscosity ratio is assumed to be an arbitrary function of r^2/t. In Section III, this function will be represented by a Fermi-Dirac function, whose parameters are determined based upon physical considerations. The solution for the pressure change is analytic except for the final step, where a numerical integration is called for. We discuss the results and implications of our calculations in Section IV. Summary and concluding remarks are contained in Section V.

II. Derivation

We start with the three equations:

Eq. of continuity
$$\frac{\partial}{\partial t}(\rho\phi) = -\nabla \cdot \rho\underset{\sim}{v}, \qquad (1)$$

Darcy's law
$$\underset{\sim}{v} = -\frac{k}{\mu}\nabla P = -K\nabla P, \qquad (2)$$

Eq. of state
$$\rho = A(T)e^{\beta P}, \qquad (3)$$

where the pertinent variables are ρ(density), ϕ(porosity), $\underset{\sim}{v}$(velocity), k(permeability), μ(viscosity), β(compressibility) and P(pressure). A new variable K is defined in terms of the permeability and viscosity ($K = k/\mu$). The porosity and compressibility of the medium is assumed to be constant in the following derivation. Working in the cylindrical coordinates and combining equations (1), (2), and (3), one obtains:

$$\rho\phi\left(\beta\frac{\partial P}{\partial t} + \frac{\partial \ell nA}{\partial t}\right) = \left(\frac{\rho K}{r} + \rho\frac{\partial K}{\partial r}\right)\frac{\partial P}{\partial r} + \rho\beta K\left(\frac{\partial P}{\partial r}\right)^2 + \rho K\frac{\partial^2 P}{\partial r^2}. \qquad (4)$$

For water, the percentage variation of density with temperature is much smaller than the corresponding viscosity variations over the same temperature range. Under these conditions, we may consider $\partial \ell nA/\partial t$ to be small compared with other terms in the equation. Furthermore, when the variation of pressure is "smooth," it is customary to neglect the $(\partial P/\partial r)^2$ term. Then, Eq. (4) reduces to:

$$\beta\phi\frac{\partial P}{\partial t} = \left(\frac{K}{r} + \frac{\partial K}{\partial r}\right)\frac{\partial P}{\partial r} + K\frac{\partial^2 P}{\partial r^2}. \qquad (5)$$

Ideally, for incompressible fluid, the fluid front propagates as r^2/t, and it is therefore expedient to apply the Boltzmann transformation and change the variables from (r,t) to $(z = r^2/t, t)$. One obtains from (5) the final equation that governs the pressure as a function of $z = r^2/t$;

$$\frac{d^2P}{dz^2} + \left(\frac{1}{z} + \frac{c}{4K(z)} + \frac{d\ell nK(z)}{dz}\right) \frac{\partial P}{\partial z} = 0 \qquad (6)$$

where the constant $\beta\phi$ is now written as c. The boundary conditions for Eq. (6) are:

(i) $P = P_o$ at $r = \infty$ and $t = 0$,

i.e., $$\lim_{z\to\infty} P(z) = P_o \quad . \qquad (7)$$

(ii) Incompressible fluid flow through a cylindrical surface around a line source implies

$$\lim_{r\to o}(2\pi rh)v = -(2\pi rh)\ K \frac{\partial P}{\partial r} = Q \qquad (8)$$

where Q is the pumping rate and h is the aquifer thickness. Applying the Boltzmann transformation on Eq. (8), we obtain, in the variable $z = r^2/t$:

$$\lim_{z\to o} K(z)\ z \frac{\partial P}{\partial z} = -\frac{Q}{4\pi h} \quad . \qquad (9)$$

We have now reduced the physical problem to the solving of a first-order differential equation for dP/dz, provided that the relevant permeability-viscosity function of the system is known. Grouping equations (6), (7), and (9) together, we have:

$$d^2P/dz^2 + \left(\frac{1}{z} + \frac{c}{4K(z)} + \frac{d\ell nK(z)}{dz}\right) \frac{dP}{dz} = 0, \qquad (10a)$$

$$\lim_{z\to o} K(z)z \frac{\partial P}{\partial z} = -\frac{Q}{4\pi h}\ , \qquad (10b)$$

$$\lim_{z\to\infty} P(z) = P_o. \qquad (10c)$$

III. Solution

We assume that $K(z) = k/\mu$ may be represented by a Fermi-Dirac function given by:

$$K(z) = \frac{(K_R - K_I)}{1+e^{-(z-d)/a}} + K_I. \tag{11}$$

The function takes on the values of K_I, K_R, and $(K_I + K_R)/2$ respectively at $z = 0$, $z = \infty$, and $z = d$ (see Figure 2a). The function varies appreciably only in the neighborhood of $z = d$; the parameter a characterizes the range of z over which K(z) is appreciably different from K_I and K_R. The derivative dK/dz is a symmetrical function about $z = d$. The full-width half-maximum of dK/dz about this point may be shown to be 3.52 a (see Figure 2b). This behavior of K(z) may be understood as follows: Near the wellbore the function takes on the value of $K = k/\mu = K_I$, equal to that of injected water; and it takes on the value K_R, equal to that of the reservoir at large radial distances from the well. If we assume a sharp temperature front between the cold injected water and the hot reservoir water, then the location of this transition from K_I to K_R is given by:

$$Qt = \pi r^2 h \frac{\rho_a C_a}{\rho_w C_w} \tag{12}$$

where ρ_w, C_w, ρ_a, C_a are the densities and heat capacities of water and aquifer, respectively. Eq. (12) implies a constant value for $r^2/t = d$, given by:

$$d = \frac{Q\rho_w C_w}{\pi h \rho_a C_a} \tag{13}$$

which is the same parameter d used in the Fermi-Dirac function. The fact that the temperature front is not sharp is accounted for by the width of variation from K_I to K_R, given earlier by the parameter a.

Avdonin has solved the problem of the propagation of temperature front with the injection of hot water into cold water in an aquifer. In the limit, where there is no vertical heat loss, Avdonin's solution is given by:

$$\frac{T-T_R}{T_I-T_R} = \frac{\operatorname{erfc}(o)}{\Gamma(\nu)} \frac{(C_a\rho_a)^\nu}{4\kappa_a} \left(\frac{r^2}{t}\right)^\nu \int_0^1 \exp\left[-\frac{1}{4S}\frac{C_a\rho_a}{\kappa_a}\left(\frac{r^2}{t}\right)\right] \frac{dS}{S^{\nu+1}} \tag{14}$$

$$\nu = Q\, C_w\rho_w/4\pi h\kappa_a$$

where T_R = initial aquifer temperature

T_I = temperature of injection fluid

κ_a = aquifer conductivity.

We note that in Eq. (14) the temperature again varies as r^2/t, as in the case of K(z). Since the viscosity is a function of temperature, one expects the variation of $K(z) = k(z)/\mu(z)$ in Eq. (11) to be intimately related to $(T-T_R)/(T_I-T_R)$ here. In particular, we may relate the widths of $dK(z)/dz$ and $(d/dz)(T-T_R)/(T_I-T_R)$. The full-width half-maximum of the curve $d/dz(T-T_R)/(T_I-T_R)$ is governed by a transcendental equation. However, in the limit of "narrow width," the full-width half-maximum can be shown to be $4\sqrt{2}\kappa_a/(C_a\rho_a)$. Equating the two full-width half-maxima, we arrive at the simple expression:

$$a = 1.605 \frac{\kappa_a}{C_a \rho_a} \tag{15}$$

which relates the parameter a, in the theoretical model for K(z), to the physical property of the aquifer.

Integrating Eq. (10a) and applying the boundary conditions (10b), one gets

$$\frac{dP}{dz} = - \frac{Q}{4\pi h} \frac{1}{K(z)z} \exp \left(- \frac{c}{4} \int_o^z \frac{1}{K(z')} dz' \right) . \tag{16}$$

Integrating (16) and applying the boundary condition (10c), we get

$$P(z) = P_o - \frac{Q}{4\pi h} \int_z^\infty \frac{1}{K(z)z} \exp \left(- \frac{c}{4} \int_o^z \frac{1}{K(z')} dz' \right) dz . \tag{17}$$

Given the Fermi-Dirac function for K(z) (Eq. 11), we have

$$\int_o^z \frac{c}{4K(z')} dz' = \frac{c}{4} \frac{z}{K_R} + \frac{ca}{4} \left(\frac{1}{K_R} - \frac{1}{K_I} \right) \ell n \frac{K_I \exp(-(z-d)/a) + K_R}{K_I \exp(d/a) + K_R} . \tag{18}$$

Then, Eq. (17) reduces to

$$P(z) = P_o - \frac{Q}{4\pi h} \exp\left(\frac{-cd}{4K_I}\right) \int_z^\infty \frac{1 + \exp(-(z'-d)/a)}{K_R + K_I \exp(-(z'-d)/a)} \frac{1}{z'} \cdot \tag{19}$$

$$\cdot \frac{[K_R + K_I \exp(-(z'-d)/a)]^{(1/K_I - 1/K_R)ca/4}}{\exp\left(\frac{c}{4K_R} z'\right)} dz' .$$

Eq. (19) is integrated numerically. Figures 3 and 4 show the variation of $P(z) - P_o$ with z for various values of d and a. Table 1 summarizes the parameters used.

IV. Results and Discussion

The most interesting feature of these plots is that the curve follows, for small values of t/r^2, a Theis line with parameters corresponding to those of the native hot water, and for large t/r^2 it approaches a line parallel to a Theis line with parameters corresponding to those of the injected water. The transition occurs at $z = d$, or $t/r^2 = 1/d$, where d may be expressed in terms of the flowrate, heat capacities, and reservoir thickness (see Eq. 13). Thus, injection well test data can yield the transition point d and the separation Δ. These two additional parameters, when coupled with the two which are normally obtained (transmissivity kh and storativity $\phi\beta h$) affords the possibility of determining the parameters h, ϕ, and k separately, provided the heat capacities are known.

To make the solution more transparent, we break up the K function into three sections as shown in Figure 2. Thus:

$$\begin{aligned} K &= K_I && z < d-w \\ K &= K_{FD} && d-w < z < d+w \\ K &= K_R && d+w < z. \end{aligned} \tag{20}$$

Here, $(d - w, d + w)$ defines the interval in z where K changes from K_I to K_R, and K_{FD} represents the Fermi-Dirac function given in Eq. (11).

Now Equation (17) gives the general pressure solution:

$$P = P_o - \frac{Q}{4\pi h} \int_z^\infty \frac{1}{Kz} \exp\left(-\int_o^z \frac{c}{4K(z')}\, dz'\right) dz \quad .$$

With K given by Eq. (20), we have

$$\begin{aligned} \int_o^z \frac{c}{4K}\, dz' &= \frac{c}{4K_I}\, z && \text{for } z < d-w \\ &= \frac{c}{4K_I}\,(d-w) + \int_o^z \frac{c}{4K_{FD}}\, dz' && d-w < z < d+w \\ &= \frac{c}{4K_I}\,(d-w) + \int_o^{d+w} \frac{c}{4K_{FD}}\, dz' + \frac{c}{4K_R}\,(z-d-w) && z > d+w \ . \end{aligned} \tag{21}$$

Then, the solution is given for

(a) $z > d+w$

$$P_1(z) = P_o + \frac{Q}{4\pi h K_R} C_1 \, Ei\left(-\frac{c}{4K_R} z\right) \tag{22}$$

where

$$C_1 = \exp\left(\frac{cw}{4K_I}\right) \left(K_R + K_I \exp\left(-\frac{w}{a}\right)\right)^{\frac{ca}{4}\left(\frac{1}{K_I} - \frac{1}{K_R}\right)}$$

(b) $d+w > z > d-w$

$$P_2(z) = P_1(d+w) - \frac{Q}{4\pi h} \exp\left(-\frac{c}{4K_I}(d-w)\right) \int_z^{d+w} \frac{1}{K_{FD} z} \exp\left(-\int_o^z \frac{c}{4K_{FD}} dz'\right) dz \tag{23}$$

(c) $z < d-w$

$$P_3(z) = P_2(d-w) + \frac{Q}{4\pi K_I h} Ei\left(-\frac{c}{4K_I} z\right) \tag{24}$$

For large z or small t/r^2, the solution behaves as a constant times the Theis solution using reservoir water parameters (Eq. 22). This constant is approximately one, since w and a are "small" quantities describing the transition width from K_I to K_R.

On the other hand, for small z or large t/r^2, pressure behaves as the Theis solution with injected water parameters, but with a constant shift, Δ, given by the first term in Eq. (24), i.e.,

$$\Delta = P_2(d-w) - P_o$$

$$= \frac{Q}{4\pi h} \left\{ \frac{C_1}{K_R} Ei\left(-\frac{c}{4K_R}(d+w)\right) - \exp\left(-\frac{c}{4K_I}(d-w)\right) \int_{d-w}^{d+w} \frac{1}{K_{FD} z} \cdot \right.$$

$$\left. \cdot \exp\left(-\int_o^z \frac{c}{4K_{FD}} dz'\right) dz \right\}$$

where the second term may be obtained by numerical integration (see Eq. 19) or by assuming the integrand to be approximately constant over the interval (d - w, d + w).

In well-test analysis, Figures 3 and 4 may be used directly. The early data may first be compared with the curve for $t/r^2 = 1/d$ yielding kh and $\phi\beta h$ values. Matching of later data will give parameter d from which h may be estimated (see Eq. 13). Thus, k, $\phi\beta$, and h are evaluated. Of course, in actual field-data analysis other possible effects (e.g., boundaries) may enter and great care has to be exercised.

V. Summary

A governing equation is obtained assuming temperature-dependent viscosity. The solution is obtained by assuming the parameter k/μ to be a Fermi-Dirac function of r^2/t. The constants in the function are related to the cold water injection problem by a comparison with Avdonin's solution. The result displays an interesting transient pressure curve which initially (small t/r^2 values) follows the Theis solution with parameters corresponding to reservoir hot water and at large t/r^2 values, turns and becomes parallel to the Theis solution with cold water parameters. Use of these results for cold water injection well-test analysis is briefly discussed.

Work performed under the auspices of the U.S. Department of Energy.

Table 1

Parameters Used in Calculations

$$Q = 80 \text{ kg/sec}$$

$$h = 150 \text{ m}$$

$$c = \phi\beta = 1.2168 \times 10^{-8} \text{ ms}^2/\text{kg}$$

$$K(300^\circ\text{C}) = \left(\frac{k}{\mu}\right)_{300^\circ\text{C}} = 5.4705 \times 10^{-10} \text{ m}^3\text{s/kg}$$

$$K(100^\circ\text{C}) = \left(\frac{k}{\mu}\right)_{100^\circ\text{C}} = 1.7857 \times 10^{-10} \text{ m}^3\text{s/kg}$$

$$d = \begin{cases} 3.2568 \\ 4.2568 \\ 5.2566 \end{cases} \times 10^{-4} \text{ m}^2/\text{s}$$

$$a = \begin{cases} 0.1 \\ 1.0 \\ 2.0 \end{cases} \times 10^{-4} \text{ m}^2/\text{s}$$

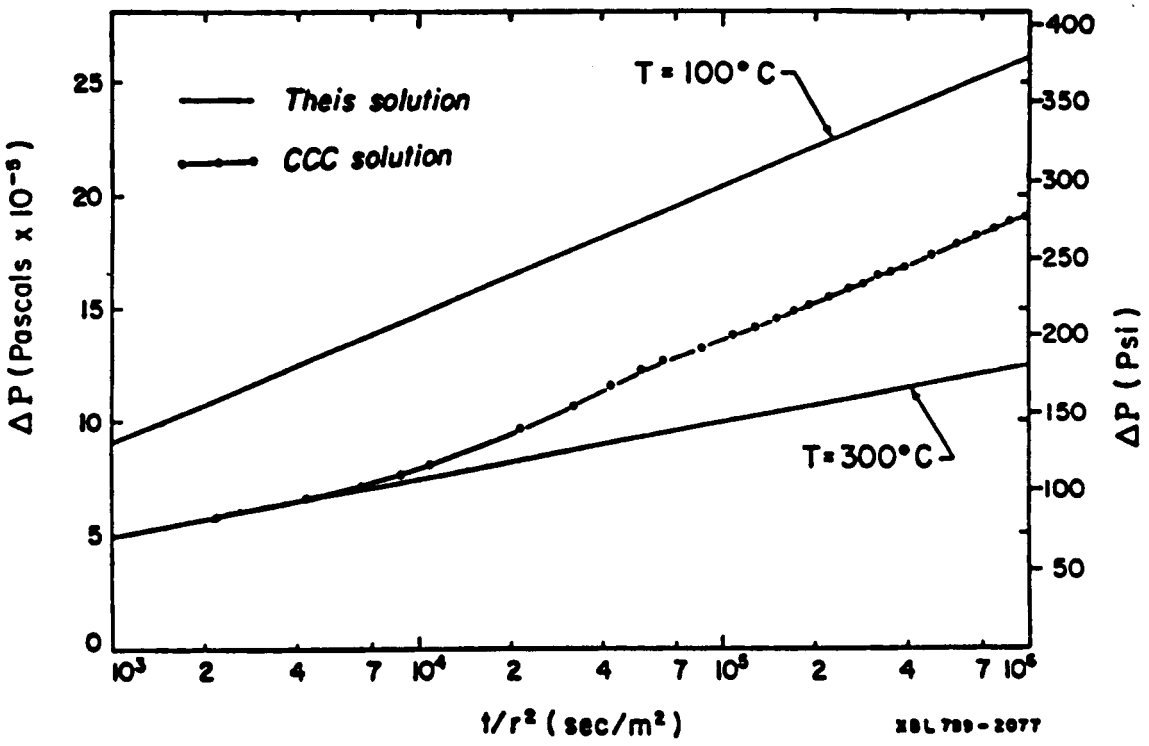

FIGURE 1

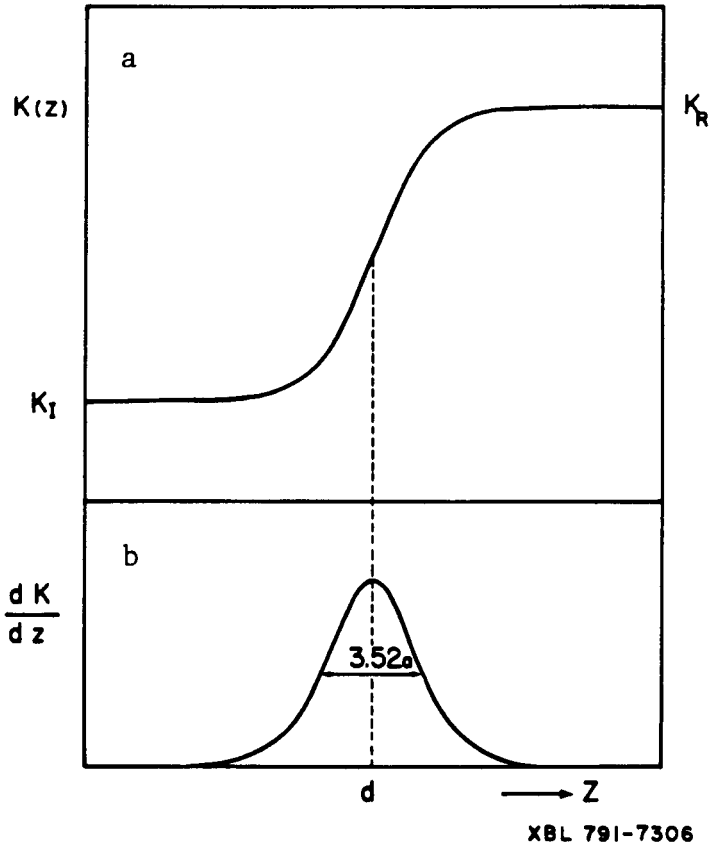

FIGURE 2

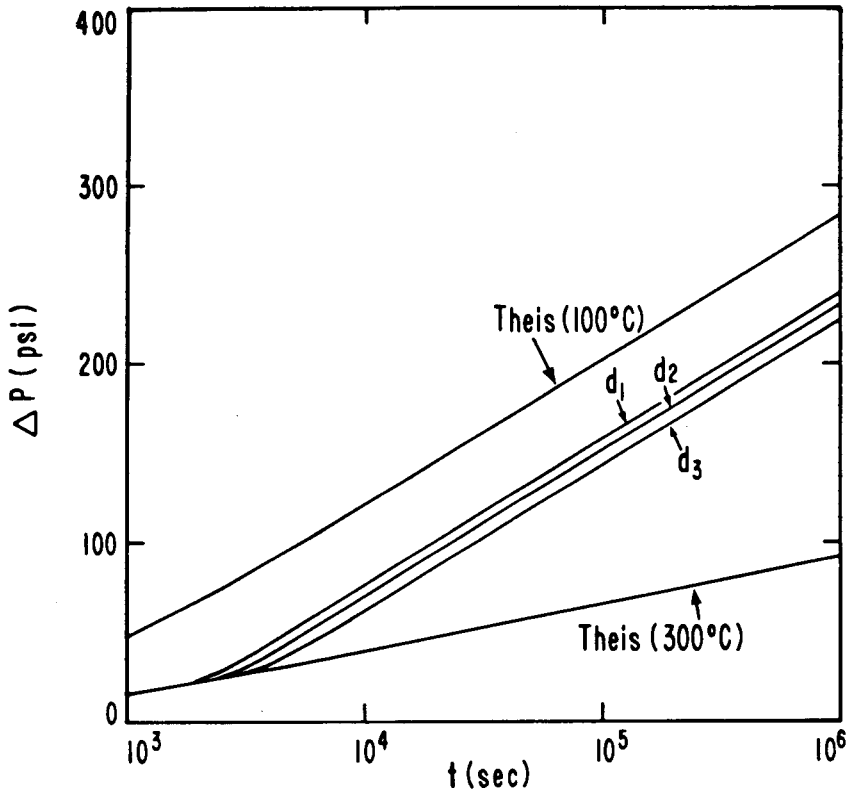

FIGURE 3

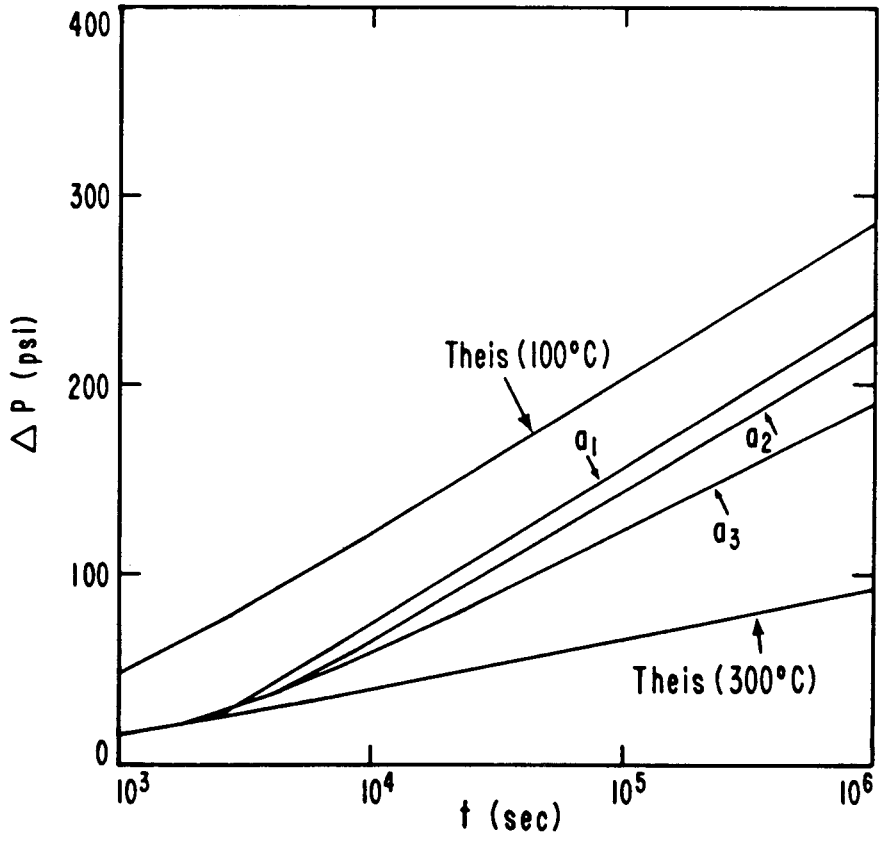

FIGURE 4

SIMULATION OF THE BROADLANDS GEOTHERMAL FIELD, NEW ZEALAND

G.A. Zyvolski* and M.J. O'Sullivan
University of Auckland, New Zealand

Abstract

The governing equations for a two phase geothermal reservoir are presented for the case when a substantial amount of carbon dioxide is present. Sample results for a model reservoir based on the Broadlands geothermal field are given.

Introduction

The Broadlands geothermal field is the next field in New Zealand which will be extensively developed. Like the Bagnore field in Italy and the Ngawha field in New Zealand, the Broadlands field is characterized by a relatively high (2-4% by mass) content of carbon dioxide. The presence of carbon dioxide has depressed the boiling surface sufficiently deep to make the production zone two phase. Because of the importance of the gas content in influencing the design of geothermal energy conversion systems it is important to understand and to predict the behaviour of carbon dioxide in the reservoir.

Lumped parameter models of gassy (carbon dioxide) geothermal reservoirs have recently been studies.[1,2,3] They have shown that the reservoir properties are sensitive to changes in the carbon dioxide content. This report presents some of the initial results of a simulation of the behaviour of a multi-dimensional carbon dioxide dominated reservoir.

Basic Field Equations

A thorough discussion of the governing equations for the carbon dioxide water geothermal system is given by Zyvoloski and O'Sullivan.[4] Here we present only the final results (see notation section).

*Presently at the University of California at Santa Barbara, California 92706.

Conservation of mass:

$$\Delta \cdot (D_m \Delta p) - q_m - \frac{\partial A_m}{\partial t} = 0 \qquad (1)$$

Conservation of energy:

$$\nabla.(D_m \nabla p) - q_e - \frac{\partial A_e}{\partial t} = 0 \qquad (2)$$

Conservation of carbon-dioxide:

$$\nabla.(D_c \nabla p) - q_e - \frac{\partial A_c}{dt} = 0 \qquad (3)$$

where

$$A_m = \phi (S_v \rho_v + S_\ell \rho_\ell)$$

$$A_e = (1-\phi) \rho_r U_r + \phi (S_v \rho_v U_v + S_\ell \rho_\ell U_\ell)$$

$$A_c = \phi (S_v \rho_v n_v + S_\ell \rho_\ell n_\ell)$$

The transmissibilities D_m, D_e, and D_c are given by

$$D_m = D_{mv} + D_{m\ell}$$

$$D_e = H_v D_{mv} + H_\ell D_{m\ell}$$

$$D_c = n_v D_{mv} + n_\ell Dm_\ell$$

with

$$D_{mv} = \frac{kR_v \rho_v}{\mu_v}, \quad D_{m\ell} = \frac{kR_v \rho_v}{\mu_\ell}$$

We note here that in equations (1), (2) and (3), use was made of Darcy's law. The forms of the relative permeabilities are those suggested by Corey.[5]

The independent variables used are the total pressure p, the mixture enthalpy H and the temperature T. The variables H and T do not appear explicitly in equations (1), (2), and (3) but the variables D_α, $A\alpha(\alpha = m, e, c)$ depend on them. The mixture enthalpy is defined by

$$H = (\rho_\ell H_\ell S_\ell + \rho_v H_v S_v)/(\rho_\ell S_\ell + \rho_v S_v)$$

This equation is used to solve for $S_v(S_\ell = 1-S_v)$ in terms of other quantities which depend only on p and T.

Thermodynamics

The thermodynamics formulae used are similar to those used by Sutton and McNabb[6], Grant[1], Zyvoloski and O'Sullivan[4], Atkinson et al[3], and Mercer and Faust[7] and are not reproduced here.

The sink terms q_e and q_c are calculated from the prescribed mass withdrawal q_m using the formulae

$$q_e = q_v H_v + q_\ell H_\ell$$

$$q_c = q_v n_v + q_\ell n_\ell$$

Here q_v and q_ℓ, the mass withdrawals of vapour and liquid respectively, are calculated using the equations below (Mercer and Faust[7])

$$q_v = \sigma q_m \quad q_e = (1 - \sigma) q_m$$

with

$$\sigma = 1/(1 - \rho_\ell R_\ell \mu_v / \rho_v R_v \mu_\ell)$$

For a presentation of the numerical procedures used the reader is referred to Zyvoloski and O'Sullivan.[4]

RESULTS

Two examples were chosen to investigate the effect of the presence of carbon dioxide on reservoir behaviour. The first is a hypothetical two-phase, two-dimensional reservoir with field properties similar to those found in the Broadlands (New Zealand) geothermal field. The data for the problem are given in Table 1. The problem is similar to one considered previously for a pure water field by Faust and Mercer[7], Toronyi and Farouq Ali[8] and Thomas and Pierson[9]. The results in Figures 1 and 2 give contours for pressure and saturation, after the field has been discharging for 500 days. The results clearly show that the pressure changes are propagated more rapidly across the field when carbon dioxide is present corresponding to a decrease in the compressibility of the fluid.

The second example considered was designed to test the effect of carbon dioxide on the short term transient behaviour of a geothermal aquifer. The data for the problem are given in Table 2. Two initial liquid saturations of 0.99, 0.2 and three initial carbon dioxide contents are considered. The pressure of the wellbore as a function of time for these six cases is shown in Figures 3 and 4. The qualitative difference between the behaviour at high saturation (Figure 3) and low saturation (Figure 4) can be explained in terms of the carbon dioxide content. With a high liquid saturation there is a very small amount of carbon dioxide in the discharge (see equation 18) because the discharge is mainly from the liquid phase in which the carbon dioxide content is small. In this situation the carbon dioxide primarily affects the system by decreasing the compressibility of the two-phase fluid. At the low liquid saturation the discharge comes mainly from the vapour phase and is rich in carbon dioxide. This removal of carbon dioxide, or "de-gassing", dominates the pressure response and consequently the pressure drops significantly as a result of the decrease of the partial pressure of carbon dioxide in the vapour. Figures 5 and 6 show the radial pressure profiles at the different saturations. The compressibility and de-gassing effects are evident.

CONCLUSIONS

The spatial behaviour of gas-dominated reservoirs is substantially different from pure water reservoirs. The qualitative behaviour of the pressure transients is affected by the saturation and the presence of carbon dioxide. Careful monitoring of the gas content in the discharge may be required to allow correct interpretation of pressure transients in gassy geothermal fields.

Nomenclature and Notation

A	-	Accumulation term
D	-	Transmissibility
H	-	Enthalpy
k	-	Field permeability
n	-	Mass fraction carbon dioxide
P	-	Field pressure
q	-	Sink
R	-	Relative permeability
S	-	Saturation
T	-	Temperature
t	-	Time
U	-	Specific internal energy
ϕ	-	Field porosity
ρ	-	Density
μ	-	Viscosity

Subscripts

c	-	carbon dioxide
m	-	mass
e	-	energy
ℓ	-	liquid phase
v	-	vapour phase
r	-	rock

REFERENCES

1. Grant, M.A., "Broadlands - a Gas-dominated Field", Geothermics, (1977), Vol. 6, 9-29

2. Zyvoloski, G.A. and O'Sullivan, M.J., "A Simple Model of the Broadlands Geothermal Field", N.Z.J.Sci., in press.

3. Atkinson, P., Celati, R., Corsi, R., and Kucuk, F., "Behaviour of two-Component Vapour-Dominated Geothermal Reservoirs", paper SPE 7132 presented at the 1978 California Regional Meeting, San Francisco, California, April 12-14, 1978.

4. Zyvoloski, G.A., and O'Sullivan, M.J., "Simulation of a Gas-Dominated Two Phase Geothermal Reservoir", to be published.

5. Corey, A.T., "The Interrelation Between Gas and Oil Relative Permeabilities", Producers Monthly (1954) Vol.19, 38-41

6. Sutton, F.M., "Pressure-temperature Curves for a Two-Phase Mixture of Water and Carbon Dioxide", N.Z.J.Sci. (1976), Vol.19, 297-301.

7. Mercer, J.W., and Faust, C.R., "Simulation of Water-and Vapour-dominated hydrothermal reservoirs", paper SPE 5520 presented at the SPE-AIME 50th Annual Fall Meeting, Dallas, Sept.28 - Oct 1, 1975.

8. Toronyi, R.M., and Farouq Ali, S.M., "Two-Phase two-Dimensional Simulation of a Geothermal Reservior and Wellbore System", Soc. Pet. Eng. J (June 1977) 171-183.

9. Thomas, L.K., and Pierson, R.G., "Three-Dimensional Geothermal Reservoir Simulation", Soc. Pet. Eng. J. (April 1978) 573-592.

TABLE 1 - A MODEL TEST TWO-PHASE RESERVOIR

Permeability	k	=	$3(10^{-14})$ m^2
Porosity	ϕ	=	0.20
Thermal conductivity	K	=	2.5 W/m.K
Rock density	ρ_r	=	2500 kg/m^3
Rock specific heat	C_r	=	1.0 kJ/kg.K
Aquifer dimensions:	Length	=	1760 m
	Width	=	880 m
	Thickness	=	250 m
Number of blocks	NX x NY	=	11 x 11
Time step	Δt	=	10 days
Production rate	q_m	=	80 kg/sec
Initial pressure	$p^0_{i,j}$	=	62 bars
Initial liquid saturation	$S^0_{\ell i,j}$	=	0.85
Initial partial pressure of CO_2	$p^0_{ci,j}$	=	0.0 or 15.0 bars

TABLE 2 - RADIAL PRESSURE TRANSIENT TEST

Permeability	$k = 6(10^{-14})$ m^2
Porosity	$\phi = 0.2$
Thermal conductivity	$K = 2.5$ W/m.k
Rock density	$\rho_r = 2500$ kg/m^3
Rock specific heat	$C_r = 1.0$kJ/kg.K
Aquifer radius	$= 12$ m
Aquifer thickness	$= 100$ m
Number of blocks	$= 35$
Time step	$\Delta t = 43.2$s
Discharge rate	$q_m = 16.7$ kg/s
Initial pressure	$p^0_{i,j} = 50$ bars
Initial liquid saturation	$S^0_{\ell i,j} = 0.2$ or 0.99
Initial partial pressure of CO_2	$p^0_{ci,j} = 0.0$, 4.0 or 12.0 bars

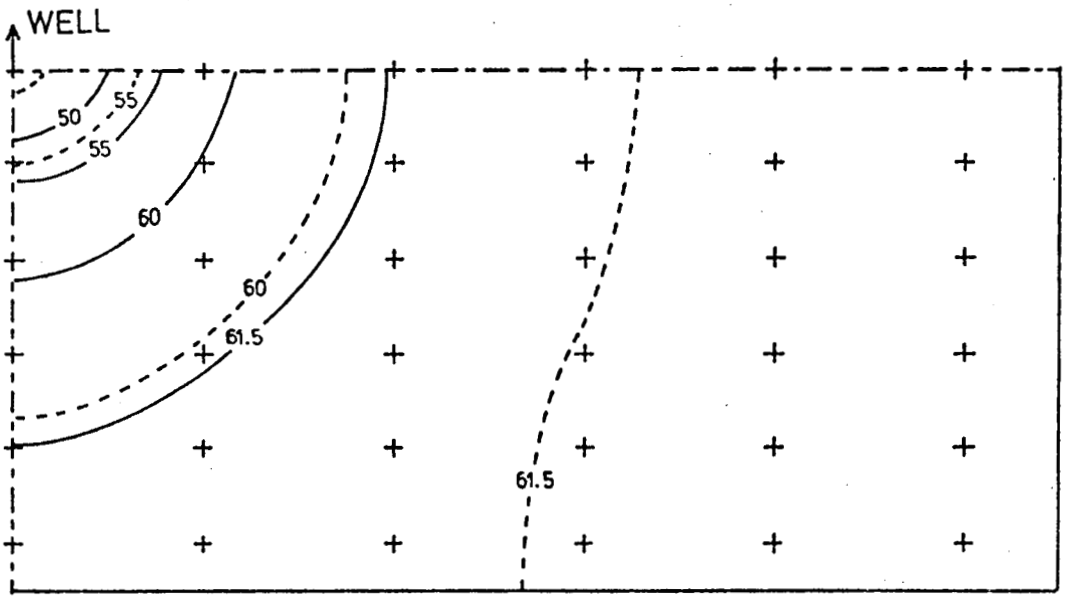

Figure 1. Pressure contours in the model reservoir after 200 days. _____ no CO_2, -------- 15 bar initial partial pressure of CO_2.

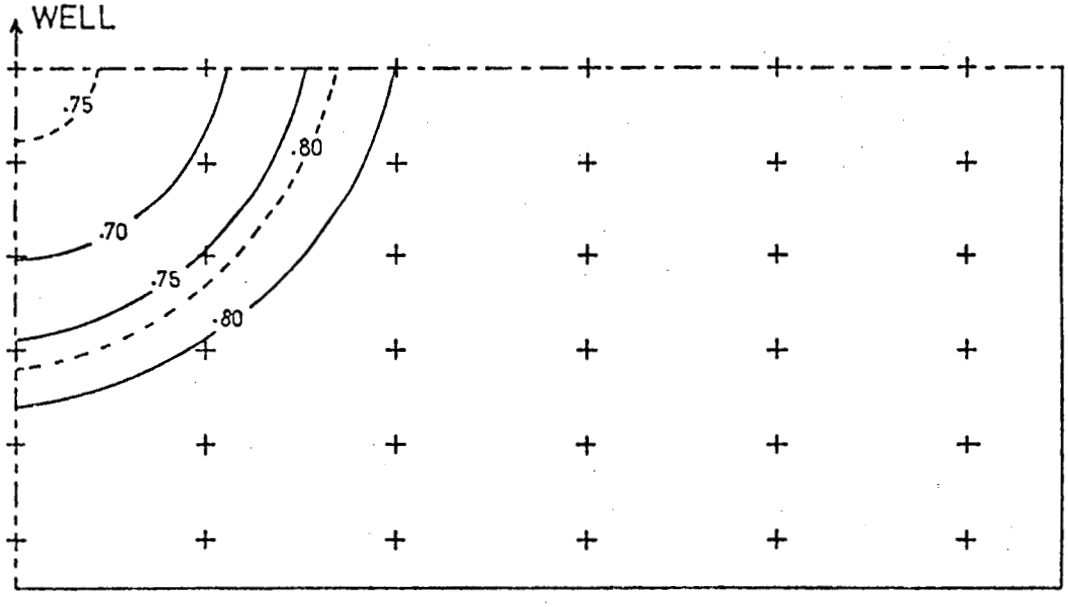

Figure 2. Liquid saturation contours in the model reservoir after 200 days. _____ no CO_2, -------- 15 bar initial partial pressure of CO_2.

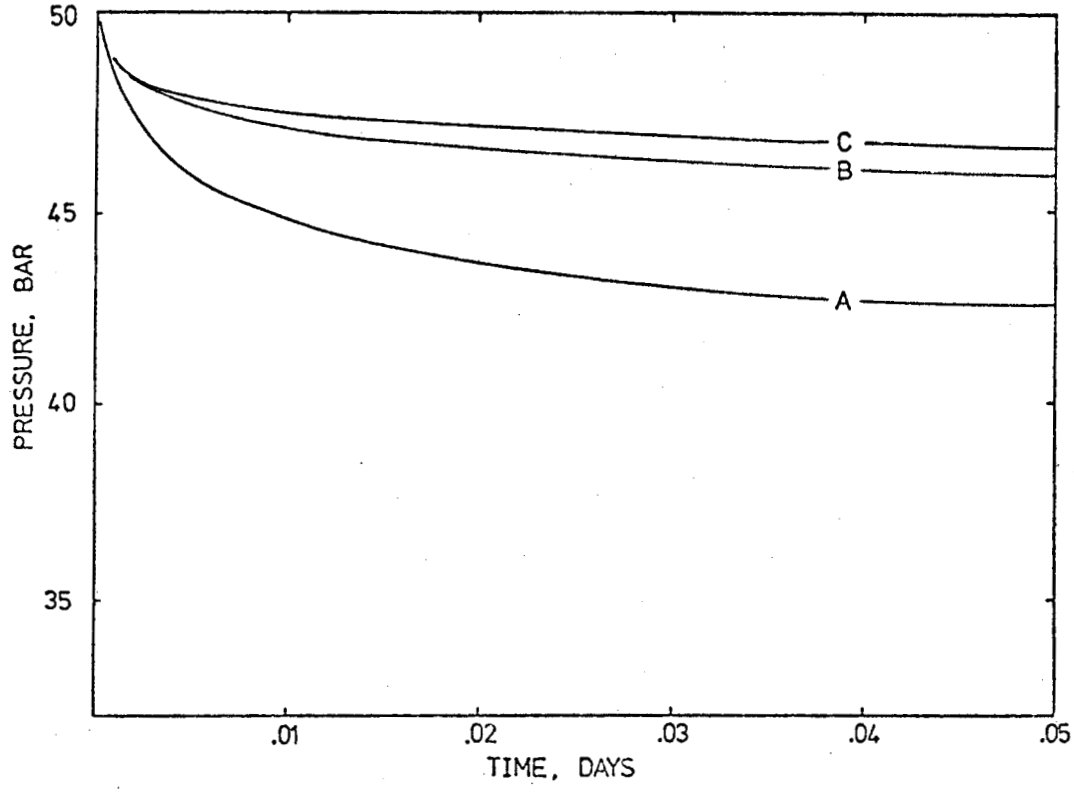

Figure 3. Transient pressure response of a model aquifer with an initial liquid saturation of 0.99 and varying CO_2 concentrations A - no CO_2, B - 4 bar CO_2, C - 12 bar CO_2.

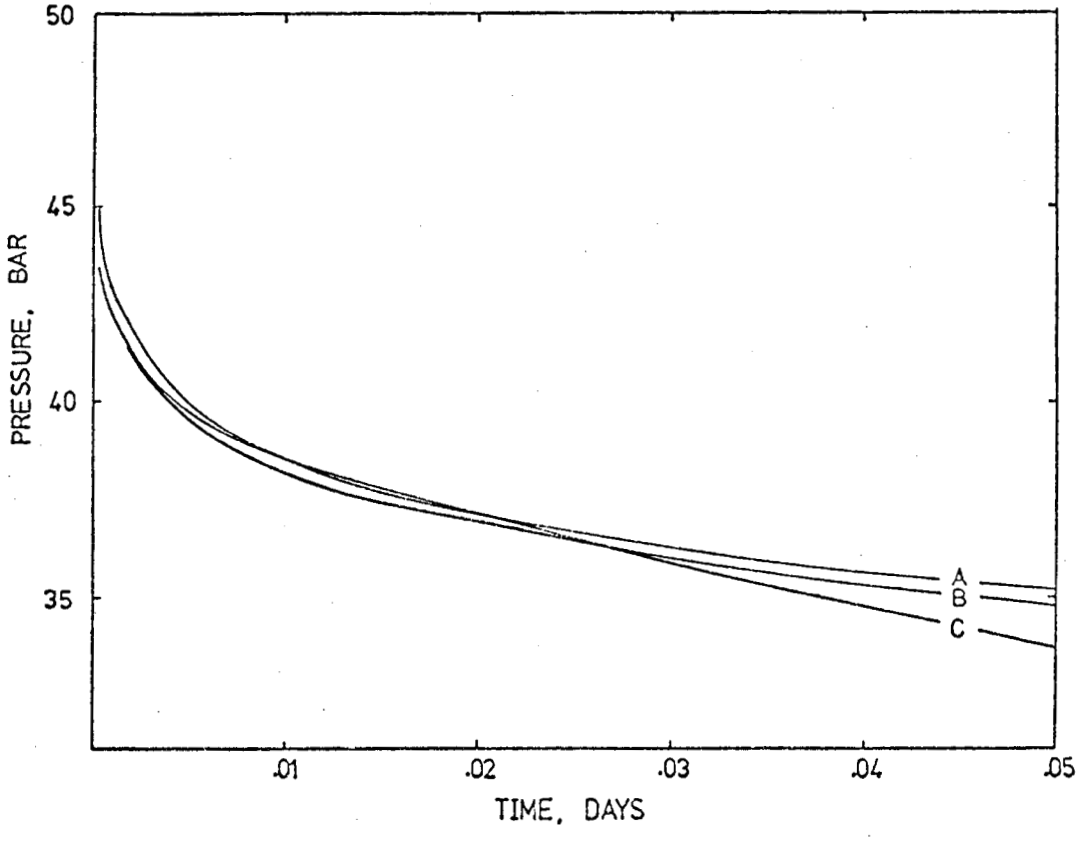

Figure 4. Transient pressure response of a model aquifer with an initial saturation of 0.20 and varying CO_2 concentrations. A - no CO_2, B - 4 bar CO_2, C - 12 bar CO_2.

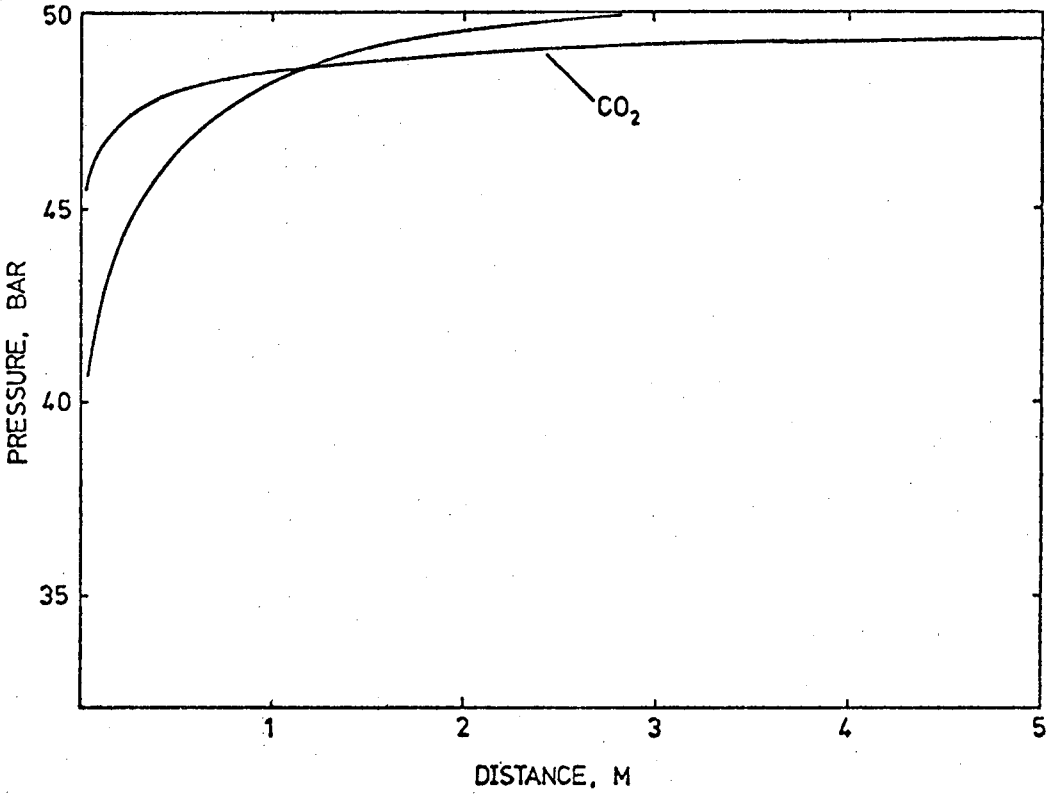

Figure 5. Pressure profiles in a model aquifer after 0.050 days. Initial liquid saturation 0.99. No CO_2 and 12 bars initial partial pressure of CO_2 respectively.

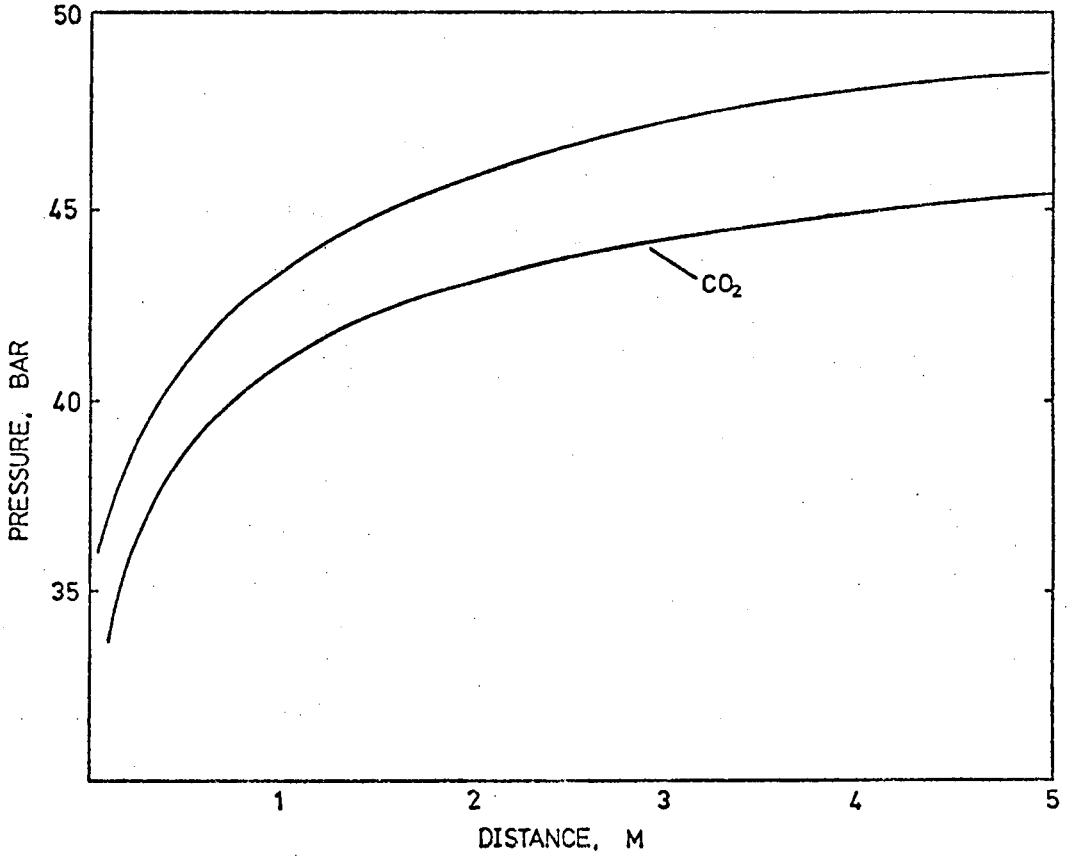

Figure 6. Pressure profiles in a model aquifer after 0.050 days Initial liquid saturation 0.20. No CO_2 and 12 bars initial partial pressure of CO_2 respectively.